TRANSNUCLEAR

NUHOMS®-MP187 MULTI-PURPOSE CASK

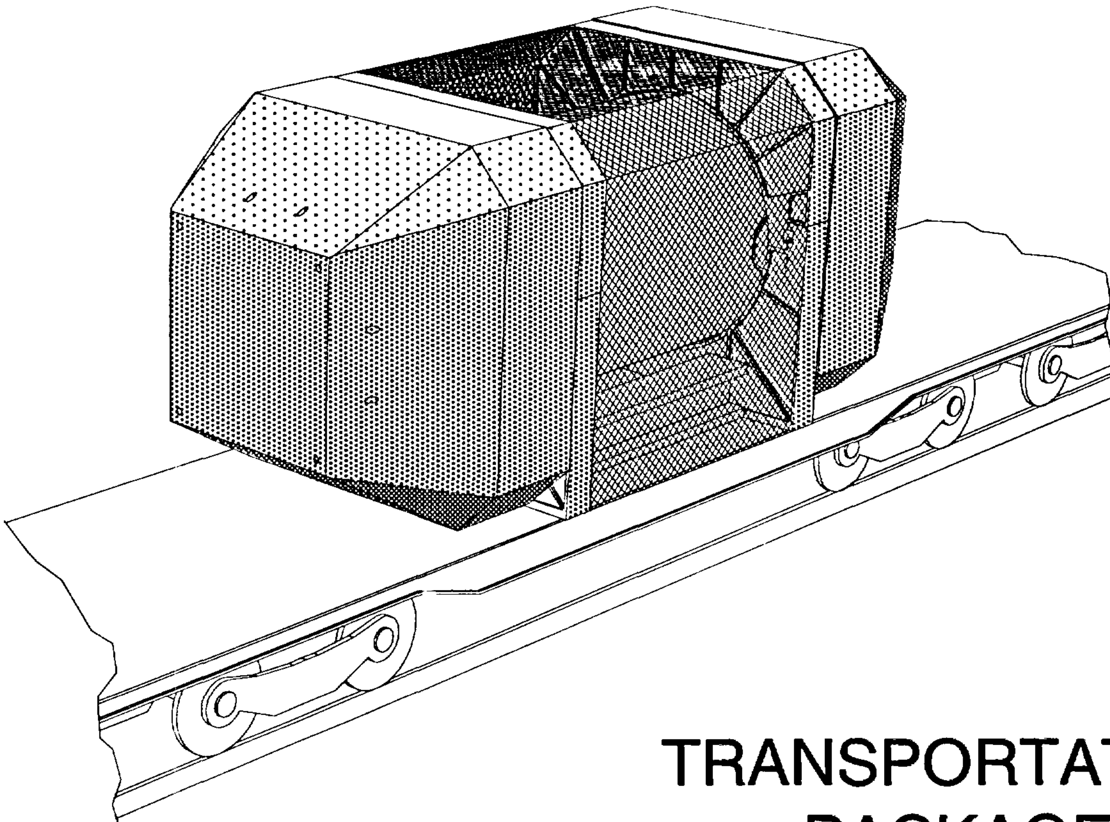

TRANSPORTATION PACKAGE

SAFETY ANALYSIS REPORT

NON-PROPRIETARY DATA

DOCUMENT NO. NUH-05-151
Volume II OF III

2.10 Appendices

2.10.1 References

2.1 "Packaging and Transportation of Radioactive Materials," Title 10, Code of Federal Regulations, Part 71 (10CFR71), USNRC, 5/31/88

2.2 ASME Boiler and Pressure Vessel Codes, 1992 Edition with 1993 Addenda.

2.3 Regulatory Guide 7.8, "Load Combinations for the Structural Analysis of Shipping Casks for Radioactive Material," Rev. 1, U. S. Nuclear Regulatory Commission, March 1989.

2.4 Regulatory Guide 7.6, "Design Criteria for the Structural Analysis of Shipping Cask Containment Vessels," Rev. 1, U. S. Nuclear Regulatory Commission, March 1978.

2.5 U.S. Nuclear Regulatory Commission (U.S. NRC), "Shock and Vibration Environments for a Large Shipping Container During Truck Transport (Part II)," NUREG/CR-0128, May 1978.

2.6 Swanson Analysis Systems, Inc., "ANSYS Engineering Analysis System User's Manual for ANSYS Revision 4.4/4.4A," Houston, PA.

2.7 Young, W. C., Roark's Formulas for Stress and Strain, Sixth Edition, McGraw-Hill Book Company, 1989.

2.8 SMUD Technical Specification, "NUHOMS Spent Nuclear Fuel Transport and Cask Storage System," Specification No. M41.01, Revision 2, September 1992.

2.9 U.S. Department of Energy Office of Civilian Radioactive Waste Management, "Characteristics of Potential Repository Wastes," DOE/RW-0184-R1, July 1992.

2.10 Boresi and Sidebottom, Advanced Mechanics of Materials, Fourth Edition, John Wiley & Sons, Inc., 1985.

2.11 Blevins, Robert D., Formulas for Natural Frequency and Mode Shape, Van Nostrand Reinhold Company, 1979.

2.12 Newmark and Rosenblueth, Fundamentals of Earthquake Engineering, Prentice-Hall, Inc., Englewood Cliffs, N.J., 1971.

2.13 Regulatory Guide 7.9, "Standard Format and Content of Part 71 Applications for Approval of Packaging of Type B, Large Quantity, and Fissile Radioactive Material", Rev. 1, U. S. Nuclear Regulatory Commission, January 1980.

2.14 Teitz, T. E., "Determination of the Mechanical Properties of a High Purity Lead and a 0.058% Copper-Lead Alloy," WADC Technical Report 57-695, ASTIA Document No. 151165 Stanford Research Institute, Menlo Park, CA, April 1958.

2.15 Shigley, J. E., Mechanical Engineering Design, Third Edition, McGraw-Hill Book Company, 1977.

2.16 Nelms, A., "Structural Analysis of Shipping Casks, Effect of Jacket Physical Properties and Curvature and Puncture Resistance," Vol. 3, ORNL TM-1312, Oak Ridge National Laboratory, Oak Ridge, Tennessee, June 1968.

2.17 Welding Research Council, Bulletin No. 297, "Local Stresses in Cylindrical Shells Due to External Loadings on Nozzles -Supplement to WRC Bulletin No. 107," August 1984

2.18 NUREG/CR-1815, "Recommendations for Protecting Against Failure by Brittle Fracture in Ferritic Steel Shipping Containers up to Four Inches Thick," Lawrence Livermore National Laboratory, August 1981.

2.19 Society of Allied Weight Engineers, Weight Engineers Handbook, Society of Allied Weight Engineers, Inc., 1986 Edition.

2.20 NUREG/CR-6007, "Stress Analysis of Closure Bolts for Shipping Casks," Lawrence Livermore National Laboratory, April 1992.

2.21 Boucher, Raymond C., "Speeds Calculation of Strength of Threads," Product Engineering, November 27, 1961.

2.22 Baumeister, et al, Mark's Standard Handbook for Mechanical Engineers, Eighth Edition, McGraw Hill Book Company, 1979.

2.23 Pacific Nuclear, "Consolidated Safety Analysis Report for the NUPAC 125-B Fuel Shipping Cask," NRC Docket No. 71-9200, April 1991.

2.24 Frank Kreith, Principles of Heat Transfer, Third Edition, Harper and Row Publishers.

2.25 Cases of ASME Boiler and Pressure Vessel Code, Case N-284, "Metal Containment Shell Buckling Design Methods, Section III, Division 1, Class MC," August 25, 1980.

2.26 IAEA Safety Guides, "Advisory Material for the Application of the IAEA Transport Regulations," Safety Series No. 37.

2.27 "General Plastics Last-a-Foam® FR-3700 for Crash and Fire Protection of Nuclear Material Shipping Containers," General Plastics Manufacturing, Tacoma, WA, September 1992.

2.28 "Numerical and Analytical Methods for Approximating the Eccentric Impact Response (Slapdown) of Deformable Bodies," G. D. Sjaarddema and W. Wellman, Sandia Report SAND88-0616.UC-71, March 1988.

2.29 "SCANS - A Microcomputer Based Analysis System for Shipping Cask Design Review," M. A. Gerhard, J. Trummer, G. L. Johnson, and G. C. Mok, NUREG/CR 4554.

2.30 Correspondence from PACTEC to Transnuclear West, "Impact Limiter Design and Performance Evaluation," September 1993.

2.31 Transnuclear West Correspondence, "Results of 1/16th Bench Test Model," File No. NUH005.0014, July 6, 1993

2.32 Helicoflex FAX dated September 30, 1994, from Ken Morales of Helicoflex to Joe Nichols of Transnuclear West, with attached sketch of Helicoflex part no. sk U200858, type O-ring (port closure bolt o-rings). See Transnuclear West Vendor File No. NUH005.0016.14.

2.33 Helicoflex FAX dated September 13, 1994, from Ken Morales of Helicoflex to Joe Nichols of Transnuclear West, with attached sketch of Helicoflex part nos. sk H-34101, Type HN 200 and sk H-304102, Type HN200 (top cover plate o-rings) and sketch of Helicoflex part nos. sk H-304103 Type HN 200 and sk H-304104, Type HN 200 (ram access closure plate o-rings). See Transnuclear West Vendor File No. NUH005.0016.14.

2.34 Bickford, An Introduction to the Design and Behavior of Bolted Joints, Marcel Dekker, Inc., 1990.

2.35 American National Standard Institute, Inc. (ANSI), "American National Standard for Radioactive Materials - Leakage Test on Packages for Shipment," ANSI N14.5, 1987

2.36 U. S. Nuclear Regulatory Commission (U.S. NRC), "Recommended Welding Criteria for Use in the Fabrication of Shipping Containers for Radioactive Materials," NUREG/CR-3019, UCRL-53044, May 1978.

2.37 U.S. Nuclear Regulatory Commission (U.S. NRC), "An Assessment of Stress-Strain Data Suitable for Finite-Element Elastic-Plastic Analysis of Shipping Containers," NUREG/CR-0481, SAND77-1872, September 1978.

2.38 U.S. Energy Research and Development Administration, "A Survey of Strain Rate Effects for Some Common Structural Materials Used in Radioactive Material Packaging and Transportation Systems," Battelle Columbus Laboratories, August, 1976.

2.39 Swanson Analysis Systems, Inc., "ANSYS Engineering Analysis System User's Manual for ANSYS, Revision 5.0A," Houston, PA

2.40 Heap, James, "Formulas for Circular Plates Subjected to Symmetrical Loads and Temperatures," Argonne National Laboratory, December 1967.

2.41 U.S. Nuclear Regulatory Commission (U.S. NRC), "Stress Analysis of Closure Bolts for Shipping Casks," NUREG/CR-6007, Lawrence Livermore National Laboratory, April 1992.

2.42 Letter from HELICOFLEX to Transnuclear West dated 11/7/95, including test data of HN 200 seal.

2.43 Transnuclear West Calculation No. NUH005.0350, "Rancho Seco NUHOMS® Mass Properties Calculation." Revision 8

2.44 Miller, C.D., "Research Related to Buckling Design of Nuclear Containment," Nuclear Engineering and Design Proceeding of the Smirt-7 Session, Status of Research in Structures and Mechanical Engineering for Nuclear Power Plants, August 24, 1983.

2.45 Shappert, L.B., et. al., "Cask Designers Guide - A Guide for the Design, Fabrication, and Operation of Shipping Casks for Nuclear Applications," Oak Ridge National Laboratory Report ORNL-NSIC-68, February 1970.

2.46 Bushnell, D., "Elastic-Plastic Buckling of Axially Compressed Ring Stiffened Cylinders - Test vs. Theory," Welding Research Council Bulletin 282, Welding Research Council, New York, November 1982.

2.47 Timoshenko and Gere, Theory of Elastic Stability, Second Edition, McGraw-Hill Book Company, New York, 1961.

2.48 NUREG 0612, "Control of Heavy Loads at Nuclear Power Plants," U.S. NRC.

2.49 ANSI N14.6 - 1986, "American National Standard for Radioactive Materials - Special Lifting Devices for Shipping Containers Weighing 10,000 pounds (4,500 kg) or More," American National Standards Institute, July 1987.

2.50 Harvey, John F., Pressure Component Construction, Design and Materials Application, Van Nostrand Reinhold Company, New York, 1980.

2.51 Manual of Steel Construction, Allowable Stress Design, Ninth Edition, American Institute of Steel Construction, Chicago, 1989. (Part 1 - Dimensions and Properties).

2.52 ASME B1.1, Unified Inch Screw Threads (UN and U NR Thread Form).

2.53 U.S. Nuclear Regulatory Commission (U.S. NRC), "Fabrication Criteria for Shipping Containers," NUREG/CR-3854, Lawrence Livermore National Laboratory Report No. UCRL-53544, March 1985.

2.54 Wichman, K.R., et al, "Local Stresses in Spherical and Cylindrical Shells due to External Loadings," Welding Research Council (WRC) Bulletin 107, August 1965.

2.55 Biggs, John M., Introduction to Structural Dynamics, McGraw-Hill Book Company, New York, 1964.

2.56 Roark, R. J., and Young, W. C., Formulas for Stress and Strain, Fifth Edition, McGraw-Hill Book Company, New York, 1975.

2.57 Timoshenko, S., Strength of Materials, Part II, Advanced Theory and Problems, Third Edition, D. Van Nostrand Company, Inc., Princeton, New Jersey, 1956.

2.58 Blevins, R. D., Formulas for Natural Frequency and Mode Shape, Robert Krieger Publishing Company, Malabar, Florida, 1984.

2.59 NRC Bulletin 96-04, "Chemical, Galvanic or other Reactions in Spent Fuel Storage and Transportation Casks."

2.60 Transnuclear West Report, "An Assessment of Chemical, Galvanic and Other Reactions in NUHOMS® Spent Fuel Storage and Transportation Casks, Part I," Document No. 31-B9604-102, Revision 2.

2.61 NRC Safety Evaluation of Transnuclear West's Response to NRC Bulletin 96-04 for the NUHOMS®-24P and NUHOMS®-7P Dry Spent Fuel Storage Systems, Docket 72-1004, November 1997.

2.62 ASTM Standard B656, "Standard Guide for Autocatalytic (Electroless) Nickel-Phosphorous Deposition on Metals for Engineering Use."

2.63 Mil-C-26074B, "Military Specification Requirements for Electroless Nickel Coatings," 1959 and 1971.

2.64 American Society for Metals, "Metals Handbook," 1985.

2.65 "Corrosion Resistance of High-Phosphorus Electroless Nickel Coatings," Plating and Surface Finishing, July 1986, pp 52-57, R. N. Duncan.

2.66 NWT Report NWT 563, "Determination of Hydrogen Generation Rates from Interaction of Spent Fuel Pool Water with Dry DSC Materials, -Part 3," January 1998.

2.67 M. G. Bale, K. Schafer, "Observations on Hydrogen Generation in Boron Carbide/Aluminum/Water Systems," 1990.

2.10.2 NUHOMS®-MP187 Cask Finite Element Analysis

2.10.2.1 Finite Element Model Descriptions

The NUHOMS®-MP187 cask is evaluated for the Normal Conditions of Transport (NCT) and the Hypothetical Accident Conditions (HAC) defined in 10CFR71 [2.1] using the finite element models described in the following sections. Five separate models are used for the cask evaluation; a half symmetry cask shell/trunnion model, an axisymmetric cask model used for mechanical loads, an axisymmetric cask model used for thermal loads, a half symmetry cask bottom end detail model, and a half symmetry cask top end detail model.

The finite element models are generated using the ANSYS version 4.4A and 5.0a program. The finite element meshes are created using finite element practices; maintaining reasonable aspect ratios and mesh densities. The number of 3-node quadrilateral shell (constant strain) elements are minimized to avoid increasing the stiffness of the structure, minimizing inaccuracies in the model solutions.

2.10.2.1.1 Cask Shell/Trunnion Half Symmetry Model

2.10.2.1.1.1 Model Description

The cask shell/trunnion half symmetry model shown in Figure 2.10.2-1 is used for the cask lifting analysis. The finite element model is used to determine the maximum stresses in the cask outer shell due to the controlling lifting condition (i.e. vertical lift from fuel pool.) The model conservatively ignores any support provided by the neutron shield and lead shielding materials.

The cask outer shell and trunnion sleeves are modeled using quadrilateral shell elements, having three rotational degrees of freedom and three translational degree of freedom at each node. The shell element thicknesses are input using real constants. Rigid beam elements are used to transfer the loads from the points of application to the upper and lower trunnion sleeves. The trunnion sleeves are modeled only to transfer the load to the cask shell. The use of shell elements for the trunnion sleeves is not appropriate for stress calculations since the trunnion sleeve R/t (3.50) is much less than the minimum value of 10 to 15 recommended for thin shell theory. Therefore, the trunnion stresses are determined using hand calculations.

The cask outer shell and trunnion sleeves are modeled using mild stainless steel and high strength stainless steel material properties at 70°F.

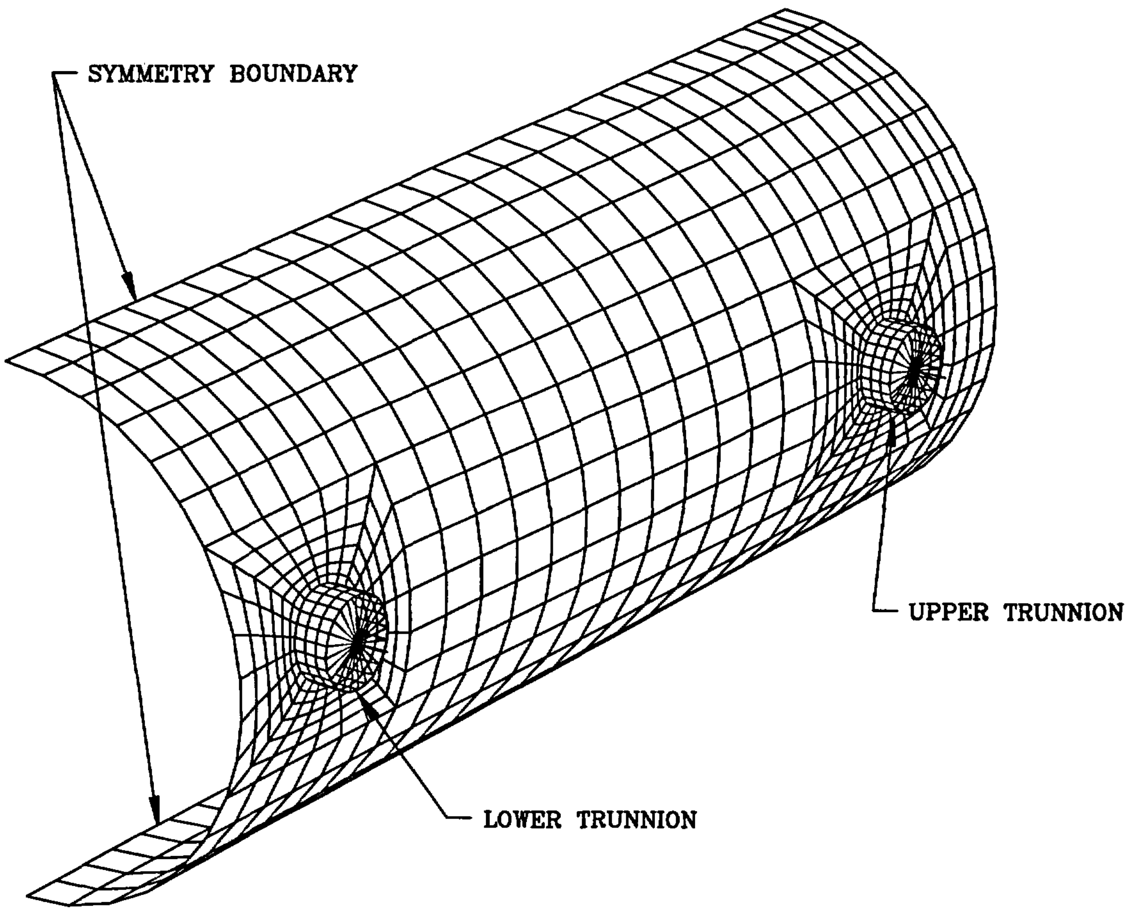

Figure 2.10.2-1
Cask Vertical Lift Half Symmetry Analytical Model

2.10.2.1.1.2 Boundary Conditions

The nodes at the top end of the cask outer shell are restrained from translating in the radial, circumferential and meridional directions and from rotating about the circumferential axis. Similarly, the nodes at the bottom end of the cask shell are restrained from translating in the radial and circumferential direction and from rotating about the circumferential axis. The boundary conditions applied to the cask shell ends represent the restraint provided by the welds between the cask shell and the top flange and bottom end closure.

2.10.2.1.1.3 Loading

The loaded MP187 cask is lifted vertically by the upper trunnions using the fuel building crane when removed from the fuel pool. For the vertical lift from the fuel pool the cask and DSC are filled with water and the cask top cover plate and DSC top plates are not in place. The temperature of the cask will remain below 100°F since the spent fuel pool water temperature is maintained near room temperature. The maximum dead load for the vertical lift from the fuel pool is 244,400 pounds (Section 2.2, Cask/FC-DSC w/ fuel, water & w/o cover plates). The MP187 cask is analyzed for the vertical lift from the fuel pool conservatively assuming a dead weight of 250,000 pounds distributed evenly to the two upper trunnions. The dead load on each of the upper trunnions is 125 kips. This load is applied to the node on the trunnion rigid link element corresponding to the furthest possible outboard centerline location of the lifting hook in order to maximize the lifting load moment arm.

2.10.2.1.2 Cask Axisymmetric Model

2.10.2.1.2.1 Model Description

The axisymmetric cask finite element model shown in Figure 2.10.2-2 through Figure 2.10.2-7 is used to analyze the cask stresses due to the thermal and mechanical loads which are axisymmetric in nature. These include the following normal and hypothetical accident conditions:

a) Internal Design Pressure (50 psig)
b) Internal Design Pressure (50 psig) + Bolt Preload
c) Thermal Case #1 (100°F Ambient, Maximum Fuel Decay Heat)
d) Thermal Case #2 (-20°F Ambient, Maximum Fuel Decay Heat)
e) Thermal Case #3 (-20°F Ambient, No Fuel Decay Heat)
f) Thermal Case #4 (-40°F Ambient, Maximum Fuel Decay Heat)

g) Thermal Fire Transient (1,475°F Fire of 30 Minute Duration)

h) 30-foot Top End Drop, Max. Impact Load (100°F Ambient, Max. Fuel Decay Heat)

i) 30-foot Top End Drop, Max. Impact Load (-20°F Ambient, No Fuel Decay Heat)

j) 30-foot Bottom End Drop, Max. Impact Load (100°F Amb., Max. Fuel Decay Heat)

k) 30-foot Bottom End Drop, Max. Impact Load (-20°F Ambient, No Fuel Decay Heat)

l) Top and Bottom Center Puncture

m) 200m Immersion

The model includes 2-D isoparametric solid elements (PLANE42), 2-D spar elements (LINK1), 2-D beam elements (BEAM3), and 2-D gap elements (CONTAC12). The 2-D isoparametric solid elements are used to model the cask inner shell, outer shell, top closure plate, top flange, bottom end closure forging, ram closure plate, lead shielding, neutron shielding, neutron shield rings, and neutron shield jacket. The neutron shield support angles are considered non-structural components. As such they are not modeled but their weight is accounted for by adjusting the weight density of the neutron shielding material as follows:

$$\rho' = [\rho_{NS}(A_{NS}) + \rho_{SS}(A_{SA}) + \rho_{AL}(A_{AL})]/(A_{NS} + A_{SA} + A_{AL})$$

where;

ρ_{NS} = 0.0637 lb/in^3, Solid neutron shielding material density

ρ_{SS} = 0.2853 lb/in^3, Stainless steel material density

ρ_{AL} = 0.098 lb/in^3, Aluminum material density

A_{SA} = Area of neutron shield support angles

= 24 x (14" x 0.12")

= 40.3 in^2

A_{AL} = Area of aluminum angles

= (14" x 0.125")

= 42.0 in^2

A_{NS}	=	Area of solid neutron shielding material
	=	$\pi(46.06^2 - 41.75^2) - 40.3 - 42.0$
	=	1.106.7 in^2

Therefore, the adjusted weight density of the neutron shield is:

ρ'	=	[0.0637(1,106.7) + 0.2853(40.3) + 0.098(42.0)]/(1,189.0)
	=	0.0724 lb/in^3

A bounding weight density of 0.0808 lb/in^3 is conservatively used in the axisymmetric finite element model.

Each 2-D isoparametric element consists of four nodes, each node having two degrees of freedom (UX and UY). The 2-D spar elements are used to model the top and bottom end closure bolts. The beam elements are consist of 2 nodes, each having two translational and one rotational degree of freedom (UX, UY, and ROTZ). The geometric properties defining the 2-D beam elements are the area, moment of inertia, height (diameter), and initial strain. When the beam elements are used to model the bolts, the bolt area is input on a 360° basis, modeling the bolts as a ring with the equivalent total area.. The areas of the top and bottom closure bolts are:

Top closure bolts:

Number of bolts	=	36
Bolt diameter	=	2.0 in.
Bolt Stress area	=	2.77 $in.^2$
Total bolt area	=	99.7 $in.^2$

Bottom closure bolts:

Number of bolts	=	12
Bolt Diameter	=	1.0 in
Bolt Stress Area	=	0.6051 in^2
Total Bolt Area	=	7.261 in^2

The 2-D gap elements are used at the regions of the seals at the ram closure plate/bottom end closure forging interface and the top closure plate/top flange interface to predict the seal behavior during the postulated puncture loading. For the design pressure and bolt preload case, and for the thermal load cases, gap elements are used to model the interface between the lead gamma shield and the cask shells. The gap elements have no stiffness when separated and a large stiffness normal to the contact surface when closed. Gap elements allow the contact surfaces to slide relative to one another and are capable of modeling static and sliding friction effects. For the purpose of this analysis, friction between the lead and steel shells is conservatively ignored. The geometric properties defining the gap elements are the gap orientation angle (THETA), the gap stiffness (KN), the initial gap size (INTF) and the initial element status (START). The orientation of the gap elements is defined such that THETA=0 for gaps between surfaces normal to the cask axial direction. The gap element compressive stiffness is modeled as an order or two greater in magnitude than the adjacent surfaces, as recommended in the ANSYS user's manual [2.6]. All gap elements are modeled as initially closed and not sliding (INTF=0.0 and START=1.0).

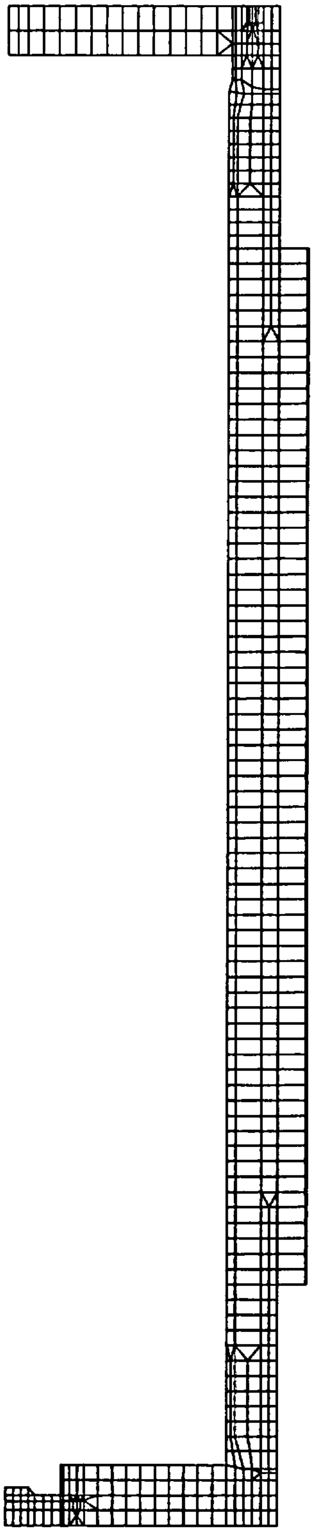

Figure 2.10.2-2

Axisymmetric Cask Model

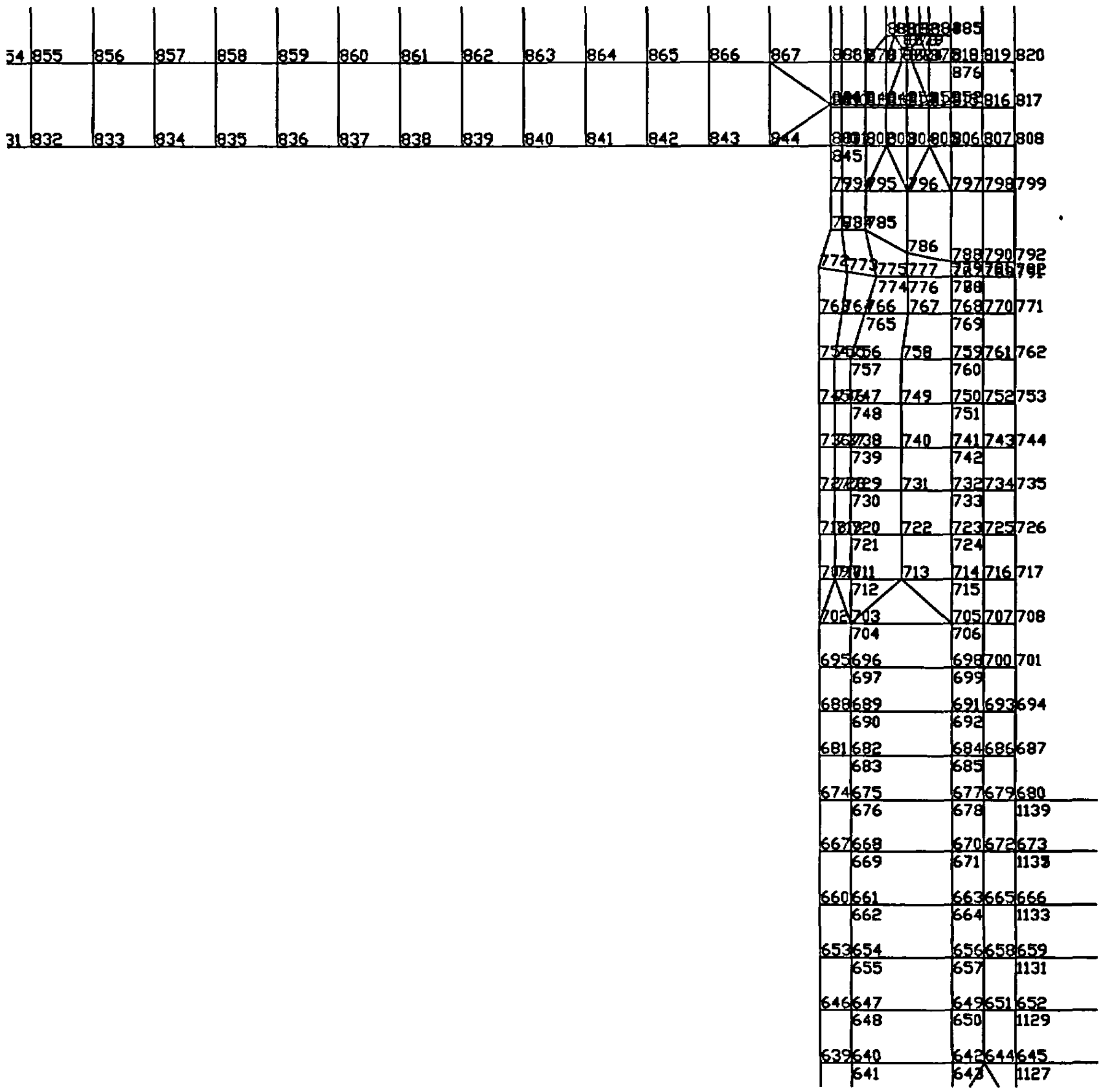

Figure 2.10.2-3

Cask Axisymmetric Model Top End Node Numbers

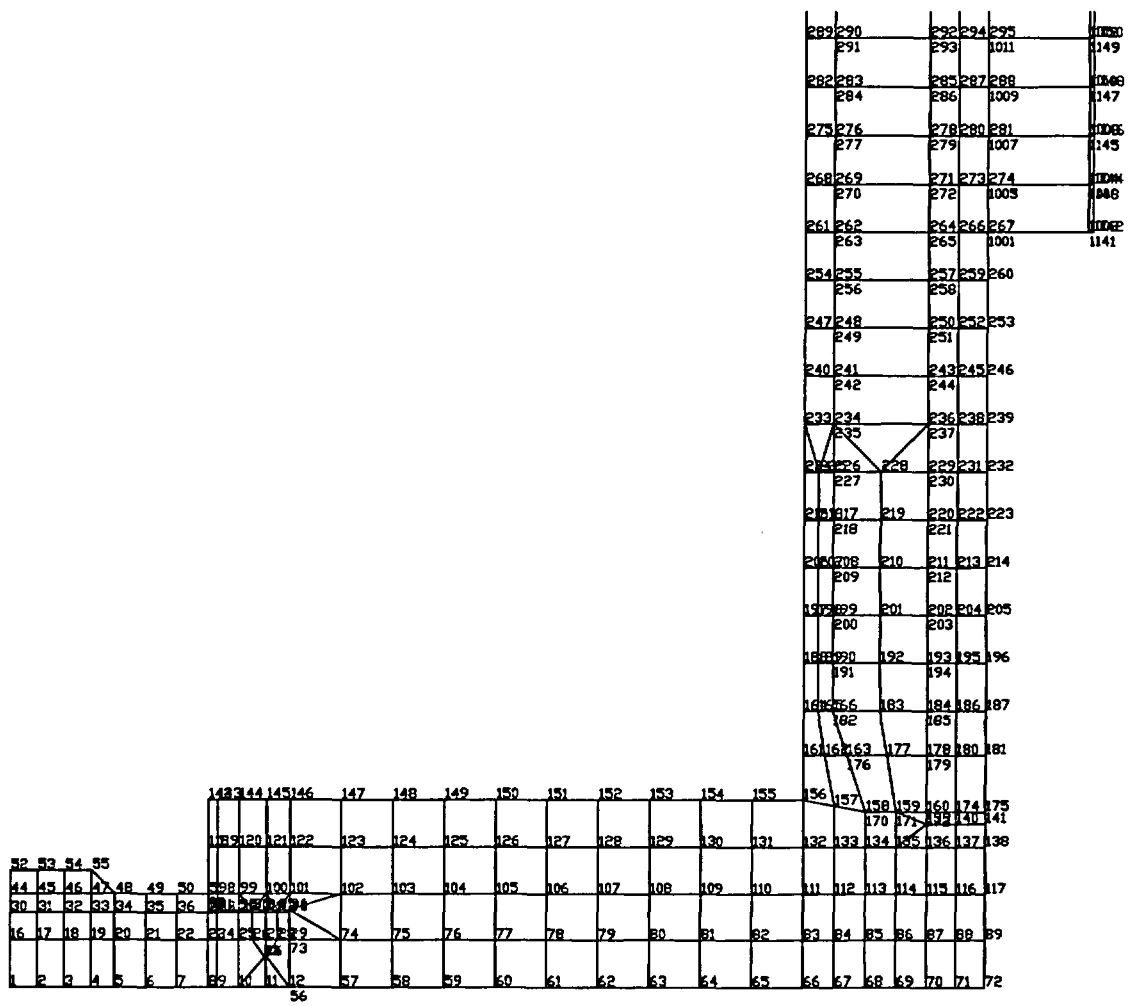

Figure 2.10.2-4

Cask Axisymmetric Model Bottom End Node Numbers

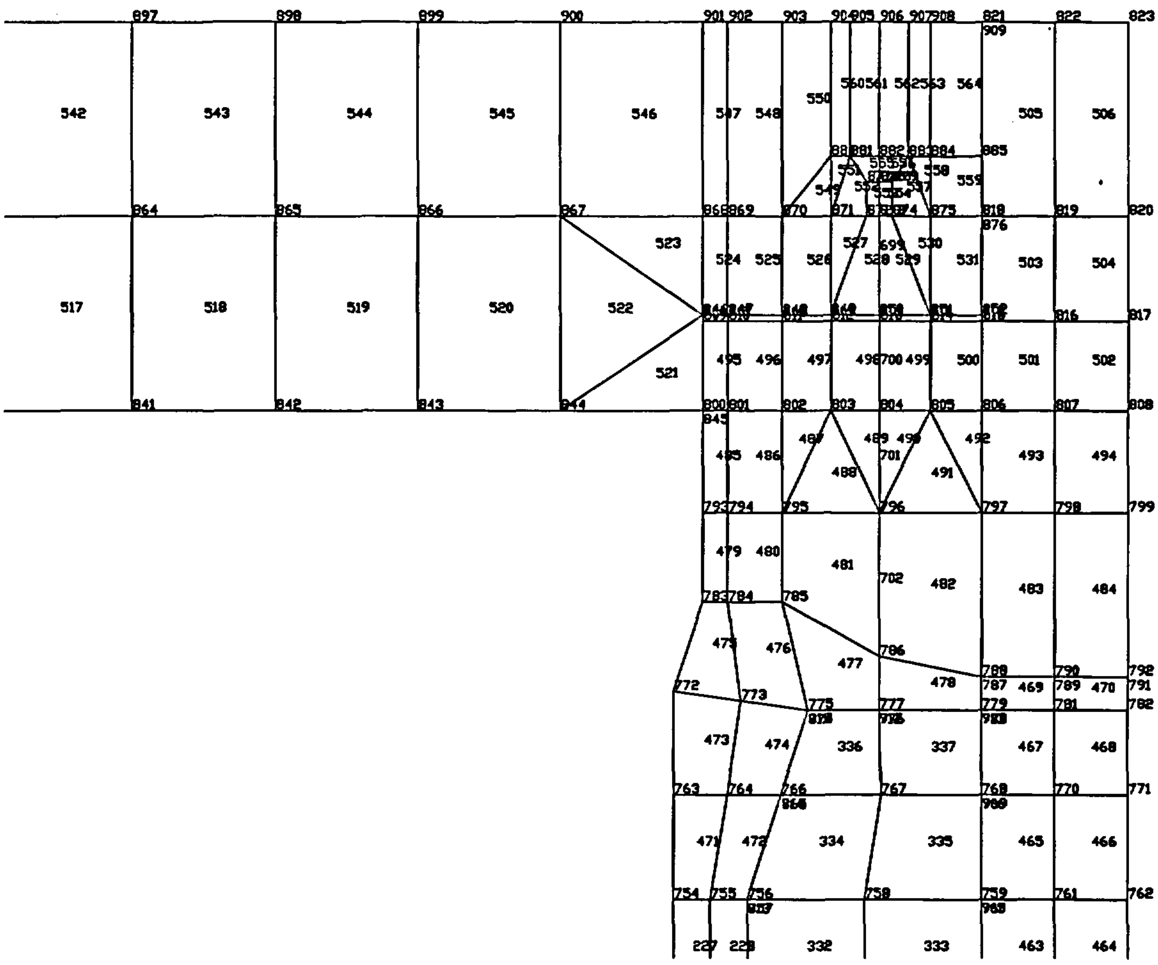

Figure 2.10.2-5

Cask Axisymmetric Model Top Corner Node and Element Numbers

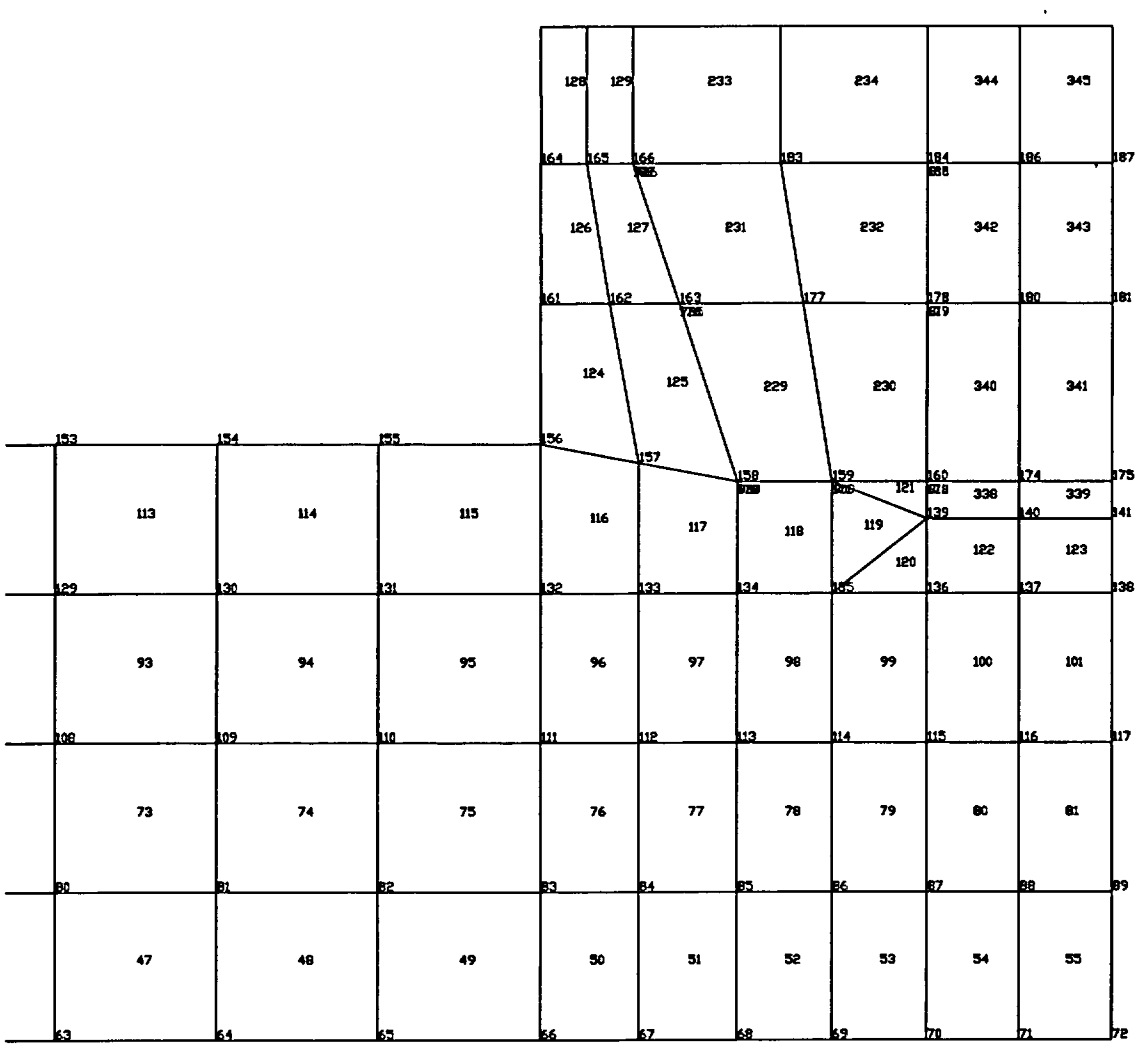

Figure 2.10.2-6

Cask Axisymmetric Model Bottom Corner Node and Element Numbers

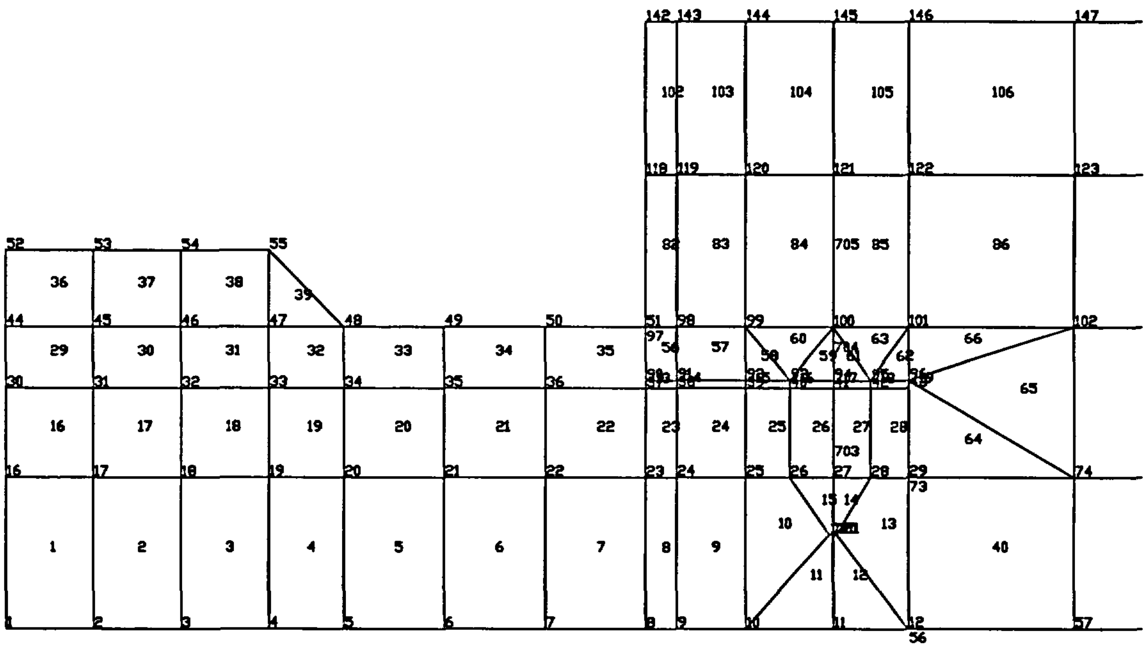

Figure 2.10.2-7

Cask Axisymmetric Model Bottom Center Node and Element Numbers

2.10.2.1.2.2 Boundary and Initial Conditions

For the model used for pressure and puncture analyses, no shear transfer is assumed between the shielding materials and the steel casing. These boundary conditions are modeled by coupling coincident nodes of the shielding material elements and the steel casing elements normal to the contact surfaces, while allowing the nodes to move relative to one another tangential to the contact surfaces. The nodes at the top of the cask are restrained in the axial (UY) direction. These nodes are sufficiently far removed from the region of interest, and have no impact on the results.

Initial strain is used to model the bolt preload.

For the bottom end drop loading condition, all nodes along the bottom edge of the model were restrained in the vertical (Y) direction. For top end loading, all nodes along the top edge of the model were restrained vertically. For this axisymmetric model, no other boundary conditions were required.

2.10.2.1.2.3 Loading

2.10.2.1.2.3.1 Internal Pressure Load

The cask internal pressure under normal conditions is 22.2 psia, as shown in Chapter 3.6. The maximum cask internal accident pressure resulting from the post fire steady state condition is 48.0 psia. A design internal pressure of 50 psig, which bounds all normal and accident condition internal pressures, is conservatively assumed for the cask normal conditions.

2.10.2.1.2.3.2 External Pressure Load

Section 71.71(c)(3) of the Part 71 regulations [2.1] include a reduced external pressure of 3.5 psia. The internal pressure of the NUHOMS®-MP187 cask is assumed to be one atmosphere (14.7 psia). Therefore, the reduced external pressure condition will result in a net internal pressure of 11.2 psig on the cask inner surface. In addition, the cask is analyzed for the external pressure load resulting from the 200 meter immersion accident condition. The external pressure due to a head of 200 meters is 284.3 psia. The cask internal pressure for these conditions is conservatively assumed to be zero. Therefore, a gauge pressure of 284.3 psig is used for the 200 meter immersion analysis.

A 1 psig unit external pressure load is applied as a uniform pressure to all element surfaces on the outer surface of the cask containment boundary (i.e. top closure plate, top flange, inner shell, bottom end closure, and ram closure plate). The cask stresses resulting from the 1psig external pressure are factored by the appropriate external gage pressures to obtain the stresses for the each normal and accident condition.

2.10.2.1.2.3.3 Puncture Loads

The maximum possible puncture load that the cask can experience is that at which the puncture bar experiences dynamic flow or plastic collapse. The dynamic flow stress of the mild steel (ASTM A-36 carbon steel) puncture bar is conservatively assumed to be 50,000 psi. A pressure load, equal to the 50,000 psi dynamic flow stress of the puncture bar, is applied to the center of the ram closure plate over a 3.0 inch radius circle. The definition of the applied puncture loads is described in Section 2.7.2.

2.10.2.1.3 Cask Three-Dimensional Half Symmetry Model

Many of the loads experienced by the cask during normal and accident transportation conditions are not axisymmetric. These load conditions include dead weight and vibration loads during horizontal transport as well as horizontal side and oblique impact loads due to normal and accident drop conditions. The cask contents load and impact limiter reaction loads due to these load conditions act normal to the surface of the shells (i.e. radially) and are assumed to be symmetric about a vertical plane passing through the cask centerline. For these load conditions, a half symmetry three-dimensional finite element model is used to accurately represent the cask loading and response.

The NUHOMS®-MP187 cask is evaluated for the non-axisymmetric loads using the half symmetry three-dimensional finite element model shown in Figure 2.10.2-9. The model consists of 10,850 nodes and 5,876 elements representing the ram closure plate, bottom forging, cask inner shell, outer shell, top flange, top closure plate, and lead gamma shield. Solid brick elements, defined by eight nodes, each having three translational degrees of freedom, are used to model all of the cask components. The neutron shield is not included in the three-dimensional model, conservatively ignoring its structural capacity. However, the weight of the neutron shield in accounted for by adjusting the density of the outer shell in the region of the neutron shield accordingly. The node numbering pattern at the 0° azimuth are shown in Figure 2.10.2-10 and Figure 2.10.2-11. The node numbers are incremented by 1000 for each circumferential increment.

The finite element model mesh density is fine near the top and bottom ends of the cask shells where stresses are expected to be highest due to the structural discontinuities of the ends. A coarse mesh is used in the mid-region of the cask shells away from the structural discontinuities of the ends and in the top and bottom closures. The circumferential distribution of the elements over the half symmetry model includes 13 elements. The first three circumferential elements each span an arc of 10 degrees and the remaining ten circumferential elements each span an arc of 15 degrees. The element arc length is sufficiently small to represent the curved surface of the cask shells. The smaller arc span is used in the region of the peak impact loads where the stresses are expected to be highest. The finite element model mesh chosen provides accurate predictions of the cask response (i.e. displacements and stresses) while maintaining a reasonable model size.

The behavior of the cask top and bottom closures is best modeled using interface (gap) elements. The gap elements are non-linear and require an iterative solution which greatly increases the computer processing time required. The cask closures are designed to remain leak-tight during and after all normal and accident conditions. In order to achieve this, the closure plates are fastened to the cask using a large number of bolts with high bolt preloads. The clamping force from the bolts maintains contact over the sealing surface. Therefore, the interface between the closure plates and sealing surfaces are modeled using coupled nodal degrees of freedom between coincident nodes at the interface of the different components. A more detailed analysis of the closure and bolts is performed using a finite element model which includes gap elements to represent the closure behavior, as discussed in Appendix 2.10.5.

In the event of a drop accident, the lead gamma shield is primarily supported by the cask inner and outer shells since it has little strength itself. In addition to the longitudinal and tangential loading from the lead in the plane of impact, lateral pressures will develop between the lead and cask shells due to lead slump. The effect of the lateral pressure loading on the cask shells due to the lead slump is considered in the analysis by coupling the nodal displacements between the lead and cask shells in the radial direction such that radial forces are transferred across the interfaces. The lateral pressure loads from the lead produce friction forces between the lead and cask . Neglecting these frictional forces increases the critical hoop stresses in the shells by forcing the shells to support the "hydrostatic" pressure imposed by the lead. The lead column is supported in the longitudinal direction at the end of the impact. This allows a gap to form between the lead column and the steel at the end opposite the impact. The stresses in the lead column are maximized at the impact end, thus producing maximum lateral forces on the cask inner and outer shells.

The cask components included in the half symmetric three-dimensional cask finite element model are manufactured from SA-240, Type 304 and Type XM-19 stainless steel plate, SA-182, Type 304 stainless steel forging material, and lead. The material density and Poisson' ratio for steel and lead are assumed constant. The density and Poisson' ratio for stainless steel are 0.2853 pounds per cubic inch and 0.29, respectively. The density and Poisson' ratio for lead are 0.408 pounds per cubic inch and 0.4, respectively. The linear elastic temperature dependent material properties of stainless steel given in Section 2.3.1 are used in the model. The properties of lead vary greatly with temperature and strain rate effects. At elevated temperatures, lead experiences a significant reduction in strength. As shown in the thermal analysis, the temperature of the lead gamma shield resulting from the heat condition (i.e. 100°F ambient with maximum fuel decay heat load) ranges from 182°F to 283°F, with an approximate volume average temperature of 230°F. The lead shielding material is modeled using the elastic plastic material properties at 230°F given in Table 2.3.4-3. The elastic plastic material properties of the lead are modeled assuming multi-linear kinematic hardening behavior which represents the stress strain relationship as piecewise linear.

As discussed previously, the neutron shield is not included in the half-symmetry three dimensional cask finite element model but its weight is accounted for by adjusting the weight density of the cask outer shell in the neutron shield region. The equivalent density used for the cask outer shell is calculated as follows:

$$\rho' = (W_{NS} + W_{SS})/V_{SS}$$

where;

V_{SS} = Volume of cask outer shell in neutron shield region

= $\pi(41.75^2 - 39.25^2)(137.50)$

= 87,500 in^3

W_{NS} = 15,400 lb., Weight of the neutron shield

W_{SS} = Weight of cask outer shell in neutron shield region

= (87,500)(0.2853)

= 25,000 pounds

Therefore, the adjusted density of the cask outer shell in the region of the neutron shield is:

$$\rho' = (15{,}400 + 25{,}000)/87{,}500$$

$$= 0.462 \text{ lb/in}^3$$

An adjusted density of 0.4588 pounds per cubic inch is used in the model. This equates to a difference in the total cask weight of approximately 200 pounds, or 0.1% of the total cask weight, which is insignificant.

2.10.2.1.3.1 Impact Loading

In the event of an oblique drop, corner drop, or side drop condition, the cask body is loaded by the DSC and the impact limiters in addition to its own self weight. The inertial loads due to the cask self weight are accounted for by applying the appropriate acceleration loads to the model. The loads from the DSC and impact limiters act on the internal and external surfaces of the cask, respectively. These loads are applied as element pressures to the finite element model.

For oblique and corner drop conditions, the DSC is supported by the cask end plate located at the impact end. The load from the DSC is modeled as a uniform pressure load on the inner surface of the supporting cask end plate. For top end impacts, the DSC longitudinal pressure load is applied to the inner surface of the top cover plate. For bottom end impacts, the DSC longitudinal pressure load is applied to the inner surface of the bottom end forging. The DSC longitudinal pressure load determined as follows:

$$q_{L,DSC} = W_{DSC}G_L/A_C$$

where;

W_{DSC} = Weight of the DSC

G_L = Equivalent static g-load acting in longitudinal direction

A_C = Contact area

= $\pi(34.50)^2$

= 3,739 in^2 (Top Closure Plate)

= $\pi[(34.00)^2 - (8.50)^2]$

= 3,405 in^2 (Bottom End Forging excluding Ram Closure Plate)

The longitudinal load due to the impact limiters is applied as a uniform pressure load to the external surface of the cask ends. At the end opposite the impact, the pressure load is calculated as follows:

$$q_{L,IL} = W_{IL}G_L/A_{end}$$

where;

W_{IL} = 15,800 lb., Weight of a single impact limiter

G_L = Equivalent static longitudinal g-load

A_{end} = Area of cask end

$= \pi(41.75)^2$

$= 5{,}476 \text{ in}^2$

At the end of the impact, the pressure load is calculated as follows:

$$q_{L,IL} = R_L/A_{end}$$

where R_L is the longitudinal reaction load resulting from drop condition and A_{end} is the area of the cask end shown above. In some cases, the pressure distribution on the impact end in the longitudinal direction is varied in order to provide moment equilibrium. These conditions are discussed in the respective sections of the cask drop analysis.

The impact load acting in the transverse direction is applied as a pressure load over the contact area between the impact limiter and the outer surface of the cask. The pressure distribution is assumed to be uniform in the longitudinal direction over the 32 inch long impact limiter overhang and vary with a cosine distribution around the circumference of the cask. For the impact conditions, the angle of contact is dependent upon the amount of crush occurring in the impact limiter. The most severe loads result from impacts on the flatside of the impact limiter. For these load conditions, the contact angle between the impact limiter and cask outer surface will be approximately 180 degrees. A contact angle of 150 degrees (75 degree half angle of contact) is conservatively used for the cask impact analysis. The circumferential cosine pressure distribution over a half angle, θ, is calculated as follows:

$$P_i = P_{max} \cos(\pi\theta_i/2\theta)$$

where;

P_i	=	Pressure load at angle θ_i
P_{max}	=	Peak pressure load, at point of impact
θ_i	=	Angle corresponding to point of interest

The circumferential pressure distribution is illustrated in Figure 2.10.2-8.

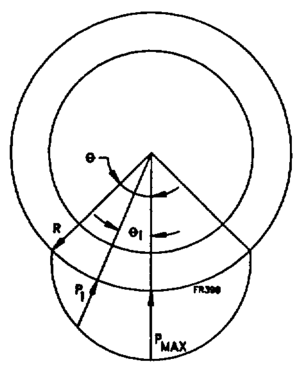

Figure 2.10.2-8

Circumferential Pressure Load Distribution

The peak pressure load, P_{max}, is determined by setting the integral of the vertical pressure components, Q_i, equal to the total transverse impact load, F_t, as follows:

$$F_t = \int_{-\theta}^{\theta} Q_i LR d\theta_i = \int_{-\theta}^{\theta} P_i \cos(\theta_i) LR d\theta_i = \int_{-\theta}^{\theta} P_{max} \cos\left(\frac{\pi\theta_i}{2\theta}\right) \cos(\theta_i) LR d\theta_i$$

$$= \frac{P_{max} LR}{2} \int_{-\theta}^{\theta} [\cos\left(\frac{\pi\theta_i}{2\theta} + \theta_i\right) + \cos\left(\frac{\pi\theta_i}{2\theta} - \theta_i\right)] d\theta_i$$

$$= P_{max}\, LR \left[\frac{\sin\left(\frac{\pi}{2} + \theta\right)}{\left(\frac{\pi}{2\theta}\right) + 1} + \frac{\sin\left(\frac{\pi}{2} - \theta\right)}{\left(\frac{\pi}{2\theta}\right) - 1} \right]$$

Rearranging terms gives the peak pressure, P_{max}, as follows:

$$P_{max} = \frac{F_t}{LR}\left[\frac{\sin\left(\frac{\pi}{2}+\theta\right)}{\left(\frac{\pi}{2\theta}\right)+1}+\frac{\sin\left(\frac{\pi}{2}-\theta\right)}{\left(\frac{\pi}{2\theta}\right)-1}\right]^{-1}$$

Therefore, the pressure at any circumferential location is given by:

$$P_i = \frac{F_t}{LR}\left[\frac{\sin\left(\frac{\pi}{2}+\theta\right)}{\left(\frac{\pi}{2\theta}\right)+1}+\frac{\sin\left(\frac{\pi}{2}-\theta\right)}{\left(\frac{\pi}{2\theta}\right)-1}\right]^{-1}\cos\left(\frac{\pi\theta_i}{2\theta}\right)$$

Element pressure loads applied to an ANSYS model can only be varied linearly over the surface of an element. Therefore, the cosine distribution is approximated as a piecewise linear distribution in the finite element analysis. As discussed previously, the element sizes are varied around the circumference of the cask model. The first three elements each span an arc of 10 degrees and all other elements span arcs of 15 degrees. For the assumed 75 degree half angle of contact and a unit impact load, F_t, the resulting circumferential pressure distribution is as follows:

Circumferential Location	Pressure Load
0°	0.708 x F_t/RL
10°	0.693 x F_t/RL
20°	0.647 x F_t/RL
30°	0.573 x F_t/RL
45°	0.416 x F_t/RL
60°	0.219 x F_t/RL
75°	0.000 x F_t/RL

The pressure load on the inner surface of the cask due to the DSC is calculated assuming a 150 degree contact angle for all accident drop conditions, equal to the contact angle assumed for the tangential impact loads. For drop orientations such as the side drop and corner drop, the distribution of the pressure load is assumed to be uniform over the length of the DSC.

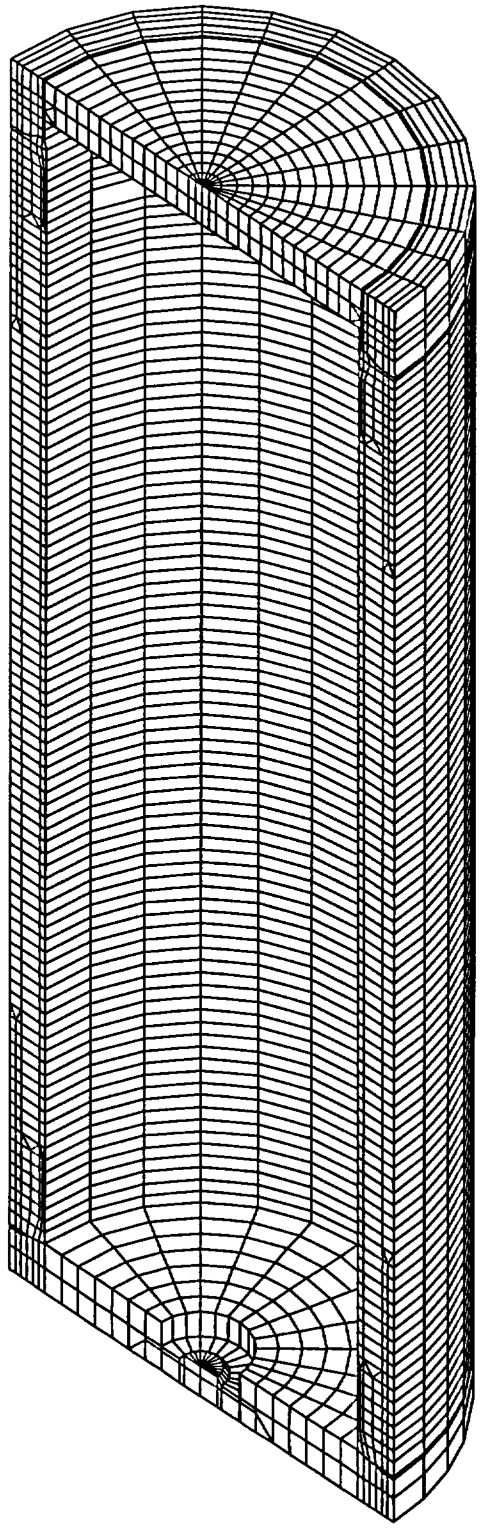

Figure 2.10.2-9

Half Symmetry Three-Dimensional Cask Finite Element Model

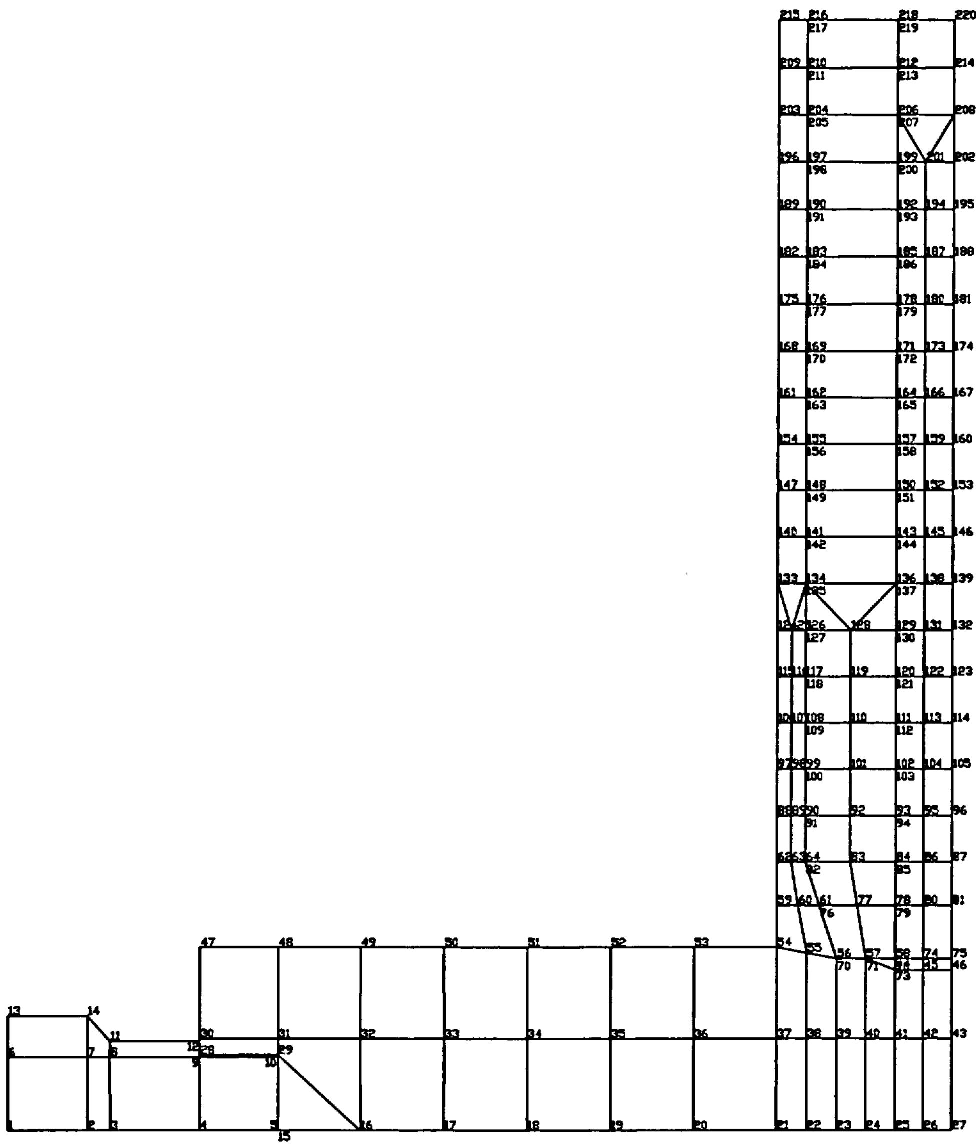

Figure 2.10.2-10

Bottom End Node Numbers at 0° Azimuth - Three-Dimensional Cask Model

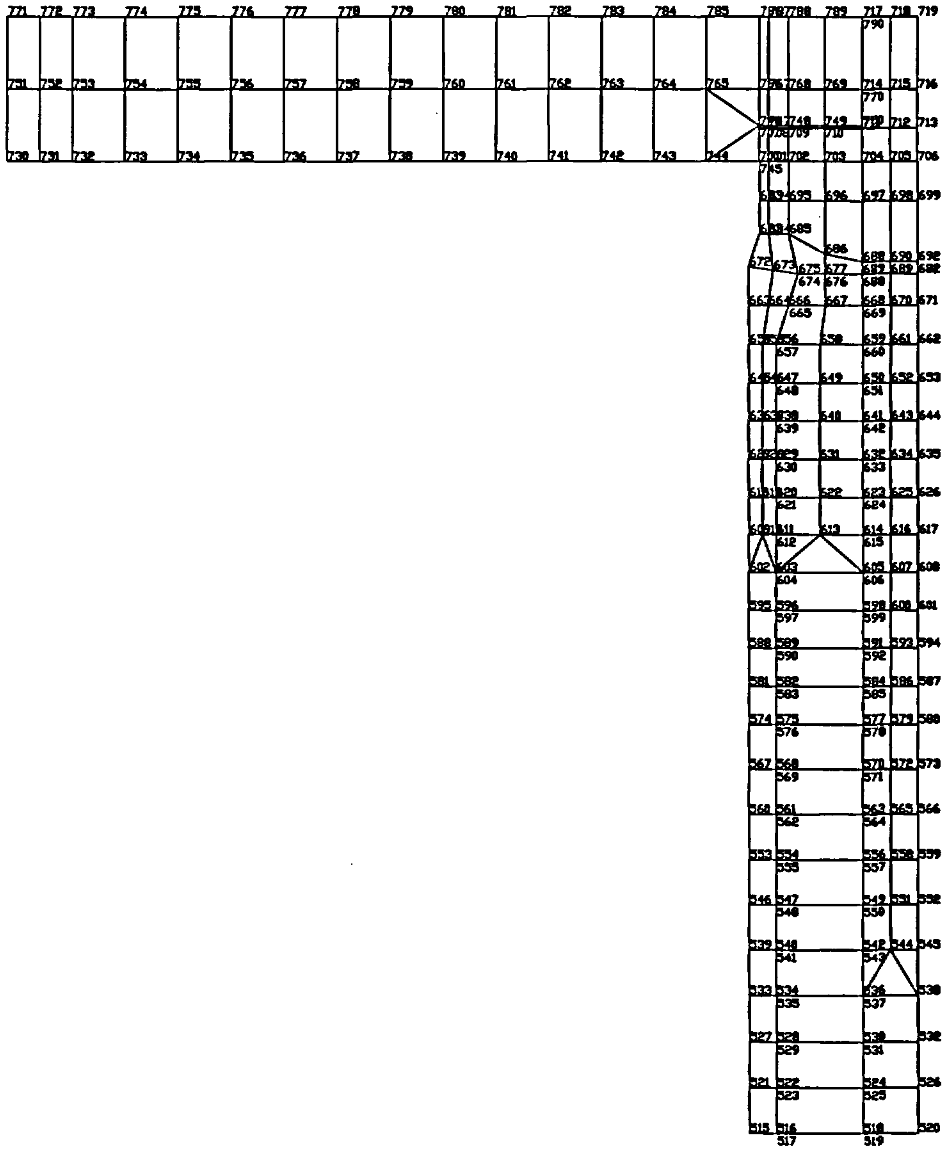

Figure 2.10.2-11

Top End Node Numbers at 0° Azimuth - Three-Dimensional Cask Model

2.10.2.1.4 Cask Half Symmetry Bottom End Detail Model

The cask half symmetry bottom end detail model is used only to analyze the cask for an off-center bottom end puncture. A detailed description of the model construction, boundary conditions, and loading follows.

2.10.2.1.4.1 Model Description

The bottom end off-center puncture is performed using the half symmetry finite element model shown in Figure 2.10.2-12. The analytical model consists of 3-D isoparametric brick elements representing the ram closure plate, bottom end closure forging, inner shell and outer shell. The lead shielding in the annulus between the inner and outer shells is assumed to have no structural significance, and consequently is not included in the analytical model. The 3-D isoparametric brick elements consist of eight nodes, each having three translational degrees of freedom. The cask inner and outer shells are included in the model to accurately model the rotational stiffness they provide to the bottom end closure forging. The shells are modeled with sufficient length to permit displacements independent of the boundary conditions.

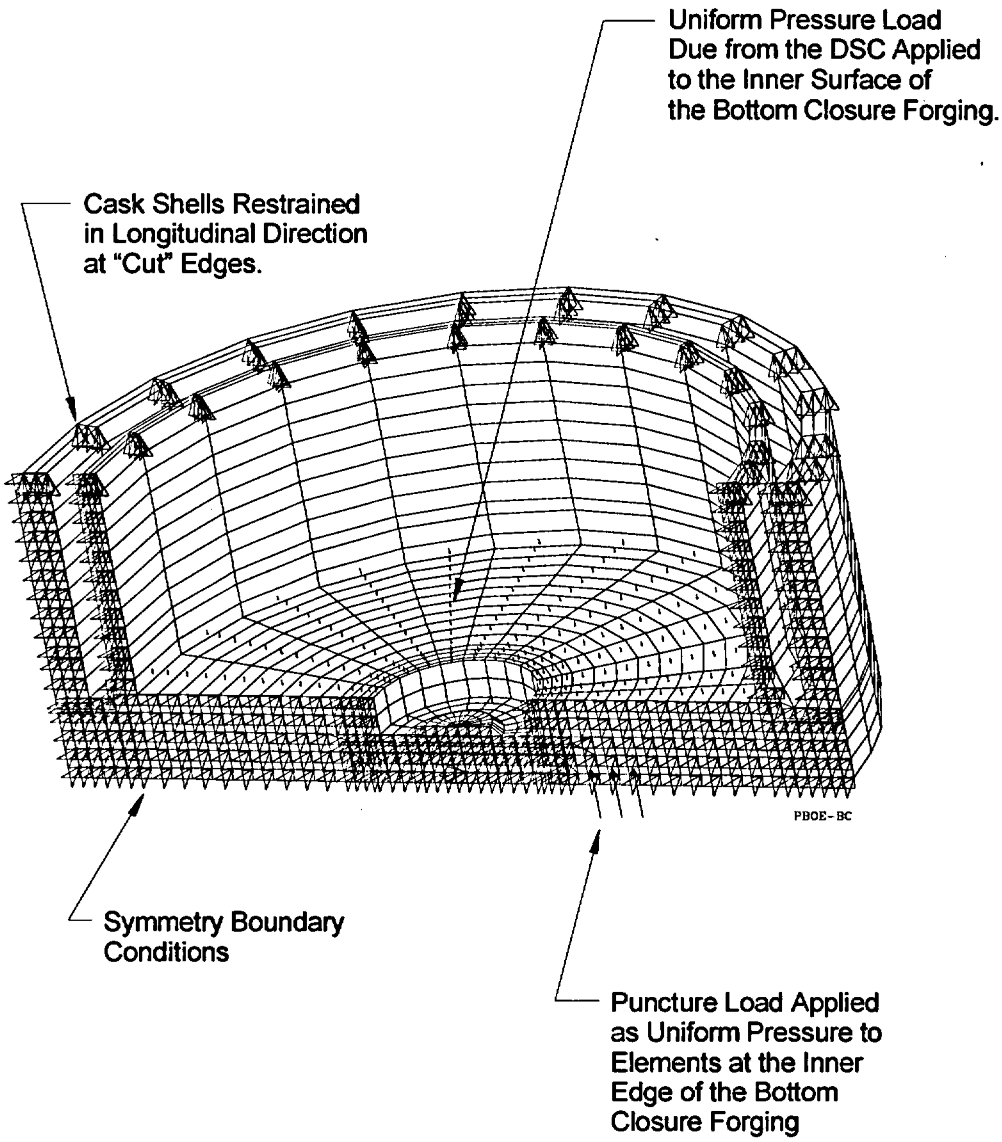

Figure 2.10.2-12
Bottom End Off-Center Puncture Analytical Model

The interface between the ram closure plate and the cask bottom end closure forging is modeled using 3-D gap elements. The 3-D gap elements operate bilinearly, having a small stiffness (1.0 x 10^{-6} lb/in.) for a separated interface (to provide stability) and a constant stiffness (1.0 x 10^{10} lb/in.) for a closed interface. The initial status of all gaps is modeled as closed and not sliding (STAT=1.0).

Three dimensional spar elements are used to model the twelve 1-8UNC-2A x 3.5 inch long bottom end closure bolts. The 3-D spar elements are uniaxial tension-compression elements consisting of 2 nodes, each having three translational degrees of freedom (UX, UY and UZ). The geometric properties defining the 3-D spar elements are the area and initial strain. The stress area of each 1 inch diameter bolt is 0.6051 square inches. The initial strain used to model the bolt preload is equal to 50% of yield in the bolts, or 0.176%, as calculated in Section 2.7.2.1.

The analytical model node numbers at the Y=0 plane (0 circumference) are shown in Figure 2.10.2-13. The nodes are generated at 7.5° increments over the first 15° circumference and at 15° increments over the remaining 165° circumference for a total angle of 90° using the node pattern shown in Figure 2.10.2-13, applying a node number increment of 300. The element numbers for the elements adjacent to the 0° azimuth are shown in Figure 2.10.2-14.

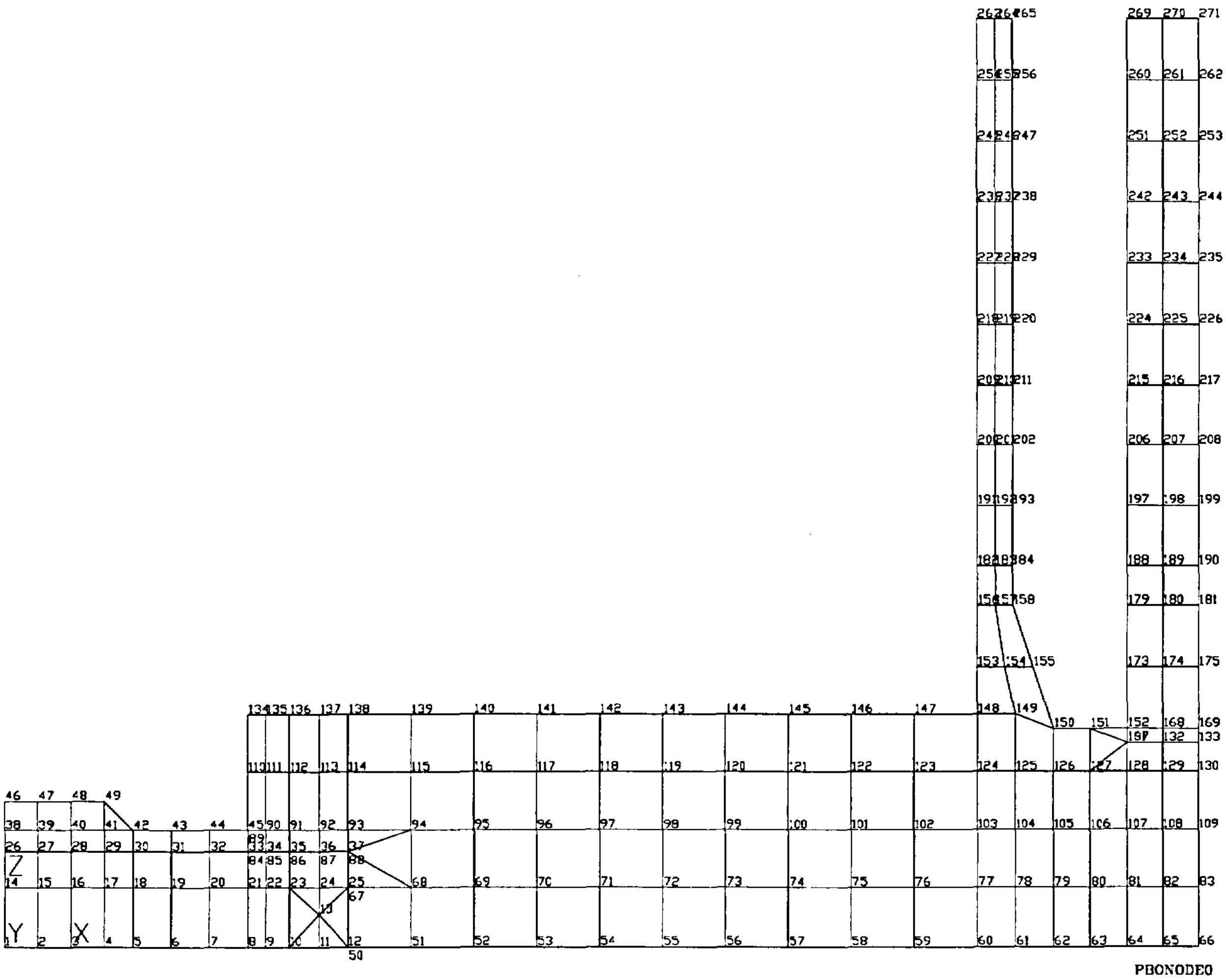

Figure 2.10.2-13

Bottom Off-Center Puncture Model Node Numbers at Y=0

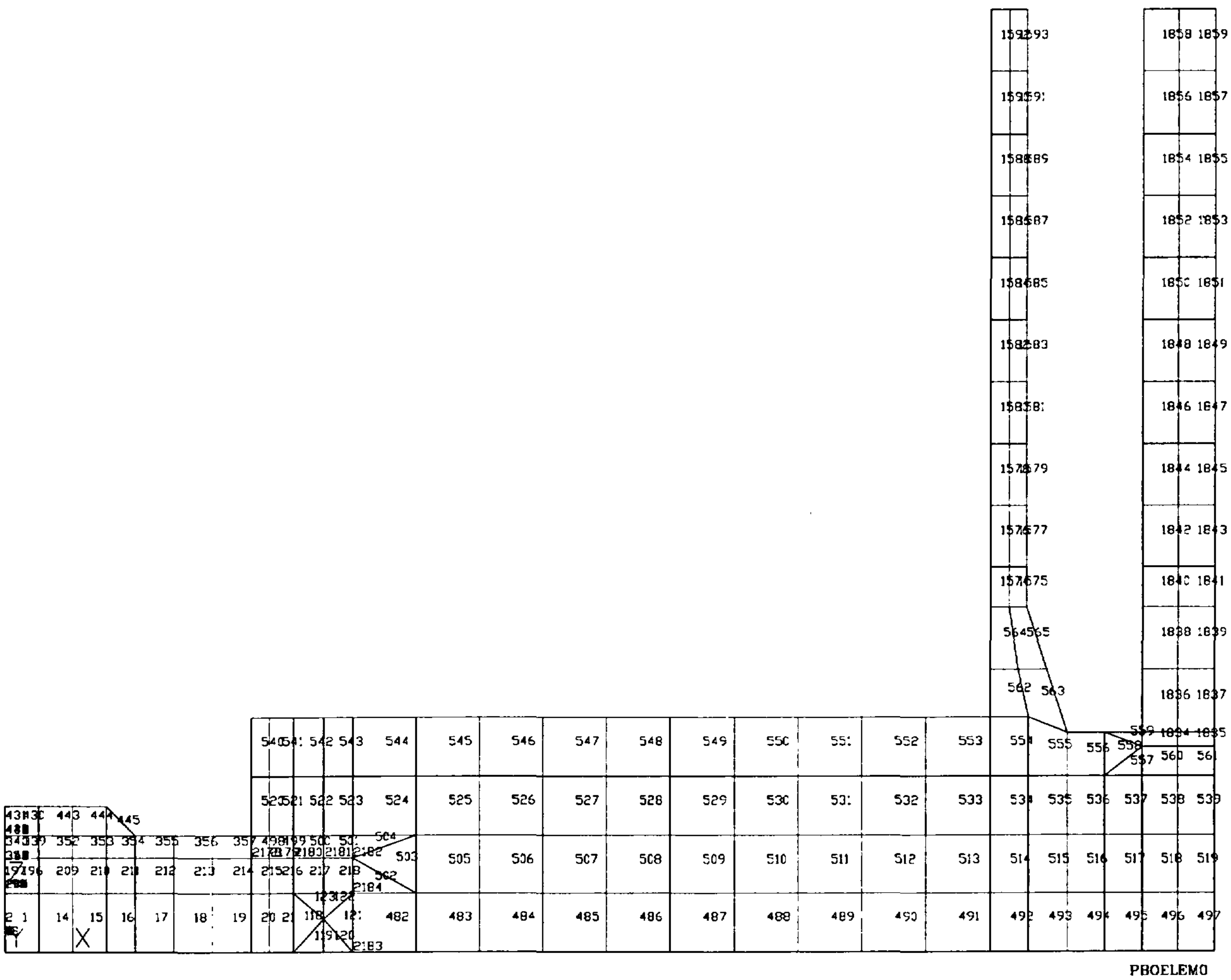

Figure 2.10.2-14

Bottom Off-Center Puncture Model Element Numbers at Y=0

2.10.2.1.4.2 Boundary Conditions

The nodes lying on the "cut" surfaces of the cask inner and outer shells are restrained from translating in the longitudinal direction (UZ = 0). Symmetry boundary conditions are applied to the nodes lying on the symmetry plane.

2.10.2.1.4.3 Loading

The flow stress of the mild steel puncture bar is applied as the puncture load to the outer surface of the bottom end closure forging adjacent to the edge of the ram closure plate. The dynamic flow stress of the puncture bar is 50,000 psi, as described in Section 2.7.2. The puncture loading is applied to elements 482 through 484 which have a total area of 13.22 square inches, or 26.44 square inches due to the symmetry plane. The area of the 6.0 inch diameter puncture bar is 28.27 square inches. The pressure load is factored by the ratio of the puncture bar area to the area of load application to apply the total puncture load. The factored puncture pressure is:

$$
\begin{aligned}
P &= (50{,}000)(28.27/26.44) \\
&= 53{,}460 \text{ psi}
\end{aligned}
$$

The load due to the cask contents (DSC + fuel) is applied to the inner surface of the bottom end closure forging as a 114 psi uniform pressure load, as discussed in Section 2.7.2.

2.10.2.1.5 Cask Half Symmetry Top End Detail Model

The cask half symmetry top end detail model is used only to analyze the cask for an off-center top end puncture. A detailed description of the model construction, boundary conditions, and loading follows.

2.10.2.1.5.1 Model Description

The top end off-center puncture is performed using the half symmetry finite element model shown in Figure 2.10.2-15. The analytical model consists of 3-D isoparametric brick elements representing the top cover plate, top flange, inner shell and outer shell. The lead shielding in the annulus between the inner and outer shells is assumed to have no structural significance, and consequently is not included in the analytical model. The 3-D isoparametric brick elements consist of eight nodes, each having three translational degrees of freedom. The cask inner and outer shells are included in the model to accurately model the rotational stiffness they provide to the top end corner forging. The shells are modeled with sufficient length to permit displacements independent of the boundary conditions. The node and element numbers at the Y=0 location are shown in Figure 2.10.2-16 and Figure 2.10.2-17, respectively. Nodes are generated from the node patters at the y=0 plane at 5° increments for the first 10° and at 10° increments for the next 170° applying node increments of 300.

The interface between the top closure plate and the top flange is modeled using 3-D gap elements. The 3-D gap elements operate bilinearly, having a small stiffness (1.0 x 10^{-6} lb/in.) for a separated interface (to provide stability) and a constant stiffness (1.0 x 10^{10} lb/in.) for a closed interface. The initial status of all gaps is modeled as closed and not sliding (STAT=1.0).

Three dimensional spar elements are used to model the 36 2-12UN-2A top closure bolts. The 3-D spar elements are uniaxial tension-compression elements consisting of 2 nodes, each having three translational degrees of freedom (UX and UY). The geometric properties defining the 3-D spar elements are the area and initial strain. The stress area of each 2 inch diameter 12UN bolt is 2.767 square inches ([2.22], pg. 8-13, Table 4). The initial strain used to model the bolt preload is equal to 50% of yield in the bolts, or 0.176%, as calculated in Section 2.7.2.1. The analytical model node numbers at the Y=0 plane (0° circumference) are shown in Figure 2.10.2-16. The nodes are generated at 5° increments over the first 10° circumference and at 10° increments over the remaining 170° circumference for a total angle of 180° using the node pattern shown in Figure 2.10.2-16, applying a node number increment of 200. The element numbers for the elements adjacent to the 0° azimuth are shown in Figure 2.10.2-17.

2.10.2.1.5.2 Boundary Conditions

The nodes lying on the free surface of the cask inner and outer shells are restrained from translating in the longitudinal direction (UZ = 0). Symmetry boundary conditions are applied to the nodes lying on the symmetry plane.

2.10.2.1.5.3 Loading

The flow stress of the mild steel puncture bar is applied as the puncture load to the outer surface of the top cover plate in the region of the seals. The dynamic flow stress of the puncture bar is 50,000 psi. The puncture loading is applied to the outer surface of the top cover plate in the region of the seals (elements 1079 and 1080) over a total area of 13.565 square inches, or 27.13 square inches due to the symmetry plane. The area of the 6.0 inch diameter puncture bar is 28.27 square inches. The dynamic flow stress of the puncture bar is factored by the ratio of the puncture bar area to the area of load application to apply the total puncture load. The factored puncture pressure is:

$$\begin{aligned} P &= (50{,}000)(28.27/27.13) \\ &= 52{,}100 \text{ psi} \end{aligned}$$

The load due to the cask contents (DSC + fuel) is applied to the inner surface of the top cover plate as a 114 psi uniform pressure load, as discussed in Section 2.7.2.

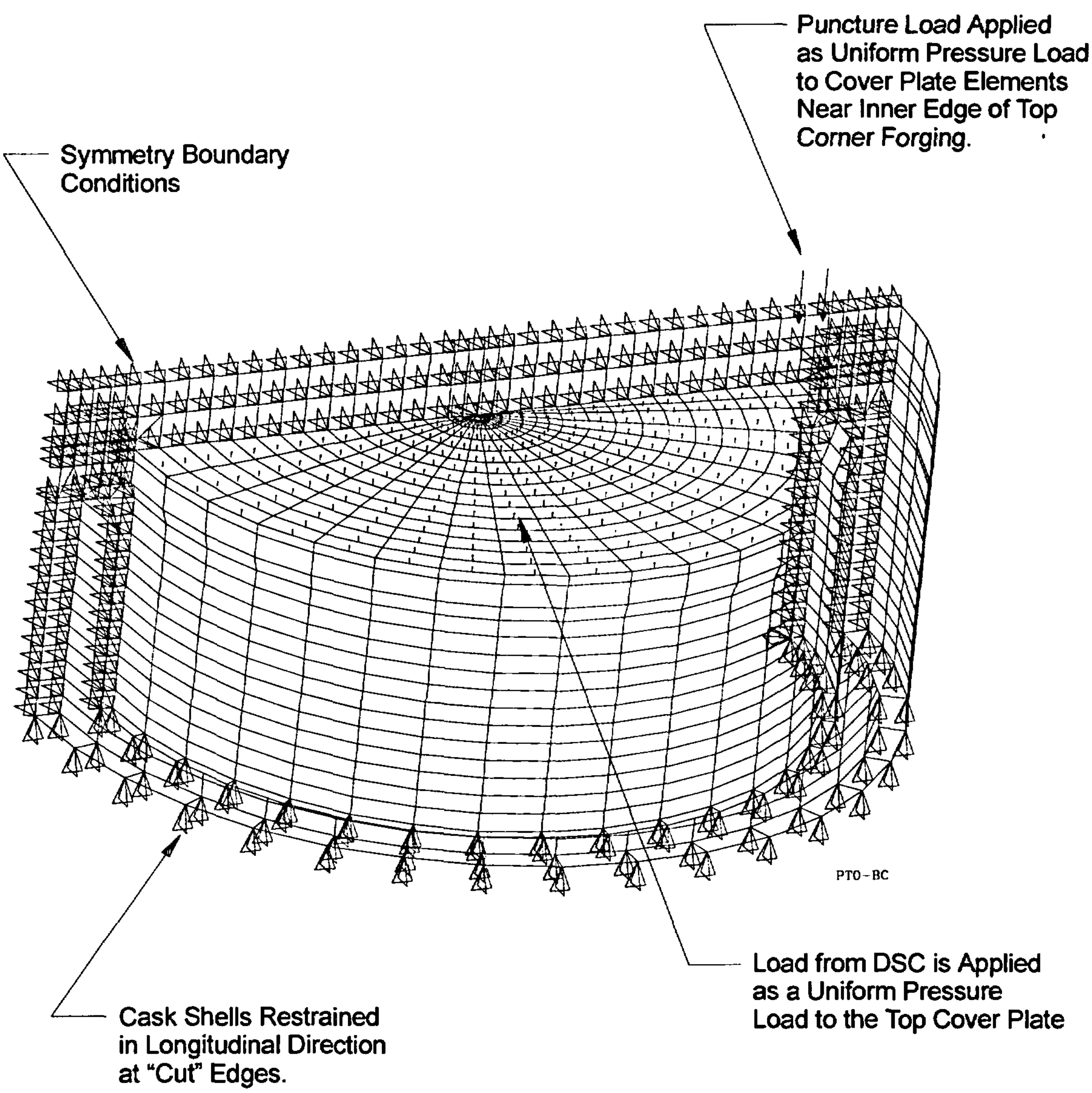

Figure 2.10.2-15

Top Off-Center Puncture Analytical Model

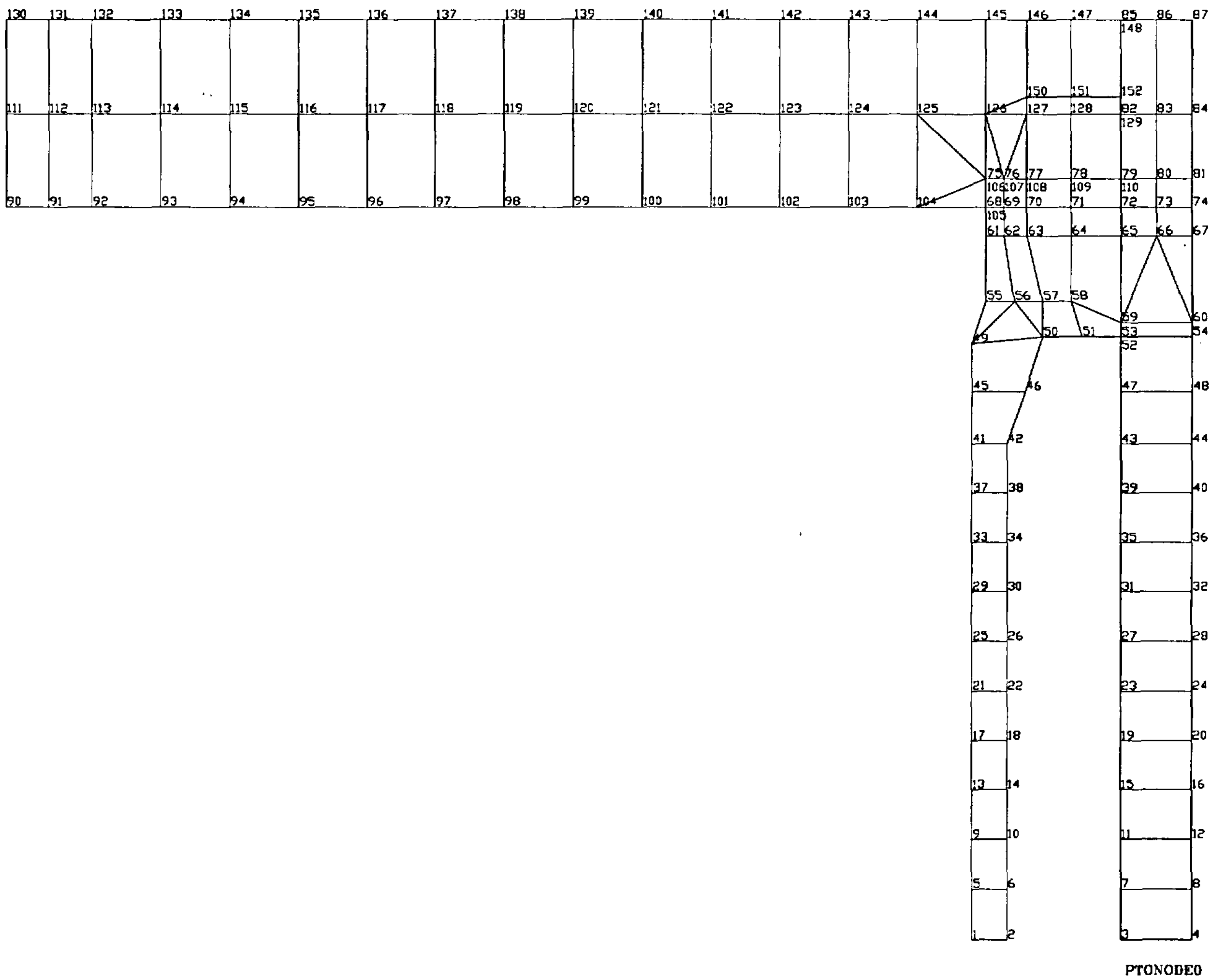

Figure 2.10.2-16

Top Off-Center Puncture Model Node Numbers at Y=0

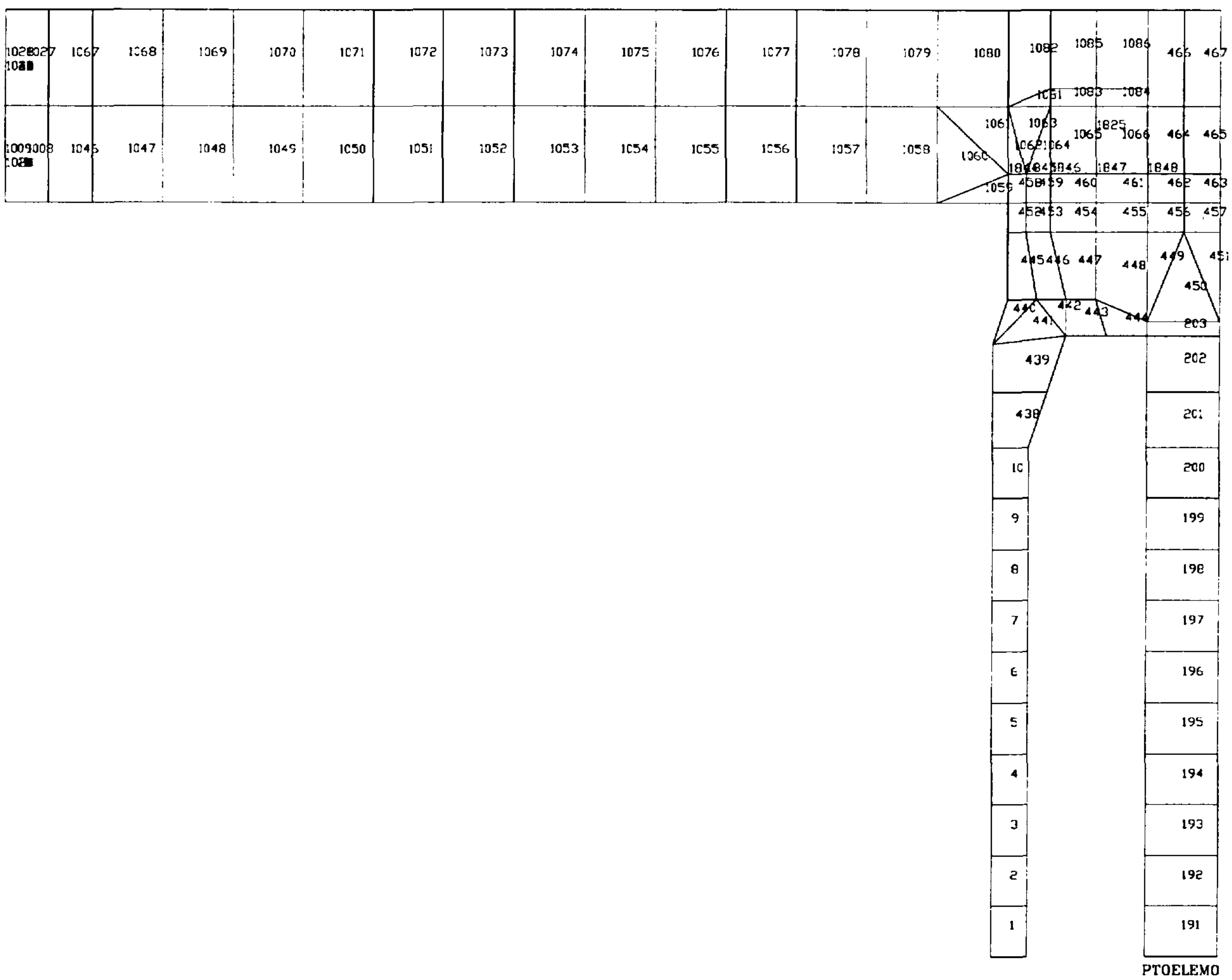

Figure 2.10.2-17

Top Off-Center Puncture Model Element Numbers at Y=0

2.10.2.2 Finite Element Model Input Files

THIS SECTION CONTAINS
PROPRIETARY INFORMATION

2.10.3 FO- and FC-DSC Basket Assembly Finite Element Analysis

The structural evaluation of the FO- and FC-DSC basket assembly components is performed using a combination of classical solutions and finite element analysis. Section 2.10.3.1 of this appendix provides a detailed description of each of the finite element models employed, including the model geometry, boundary condition, and loading. In addition, the input files for each of the finite element analyses are provided in Section 2.10.3.1.7. Detailed descriptions of the analysis results are provided in the respective sections of Chapter 2.

The finite element model applied loads used in this Appendix are based on the spacer disc configuration described in Table 2.10.3-1. Table 2.10.3-4 provides the spacer disc tributary weights used for the detailed analyses presented in this Appendix. Table 2.10.3-2 and Table 2.10.3-5 provide the spacer disc tributary weights for the revised spacer disc configuration. As shown by a comparision of these tables, the revised maximum spacer disc configuration loads are enveloped by the results presented for the bounding spacer disc. Therefore, the analyses presented in this Appendix provide a bounding spacer disc analysis.

2.10.3.1 Finite Element Model Descriptions

The FO- and FC-DSC basket assemblies are evaluated for the Normal Conditions of Transport (NCT) and the Hypothetical Accident Conditions (HAC) defined in the Regulations [2.1] using the finite element models described in the following sections. Four separate models are used for the spacer disc evaluation; a quarter symmetry model, a half symmetry flatside impact model, a half symmetry corner impact model, and a full disc model. The guide sleeves are evaluated for the side drop loading using a half symmetry periodic model. The DSC shell stiffness is evaluated using a half symmetry model of the DSC shell. The finite element models are generated using the ANSYS version 5.0A [2.39] and ANSYS version 4.4A [2.6] programs. The finite element meshes are created using good finite element practices; maintaining low aspect ratios and reasonably fine mesh densities. The number of 3-node triangular shell (constant strain) elements are minimized to avoid inaccuracies in the model solutions. All spacer disc ligaments are modeled using at least two elements through the depth to accurately capture the bending behavior resulting from the in-plane fuel load.

2.10.3.1.1 Spacer Disc 1/4 Symmetry Model

2.10.3.1.1.1 Model Description

The spacer disc 1/4 symmetry model, shown in Figure 2.10.3-1, is used for the 30 foot end drop and out-of-plane modal analyses. The model consists of 655 nodes and 494 elements. The spacer disc model node numbers and mesh are shown in Figure 2.10.3-2. The spacer disc is modeled with conservative ligament widths of 1.660 inches, 1.190 inches, 0.990 inches, 0.810 inches, and 0.675 inches, based on the specified minimum material condition. The 1.25 inch thickness of the spacer disc is defined by a real constant, and is assumed constant over the element area.

The spacer disc is modeled using elastic shell elements (SHELL63), defined by four nodes. Each node has a total of six degrees of freedom (UX, UY, UZ, ROTX, ROTY, and ROTZ), thus permitting both in-plane and normal loads. Element output is provided at the top, middle, and bottom fibers through the spacer disc thickness. Middle fiber stress results provide membrane and in-plane bending stresses. The top and bottom fiber results give the bending stresses resulting from both in-plane and out-of-plane (normal) bending.

The support rods provide in-plane membrane stiffness and out-of-plane bending stiffness to the spacer disc in the event of an end drop. The in-plane membrane stiffness provided by the support rods is conservatively ignored. The bending stiffness of the support rods is modeled using torsional spring elements (COMBIN14.) The support rod bending stiffness, conservatively based on only the stiffness of the support rod sleeves, k, is calculated as twice the stiffness of a simply supported beam subjected to a unit moment, M_o, at one end, as follows:

$$k = (2*M/\theta)$$

where;

$$\theta = M_oL/3EI, \text{ Angle of rotation due to applied moment}$$

Therefore,

$$k = 2*M/(ML/3EI)$$

$k = 6*EI/L$

and,

E = 26.7×10^6 psi, Elastic Modulus of ASME SA-564, Type 630 Stainless steel at 500°F.

$I = \pi(D_o^4 - D_i^4)/64$

$= \pi(3.00^4 - 2.08^4)/64$

$= 3.06 \text{ in}^4$

L = 2.35 in., 1/2 of support rod sleeve length (4.70".)

Therefore,

$k = 6 * (26.7 \times 10^6 * 3.06/ 2.35)$

$k = 2.09 \times 10^8$ in-lb/radian

A support rod stiffness of 1.0×10^8 in-lb/radian is conservatively used for the support rod stiffness in the quarter symmetry spacer disc model.

2.10.3.1.1.2 Boundary Conditions

Symmetry boundary constraints are applied to the nodes lying on the 1/4 symmetry planes of the spacer disc. The spacer disc is restrained from translating in the longitudinal direction (UZ) at the node nearest the centerline location of the support rod assembly. The support rod spring element ground nodes are restrained in all degrees of freedom.

2.10.3.1.1.3 Loading

The 1/4 symmetry spacer disc model is used only for the spacer disc 30 foot end drop and out-of-plane bending modal analyses. For these load conditions, the load from the fuel assemblies is transferred directly through the DSC shell end plugs to the cask body. Because the guide sleeves are not attached to the spacer discs, they will be supported in the longitudinal direction by the DSC end plugs. Therefore, the spacer discs support only their own self weight in the longitudinal direction for the accident drop conditions. The loading applied to the model for the 30 foot end drop condition consists of the equivalent static end drop acceleration only.

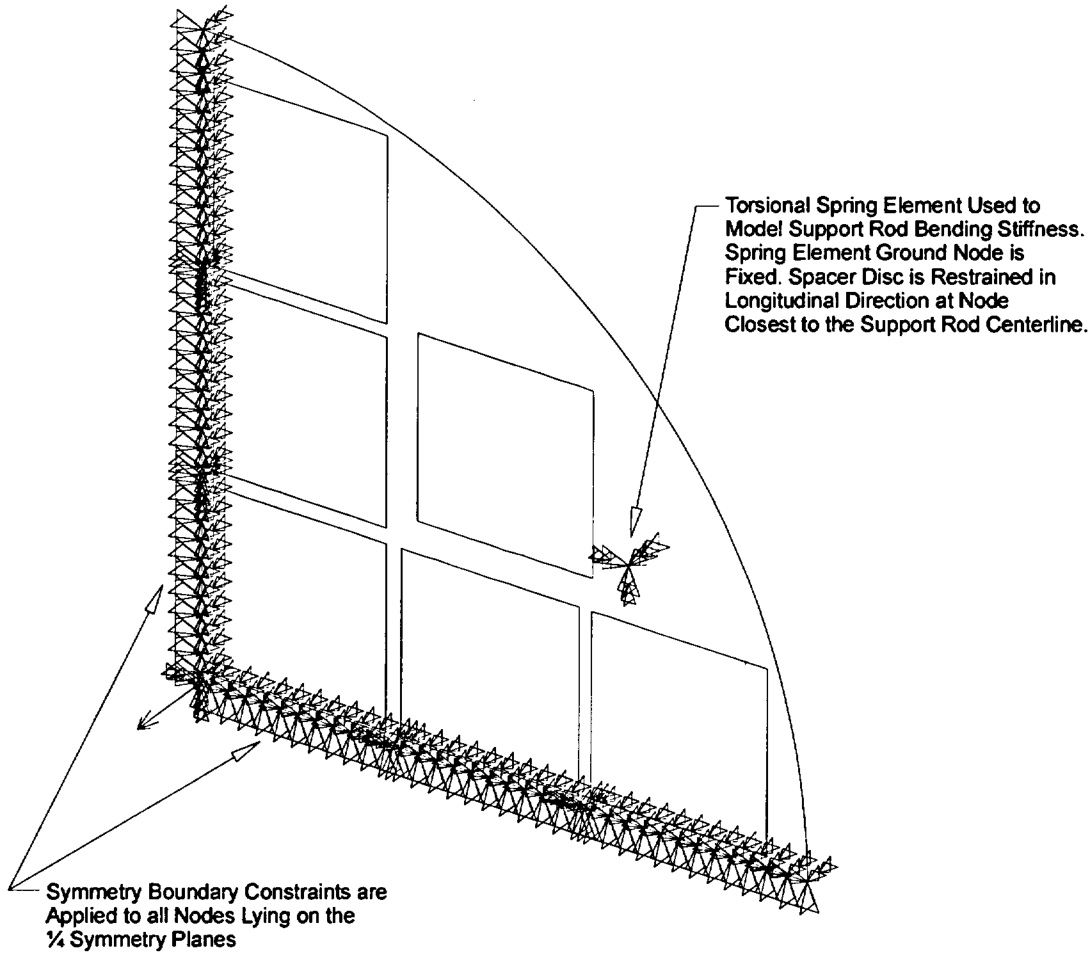

Figure 2.10.3-1
FC Spacer Disc 1/4 Symmetry Model

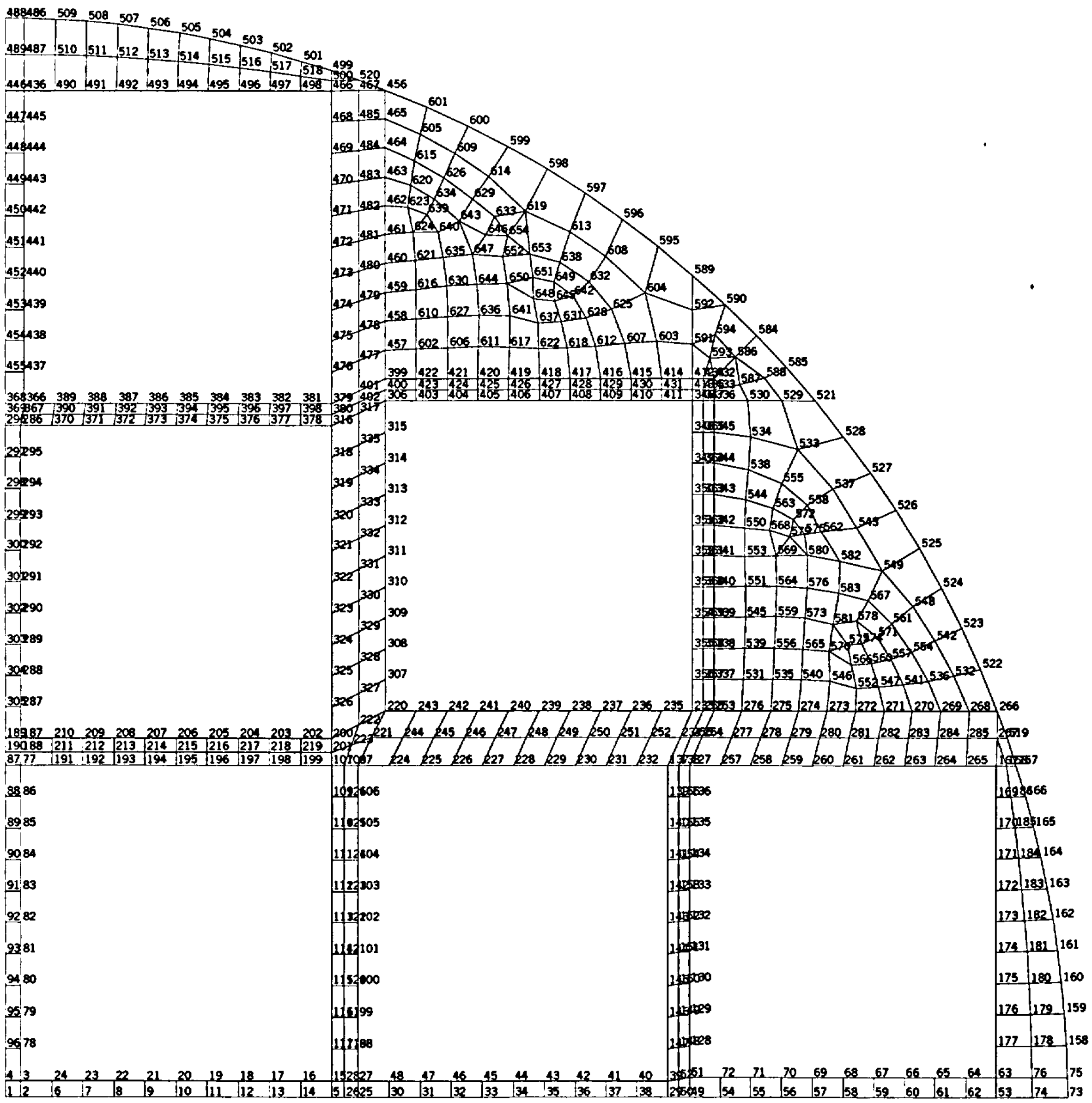

Figure 2.10.3-2
Spacer Disc 1/4 Symmetry Model Node Numbers

2.10.3.1.2 Spacer Disc Flatside Impact 1/2 Symmetry Model

2.10.3.1.2.1 Model Description

The spacer disc flatside impact 1/2 symmetry finite element model, shown in Figure 2.10.3-3, is used for the flatside ovalling modal, vibration, one foot drop, and all 30 foot flatside impact drop analyses. The model consists of 1363 nodes and 1077 elements. The half symmetry spacer disc is generated by symmetry reflection from the 1/4 symmetry spacer disc model described in Section 2.10.3.1.1. The spacer disc model node numbers and mesh in the upper and lower quadrants are shown in Figure 2.10.3-2 and Figure 2.10.3-4, respectively. The spacer disc is modeled with conservative ligament widths of 1.660 inches, 1.190 inches, 0.990 inches, 0.810 inches, and 0.675 inches, based on the specified minimum material condition. The 1.25 inch thickness of the spacer disc is defined by a real constant, and is assumed constant over the element area.

The spacer disc is modeled using 2-D plane stress elements with input thickness (PLANE42) for those load condition in which only in-plane response is expected (i.e. in-plane modal analysis, vibration, and 1' side drop,) and elastic shell elements (SHELL63) for load conditions in which normal loads exist (30' flatside oblique drops.) Gap elements (CONTAC12) used to model the interface between the spacer disc and DSC shell. The gap elements are defined by an orientation angle (THETA), a contact stiffness (KN), an initial gap size (GAP) and an initial gap status (STAT). The spacer disc is modeled with uniform gaps of 0.19 inches around the entire circumference, assuming that the spacer disc and DSC shell are initially concentric. The gap orientation angles are defined as the angle to the radial line from the DSC shell node to the spacer disc node, measured positive counterclockwise from the positive Y-axis in degrees.

The contact stiffness is used to model the stiffness of the DSC shell. The radial stiffness of the DSC shell depends on both the radial and longitudinal locations. The shell is stiffest near the top and bottom ends where it is supported radially by the top and bottom end plates and least stiff at the mid-length of the DSC cavity. The stiffness of the shell also increases near the point of contact with the cask inner shell.

The DSC shell stiffness is analyzed using the ANSYS version 4.4A [2.6] half symmetry finite element model discussed in Section 2.10.3.1.5. The shell stiffness at the mid-length of the DSC cavity is conservatively used for the spacer disc drop analyses. The shell stiffness is determined by displacing each node located at the mid-length of the DSC cavity, individually, by 1 inch in the radial direction. The stiffness of the shell at the location of the displaced node is equal to twice the reaction force at the displaced node since the nodes are located on the 1/2 symmetry plane. The stiffness of the DSC shell at the DSC cavity mid-length is determined for circumferential locations of 5° to 60°, at 5° increments, from the point of contact with the cask inner shell. The resulting shell stiffnesses are summarized in Table 2.10.3-6.

The DSC shell stiffness analysis results show that the shell stiffness increases significantly near the point of contact with the cask inner shell. The maximum shell stiffness is assumed to be equal to the shell stiffness at 10° from the initial point of contact. This stiffness is used for all gap elements which are less than 10° from the initial point of contact (45° azimuth). The shell stiffnesses for angles greater than 10° from the initial point of contact are calculated using 5^{th} order polynomial equation curve fit, shown in Figure 2.10.3-5, and given by:

$$K = 1.286e6 - 1.356e5\theta + 7.157e3\theta^2 - 1.843e2\theta^3 + 2.290\theta^4 - 1.100e\text{-}2\theta^5$$

For the oblique drop condition, in which the spacer disc is loaded in the longitudinal direction, the bending stiffness of the support rods is modeled using torsional spring elements, as discussed in Section 2.10.3.1.1. A lower bound support rod bending stiffness of 1.0×10^8 in-lb/radian is conservatively used in the model. The torsional spring elements are attached to the spacer disc nodes nearest the support rod centerline location.

For the modal analysis, the fuel assemblies and guide sleeves assemblies are modeled as mass elements (MASS21) attached to the supporting spacer disc ligament. The fuel assembly and guide sleeve assembly weights tributary to each of the FC-DSC spacer disc ligaments are calculated in the following paragraphs.

Guide Sleeve Assy. Type "A":

Wt. = 237 lb., Weight of Type "A" guide sleeve assembly

w = 237/161.5

$= \quad 1.47$ lb/in.

Guide Sleeve Assy. Type "B":

Wt.	=	274 lb., Weight of Type "B" guide sleeve assembly
w	=	274/161.5
	=	1.70 lb/in.

The weight of the 24 guide sleeve assemblies tributary to each disc is calculated as follows:

$$W_{gs1} = 12(1.47 + 1.70)(11.60 - 0.50)$$
$$= 422.2 \text{ lb.}$$

$$W_{gs2} \text{ through } W_{gs23} = 12(1.47 + 1.70)(5.95)$$
$$= 226.3 \text{ lb.}$$

$$W_{gs24} = 12(1.47 + 1.70)(7.175)$$
$$= 272.9 \text{ lb.}$$

$$W_{gs25} = 12(1.47 + 1.70)(7.637)$$
$$= 290.5 \text{ lb.}$$

$$W_{gs26} = 12(237 + 274) - 422.2 - 22(226.3) - 272.9 - 290.5$$
$$= 167.8 \text{ lb.}$$

As shown in Table 2.10.3-7, the maximum weight of a single PWR fuel assembly and control component are 1,530 pounds and 135 pounds, respectively, for a total weight of 1,665 pounds per fuel assembly [2.8]. The weight distribution of a B&W 15X15 Mark B (PWR) fuel assembly over the four major axial regions are summarized in Table 2.10.3-7.

The weight of a PWR fuel assembly varies along its length. The heaviest portion of the fuel assembly is in the active fuel region. Per Table 2.10.3-7 the fuel assembly plus control component weight distributed over the in-core region is 1537 lbs. The control components weigh 135 pounds each [2.8] and are located within the active fuel region, plenum region, top region, and above the top region. The control component spider, which weighs 32 pounds [2.9], is located above the top region. The remainder of the control components are assumed to be distributed evenly over the active fuel region (141.80 inches), plenum region, and top region (total length = 157.32 inches).

Therefore, the line load for a fuel assembly and control is developed by conservatively assuming all of the fuel component weight is distributed over the in-core region as follows:

$$w = 1{,}537/141.8$$

$$= 10.84 \text{ lb/in.}$$

A bounding line load of 10.84 pounds per inch is used for the fuel assembly and control components.

Using the fuel assembly line loads for each fuel region presented in Table 2.10.3-7, the weight of the 24 fuel assemblies tributary to each spacer disc for the analytical model geometry, described in Table 2.10.3-4 is calculated as follows:

$$W_{F1} = [3.55(8.63) + 10.84(11.60 - 8.63)](24)$$

$$= 1{,}508.0 \text{ lbs.}$$

$$W_{F2} \text{ thru } W_{F23} = 10.84(5.95)(24)$$

$$= 1{,}548.0 \text{ lbs.}$$

$$W_{F24} = 10.84(7.175)(24)$$

$$= 1866.6 \text{ lbs.}$$

$$W_{F25} = [10.84(150.430 - 149.675) + 3.34(157.313 - 150.430)](24)$$

$$= 748.1 \text{ lbs.}$$

$$W_{F26} = 24(1{,}665.0) - 1{,}508.0 - 22(1{,}548.0) - 1{,}866.6 - 748.1$$

$$= 1{,}781.3 \text{ lbs}$$

The mass of the fuel assemblies and guide sleeve assemblies are distributed evenly over the length of the supporting spacer disc ligaments. The total mass of fuel assembly and guide sleeve assembly tributary to each spacer disc ligament is:

Type "A": m_A = [1866.6 + 272.9(1.47)/(1.47 + 1.70)]/(24 x 386.4)

= 0.215 lb-s²/in

Type "B": m_B = [1866.6 + 272.9(1.70)/(1.47 + 1.70)]/(24 x 386.4)

= 0.217 lb-s²/in

Bounding masses of 0.231 lb-s^2/in. and 0.235 lb-s^2/in. are conservatively used for the type "A" and "B" ligaments, respectively. The additional mass applied to the disc represents a 7% to 8% increase in the tributary fuel and guide sleeve tributary weight. The effect of the additional tributary weight reduces the vibration frequency of the spacer disc. The spacer disc vibration frequency is used to determine the DLFs applied to the spacer disc for the various impact load conditions. As shown in Appendix 2.10.10, the DLF is higher at lower frequencies. Therefore, the additional mass applied to the spacer disc model is conservative. The total tributary mass is uniformly distributed over the entire width of the supporting spacer disc ligament.

2.10.3.1.2.2 Boundary Conditions

Symmetry boundary constraints are applied to the nodes lying on the 1/2 symmetry plane of the spacer disc. The spacer disc is restrained from translating in the longitudinal direction (UZ) at the node nearest the centerline location of the support rod assemblies. The gap element and support rod spring element ground nodes are restrained in all degrees of freedom.

2.10.3.1.2.3 Loading

Each drop analysis is performed for the single spacer disc which supports the largest total tributary weight. The spacer disc tributary weight includes the spacer disc self weight and the tributary weight of the four support rods, 24 fuel assemblies, and 24 guide sleeve assemblies. The tributary weights used for the bounding analysis for each of the 26 spacer discs are calculated as described below and summarized in Table 2.10.3-1. Each spacer disc weighs approximately 417 pounds. The tributary weight of the four support rods for each spacer disc is calculated as follows:

$$W_{sr,i} = (4)[A_{rod}(b_i) + A_{sleeve}(b_i - 1.25)](0.2853)$$

$$= (4)[3.14b_i + 3.67(b_i - 1.25)](0.2853)$$

$$= 7.77b_i - 5.24$$

where the spacer disc tributary widths, bi, are taken from the free end to the mid-span of the adjacent spacer disc for the top and bottom end discs and from mid-span to mid-span of the adjacent spacer discs for interior spacer discs. The spacer disc tributary widths used in the bounding analysis are summarized in Table 2.10.3-1. The actual spacer disc loads shown in Table 2.10.3-2 show a more uniform load distribution over the middle spacer discs and lighter loads at the package ends. As described below, this results in lower spacer disc loads for all drop orientations and results in the analytical loads, shown in Table 2.10.3-4, enveloping all revised spacer disc loads shown in Table 2.10.3-5.

Table 2.10.3-1
Spacer Disc Analytical Tributary Weight Distribution

Spacer Disc Number	Disc Axial Centerline Location (in.)	Spacer Disc Tributary Width (in.)	Spacer Disc Self Weight (lb.)	Tributary Fuel Assy. Weight (lb.)	Tributary Guide Sleeve Weight (lb.)	Tributary Support Rod Weight (lb.)	Total Disc Tributary Weight (lb.)
1	8.625	11.600	416.6	1508.0	422.2	84.9	2431.7
2	14.575	5.950	416.6	1548.0	226.3	41.0	2231.9
3	20.525	5.950	416.6	1548.0	226.3	41.0	2231.9
4	26.475	5.950	416.6	1548.0	226.3	41.0	2231.9
5	32.425	5.950	416.6	1548.0	226.3	41.0	2231.9
6	38.375	5.950	416.6	1548.0	226.3	41.0	2231.9
7	44.325	5.950	416.6	1548.0	226.3	41.0	2231.9
8	50.275	5.950	416.6	1548.0	226.3	41.0	2231.9
9	56.225	5.950	416.6	1548.0	226.3	41.0	2231.9
10	62.175	5.950	416.6	1548.0	226.3	41.0	2231.9
11	68.125	5.950	416.6	1548.0	226.3	41.0	2231.9
12	74.075	5.950	416.6	1548.0	226.3	41.0	2231.9
13	80.025	5.950	416.6	1548.0	226.3	41.0	2231.9
14	85.975	5.950	416.6	1548.0	226.3	41.0	2231.9
15	91.925	5.950	416.6	1548.0	226.3	41.0	2231.9
16	97.875	5.950	416.6	1548.0	226.3	41.0	2231.9
17	103.825	5.950	416.6	1548.0	226.3	41.0	2231.9
18	109.775	5.950	416.6	1548.0	226.3	41.0	2231.9
19	115.725	5.950	416.6	1548.0	226.3	41.0	2231.9
20	121.675	5.950	416.6	1548.0	226.3	41.0	2231.9
21	127.625	5.950	416.6	1548.0	226.3	41.0	2231.9
22	133.575	5.950	416.6	1548.0	226.3	41.0	2231.9
23	139.525	5.950	416.6	1548.0	226.3	41.0	2231.9
24	145.475	7.175	416.6	1866.6	272.9	50.5	2606.7
25	153.875	7.637	416.6	748.1	290.5	54.1	1509.4
26	160.750	15.188	416.6	1782.8	167.8	112.8	2480.0

Note:

1. The spacer disc locations presented in this Table are obsolete and are only used to develop the bounding spacer disc loads.

For oblique drop conditions, the spacer disc tangential (i.e. in-plane) impact load varies with the longitudinal distance from the package center of gravity, x, as follows:

$$P_i = W_i(G_{cg} + \alpha x)(DLF)$$

where tangential acceleration at the package center of gravity, G_{cg}, and the angular acceleration of the package, α, are calculated for each oblique drop condition in Appendix 2.10.9, and the spacer disc DLF corresponding to each impact condition are summarized in Table 2.10.3-3.

Table 2.10.3-2
Spacer Disc Actual Tributary Weight Distribution

Disc No.:	Centerline Location (inches)	Tributary Span (inches)	Disc Self Wt. (lbs)	Tributary Weights (lbs) Fuel Weight	Sleeve Weight	Rod Weight	Total Weight, W_{TOT}(lb)
1	6.875	9.625	424.3	994.1	346.8	69.2	1,834.4
2	12.375	5.500	424.3	1,430.9	209.0	37.3	2,101.5
3	17.875	5.500	424.3	1,430.9	209.0	37.3	2,101.5
4	23.375	5.750	424.3	1,495.9	218.5	39.2	2,178.0
5	29.375	6.250	424.3	1,626.0	237.5	43.1	2,330.9
6	35.875	6.625	424.3	1,723.6	251.8	46.0	2,445.6
7	42.625	6.750	424.3	1,756.1	256.5	47.0	2,483.8
8	49.375	6.750	424.3	1,756.1	256.5	47.0	2,483.8
9	56.125	6.750	424.3	1,756.1	256.5	47.0	2,483.8
10	62.875	6.750	424.3	1,756.1	256.5	47.0	2,483.8
11	69.625	6.750	424.3	1,756.1	256.5	47.0	2,483.8
12	76.375	6.750	424.3	1,756.1	256.5	47.0	2,483.8
13	83.125	6.750	424.3	1,756.1	256.5	47.0	2,483.8
14	89.875	6.750	424.3	1,756.1	256.5	47.0	2,483.8
15	96.625	6.750	424.3	1,756.1	256.5	47.0	2,483.8
16	103.375	6.750	424.3	1,756.1	256.5	47.0	2,483.8
17	110.125	6.750	424.3	1,756.1	256.5	47.0	2,483.8
18	116.875	6.625	424.3	1,723.6	251.8	46.0	2,445.6
19	123.375	6.500	424.3	1,691.0	247.0	45.0	2,407.4
20	129.875	6.500	424.3	1,691.0	247.0	45.0	2,407.4
21	136.375	6.500	424.3	1,691.0	247.0	45.0	2,407.4
22	142.875	6.250	424.3	1,626.0	237.5	43.1	2,330.9
23	148.875	5.875	424.3	1,528.4	223.3	40.2	2,216.2
24	154.625	5.313	424.3	458.3	201.9	35.9	1,120.3
25(3)	159.500	3.063	424.3	245.5	116.4	18.5	1,589.4
26(3)	160.750	12.375	424.3	1,676.9	182.5	90.4	1,589.4
		Totals:	11,032	40,350	6,248	1,198	58,828

Notes: 1. Sleeve weight of 38.00 lb/in is applied from 0.5 inch to 162.3 inches (161.8 + 0.5) where there is a 0.5 inch gap between the bottom of the fuel cavity and the bottom of the

trib_wt7.xls

2. An additional weight of 99.84 lb(24 sleeves * 4 angles/sleeve * 6.5"/angle * 1.92 lb/ft) applied to the sleeve weight for the top spacer disk.
3. Discs 25 & 26 are immediately adjacent to each other (i.e. no gap between the discs). The load is assumed to be evenly distributed between these 2 discs.

Table 2.10.3-3
FC Spacer Disc Oblique Drop Bounding Impact Loads

Impact Orientation	Ambient Condition	Tangential Acceleration at C.G. (g's)	Angular Acceleration at C.G. (rad/sec^2)	Dynamic Load Factor (DLF)
Flatside 30° Primary Impact	Cold	29.5	188.0	1.10
	Hot	16.5	86.2	1.07
Flatside 30° Slapdown Impact	Cold	29.8	193.0	1.28
	Hot	19.5	133.0	1.27
Flatside 60° Primary Impact	Cold	18.5	118.0	1.02
	Hot	9.5	43.5	1.01

The resulting spacer disc in-plane loads for each of the flatside oblique drop conditions are summarized in Table 2.10.3-4 for the bounding analysis and Table 2.10.3-3b for the actual configuration. As shown in Table 2.10.3-4, spacer disc #26 (i.e. the top end spacer disc) is the most heavily loaded spacer disc for all flatside oblique drop conditions, and the resulting loads are used for all spacer disc analyses. These results bound the revised loads shown in Table 2.10.3-5b.

Table 2.10.3-4
FC Spacer Disc Flatside Oblique Impact Bounding Analytical Tangential Loads

Spacer Disc Number	Disc Axial Centerline Location (in.)	Distance from C.G. (in.)	Cold Flatside 30° Impact Load (kips)	Hot Flatside 30° Impact Load (kips)	Cold Flatside Slapdown Impact Load (kips)	Hot Flatside Slapdown Impact Load (kips)	Cold Flatside 60° Impact Load (kips)	Hot Flatside 60° Impact Load (kips)
1	8.625	76.76	178.	87.5	212.	141.	104.	44.6
2	14.57	70.8	157.	77.	186.	124.	91.	39.4
3	20.525	64.86	149.	74.0	177.	118.	87.2	37.9
4	26.475	58.9	142.	70.8	169.	112.	83.	36.4
5	32.425	52.96	135.	67.6	160.	106.	78.9	34.9
6	38.375	47.0	128.	64.4	152.	101.	74.8	33.3
7	44.325	41.0	121.	61.	143.	95.3	70.7	31.
8	50.275	35.1	114.	58.	135.	89.5	66.5	30.3
9	56.225	29.1	107.	54.9	126.	83.7	62.4	28.8
1	62.17	23.2	100.	51.	118.	77.9	58.2	27.3
1	68.12	17.2	93.0	48.6	109.	72.	54.	25.8
1	74.075	11.3	85.9	45.4	101.	66.3	50.0	24.3
1	80.025	5.35	78.8	42.3	92.8	60.5	45.8	22.8
1	85.975	0.60	73.	39.7	86.0	55.9	42.5	21.
1	91.92	6.55	80.2	42.9	94.5	61.	46.7	23.
1	97.875	12.5	87.4	46.	103.	67.5	50.8	24.6
1	103.82	18.4	94.5	49.2	111.	73.3	54.9	26.
1	109.77	24.40	101.	52.4	119.	79.	59.	27.6
1	115.72	30.35	108.	55.6	128.	84.9	63.2	29.
20	121.67	36.30	115.	58.7	136.	90.7	67.3	30.6
2	127.62	42.25	122.	61.	145.	96.5	71.	32.
22	133.57	48.20	130.	65.	153.	102.	75.6	33.6
23	139.52	54.1	137.	68.3	162.	108.	79.8	35.2
24	145.47	60.1	168.	83.4	199.	133.	98.0	42.8
25	153.87	68.50	104.	51.	123.	82.6	60.7	26.2
26	160.75	75.37	180.4	88.4	214.0	143.1	105.0	45.0
Maximum Impact Load (kips)			180.	88.4	214.	143.	105.	45.0

Table 2.10.3-5
FC Spacer Disc Flatside Oblique Impact Actual Tangential Loads

Spacer Disk Number	Spacer Disc Location		Disc Total Dead Load (lb)	Cold 30' Flatside Drop Load (kips)		
	Centerline Location	Dist. From CG (in)		30° Primary Impact	Flatside Slapdown	60° Primary Impact
1	6.88	78.645	1,834.4	137.2	169.3	80.5
2	12.38	73.145	2,101.5	150.9	186.2	88.6
3	17.88	67.645	2,101.5	144.7	178.5	84.9
4	23.38	62.145	2,178.0	143.4	177.0	84.2
5	29.38	56.145	2,330.9	146.0	180.0	85.7
6	35.88	49.645	2,445.6	144.6	178.3	84.9
7	42.63	42.895	2,483.8	137.8	169.8	80.9
8	49.38	36.145	2,483.8	128.7	158.6	75.6
9	56.13	29.395	2,483.8	119.7	147.4	70.3
10	62.88	22.645	2,483.8	110.6	136.2	64.9
11	69.63	15.895	2,483.8	101.6	124.9	59.6
12	76.38	9.145	2,483.8	92.5	113.7	54.3
13	83.13	2.395	2,483.8	83.4	102.5	49.0
14	89.88	4.355	2,483.8	86.1	105.8	50.6
15	96.63	11.105	2,483.8	95.1	117.0	55.9
16	103.38	17.855	2,483.8	104.2	128.2	61.2
17	110.13	24.605	2,483.8	113.2	139.4	66.5
18	116.88	31.355	2,445.6	120.4	148.3	70.7
19	123.38	37.855	2,407.4	127.0	156.5	74.5
20	129.88	44.355	2,407.4	135.4	167.0	79.5
21	136.38	50.855	2,407.4	143.9	177.4	84.5
22	142.88	57.355	2,330.9	147.5	181.9	86.6
23	148.88	63.355	2,216.2	147.4	181.9	86.5
24	154.63	69.105	1,120.3	78.0	96.3	45.8
25	159.50	73.980	1,589.4	114.8	141.7	67.4
26	160.75	75.230	1,589.4	115.9	143.1	68.0
Flatside Drop Maximums:				**150.9 kip**	**186.2 kip**	**88.6 kip**

Note: Hot drop loads are enveloped by cold drop loads. Thus, only cold drop loads are listed.

trib_wt7.xls

The in-plane loads due to the weight of the fuel assemblies and guide sleeve assemblies tributary to the spacer disc are modeled as a uniform pressure load acting on the supporting spacer disc ligaments. Edge pressures applied to elastic shell elements are input on a force per unit length basis. Therefore, the in-plane pressure loads applied to the type "A" and "B" ligaments due to an equivalent static deceleration, G, for the 1-foot and 30-foot flatside horizontal drop conditions are calculated as follows:

$$q = WG/b$$

where;

$$W = 1{,}866.6/24 + 272.9(237)/[(237 + 274)(12)]$$

$$= 88.3 \text{ lb. (type "A" ligaments)}$$

$$W = 1{,}866.6/24 + 272.9(274)/[(237 + 274)(12)]$$

$$= 90.0 \text{ lb. (type "B" ligaments)}$$

G = Equivalent static in-plane g-load

b = 9.47 in., Type "A" modeled ligament width

= 9.57 in., Type "B" modeled ligament width

Therefore,

$$q_A = (88.3 \text{ x } G)/(9.47)$$

$$= 9.32G \text{ psi}$$

$$q_B = (90.0 \text{ x } G)/(9.57)$$

$$= 9.40G \text{ psi}$$

The in-plane pressure loads applied to the type "A" and "B" ligaments due to an equivalent static deceleration, G, for the 30-foot flatside oblique drop conditions are calculated as follows:

$$q = WG/b$$

where;

$$W = 1{,}782.8/24 + 167.8(237)/[(237 + 274)(12)]$$
$$= 80.7 \text{ lb. (type "A" ligaments)}$$

$$W = 1{,}782.8/24 + 167.8(274)/[(237 + 274)(12)]$$
$$= 81.8 \text{ lb. (type "B" ligaments)}$$

G = Equivalent static in-plane g-load

b = 9.47 in., Type "A" modeled ligament width

= 9.57 in., Type "B" modeled ligament width

Therefore,

$$q_A = (80.8 \text{ x } G)/(9.47)$$
$$= 8.53G \text{ psi}$$

$$q_B = (81.8 \text{ x } G)/(9.57)$$

$$= 8.55G \text{ psi}$$

In addition to the in-plane pressure loads due to the fuel assemblies and guide sleeve assemblies, longitudinal equivalent static accelerations are applied for the oblique drop conditions to determine the out-of-plane bending stresses due to the spacer disc self weight.

The spacer disc loading is applied in the following sequence:

1.) A vertical displacement of 0.1901 inches is applied to the node at the bottom edge on the symmetry plane in the first load step to bring the spacer disc into contact with the DSC shell.

2.) The vertical displacement constraint applied to the spacer disc to close the gaps in the initial contact region is removed. The spacer disc drop loads are applied.

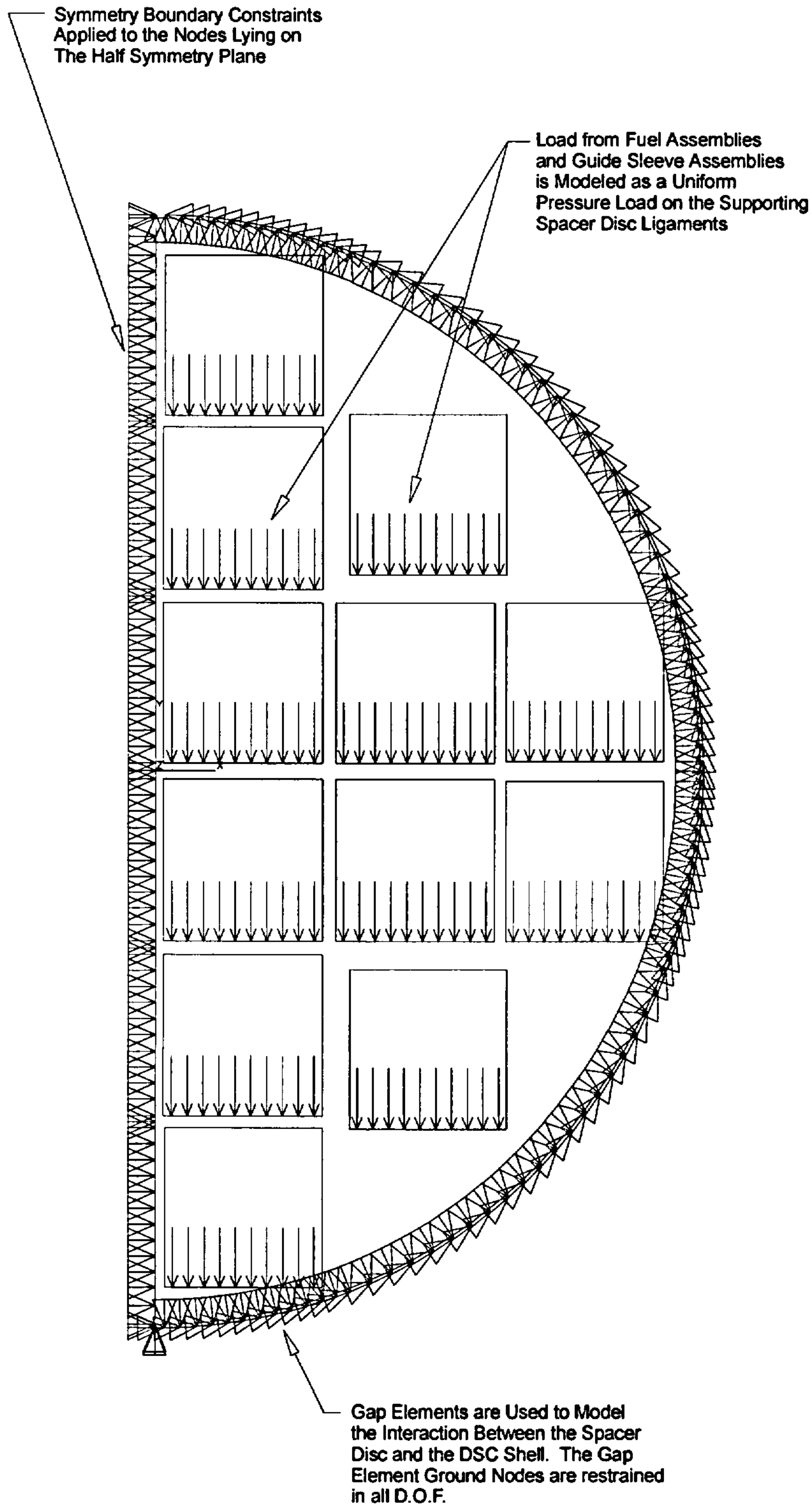

Figure 2.10.3-3
Spacer Disc 1/2 Symmetry Model

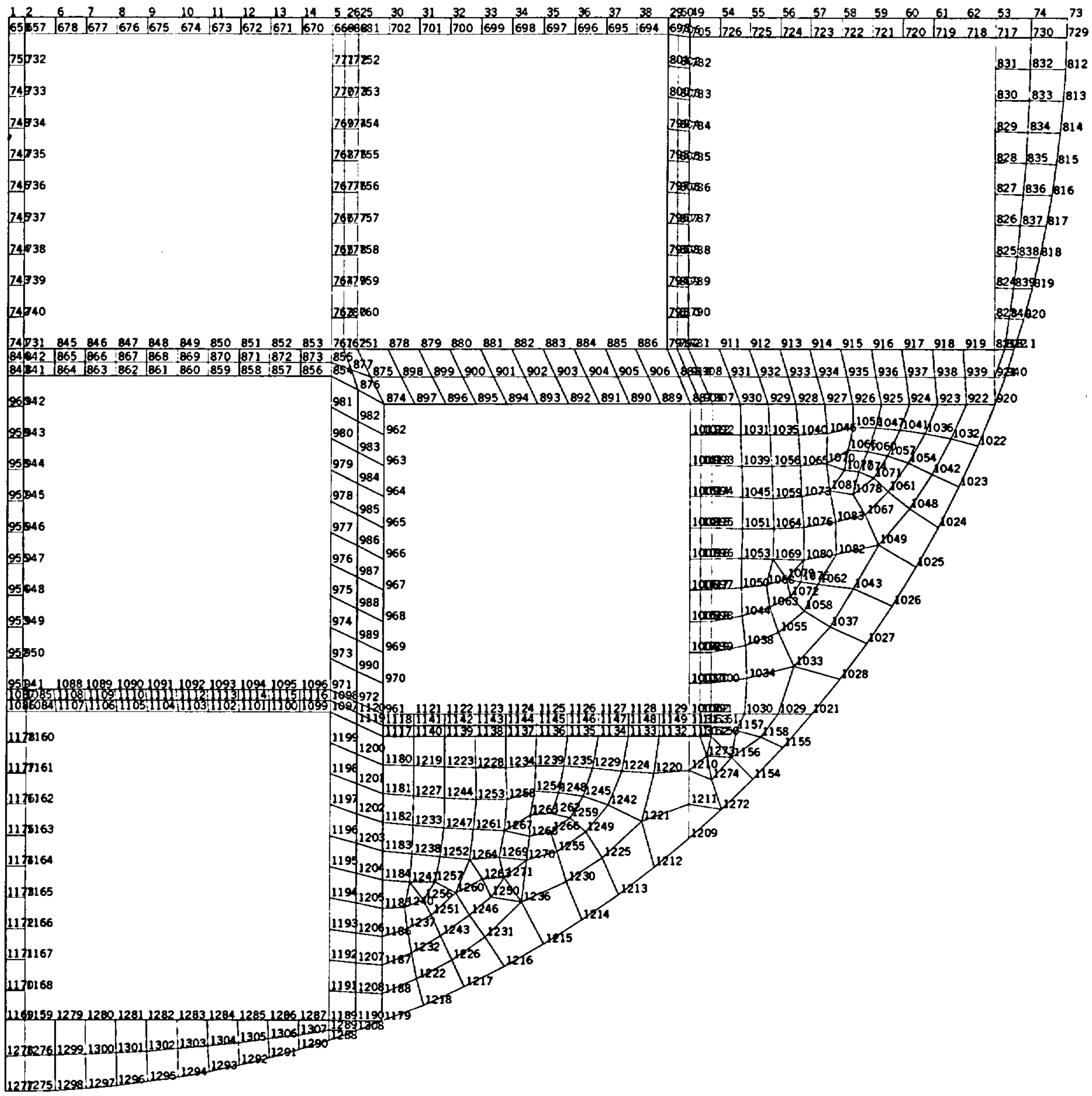

Figure 2.10.3-4
Spacer Disc 1/2 Symmetry Model Node Numbers - Lower Quadrant

Table 2.10.3-6
DSC Shell Stiffness Analysis Results

Node Number	Load Step	Angle(1) (Degrees)	Reaction Force (10^5 lbs.)	Stiffness (10^5 lb/in.)
1122	1	5	5.92	11.84
1123	2	10	2.42	4.84
1124	3	15	1.72	3.44
1125	4	20	1.49	2.98
1126	5	25	1.39	2.78
1127	6	30	1.34	2.68
1128	7	35	1.30	2.60
1129	8	40	1.24	2.48
1130	9	45	1.17	2.34
1131	10	50	1.10	2.20
1132	11	55	1.04	2.08
1133	12	60	0.98	1.96

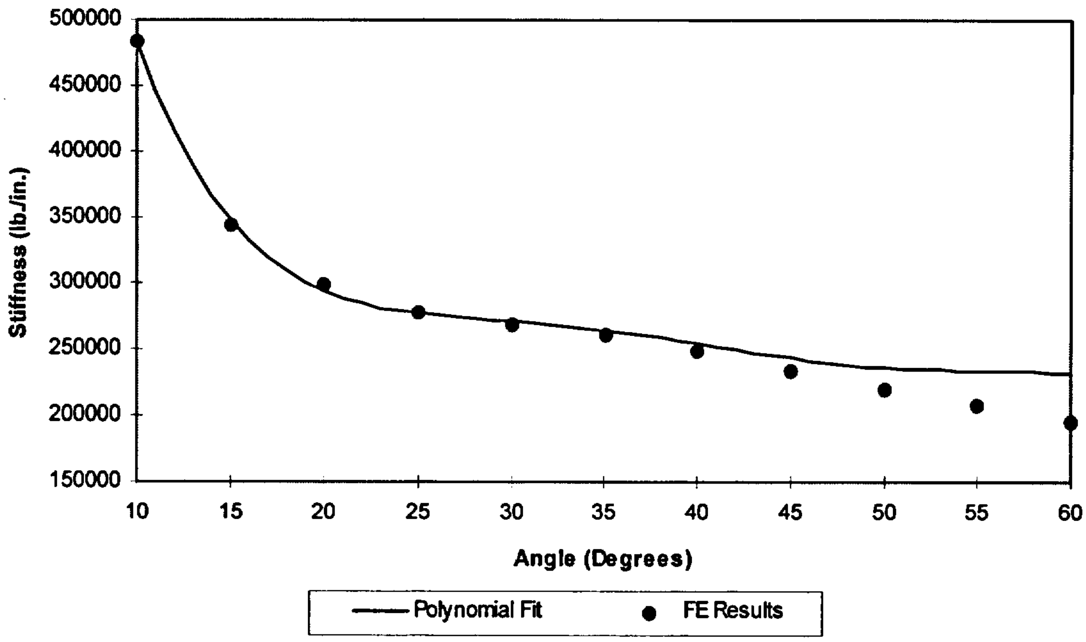

Figure 2.10.3-5
DSC Shell Stiffness Vs. Angle

Table 2.10.3-7
Summary of PWR Fuel Assembly Weights

Fuel Region	Fuel Assembly Component	Weight(1)		Line Load (lb./in.)
		kilograms	pounds	
Bottom Region (8.63")	Grid Spacer	1.30	2.87	-
	Bottom Nozzle/Misc. Steel	8.31	18.32	-
	Support Spacers	4.27	9.42	-
	Region Totals	13.88	30.61	3.55
In-Core Region (141.8")	Fuel(2)	534.39	1,178.33	-
	Cladding	107.10	236.16	-
	Guide/Inst. Tubes	7.97	17.57	-
	Grid Spacers	4.90	10.80	-
	Grid Supports	0.64	1.41	-
	Control Components(3)	42.14	92.92	-
	Region Totals	697.15	1,537.22	10.84
Plenum Region (11.72")	Grid Spacer	1.04	2.29	-
	Guide/Inst. Tubes	0.67	1.48	-
	Cladding	8.28	18.26	-
	Support Spacers	4.27	9.42	-
	Control Components(3)	3.48	7.67	-
	Region Totals	17.74	39.12	3.34
Top Region (3.73")	Holddown Springs	1.80	3.97	-
	Top Nozzle/Misc. Steel	8.96	19.76	-
	Control Components(3)	1.11	2.45	-
	Region Totals	11.87	26.17	7.01
Above Top Region (5.125")	Spider(4)	14.5	31.97	6.24
Fuel Assembly Totals (w/ Control Components)		755.14	1,665.0	-

Notes:

(1) All fuel assembly component weights are taken from Reference [2.8], except as noted.

(2) The weight of the fuel is calculated as the difference between the maximum fuel weight (1,530 pounds) and the total of all other fuel assembly components (not including control components).

(3) The weight of the control components (less the weight of the spider) is assumed to be distributed evenly over the in-core fuel, plenum and top regions.

(4) The reported weight includes the weight of the spider assembly (7.8 pounds per Reference [2.9]) plus the weight of the control components in the above top region.

2.10.3.1.3 Spacer Disc Corner Impact Half Symmetry Model

2.10.3.1.3.1 Model Description

The FC-DSC spacer disc corner impact half symmetry model, shown in Figure 2.10.3-6, is used only to determine the in-plane corner ovalling fundamental frequency. The spacer disc is modeled using 2-D structural solid elements (PLANE42), using the plane stress option with input thickness. Each element consists of 4 nodes, each having two translational degrees of freedom (UX and UY.) The spacer disc plate thickness (1.25 inches) is input as a real constant. The spacer disc is conservatively modeled with ligament widths of 1.660 inches, 1.190 inches, 0.990 inches, 0.810 inches, and 0.675 inches, which are less than the nominal ligament widths of 1.680 inches, 1.210 inches, 1.010 inches, 0.830 inches, and 0.695 inches, respectively.

The spacer disc supports the mass of the fuel assemblies and guide sleeve assemblies in the in-plane direction. The mass of the fuel assemblies and guide sleeves are modeled as structural mass elements (MASS21) distributed to the supporting spacer disc ligaments. The bounding fuel assembly and guide sleeve assembly mass tributary to each of the type "A" and "B" fuel cell openings of 0.231 lb-s^2/inch and 0.235 lb-s^2/inch, respectively, as calculated in Section 2.10.3.1.2.1, are applied to the supporting spacer disc ligaments. Each fuel assembly and guide sleeve is supported by two spacer disc ligaments, having a total of 40 elements with equal widths. The fuel assembly and guide sleeve mass is distributed to the supporting spacer disc ligament nodes based on the nodal tributary widths. Therefore, the fuel and guide sleeve assembly mass is distributed as follows:

Type "A":	Corner nodes	=	0.231/80	=	0.00289 lb/in/sec^2/node
	Mid-span nodes	=	0.231/40	=	0.00578 lb/in/sec^2/node
Type "B":	Corner nodes	=	0.235/80	=	0.00294 lb/in/sec^2/node
	Mid-span nodes	=	0.235/40	=	0.00588 lb/in/sec^2/node

2.10.3.1.3.2 Boundary Conditions

The spacer disc is restrained from radial translation (UX) in the region of contact expected for a typical 30 foot drop through the impact limiter corner. Symmetry boundary displacement constraints are also applied to the nodes lying on the symmetry plane.

2.10.3.1.3.3 Loading

No loads are applied to the spacer disc for the free vibration modal analysis.

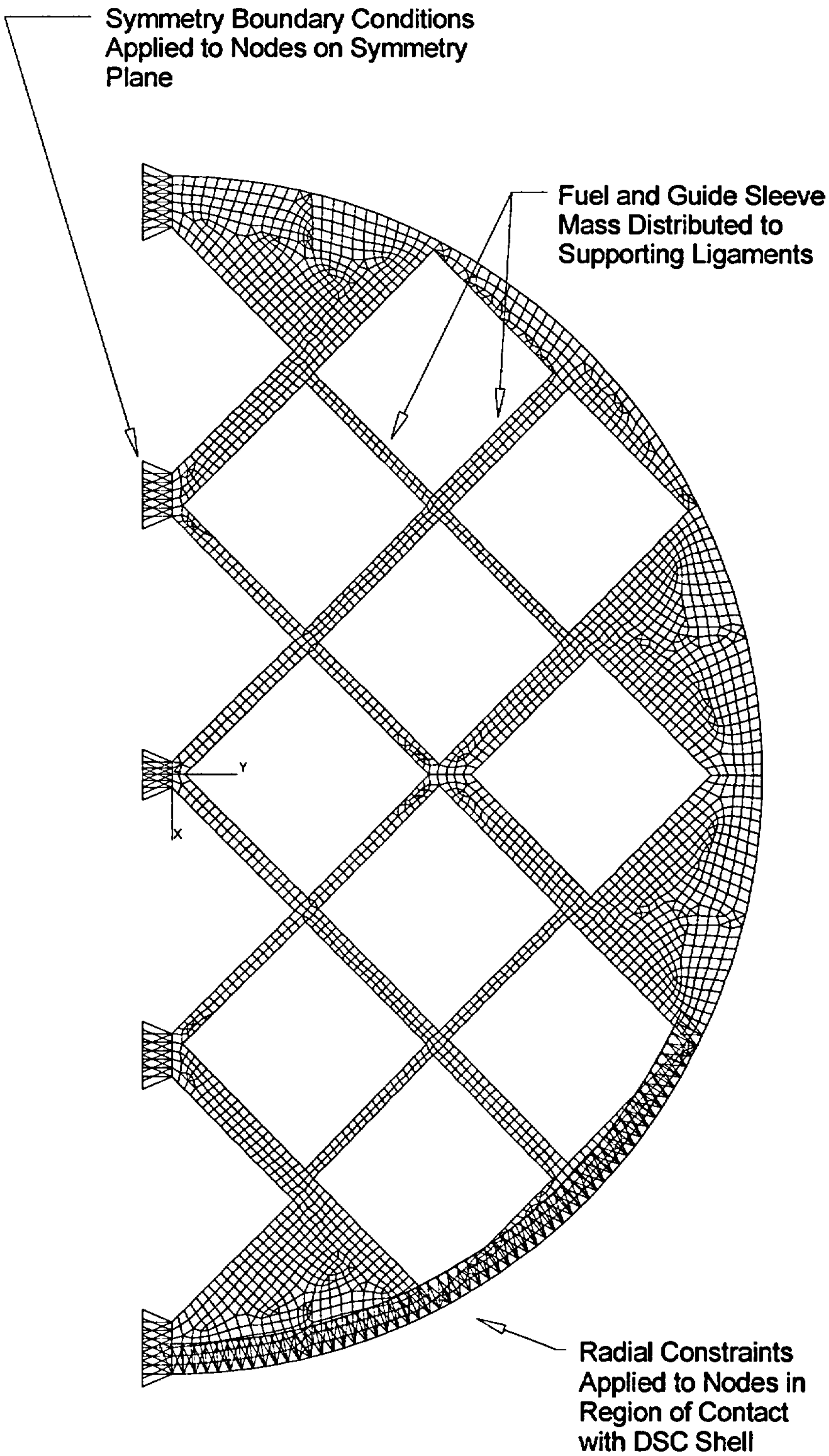

Figure 2.10.3-6
FC Spacer Disc Corner Impact Half Symmetry Model

2.10.3.1.4 Spacer Disc Full Model

2.10.3.1.4.1 Model Description

The full spacer disc finite element model, shown in Figure 2.10.3-7, is used for the corner ovalling modal analysis and all 30 foot corner impact drop analyses. The model consists of 2653 nodes and 2160 elements. The ovalling analysis uses the fundamental frequencies developed in Section 2.10.3.1.3. The full spacer disc is generated by symmetry reflection from the 1/2 symmetry spacer disc model described in Section 2.10.3.1.2. The spacer disc model node numbers and mesh in the upper and lower right side quadrants are shown in Figure 2.10.3-2 and Figure 2.10.3-4, respectively. The node numbers and mesh in the upper and lower left side quadrants are shown in Figure 2.10.3-8 and Figure 2.10.3-9, respectively. The spacer disc is modeled with conservative ligament widths of 1.660 inches, 1.190 inches, 0.990 inches, 0.810 inches, and 0.675 inches based on the specified minimum material condition. The 1.25 inch thickness of the spacer disc is defined by a real constant, and is assumed constant over the element area.

The spacer disc is modeled using 2-D plane stress elements with input thickness (PLANE42) for those load condition in which only in-plane response is expected (i.e. in-plane modal analysis, 30' side drop, and 30' c.g. over corner drop,) and elastic shell elements (SHELL63) for load conditions in which normal loads exist (30' corner oblique drops.) Gap elements (CONTAC12) used to model the interface between the spacer disc and DSC shell. The gap elements are defined by an orientation angle (THETA), a contact stiffness (KN), an initial gap size (GAP) and an initial gap status (STAT). The spacer disc is modeled with uniform gaps of 0.19 inches around the entire circumference, assuming that the spacer disc and DSC shell are initially concentric. The gap orientation angles are defined as the angle to the radial line from the DSC shell node to the spacer disc node, measured positive counterclockwise from the positive Y-axis in degrees.

The contact stiffness is used to model the stiffness of the DSC shell. The radial stiffness of the DSC shell depends on both the radial and longitudinal locations. The shell is stiffest near the top and bottom ends where it is supported radially by the top and bottom end plates and least stiff at the mid-length of the DSC cavity. The stiffness of the shell also increases near the point of contact with the cask inner shell.

The DSC shell stiffness is analyzed using the ANSYS version 4.4A [2.6] half symmetry finite element model discussed in Section 2.10.3.1.5. The shell stiffness at the mid-length of the DSC cavity is conservatively used for the spacer disc drop analyses. The shell stiffness is determined by displacing each node located at the mid-length of the DSC cavity, individually, by 1 inch in the radial direction. The stiffness of the shell at the location of the displaced node is equal to twice the reaction force at the displaced node since the nodes are located on the 1/2 symmetry plane. The stiffness of the DSC shell at the DSC cavity mid-length is determined for circumferential locations of 5° to 60°, at 5° increments, from the point of contact with the cask inner shell. The resulting shell stiffnesses are summarized in Table 2.10.3-6.

The DSC shell stiffness analysis results show that the shell stiffness increases significantly near the point of contact with the cask inner shell. The maximum shell stiffness is assumed to be equal to the shell stiffness at 10° from the initial point of contact. This stiffness is used for all gap elements which are less than 10° from the initial point of contact (45° azimuth). The shell stiffnesses for angles greater than 10° from the initial point of contact are calculated using 5th order polynomial equation curve fit, shown in Figure 2.10.3-5, and given by:

$$K = 1.286 \cdot 10^6 - 1.356 \cdot 10^5 \cdot \theta + 7.157 \cdot 10^3 \cdot \theta^2 - 1.843 \cdot 10^2 \cdot \theta^3 + 2.290\theta^4 - 1.100 \cdot 10^{-2} \cdot \theta^5$$

For the oblique drop condition, in which the spacer disc is loaded in the longitudinal direction, the bending stiffness of the support rods is modeled using torsional spring elements, as discussed in Section 2.10.3.1.1.1. A lower bound support rod bending stiffness of 1.0×10^8 in-lb/radian is conservatively used in the model. The torsional spring elements are attached to the spacer disc nodes nearest the support rod centerline location.

In the case of the modal analysis, the tributary mass of the fuel assemblies and guide sleeve assemblies are modeled as mass elements (MASS21) uniformly distributed to the supporting spacer disc ligaments, as discussed in Section 2.10.3.1.2.1. The full model is used to determine the corner in-plane ovalling mode. For this condition, each fuel assembly and guide sleeve assembly is supported by two adjacent sides of the fuel cell cutout. The mass elements are assumed to act only normal to the ligaments. Therefore, the masses are multiplied by 0.707 so that the resultant mass for the corner ovalling mode equals the total tributary mass.

2.10.3.1.4.2 Boundary Conditions

The full spacer disc model is restrained in the circumferential direction at the nodes located at the initial point of contact and the node 180° away on the perimeter of the disc. The gap element and spring element ground nodes are restrained in all degrees of freedom. The spacer disc nodes nearest the support rod centerline locations are restrained in the longitudinal direction (UY.)

2.10.3.1.4.3 Loading

The spacer disc loading for the full model is developed using the methodology described in Section 2.10.3.1.2.3. As shown in Table 2.10.3-1, spacer disc #24 (i.e., third spacer disc from the top end basket assembly) supports the largest tributary weight and envelopes the maximum spacer disc loads described in Table 2.10.3-2. Therefore, spacer disc #24 provides the bounding spacer disc loads for the 1-foot and 30-foot horizontal side drop conditions.

For oblique drop conditions, the spacer disc tangential (i.e., in-plane) impact load varies with the longitudinal distance from the package center of gravity, x, as follows:

$$P_i \quad = \quad W_i(G_{cg} + \alpha x)(DLF)$$

where tangential acceleration at the package center of gravity, G_{cg}, and the angular acceleration of the package, α, which are calculated for each corner oblique drop condition in Appendix 2.10.9, and the spacer disc DLF corresponding to each impact condition are summarized in Table 2.10.3-10.

The bounding spacer disc in-plane loads for each of the corner oblique drop conditions are summarized in Table 2.10.3-8 and Table 2.10.3-9 for the actual configuration. A review of the tabulated values shows that spacer disc #26 (i.e., the top end spacer disc in Table 2.10.3-8 is the most heavily loaded spacer disc for all corner oblique drop conditions. Therefore, the spacer disc corner oblique drop impact analyses are all performed using the bounding loads from spacer disc #26.

Table 2.10.3-8
FC Spacer Disc Corner Oblique Impact Bounding AnalyticalTangential Loads

Spacer Disc Number	Disc Axial Centerline Location (in.)	Distance from C.G. (in.)	Cold Corner 30° Primary Impact Load (kips)	Hot Corner 30° Primary Impact Load (kips)	Cold Corner Slapdown Impact Load (kips)	Hot Corner Slapdown Impact Load (kips)	Cold Corner 60° Primary Impact Load (kips)	Hot Corner 60° Primary Impact Load (kips)
1	8.625	76.76	114.5	72.9	178.0	125.9	79.9	31.9
2	14.575	70.81	100.5	64.1	156.2	110.4	70.1	28.2
3	20.525	64.86	95.9	61.4	149.1	105.2	66.9	27.0
4	26.475	58.91	91.3	58.7	142.0	100.0	63.7	25.9
5	32.425	52.96	86.7	55.9	134.8	94.9	60.5	24.7
6	38.375	47.01	82.1	53.2	127.7	89.7	57.3	23.6
7	44.325	41.06	77.5	50.5	120.6	84.6	54.1	22.5
8	50.275	35.11	72.9	47.8	113.5	79.4	50.9	21.3
9	56.225	29.16	68.3	45.0	106.3	74.3	47.7	20.2
10	62.175	23.21	63.7	42.3	99.2	69.1	44.6	19.0
11	68.125	17.26	59.1	39.6	92.1	64.0	41.4	17.9
12	74.075	11.31	54.5	36.8	85.0	58.8	38.2	16.7
13	80.025	5.35	49.9	34.1	77.8	53.7	35.0	15.6
14	85.975	0.60	46.2	31.9	72.1	49.5	32.4	14.7
15	91.925	6.55	50.8	34.6	79.3	54.7	35.6	15.8
16	97.875	12.50	55.4	37.4	86.4	59.8	38.8	17.0
17	103.825	18.45	60.0	40.1	93.5	65.0	42.0	18.1
18	109.775	24.40	64.6	42.8	100.6	70.1	45.2	19.3
19	115.725	30.35	69.2	45.6	107.8	75.3	48.4	20.4
20	121.675	36.30	73.8	48.3	114.9	80.5	51.6	21.5
21	127.625	42.25	78.4	51.0	122.0	85.6	54.8	22.7
22	133.575	48.20	83.0	53.8	129.1	90.8	58.0	23.8
23	139.525	54.15	87.6	56.5	136.3	95.9	61.2	25.0
24	145.475	60.10	107.7	69.2	167.5	118.1	75.2	30.5
25	153.875	68.50	66.8	42.7	103.8	73.3	46.6	18.8
26	160.750	75.37	**115.6**	**73.6**	**179.6**	**127.0**	**80.6**	**32.3**
Maximum Impact Load (kips)			115.6	73.6	179.6	127.0	80.6	32.3

Table 2.10.3-9
FC Spacer Disc Corner Oblique Impact Actual Tangential Loads

Spacer Disk Number	Spacer Disc Location: Centerline Location	Spacer Disc Location: Dist. From CG (in)	Disc Total Dead Load (lb)	Cold 30' Corner Drop Load (kips): 30° Primary Impact	Cold 30' Corner Drop Load (kips): Corner Slapdown	Cold 30' Corner Drop Load (kips): 60° Primary Impact
1	6.88	78.645	1,834.4	88.8	142.1	65.3
2	12.38	73.145	2,101.5	97.7	156.3	71.8
3	17.88	67.645	2,101.5	93.6	149.8	68.8
4	23.38	62.145	2,178.0	92.8	148.5	68.2
5	29.38	56.145	2,330.9	94.4	151.0	69.4
6	35.88	49.645	2,445.6	93.4	149.5	68.7
7	42.63	42.895	2,483.8	89.0	142.4	65.5
8	49.38	36.145	2,483.8	83.1	133.0	61.1
9	56.13	29.395	2,483.8	77.1	123.6	56.8
10	62.88	22.645	2,483.8	71.2	114.1	52.5
11	69.63	15.895	2,483.8	65.3	104.7	48.1
12	76.38	9.145	2,483.8	59.4	95.3	43.8
13	83.13	2.395	2,483.8	53.5	85.8	39.4
14	89.88	4.355	2,483.8	55.2	88.6	40.7
15	96.63	11.105	2,483.8	61.1	98.0	45.0
16	103.38	17.855	2,483.8	67.0	107.4	49.4
17	110.13	24.605	2,483.8	73.0	116.9	53.7
18	116.88	31.355	2,445.6	77.7	124.4	57.2
19	123.38	37.855	2,407.4	82.0	131.2	60.3
20	129.88	44.355	2,407.4	87.5	140.0	64.4
21	136.38	50.855	2,407.4	93.0	148.8	68.4
22	142.88	57.355	2,330.9	95.4	152.6	70.2
23	148.88	63.355	2,216.2	95.4	152.6	70.1
24	154.63	69.105	1,120.3	50.5	80.8	37.1
25	159.50	73.980	1,589.4	74.4	118.9	54.7
26	160.75	75.230	1,589.4	75.1	120.0	55.2
Corner Drop Maximums:				**97.7 kip**	**156.3 kip**	**71.8 kip**

Note: Hot drop loads are enveloped by cold drop loads. Thus, only cold drop loads are listed.

trib_wt7.xls

Table 2.10.3-10
FC Spacer Disc Corner Oblique Drop Impact Loads

Impact Orientation	Ambient Condition	Tangential Acceleration at C.G. (g's)	Angular Acceleration at C.G. (rad/sec.)	Dynamic Load Factor (DLF)
Corner 30° Primary Impact	Cold	19.9	130.0	1.03
	Hot	13.9	77.9	1.02
Corner 30° Slapdown Impact	Cold	25.0	162.0	1.28
	Hot	18.3	125.0	1.20
Corner 60° Primary Impact	Cold	14.1	91.1	1.02
	Hot	6.4	32.6	1.02

The in-plane loads due to the weight of the fuel assemblies and guide sleeve assemblies tributary to the spacer disc are modeled as a uniform pressure load acting on the supporting spacer disc ligaments. Edge pressures applied to elastic shell elements are input on a force per unit length basis. As shown in Section 2.10.3.1.2.3, the in-plane pressure loads due on the type "A" and "B" ligaments to an equivalent static deceleration, G, for the 1-foot and 30-foot flatside horizontal drop conditions are 9.32xG psi and 9.40xG psi, respectively. Similarly, the in-plane pressure loads due on the type "A" and "B" ligaments due to an equivalent static deceleration, G, for the 30-foot flatside oblique drop conditions are 8.53xG psi and 8.55xG psi, respectively.

In addition to the in-plane pressure loads due to the fuel assemblies and guide sleeve assemblies, longitudinal equivalent static accelerations are applied for the oblique drop conditions to determine the out-of-plane bending stresses due to the spacer disc self weight.

The spacer disc loading is applied in the following sequence:

1.) A vertical displacement of 0.1901 inches is applied to the node at the initial point of contact (θ = -45°) in the first load step to bring the spacer disc into contact with the DSC shell.

2.) The vertical displacement constraint applied to the spacer disc to close the gaps in the initial contact region is removed. The spacer disc drop loads are applied.

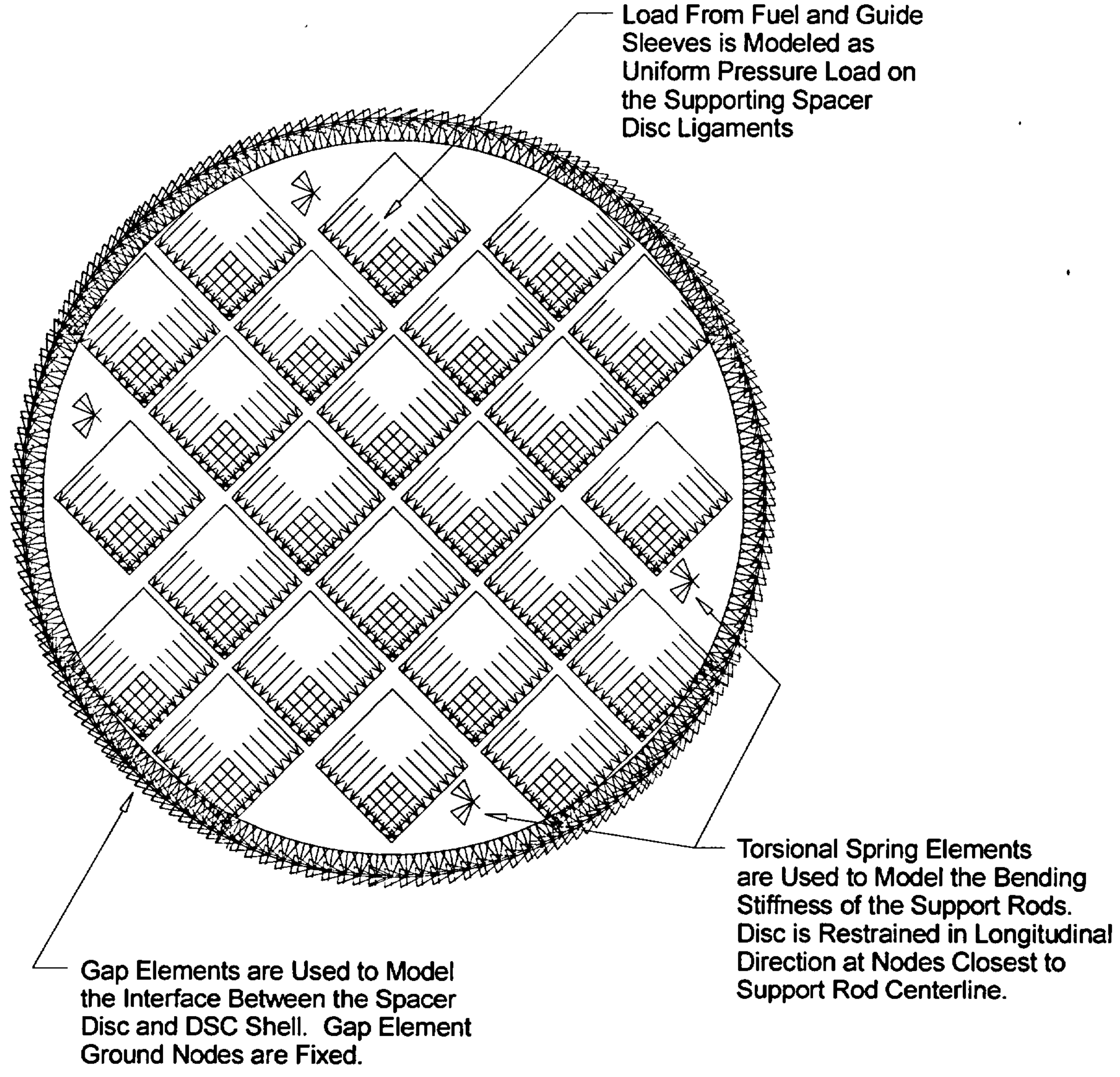

Figure 2.10.3-7
FC-DSC Spacer Disc Full Model

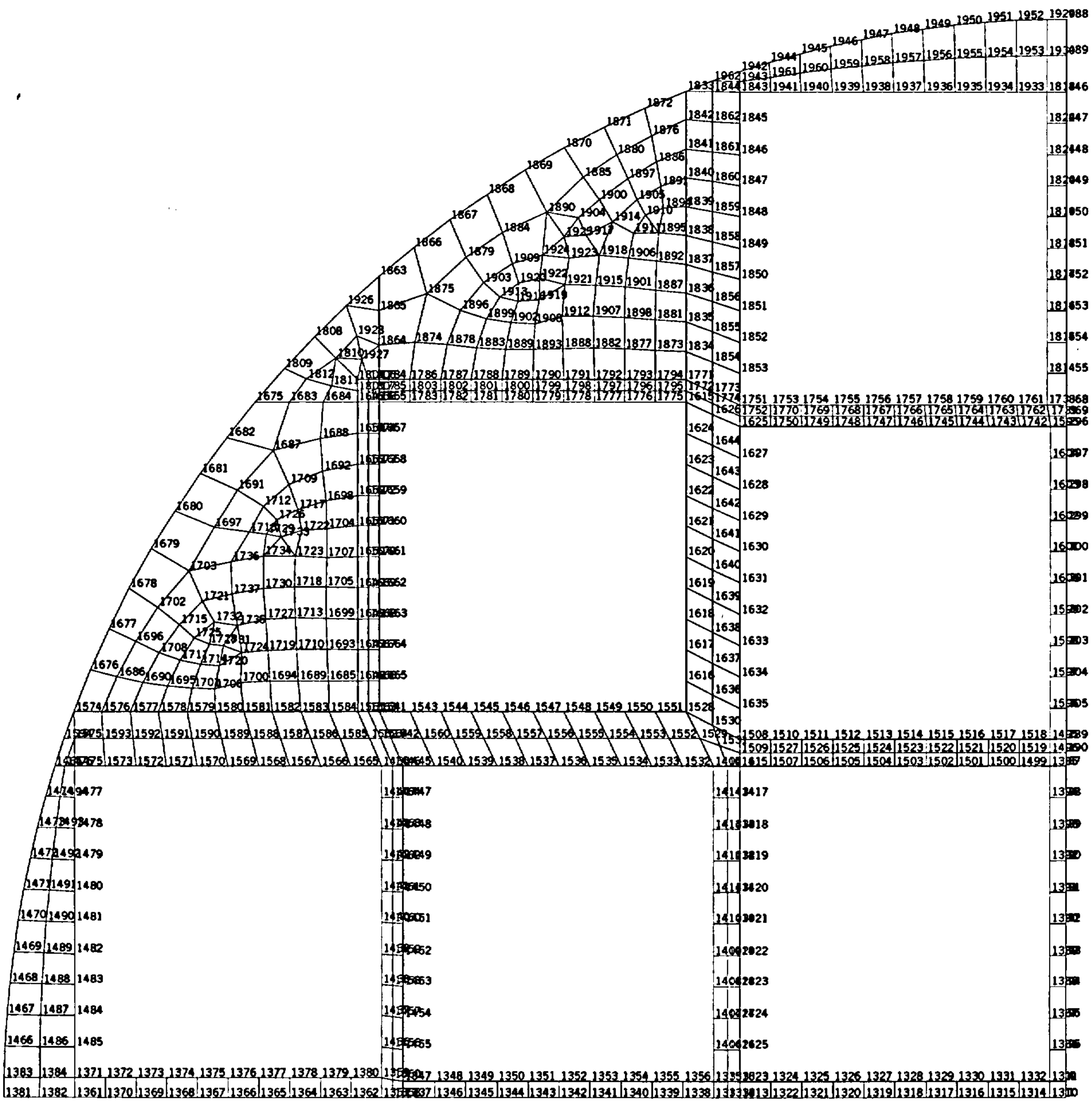

Figure 2.10.3-8
FC Spacer Disc Full Model Node Numbers - Upper Left Quadrant

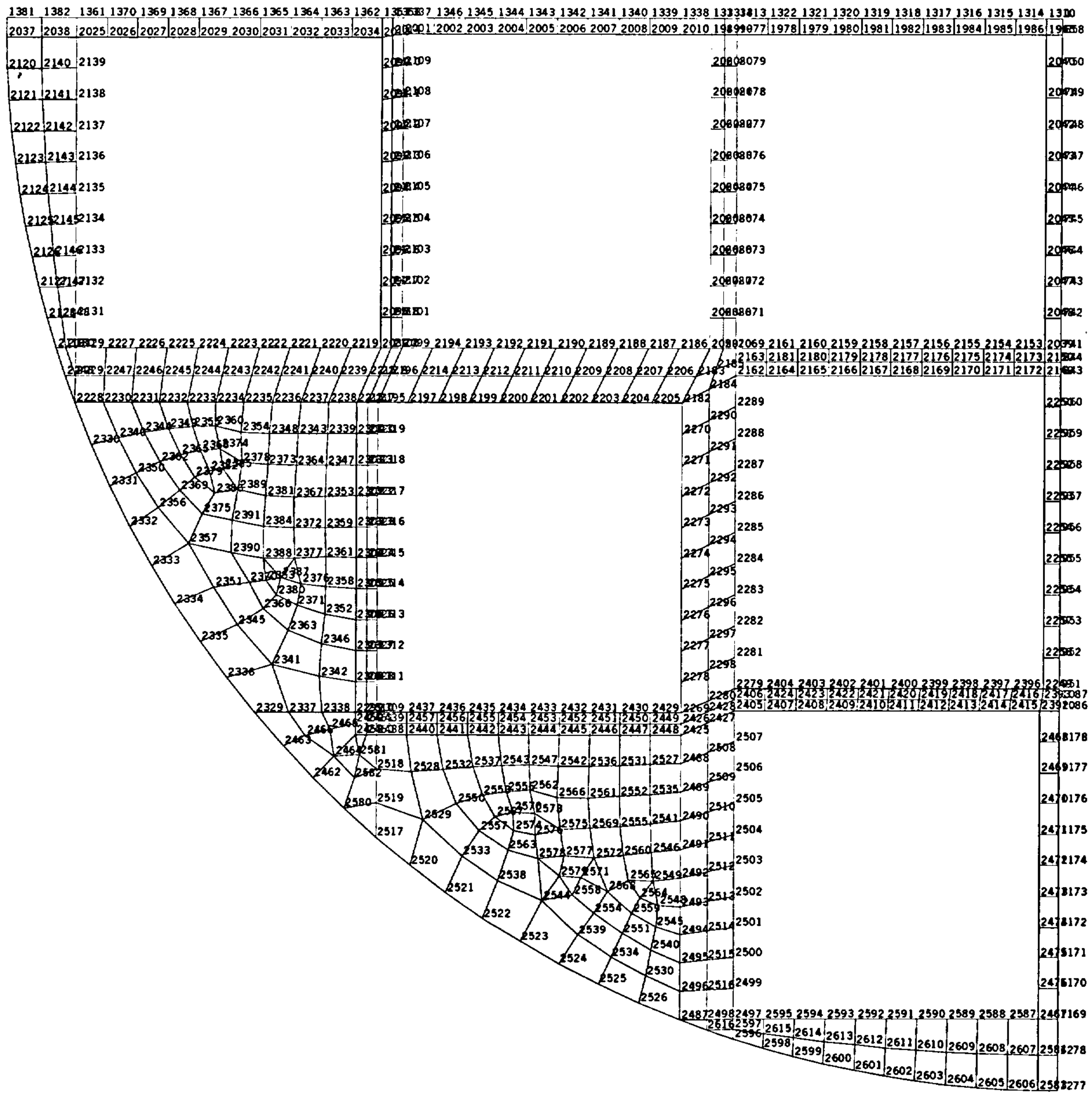

Figure 2.10.3-9
FC Spacer Disc Full Model Node Numbers - Lower Left Quadrant

2.10.3.1.5 DSC Shell 1/2 Symmetry Model

2.10.3.1.5.1 Model Description

The DSC shell stiffness is analyzed using the ANSYS v4.4A [2.6] half symmetry finite element model shown in Figure 2.10.3-10. The model includes the DSC shell modeled from the mid-span to the bottom end of the DSC cavity. The DSC shell is modeled using quadrilateral shell elements (STIF63) defined by four nodes, each having 3 translational and 3 rotational degrees of freedom. The 0.625 inch thickness of the DSC shell is input as a real constant.

2.10.3.1.5.2 Boundary Conditions

Symmetry boundary conditions are applied to the nodes located at the mid-span of the DSC shell cavity and along the half-symmetry plane. The nodes located at the bottom end of the cavity are restrained in all degrees of freedom. The analytical model boundary conditions are shown in Figure 2.10.3-10.

2.10.3.1.5.3 Loading

The shell stiffness at the mid-length of the DSC cavity is conservatively used for the spacer disc drop analyses. The shell stiffness is determined by displacing each node located at the mid-length of the DSC cavity, individually, by 1 inch in the radial direction. The stiffness of the shell at the location of the displaced node is equal to twice the reaction force at the displaced node since the nodes are located on the 1/2 symmetry plane. The stiffness of the DSC shell at the DSC cavity mid-length is determined for circumferential locations of 5° to 60°, at 5° increments, from the point of contact with the cask inner shell.

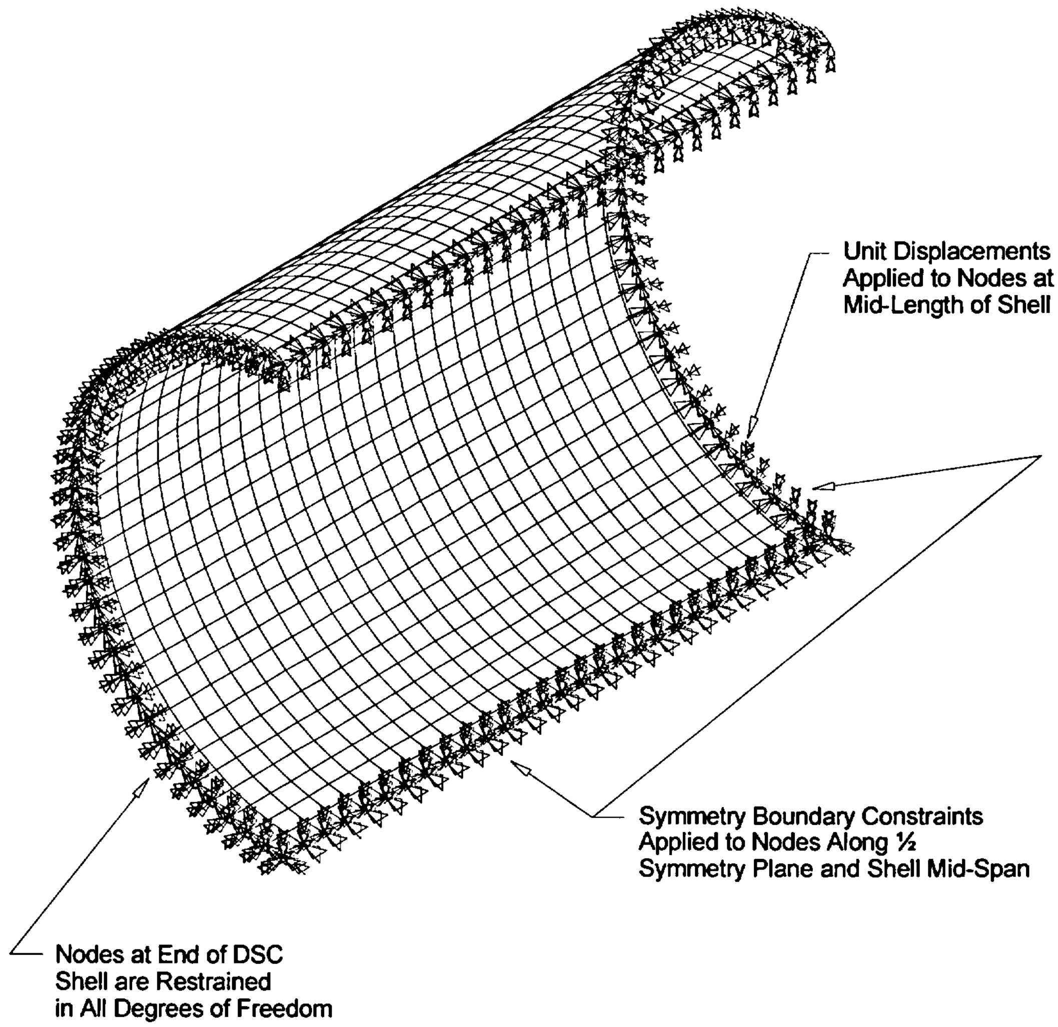

Figure 2.10.3-10
DSC Shell 1/2 Symmetry Model

2.10.3.1.6 Guide Sleeve 1/2 Symmetry Periodic Model

2.10.3.1.6.1 Model Description

The NUHOMS®-MP187 guide sleeves are analyzed for the 1' side drop conditions using the half symmetry finite element model shown in Figure 2.10.3-12. As illustrated in Figure 2.10.3-11, a periodic longitudinal section of the guide sleeve, from the centerline of a spacer disc to the middle of the span between spacer discs, is modeled, taking advantage of symmetry. The guide sleeve is modeled using 3-D shell elements having a uniform thickness of 0.12 inches.

The mass of the neutron absorber sheets and oversleeves are accounted for by adjusting the material density used for the guide sleeve as follows:

$$\rho' = [\rho_{ss}(A_{gs} + A_{os}) + \rho_{al}A_{nas}]/A_{gs}$$

where;

ρ_{ss} = 0.2853 lb/in^3, Density of Stainless Steel

ρ_{al} = 0.098 lb/in^3, Density of Aluminum

A_{gs} = Area of guide sleeve

= $4(8.90 + 0.12)(0.12)$

= 4.33 in^2

A_{os} = Area of Oversleeves

= $4(8.71 + 2(0.12 + 0.085))(0.0178)$

= 0.65 in^2

A_{nas} = Area of Neutron Absorber Sheets

= $4(8.59)(0.085)$

= 2.92 in^2

Therefore, the adjusted density of the guidesleeve is:

$$\rho' = [0.2853(4.33 + 0.65) + 0.098(2.92)]/4.33$$

$$= 0.3942 \text{ lb/in}^3$$

Gap elements are used to model the interface between the guide sleeve bottom panel and the spacer disc ligament. The gap elements are oriented normal to the surface of the guide sleeve bottom panel and assumed to be initially closed and not sliding. An interface stiffness of 1.0×10^6 pounds per inch is used for the gap elements.

2.10.3.1.6.2 Boundary Conditions

Symmetry boundary displacement constraints are applied to the nodes lying on the half symmetry plane, on the plane located at the spacer disc centerline, and on the plane at the midspan between the spacer discs. The gap element ground nodes are restrained in all degrees of freedom.

2.10.3.1.6.3 Loading

The pressure load due to the fuel assembly and the equivalent static acceleration load are applied to the model for the hot and cold 1' side drop conditions. The equivalent static pressure load on the guide sleeve panel due to the fuel assembly weight is calculated as follows:

$$p = Gw/b$$

where the fuel line load, w, is 10.84 pounds per inch and the guide sleeve panel width, b, is the width of the bottom panel of the guide sleeve.

An equivalent static acceleration load is also applied to the model to account for the load due to the self weight of the guide sleeve assembly.

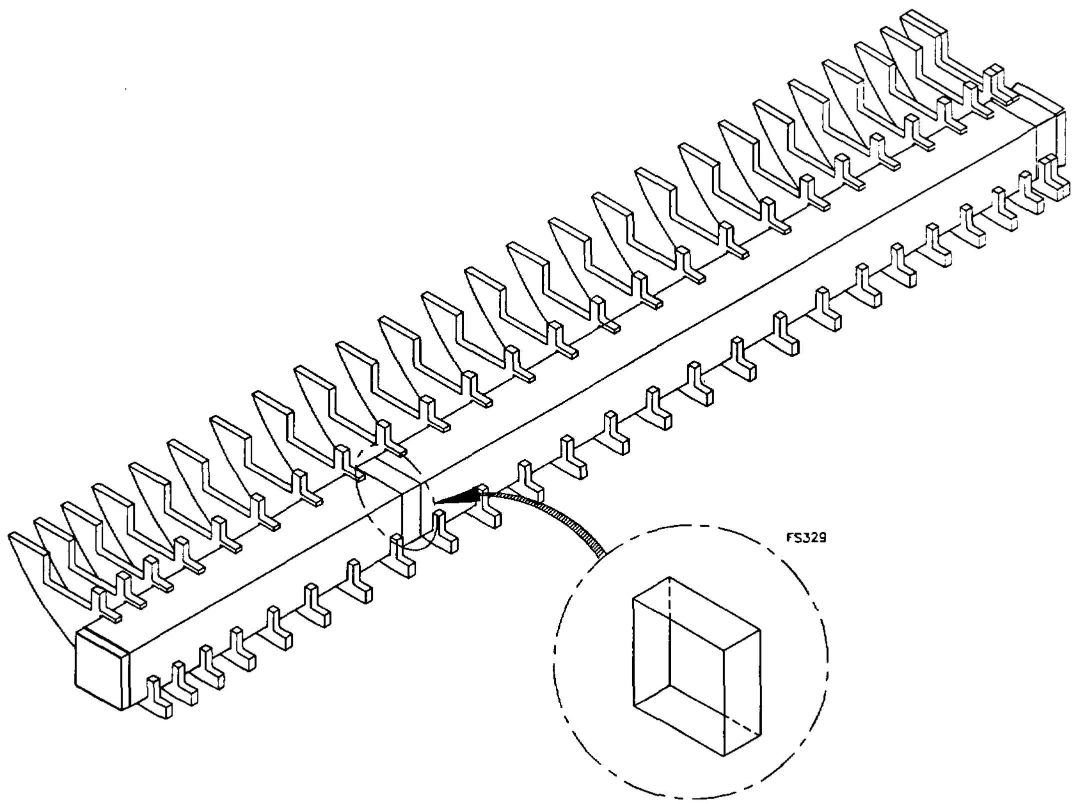

Figure 2.10.3-11
Guide Sleeve Model Periodic Segment

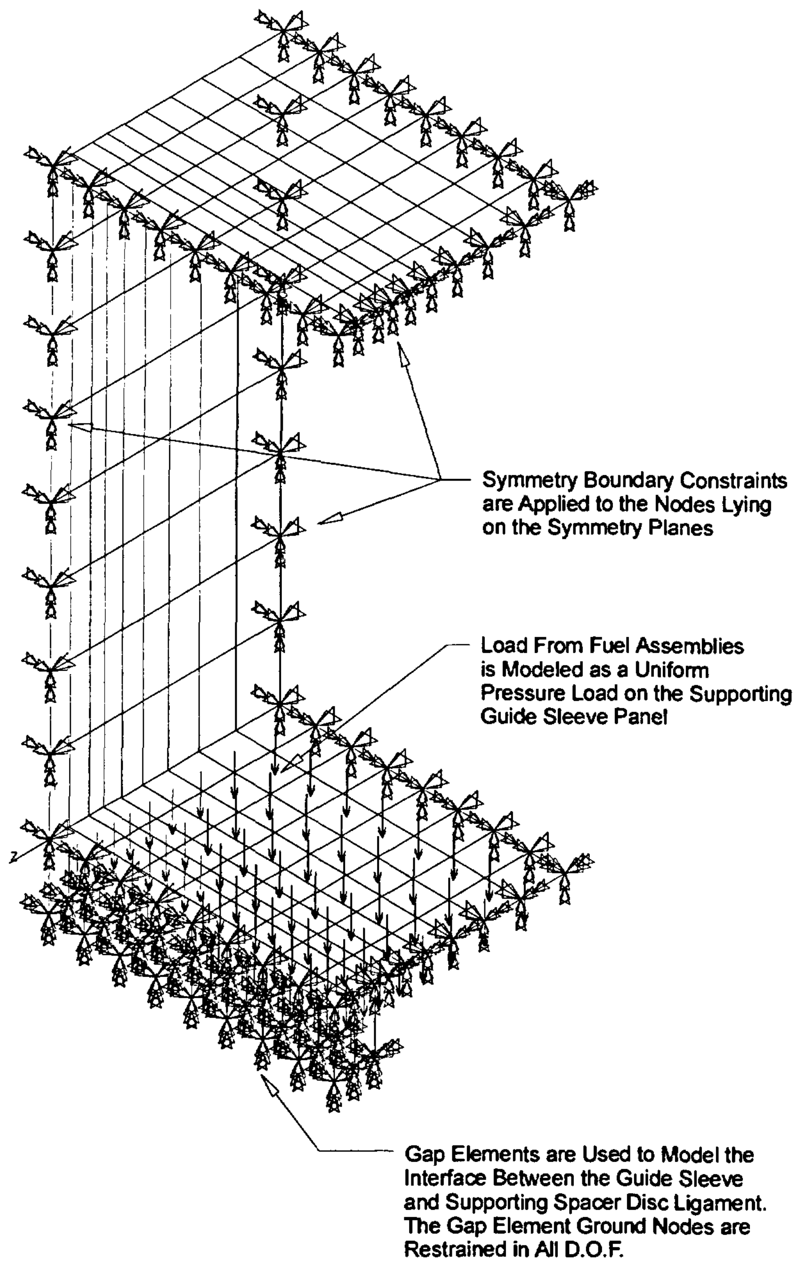

Figure 2.10.3-12
Guide Sleeve 1/2 Symmetry Periodic Model

2.10.3.1.7 Finite Element Model Input Files

THIS SECTION CONTAINS
PROPRIETARY INFORMATION

2.10.4 FF-DSC Basket Assembly Finite Element Analysis

2.10.4.1 FF-DSC Basket Assembly Model Descriptions

The complete analysis of the FF-DSC Basket Assembly was performed using a combination of classical hand calculations and finite element analysis. Only the spacer discs are analyzed using the finite element method. All of the FF-DSC basket assembly finite element analysis models were generated using the ANSYS PREP7 routine. The type of element varies depending on the type of analysis, and the choice of element is discussed in the relevant sections. The loads are applied as discussed in Section 2.10.4.1.1. While the canister is not modeled, the interactions between the spacer discs and the canister and/or the support plates are considered, and when necessary, these effects are included in the finite element models. The formulation of the spacer disc and canister interaction, and other boundary conditions, is discussed in Section 2.10.4.1.2.

The analyses documented herein are based on the SA-537, Class 2 carbon steel basket option for fabrication of the FF-DSC. Appendix 2.10.13 provides an evaluation of the XM-19 basket design option for the FF-DSC which addresses the alternate basket assembly material (SA-240, Type XM-19 austenitic stainless steel) as well as other configuration modifications.

2.10.4.1.1 Loading

2.10.4.1.1.1 Thermal Loading

The spacer disc temperature distribution resulting from normal and hypothetical accident thermal conditions are applied to the spacer disc finite element model as nodal temperature constraints (note: the spacer disc temperature distributions bound the Thermal Evaluation presented in Chapter 3). The FF-DSC spacer disc thermal stresses are determined for two conditions: (1) -20°F ambient temperature, maximum decay heat and zero insolation, and (2) 100°F ambient temperature, maximum decay heat and maximum insolation. The spacer disc thermal gradients resulting from the cold normal condition (-40°F ambient temperature, zero insolation, maximum decay heat) are approximately equal to those due to the -20°F ambient condition. Consequently, the -20°F ambient thermal condition is used for the cold thermal condition analysis.

The spacer disc temperature distributions for the 100°F and -20°F ambient conditions are shown in Figure 2.10.4-1 and Figure 2.10.4-2, respectively.

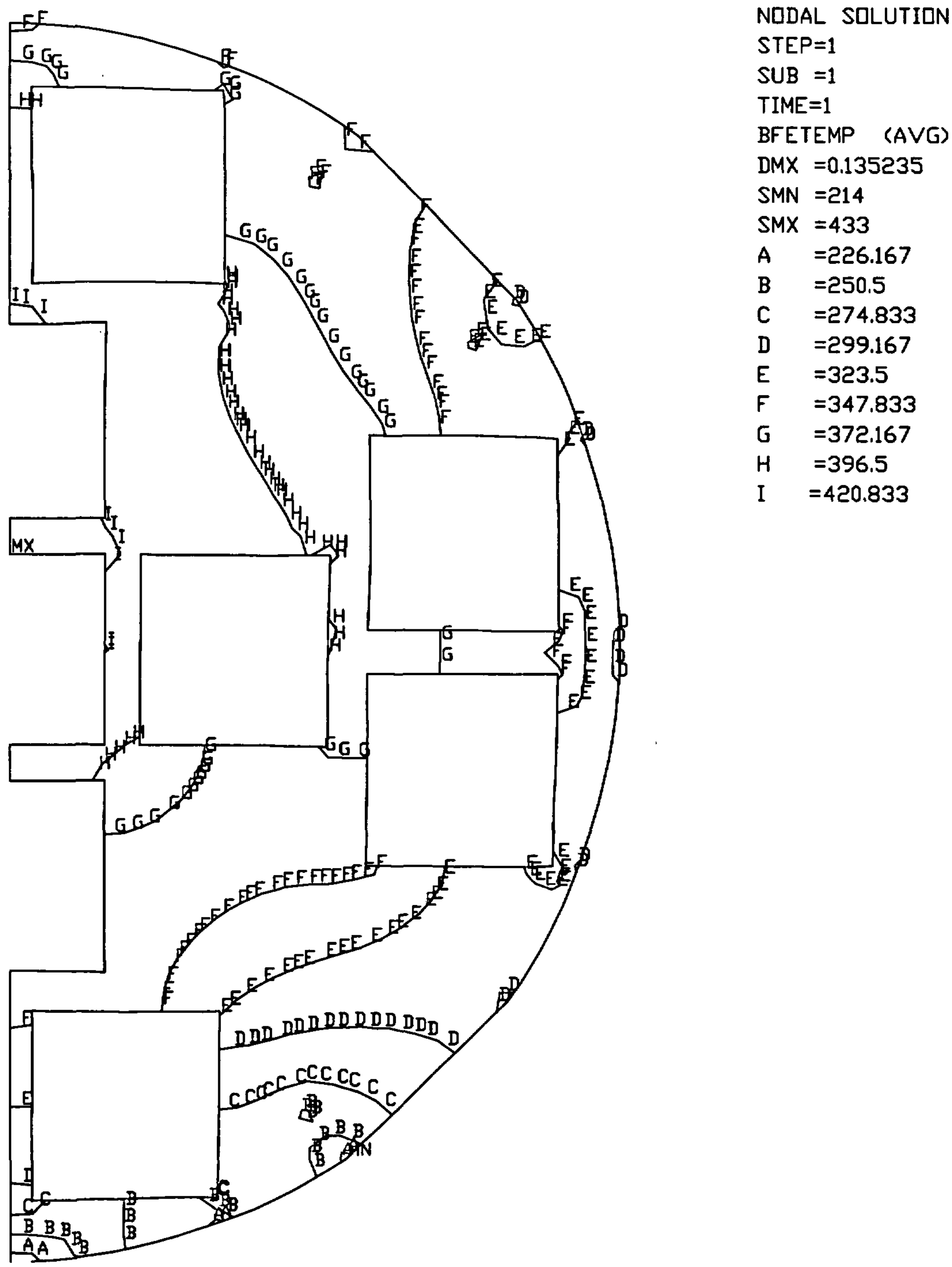

Figure 2.10.4-1
FF Spacer Disc Temperature Distribution for 100°F Ambient Condition

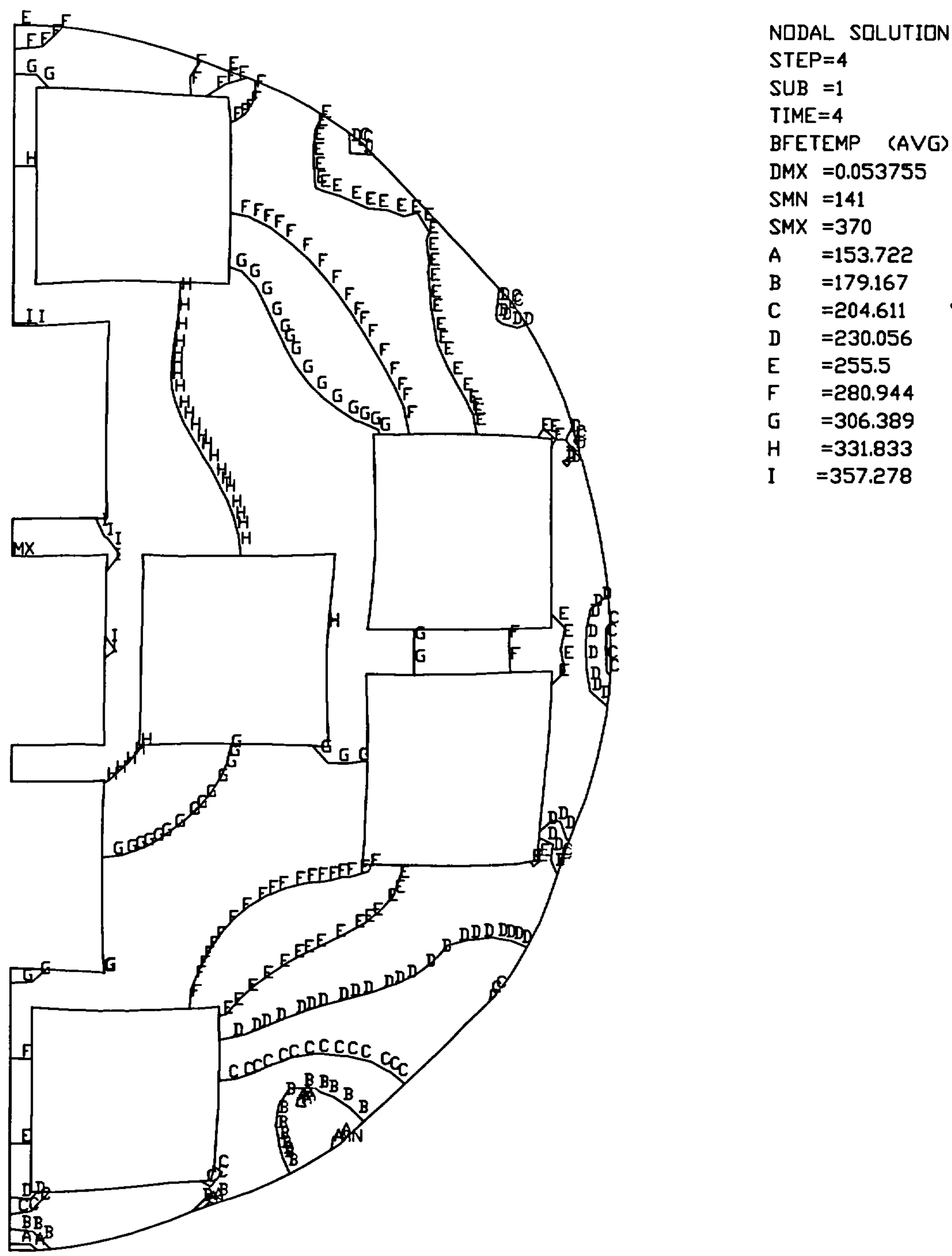

Figure 2.10.4-2
FF Spacer Disc Temperature Distribution for -20°F Ambient Condition

2.10.4.1.1.2 Drop Loading

The drop analysis is performed for the single spacer disc which supports the largest total tributary weight of the fuel assemblies and fuel can assemblies in addition to its own self weight. The maximum weight of a single PWR fuel assembly is 1,530 pounds [2.8]. The weight distribution of a B&W 15X15 Mark B (PWR) fuel assembly over the four major axial regions is summarized in Table 2.10.4-1. The fuel assembly tributary weights are determined by multiplying the fuel region line loads by the respective tributary widths.

Each fuel can assembly consists of a fuel can body (tube), top lid subassembly, and bottom lid subassembly. The weight of the fuel can body tributary to each spacer disc is calculated by multiplying the fuel can body line load by the spacer disc tributary widths. The line weight of a single fuel can body, w_{tube}, is:

$$w_{tube} = (9.5^2 - 9.0^2)(0.2853)$$

$$= 2.64 \text{ lbs./in.}$$

The weights of the remaining fuel can assembly components are distributed to the spacer discs based on location. The weights of the other fuel can assembly components are:

Fuel can top lid subassembly = 52.64 lbs.

Fuel can bottom lid subassembly = 18.39 lbs.

The weight of the support plates tributary to each spacer disc is calculated by multiplying the support plate line load by the spacer disc tributary widths. The support plate line load, w_{supt}, is:

$$w_{supt} = 4x(12.0 \times 4.0)(0.2835)$$

$$= 54.4 \text{ lbs./in.}$$

The tributary widths of the spacer discs are calculated as follows:

$$b_{\#1}\text{(bottom)} = 8.00 + (11.25/2)$$

	=	13.63 in.
$b_{\#2\text{-}\#13}$	≡	11.25 in.
$b_{\#14}$	=	(11.25 + 9.50)/2
	=	10.38
$b_{\#15}$(top)	=	(9.50/2) + (172.50 - 163.75)
	=	13.50 in.

Therefore, the weight of fuel can, fuel and support plate tributary to the spacer disc through 15 are:

$$W_i = W_{\text{fuel can body}} + W_{\text{fuel}} + W_{\text{support plate}}$$

$$W_1 = [18.39 + (2.64)(13.63) + (8.63)(3.55) + (13.63 - 8.63)(10.19)](13) + (54.4)(13.63)$$

$$= 2{,}509 \text{ lbs.}$$

$$W_2 - W_{13} = (2.64 + 10.19)(11.25)(13) + (54.4)(11.25)$$

$$= 2{,}488 \text{ lbs.}$$

$$W_{14} = [(2.64)(10.38) + (10.19)(10.38 + 13.50 - 4.00 - 3.73 - 11.72) + (2.68)(4.00 + 3.73 + 11.72 - 13.50)](13) + (54.4)(10.38) = 1{,}715 \text{ lbs.}$$

$$W_{15} = [(2.64)(13.50) + 52.64 + (2.68)(13.5 - 4.0 - 3.73) + (6.36)(3.73)](13) + (54.4)(13.50)$$

$$= 2{,}391.5 \text{ lbs.}$$

Spacer disc #1 (bottom end disc) supports the largest tributary weight. Therefore, the spacer disc drop analysis will be performed for the bottom end spacer discs only.

The spacer discs support the load due to the fuel cans and fuel assemblies in the tangential direction (in-plane) only. The fuel cans and fuel assemblies are not mechanically fastened to the basket structure, and thus, are free to move in the longitudinal direction. Therefore, the longitudinal loads due to the fuel can and fuel assemblies are transferred directly through the

DSC end plates to the cask body. The in-plane load due to the weight of the fuel assemblies and fuel can assemblies is modeled as a uniform pressure load acting on the supporting spacer disc ligaments. The in-plane pressure load due to an impact equivalent static deceleration (G_s) is calculated as follows:

$$q = WG_s/bt$$

where;

W	≡	Tributary weight of a single fuel can and fuel assembly
	=	18.39 + (2.64)13.63 + (8.63)3.55 + (13.63 - 8.63)10.19
	=	136 lb.
G_s	≡	Equivalent static tangential deceleration due to drop condition
b	=	10.15 in., Modeled ligament width
t	=	2.0 in, spacer disc thickness

Therefore,

$$q = (136 \times G_s)/(10.15 \times 2.0)$$

$$= 6.7 \times G_s \text{(psi)}$$

The equivalent static deceleration value is arrived at by multiplying the appropriate DLF (Appendix 2.10.10) by the peak rigid body impact deceleration (Appendix 2.10.9). The resulting values are listed in Table 2.7.7-2.

Table 2.10.4-1
Summary of PWR Fuel Assembly Weights

Fuel Region	Fuel Assembly Component	Weight[1]		Line Load
		kilograms	pounds	(lb./in.)
Bottom Region (8.63")	Grid Spacer	1.30	2.87	-
	Bottom Nozzle/Misc. Steel	8.31	18.32	-
	Support Spacers	4.27	9.42	-
	Region Totals	**13.88**	**30.61**	**3.55**
In-Core Region (141.8")	Fuel[2]	534.39	1,178.33	-
	Cladding	107.10	236.16	-
	Guide/Inst. Tubes	7.97	17.57	-
	Grid Spacers	4.90	10.80	-
	Grid Supports	0.64	1.41	-
	Region Totals	**655.12**	**1,444.3**	**10.19**
Plenum Region (11.72")	Grid Spacer	1.04	2.29	-
	Guide/Inst. Tubes	0.67	1.48	-
	Cladding	8.28	18.26	-
	Support Spacers	4.27	9.42	-
	Region Totals	**14.27**	**31.45**	**2.68**
Top Region (3.73")	Hold Down Springs	1.80	3.97	-
	Top Nozzle/Misc. Steel	8.96	19.76	-
	Region Totals	**10.76**	**23.72**	**6.36**
Fuel Assembly Totals (w/o Control Components)		694.0	1,530.0	-

Note:

(1) The weight of the fuel is calculated as the difference between the maximum fuel weight (1,530 pounds) and the total of all other fuel assembly components (not including control components).

2.10.4.1.1.3 Vibration Loading

As presented in Section 2.6.4, a 2g vertical vibration load is applied to the disc in the orientation in which it is transported.

2.10.4.1.1.4 Modal Mass Loadings

In the case of the modal analyses only, the mass of the fuel assemblies and fuel can bodies are modeled as structural mass elements (MASS21) distributed to the supporting spacer disc ligaments. The fuel assemblies and fuel can body assemblies are supported by the DSC shield plugs in the axial direction. Therefore, the spacer discs support the weight of the fuel assemblies and fuel can body assemblies in only the transverse (radial) direction. The load on the spacer disc ligaments resulting from the decelerated mass of the fuel assemblies and fuel can bodies is applied as nodal mass elements on the spacer disc ligaments as follows:

The maximum weight of the PWR fuel assemblies is in the active fuel region. The line load for a fuel assembly is developed by assuming that all of the fuel component weight (Table 2.10.4-1) is distributed over the in-core region (141.8 inches) as follows:

$$\begin{aligned} W &= 1444.3/141.8 \\ &= 10.19 \text{ lb/in} \end{aligned}$$

Therefore, the fuel assembly tributary weight supported per disc is:

$$\begin{aligned} \text{Fuel} &= (10.19)(11.25) \\ &= 115 \text{ lbs.} \end{aligned}$$

The tributary weight of a single fuel can body is:

$$\begin{aligned} \text{Tube} &= (0.25)(4\text{x}9.0)(11.25)(0.2853) \\ &= 29 \text{ lbs.} \end{aligned}$$

The total tributary weight of a fuel assembly and fuel can body on each spacer disc ligament is:

$$W_t = 115 + 29$$
$$= 144 \text{ lbs.}$$

The mass of the fuel assemblies and fuel can bodies is distributed uniformly to the supporting spacer disc ligaments as lump masses at ligament nodes based on the nodal tributary widths.

2.10.4.1.2 Boundary Conditions

2.10.4.1.2.1 DSC Interface with Spacer Discs

The interface between the spacer disc and DSC shell is modeled using 2-D interface (gap) elements. The gap is defined by an orientation angle (THETA), a contact stiffness (KN), an initial gap size (GAP) and an initial gap status (STAT). The spacer disc is modeled with uniform gaps of 0.22 inches around the entire circumference, assuming that the spacer disc and DSC shell are initially concentric. The gap orientation angles are defined as the angle to the radial line from the DSC shell node to the spacer disc node, measured positive counterclockwise from the positive Y-axis in degrees. The shell stiffnesses at an angle, θ, measured relative to the initial point of contact, are calculated using 5^{th} order polynomial equation curve fit. The contact stiffness formulation was developed in Appendix 2.10.3.

$$KN = 1.286 \cdot 10^6 - 1.356 \cdot 10^5 \cdot \theta + 7.157 \cdot 10^3 \cdot \theta^2 - 1.843 \cdot 10^2 \cdot \theta^3 + 2.290 \cdot \theta^4 - 1.100 \cdot 10^{-2} \cdot \theta^5$$

2.10.4.1.2.2 Support Plate Interface with Spacer Disc

The support plates provide rotational stiffness to the spacer discs for out-of-plane bending. The bending stiffness of the support plates is modeled using torsional spring elements to model the rotational stiffness of the support plates. The support plate rotational stiffness is calculated as follows:

$$k = M_o/\theta$$
$$\theta = (M_o/2)L/3EI, \text{ Assuming moment equally distributed}$$
$$k = 6EI/L$$

where;

E	=	27.7×10^6 psi, Elastic Modulus of carbon steel at 500°F
I	=	$bh^3/12$, Moment of Inertia of a single support plate
	=	$(12)(2.0)^3/12$
	=	$8.0\ in^4$
L	=	5.625 inches, 1/2 of spacer disc pitch

therefore,

$$k = (6)(27.7 \cdot 10^6)(8.0)/(5.625)$$
$$= 2.36 \times 10^8 \text{ in-lb/radian}$$

The support plate stiffness is evenly distributed to the eleven nodes on the outer edge of the spacer disc in the support plate region. The spring stiffness per node is 2.15×10^7 in-lb/radian ($=2.36 \times 10^8/11$). A lower bound spring stiffness of 2.2×10^7 in-lb/radian is conservatively used only in the spacer disc 1/4 symmetry model for end drop analysis. The moment reactions due to the end drop are used for the spacer disc to support plate weld evaluation.

2.10.4.1.2.3 Other Boundary Condition

The spacer disc is restrained in the longitudinal direction at the nodes along the outer edge of the support plate region. Symmetry boundary conditions are applied to the nodes lying on the 1/4 or 1/2 symmetry planes. The support plate torsional spring element ground nodes are restrained in all DOF.

2.10.4.1.3 Quarter Symmetry Models

Only the 30 foot end drop was analyzed using the quarter symmetry model shown in Figure 2.10.4-3 and Figure 2.10.4-4. The model consists of 588 nodes and 525 elements. The boundary conditions and loadings are applied as shown in Figure 2.10.4-3. The spacer disc node numbers are shown in Figure 2.10.4-4. The spacer disc is modeled using quadrilateral stress elements (SHELL63) having 3 transitional and 3 rotational degrees of freedom and input thickness. The input file for this model is provided in Section 2.10.4.2.2.

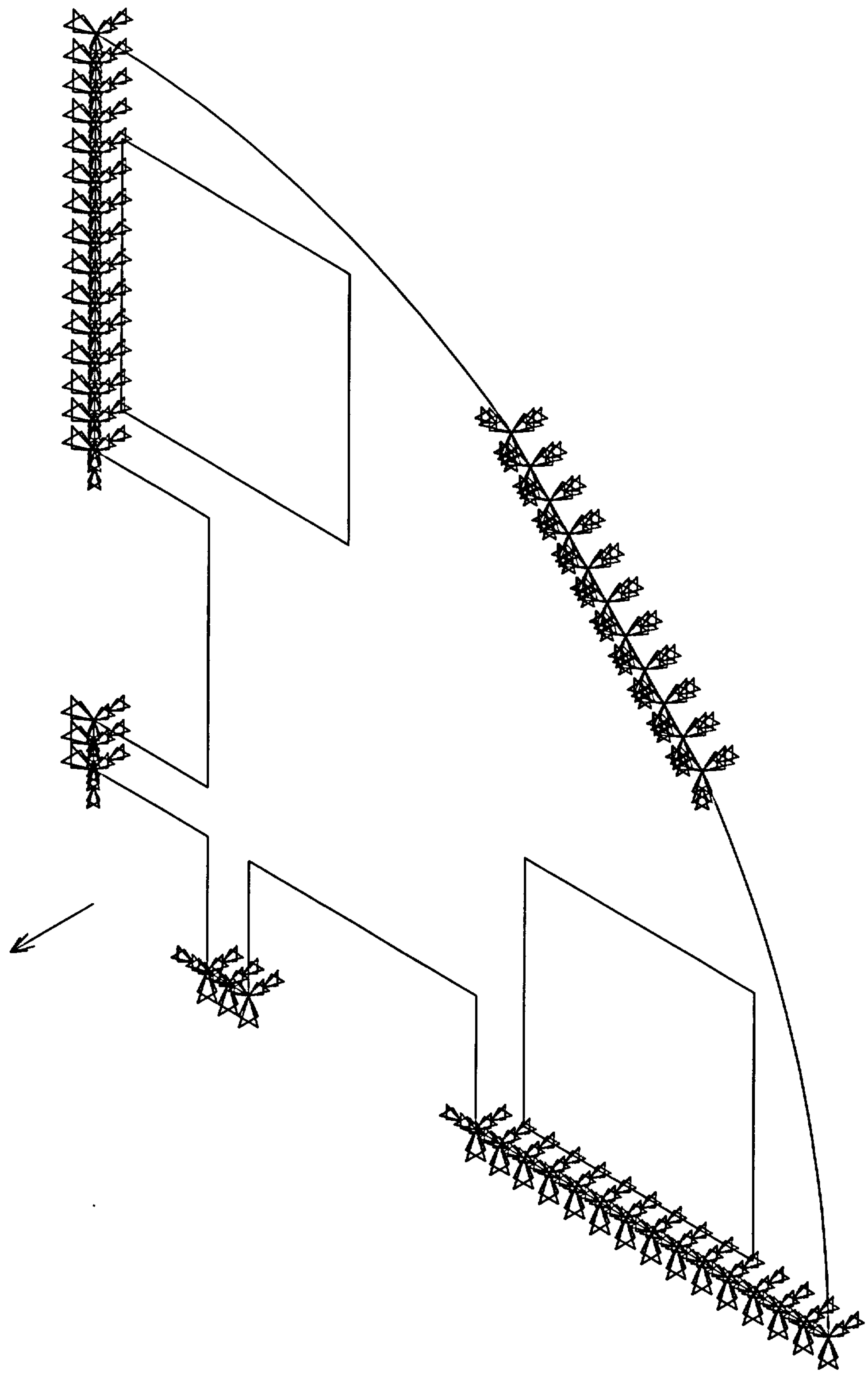

Figure 2.10.4-3
FF Spacer Disc Quarter Symmetry End Drop Model

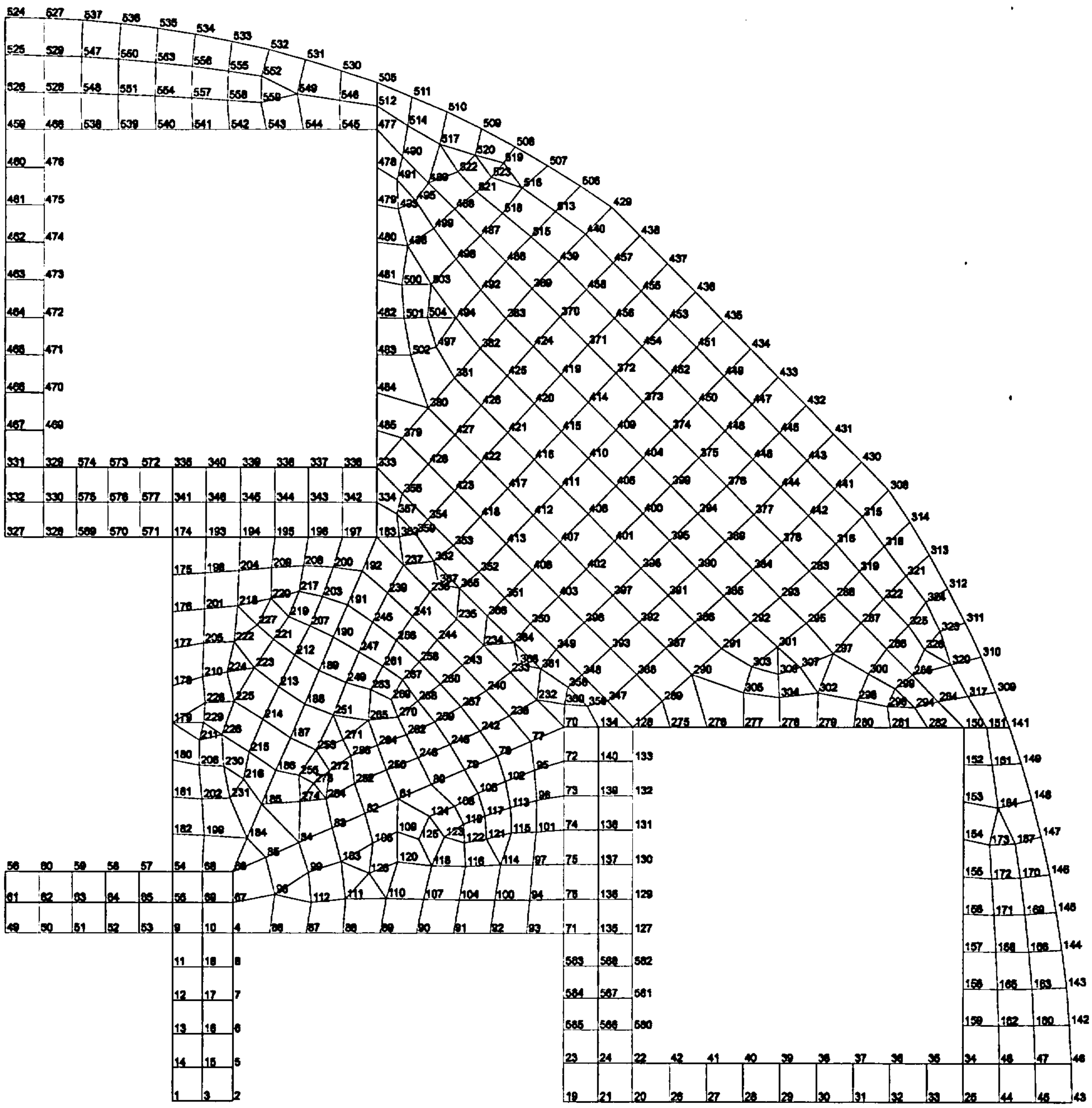

Figure 2.10.4-4
Node Plot of the Quarter Symmetry Model

2.10.4.1.4 Half Symmetry Models

The half symmetry model is used for the NCT Thermal, Vibration, and 1 foot Side Drop, as well as the 30 foot Side Drop and Flatside Buckling analysis. The equivalent static accelerations are in the plane of symmetry and the thermal conditions are symmetric across half the spacer disc, thus a half symmetry model is warranted. The model consists of 1204 nodes and 1149 elements.

The spacer disc modal analysis is modeled using quadrilateral solid elements (PLANE42), with the plane stress option and input thickness. Each node has 2 translational degrees of freedom (UX and UY). The spacer disc modal analysis is performed using the reduced (Householder) method and 300 translational master degrees of freedom. The model boundary conditions and loading for the corner slapdown condition are determined using the same methodology as outlined in Section 0 and Section 2.10.4.1.2.

For NCT in which the loads act only in the plane of the disc, the spacer disc is modeled using quadrilateral plane stress elements (SOLID42) with two degrees of freedom and input thickness. For HAC conditions, the spacer disc is modeled using quadrilateral stress elements (SHELL63) with 6 degrees of freedom (to permit out-of-plane bending) and input thickness.

The modal analysis model is shown in Figure 2.10.4-5. The boundary conditions for the stress analysis and loadings are applied as shown in Figure 2.10.4-6. The spacer disc node numbers in the upper and lower regions are shown in Figure 2.10.4-7 and Figure 2.10.4-8, respectively.

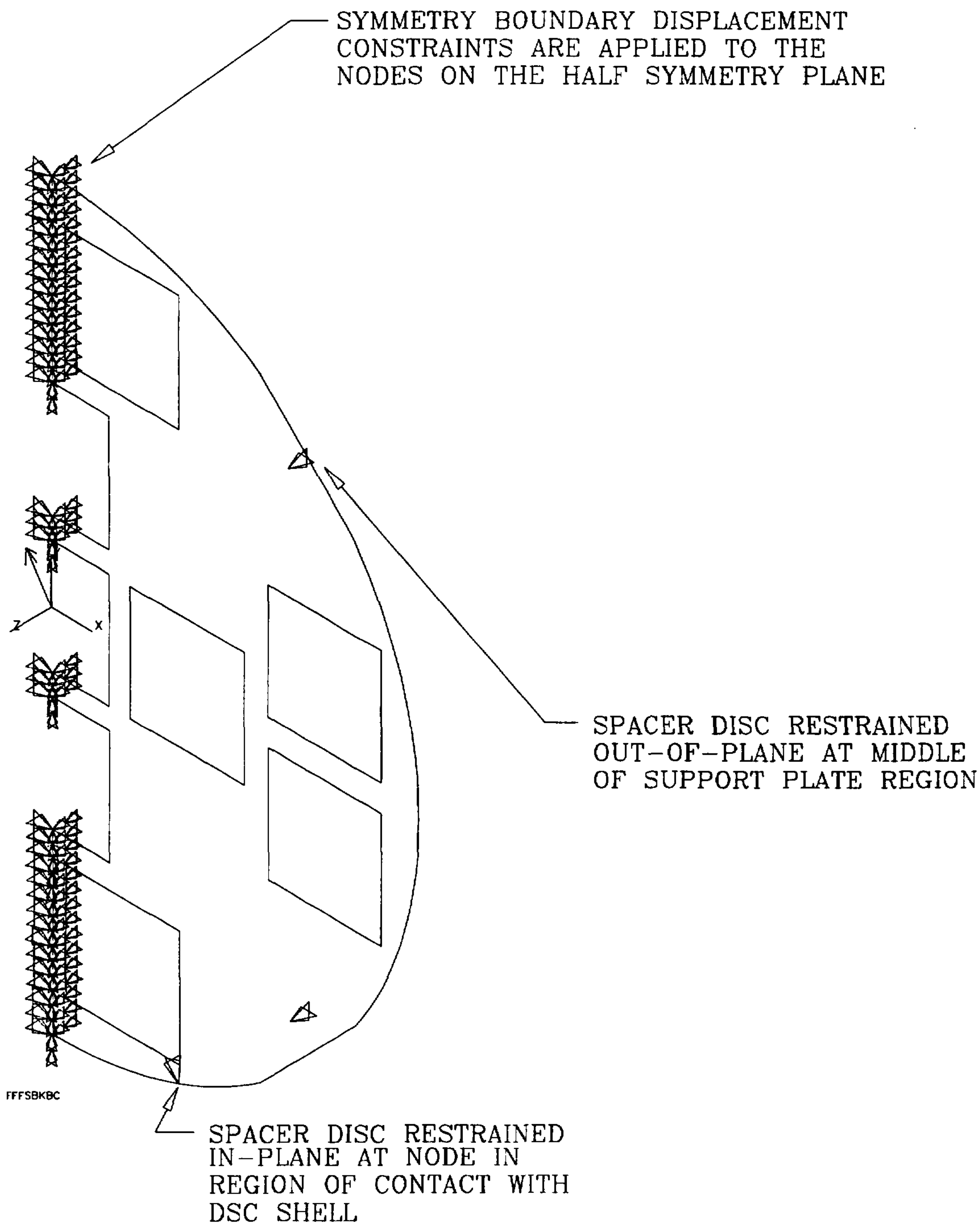

Figure 2.10.4-5
Modal Analysis Half Symmetry Model

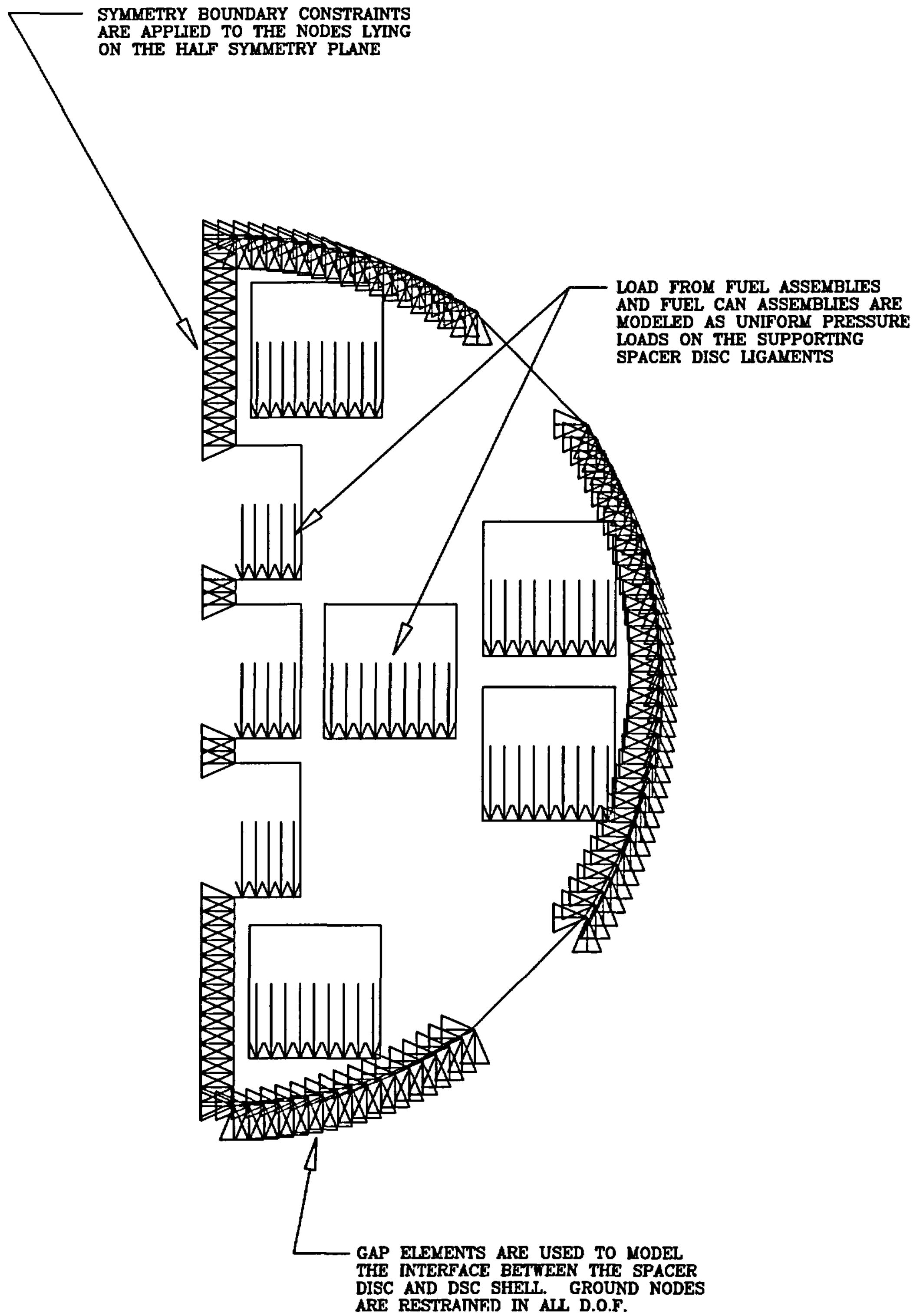

Figure 2.10.4-6
Stress Analysis Half Symmetry Model

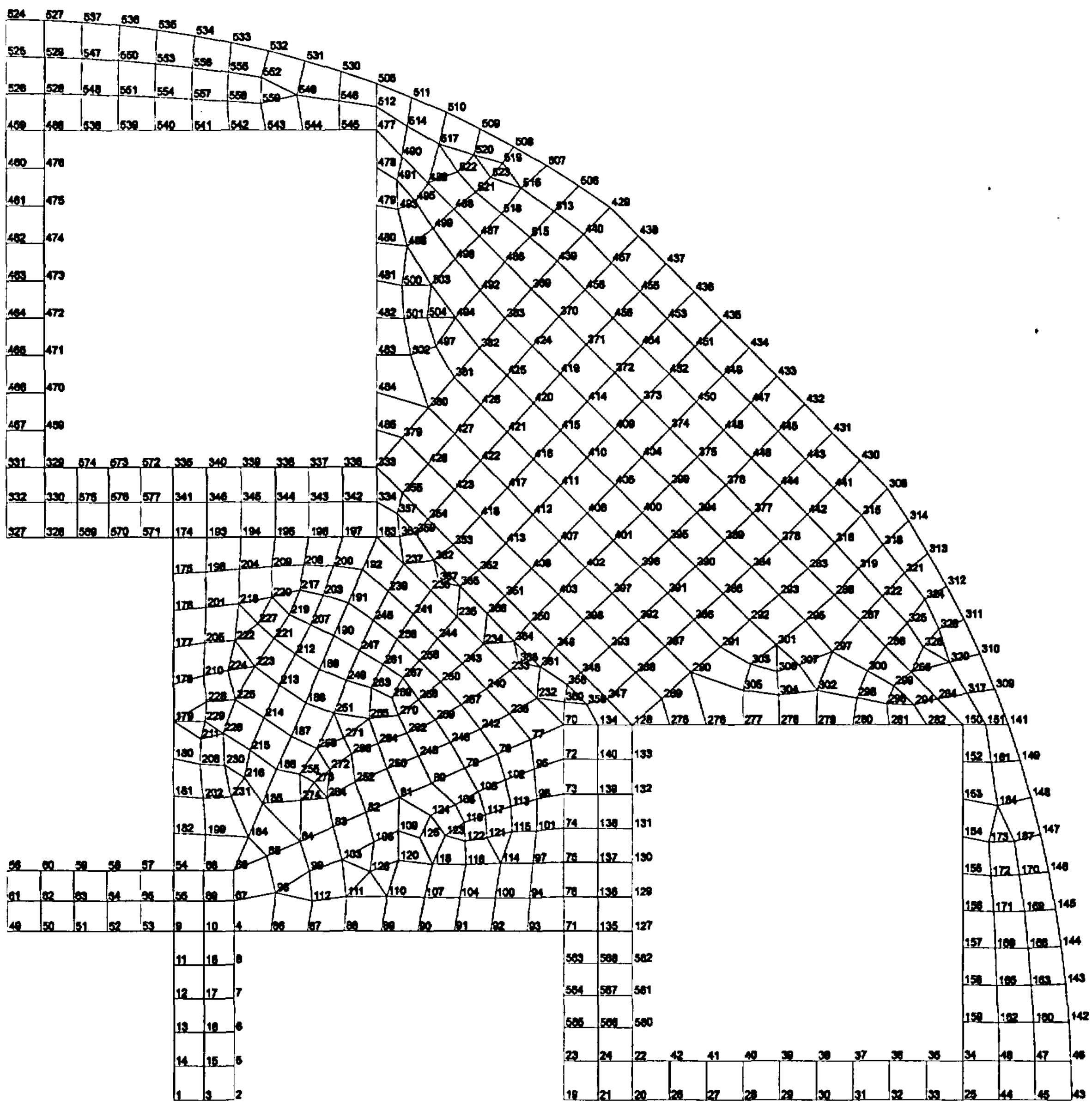

Figure 2.10.4-7
Node Plot of Half Symmetry Model (Top Half)

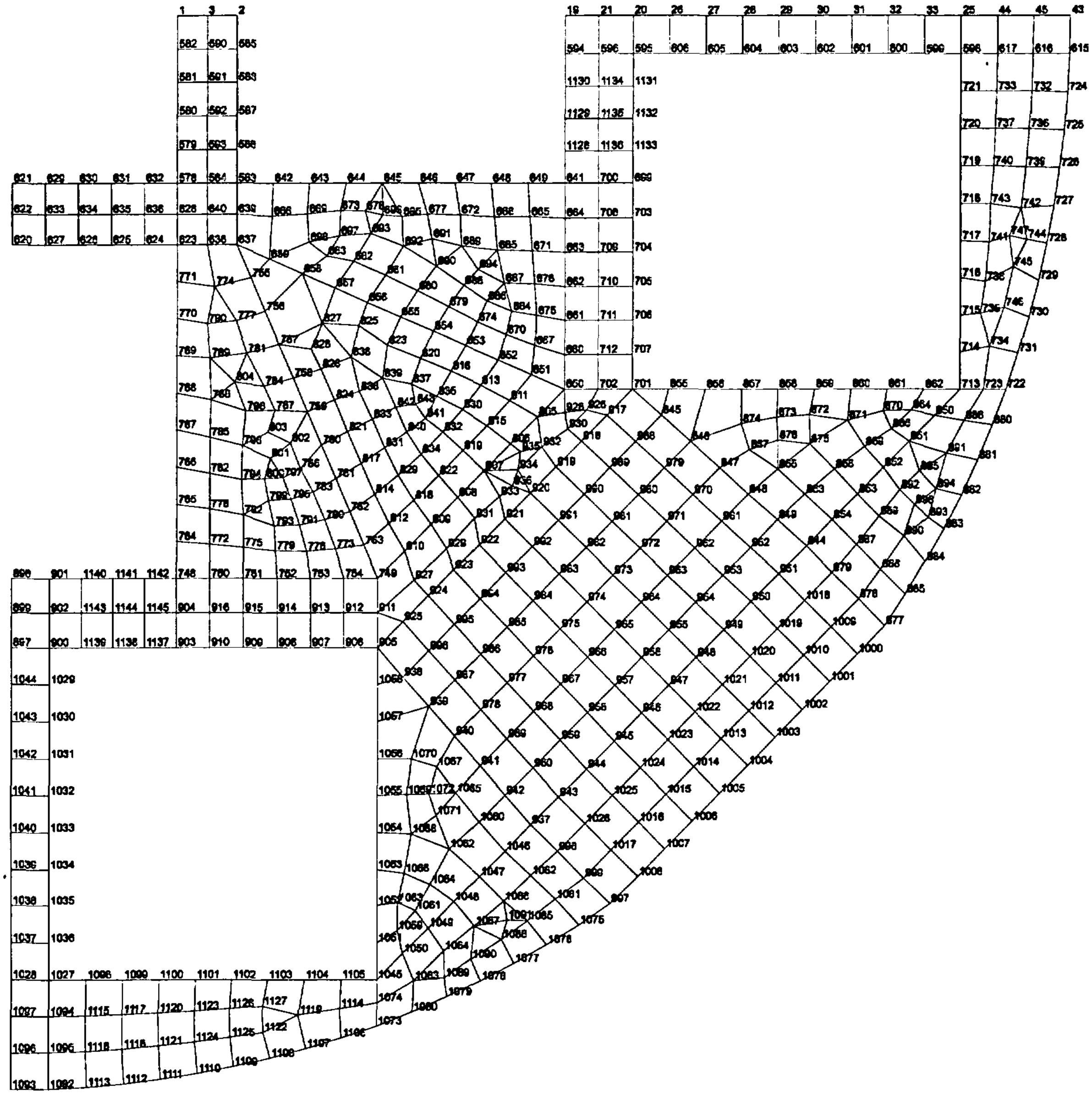

Figure 2.10.4-8
Node Plot of Half Symmetry Model (Bottom Half)

2.10.4.1.5 Full Model

The oblique corner impact, corner slapdown impact, and corner impact buckling spacer disc analyses are performed using a full disc model shown in Figure 2.10.4-10, and the modal analysis is performed using the model shown in Figure 2.10.4-9. The model is generated by symmetry reflection from the half symmetry model discussed in Section 2.10.4.1.4. Although loading and geometric properties do warrant a half symmetry model, the most efficient method of generating the model was to base it on a previous model (using symmetry reflection), rather than building an entirely new model. The model consists of 2370 nodes and 2294 elements.

The spacer disc modal analysis is modeled using quadrilateral solid elements (PLANE42), with the plane stress option and input thickness. Each node has 2 translational degrees of freedom (UX and UY). The spacer disc modal analysis is performed using the reduced (Householder) method and 300 translational master degrees of freedom. The model boundary conditions and loading for the corner slapdown condition are determined using the same methodology as outlined in Section 0 and Section 2.10.4.1.2.

The spacer disc stress analysis is modeled using quadrilateral stress elements (SHELL63) with 6 degrees of freedom and input thickness. The model boundary conditions and loading for the corner slapdown condition are determined using the same methodology as outlined in Section 0 and Section 2.10.4.1.2. The full spacer disc model node numbers are shown in Figure 2.10.4-11, Figure 2.10.4-12, Figure 2.10.4-13, and Figure 2.10.4-14.

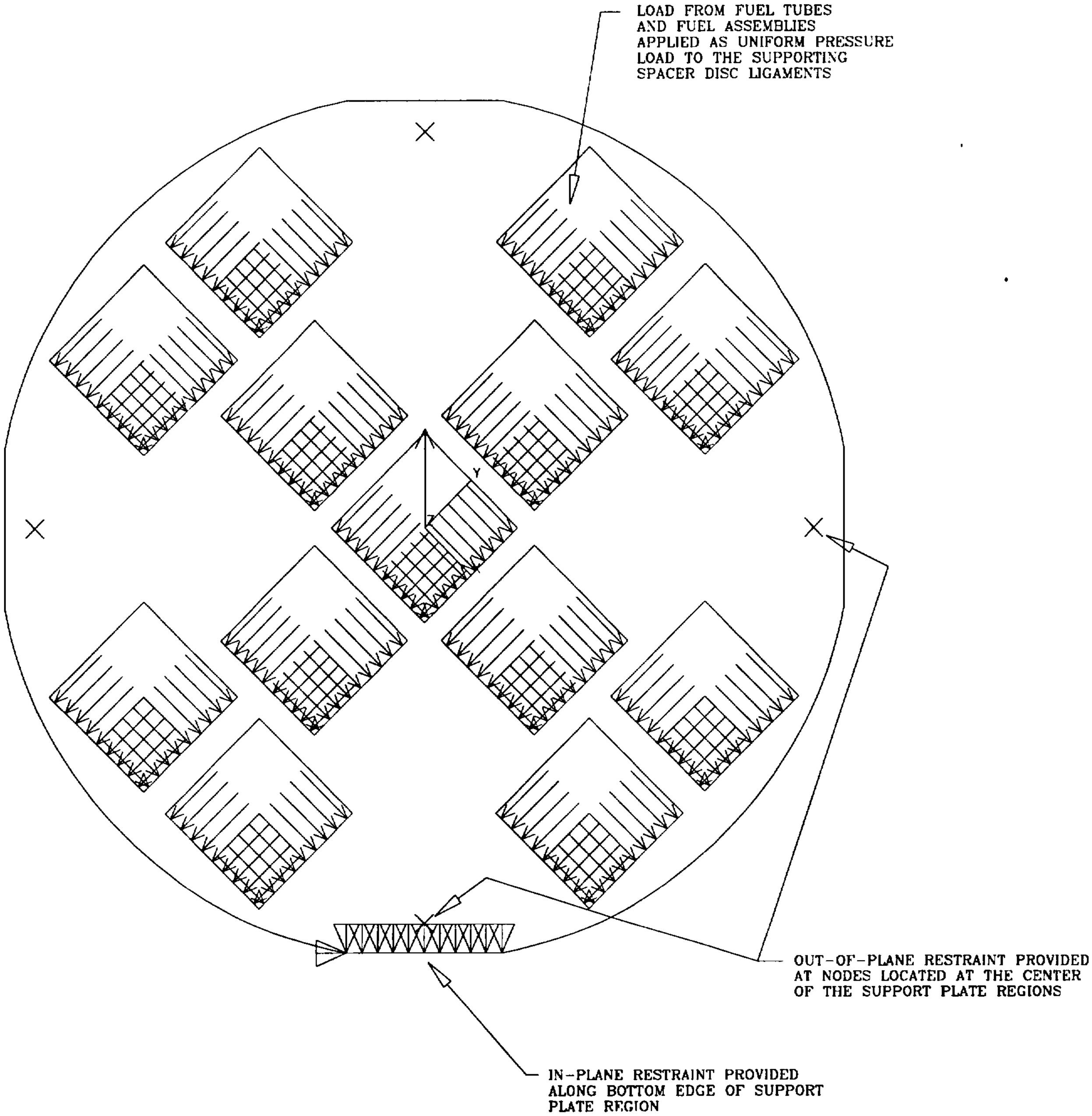

Figure 2.10.4-9
Modal Analysis Full Model

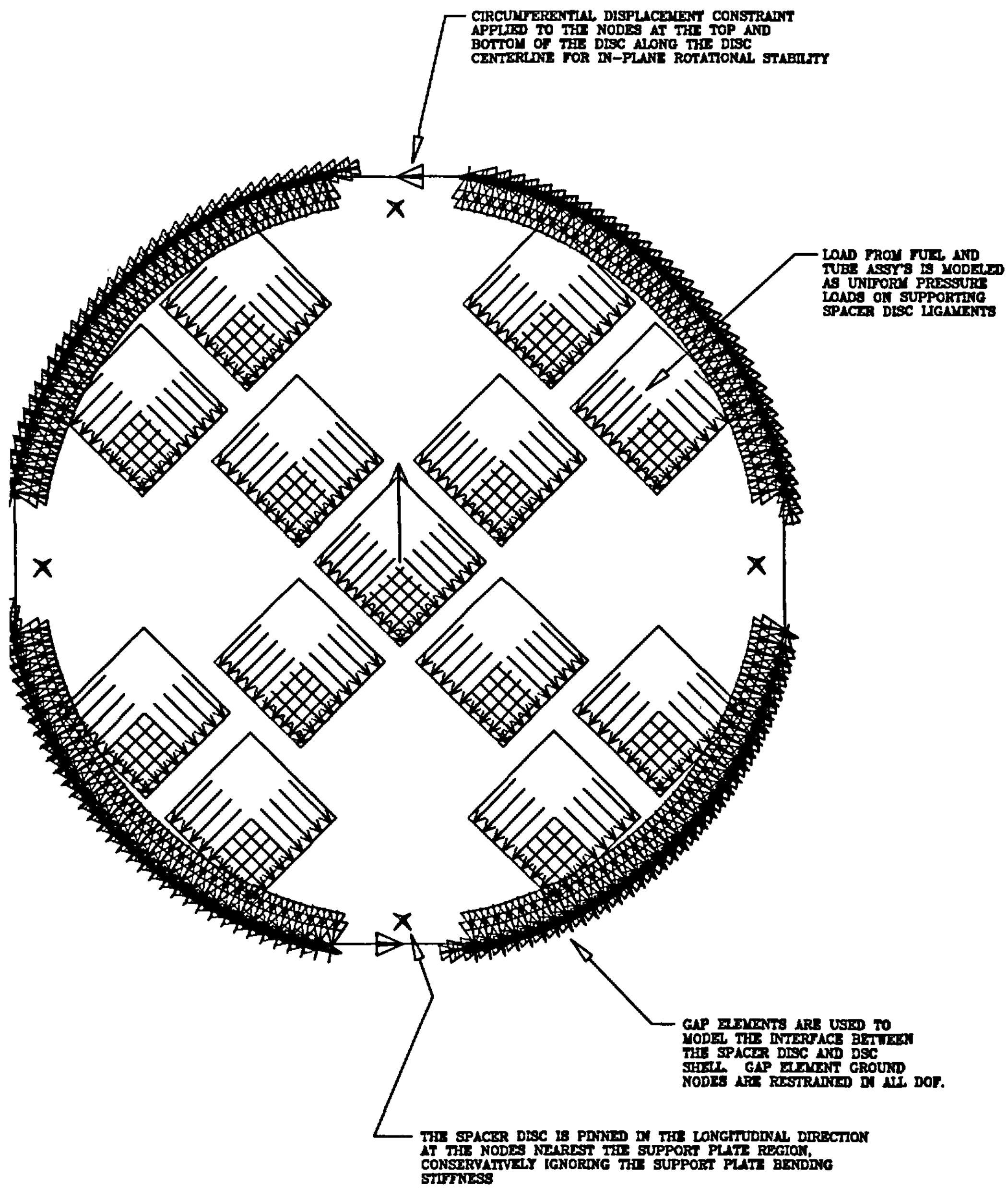

Figure 2.10.4-10
Stress Analysis Full Model

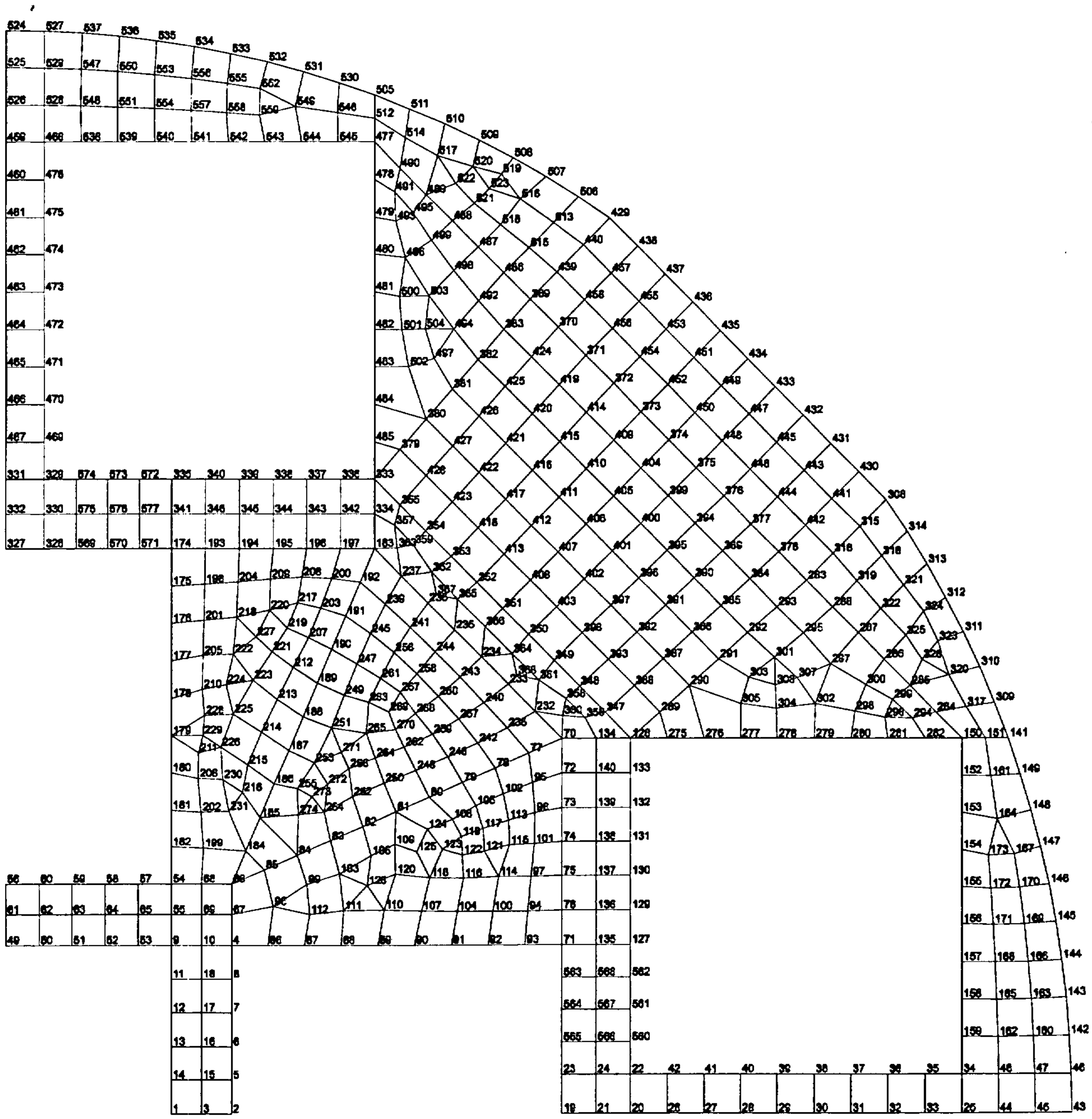

Figure 2.10.4-11
Full Model Node Plot, Right Top Quadrant

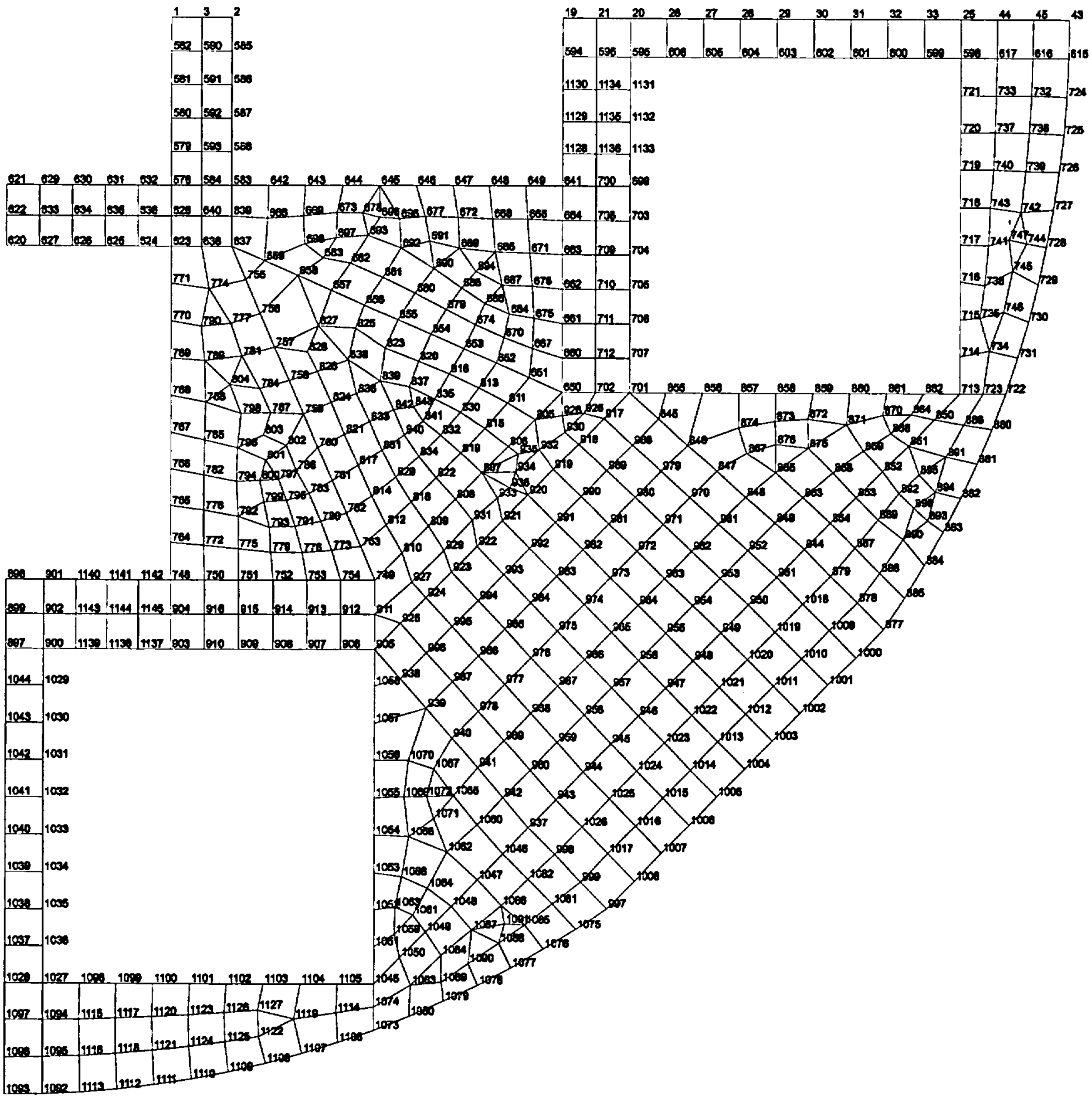

Figure 2.10.4-12
Full Model Node Plot, Right Bottom Quadrant

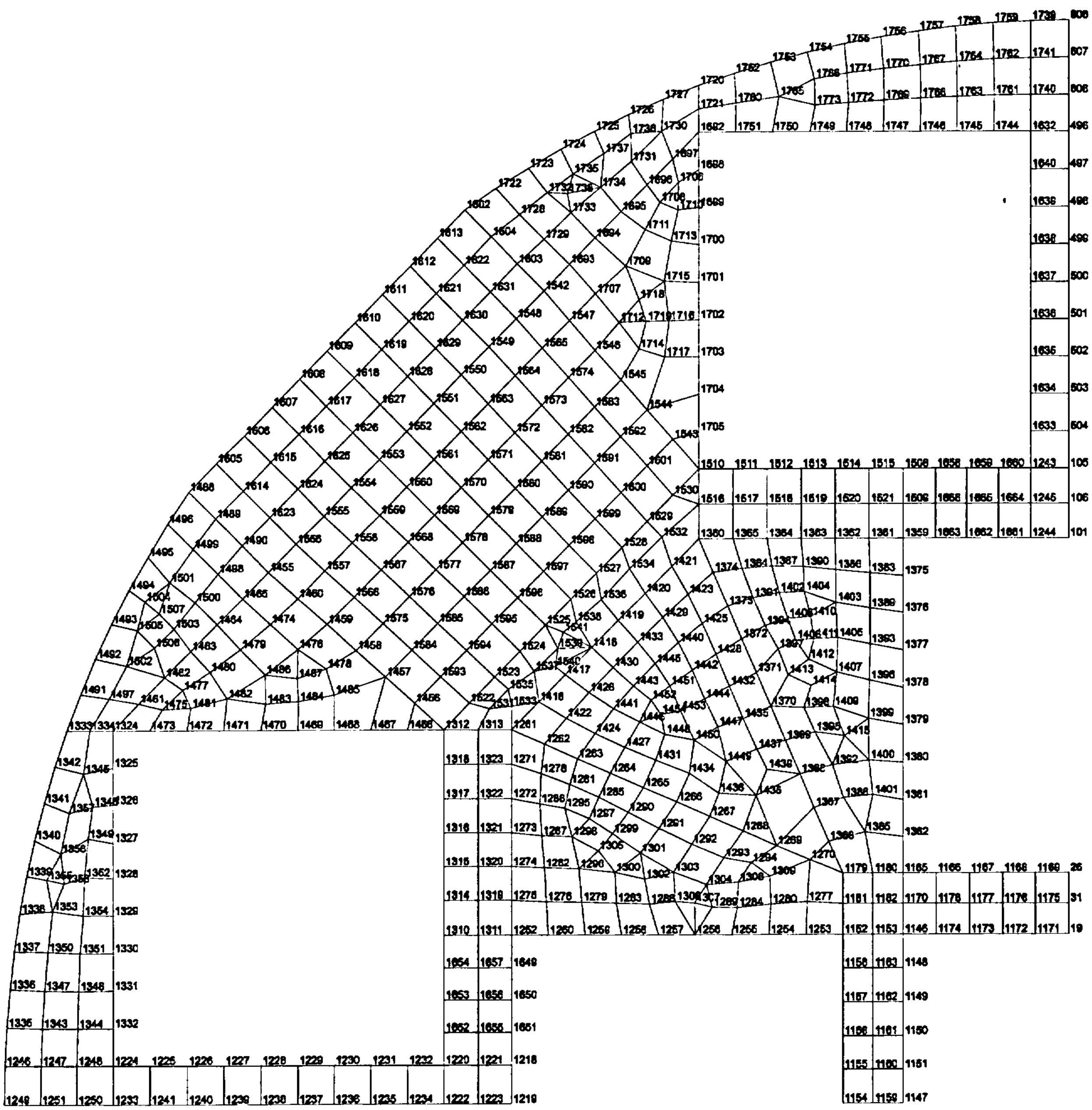

Figure 2.10.4-13
Full Model Node Plot, Left Top Quadrant

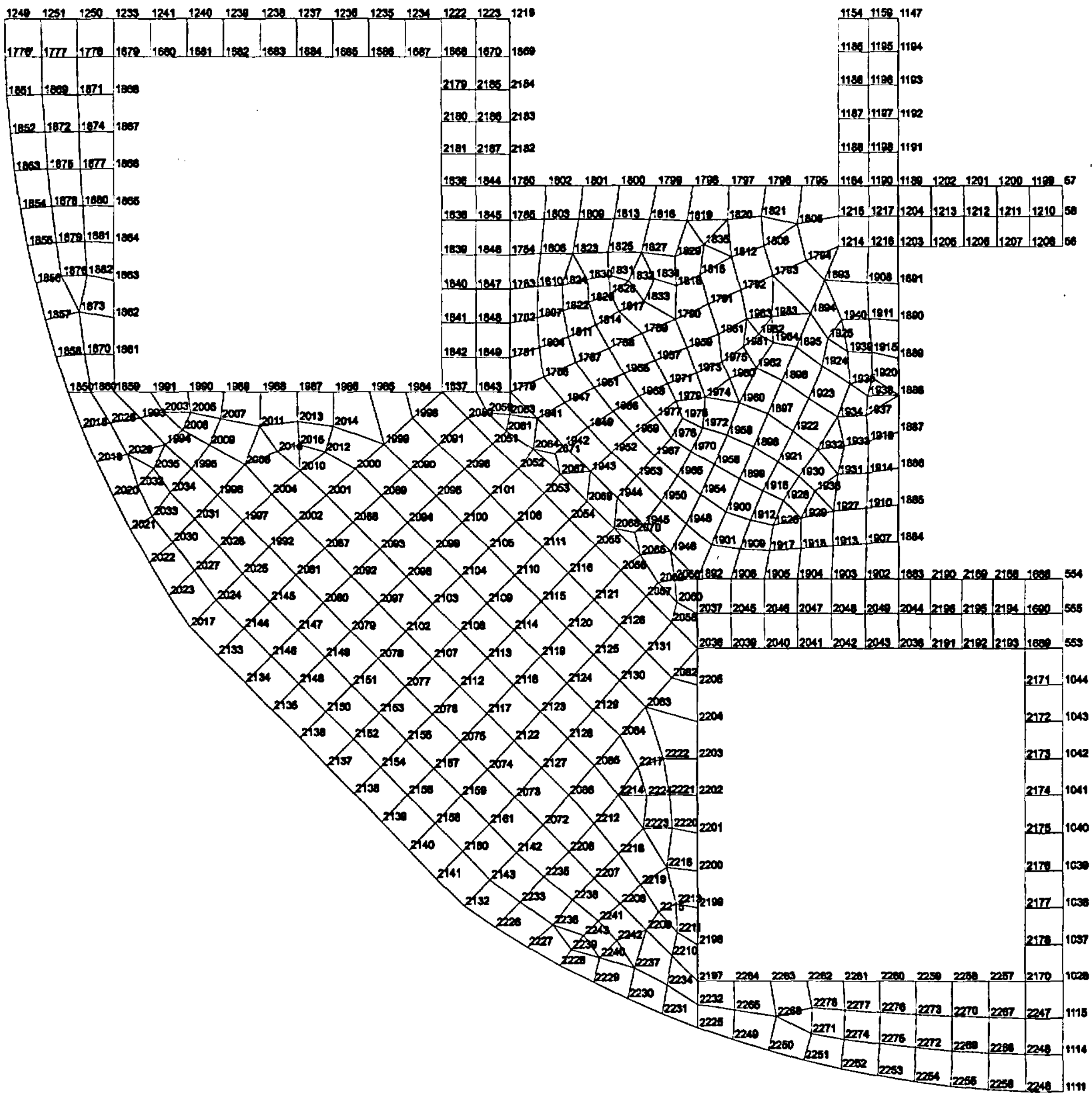

Figure 2.10.4-14
Full Model Node Plot, Left Bottom Quadrant

2.10.4.2 FF-DSC Basket Assembly Finite Element Analysis Input Files

THIS SECTION CONTAINS
PROPRIETARY INFORMATION

2.10.5 Bolt Evaluation

2.10.5.1 Introduction

THIS SECTION CONTAINS
PROPRIETARY INFORMATION

2.10.6 Buckling Evaluation

THIS SECTION CONTAINS
PROPRIETARY INFORMATION

2.10.7 Cask Lead Slump Finite Element Analysis

In the event of a cask drop, permanent deformation of the lead gamma shield may result for certain impact orientations. The lead gamma shield is supported by friction between the lead and cask shells, in addition to bearing at the end of the lead column. During fabrication, a small gap may develop between the lead gamma shield and the cask structural shell due to differential thermal expansion of the dissimilar materials during cooling after the lead pour. Thus, for the cold end drop condition the lead will initially flow outward until it contacts the cask structural shell. After the lead comes in contact with the cask structural shell, hoop stresses will begin to develop in the cask shells due to the lateral pressure from the lead. Therefore, the effect of the gap between the lead and structural shell is to reduce the stresses in the cask shells due to the postulated end drop, while maximizing the amount of permanent deformation in the lead column (i.e. lead slump). Therefore, for purposes of demonstrating the conservatism of the cask lead slump stress calculations, the lead is assumed to initially be in contact with both the cask inner and structural shells.

The cask shell stresses due to the lead slump effects resulting from the end drop are determined in Section 2.7.1.1 using conservative hand calculations. In order to verify the conservatism of these calculations and to quantify the amount of lead slump resulting from the postulated 30 foot end drop, a finite element analysis is performed. The cask axisymmetric finite element model described in Section 2.10.2.1.2 is used for the cask end drop lead slump analysis. Gap elements are used to model the interaction between the lead gamma shield and cask shells. The gap elements transfer both normal forces and friction forces between the lead and cask shells. The coefficient of static friction for lead on mild steel varies from 0.5 for lubricated surfaces to 0.95 for dry surfaces [2.22]. A lower bound coefficient of static friction of 0.5 is conservatively used for the lead slump analysis.

In order to determine the amount of permanent lead slump for the postulated end drop, an elastic-plastic analysis is required. Only the lead gamma shield is modeled with elastic-plastic material properties. The lead gamma shield elastic-plastic material properties are based on the quasistatic stress-strain properties for chemical lead loaded in compression provided in Figure 25 of

NUREG/CR-0481, "An Assessment of Stress-Strain Data Suitable for Finite-Element Elastic-Plastic Analysis of Shipping Containers" [2.37]. The strain-rate effects on lead properties, which are shown to be significant in Reference [2.37], are conservatively ignored for this analysis. The initial elastic modulus of lead is conservatively modeled as 2.0 x 10^6 psi and the proportional limit as 1,000 psi [2.37].

An equivalent static end drop acceleration load of 43.0 g's, resulting from the cold drop condition, is conservatively used with lead material properties at 300°F. Both top and bottom end drop conditions are evaluated. The membrane, membrane plus bending, and primary plus secondary stress intensities resulting from the bottom end drop are reported for the 52 cask stress points shown in Figure 2.10.7-1 are presented in Table 2.10.7-1 through Table 2.10.7-3, respectively. Similarly, the membrane, membrane plus bending, and primary plus secondary stress intensities resulting from the top end drop are reported for the 52 cask stress points shown in Figure 2.10.7-1 are presented in Table 2.10.7-4 through Table 2.10.7-6, respectively. The maximum primary membrane stress intensities in the cask shells due to the bottom and top end drops are 6.4 ksi (stress points 39 and 40) and 2.9 ksi (stress point 27 and 28), respectively. The cask cold end drop stresses at the corresponding stress points determined using hand calculations are 8.2 ksi and 8.4 ksi, respectively, as shown in Section 2.7.1.1.

The results show that the cask end drop stresses determined using the finite element analysis are much lower than those calculated by hand. This confirms the conservatism of the hand calculations.

The amount of shortening of the lead column due to the worst case end drop condition will be minimal. A conservative hand calculation is performed to determine an upper bound value for the lead slump for both the hot and cold end drop conditions. The methodology used to determine the amount of permanent lead slump assumes that the portion of the lead column which is loaded beyond its elastic limit flows to fill any gaps existing between the lead and cask shells prior to the drop. The lead column is assumed to be supported only at its base, conservatively ignoring the friction forces developed between the lead and cask inner and outer shells. The steps followed to determine the lead slump are:

1.) Determine the lead cavity volume at the solidification temperature of lead (620°F)

2.) Calculate the volume of lead in the cavity at the drop temperature (175°F and 300°F for cold and hot drop conditions, respectively)

3.) Calculate the axial and radial gaps developed between the lead and the cavity at the temperature of the drop condition

4.) Find the height of the lead column which is loaded beyond its elastic limit

5.) Determine the amount of lead slump due to plastic flow of the lead filling the radial gap within the yielded height of the lead column

6.) Add the lead slump and axial lead shrinkage to determine the total axial gap existing after the postulated drop event.

The nominal dimensions of the cask cavity at room temperature are:

R_o = 39.25 in., Outer radius of lead cavity

R_i = 35.25 in., Inner radius of lead cavity

L = 182.44 in., Length of lead cavity

The volume of the lead cavity at the solidification temperature of lead (620°F) is:

$$V_{620} = \pi L(R_o^2 - R_i^2)(1 + \alpha_{ss}\Delta T)$$

where α_{ss} is the mean coefficient of thermal expansion of stainless steel, calculated as the average value of the instantaneous coefficient thermal expansion in the temperature range of interest, ΔT. The instantaneous coefficient of thermal expansion of stainless steel at 70°F and 600°F are 8.46×10^{-6} in/in-°F and 10.38×10^{-6} in/in-°F, respectively. Therefore, the lead cavity volume at 620°F is:

$$V_{620} = \pi(182.44)(39.25^2 - 35.25^2)[1 + (9.42 \times 10^{-6})(620 - 70)]$$
$$= 171{,}684 \text{ in}^3$$

Using the same methodology, the volume of the lead cavity at 300°F reduces to:

$$V_{SS,300} = \pi(182.44)(39.25^2 - 35.25^2)[1 + (8.96 \times 10^{-6})(300 - 70)]$$
$$= 171{,}151 \text{ in}^3$$

The liquid lead is assumed to fill the entire lead cavity prior to solidifying. The volume of the lead at a temperature of 300°F, corresponding to the hot drop condition, is calculated using the average instantaneous coefficient of thermal expansion of lead between the temperatures of 620°F and 300°F. The instantaneous coefficient of thermal expansion of lead at 620°F and 300°F are 20.39×10^{-6} in/in-°F and 17.54×10^{-6} in/in-°F, respectively. Therefore, the lead volume at 300°F is:

$$V_{PB,300} = (171{,}684)[1 - (18.97 \times 10^{-7})(620 - 300)]$$
$$= 170{,}642 \text{ in}^3$$

The length of the lead column at 300°F is:

$$L_{300} = (L_{620})[1 - (18.97 \times 10^{-7})(620 - 300)]$$

where L_{620} is the length of the lead cavity at 620°F, calculated as follows:

$$L_{620} = (182.44)[1 + (9.42 \times 10^{-6})(620 - 70)]$$
$$= 183.39 \text{ in.}$$

Therefore, the length of the lead at 300°F is:

$$L_{PB,300} = (183.39)[1 - (18.97 \times 10^{-6})(620 - 300)]$$

$$= \quad 182.28 \text{ in.}$$

The length of the cask cavity at 300°F is:

$$L_{SS,300} = (183.39)[1 - (9.92 \times 10^{-6})(620 - 300)]$$

$$= \quad 182.81 \text{ in.}$$

Therefore, the axial gap developed due to differential thermal shrinkage of the lead and stainless steel cavity is:

$$\delta_a = 182.81 - 182.28$$

$$= \quad 0.53 \text{ inches}$$

The radial gap developed between the lead and outer shell at 300°F is determined based on the difference between the cask lead cavity volume and lead volume at 300°F. The inner radius of the lead will be equal to that of the cask lead cavity at 300°F. The inner and outer radii of the lead cavity at 300°F are calculated as follows:

$$R_{ic,300} = (35.25)[1 + (8.96 \times 10^{-6})(300 - 70)]$$

$$= \quad 35.32 \text{ in.}$$

$$R_{oc,300} = (39.25)[1 + (8.96 \times 10^{-6})(300 - 70)]$$

$$= \quad 39.33 \text{ in.}$$

The outer radius of the lead at 300°F is calculated as follows:

$$R_{ol} = [(V_{PB,300}/\pi L_{PB,300}) + R_{ic}^2]^{1/2}$$

$$= \quad [(170{,}642)/(\pi \times 182.28) + 35.32^2]^{1/2}$$

$$= \quad 39.31 \text{ in.}$$

Therefore, the radial gap between the lead and cask outer shell at 300°F is:

$$\delta_r = R_{oc,300} - R_{ol}$$

$$= 39.33 - 39.31$$

$$= 0.02 \text{ in.}$$

Following the same procedure, the radial axial and radial gaps between the lead and cavity at 175°F are 0.73 inches and 0.04 inches, respectively.

The equivalent static g-loads for the hot and cold end drop conditions are 26.6 g's and 43.0 g's, as shown in Section 2.7.1. As shown in Chapter 3, the maximum temperature of the lead for the hot thermal condition (100°F ambient) is less than 300°F. Similarly, the maximum temperature of the lead for the -20°F drop condition with the maximum decay heat load is less than 175°F. An additional cold drop condition is considered in which the -20°F ambient temperature exists in combination with zero decay heat, resulting in a uniform temperature of -20°F throughout the cask. The dynamic yield strength of lead at a strain rate of 10 s^{-1} and room temperature is approximately 1000 psi, as shown in Figure 25 of Reference 2.37. As shown in Figure 23 of Reference 2.37, the yield strength of lead reduces by approximately 20% at 175°F and by 50% at 300°F. Therefore, the approximate dynamic yield strengths of lead at 175°F and 300°F are 800 psi and 500 psi, respectively. A bounding cold drop condition is considered for which the axial gap due to lead shrinkage for a lead temperature of -20°F is combined with the lead slump based on lead properties at 175°F.

For the hot drop condition, the height of the lead column in which the stresses exceed the 500 psi dynamic yield strength is:

$$h' = L_{PB,300} - \sigma_y/(\rho_{PB}G)$$

where G is the equivalent static end drop load (26.6 g's) and ρ_{PB} is the density of lead (0.408 lb/in^3.) Therefore,

$$h' = 182.28 - 500/(0.408 \times 26.6)$$

$$= 136.2 \text{ in.}$$

The change in the height of the lead column due to plastic flow of the lead for the hot end drop is:

$$\Delta h = (h')(R_{oc,300}^2 - R_{ol}^2)/(R_{ol}^2 - R_{ic,300}^2)$$

$$= (136.2)(39.33^2 - 39.31^2)/(39.31^2 - 35.32^2)$$

$$= 0.72 \text{ inches}$$

Therefore, the total axial gap between the lead and cavity after the hot end drop is 1.25 inches (=0.53 + 0.72). Following the same procedure for the cold drop condition the axial gap due to lead shrinkage, based on a uniform temperature of -20°F, is 1.01 inches. The change in height of the lead column due to the cold end drop, using lead material properties at 175°F, is 0.56 inches. Therefore, the total axial gap between the lead and cavity after the cold end drop is 1.57 inches.

An upper bound lead slump of 2.5 inches is conservatively assumed for the post-drop shielding evaluation in Chapter 5.

FIGURE WITHHELD UNDER 10 CFR 2.390

Table 2.10.7-1

Cask Primary Membrane S.I. Summary - Bottom End Drop Lead Slump

Cask Component	Stress Point	Node Number	Stress Components (ksi)				Principal Stresses (ksi			SI (ksi)
			Sx	Sy	Sz	Sxy	S1	S2	S3	
Top Cover	1	1390	0.0	0.0	0.0	0.0	0.0	0.0	0.0	0.0
	2	1430	0.0	0.0	0.0	0.0	0.0	0.0	0.0	0.0
	3	1398	0.0	0.0	0.0	0.1	0.1	0.0	-0.1	0.2
	4	1438	0.0	0.0	0.0	0.1	0.1	0.0	-0.1	0.2
	5	1369	0.0	0.0	-0.2	0.2	0.2	-0.2	-0.3	0.4
	6	1445	0.0	0.0	-0.2	0.2	0.2	-0.2	-0.3	0.4
Top Flange	7	1373	-0.1	0.0	0.2	0.0	0.2	0.0	-0.1	0.3
	8	1375	-0.1	0.0	0.2	0.0	0.2	0.0	-0.1	0.3
	9	1334	0.1	-0.6	-0.1	-0.1	0.1	-0.1	-0.7	0.7
	10	1336	0.1	-0.6	-0.1	-0.1	0.1	-0.1	-0.7	0.7
Inner Shell	11	1316	0.0	-1.2	-0.5	-0.1	0.0	-0.5	-1.2	1.1
	12	1318	0.0	-1.2	-0.5	-0.1	0.0	-0.5	-1.2	1.1
	13	1235	0.0	-1.5	0.0	0.0	0.0	0.0	-1.5	1.5
	14	1237	0.0	-1.5	0.0	0.0	0.0	0.0	-1.5	1.5
	15	1092	0.0	-1.7	0.0	0.0	0.0	0.0	-1.7	1.7
	16	1094	0.0	-1.7	0.0	0.0	0.0	0.0	-1.7	1.7
	17	742	0.0	-2.4	0.0	0.0	0.0	0.0	-2.4	2.4
	18	744	0.0	-2.4	0.0	0.0	0.0	0.0	-2.4	2.4
	19	392	0.0	-3.0	-0.8	0.0	0.0	-0.8	-3.0	3.0
	20	394	0.0	-3.0	-0.8	0.0	0.0	-0.8	-3.0	3.0
	21	263	0.0	-3.2	-1.1	0.0	0.0	-1.1	-3.2	3.2
	22	265	0.0	-3.2	-1.1	0.0	0.0	-1.1	-3.2	3.2
	23	156	-0.2	-3.1	-1.6	-0.5	-0.1	-1.6	-3.2	3.1
	24	158	-0.2	-3.1	-1.6	-0.5	-0.1	-1.6	-3.2	3.1
	25	148	0.7	-1.8	0.2	-0.4	0.7	0.2	-1.8	2.6
	26	150	0.7	-1.8	0.2	-0.4	0.7	0.2	-1.8	2.6
Outer Shell	27	1342	0.0	-0.3	0.0	0.0	0.0	0.0	-0.3	0.3
	28	1344	0.0	-0.3	0.0	0.0	0.0	0.0	-0.3	0.3
	29	1241	-0.1	-0.6	0.2	-0.1	0.2	-0.1	-0.6	0.8
	30	1243	-0.1	-0.6	0.2	-0.1	0.2	-0.1	-0.6	0.8
	31	1098	0.0	-1.2	0.0	0.0	0.0	0.0	-1.2	1.2
	32	1100	0.0	-1.2	0.0	0.0	0.0	0.0	-1.2	1.2
	33	747	0.0	-1.8	1.1	0.0	1.1	0.0	-1.8	2.9
	34	750	0.0	-1.8	1.1	0.0	1.1	0.0	-1.8	2.9
	35	399	0.0	-2.4	2.4	0.0	2.4	0.0	-2.4	4.8
	36	400	0.0	-2.4	2.4	0.0	2.4	0.0	-2.4	4.8
	37	269	-0.8	-3.0	1.8	0.1	1.8	-0.8	-3.0	4.8
	38	271	-0.8	-3.0	1.8	0.1	1.8	-0.8	-3.0	4.8
	39	131	1.7	-4.6	-0.1	0.7	1.8	-0.1	-4.7	6.4
	40	133	1.7	-4.6	-0.1	0.7	1.8	-0.1	-4.7	6.4
Bottom Forging	41	148	0.3	-2.1	-0.2	0.0	0.3	-0.2	-2.1	2.4
	42	60	0.3	-2.1	-0.2	0.0	0.3	-0.2	-2.1	2.4
	43	143	0.3	0.0	0.4	0.1	0.4	0.3	0.0	0.4
	44	55	0.3	0.0	0.4	0.1	0.4	0.3	0.0	0.4
	45	82	0.2	-0.1	0.6	0.0	0.6	0.2	-0.1	0.7
	46	48	0.2	-0.1	0.6	0.0	0.6	0.2	-0.1	0.7
Ram Access Cover Plate	47	32	0.0	0.0	0.0	0.0	0.0	0.0	0.0	0.0
	48	13	0.0	0.0	0.0	0.0	0.0	0.0	0.0	0.0
	49	31	0.0	0.0	0.0	0.0	0.0	0.0	0.0	0.0
	50	10	0.0	0.0	0.0	0.0	0.0	0.0	0.0	0.0
	51	29	0.0	0.0	0.0	0.0	0.0	0.0	0.0	0.0
	52	1	0.0	0.0	0.0	0.0	0.0	0.0	0.0	0.0

Table 2.10.7-2

Cask Membrane Plus Bending S.I. Summary - Bottom End Drop Lead Slump

Cask Component	Stress Point	Node Number	Stress Components (ksi)				Principal Stresses (ksi			SI (ksi)
			Sx	Sy	Sz	Sxy	S1	S2	S3	
Top Cover	1	1390	3.3	0.0	3.3	0.0	3.3	3.3	0.0	3.3
	2	1430	-3.2	0.0	-3.2	0.0	0.0	-3.2	-3.2	3.2
	3	1398	2.5	0.0	2.8	0.1	2.8	2.5	0.0	2.8
	4	1438	-2.5	0.0	-2.8	0.1	0.0	-2.5	-2.8	2.8
	5	1369	0.5	0.1	1.2	0.3	1.2	0.6	-0.1	1.3
	6	1445	-0.6	-0.1	-1.7	0.2	-0.1	-0.6	-1.7	1.6
Top Flange	7	1373	-0.2	-0.1	0.2	0.0	0.2	-0.1	-0.2	0.3
	8	1375	0.0	0.0	0.2	0.0	0.2	0.1	0.0	0.2
	9	1334	0.0	-0.8	-0.2	-0.1	0.0	-0.2	-0.8	0.8
	10	1336	0.1	-0.5	0.0	-0.1	0.2	0.0	-0.5	0.6
Inner Shell	11	1316	0.0	-0.4	-0.3	0.0	0.0	-0.3	-0.4	0.4
	12	1318	0.0	-1.9	-0.7	-0.2	0.0	-0.7	-1.9	1.9
	13	1235	0.0	-1.6	0.0	0.0	0.0	0.0	-1.6	1.6
	14	1237	0.0	-1.4	0.0	0.0	0.0	0.0	-1.4	1.5
	15	1092	0.0	-1.7	0.0	0.0	0.0	0.0	-1.7	1.7
	16	1094	0.0	-1.7	0.0	0.0	0.0	0.0	-1.7	1.7
	17	742	0.0	-2.3	0.0	0.0	0.0	0.0	-2.3	2.4
	18	744	0.0	-2.4	0.0	0.0	0.0	0.0	-2.4	2.4
	19	392	0.0	-3.0	-0.8	0.0	0.0	-0.8	-3.0	3.0
	20	394	0.0	-3.0	-0.8	0.0	0.0	-0.8	-3.0	2.9
	21	263	0.0	-3.3	-1.2	0.0	0.0	-1.2	-3.3	3.3
	22	265	0.0	-3.1	-1.1	0.0	0.0	-1.1	-3.1	3.0
	23	156	-0.1	-3.8	-1.8	-0.3	-0.1	-1.8	-3.8	3.7
	24	158	-0.3	-2.4	-1.4	-0.7	-0.1	-1.4	-2.6	2.5
	25	148	-0.2	-4.3	-0.8	-0.1	-0.2	-0.8	-4.3	4.1
	26	150	1.5	0.7	1.2	-0.8	2.0	1.2	0.3	1.7
Outer Shell	27	1342	0.0	0.0	0.1	0.0	0.1	0.0	0.0	0.1
	28	1344	0.0	-0.6	-0.1	0.0	0.0	-0.1	-0.6	0.7
	29	1241	0.0	-1.3	0.0	0.0	0.0	0.0	-1.3	1.3
	30	1243	-0.1	0.2	0.4	-0.1	0.4	0.2	-0.2	0.6
	31	1098	0.0	-1.3	0.0	0.0	0.0	0.0	-1.3	1.3
	32	1100	0.0	-1.1	0.1	0.0	0.1	0.0	-1.1	1.2
	33	747	-0.1	-1.8	1.1	0.0	1.1	-0.1	-1.8	2.9
	34	750	0.0	-1.8	1.1	0.0	1.1	0.0	-1.8	2.9
	35	399	-0.1	-2.4	2.4	0.0	2.4	-0.1	-2.4	4.8
	36	400	0.0	-2.4	2.3	0.0	2.3	0.0	-2.4	4.7
	37	269	-0.5	-1.8	2.2	0.2	2.2	-0.5	-1.8	4.1
	38	271	-1.1	-4.2	1.4	-0.1	1.4	-1.1	-4.2	5.6
	39	131	2.9	-1.9	1.0	1.0	3.1	1.0	-2.1	5.2
	40	133	0.4	-7.3	-1.1	0.4	0.5	-1.1	-7.4	7.8
Bottom Forging	41	148	0.7	-3.5	-0.3	-0.1	0.7	-0.3	-3.5	4.2
	42	60	-0.1	-0.7	0.0	0.1	0.0	0.0	-0.7	0.7
	43	143	0.5	0.0	0.5	0.1	0.5	0.5	0.0	0.5
	44	55	0.1	0.0	0.4	0.0	0.4	0.1	0.0	0.4
	45	82	0.3	0.0	0.6	0.1	0.6	0.3	0.0	0.6
	46	48	0.1	-0.1	0.6	0.0	0.6	0.1	-0.1	0.7
Ram Access Cover Plate	47	32	0.0	0.0	0.0	0.0	0.0	0.0	0.0	0.0
	48	13	0.0	0.0	0.0	0.0	0.0	0.0	0.0	0.0
	49	31	0.0	0.0	0.0	0.0	0.0	0.0	0.0	0.0
	50	10	0.0	0.0	0.0	0.0	0.0	0.0	0.0	0.0
	51	29	0.0	0.0	0.0	0.0	0.0	0.0	0.0	0.0
	52	1	0.0	-0.1	0.0	0.0	0.0	0.0	-0.1	0.1

Table 2.10.7-3

Cask Primary Plus Secondary S.I. Summary - Bottom End Drop Lead Slump

Cask Component	Stress Point	Node Number	Stress Components (ksi)				Principal Stresses (ksi)			SI (ksi)
			Sx	Sy	Sz	Sxy	S1	S2	S3	
Top Cover	1	1390	3.3	0.0	3.3	0.0	3.3	3.3	0.0	3.3
	2	1430	-3.2	0.0	-3.2	0.0	0.0	-3.2	-3.2	3.2
	3	1398	2.5	0.0	2.8	0.0	2.8	2.5	0.0	2.8
	4	1438	-2.5	0.0	-2.8	0.0	0.0	-2.5	-2.8	2.8
	5	1369	0.0	0.0	0.3	0.0	0.3	0.0	0.0	0.3
	6	1445	-0.5	-0.1	-1.7	0.1	0.0	-0.6	-1.7	1.7
Top Flange	7	1373	-0.2	0.0	0.2	0.0	0.2	0.0	-0.2	0.4
	8	1375	0.0	0.1	0.2	0.0	0.2	0.1	0.0	0.3
	9	1334	0.0	-0.7	-0.2	-0.1	0.0	-0.2	-0.8	0.8
	10	1336	0.0	0.0	0.0	0.0	0.0	0.0	0.0	0.0
Inner Shell	11	1316	0.0	-0.5	-0.3	0.0	0.0	-0.3	-0.5	0.4
	12	1318	0.0	-1.9	-0.7	-0.2	0.0	-0.7	-2.0	1.9
	13	1235	0.0	-1.6	0.0	0.0	0.0	0.0	-1.6	1.6
	14	1237	0.0	-1.4	0.0	0.0	0.0	0.0	-1.4	1.5
	15	1092	0.0	-1.7	0.0	0.0	0.0	0.0	-1.7	1.7
	16	1094	0.0	-1.7	0.0	0.0	0.0	0.0	-1.7	1.7
	17	742	0.0	-2.3	0.0	0.0	0.0	0.0	-2.3	2.4
	18	744	0.0	-2.4	0.0	0.0	0.0	0.0	-2.4	2.4
	19	392	0.0	-3.0	-0.8	0.0	0.0	-0.8	-3.0	3.0
	20	394	0.0	-3.0	-0.8	0.0	0.0	-0.8	-3.0	2.9
	21	263	0.0	-3.3	-1.2	0.0	0.0	-1.2	-3.3	3.3
	22	265	0.0	-3.1	-1.1	0.0	0.0	-1.1	-3.1	3.0
	23	156	-0.1	-3.8	-1.8	-0.4	0.0	-1.8	-3.8	3.8
	24	158	-0.3	-2.4	-1.4	-0.8	0.0	-1.4	-2.6	2.7
	25	148	0.0	-4.7	-0.9	-0.2	0.0	-0.9	-4.8	4.7
	26	150	1.7	0.5	1.2	-1.0	2.2	1.2	-0.1	2.3
Outer Shell	27	1342	0.0	0.0	0.0	0.0	0.0	0.0	0.0	0.0
	28	1344	0.0	-0.6	-0.1	0.0	0.0	-0.1	-0.6	0.7
	29	1241	0.0	-0.3	0.0	0.0	0.0	0.0	-0.3	0.3
	30	1243	-0.1	0.2	0.4	-0.1	0.4	0.2	-0.2	0.6
	31	1098	0.0	-0.7	-0.1	0.0	0.0	-0.1	-0.7	0.7
	32	1100	0.0	-1.1	0.1	0.0	0.1	0.0	-1.1	1.2
	33	747	-0.1	-1.6	-0.7	0.0	-0.1	-0.7	-1.6	1.5
	34	750	0.0	-1.8	1.1	0.0	1.1	0.0	-1.8	2.9
	35	399	-0.1	-2.4	2.4	0.0	2.4	-0.1	-2.4	4.8
	36	400	0.0	-2.4	2.3	0.0	2.3	0.0	-2.4	4.7
	37	269	-0.2	-2.8	-1.3	0.0	-0.2	-1.3	-2.8	2.6
	38	271	-1.1	-4.2	1.3	-0.1	1.3	-1.1	-4.2	5.5
	39	131	2.7	-1.9	1.0	0.9	2.9	1.0	-2.0	4.9
	40	133	0.2	-7.3	-1.2	0.3	0.2	-1.2	-7.3	7.5
Bottom Forging	41	148	0.0	-4.7	-0.9	-0.2	0.0	-0.9	-4.8	4.7
	42	60	-0.1	-1.4	-0.2	0.0	-0.1	-0.2	-1.4	1.3
	43	143	0.5	0.0	0.5	0.1	0.5	0.5	0.0	0.5
	44	55	0.1	0.0	0.4	0.0	0.4	0.1	0.0	0.4
	45	82	0.3	0.0	0.6	0.1	0.6	0.3	0.0	0.6
	46	48	0.0	0.0	0.0	0.0	0.0	0.0	0.0	0.0
Ram Access Cover Plate	47	32	0.0	0.0	0.0	0.0	0.0	0.0	0.0	0.0
	48	13	0.0	0.0	0.0	0.0	0.0	0.0	0.0	0.0
	49	31	0.0	0.0	0.0	0.0	0.0	0.0	0.0	0.0
	50	10	0.0	0.0	0.0	0.0	0.0	0.0	0.0	0.0
	51	29	0.0	0.0	0.0	0.0	0.0	0.0	0.0	0.0
	52	1	0.0	-0.1	0.0	0.0	0.0	0.0	-0.1	0.0

Table 2.10.7-4

Cask Primary Membrane S.I. Summary - Top End Drop Lead Slump

Cask Component	Stress Point	Node Number	Stress Components (ksi)				Principal Stresses (ksi)			SI (ksi)
			Sx	Sy	Sz	Sxy	S1	S2	S3	
Top Cover	1	1390	0.0	0.0	0.0	0.0	0.0	0.0	0.0	0.1
	2	1430	0.0	0.0	0.0	0.0	0.0	0.0	0.0	0.1
	3	1398	0.0	0.0	0.0	0.0	0.0	0.0	0.0	0.0
	4	1438	0.0	0.0	0.0	0.0	0.0	0.0	0.0	0.0
	5	1369	0.0	-0.2	0.0	0.0	0.0	0.0	-0.2	0.2
	6	1445	0.0	-0.2	0.0	0.0	0.0	0.0	-0.2	0.2
Top Flange	7	1373	-0.8	-7.4	1.9	-0.1	1.9	-0.8	-7.4	9.3
	8	1375	-0.8	-7.4	1.9	-0.1	1.9	-0.8	-7.4	9.3
	9	1334	-0.2	0.0	0.3	-0.1	0.3	0.1	-0.3	0.6
	10	1336	-0.2	0.0	0.3	-0.1	0.3	0.1	-0.3	0.6
Inner Shell	11	1316	-0.1	-0.9	-2.1	-0.3	0.0	-1.0	-2.1	2.1
	12	1318	-0.1	-0.9	-2.1	-0.3	0.0	-1.0	-2.1	2.1
	13	1235	0.0	-0.8	0.1	0.0	0.1	0.0	-0.8	0.9
	14	1237	0.0	-0.8	0.1	0.0	0.1	0.0	-0.8	0.9
	15	1092	0.0	-0.5	0.0	0.0	0.0	0.0	-0.5	0.5
	16	1094	0.0	-0.5	0.0	0.0	0.0	0.0	-0.5	0.5
	17	742	0.0	0.1	0.0	0.0	0.1	0.0	0.0	0.1
	18	744	0.0	0.1	0.0	0.0	0.1	0.0	0.0	0.1
	19	392	0.0	0.7	-0.3	0.0	0.7	0.0	-0.3	0.9
	20	394	0.0	0.7	-0.3	0.0	0.7	0.0	-0.3	0.9
	21	263	0.0	0.9	-0.8	0.0	0.9	0.0	-0.8	1.8
	22	265	0.0	0.9	-0.8	0.0	0.9	0.0	-0.8	1.8
	23	156	0.2	1.0	1.9	-0.4	1.9	1.1	0.1	1.9
	24	158	0.2	1.0	1.9	-0.4	1.9	1.1	0.1	1.9
	25	148	0.4	1.2	1.5	-0.3	1.5	1.3	0.3	1.2
	26	150	0.4	1.2	1.5	-0.3	1.5	1.3	0.3	1.2
Outer Shell	27	1342	0.6	-2.0	0.1	-0.7	0.7	0.1	-2.2	2.9
	28	1344	0.6	-2.0	0.1	-0.7	0.7	0.1	-2.2	2.9
	29	1241	0.1	-1.7	0.0	0.2	0.1	0.0	-1.7	1.8
	30	1243	0.1	-1.7	0.0	0.2	0.1	0.0	-1.7	1.8
	31	1098	0.0	-0.9	0.3	0.0	0.3	0.0	-0.9	1.2
	32	1100	0.0	-0.9	0.3	0.0	0.3	0.0	-0.9	1.2
	33	747	0.0	-0.3	0.0	0.0	0.0	0.0	-0.3	0.3
	34	750	0.0	-0.3	0.0	0.0	0.0	0.0	-0.3	0.3
	35	398	0.0	0.3	0.0	0.0	0.3	0.0	0.0	0.4
	36	400	0.0	0.3	0.0	0.0	0.3	0.0	0.0	0.4
	37	269	0.2	0.9	0.3	0.0	0.9	0.3	0.2	0.7
	38	271	0.2	0.9	0.3	0.0	0.9	0.3	0.2	0.7
	39	131	-1.7	0.1	0.1	0.2	0.1	0.1	-1.7	1.9
	40	133	-1.7	0.1	0.1	0.2	0.1	0.1	-1.7	1.9
Bottom Forging	41	148	-0.2	-0.2	-0.3	-0.1	0.0	-0.3	-0.3	0.3
	42	60	-0.2	-0.2	-0.3	-0.1	0.0	-0.3	-0.3	0.3
	43	143	-0.1	0.0	-0.4	-0.1	0.1	-0.2	-0.4	0.5
	44	55	-0.1	0.0	-0.4	-0.1	0.1	-0.2	-0.4	0.5
	45	82	0.3	0.0	1.0	-0.1	1.0	0.4	0.0	1.0
	46	48	0.3	0.0	1.0	-0.1	1.0	0.4	0.0	1.0
Ram Access Cover Plate	47	32	0.0	0.0	0.0	-0.1	0.1	0.0	0.0	0.1
	48	13	0.0	0.0	0.0	-0.1	0.1	0.0	0.0	0.1
	49	31	0.0	0.0	0.0	0.0	0.0	0.0	0.0	0.1
	50	10	0.0	0.0	0.0	0.0	0.0	0.0	0.0	0.1
	51	29	0.0	0.0	0.0	0.0	0.0	0.0	0.0	0.0
	52	1	0.0	0.0	0.0	0.0	0.0	0.0	0.0	0.0

Table 2.10.7-5

Cask Membrane Plus Bending S.I. Summary - Top End Drop Lead Slump

Cask Component	Stress Point	Node Number	Stress Components (ksi)				Principal Stresses (ksi			SI (ksi)
			Sx	Sy	Sz	Sxy	S1	S2	S3	
Top Cover	1	1390	0.0	0.0	0.0	0.0	0.0	0.0	0.0	0.0
	2	1430	0.0	-0.1	0.0	0.0	0.0	0.0	-0.1	0.1
	3	1398	0.0	0.0	0.0	0.0	0.0	0.0	0.0	0.0
	4	1438	0.0	-0.1	0.0	0.0	0.0	0.0	-0.1	0.1
	5	1369	0.1	-0.1	0.2	0.1	0.2	0.1	-0.1	0.4
	6	1445	-0.1	-0.3	-0.2	0.0	-0.1	-0.2	-0.3	0.2
Top Flange	7	1373	-1.1	-11.3	0.8	-0.7	0.8	-1.0	-11.4	12.1
	8	1375	-0.4	-3.5	3.1	0.5	3.1	-0.4	-3.5	6.6
	9	1334	0.1	1.7	0.8	0.2	1.7	0.8	0.1	1.6
	10	1336	-0.5	-1.7	-0.2	-0.5	-0.2	-0.3	-1.9	1.6
Inner Shell	11	1316	-0.1	3.4	-0.8	0.1	3.4	-0.1	-0.8	4.3
	12	1318	-0.1	-5.1	-3.3	-0.7	-0.1	-3.3	-5.2	5.2
	13	1235	0.0	-1.1	0.0	0.0	0.0	0.0	-1.1	1.1
	14	1237	0.0	-0.5	0.2	0.0	0.2	0.0	-0.5	0.6
	15	1092	0.0	-0.5	0.0	0.0	0.0	0.0	-0.5	0.5
	16	1094	0.0	-0.5	0.0	0.0	0.0	0.0	-0.5	0.5
	17	742	0.0	0.1	0.0	0.0	0.1	0.0	0.0	0.1
	18	744	0.0	0.1	0.0	0.0	0.1	0.0	0.0	0.1
	19	392	0.0	0.7	-0.3	0.0	0.7	0.0	-0.3	0.9
	20	394	0.0	0.7	-0.2	0.0	0.7	0.0	-0.2	1.0
	21	263	0.0	0.9	-0.8	0.0	0.9	0.0	-0.8	1.8
	22	265	0.0	0.9	-0.8	0.0	0.9	0.0	-0.8	1.7
	23	156	0.1	-2.3	1.0	0.0	1.0	0.1	-2.3	3.3
	24	158	0.3	4.3	2.9	-0.7	4.4	2.9	0.2	4.3
	25	148	-0.3	-1.5	0.7	0.1	0.7	-0.3	-1.5	2.2
	26	150	1.2	3.9	2.4	-0.8	4.1	2.4	0.9	3.2
Outer Shell	27	1342	0.4	6.4	2.4	-1.4	6.7	2.4	0.1	6.6
	28	1344	0.7	-10.4	-2.3	0.0	0.7	-2.3	-10.4	11.1
	29	1241	-0.1	-0.7	0.2	0.1	0.2	-0.1	-0.7	0.9
	30	1243	0.3	-2.7	-0.2	0.2	0.3	-0.2	-2.7	3.0
	31	1098	0.0	-0.7	0.4	0.0	0.4	0.0	-0.7	1.1
	32	1100	0.0	-1.1	0.3	0.0	0.3	0.0	-1.1	1.4
	33	747	0.0	-0.3	0.0	0.0	0.0	0.0	-0.3	0.3
	34	750	0.0	-0.3	0.0	0.0	0.0	0.0	-0.3	0.3
	35	398	0.0	0.3	-0.1	0.0	0.3	0.0	-0.1	0.4
	36	400	0.0	0.4	0.0	0.0	0.4	0.0	0.0	0.4
	37	269	0.1	0.4	0.1	-0.1	0.5	0.1	0.1	0.3
	38	271	0.3	1.4	0.5	0.1	1.4	0.5	0.3	1.1
	39	131	-2.8	-5.1	-1.6	0.1	-1.6	-2.8	-5.1	3.5
	40	133	-0.6	5.2	1.8	0.3	5.2	1.8	-0.7	5.9
Bottom Forging	41	148	0.1	-0.8	1.1	-0.1	1.1	0.1	-0.8	1.8
	42	60	-0.5	0.4	-1.7	-0.2	0.5	-0.5	-1.7	2.2
	43	143	0.9	0.0	2.0	-0.1	2.0	1.0	0.0	2.1
	44	55	-1.2	0.0	-2.8	-0.1	0.0	-1.2	-2.8	2.8
	45	82	0.9	0.0	3.3	0.0	3.3	0.9	0.0	3.4
	46	48	-0.3	0.0	-1.4	-0.2	0.0	-0.3	-1.4	1.5
Ram Access Cover Plate	47	32	0.2	0.1	0.2	-0.1	0.3	0.2	0.0	0.2
	48	13	-0.2	0.0	-0.3	0.0	0.0	-0.2	-0.3	0.3
	49	31	0.4	0.1	0.3	-0.1	0.4	0.3	0.0	0.3
	50	10	-0.4	0.0	-0.3	0.0	0.0	-0.3	-0.4	0.4
	51	29	0.4	0.0	0.4	0.0	0.4	0.4	0.0	0.4
	52	1	-0.3	0.0	-0.3	0.0	0.0	-0.3	-0.3	0.3

Table 2.10.7-6

Cask Primary Plus Secondary S.I. Summary - Top End Drop Lead Slump

Cask Component	Stress Point	Node Number	Stress Components (ksi)				Principal Stresses (ksi)			SI (ksi)
			Sx	Sy	Sz	Sxy	S1	S2	S3	
Top Cover	1	1390	0.0	0.0	0.0	0.0	0.0	0.0	0.0	0.0
	2	1430	0.0	-0.1	0.0	0.0	0.0	0.0	-0.1	0.1
	3	1398	0.0	0.0	0.0	0.0	0.0	0.0	0.0	0.0
	4	1438	0.0	-0.1	0.0	0.0	0.0	0.0	-0.1	0.1
	5	1369	0.1	0.2	5.1	0.2	5.1	0.4	0.0	5.2
	6	1445	-0.1	-0.2	-0.1	0.0	-0.1	-0.1	-0.2	0.1
Top Flange	7	1373	-1.2	-10.7	0.9	-0.8	0.9	-1.1	-10.8	11.7
	8	1375	-0.5	-2.9	3.2	0.4	3.2	-0.4	-2.9	6.1
	9	1334	0.0	1.9	0.8	0.3	1.9	0.8	-0.1	2.0
	10	1336	-0.1	-2.4	-1.2	-0.2	-0.1	-1.2	-2.5	2.4
Inner Shell	11	1316	-0.1	3.4	-0.8	0.0	3.4	-0.1	-0.8	4.3
	12	1318	-0.2	-5.2	-3.3	-0.7	-0.1	-3.3	-5.3	5.2
	13	1235	0.0	-1.1	0.0	0.0	0.0	0.0	-1.1	1.1
	14	1237	0.0	-0.5	0.2	0.0	0.2	0.0	-0.5	0.6
	15	1092	0.0	-0.5	0.0	0.0	0.0	0.0	-0.5	0.5
	16	1094	0.0	-0.5	0.0	0.0	0.0	0.0	-0.5	0.5
	17	742	0.0	0.1	0.0	0.0	0.1	0.0	0.0	0.1
	18	744	0.0	0.1	0.0	0.0	0.1	0.0	0.0	0.1
	19	392	0.0	0.7	-0.3	0.0	0.7	0.0	-0.3	0.9
	20	394	0.0	0.7	-0.2	0.0	0.7	0.0	-0.2	1.0
	21	263	0.0	0.9	-0.8	0.0	0.9	0.0	-0.8	1.8
	22	265	0.0	0.9	-0.8	0.0	0.9	0.0	-0.8	1.7
	23	156	0.2	-2.2	1.0	-0.1	1.0	0.2	-2.2	3.2
	24	158	0.3	4.4	2.9	-0.8	4.6	2.9	0.2	4.4
	25	148	-0.3	-1.3	0.7	-0.1	0.7	-0.3	-1.3	2.0
	26	150	1.3	4.2	2.6	-1.0	4.5	2.6	1.0	3.6
Outer Shell	27	1342	-0.4	-1.9	-0.9	0.0	-0.4	-0.9	-1.9	1.5
	28	1344	0.7	-8.5	-1.7	0.1	0.7	-1.7	-8.5	9.2
	29	1241	0.0	-1.3	-0.4	0.0	0.0	-0.4	-1.3	1.2
	30	1243	0.3	-2.8	-0.2	0.2	0.3	-0.2	-2.8	3.1
	31	1098	0.0	-1.0	-0.1	0.0	0.0	-0.1	-1.0	1.0
	32	1100	0.0	-1.1	0.3	0.0	0.3	0.0	-1.1	1.4
	33	747	0.0	-0.1	0.0	0.0	0.0	0.0	-0.1	0.1
	34	750	0.0	-0.3	0.0	0.0	0.0	0.0	-0.3	0.3
	35	398	0.0	0.9	0.1	0.0	0.9	0.1	0.0	0.9
	36	400	0.0	0.4	0.0	0.0	0.4	0.0	0.0	0.4
	37	269	0.0	1.2	0.3	0.0	1.2	0.3	0.0	1.2
	38	271	0.3	1.5	0.5	0.1	1.5	0.5	0.3	1.1
	39	131	-2.5	-5.9	-1.7	-0.1	-1.7	-2.5	-5.9	4.1
	40	133	-0.4	4.4	1.7	0.1	4.4	1.7	-0.4	4.7
Bottom Forging	41	148	-0.3	-1.3	0.7	-0.1	0.7	-0.3	-1.3	2.0
	42	60	-0.5	0.1	-1.9	-0.1	0.1	-0.5	-1.9	1.9
	43	143	0.9	0.0	2.0	0.0	2.0	0.9	0.0	2.0
	44	55	-1.2	0.0	-2.8	0.0	0.0	-1.2	-2.8	2.8
	45	82	0.9	0.0	3.4	0.1	3.4	1.0	0.0	3.4
	46	48	0.0	-0.1	0.1	0.0	0.1	0.0	-0.1	0.2
Ram Access Cover Plate	47	32	0.3	0.1	0.2	-0.1	0.3	0.2	0.0	0.2
	48	13	-0.2	0.0	-0.3	0.0	0.0	-0.2	-0.3	0.3
	49	31	0.4	0.1	0.3	-0.1	0.4	0.3	0.0	0.4
	50	10	-0.4	0.0	-0.4	0.0	0.0	-0.4	-0.4	0.4
	51	29	0.4	0.0	0.4	0.0	0.4	0.4	0.0	0.4
	52	1	-0.3	0.0	-0.3	0.0	0.0	-0.3	-0.3	0.3

2.10.8 Impact Limiter Energy Absorbing Material Bench Tests

THIS SECTION CONTAINS
PROPRIETARY INFORMATION

2.10.9 Impact Limiter Design and Performance Evaluation

THIS SECTION CONTAINS
PROPRIETARY INFORMATION

2.10.10 Determination of Dynamic Load Factors for Free Drop Analysis

2.10.10.1 Introduction

The NUHOMS®-MP187 transportation package is analyzed for the 1 foot and 30 foot free drop conditions specified in the Part 71 Regulations [2.1] using equivalent static methods. The equivalent static loads used for the drop stress evaluations of the MP187 package components are determined by multiplying the peak rigid body accelerations from the respective time histories by the corresponding dynamic load factor (DLF). The purpose of this analysis is to determine the dynamic load factors for use in the 1 foot and 30 foot free drop equivalent static structural analyses.

2.10.10.2 Technical Approach

The structural response of the various MP187 package structural components to the 1 foot and 30 foot free drop loading depends upon the dynamic loading characteristics (i.e. shape of the loading function and duration of loading) and the frequency content of the structural components. The dynamic loading characteristics are provided by the acceleration time histories calculated in Section 2.10.9, the drop evaluation. Using the acceleration time histories for the various drop conditions, the dynamic load factor is calculated for frequencies between 1 and 200 Hz for damping values of 0%, 2%, 5%, 10%, and 20% using the computer program "DLF". The accuracy of the "DLF" program is verified in Section 2.10.10.6.

The fundamental frequencies of the NUHOMS®-MP187 Multi-Purpose Cask, FO-DSC, FC-DSC and FF-DSC structural components are determined using a combination of computer models and hand calculations. Based on the fundamental frequencies of the structural components, the dynamic load factors are determined from the DLF versus frequency curves.

2.10.10.3 Dynamic Load Factor Curves

As discussed in Section 2.10.10.2, dynamic amplification is a function of the characteristics of the dynamic loading as well as the characteristics of the structure. The most important characteristics of dynamic loading upon the DLF are the rise time (i.e., time to reach peak acceleration) and the duration of loading. Due to the geometry of the impact limiters, each drop condition will yield a different acceleration time history. Therefore, a range of drop conditions is considered for the purpose of this analysis. The drop cases considered in this analysis are listed below:

Normal (1 foot) Drop Conditions

- Flat Side 1 foot Horizontal Drop

Accident (30 foot) Drop Conditions

- Flat Side Slapdown
- Corner Slapdown
- Flat Side 30° Drop
- Corner 30° Drop
- Flat Side 60° Drop
- Corner 60° Drop
- Corner 72° Drop (C.G. over Flat Side)
- Corner 72° Drop (C.G. over Corner)
- Vertical End Drop
- Flat Side Horizontal Drop
- Corner Horizontal Drop

Each of the conditions listed above is analyzed for both hot and cold conditions. The acceleration time history data used for the analysis is from the vertical direction at the package center of gravity. Since the acceleration time history loading characteristics are similar for both the longitudinal and tangential direction, and vary only in magnitude along the length of the package, the DLF versus frequency results for the vertical direction can be applied to both of the axes at all axial locations.

The characteristics of the structure which influence the response are the frequency content of the structure, the type and condition of the structure and the stress levels in the structure resulting from the dynamic loading. The amount of structural damping is highly dependent upon the type and condition of the structure and the stress levels in the structure. The type and condition of the MP187 transportation package is best characterized as a relatively loose fitting series of structures captured one inside another. This type of structure exhibits a significant amount of damping due to sliding friction between various components and plastic deformation of the cask and DSC shielding materials when subjected to accident drop type loads. The amount of damping is expected to be greater than or equal to that observed in typical bolted or riveted steel structures. The percentage of critical damping in bolted steel structures for various stress levels is shown below (Table 13.1 of [2.12]):

Stress Level	% Critical Damping
At 1/2 of yield point	5 - 7
At or just below yield point	10 - 15
Beyond yield point	20

Based upon these considerations, damping values of 10% and 20% are reasonable for the normal drop and accident drop conditions, respectively. For the purposes of this analysis, damping is conservatively ignored for normal and accident drop conditions. The DLF values for frequencies between 1 and 200 Hz are determined for 0% damping using the "DLF" program which determines the dynamic and static response (i.e. deflection) of a single degree of freedom (SDOF) oscillator for a given dynamic load and calculates the DLF as the ratio of the dynamic response to the static response. Selected computer run output is included in Section 2.10.10.7. Figures illustrating the various normal and accident drop conditions and the corresponding acceleration time history and DLF versus frequency results are shown in Figure 2.10.10-1 through Figure 2.10.10-33.

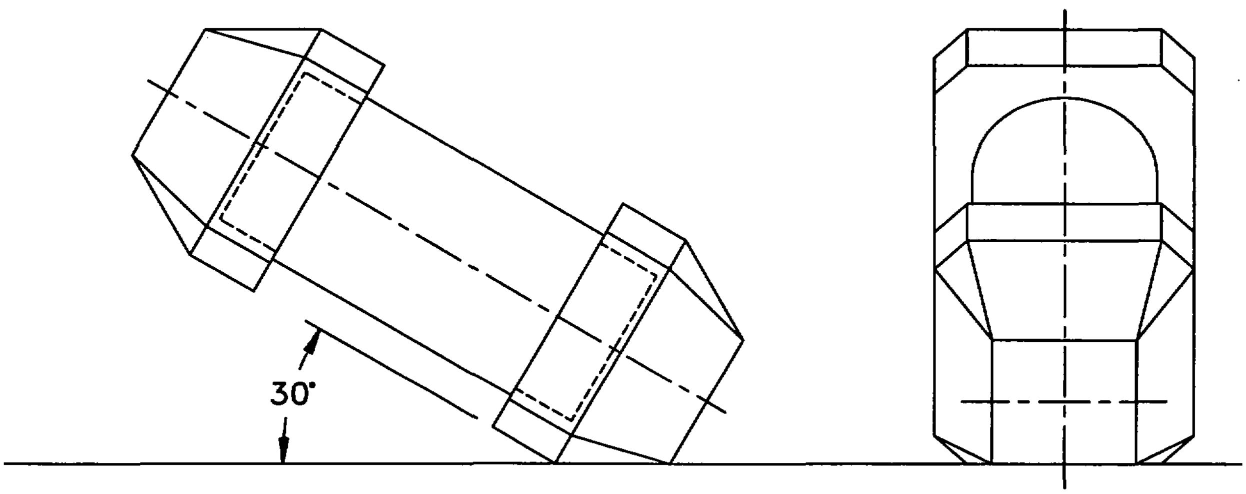

Figure 2.10.10-1

Flat Side 30° Drop Orientation

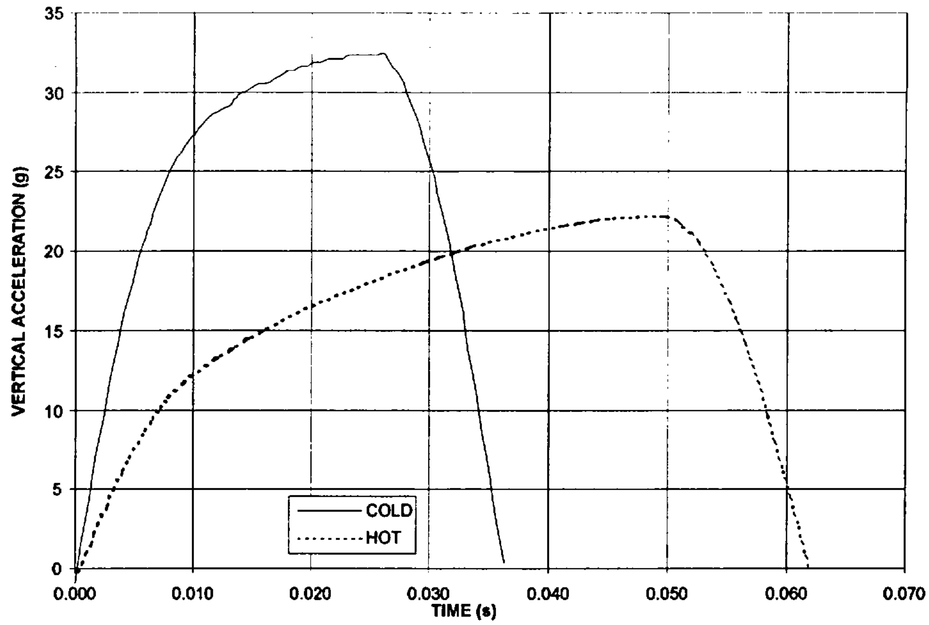

Figure 2.10.10-2

Flat Side 30° Drop Primary Impact Acceleration Time Histories

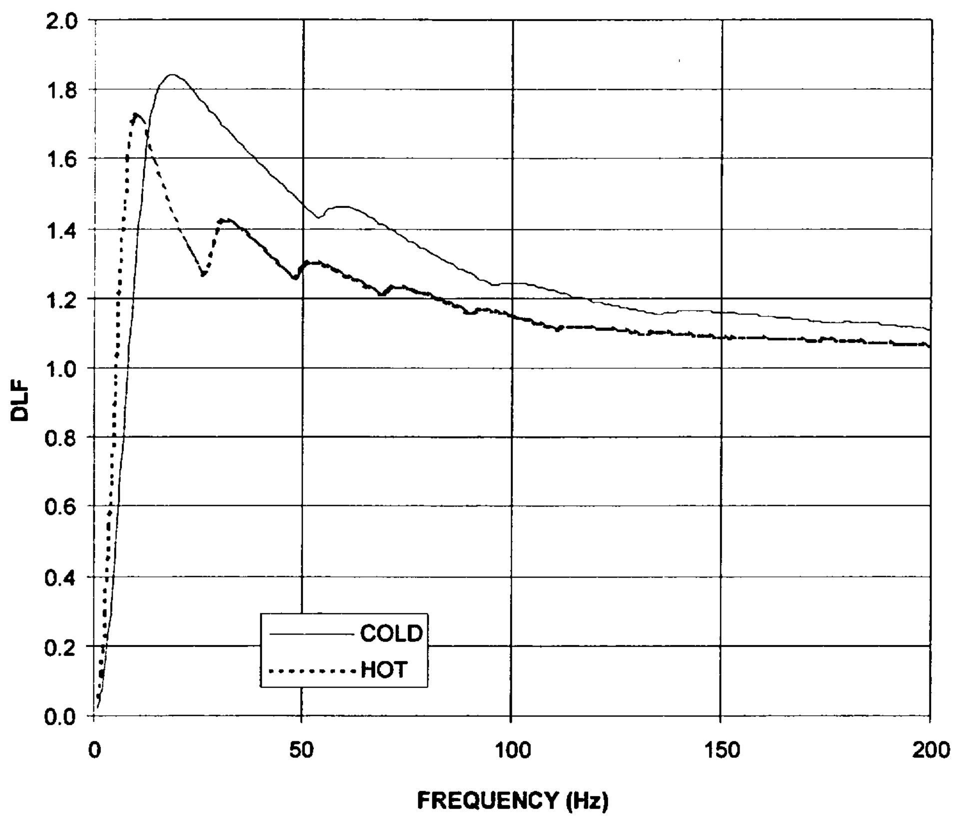

Figure 2.10.10-3

Flat Side 30° Primary Impact DLFs

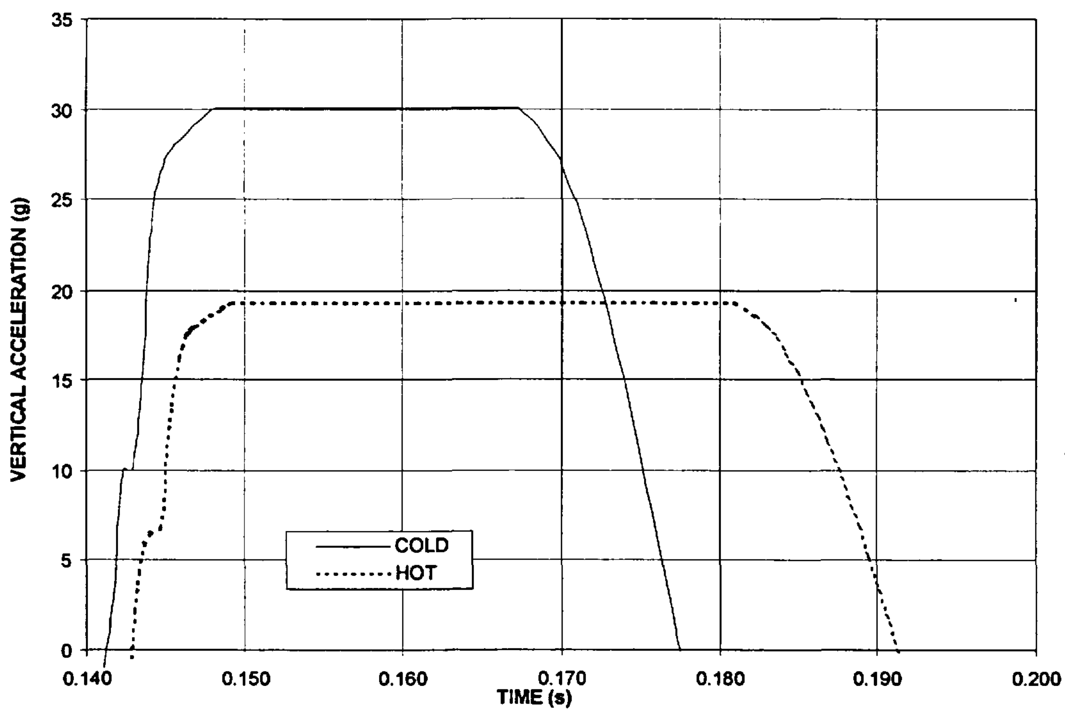

Figure 2.10.10-4

Flat Side Slapdown Acceleration Time Histories

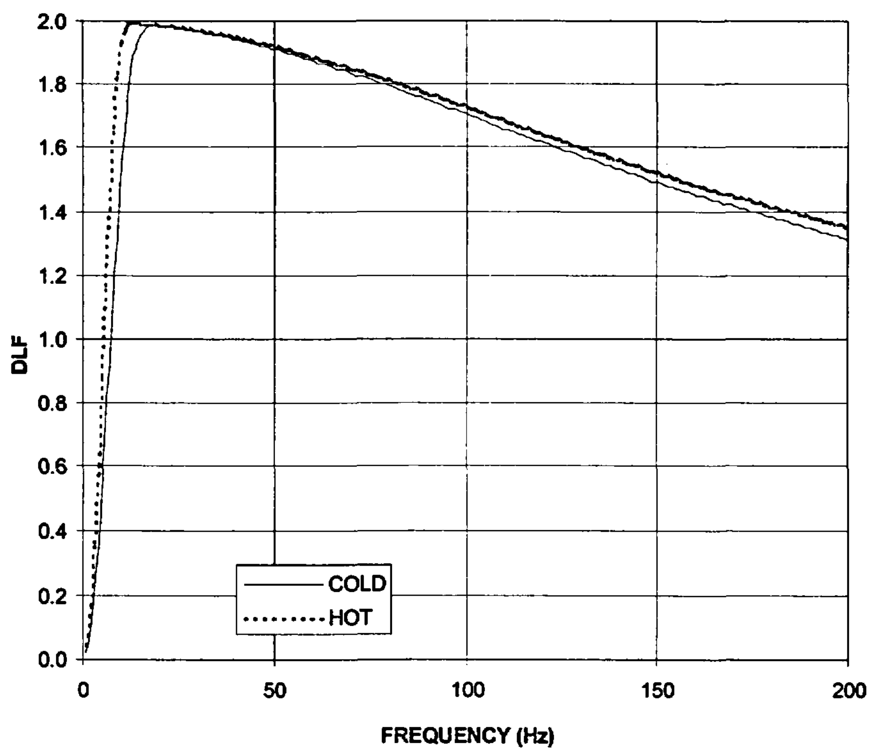

Figure 2.10.10-5

Flat Side Slapdown DLFs

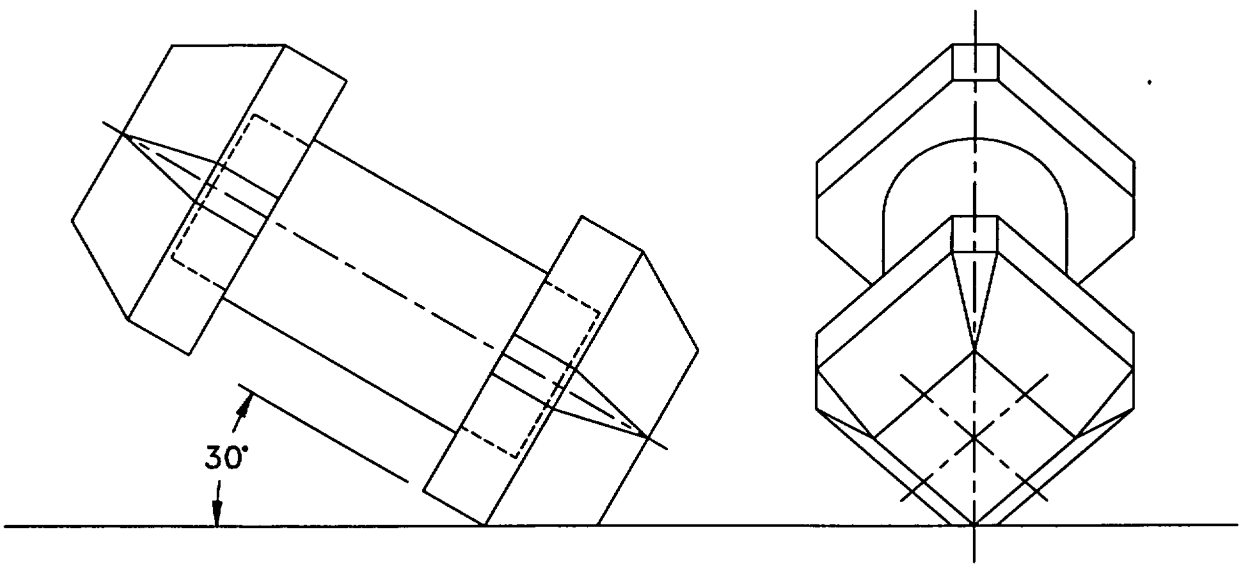

Figure 2.10.10-6

Corner 30° Drop Orientation

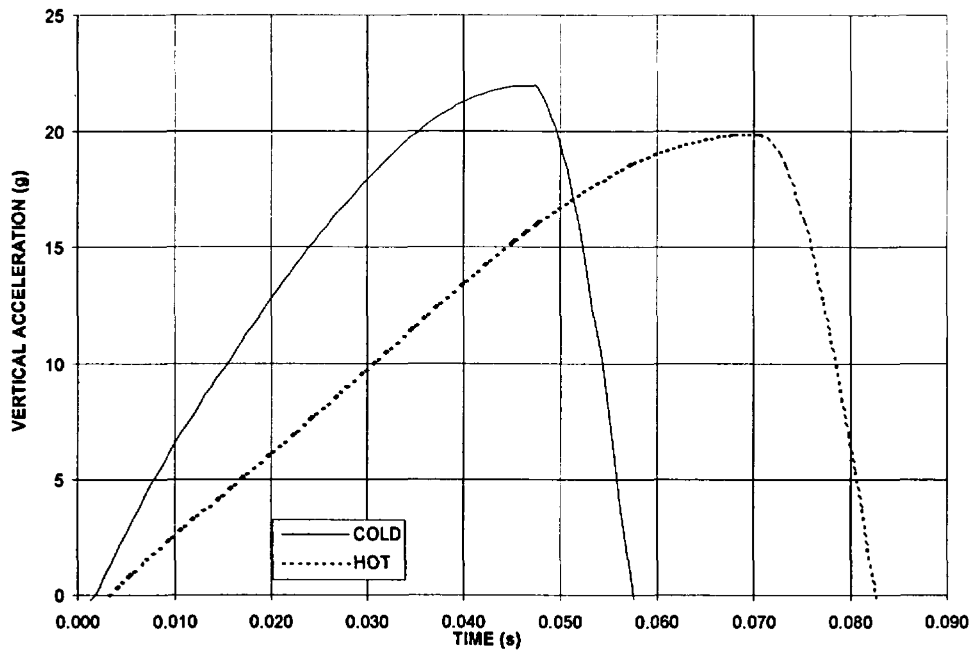

Figure 2.10.10-7

Corner 30° Primary Impact Acceleration Time Histories

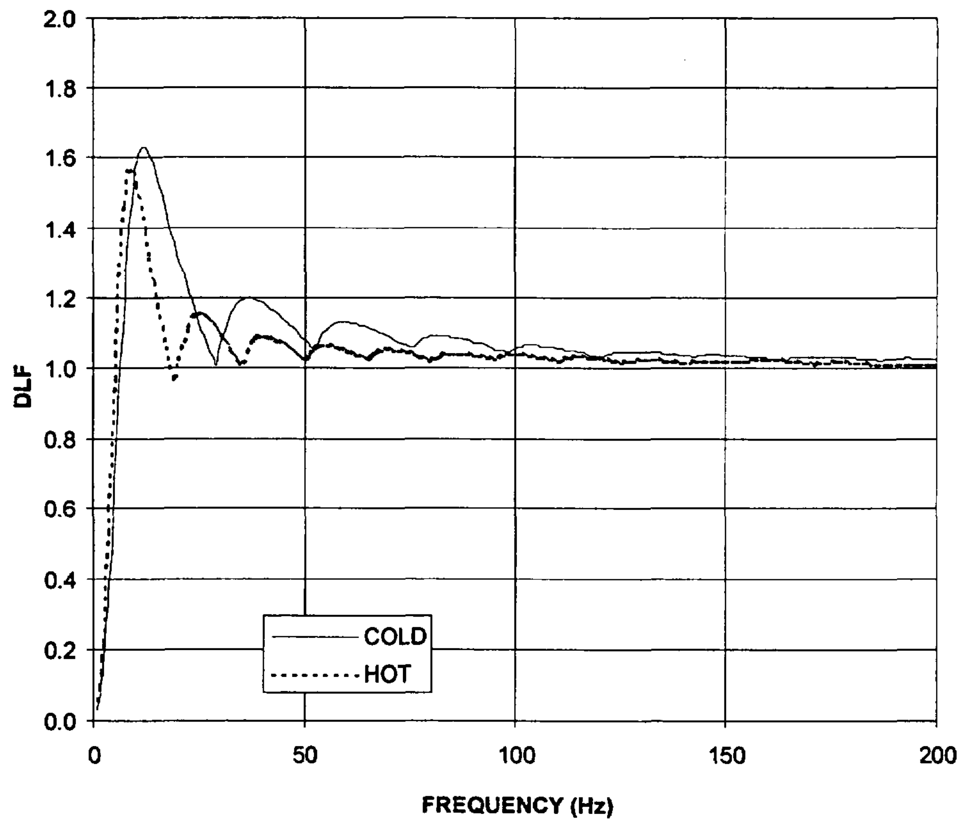

Figure 2.10.10-8

Corner 30° Primary Impact DLFs

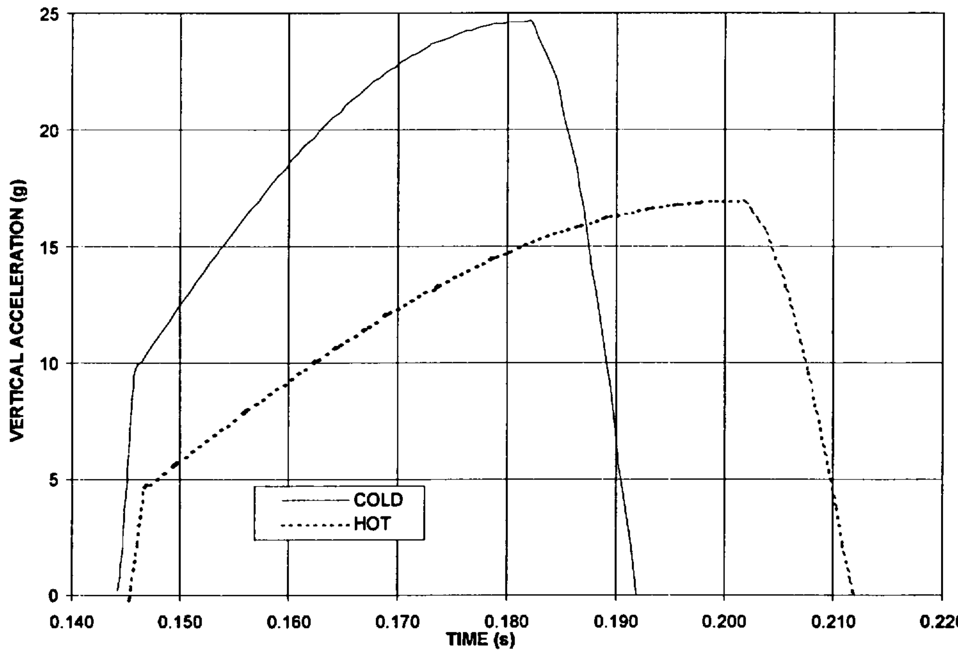

Figure 2.10.10-9

Corner Slapdown Acceleration Time Histories

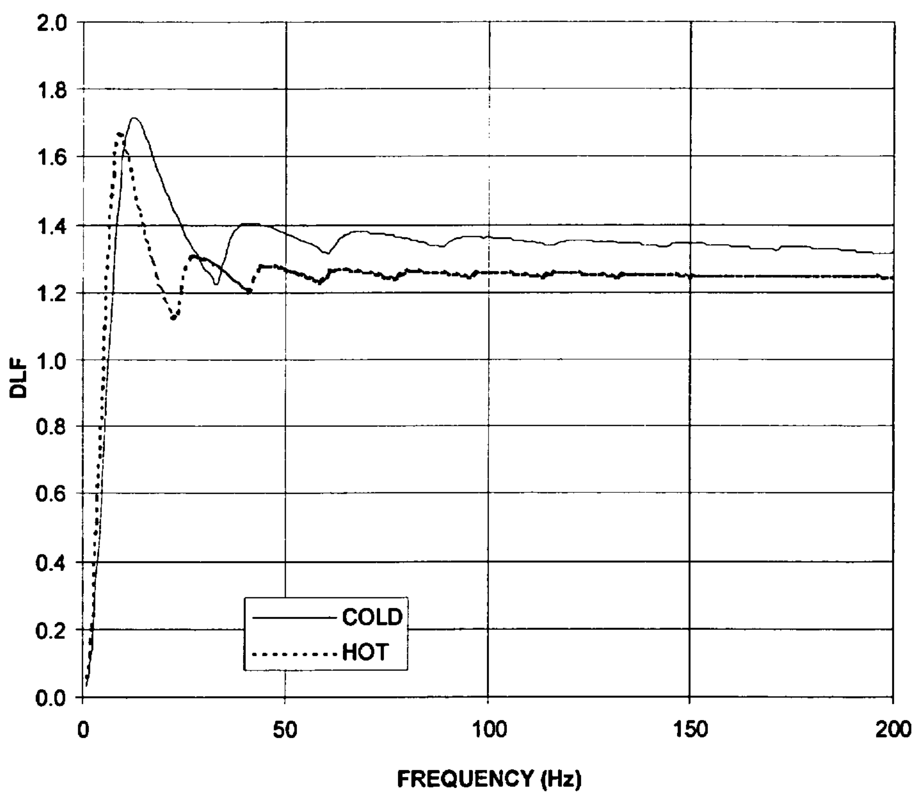

Figure 2.10.10-10

Corner Slapdown DLFs

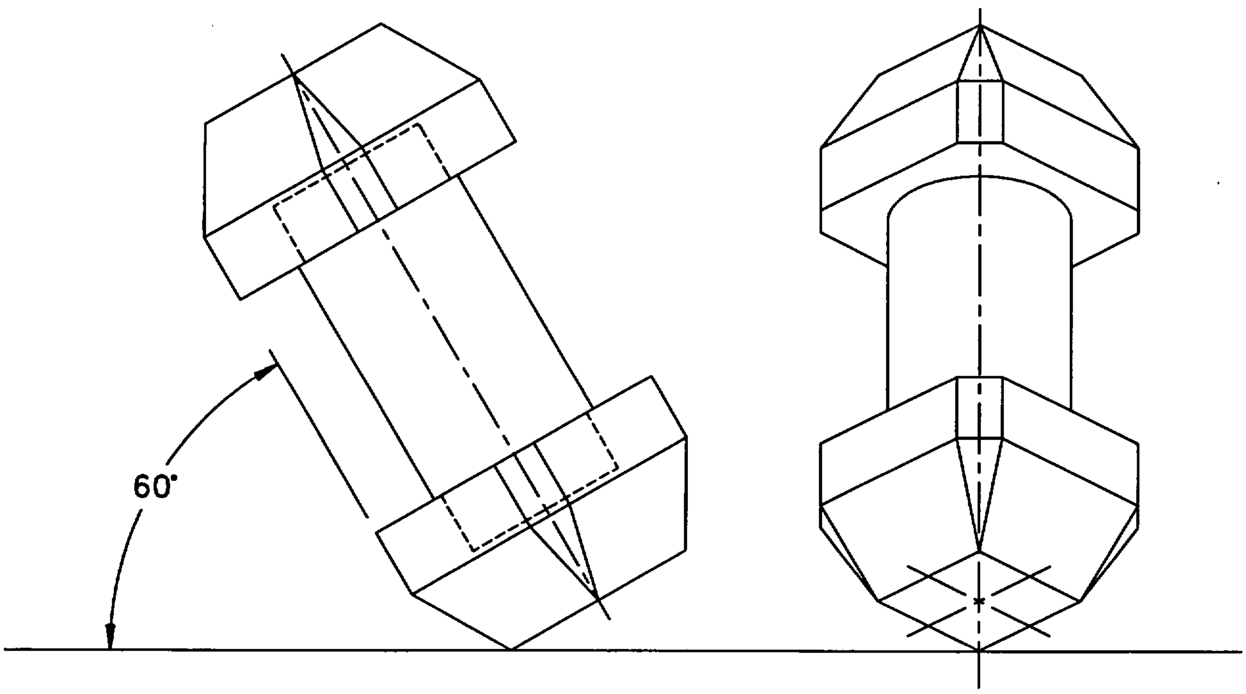

Figure 2.10.10-11

Corner 60° Drop Orientation

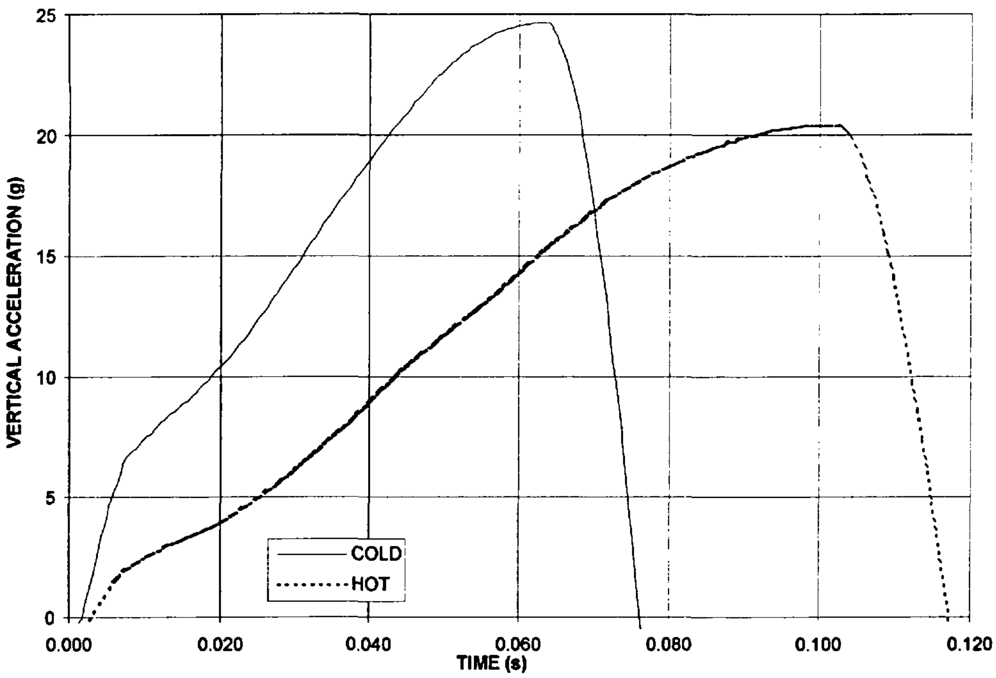

Figure 2.10.10-12

Corner 60° Drop Acceleration Time Histories

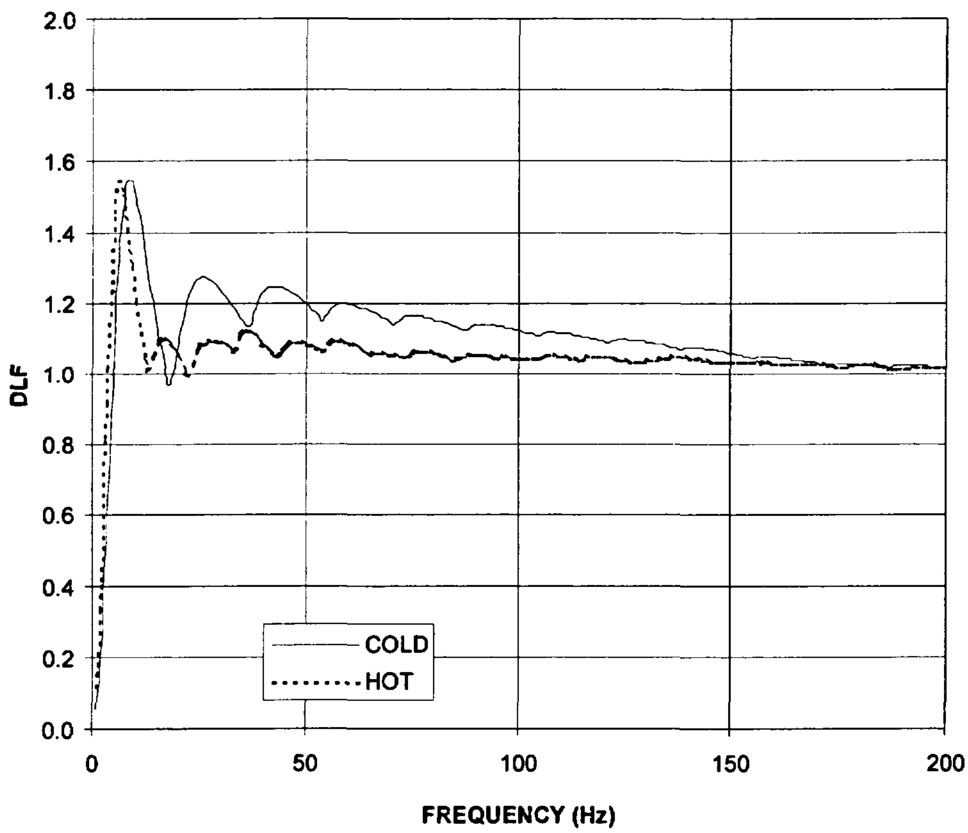

Figure 2.10.10-13

Corner 60° Drop DLFs

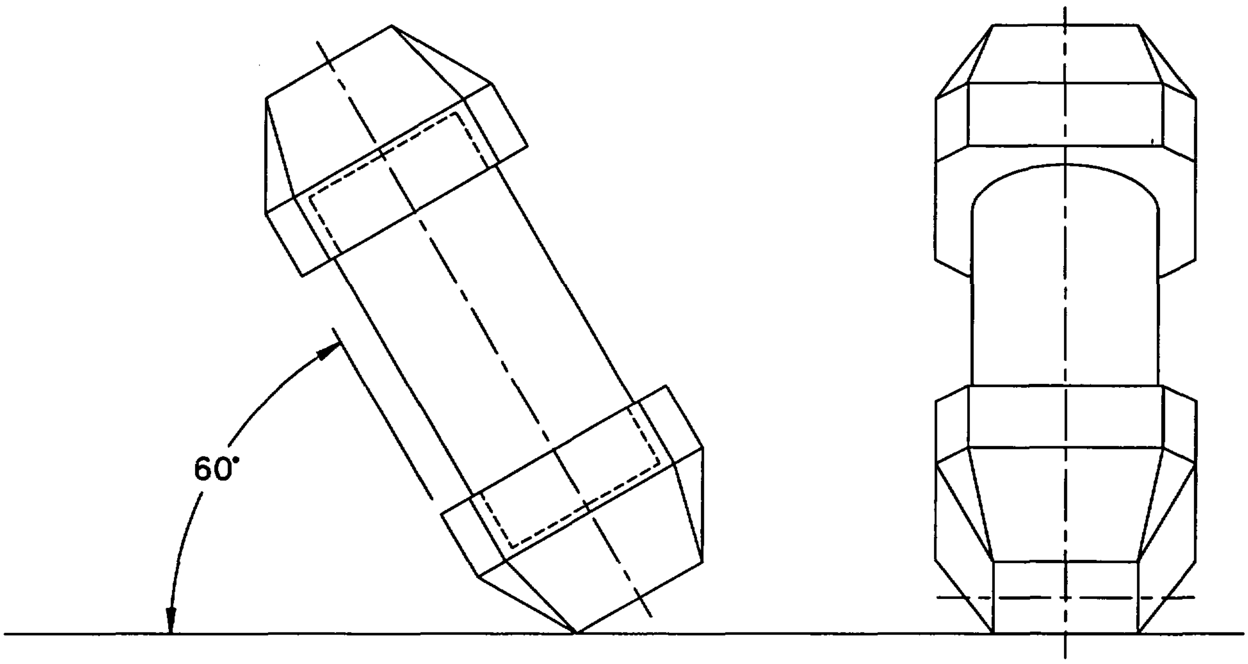

Figure 2.10.10-14

Flat Side 60° Drop Orientation

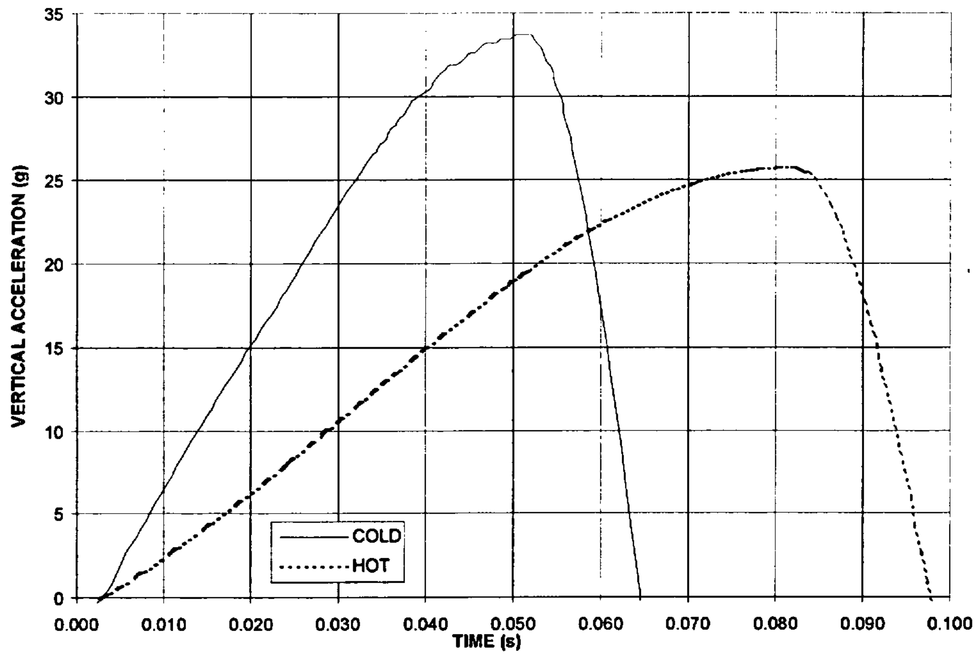

Figure 2.10.10-15

Flat Side 60° Drop Acceleration Time Histories

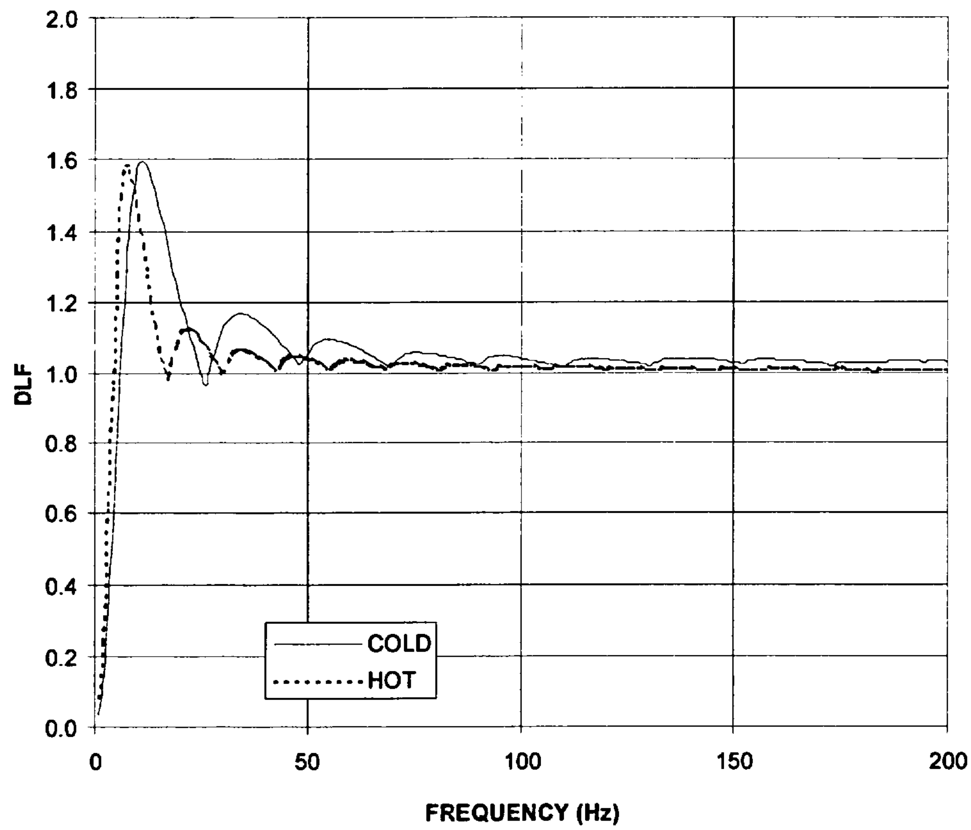

Figure 2.10.10-16

Flat Side 60° Drop DLFs

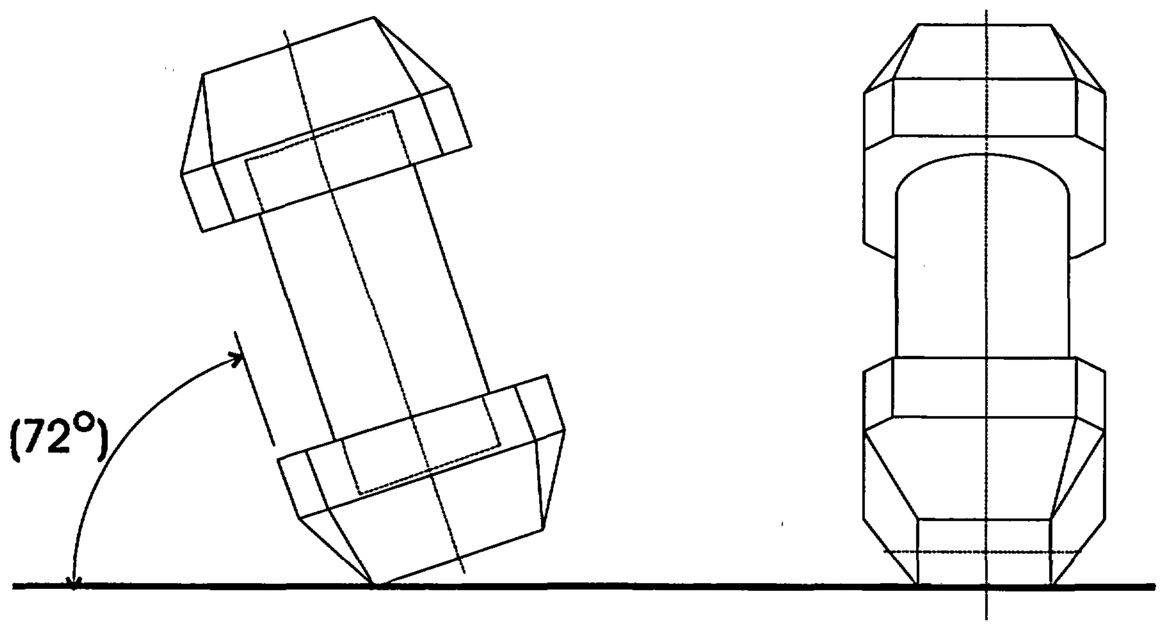

Figure 2.10.10-17
Flat 72° Drop Orientation (C.G. over Flat)

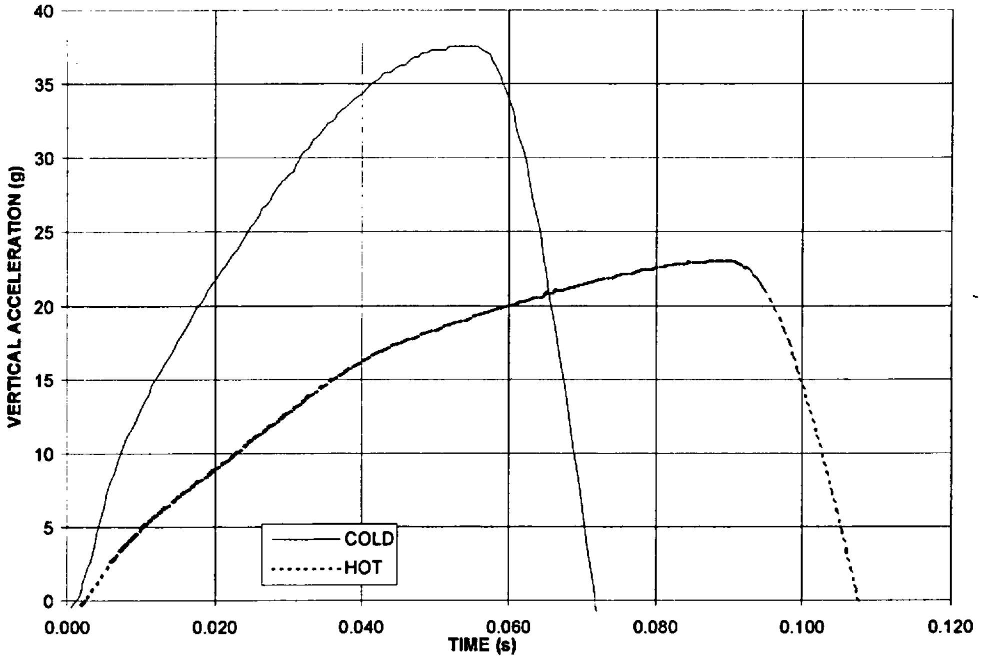

Figure 2.10.10-18

Flat 72° (C.G. over Flat) Acceleration Time Histories

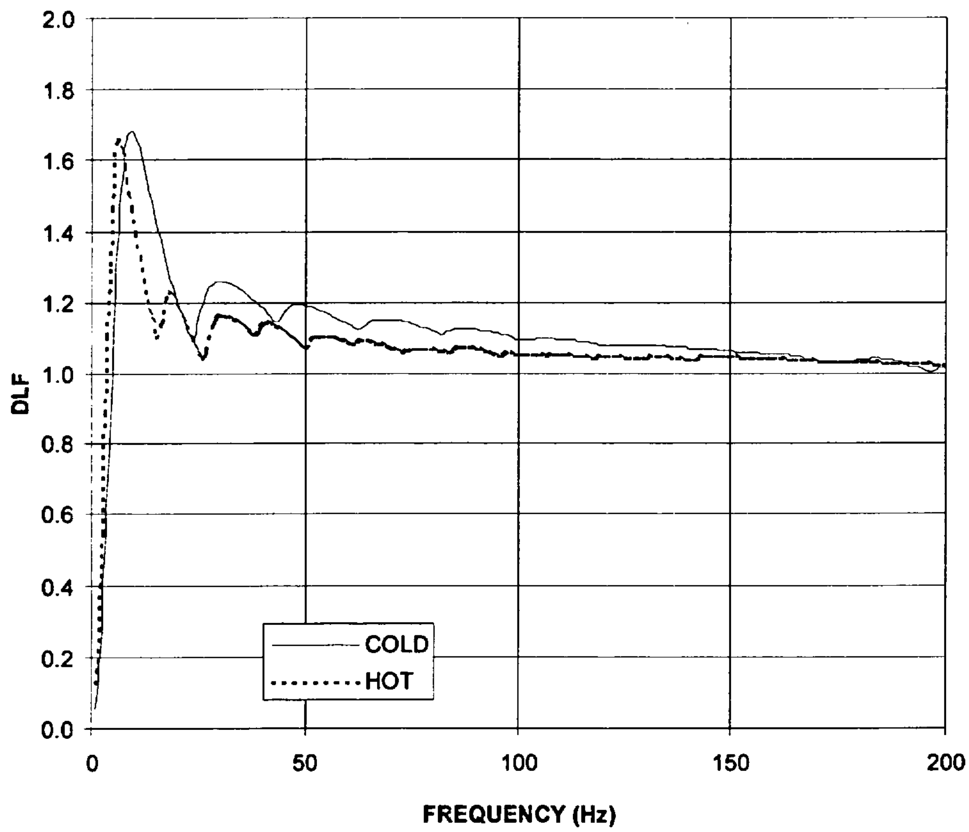

Figure 2.10.10-19

Flat 72° (C.G. over Flat) Drop DLFs

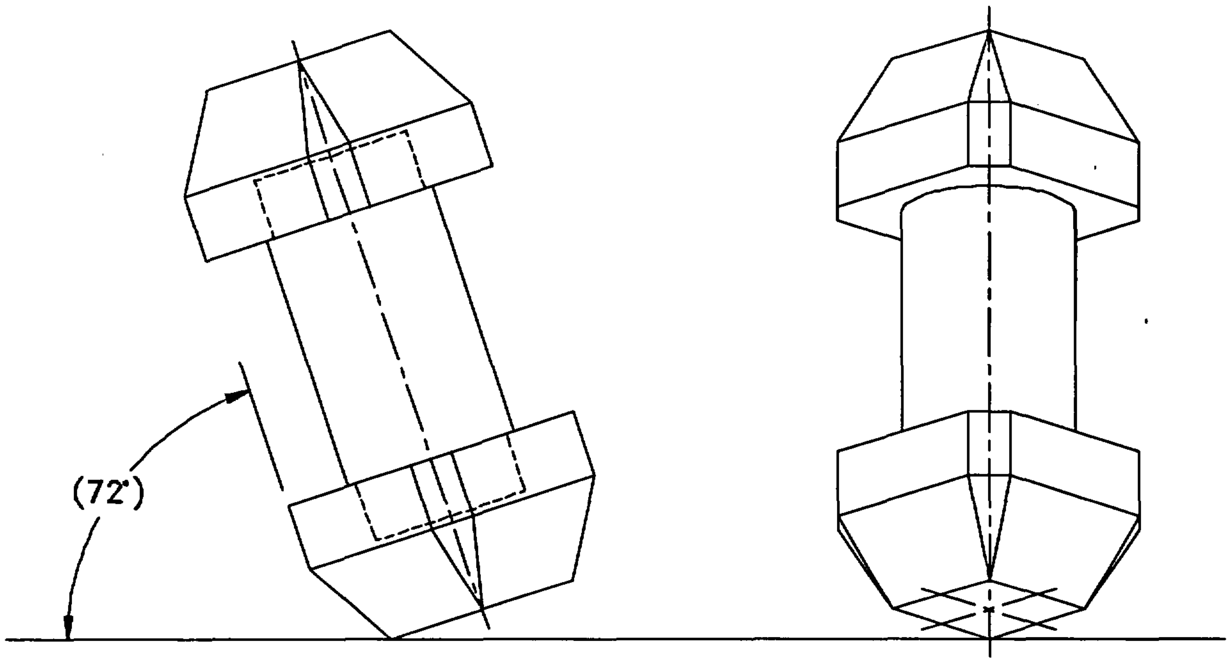

Figure 2.10.10-20

Corner 72° Drop Orientation (C.G. over Corner)

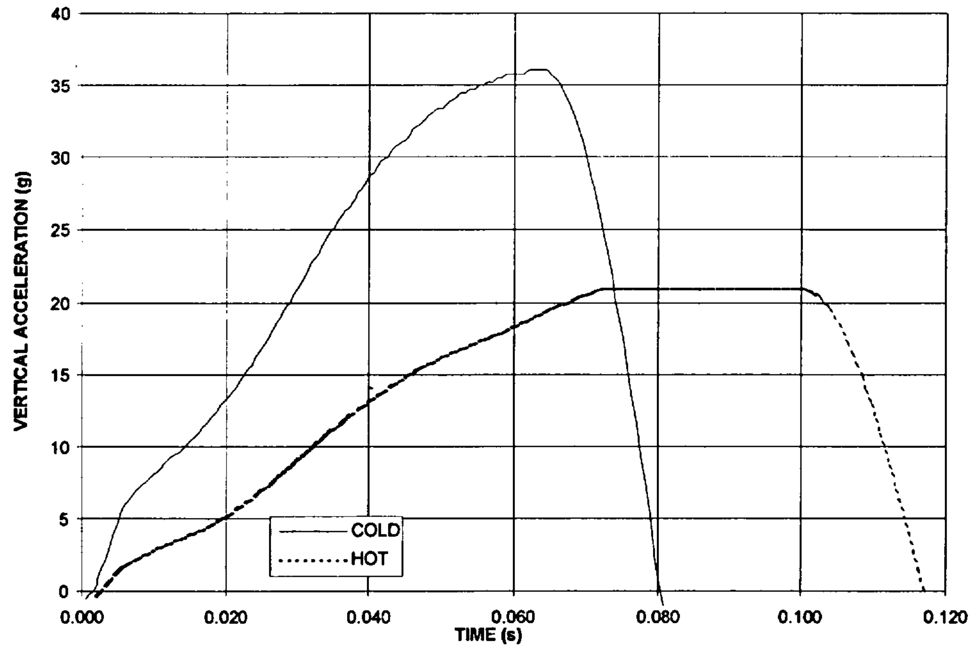

Figure 2.10.10-21

Corner 72° (C.G. over Corner) Acceleration Time Histories

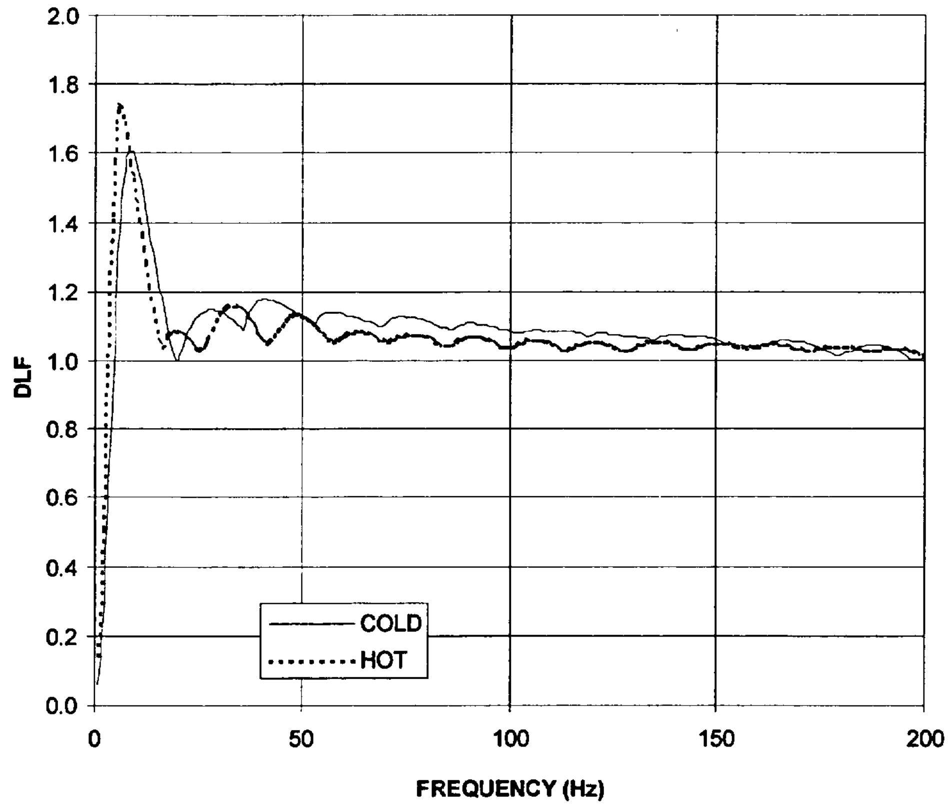

Figure 2.10.10-22

Corner 72° (C.G. over Corner) Drop DLFs

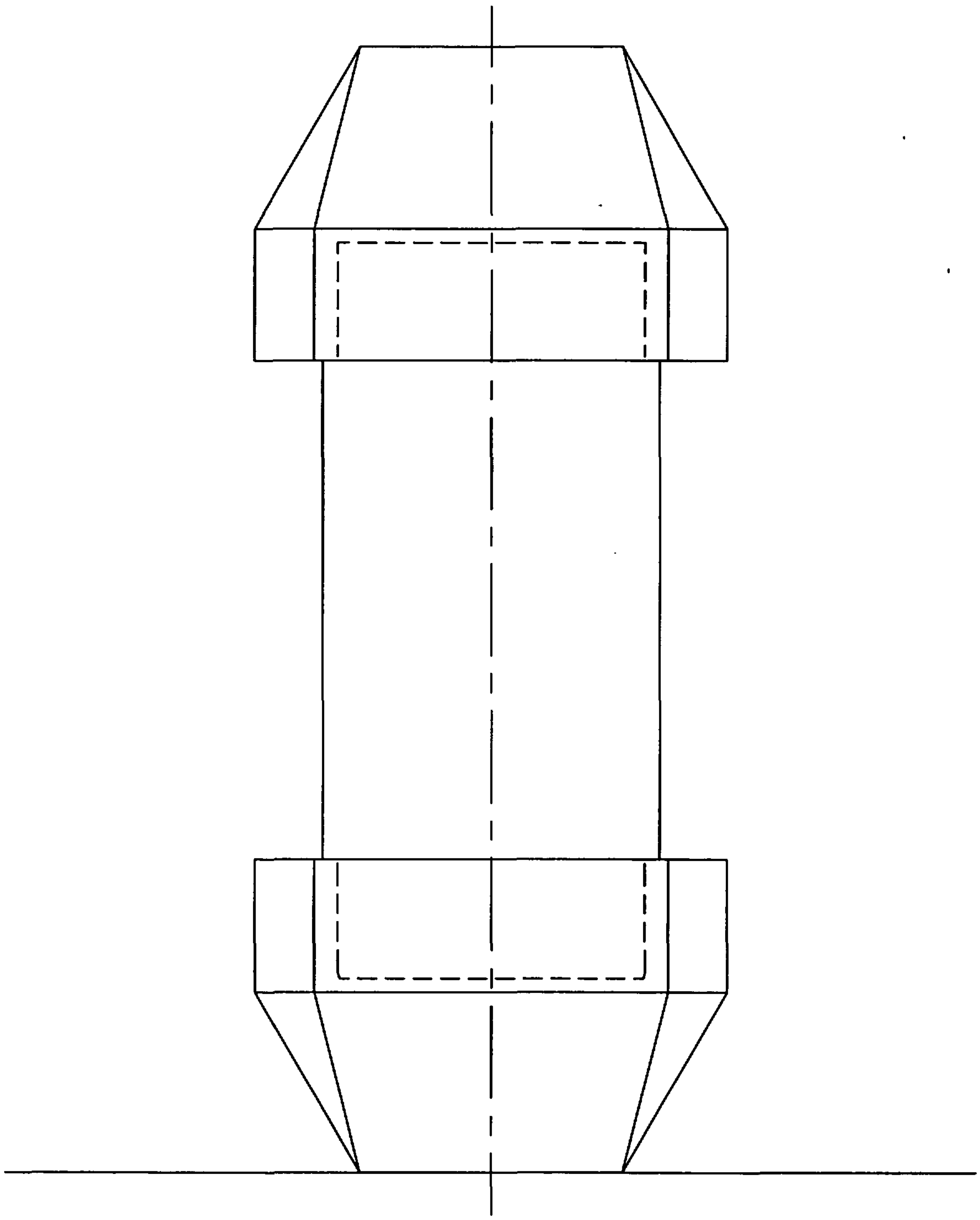

Figure 2.10.10-23

Vertical End Drop Orientation

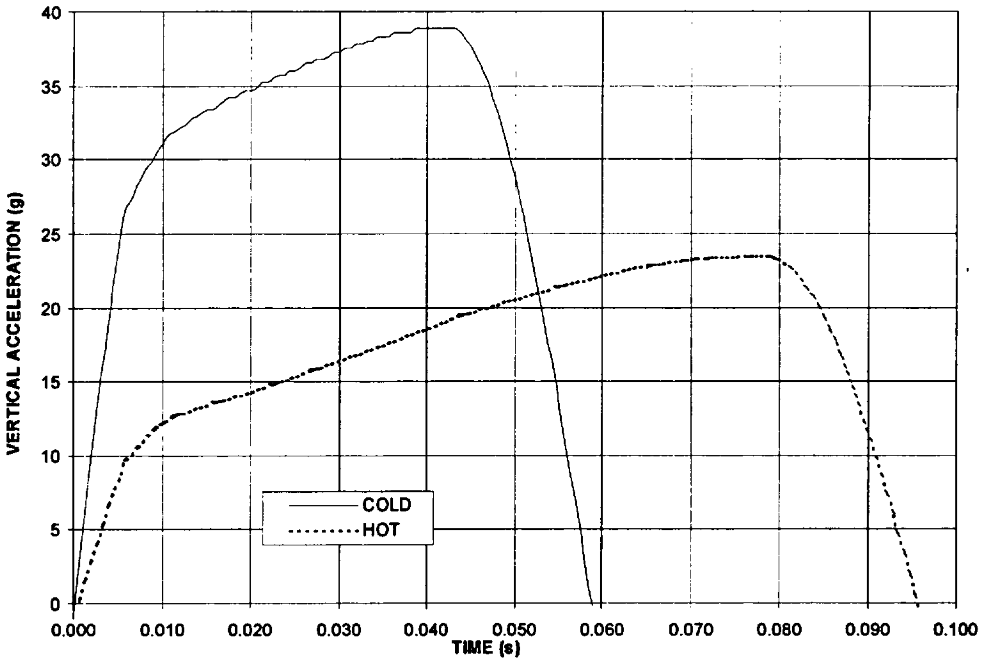

Figure 2.10.10-24

End Drop Acceleration Time Histories

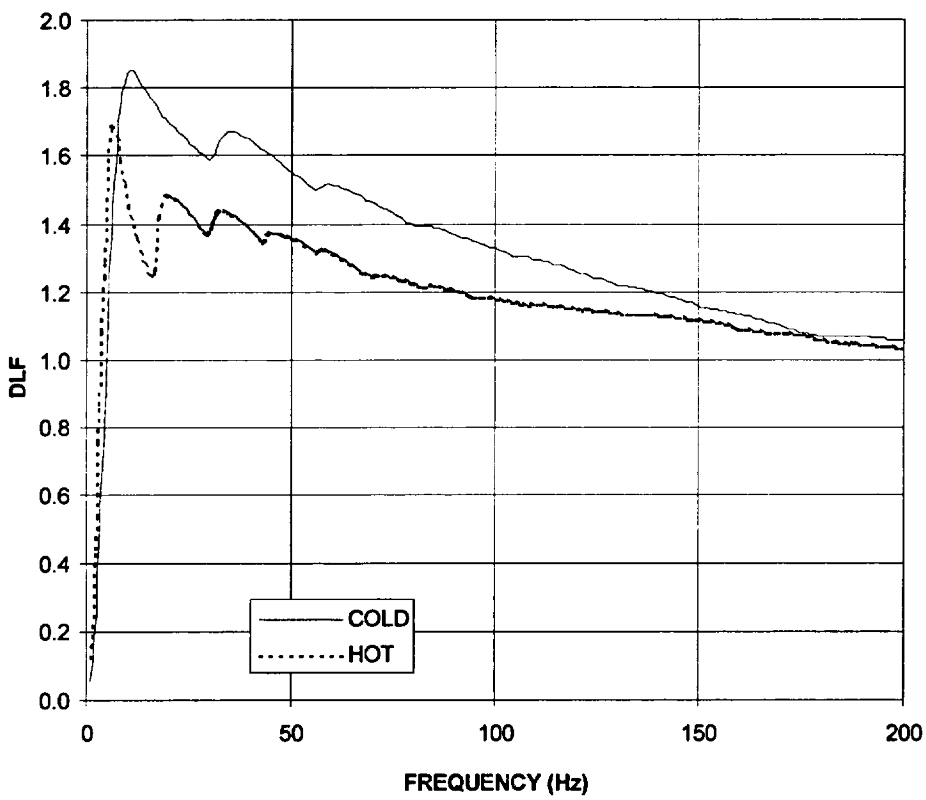

Figure 2.10.10-25

End Drop DLFs

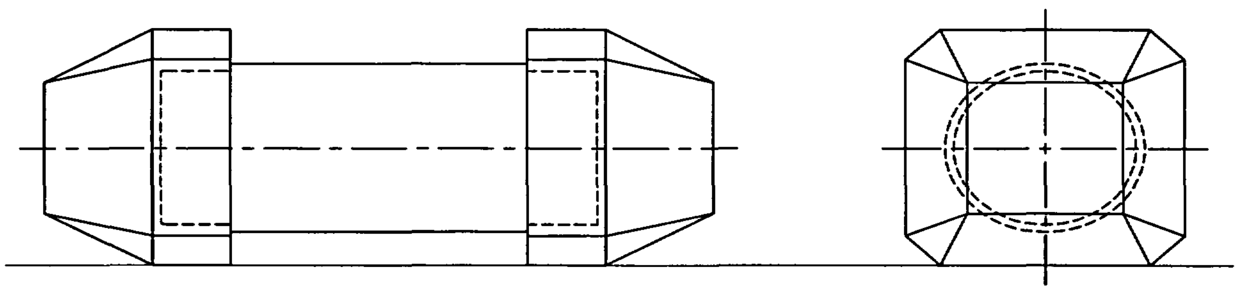

Figure 2.10.10-26

Flat-Side Horizontal Drop Orientation

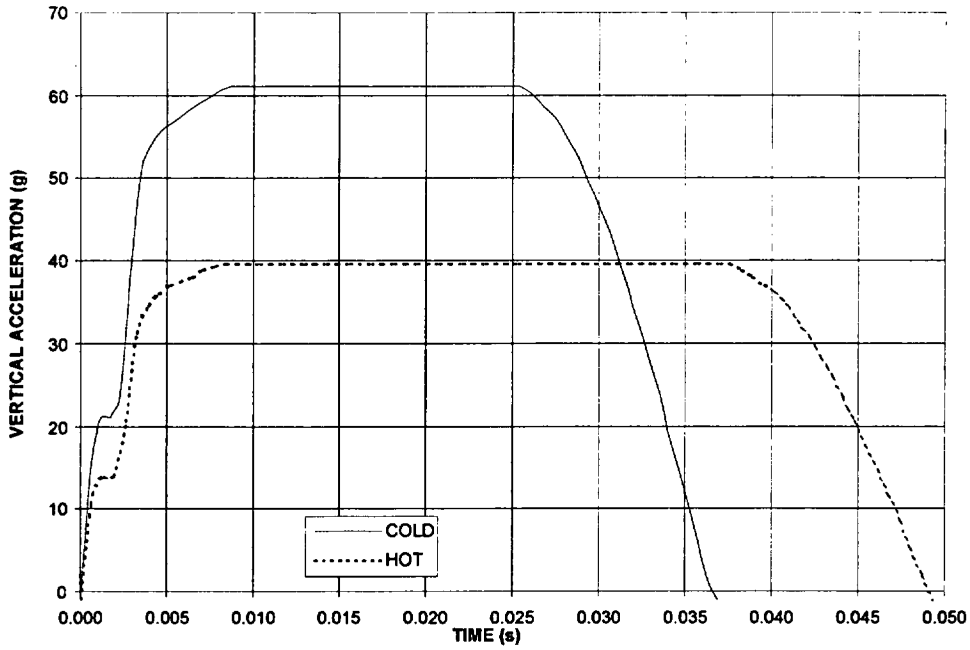

Figure 2.10.10-27

Flat Side Horizontal 30' Drop Acceleration Time Histories

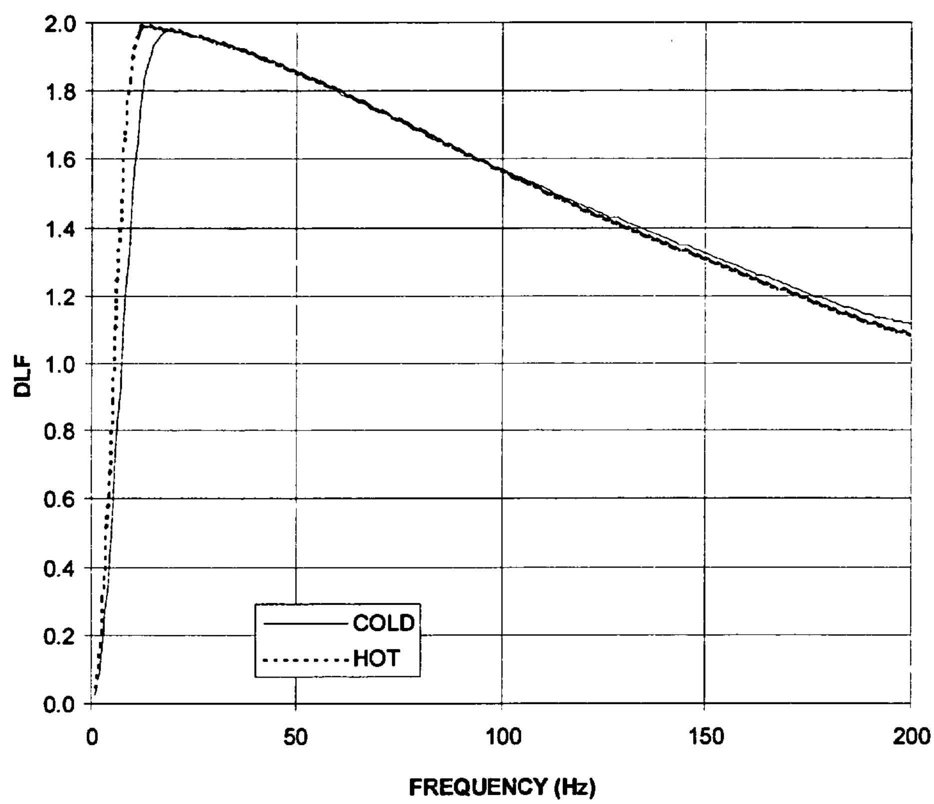

Figure 2.10.10-28

Flat Side Horizontal 30' Drop DLFs

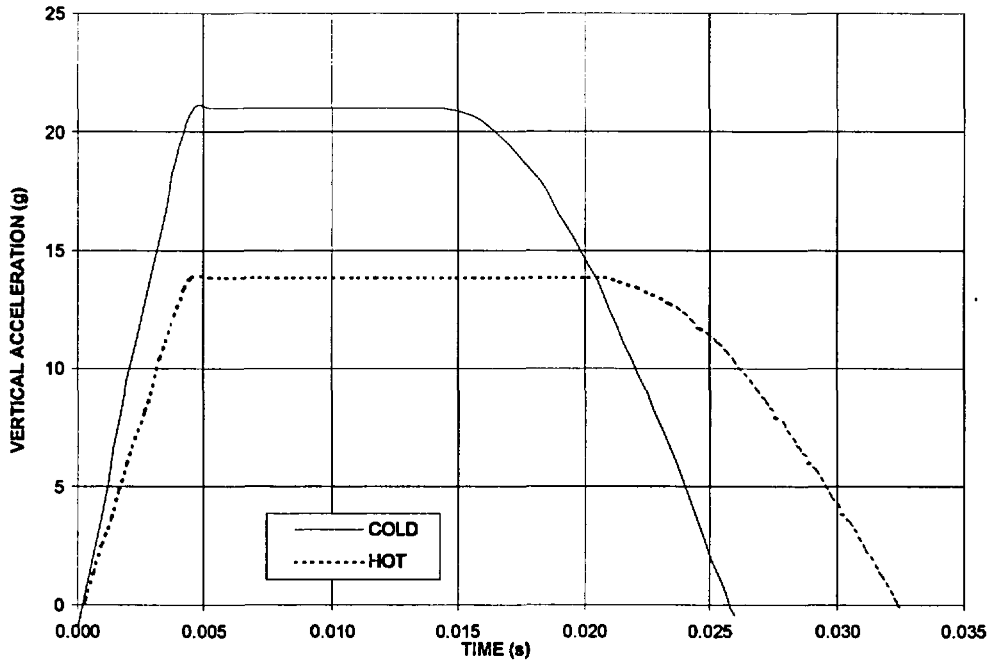

Figure 2.10.10-29

Flat Side Horizontal 1' Drop Acceleration Time Histories

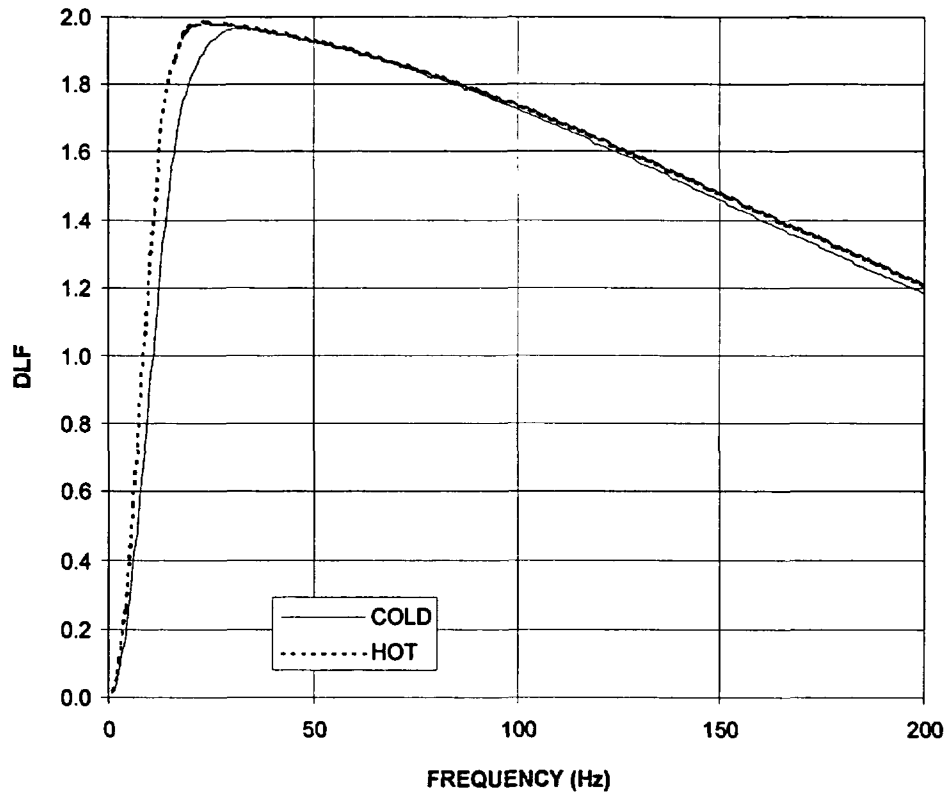

Figure 2.10.10-30

Flat Side Horizontal 1' Drop DLFs

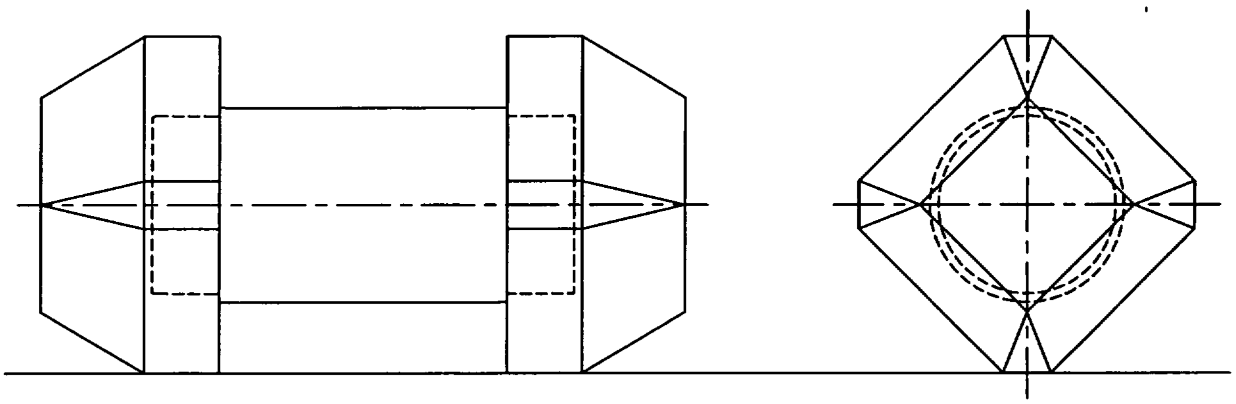

Figure 2.10.10-31

Corner Horizontal Drop Orientation

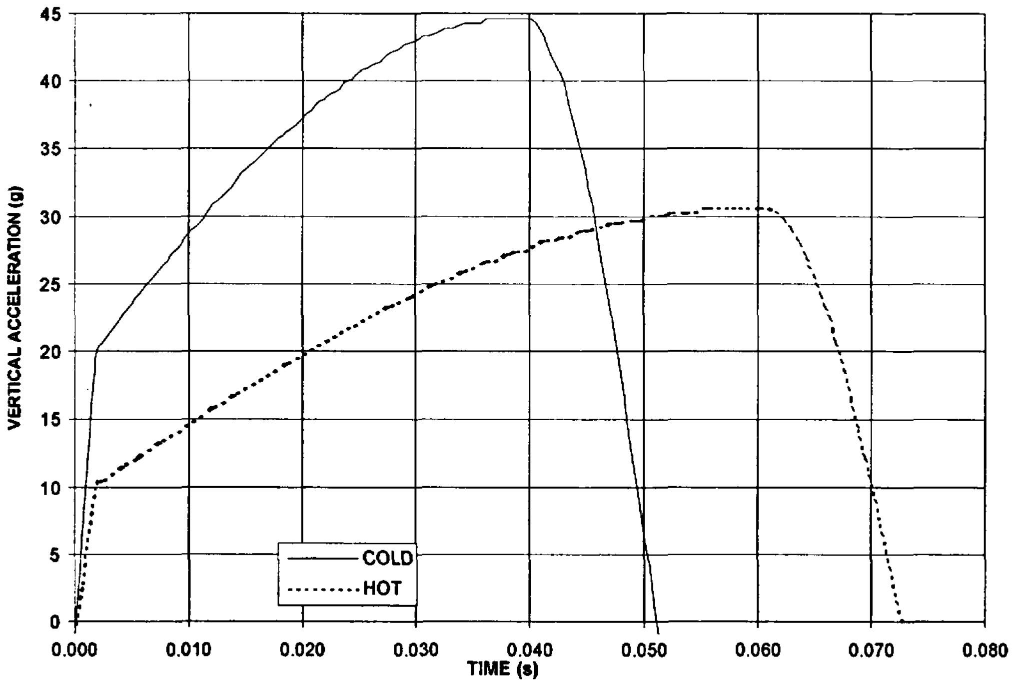

Figure 2.10.10-32

Corner Horizontal Drop Acceleration Time Histories

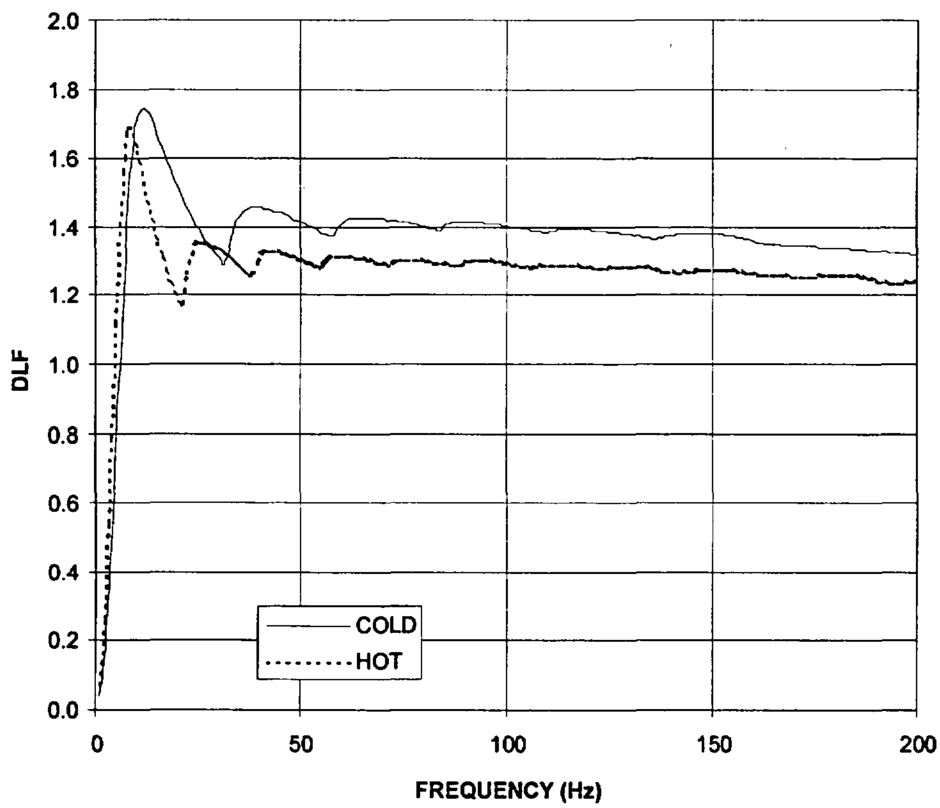

Figure 2.10.10-33

Corner Horizontal Drop DLFs

2.10.10.4 MODAL ANALYSIS

The frequency content of the various NUHOMS®-MP187 transportation package components are determined using a combination of computer models and hand calculations. The main components of the MP187, Fuel Only Dry Shielded Canister (FO-DSC), Fuel with Control Components Dry Shielded Canister (FC-DSC) and Failed Fuel Dry Shielded Canister (FF-DSC) are analyzed in the following sections. A summary of the significant structural modes of each major component is presented in Table 2.10.10-1, which can be found in Section 2.10.10.5, Summary of Results.

2.10.10.4.1 FC- and FO-DSC

The configuration of the FC-DSC and the FO-DSC are similar in almost all respects. Minor differences exist between the two designs in order to accommodate fuel with and without control components. In order to limit the number of calculations, only the controlling natural frequencies for the FO- and FC-DSC components are calculated and conservatively used for the analysis of both designs.

2.10.10.4.1.1 Spacer Disc

The dimensions and material of FO- and FC-DSC spacer discs are identical. The FC-DSC spacer discs support slightly heavier fuel due to the weight of the control components. Therefore, the natural frequencies of the FC-DSC spacer discs will be slightly lower than those of the FO-DSC spacer discs. Therefore, the spacer disc frequency calculations are conservatively based on the FC-DSC. The fundamental frequencies of the spacer disc which have the most significant effect on the spacer disc response, and the corresponding load conditions affected by the fundamental modes, are:

1. In-Plane Flat Side Ovalling - Horizontal and oblique flat side impacts
2. In-Plane Corner Ovalling - Horizontal and oblique corner impacts
3. Out-of-Plane Bending - Vertical and oblique impacts.

The fundamental frequencies of the FC-DSC spacer discs are determined using finite element modal analysis. Detailed descriptions of the FC-DSC spacer disc modal analyses are presented in the following sections.

2.10.10.4.1.1.1 In-Plane Flat Side Ovalling Modal Analysis

The modal analysis of the FC-DSC spacer disc for the in-plane flat side impact loading conditions is performed using the half symmetry ANSYS finite element model described in Section 2.10.3.1.2.

A modal analysis is performed using the ANSYS version 5.0A program [ANSYS v5.0A]. The lowest in-plane spacer disc flat side ovalling mode, shown in Figure 2.10.10-34, occurs at 297 Hz. This mode most significantly influences the response of the spacer disc for side drops on the flat side of the impact limiters (0°, 90°, 180° and 360° azimuths) and has a lesser influence on all other side drops and oblique drops.

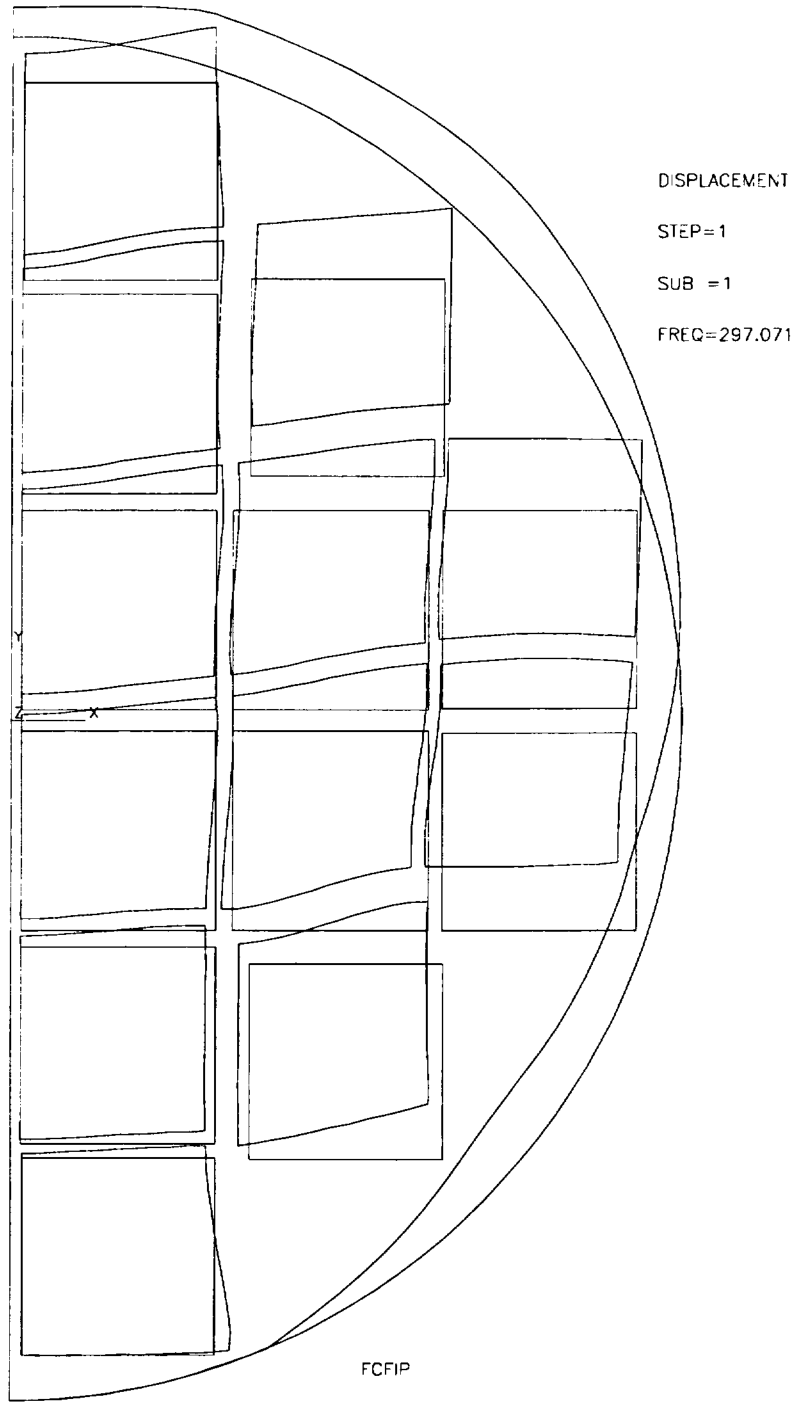

Figure 2.10.10-34

FC-DSC Spacer Disc In-Plane Flat Side Ovalling Mode

2.10.10.4.1.1.2 <u>In-Plane Corner Ovalling Modal Analysis</u>

The FC-DSC spacer disc fundamental frequency for the corner drop analyses is determined using the corner impact half spacer disc finite element model described in Section 2.10.3.1.3. The spacer disc is conservatively modeled with ligament widths of 1.660 inches, 1.190 inches, 0.990 inches, 0.810 inches, and 0.675 inches, which are less than the nominal ligament widths of 1.680 inches, 1.210 inches, 1.010 inches, 0.830 inches, and 0.695 inches, respectively.

The modal analysis of the spacer disc is performed using the reduced (Householder) method. The lowest in-plane spacer disc corner ovalling mode, shown in Figure 2.10.10-35, occurs at 131 Hz. This mode most significantly influences the response of the spacer disc for side drops on the corners of the impact limiters (45°, 135°, 225° and 315° azimuths) and has a lesser influence on all other side drops and oblique drops.

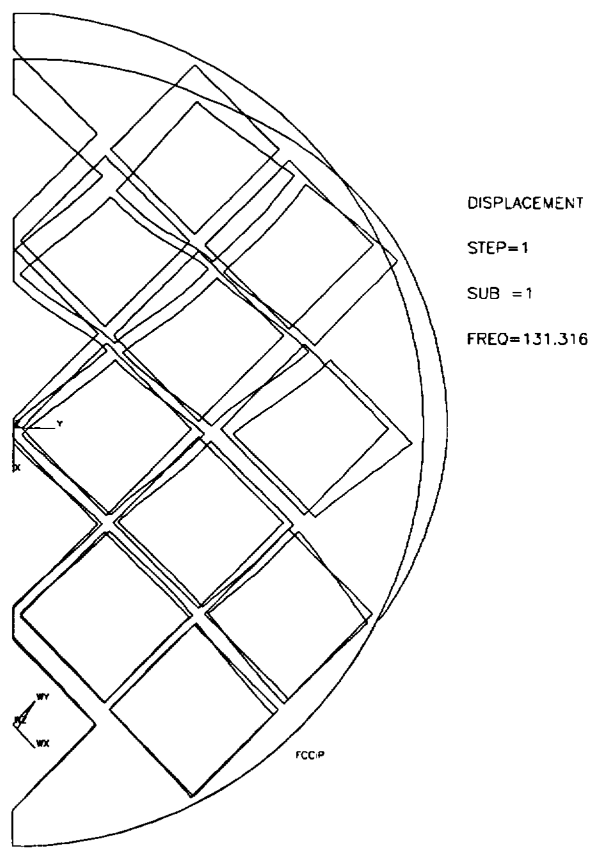

Figure 2.10.10-35

FC-DSC Spacer Disc In-Plane Corner Ovalling Mode

2.10.10.4.1.1.3 Out-of-Plane Bending Modal Analysis

The FC-DSC spacer disc out-of-plane bending mode fundamental frequency is determined using the quarter symmetry finite element model described in Section 2.10.3.1.1.

The lowest out-of-plane spacer disc bending mode, shown in Figure 2.10.10-36, occurs at 61 Hz. This mode most significantly influences the out-of-plane response of the spacer disc for vertical end drops and oblique drops.

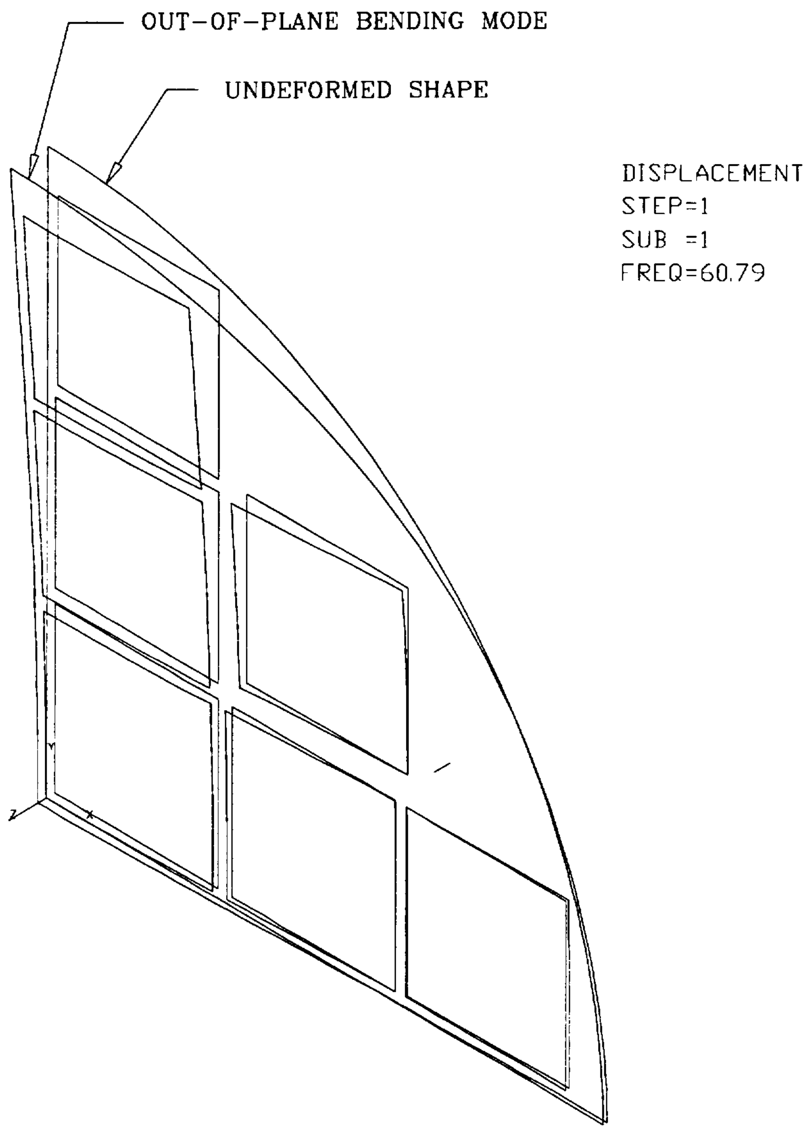

Figure 2.10.10-36

FC Spacer Disc Out-of-Plane Bending Mode

2.10.10.4.1.2 Support Rods

The FO- and FC-DSC support rods consist of a 2.0 inch O.D. rod, which is inserted through the spacer disc support rod cutout holes, and 3.0 inch O.D. x 2.06 inch I.D. sleeves which fit over the support rod between the spacer discs and at the top and bottom ends. Longitudinal loads are carried by the sleeves in axial compression and lateral loads by the support rod in bending.

The two modes of vibration of interest for the support rods are the axial compression mode and the beam bending mode. The frequencies associated with these two modes of vibration are determined using hand calculations in the following paragraphs.

(a) Axial Compression

The support rod axial compression mode of vibration is analyzed assuming the support rod sleeves act as a series of springs to which equal masses are attached. This assumption is valid since the mass of the support rod sleeves is insignificant in comparison to the mass of the spacer discs which are supported by the support rod sleeves in the axial direction. The natural frequency of vibration for the support rod sleeves axial compression mode is:

$$f_i = \frac{\sin\left(\frac{(2i-1)}{(2N+1)}\frac{\pi}{2}\right)}{\pi}\sqrt{\frac{k}{M}} \qquad \text{([2.11], Table 6-2, Case 5)}$$

where;

i	=	1 for the first (lowest) axial mode
N	=	26, Number of masses (spacer discs)
L	=	Average center to center span distance of spacer discs
	=	6.75 inches

A	=	Cross section area of support rod sleeves
	=	$\pi[(3.00/2)^2 - (2.08/2)^2]$
	=	3.67 in^2
E	=	26.7 x 10^6 psi, Modulus of Elasticity of support rod ASME SA-564 Type 630 SS at 500°F
k	=	Support rod spring stiffness
	=	AE/L
	=	14.52 x 10^6 lb/in.
M	=	Tributary mass of spacer disc plus support rod
	=	{(417/4) + [6.75(3.67)(0.2835)]}/386.4
	=	0.288 lb-s^2/in

Therefore, the fundamental axial compression frequency of the support rods is:

f_l = 67 Hz

(b) Beam Bending

The beam bending mode of the support rods is calculated for a free-free multiple span beam with pinned intermediate supports (i.e. spacer discs). The fundamental support rod bending frequency is given by:

$$f_i = \frac{\lambda_i^2}{2\pi L^2}\sqrt{\frac{EI}{m}} \qquad \text{([2.11], Table 8-3a)}$$

where;

E is defined above in Section 2.10.10.4.1.2(a)

λ_1 = 1.539 for 8 spans or greater

L	=	6.75 in., Center to center distance between spacer discs
I	=	$\pi R^4/4$, Moment of inertia of support rod
	=	$0.79\ in^4$
m	=	mass per unit length of support rod
	=	$\pi(1.5)^2(1.0)(0.2835/386.4)$
	=	$0.00519\ lb\text{-}s^2/in/in.$

Therefore,

f_1 = 527 Hz

2.10.10.4.1.3 FC/FO-DSC Guide Sleeves

The two modes of vibration of interest for the guide sleeves are the axial compression mode and the panel bending mode. The frequencies associated with these two modes of vibration are determined using hand calculations in the following paragraphs.

(a) Axial Compression

The guide sleeves axial compression mode of vibration is analyzed assuming the guide sleeves act as a fixed beam with weight of the 4 neutron absorber sheets lumped at the free end. The natural frequency of vibration for the guide sleeve axial compression mode is approximated as:

$$f_i = \frac{\lambda_i}{2\pi L}\sqrt{\frac{E}{\mu}}, \quad i = 1,\ 2,\ 3,\ \ldots \qquad \text{([2.11], Table 8-16)}$$

where;

E	=	24.8×10^6 psi, Modulus of Elasticity of ASME SA-240, Type 304 stainless steel at 700°F [2.2]
μ	=	Mass density of guide sleeve

= 275/[4(9.02)(0.12)(161.8)(386.4)]

= 0.00102 $lb\text{-}s^2/in^4$

L = 161.8 in., length of guide sleeves

λ_1 = $(2i - 1)\pi/2$ ([2.11], Table 8-16, case 2)

= $\pi/2$

Therefore, the fundamental longitudinal vibration frequency of the FO- and FC-DSC guide sleeve is:

f_1 = 241 Hz

(b) Panel Bending

The FO- and FC-DSC guide sleeves are loaded by the weight of the fuel assemblies, oversleeves, neutron absorber sheets, and their own self weight for all side drop and oblique drop conditions. The most significant loading on the guide sleeve for these drop conditions is due to the fuel assemblies. Since nearly all of the load on the guide sleeve bottom panel is due to the fuel assembly, the loading on the guide sleeve bottom panel will be controlled by the response of the fuel assembly. Therefore, the fundamental bending frequency of a single fuel rod, conservatively ignoring friction between fuel rods within a fuel assembly, is used to determine the DLFs for the guide sleeve panel bending mode. The fundamental frequency of the fuel assembly fuel tubes in bending is calculated for a single span of 6.75 inches, assuming fixed boundary conditions at both ends. Structural credit is taken only for the fuel cladding. The fundamental frequency is calculated as follows:

$$f_i = \frac{\lambda_i^2}{2\pi L^2}\sqrt{\frac{EI}{m}}$$ ([2.11], Table 8-1, case 7)

where;

λ_1 = 4.73 ([2.11], Table 8-1, case 7)

L = 6.75 in., Maximum span between spacer disc supports

E = 9×10^6 psi, Young's Modulus for Zircaloy @ 800°F [2.38]

R = 0.2150 in., Outer radius of cladding tube [2.9]

r = 0.1885 in., Inner radius of cladding tube [2.9]

I = $(R^4 - r^4)/4$, Cross section inertia of cladding tube

= 0.000687 in^4

w = 10.84 lbs/in., fuel assembly line load in active fuel region

N = 208, Number of fuel rods per 15x15 PWR fuel assembly[2.9]

g = 386.4 in/s^2, gravitational constant

m = Mass distribution of fuel tube per unit length

= w/Ng

= 0.000135 $lb\text{-}s^2/in/in.$

Therefore, the fundamental bending frequency of a fuel rod, used to determine the DLF for the guide sleeve panel bending mode, is:

$$f_1 = \frac{4.73^2}{2\pi(6.75)^2}\sqrt{\frac{(9x10^6)(0.000687)}{0.000135}}$$

$$= 529 \text{ Hz}$$

2.10.10.4.2 <u>FF-DSC</u>

The main components of the FF-DSC include the spacer discs, support plates and fuel can bodies. The modal analyses of each of these components are presented in the following sections.

2.10.10.4.2.1 Spacer Disc

The fundamental frequencies of the spacer disc which have the most significant effect on the spacer disc response, and the corresponding load conditions affected by the fundamental modes, are:

1. In-Plane Flat Side Ovalling - Horizontal and oblique flat side impacts
2. In-Plane Corner Ovalling - Horizontal and oblique corner impacts
3. Out-of-Plane Bending - Vertical and oblique impacts.

The fundamental frequencies of the FC-DSC spacer discs are determined using finite element modal analysis. Detailed descriptions of the FC-DSC spacer disc modal analyses are presented in the following sections.

2.10.10.4.2.1.1 Flat Side Ovalling and Out-of-Plane Bending Modes

The fundamental frequency of the FF-DSC spacer discs for the corner side drop and corner oblique drop conditions is determined using the ANSYS finite element model described in Section 2.10.4. This half disc model is used to calculate the spacer disc in-plane natural frequencies for side and oblique drops on the corner of the impact limiters.

A modal analysis is performed using the reduced (Householder) method and 300 master degrees of freedom. The lowest natural frequency of the FF-DSC spacer disc is an out-of-plane bending mode occurring at 66 Hz, as shown in Figure 2.10.10-37. The out-of-plane bending mode (or plate bending mode) of the spacer disc is most significant for spacer disc response for vertical end drops and also contributes to the spacer disc response for oblique impact drops.

The lowest FF-DSC spacer disc in-plane flat side ovalling mode occurs at 213 Hz, as shown in Figure 2.10.10-38. This mode contributes to the spacer disc response for side drops on the flat side of the impact limiters (0°, 90°, 180° and 360° azimuths).

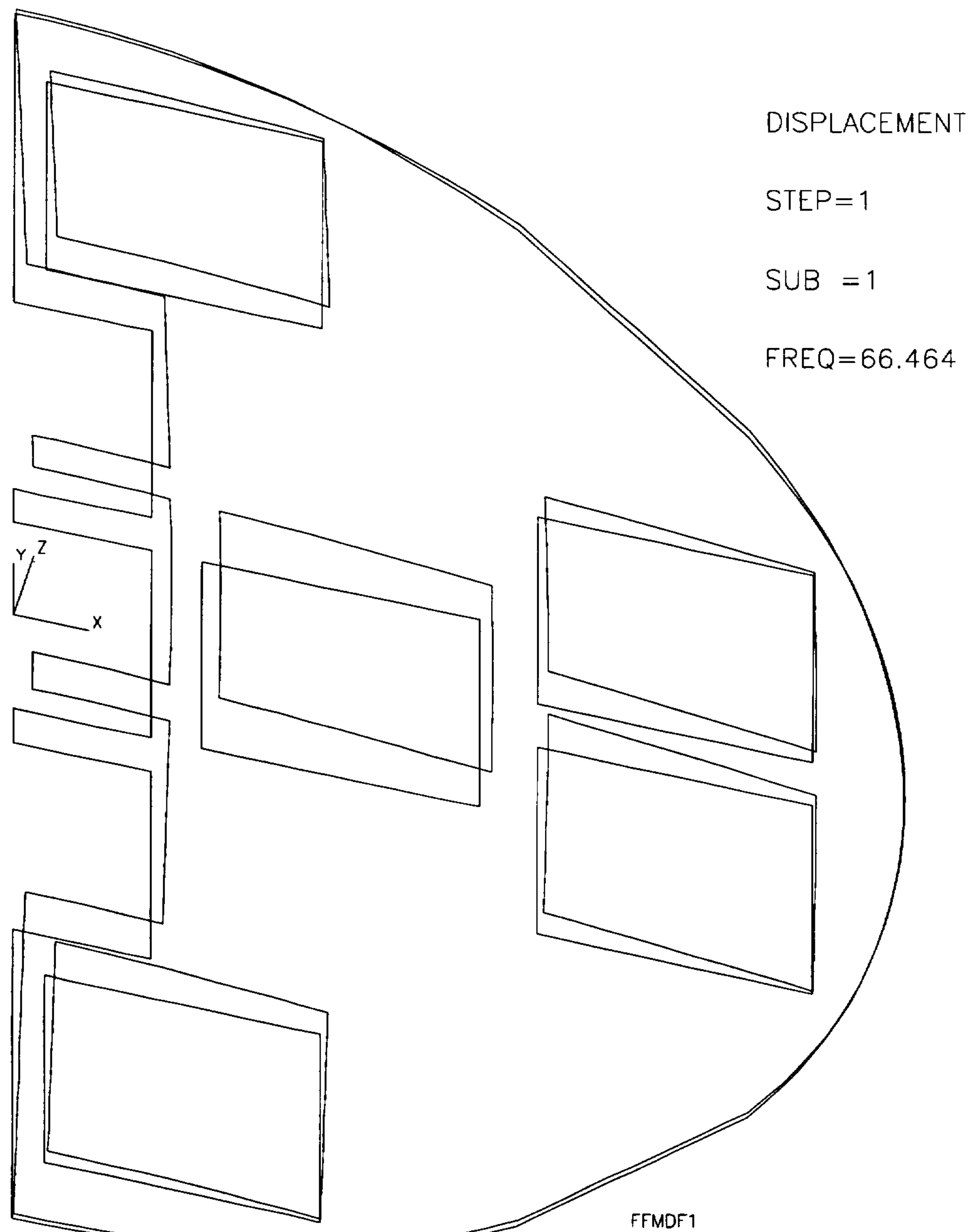

Figure 2.10.10-37

FF-DSC Spacer Disc Out-Of-Plane Bending Mode

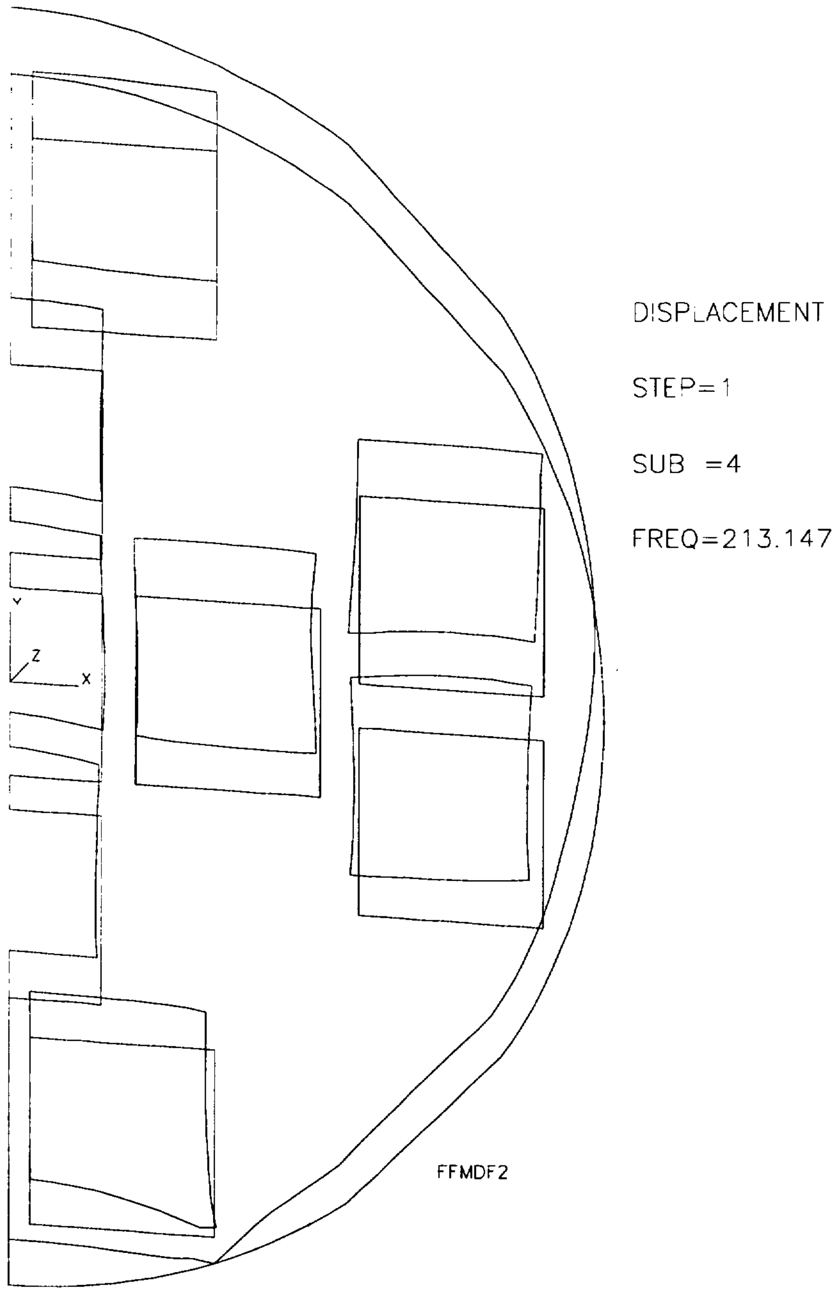

Figure 2.10.10-38

FF-DSC Spacer Disc Flat Side Ovalling Mode

2.10.10.4.2.1.2 Corner Ovalling Mode

The fundamental frequency of the FF-DSC spacer discs for the corner side drop and corner oblique drop conditions is determined using the ANSYS finite element model described in Section 2.10.4.

A modal analysis is performed using the reduced (Householder) method and 300 translational master degrees of freedom. The lowest in plane spacer disc corner ovalling mode occurs at 105 Hz, as shown in Figure 2.10.10-39. This mode contributes to the spacer disc response for side drops on the corner (small facet) of the impact limiters (45°, 135°, 225° and 315° azimuths).

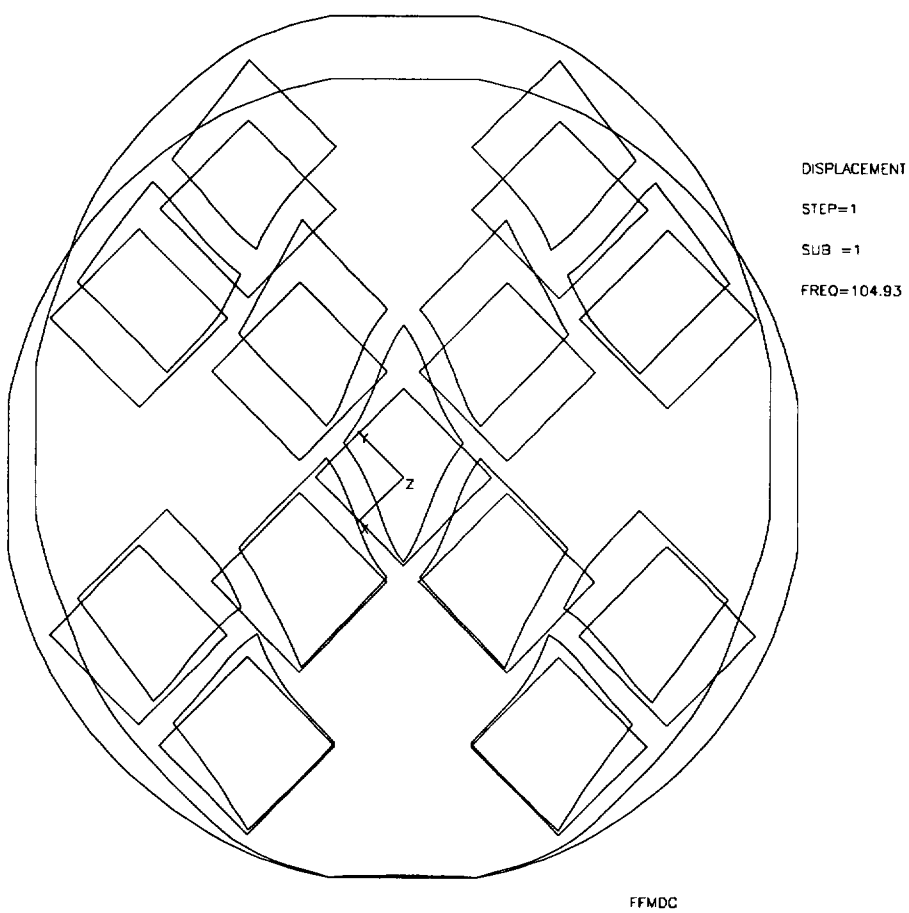

Figure 2.10.10-39
FF-DSC Spacer Disc Corner Ovalling Mode

2.10.10.4.2.2 Support Plates

The two modes of vibration of interest for the support plates are the axial compression mode and the beam bending mode. The frequencies associated with these two modes of vibration are determined using hand calculations in the following paragraphs.

(a) Axial Compression

The support plates axial compression mode of vibration is analyzed assuming the support plates act as a series of springs to which equal masses are attached. The natural frequency of vibration for the support rod axial compression mode is:

$$f_i = \frac{\sin\left(\frac{(2i-1)}{(2N+1)}\frac{\pi}{2}\right)}{\pi}\sqrt{\frac{k}{M}} \qquad \text{([2.11], Table 6-2, Case 5)}$$

where;

i	=	1 for the first (lowest) axial mode
N	=	15, Number of masses (spacer discs)
L	=	11.25 in., Average center to center span distance of spacer discs
A	=	[8(2x12)] = 192.0 in^2, Cross section area of support plates
E	=	27.3×10^6 psi, Modulus of Elasticity at 500°F
k	=	AE/L, Support plates spring stiffness
	=	$(192)(27.3 \times 10^6)/11.25$
	=	4.66×10^8 lb/in.
M	=	Mass of each spacer disc plus tributary support plates mass
	=	{1065 + [(192)(11.25)(0.2835)]}/386.4
	=	4.34 lb-s^2/in

Therefore, the fundamental axial compression frequency of the support rods is:

$f_1 \quad = \quad 167 \text{ Hz}$

(b), Beam Bending

The beam bending mode of the support plates is calculated for a free-free multiple span beam with pinned intermediate supports (i.e., spacer discs). The fundamental support rod bending frequency is given by:

$$f_i = \frac{\lambda_i^2}{2\pi L^2}\sqrt{\frac{EI}{m}}$$ ([2.11], Table 8-3a)

where;

E is defined above in Section (a)

$\lambda_1 \quad = \quad$ 1.539 for 8 spans or greater

$L \quad = \quad$ 11.25 in., Center to center distance between spacer discs

$I \quad = \quad [b(h)^3]/12$, Weak axis moment of inertia of one support plate

$\quad = \quad [12(2)^3]/12$

$\quad = \quad 8 \text{ in}^4$

$m \quad = \quad (w/g)/L$, Mass per unit length of one support plate

$\quad = \quad [(0.2835(2x12)172.5)/386.4]/172.5$

$\quad = \quad 0.01761 \text{ lb-s}^2\text{/in/in.}$

Therefore,

$f_1 \quad = \quad 331 \text{ Hz}$

2.10.10.4.2.3 Fuel Can Bodies

The two modes of vibration of interest for the fuel cans are the axial compression mode and the beam bending mode. The frequencies associated with these two modes of vibration are determined using hand calculations in the following paragraphs.

(a) Axial Compression

The fuel can axial compression mode of vibration is calculated for a free-free uniform beam. The natural frequency of vibration for the fuel can axial compression mode is approximated as follows:

$$f_i = \frac{\lambda_i}{2\pi L}\sqrt{\frac{E}{\mu}}$$ ([2.11], Table 8-16, Case 1)

where;

i	=	1 for the first (lowest) axial mode		
L	=	171.25 in., Length of Fuel Can Assembly		
E	=	25.8×10^6 psi, Modulus of Elasticity at 500°F		
μ	=	0.2835/386.4	=	0.000734 $lb\text{-}s^2/in^4$
λ_i	=	π		

Therefore, the fundamental axial compression frequency of the fuel can is:

f_1 = 547 Hz

(b) Beam Bending

The beam bending mode of the support plates is calculated for a free-free multiple span beam with pinned intermediate supports (i.e., spacer discs). The fundamental fuel can bending frequency is given by:

$$f_i = \frac{\lambda_i^2}{2\pi L^2}\sqrt{\frac{EI}{m}} \qquad \text{([2.11], Table 8-3a)}$$

where;

E is defined above in Section (a)

λ_1 = 1.539 for 8 spans or greater

L = 11.25 in., Center to center distance between spacer discs

I = $t[(b^3/6) + (ab^2/2)]$ (Table 5-1, Case 9 [2.11])

= $0.25[(9.5)^3/6 + (9.5)^3/2) = 142.9\ in^4$

m = mass per unit length of one can plus fuel

= {[[(0.2835)(9)(172.5)/172.5]+10.35]/386.4}

= 0.03339 $lb\text{-}s^2/in/in.$

Therefore,

f_1 = 990 Hz

2.10.10.4.3 Multi-Purpose Cask

2.10.10.4.3.1 Cask Shells

Two modes of vibration are considered in the cask shells modal analysis. These modes are:

1. Beam Bending
2. Axial Compression

The cask shells vibration frequencies are determined using hand calculations in the following paragraphs. These hand calculations are performed based on the assumption that the lead shielding, neutron shielding, neutron shield jacket, shear key and trunnions provide no additional stiffness to the cask shells. The mass of these components are accounted for by adjusting the density of the cask shells accordingly. The cask shell properties used in the frequency calculations are as follows:

Outer shell area	=	$\pi(83.5^2 - 78.5^2)/4$
	=	636.17 in^2
Inner shell area	=	$\pi(70.5^2 - 68^2)/4$
	=	271.94 in^2
Total shell area (A)	=	908.11 in^2
Avg. length of shells (L)	=	(183.50 + 173.75)/2
	=	178.63 in
Avg. thickness of shells (L)	=	(1.25 + 2.5)/2
	=	1.875 in
Weighted mean radius (R)	=	[40.5(636.17) + 34.625(271.94)]/908.11
	=	38.74 in

The adjusted mass density of the cask shell region excluding the steel on the top and bottom ends of the cask (μ') is calculated as follows:

Weight of Cask Assy.	=	158,580 lbs. [Table 2.1.2-5]
Weight of Cask Top Steel	=	$[\pi(83.5^2)/4](6.5)(0.2853)$
	=	10,160 lbs.
Weight of Cask Btm Steel	=	$[\pi(83.5^2)/4](8)(0.2853)$
	=	12,500 lbs.

Therefore, the total weight of the cask shells, lead shielding, neutron shielding, shear key and trunnions, W_T, is:

$$W_T = 158{,}580 - (10{,}160 + 12{,}500)$$

$$= 135{,}920 \text{ lbs.}$$

The adjusted density of the cask shells is:

$$\mu' = w/(gV)$$

$$= 135{,}920/[(386.4)(178.63 \times 908.11)]$$

$$= 0.00217 \text{ lb-s}^2/\text{in}^4.$$

(a) Beam Bending Mode

The first beam bending mode of the cask shell is calculated for a simply supported cylindrical shell with no axial support. The natural frequency, f_{ij}, for the case of i=1 and j=1 is calculated using the formula presented below.

$$f_{ij} = \frac{\lambda_{ij}}{2\pi R}\sqrt{\frac{E}{\mu(1-\nu^2)}} \qquad \text{([2.11], Table 12-2, Case 4)}$$

Where;

R	=	Weighted mean radius
	=	38.74 in
L	=	Average length
	=	178.63 in
h	=	Average thickness for inner and outer shell
	=	(1.25 + 2.5)/2
	=	1.875
E	=	Elastic modulus of ASME SA-240, Type 304 stainless steel at 400°F [2]
	=	26.5x106 psi
μ	=	Adjusted density
	=	0.00217 $lb\text{-}s^2/in^4$
ν	=	Poisson ratio
	=	0.29
L/jR	=	178.63/38.74
	=	4.61 ⟨ 8

Beam theory formula for L/jR > 8 ([2.11], Table 12-2, Case 4) can not be used.

R/h	=	38.74/1.875	
	=	20.7	
λ_{ij}	=	0.25 for R/h = 20	([2.11], Fig. 12-5 - Flügge Shell Theory)

Therefore, the first beam bending frequency of the cask shell is:

f_1 = 119 Hz

(b) Axial Compression

The axial compression mode of the cask shell is calculated assuming the cask acts as a uniform beam with lumped masses at the ends. The heavier mass of the bottom end closure assembly is conservatively used for both the top and bottom end masses for the purpose of this calculation. The lowest axial vibration frequency is given by:

$$f_i = \frac{\lambda_i}{2\pi L}\sqrt{\frac{E}{\mu}},\quad i = 1, 2, 3, \ldots$$ ([2.11], Table 8-16, case 6)

where;

E	=	27.0 x 10^6 psi, Modulus of Elasticity of ASME SA-240, Type 304 stainless steel at 300°F [2.2]
M	=	Mass of bottom plate
	=	12,500/386.4 = 32.3 lb-s^2/in
A	=	908.11 in^2
μ	=	0.00217 lb-s^2/in^4
L	=	89.32 in., half of the average length
λ_1	=	1.33 for $\beta = \mu AL/M = 5.45$ ([2.11], Figure 8-23)

Therefore, the fundamental longitudinal vibration frequency of the cask shell is:

f_1 = 262 Hz

2.10.10.4.3.2 Cask Bottom Plate

The first plate bending mode of the cask bottom plate is conservatively calculated for a simply supported annular plate with a free inside edge. The lowest natural frequency, f_{ij}, for the case of i=0 and j=0 is calculated using the formula presented in ([2.11], Table 11-2, case 3)

$$f_{ij} = \frac{\lambda_{ij}^2}{2\pi a^2}\sqrt{\frac{Eh^3}{12\gamma(1-\nu^2)}}$$

where,

λ_{ij}^2 = 4.76 for b/a = 0.20

b	=	(17)/2 = 8.5 in, ram access penetration radius
a	=	(83.5/2) = 41.75 in., cask outer radius
E	=	27.0 x 10^6 psi, Modulus of Elasticity of ASME SA-182, Type F304 stainless steel at 300°F [2.2]
γ	=	0.00628 lb-s^2/in^3, Mass per unit area of plate, where,
		Mass of plate (including hole) = 12,500/386.4 = 32.3 lb-s^2/in
		Area of plate (excluding hole) = $\pi(83.5^2 - 20.5^2)/4$ = 5,145.9 in^2
ν	=	0.29, Poisson's ratio for stainless steel
h	=	8.0 in., plate thickness.

Therefore, the fundamental plate bending vibration frequency of the cask bottom plate is:

f_1 = 195 Hz

2.10.10.4.3.3 Cask Top Plate

The first plate bending mode of the cask top plate is calculated assuming simply supported edge. The lowest natural frequency, f_{ij}, for the case of i=0 and j=0 is calculated using the formula presented in ([2.11], Table 11-1, case 2)

$$f_{ij} = \frac{\lambda_{ij}^2}{2\pi a^2}\sqrt{\frac{Eh^3}{12\gamma(1-\nu^2)}}$$

where,

λ_{ij}^2	=	4.977
a	=	(83.5/2) = 41.75 in., disc radius
E	=	27.0 x 10^6 psi, Modulus of Elasticity of ASME SA-240, Type 304 stainless steel at 300°F [2.2]

γ = 0.0048 lb-s^2/in^3, Mass per unit area of plate, where,

Mass of plate = 10,160 lbs / 386.4 .

Area of plate = $\pi(83.5^2)/4 = 5{,}475.99$ in^2

ν = 0.29, Poisson's ratio for stainless steel

h = 6.5 in, plate thickness.

Therefore, the fundamental plate bending vibration frequency of the cask top plate is:

f_1 = 170 Hz

2.10.10.5 Summary of Results

A summary of the NUHOMS®-MP187 transportation package component natural frequencies is shown in Table 2.10.10-1. The maximum DLFs corresponding to the natural frequencies of the NUHOMS®-MP187 FC- and FO-DSCs, FF-DSC and Multi-Purpose Cask components are reported in Table 2.10.10-2, Table 2.10.10-3 and Table 2.10.10-4 respectively. The results show that the maximum dynamic amplification results from the flat side drop and flat side slapdown drop conditions. This is due primarily to the sharp rise time associated with the acceleration time histories of these drop conditions. All other drop conditions result in little or no dynamic amplification in any of the NUHOMS®-MP187 transportation package system components.

Table 2.10.10-1

NUHOMS®-MP187 Transportation Package Component Frequency Summary

Assembly	Component	Vibration Mode	Vibration Frequency	Applicable Drop Conditions				
				End Drop	Side Drop		Oblique Drop	
					0°	45°	0°	45°
FO- and FC-DSC	Spacer Disc	Plate Bending	61	x			x	x
		Flat Side Ovalling	297		x		x	
		Corner Ovalling	131			x		x
	Guide Sleeves	Panel Bending	529		x	x	x	x
		Axial Compression	241	x			x	x
	Support Rods	Beam Bending	527		x	x	x	x
		Axial Compression	67	x			x	x
FF-DSC	Spacer Disc	Plate Bending	66	x			x	x
		Flat Side Ovalling	213		x		x	
		Corner Ovalling	105			x		x
	Fuel Can Bodies	Panel Bending	990		x	x	x	x
		Axial Compression	547	x			x	x
	Support Rods	Beam Bending	331		x	x	x	x
		Axial Compression	167	x			x	x
Multi-Purpose Cask	Shells	Axial Compression	262	x			x	x
		Beam Bending	119		x	x	x	x
	Top Cover Plate	Plate Bending	170	x			x	x
	Bottom Forging	Plate Bending	195	x			x	x

Notes:

1) The 0° and 45° side and oblique drop conditions are also referred to as drop 'through flat' and 'through diagonal'.

Table 2.10.10-2

Maximum DLF for FC- and FO-DSC Components Drop Condition

Drop Orientation	Temperature Condition	Load Case ID	Acceleration Direction	COMPONENT		
				Spacer Disk	Support Rod	Guide Sleeves
Horizontal Flat Side	Cold	1. FSHC	Tangential	1.12	1.12	1.12
	Hot	2. FSHH	Tangential	1.09	1.09	1.09
30° Flat Side	Cold	3. FS3C	Tangential	1.11	1.11	1.11
			Longitudinal	1.46	1.43	1.11
	Hot	4. FS3H	Tangential	1.07	1.07	1.07
			Longitudinal	1.27	1.23	1.07
60° Flat Side	Cold	5. FS6C	Tangential	1.03	1.03	1.03
			Longitudinal	1.08	1.04	1.03
	Hot	6. FS6H	Tangential	1.01	1.01	1.01
			Longitudinal	1.04	1.02	1.01
Horizontal Corner	Cold	7. CNHC	Tangential	1.38	1.32	1.32
	Hot	8. CNHH	Tangential	1.29	1.24	1.24
30° Corner	Cold	9. CN3C	Tangential	1.04	1.03	1.03
			Longitudinal	1.13	1.11	1.03
	Hot	10. CN3H	Tangential	1.02	1.01	1.01
			Longitudinal	1.05	1.04	1.01
60° Corner	Cold	11. CN6C	Tangential	1.09	1.02	1.02
			Longitudinal	1.19	1.17	1.02
	Hot	12. CN6H	Tangential	1.04	1.02	1.02
			Longitudinal	1.09	1.06	1.02
CG Over Flat Side	Cold	13. CGFC	Tangential	1.08	1.02	1.02
			Longitudinal	1.13	1.15	1.02
	Hot	14. CGFH	Tangential	1.05	1.02	1.02
			Longitudinal	1.08	1.09	1.02
CG Over Corner	Cold	15. CGCC	Tangential	1.07	1.01	1.01
			Longitudinal	1.13	1.11	1.01
	Hot	16. CGCH	Tangential	1.04	1.02	1.02
			Longitudinal	1.07	1.07	1.02
End	Cold	17. ENDC	Longitudinal	1.51	1.48	1.06
	Hot	18. ENDH	Longitudinal	1.31	1.26	1.04
	Special	25. ENDS	Longitudinal	1.32	1.30	1.03
Flat Side Slapdown	Cold	19. FSSC	Tangential	1.31	1.31	1.31
			Longitudinal	1.87	1.85	1.31
	Hot	20. FSSH	Tangential	1.35	1.35	1.35
			Longitudinal	1.89	1.86	1.35
Corner Slapdown	Cold	21. CNSC	Tangential	1.35	1.32	1.32
			Longitudinal	1.31	1.38	1.32
	Hot	22. CNSH	Tangential	1.25	1.24	1.24
			Longitudinal	1.26	1.27	1.24
Horizontal 1' Flat Side	Cold	23. FH1C	Tangential	1.18	1.18	1.18
	Hot	24. FH1H	Tangential	1.21	1.21	1.21

Table 2.10.10-3

Maximum DLF for FF-DSC Components

Drop Orientation	Temperature Condition	Load Case ID	Acceleration Direction	COMPONENT		
				Spacer Disk	Support Plate	Fuel Can
Horizontal Flat Side	Cold	1. FSHC	Tangential	1.12	1.12	1.12
	Hot	2. FSHH	Tangential	1.09	1.09	1.09
30° Flat Side	Cold	3. FS3C	Tangential	1.11	1.11	1.11
			Longitudinal	1.43	1.14	1.11
	Hot	4. FS3H	Tangential	1.07	1.07	1.07
			Longitudinal	1.23	1.08	1.07
60° Flat Side	Cold	5. FS6C	Tangential	1.03	1.03	1.03
			Longitudinal	1.04	1.03	1.03
	Hot	6. FS6H	Tangential	1.01	1.01	1.01
			Longitudinal	1.02	1.01	1.01
Horizontal Corner	Cold	7. CNHC	Tangential	1.39	1.32	1.32
	Hot	8. CNHH	Tangential	1.28	1.24	1.24
30° Corner	Cold	9. CN3C	Tangential	1.06	1.03	1.03
			Longitudinal	1.11	1.03	1.03
	Hot	10. CN3H	Tangential	1.03	1.01	1.01
			Longitudinal	1.03	1.02	1.01
60° Corner	Cold	11. CN6C	Tangential	1.11	1.02	1.02
			Longitudinal	1.17	1.04	1.02
	Hot	12. CN6H	Tangential	1.05	1.02	1.02
			Longitudinal	1.06	1.03	1.02
CG Over Flat Side	Cold	13. CGFC	Tangential	1.10	1.02	1.02
			Longitudinal	1.15	1.05	1.02
	Hot	14. CGFH	Tangential	1.06	1.02	1.02
			Longitudinal	1.09	1.04	1.02
CG Over Corner	Cold	15. CGCC	Tangential	1.09	1.01	1.01
			Longitudinal	1.11	1.06	1.01
	Hot	16. CGCH	Tangential	1.06	1.02	1.02
			Longitudinal	1.08	1.04	1.02
End	Cold	17. ENDC	Longitudinal	1.49	1.11	1.06
	Hot	18. ENDH	Longitudinal	1.27	1.08	1.04
	Special	25. ENDS	Longitudinal	1.31	1.09	1.03
Flat Side Slapdown	Cold	19. FSSC	Tangential	1.31	1.31	1.31
			Longitudinal	1.85	1.43	1.31
	Hot	20. FSSH	Tangential	1.35	1.35	1.35
			Longitudinal	1.87	1.46	1.35
Corner Slapdown	Cold	21. CNSC	Tangential	1.36	1.32	1.32
			Longitudinal	1.37	1.33	1.32
	Hot	22. CNSH	Tangential	1.26	1.24	1.24
			Longitudinal	1.27	1.25	1.24
Horizontal 1' Flat Side	Cold	23. FH1C	Tangential	1.18	1.18	1.18
	Hot	24. FH1H	Tangential	1.21	1.21	1.21

Table 2.10.10-4

Maximum DLF for Multi-Purpose Cask

Drop Orientation	Temperature Condition	Load Case ID	Acceleration Direction	COMPONENT		
				Shells	Top Plate	Bottom Plate
Horizontal Flat Side	Cold	1. FSHC	Tangential	1.47	N/A	N/A
	Hot	2. FSHH	Tangential	1.46	N/A	N/A
30° Flat Side	Cold	3. FS3C	Tangential	1.19	N/A	N/A
			Longitudinal	1.11	1.14	1.12
	Hot	4. FS3H	Tangential	1.12	N/A	N/A
			Longitudinal	1.07	1.08	1.07
60° Flat Side	Cold	5. FS6C	Tangential	1.04	N/A	N/A
			Longitudinal	1.03	1.03	1.03
	Hot	6. FS6H	Tangential	1.01	N/A	N/A
			Longitudinal	1.01	1.01	1.01
Horizontal Corner	Cold	7. CNHC	Tangential	1.39	N/A	N/A
	Hot	8. CNHH	Tangential	1.29	N/A	N/A
30° Corner	Cold	9. CN3C	Tangential	1.03	N/A	N/A
			Longitudinal	1.03	1.03	1.03
	Hot	10. CN3H	Tangential	1.03	N/A	N/A
			Longitudinal	1.01	1.01	1.01
60° Corner	Cold	11. CN6C	Tangential	1.10	N/A	N/A
			Longitudinal	1.02	1.03	1.02
	Hot	12. CN6H	Tangential	1.05	N/A	N/A
			Longitudinal	1.02	1.03	1.02
CG Over Flat Side	Cold	13. CGFC	Tangential	1.08	N/A	N/A
			Longitudinal	1.02	1.04	1.01
	Hot	14. CGFH	Tangential	1.04	N/A	N/A
			Longitudinal	1.02	1.04	1.03
CG Over Corner	Cold	15. CGCC	Tangential	1.07	N/A	N/A
			Longitudinal	1.01	1.06	1.02
	Hot	16. CGCH	Tangential	1.05	N/A	N/A
			Longitudinal	1.02	1.03	1.03
End	Cold	17. ENDC	Longitudinal	1.06	1.10	1.06
	Hot	18. ENDH	Longitudinal	1.04	1.08	1.04
	Special	25. ENDS	Longitudinal	1.03	1.08	1.04
Flat Side Slapdown	Cold	19. FSSC	Tangential	1.62	N/A	N/A
			Longitudinal	1.31	N/A	N/A
	Hot	20. FSSH	Tangential	1.65	N/A	N/A
			Longitudinal	1.35	N/A	N/A
Corner Slapdown	Cold	21. CNSC	Tangential	1.35	N/A	N/A
			Longitudinal	1.32	N/A	N/A
	Hot	22. CNSH	Tangential	1.26	N/A	N/A
			Longitudinal	1.24	N/A	N/A
Horizontal 1' Flat Side	Cold	23. FH1C	Tangential	1.63	N/A	N/A
	Hot	24. FH1H	Tangential	1.65	N/A	N/A

2.10.10.6 Computer Program "DLF" Verification

DLF is a computer program which calculates dynamic load factors (DLF) associated with a given general force time history. The dynamic factors are given as a function of natural frequency of a damped single degree of freedom oscillator. Linear acceleration method is employed in solving the equations of equilibrium. The program "DLF" is a PC version of the Cyber 990 Version of "DLF" at Power Computing. The program user's documentation is provided in the DLF User's Manual.

Verification of the DLF program is done by running the same set of verification problems used to verify the Cyber 990 version of the program and comparing the results. The verification problem set consists of seven different problems. The first two problems consist of rectangular pulse and triangular pulse loads applied to undamped single degree of freedom systems. The DLF from these runs at various frequencies are compared to classical solutions for the same problems in Table 2.10.10-5. The remaining five problems consist of damped single degree of freedom systems subjected to sinusoidal loading. The maximum DLF for the various damping values is compared to the classical closed form solution for the same loading in Table 2.10.10-6.

The results from the analyses show that the DLF program results are in excellent agreement with the classical solutions and the results from the Cyber 990 version of the DLF program at Power Computing.

In addition to the verification problems discussed above, a transient dynamic analysis is performed using a finite element model consisting of four SDOF damped spring oscillators, for which a range of damping values is used. The results of the analysis are compared to the solutions obtained using the DLF program for the same damping values. This analysis not only provides an additional verification of the DLF program, but also demonstrates the effect of damping on the DLF for a single pulse short duration load.

The stiffness used for the finite element model is calculated such that the natural frequency of the system is 100 Hz (T = 0.01 sec.), which is representative of the fundamental frequency of many of the MP187 package components. The stiffness is calculated as follows:

$$k = (2\pi/T)^2$$

$$= (2\pi/0.01)^2$$

$$= 3.95 \times 10^5 \text{ lb/in.}$$

A unit mass is used in the model. The values of damping used for the finite element analysis are 2%, 5%, 10% of critical damping. The critical damping value of the system is calculated as follows:

$$c_{cr} = 2(km)^{1/2}$$

$$= 2[(3.95 \times 10^5)(1)]^{1/2}$$

$$= 1{,}260 \text{ lb-s/inch}$$

Therefore, the damping values corresponding to 2%, 5%, and 10% of critical damping are 25.2 lb-s/inch, 63.0 lb-s/inch, and 126.0 lb-s/inch, respectively.

An acceleration time history load is applied to the model which is representative of that which is experienced by the MP187 package for the flat side horizontal side drop or flat side slapdown. This time history loading is chosen since it results in the highest DLFs in the frequency range of interest. The time history load applied to the model is defined as follows:

Time (seconds)	Acceleration (in/s^2)
0.000	0
0.007	10,000
0.030	10,000
0.037	0

The results of the time history analysis and the DLF program analysis are summarized in Table 2.10.10-7. The results show excellent agreement between the finite element solution and the DLF program solution. The maximum difference between the results is less than 0.1%. The results also show that the damping ratio does effect the DLF for a single pulse short duration load. Therefore, the use of damping for the DLF calculations is justified.

Table 2.10.10-5

DLF Program Verification Results - Undamped Systems

Frequency (Hz)	Rectangular Pulse		Triangular Pulse	
	Results from "DLF" Program	Classical Solution Results[1]	Results from "DLF" Program	Classical Solution Results[1]
0.5	2.00	2.00	1.20	1.20
1	2.00	2.00	1.55	1.55
2	2.00	2.00	1.76	1.76
5	2.00	2.00	1.90	1.90
10	2.00	2.00	1.95	1.95

Notes:
(1) Classical solutions for the problems are obtained from Reference 2.39.

Table 2.10.10-6

DLF Program Verification Results - Damped Systems

Frequency (Hz)	Maximum DLF		% Difference
	Results from "DLF" Program	Results from Classical Solution[1]	
2	25	25	0.0
5	10	10	0.0
10	5.0	5.0	0.0
20	2.5	2.5	0.0
30	1.71	1.67	2.4

Notes:
(1) Classical Solution Results are obtained from Reference 2.39.

Table 2.10.10-7

DLF Program Verification Results - Undamped Systems

Damping (Hz)	ANSYS Results		DLF Program Results (@ 100 Hz)	% Difference
	Peak Response (in.)	DLF [1]		
2%	0.04043	1.597	1.598	0.06
5%	0.03906	1.544	1.544	0.06
10%	0.03708	1.463	1.463	0.07

Notes:

(1) DLFs are calculated as the ratio of the peak response to the static response from Run I.D. 94101908.10A. The static response is equal to the peak response of the critically damped system of 0.02532 inches.

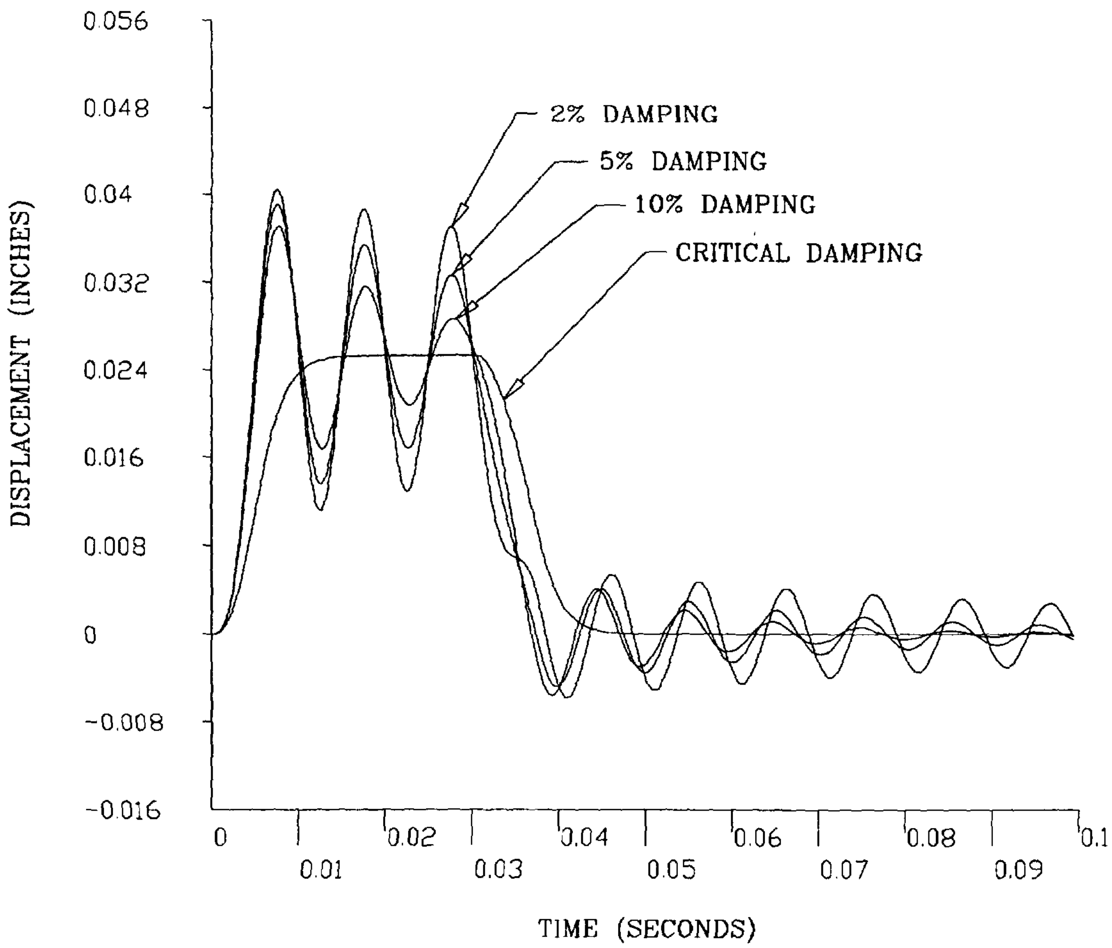

Figure 2.10.10-40

Effect of Damping on Dynamic Response

2.10.10.7 Selected Computer Run Output Files

The output files for selected computer runs referenced in this appendix are included in the following sections. Two input files are required for each run: 1) time history input files, and 2) DLF parameter input file. The output file lists the input parameters, time history loading, and DLFs in the requested frequency range for damping values of 0%, 2%, 5%, 10%, and 20%.

2.10.10.7.1 Cold Flatside Slapdown DLF (Portion) Output File

```
DLF ANALYSIS FOR LOAD CASE FSSC
SLAPDOWN RESPONSE ANALYSIS

CALCULATION PARAMETERS
 KOULIM  =        50
 FCTLIM  =      .010
 CNVFCT  =      .020
 NSPLIM  =         2
 FREQLO  =     1.000
 FREQINC =     1.000
 NFREQ   =       200

PRIMARY TIME-HISTORY STARTS AT LINE        6
PRIMARY TIME-HISTORY ENDS AT LINE         68
SECONDARY TIME-HISTORY STARTS AT LINE    244
SECONDARY TIME-HISTORY ENDS AT LINE      304
NUMBER OF TIME-HISTORY POINTS        61

TIME HISTORY DATA
    I         T         F
    1      .1417     2.927
    2      .1423    10.000
    3      .1429    10.000
    4      .1435    14.171
    5      .1441    23.756
    6      .1447    26.425
    7      .1453    27.720
    8      .1459    28.238
    9      .1465    28.756
   10      .1471    29.275
   11      .1477    29.793
   12      .1483    30.052
   13      .1489    30.052
   14      .1495    30.052
   15      .1501    30.052
   16      .1507    30.052
   17      .1513    30.052
   18      .1519    30.052
   19      .1525    30.052
   20      .1530    30.052
   21      .1536    30.052
   22      .1542    30.052
   23      .1548    30.052
   24      .1554    30.052
   25      .1560    30.052
   26      .1566    30.052
   27      .1572    30.052
   28      .1578    30.052
   29      .1584    30.052
   30      .1590    30.052
   31      .1596    30.052
   32      .1602    30.052
   33      .1608    30.052
   34      .1614    30.052
   35      .1620    30.052
   36      .1626    30.052
   37      .1632    30.052
   38      .1638    30.052
   39      .1644    30.052
   40      .1650    30.052
   41      .1656    30.052
   42      .1662    30.052
   43      .1667    30.052
   44      .1673    30.052
   45      .1679    29.534
   46      .1685    29.016
   47      .1691    28.238
   48      .1697    27.461
   49      .1703    26.166
   50      .1709    24.767
   51      .1715    23.187
   52      .1721    21.399
   53      .1727    19.456
   54      .1733    17.358
   55      .1739    15.130
   56      .1745    12.798
   57      .1751    10.337
```

58	.1757	7.798
59	.1763	5.207
60	.1769	2.567
61	.1775	.000

DLF VALUES

F	0%	2%	5%	10%	20%
1	.022	.022	.022	.022	.023
2	.089	.088	.088	.087	.087
3	.196	.194	.192	.189	.187
4	.339	.335	.330	.323	.314
5	.510	.503	.494	.480	.460
6	.703	.691	.676	.652	.617
7	.908	.890	.866	.831	.776
8	1.114	1.091	1.057	1.008	.930
9	1.314	1.283	1.239	1.175	1.071
10	1.496	1.457	1.404	1.324	1.194
11	1.652	1.607	1.543	1.449	1.295
12	1.776	1.724	1.652	1.544	1.370
13	1.860	1.803	1.725	1.608	1.420
14	1.910	1.851	1.770	1.650	1.457
15	1.944	1.885	1.802	1.680	1.483
16	1.966	1.906	1.823	1.699	1.500
17	1.978	1.918	1.835	1.711	1.511
18	1.984	1.924	1.840	1.716	1.516
19	1.986	1.925	1.842	1.718	1.518
20	1.985	1.925	1.841	1.718	1.518
21	1.984	1.924	1.840	1.717	1.517
22	1.982	1.922	1.839	1.716	1.516
23	1.980	1.920	1.837	1.714	1.515
24	1.978	1.919	1.836	1.713	1.514
25	1.977	1.917	1.834	1.712	1.514
26	1.975	1.915	1.833	1.710	1.512
27	1.973	1.914	1.831	1.709	1.511
28	1.971	1.912	1.829	1.707	1.510
29	1.969	1.910	1.827	1.706	1.509
30	1.967	1.908	1.826	1.704	1.508
31	1.965	1.906	1.824	1.703	1.507
32	1.962	1.904	1.822	1.701	1.505
33	1.960	1.901	1.820	1.699	1.504
34	1.958	1.899	1.818	1.697	1.503
35	1.955	1.897	1.815	1.696	1.501
36	1.953	1.894	1.813	1.694	1.500
37	1.950	1.892	1.811	1.692	1.498
38	1.948	1.890	1.809	1.690	1.497
39	1.945	1.887	1.807	1.688	1.495
40	1.942	1.884	1.804	1.686	1.494
41	1.939	1.881	1.802	1.684	1.492
42	1.936	1.879	1.799	1.682	1.491
43	1.933	1.876	1.797	1.679	1.489
44	1.931	1.873	1.794	1.677	1.487
45	1.928	1.871	1.791	1.675	1.485
46	1.924	1.868	1.788	1.672	1.483
47	1.921	1.864	1.785	1.670	1.482
48	1.918	1.861	1.783	1.668	1.480
49	1.915	1.859	1.781	1.665	1.478
50	1.911	1.855	1.777	1.662	1.476
51	1.908	1.852	1.775	1.660	1.474
52	1.905	1.849	1.772	1.658	1.472
53	1.901	1.846	1.769	1.655	1.470
54	1.897	1.842	1.766	1.652	1.468
55	1.894	1.839	1.763	1.650	1.466
56	1.890	1.835	1.759	1.647	1.464
57	1.887	1.832	1.757	1.644	1.462
58	1.883	1.828	1.753	1.641	1.460
59	1.880	1.825	1.750	1.639	1.457
60	1.875	1.821	1.746	1.635	1.455
61	1.872	1.818	1.744	1.633	1.453
62	1.868	1.813	1.740	1.630	1.451
63	1.865	1.811	1.737	1.627	1.448
64	1.860	1.806	1.733	1.624	1.446
65	1.857	1.803	1.730	1.620	1.444
66	1.852	1.799	1.727	1.618	1.441
67	1.848	1.795	1.722	1.615	1.439
68	1.845	1.792	1.720	1.612	1.436
69	1.840	1.788	1.716	1.609	1.434
70	1.836	1.783	1.712	1.605	1.432
71	1.833	1.780	1.709	1.602	1.429
72	1.828	1.776	1.705	1.600	1.427
73	1.824	1.772	1.701	1.595	1.425
74	1.820	1.769	1.698	1.593	1.422

75	1.815	1.765	1.695	1.590	1.419
76	1.811	1.760	1.689	1.586	1.417
77	1.808	1.757	1.687	1.582	1.414
78	1.803	1.753	1.684	1.580	1.411
79	1.799	1.748	1.679	1.577	1.409
80	1.794	1.744	1.675	1.572	1.407
81	1.790	1.741	1.672	1.569	1.404
82	1.785	1.736	1.668	1.567	1.401
83	1.781	1.731	1.664	1.563	1.399
84	1.777	1.728	1.659	1.559	1.396
85	1.773	1.724	1.657	1.556	1.393
86	1.768	1.720	1.653	1.553	1.390
87	1.763	1.714	1.648	1.550	1.388
88	1.759	1.710	1.643	1.545	1.386
89	1.755	1.707	1.641	1.542	1.383
90	1.751	1.703	1.637	1.539	1.379
91	1.745	1.698	1.633	1.536	1.377
92	1.742	1.693	1.628	1.532	1.375
93	1.737	1.690	1.624	1.528	1.372
94	1.733	1.686	1.621	1.524	1.369
95	1.728	1.682	1.618	1.522	1.366
96	1.723	1.677	1.614	1.519	1.364
97	1.719	1.671	1.609	1.515	1.361
98	1.714	1.668	1.604	1.511	1.359
99	1.710	1.665	1.601	1.507	1.356
100	1.706	1.660	1.598	1.504	1.353
101	1.700	1.655	1.594	1.501	1.350
102	1.695	1.650	1.589	1.497	1.347
103	1.692	1.647	1.585	1.493	1.344
104	1.687	1.643	1.582	1.490	1.342
105	1.682	1.638	1.578	1.487	1.339
106	1.677	1.633	1.573	1.484	1.336
107	1.673	1.629	1.569	1.480	1.334
108	1.669	1.625	1.566	1.476	1.331
109	1.664	1.621	1.562	1.473	1.329
110	1.658	1.616	1.558	1.470	1.326
111	1.655	1.612	1.553	1.466	1.323
112	1.651	1.608	1.550	1.462	1.321
113	1.646	1.604	1.546	1.459	1.318
114	1.641	1.600	1.543	1.456	1.315
115	1.636	1.595	1.538	1.453	1.312
116	1.633	1.591	1.534	1.449	1.310
117	1.629	1.587	1.530	1.445	1.307
118	1.624	1.583	1.527	1.441	1.305
119	1.620	1.579	1.523	1.439	1.303
120	1.615	1.574	1.519	1.436	1.300
121	1.611	1.569	1.514	1.432	1.297
122	1.606	1.566	1.510	1.429	1.294
123	1.603	1.562	1.507	1.425	1.292
124	1.598	1.558	1.504	1.421	1.290
125	1.594	1.553	1.500	1.419	1.287
126	1.589	1.548	1.496	1.416	1.284
127	1.586	1.544	1.491	1.412	1.281
128	1.581	1.541	1.487	1.409	1.279
129	1.577	1.537	1.484	1.405	1.277
130	1.573	1.533	1.480	1.401	1.275
131	1.568	1.528	1.476	1.398	1.272
132	1.565	1.523	1.472	1.395	1.270
133	1.561	1.518	1.468	1.392	1.267
134	1.556	1.515	1.464	1.388	1.264
135	1.551	1.511	1.460	1.384	1.261
136	1.548	1.506	1.456	1.381	1.259
137	1.543	1.501	1.452	1.378	1.257
138	1.540	1.497	1.448	1.375	1.254
139	1.534	1.493	1.444	1.372	1.252
140	1.531	1.489	1.440	1.368	1.249
141	1.527	1.485	1.437	1.364	1.247
142	1.523	1.480	1.433	1.361	1.244
143	1.519	1.475	1.429	1.358	1.242
144	1.515	1.471	1.425	1.355	1.240
145	1.511	1.468	1.420	1.352	1.237
146	1.508	1.463	1.417	1.348	1.235
147	1.503	1.459	1.414	1.344	1.232
148	1.500	1.455	1.410	1.341	1.230
149	1.495	1.450	1.406	1.338	1.228
150	1.492	1.445	1.402	1.335	1.225
151	1.487	1.442	1.397	1.332	1.223
152	1.484	1.438	1.393	1.328	1.221
153	1.480	1.433	1.390	1.325	1.218
154	1.476	1.429	1.386	1.321	1.216
155	1.473	1.424	1.383	1.318	1.213
156	1.468	1.420	1.379	1.315	1.211

157	1.465	1.415	1.375	1.312	1.209
158	1.461	1.411	1.370	1.309	1.207
159	1.457	1.407	1.366	1.305	1.204
160	1.454	1.403	1.362	1.302	1.202
161	1.450	1.399	1.359	1.299	1.200
162	1.446	1.394	1.355	1.295	1.197
163	1.443	1.390	1.351	1.291	1.195
164	1.438	1.385	1.348	1.288	1.192
165	1.435	1.381	1.343	1.285	1.190
166	1.432	1.377	1.339	1.282	1.188
167	1.428	1.373	1.335	1.279	1.186
168	1.425	1.368	1.331	1.275	1.184
169	1.421	1.364	1.328	1.272	1.181
170	1.417	1.360	1.324	1.269	1.179
171	1.414	1.356	1.319	1.266	1.177
172	1.410	1.352	1.315	1.263	1.174
173	1.407	1.347	1.312	1.259	1.172
174	1.403	1.343	1.308	1.256	1.170
175	1.399	1.338	1.304	1.253	1.168
176	1.396	1.334	1.301	1.250	1.166
177	1.392	1.330	1.297	1.246	1.164
178	1.389	1.326	1.293	1.243	1.162
179	1.385	1.321	1.289	1.240	1.159
180	1.381	1.317	1.285	1.237	1.157
181	1.378	1.313	1.281	1.234	1.155
182	1.374	1.309	1.277	1.231	1.153
183	1.371	1.306	1.274	1.228	1.151
184	1.367	1.304	1.270	1.224	1.149
185	1.363	1.301	1.266	1.221	1.147
186	1.360	1.298	1.262	1.218	1.145
187	1.357	1.295	1.259	1.215	1.143
188	1.353	1.292	1.255	1.212	1.141
189	1.350	1.289	1.251	1.209	1.139
190	1.346	1.287	1.247	1.206	1.137
191	1.342	1.283	1.243	1.203	1.135
192	1.339	1.281	1.240	1.200	1.132
193	1.335	1.278	1.236	1.197	1.130
194	1.332	1.275	1.232	1.194	1.129
195	1.328	1.272	1.229	1.191	1.127
196	1.324	1.270	1.225	1.188	1.125
197	1.321	1.266	1.221	1.184	1.123
198	1.318	1.264	1.217	1.181	1.121
199	1.314	1.261	1.213	1.178	1.119
200	1.310	1.258	1.209	1.175	1.117

2.10.10.7.2 Hot Flatside Slapdown DLF (Portion) Output File

```
DLF ANALYSIS FOR LOAD CASE FSSH
SLAPDOWN RESPONSE ANALYSIS

CALCULATION PARAMETERS
 KOULIM  =        50
 FCTLIM  =      .010
 CNVFCT  =      .020
 NSPLIM  =         2
 FREQLO  =     1.000
 FREQINC =     1.000
 NFREQ   =       200

PRIMARY TIME-HISTORY STARTS AT LINE      6
PRIMARY TIME-HISTORY ENDS AT LINE       89
SECONDARY TIME-HISTORY STARTS AT LINE  227
SECONDARY TIME-HISTORY ENDS AT LINE    301
NUMBER OF TIME-HISTORY POINTS       75

TIME HISTORY DATA
    I         T         F
    1     .1434     4.767
    2     .1440     6.451
    3     .1447     6.736
    4     .1453    13.549
    5     .1460    16.736
    6     .1466    17.720
    7     .1473    18.135
    8     .1479    18.549
    9     .1485    18.938
   10     .1492    19.326
   11     .1498    19.326
   12     .1505    19.326
   13     .1511    19.326
   14     .1518    19.326
   15     .1524    19.326
   16     .1531    19.326
   17     .1537    19.326
   18     .1544    19.326
   19     .1550    19.326
   20     .1557    19.326
   21     .1563    19.326
   22     .1570    19.326
   23     .1576    19.326
   24     .1583    19.326
   25     .1589    19.326
   26     .1596    19.326
   27     .1602    19.326
   28     .1609    19.326
   29     .1615    19.326
   30     .1622    19.326
   31     .1628    19.326
   32     .1635    19.326
   33     .1641    19.326
   34     .1648    19.326
   35     .1654    19.326
   36     .1661    19.326
   37     .1667    19.326
   38     .1674    19.326
   39     .1680    19.326
   40     .1687    19.326
   41     .1693    19.326
   42     .1700    19.326
   43     .1706    19.326
   44     .1713    19.326
   45     .1719    19.326
   46     .1725    19.326
   47     .1732    19.326
   48     .1738    19.326
   49     .1745    19.326
   50     .1751    19.326
   51     .1758    19.326
   52     .1764    19.326
   53     .1771    19.326
   54     .1777    19.326
   55     .1784    19.326
   56     .1790    19.326
```

57	.1797	19.326
58	.1803	19.326
59	.1810	19.326
60	.1816	19.016
61	.1823	18.601
62	.1829	18.031
63	.1836	17.306
64	.1842	16.425
65	.1849	15.415
66	.1855	14.249
'67	.1862	12.953
68	.1868	11.580
69	.1875	10.078
70	.1881	8.472
71	.1888	6.813
72	.1894	5.078
73	.1901	3.316
74	.1907	1.495
75	.1914	.000

DLF VALUES

F	0%	2%	5%	10%	20%
1	.042	.042	.042	.042	.042
2	.164	.163	.161	.159	.158
3	.356	.352	.347	.339	.330
4	.602	.593	.580	.563	.536
5	.879	.863	.840	.808	.756
6	1.165	1.139	1.104	1.052	.969
7	1.434	1.398	1.349	1.276	1.158
8	1.663	1.618	1.555	1.461	1.309
9	1.832	1.779	1.704	1.593	1.413
10	1.927	1.868	1.787	1.666	1.471
11	1.971	1.911	1.827	1.703	1.504
12	1.989	1.929	1.845	1.720	1.519
13	1.994	1.933	1.849	1.725	1.523
14	1.993	1.933	1.849	1.724	1.523
15	1.992	1.932	1.848	1.724	1.522
16	1.992	1.931	1.847	1.723	1.522
17	1.990	1.930	1.846	1.722	1.521
18	1.989	1.929	1.845	1.721	1.520
19	1.988	1.928	1.844	1.720	1.520
20	1.987	1.927	1.843	1.719	1.519
21	1.985	1.925	1.842	1.718	1.518
22	1.984	1.924	1.841	1.717	1.517
23	1.983	1.923	1.839	1.716	1.517
24	1.981	1.921	1.838	1.715	1.516
25	1.979	1.920	1.837	1.714	1.515
26	1.978	1.918	1.835	1.712	1.514
27	1.976	1.916	1.834	1.711	1.513
28	1.974	1.915	1.832	1.710	1.512
29	1.972	1.913	1.831	1.708	1.511
30	1.971	1.911	1.829	1.707	1.510
31	1.968	1.909	1.827	1.705	1.509
32	1.967	1.908	1.825	1.704	1.508
33	1.964	1.905	1.823	1.702	1.507
34	1.962	1.904	1.822	1.701	1.505
35	1.960	1.901	1.820	1.699	1.504
36	1.958	1.899	1.818	1.697	1.503
37	1.955	1.897	1.816	1.695	1.501
38	1.953	1.895	1.814	1.694	1.500
39	1.951	1.892	1.811	1.692	1.499
40	1.948	1.890	1.809	1.690	1.497
41	1.946	1.888	1.807	1.688	1.496
42	1.943	1.885	1.804	1.686	1.494
43	1.940	1.882	1.802	1.685	1.493
44	1.938	1.880	1.800	1.683	1.492
45	1.935	1.878	1.798	1.681	1.490
46	1.932	1.875	1.795	1.678	1.488
47	1.929	1.871	1.792	1.676	1.487
48	1.927	1.870	1.791	1.674	1.485
49	1.924	1.867	1.788	1.672	1.483
50	1.920	1.864	1.785	1.670	1.482
51	1.918	1.861	1.783	1.668	1.480
52	1.914	1.858	1.780	1.665	1.478
53	1.911	1.855	1.777	1.663	1.476
54	1.908	1.852	1.774	1.660	1.474
55	1.905	1.849	1.772	1.658	1.473
56	1.902	1.846	1.769	1.655	1.470
57	1.899	1.843	1.766	1.653	1.469
58	1.895	1.840	1.763	1.650	1.467
59	1.892	1.837	1.761	1.648	1.465
60	1.888	1.833	1.757	1.645	1.463

61	1.885	1.830	1.755	1.643	1.461
62	1.881	1.825	1.751	1.640	1.459
63	1.878	1.824	1.749	1.637	1.456
64	1.874	1.820	1.746	1.635	1.455
65	1.870	1.815	1.741	1.631	1.453
66	1.867	1.813	1.739	1.629	1.450
67	1.863	1.809	1.736	1.627	1.448
68	1.859	1.805	1.732	1.623	1.446
69	1.856	1.803	1.730	1.621	1.443
70	1.851	1.798	1.726	1.618	1.442
71	1.848	1.795	1.723	1.614	1.439
72	1.845	1.792	1.720	1.612	1.437
73	1.840	1.788	1.716	1.609	1.435
74	1.836	1.783	1.711	1.605	1.433
75	1.833	1.781	1.710	1.602	1.430
76	1.829	1.778	1.707	1.600	1.427
77	1.824	1.773	1.703	1.597	1.426
78	1.821	1.768	1.697	1.593	1.423
79	1.817	1.766	1.696	1.590	1.420
80	1.814	1.763	1.693	1.588	1.418
81	1.808	1.758	1.689	1.585	1.416
82	1.805	1.753	1.684	1.581	1.414
83	1.801	1.751	1.681	1.578	1.411
84	1.797	1.747	1.679	1.576	1.408
85	1.793	1.743	1.675	1.573	1.406
86	1.788	1.737	1.669	1.569	1.404
87	1.785	1.735	1.666	1.564	1.401
88	1.781	1.732	1.663	1.562	1.398
89	1.776	1.727	1.660	1.560	1.395
90	1.772	1.722	1.655	1.556	1.393
91	1.768	1.719	1.652	1.552	1.391
92	1.764	1.716	1.649	1.550	1.388
93	1.759	1.711	1.645	1.547	1.385
94	1.755	1.707	1.640	1.543	1.383
95	1.751	1.704	1.637	1.539	1.381
96	1.747	1.700	1.634	1.536	1.378
97	1.742	1.695	1.630	1.533	1.375
98	1.738	1.690	1.626	1.530	1.373
99	1.734	1.687	1.622	1.526	1.371
100	1.730	1.683	1.619	1.523	1.368
101	1.724	1.678	1.615	1.520	1.364
102	1.720	1.673	1.610	1.516	1.362
103	1.717	1.670	1.607	1.512	1.359
104	1.712	1.666	1.603	1.509	1.357
105	1.707	1.662	1.600	1.506	1.354
106	1.703	1.657	1.595	1.503	1.351
107	1.699	1.654	1.591	1.499	1.349
108	1.695	1.650	1.588	1.495	1.347
109	1.690	1.646	1.585	1.493	1.344
110	1.685	1.641	1.581	1.490	1.341
111	1.682	1.637	1.576	1.486	1.338
112	1.678	1.634	1.573	1.482	1.336
113	1.674	1.630	1.570	1.479	1.334
114	1.669	1.625	1.566	1.476	1.331
115	1.664	1.620	1.561	1.473	1.328
116	1.661	1.617	1.557	1.470	1.325
117	1.656	1.613	1.554	1.466	1.323
118	1.652	1.609	1.551	1.463	1.321
119	1.647	1.605	1.547	1.460	1.318
120	1.643	1.600	1.542	1.457	1.315
121	1.639	1.597	1.539	1.453	1.313
122	1.635	1.593	1.536	1.449	1.311
123	1.630	1.589	1.532	1.447	1.308
124	1.626	1.584	1.528	1.444	1.305
125	1.622	1.580	1.524	1.441	1.303
126	1.618	1.577	1.520	1.437	1.300
127	1.614	1.573	1.517	1.433	1.298
128	1.609	1.569	1.514	1.430	1.296
129	1.605	1.564	1.510	1.428	1.293
130	1.600	1.560	1.506	1.425	1.291
131	1.597	1.556	1.501	1.421	1.288
132	1.592	1.553	1.498	1.418	1.286
133	1.588	1.549	1.495	1.414	1.283
134	1.584	1.545	1.491	1.411	1.281
135	1.580	1.540	1.487	1.408	1.278
136	1.576	1.536	1.483	1.405	1.276
137	1.572	1.533	1.479	1.402	1.273
138	1.568	1.529	1.476	1.398	1.271
139	1.564	1.525	1.473	1.395	1.269
140	1.560	1.520	1.469	1.392	1.266
141	1.556	1.516	1.465	1.389	1.264
142	1.551	1.512	1.461	1.386	1.262

143	1.549	1.509	1.457	1.382	1.259
144	1.545	1.505	1.454	1.379	1.256
145	1.541	1.501	1.450	1.376	1.254
146	1.537	1.496	1.447	1.373	1.252
147	1.533	1.492	1.443	1.370	1.250
148	1.529	1.488	1.439	1.367	1.247
149	1.526	1.485	1.435	1.364	1.245
150	1.522	1.481	1.432	1.360	1.242
151	1.518	1.476	1.428	1.356	1.240
152	1.514	1.472	1.425	1.354	1.238
153	1.510	1.467	1.421	1.351	1.236
154	1.507	1.464	1.417	1.348	1.234
155	1.502	1.460	1.413	1.345	1.231
156	1.499	1.456	1.409	1.342	1.229
157	1.495	1.452	1.406	1.338	1.226
158	1.492	1.448	1.403	1.335	1.224
159	1.488	1.444	1.399	1.332	1.222
160	1.484	1.439	1.395	1.329	1.220
161	1.481	1.435	1.391	1.326	1.218
162	1.477	1.432	1.387	1.323	1.215
163	1.474	1.428	1.384	1.320	1.213
164	1.469	1.424	1.380	1.317	1.211
165	1.467	1.420	1.377	1.313	1.208
166	1.463	1.416	1.374	1.310	1.206
167	1.460	1.412	1.369	1.307	1.204
168	1.456	1.408	1.365	1.304	1.202
169	1.453	1.404	1.362	1.301	1.200
170	1.449	1.400	1.358	1.298	1.197
171	1.445	1.396	1.355	1.295	1.195
172	1.443	1.391	1.351	1.291	1.193
173	1.439	1.387	1.347	1.288	1.191
174	1.436	1.383	1.344	1.285	1.188
175	1.432	1.380	1.340	1.282	1.186
176	1.429	1.376	1.336	1.279	1.184
177	1.426	1.372	1.333	1.276	1.182
178	1.422	1.368	1.329	1.273	1.180
179	1.419	1.363	1.326	1.270	1.178
180	1.415	1.359	1.322	1.267	1.176
181	1.412	1.355	1.318	1.263	1.174
182	1.409	1.351	1.314	1.261	1.171
183	1.405	1.347	1.311	1.258	1.169
184	1.402	1.344	1.307	1.255	1.167
185	1.399	1.340	1.303	1.252	1.165
186	1.396	1.335	1.300	1.249	1.163
187	1.392	1.331	1.297	1.246	1.161
188	1.388	1.327	1.293	1.243	1.159
189	1.386	1.323	1.289	1.239	1.157
190	1.382	1.319	1.286	1.236	1.155
191	1.379	1.315	1.282	1.233	1.153
192	1.376	1.311	1.278	1.231	1.151
193	1.372	1.307	1.274	1.228	1.149
194	1.369	1.304	1.271	1.225	1.147
195	1.366	1.302	1.267	1.222	1.145
196	1.363	1.299	1.264	1.219	1.143
197	1.359	1.296	1.261	1.216	1.141
198	1.357	1.294	1.257	1.213	1.139
199	1.353	1.292	1.253	1.210	1.137
200	1.349	1.289	1.250	1.207	1.135

2.10.10.7.3 Cold Corner Slapdown DLF (Portion) Output File

```
DLF ANALYSIS FOR LOAD CASE CNSC
SLAPDOWN RESPONSE ANALYSIS

CALCULATION PARAMETERS
 KOULIM  =        50
 FCTLIM  =      .010
 CNVFCT  =      .020
 NSPLIM  =         2
 FREQLO  =     1.000
 FREQINC =     1.000
 NFREQ   =       200

PRIMARY TIME-HISTORY STARTS AT LINE       8
PRIMARY TIME-HISTORY ENDS AT LINE        98
SECONDARY TIME-HISTORY STARTS AT LINE   237
SECONDARY TIME-HISTORY ENDS AT LINE     313
NUMBER OF TIME-HISTORY POINTS       77

TIME HISTORY DATA
    I         T         F
    1      .1446     1.604
    2      .1453     5.984
    3      .1459     9.637
    4      .1465    10.078
    5      .1471    10.518
    6      .1478    10.959
    7      .1484    11.373
    8      .1490    11.788
    9      .1496    12.228
   10      .1503    12.642
   11      .1509    13.057
   12      .1515    13.472
   13      .1521    13.860
   14      .1528    14.275
   15      .1534    14.663
   16      .1540    15.052
   17      .1546    15.440
   18      .1553    15.829
   19      .1559    16.218
   20      .1565    16.580
   21      .1572    16.943
   22      .1578    17.306
   23      .1584    17.668
   24      .1590    18.005
   25      .1597    18.342
   26      .1603    18.679
   27      .1609    18.990
   28      .1615    19.326
   29      .1622    19.611
   30      .1628    19.922
   31      .1634    20.233
   32      .1640    20.518
   33      .1647    20.777
   34      .1653    21.062
   35      .1659    21.321
   36      .1665    21.554
   37      .1672    21.813
   38      .1678    22.047
   39      .1684    22.254
   40      .1690    22.487
   41      .1697    22.668
   42      .1703    22.876
   43      .1709    23.057
   44      .1716    23.238
   45      .1722    23.394
   46      .1728    23.549
   47      .1734    23.705
   48      .1741    23.834
   49      .1747    23.964
   50      .1753    24.067
   51      .1759    24.171
   52      .1766    24.249
   53      .1772    24.326
   54      .1778    24.404
   55      .1784    24.456
   56      .1791    24.508
   57      .1797    24.534
```

58	.1803	24.560
59	.1809	24.585
60	.1816	24.585
61	.1822	24.560
62	.1828	24.016
63	.1834	23.420
64	.1841	22.617
65	.1847	21.606
66	.1853	20.440
67	.1860	19.067
68	.1866	17.539
69	.1872	15.829
70	.1878	14.016
71	.1885	12.073
72	.1891	10.000
73	.1897	7.850
74	.1903	5.622
75	.1910	3.368
76	.1916	1.052
77	.1922	.000

DLF VALUES

F	0%	2%	5%	10%	20%
1	.031	.031	.031	.031	.031
2	.121	.121	.120	.118	.118
3	.265	.262	.258	.253	.247
4	.450	.444	.436	.424	.407
5	.664	.653	.638	.615	.581
6	.892	.874	.849	.813	.756
7	1.115	1.090	1.055	1.003	.920
8	1.320	1.287	1.241	1.173	1.063
9	1.490	1.450	1.394	1.311	1.177
10	1.616	1.570	1.506	1.411	1.258
11	1.689	1.640	1.571	1.469	1.304
12	1.715	1.666	1.597	1.495	1.329
13	1.718	1.669	1.602	1.501	1.338
14	1.703	1.656	1.590	1.493	1.336
15	1.676	1.631	1.568	1.474	1.324
16	1.643	1.599	1.539	1.449	1.305
17	1.609	1.566	1.508	1.421	1.283
18	1.575	1.534	1.477	1.393	1.260
19	1.543	1.503	1.447	1.365	1.237
20	1.512	1.472	1.418	1.339	1.214
21	1.482	1.443	1.390	1.313	1.191
22	1.453	1.416	1.364	1.288	1.170
23	1.427	1.390	1.339	1.264	1.149
24	1.401	1.365	1.315	1.242	1.129
25	1.377	1.341	1.292	1.220	1.109
26	1.354	1.319	1.271	1.200	1.091
27	1.333	1.298	1.250	1.180	1.073
28	1.312	1.278	1.231	1.162	1.056
29	1.293	1.259	1.213	1.145	1.040
30	1.275	1.242	1.195	1.128	1.025
31	1.258	1.225	1.179	1.113	1.010
32	1.242	1.209	1.164	1.098	.996
33	1.226	1.194	1.149	1.084	1.007
34	1.254	1.197	1.135	1.070	1.022
35	1.304	1.242	1.171	1.096	1.035
36	1.342	1.276	1.200	1.118	1.045
37	1.370	1.301	1.222	1.135	1.053
38	1.387	1.317	1.237	1.146	1.059
39	1.398	1.328	1.245	1.153	1.063
40	1.403	1.332	1.250	1.157	1.065
41	1.404	1.334	1.251	1.158	1.065
42	1.403	1.333	1.251	1.157	1.064
43	1.401	1.331	1.249	1.156	1.063
44	1.399	1.329	1.247	1.154	1.060
45	1.396	1.326	1.244	1.151	1.058
46	1.393	1.323	1.241	1.148	1.055
47	1.389	1.319	1.237	1.144	1.051
48	1.384	1.315	1.233	1.140	1.047
49	1.380	1.310	1.229	1.136	1.043
50	1.375	1.306	1.224	1.131	1.039
51	1.370	1.301	1.219	1.127	1.035
52	1.365	1.296	1.214	1.122	1.030
53	1.359	1.290	1.209	1.117	1.025
54	1.354	1.285	1.203	1.111	1.021
55	1.348	1.279	1.198	1.106	1.016
56	1.342	1.274	1.193	1.101	1.011
57	1.337	1.268	1.187	1.095	1.006
58	1.331	1.262	1.182	1.090	1.001
59	1.325	1.256	1.176	1.084	.998

60	1.319	1.251	1.170	1.079	1.003
61	1.313	1.245	1.165	1.074	1.007
62	1.331	1.239	1.159	1.068	1.010
63	1.349	1.248	1.153	1.063	1.013
64	1.362	1.260	1.158	1.069	1.016
65	1.369	1.267	1.165	1.074	1.017
66	1.374	1.272	1.168	1.077	1.019
67	1.376	1.274	1.170	1.079	1.019
68	1.376	1.274	1.171	1.079	1.019
69	1.376	1.274	1.171	1.079	1.019
70	1.376	1.274	1.171	1.079	1.019
71	1.374	1.272	1.170	1.078	1.018
72	1.374	1.272	1.169	1.077	1.017
73	1.372	1.270	1.167	1.076	1.016
74	1.371	1.269	1.166	1.075	1.015
75	1.369	1.267	1.164	1.073	1.014
76	1.367	1.265	1.163	1.071	1.012
77	1.365	1.263	1.161	1.070	1.011
78	1.363	1.261	1.159	1.068	1.009
79	1.360	1.259	1.157	1.066	1.007
80	1.357	1.256	1.154	1.063	1.005
81	1.354	1.253	1.151	1.061	1.003
82	1.351	1.250	1.149	1.058	1.001
83	1.349	1.248	1.146	1.056	.999
84	1.346	1.245	1.143	1.053	.998
85	1.343	1.242	1.141	1.050	.999
86	1.339	1.239	1.138	1.047	1.000
87	1.336	1.235	1.135	1.044	1.001
88	1.334	1.233	1.131	1.041	1.002
89	1.334	1.230	1.129	1.039	1.003
90	1.345	1.226	1.126	1.035	1.004
91	1.352	1.223	1.122	1.035	1.005
92	1.357	1.227	1.119	1.038	1.006
93	1.359	1.229	1.118	1.039	1.006
94	1.361	1.231	1.119	1.040	1.006
95	1.362	1.231	1.120	1.040	1.006
96	1.361	1.231	1.120	1.041	1.006
97	1.361	1.231	1.119	1.040	1.006
98	1.361	1.231	1.119	1.040	1.006
99	1.360	1.230	1.119	1.040	1.005
100	1.361	1.231	1.119	1.039	1.005
101	1.360	1.231	1.118	1.039	1.005
102	1.360	1.230	1.118	1.038	1.004
103	1.359	1.229	1.117	1.038	1.004
104	1.357	1.228	1.116	1.037	1.003
105	1.357	1.227	1.115	1.036	1.002
106	1.355	1.226	1.114	1.035	1.002
107	1.354	1.224	1.112	1.033	1.001
108	1.352	1.223	1.111	1.032	1.000
109	1.350	1.221	1.110	1.031	1.000
110	1.349	1.220	1.108	1.029	1.000
111	1.346	1.218	1.106	1.028	1.000
112	1.345	1.216	1.105	1.026	1.001
113	1.343	1.214	1.103	1.025	1.001
114	1.340	1.212	1.101	1.023	1.001
115	1.338	1.210	1.099	1.021	1.002
116	1.337	1.208	1.097	1.019	1.002
117	1.341	1.206	1.095	1.017	1.002
118	1.347	1.204	1.093	1.018	1.002
119	1.350	1.201	1.091	1.019	1.002
120	1.352	1.199	1.088	1.020	1.002
121	1.352	1.198	1.086	1.021	1.002
122	1.352	1.199	1.085	1.021	1.002
123	1.351	1.198	1.084	1.021	1.002
124	1.351	1.198	1.084	1.021	1.002
125	1.351	1.198	1.084	1.021	1.002
126	1.349	1.197	1.084	1.020	1.002
127	1.349	1.197	1.083	1.020	1.002
128	1.348	1.196	1.083	1.020	1.002
129	1.347	1.195	1.082	1.019	1.002
130	1.347	1.195	1.082	1.019	1.001
131	1.346	1.194	1.081	1.018	1.001
132	1.345	1.193	1.080	1.018	1.001
133	1.344	1.193	1.080	1.017	1.001
134	1.344	1.193	1.080	1.016	1.001
135	1.344	1.192	1.079	1.016	1.001
136	1.342	1.191	1.078	1.015	1.001
137	1.342	1.190	1.077	1.014	1.001
138	1.340	1.189	1.076	1.013	1.001
139	1.339	1.188	1.075	1.012	1.001
140	1.338	1.187	1.074	1.011	1.001
141	1.337	1.186	1.073	1.010	1.001

142	1.335	1.184	1.072	1.009	1.001
143	1.334	1.184	1.071	1.008	1.001
144	1.335	1.182	1.070	1.008	1.002
145	1.339	1.181	1.068	1.009	1.002
146	1.341	1.179	1.067	1.010	1.002
147	1.343	1.177	1.065	1.011	1.002
148	1.343	1.175	1.064	1.011	1.002
149	1.343	1.174	1.062	1.011	1.002
150	1.343	1.172	1.061	1.011	1.002
151	1.342	1.170	1.060	1.011	1.002
152	1.341	1.170	1.060	1.011	1.002
153	1.341	1.170	1.060	1.011	1.001
154	1.340	1.169	1.059	1.011	1.001
155	1.339	1.169	1.059	1.010	1.001
156	1.338	1.168	1.059	1.010	1.001
157	1.338	1.168	1.058	1.010	1.001
158	1.337	1.167	1.058	1.009	1.001
159	1.336	1.166	1.057	1.009	1.001
160	1.335	1.165	1.057	1.008	1.001
161	1.334	1.165	1.056	1.008	1.001
162	1.332	1.164	1.055	1.007	1.001
163	1.332	1.163	1.055	1.007	1.001
164	1.331	1.162	1.054	1.006	1.001
165	1.330	1.161	1.053	1.005	1.001
166	1.329	1.161	1.053	1.005	1.001
167	1.329	1.161	1.052	1.004	1.001
168	1.328	1.160	1.052	1.003	1.001
169	1.327	1.159	1.051	1.003	1.001
170	1.326	1.158	1.050	1.003	1.001
171	1.325	1.157	1.049	1.004	1.001
172	1.329	1.157	1.049	1.005	1.001
173	1.331	1.155	1.048	1.006	1.001
174	1.332	1.154	1.047	1.006	1.001
175	1.332	1.153	1.046	1.006	1.001
176	1.332	1.152	1.045	1.006	1.001
177	1.332	1.151	1.044	1.006	1.001
178	1.332	1.150	1.043	1.006	1.001
179	1.331	1.148	1.043	1.006	1.001
180	1.330	1.147	1.043	1.006	1.001
181	1.330	1.145	1.043	1.006	1.001
182	1.329	1.145	1.042	1.006	1.001
183	1.328	1.144	1.042	1.006	1.001
184	1.328	1.144	1.042	1.006	1.001
185	1.326	1.143	1.041	1.005	1.001
186	1.326	1.143	1.041	1.005	1.001
187	1.325	1.142	1.041	1.005	1.001
188	1.323	1.141	1.040	1.004	1.001
189	1.322	1.140	1.039	1.004	1.001
190	1.321	1.139	1.039	1.004	1.001
191	1.320	1.138	1.038	1.003	1.001
192	1.319	1.138	1.037	1.002	1.001
193	1.318	1.137	1.037	1.002	1.001
194	1.316	1.136	1.036	1.001	1.001
195	1.315	1.135	1.035	1.001	1.001
196	1.314	1.134	1.034	1.001	1.001
197	1.313	1.133	1.034	1.001	1.001
198	1.312	1.132	1.033	1.002	1.001
199	1.313	1.131	1.032	1.002	1.001
200	1.316	1.131	1.032	1.003	1.001

2.10.10.7.4 Hot Corner Slapdown DLF (Portion) Output File

```
DLF ANALYSIS FOR LOAD CASE CNSH
SLAPDOWN RESPONSE ANALYSIS

CALCULATION PARAMETERS
 KOULIM  =         50
 FCTLIM  =       .010
 CNVFCT  =       .020
 NSPLIM  =          2
 FREQLO  =      1.000
 FREQINC =      1.000
 NFREQ   =        200

PRIMARY TIME-HISTORY STARTS AT LINE      11
PRIMARY TIME-HISTORY ENDS AT LINE       122
SECONDARY TIME-HISTORY STARTS AT LINE   231
SECONDARY TIME-HISTORY ENDS AT LINE     333
NUMBER OF TIME-HISTORY POINTS       103

TIME HISTORY DATA
    I         T         F
    1     .1460     2.223
    2     .1466     4.560
    3     .1473     4.793
    4     .1479     5.026
    5     .1485     5.259
    6     .1492     5.492
    7     .1498     5.725
    8     .1505     5.959
    9     .1511     6.192
   10     .1518     6.399
   11     .1524     6.632
   12     .1531     6.865
   13     .1537     7.098
   14     .1544     7.306
   15     .1550     7.539
   16     .1557     7.772
   17     .1563     7.979
   18     .1570     8.212
   19     .1576     8.420
   20     .1583     8.653
   21     .1589     8.860
   22     .1596     9.067
   23     .1602     9.301
   24     .1609     9.508
   25     .1615     9.715
   26     .1622     9.922
   27     .1628    10.130
   28     .1635    10.337
   29     .1641    10.544
   30     .1648    10.751
   31     .1654    10.933
   32     .1661    11.140
   33     .1667    11.321
   34     .1674    11.528
   35     .1680    11.710
   36     .1687    11.917
   37     .1693    12.098
   38     .1700    12.280
   39     .1706    12.461
   40     .1713    12.642
   41     .1719    12.798
   42     .1725    12.979
   43     .1732    13.135
   44     .1738    13.316
   45     .1745    13.472
   46     .1751    13.627
   47     .1758    13.782
   48     .1764    13.938
   49     .1771    14.093
   50     .1777    14.249
   51     .1784    14.378
   52     .1790    14.534
   53     .1797    14.663
   54     .1803    14.793
   55     .1810    14.922
   56     .1816    15.052
   57     .1823    15.181
```

58	.1829	15.285
59	.1836	15.415
60	.1842	15.518
61	.1849	15.622
62	.1855	15.725
63	.1862	15.829
64	.1868	15.907
65	.1875	16.010
66	.1881	16.088
67	.1888	16.192
68	.1894	16.269
69	.1901	16.321
70	.1907	16.399
71	.1914	16.477
72	.1920	16.528
73	.1927	16.580
74	.1933	16.632
75	.1940	16.684
76	.1946	16.736
77	.1953	16.788
78	.1959	16.813
79	.1966	16.839
80	.1972	16.865
81	.1978	16.891
82	.1985	16.917
83	.1991	16.917
84	.1998	16.943
85	.2004	16.943
86	.2011	16.943
87	.2017	16.943
88	.2024	16.554
89	.2030	16.140
90	.2037	15.570
91	.2043	14.870
92	.2050	14.067
93	.2056	13.109
94	.2063	12.047
95	.2069	10.881
96	.2076	9.611
97	.2082	8.238
98	.2089	6.813
99	.2095	5.337
100	.2102	3.782
101	.2108	2.202
102	.2115	.598
103	.2121	.000

DLF VALUES

F	0%	2%	5%	10%	20%
1	.055	.054	.054	.054	.054
2	.211	.209	.206	.203	.199
3	.448	.442	.433	.421	.404
4	.733	.720	.702	.675	.634
5	1.030	1.007	.976	.930	.857
6	1.299	1.267	1.222	1.155	1.047
7	1.508	1.467	1.409	1.325	1.188
8	1.632	1.586	1.521	1.425	1.271
9	1.665	1.618	1.553	1.457	1.301
10	1.645	1.601	1.540	1.449	1.301
11	1.598	1.557	1.501	1.417	1.282
12	1.541	1.503	1.450	1.373	1.250
13	1.485	1.449	1.399	1.327	1.213
14	1.432	1.398	1.351	1.282	1.176
15	1.382	1.349	1.304	1.239	1.141
16	1.335	1.304	1.260	1.198	1.106
17	1.291	1.261	1.220	1.160	1.073
18	1.251	1.222	1.181	1.124	1.042
19	1.213	1.185	1.146	1.091	1.013
20	1.179	1.151	1.113	1.059	.984
21	1.147	1.120	1.083	1.030	.984
22	1.118	1.091	1.055	1.003	1.000
23	1.135	1.101	1.066	1.034	1.017
24	1.211	1.168	1.119	1.070	1.031
25	1.263	1.214	1.157	1.097	1.042
26	1.293	1.241	1.180	1.113	1.050
27	1.306	1.252	1.190	1.121	1.053
28	1.307	1.254	1.192	1.121	1.052
29	1.304	1.251	1.189	1.119	1.050
30	1.300	1.247	1.185	1.115	1.046
31	1.294	1.241	1.179	1.109	1.041
32	1.286	1.234	1.172	1.103	1.035
33	1.278	1.226	1.165	1.095	1.029

34	1.269	1.217	1.156	1.087	1.022
35	1.260	1.208	1.147	1.079	1.014
36	1.250	1.198	1.138	1.069	1.007
37	1.240	1.188	1.128	1.060	.999
38	1.229	1.178	1.118	1.050	.994
39	1.219	1.168	1.108	1.041	.998
40	1.208	1.157	1.098	1.031	1.003
41	1.198	1.147	1.087	1.025	1.007
42	1.234	1.164	1.096	1.040	1.011
43	1.260	1.186	1.113	1.051	1.014
44	1.273	1.198	1.123	1.057	1.016
45	1.277	1.202	1.126	1.059	1.016
46	1.278	1.202	1.127	1.060	1.016
47	1.277	1.202	1.126	1.059	1.015
48	1.275	1.200	1.124	1.057	1.014
49	1.273	1.198	1.122	1.055	1.012
50	1.270	1.195	1.119	1.052	1.010
51	1.266	1.191	1.116	1.049	1.008
52	1.262	1.188	1.113	1.046	1.005
53	1.258	1.184	1.109	1.042	1.003
54	1.254	1.179	1.104	1.038	1.000
55	1.249	1.174	1.100	1.033	1.000
56	1.244	1.170	1.095	1.029	1.001
57	1.238	1.164	1.090	1.024	1.002
58	1.233	1.159	1.085	1.018	1.003
59	1.228	1.154	1.079	1.014	1.004
60	1.240	1.148	1.074	1.021	1.005
61	1.257	1.162	1.081	1.027	1.006
62	1.265	1.169	1.087	1.030	1.006
63	1.267	1.171	1.089	1.031	1.006
64	1.268	1.172	1.089	1.031	1.006
65	1.267	1.171	1.089	1.031	1.006
66	1.266	1.171	1.088	1.030	1.005
67	1.265	1.169	1.087	1.029	1.005
68	1.263	1.168	1.085	1.027	1.004
69	1.261	1.166	1.084	1.026	1.003
70	1.259	1.164	1.081	1.024	1.003
71	1.257	1.162	1.079	1.022	1.002
72	1.254	1.159	1.077	1.019	1.002
73	1.252	1.156	1.074	1.017	1.002
74	1.249	1.154	1.071	1.014	1.002
75	1.246	1.150	1.068	1.011	1.002
76	1.242	1.147	1.065	1.008	1.002
77	1.239	1.144	1.062	1.007	1.002
78	1.242	1.140	1.058	1.011	1.003
79	1.254	1.141	1.058	1.014	1.003
80	1.260	1.146	1.062	1.016	1.003
81	1.262	1.148	1.063	1.017	1.003
82	1.262	1.148	1.064	1.017	1.003
83	1.262	1.148	1.063	1.016	1.003
84	1.261	1.148	1.063	1.016	1.003
85	1.261	1.147	1.062	1.015	1.003
86	1.261	1.147	1.062	1.015	1.002
87	1.260	1.146	1.061	1.014	1.002
88	1.258	1.144	1.060	1.013	1.002
89	1.257	1.143	1.059	1.011	1.002
90	1.255	1.142	1.057	1.010	1.002
91	1.254	1.140	1.055	1.008	1.002
92	1.252	1.138	1.053	1.007	1.002
93	1.250	1.136	1.051	1.005	1.002
94	1.248	1.134	1.049	1.003	1.002
95	1.245	1.131	1.047	1.004	1.002
96	1.244	1.129	1.045	1.006	1.002
97	1.253	1.127	1.042	1.008	1.002
98	1.257	1.128	1.045	1.009	1.002
99	1.259	1.129	1.046	1.009	1.002
100	1.259	1.129	1.046	1.009	1.002
101	1.260	1.130	1.046	1.009	1.002
102	1.259	1.129	1.046	1.009	1.002
103	1.259	1.129	1.045	1.009	1.002
104	1.258	1.128	1.045	1.008	1.002
105	1.257	1.127	1.044	1.008	1.002
106	1.256	1.126	1.043	1.007	1.002
107	1.255	1.125	1.042	1.006	1.002
108	1.253	1.124	1.041	1.005	1.002
109	1.252	1.122	1.040	1.004	1.002
110	1.250	1.121	1.038	1.002	1.002
111	1.249	1.119	1.037	1.001	1.002
112	1.247	1.118	1.035	1.001	1.002
113	1.245	1.116	1.033	1.002	1.002
114	1.244	1.115	1.032	1.004	1.002
115	1.252	1.114	1.031	1.005	1.001

116	1.256	1.112	1.032	1.005	1.001
117	1.257	1.113	1.033	1.005	1.001
118	1.257	1.113	1.033	1.005	1.001
119	1.257	1.113	1.034	1.005	1.001
120	1.257	1.113	1.033	1.005	1.001
121	1.257	1.113	1.033	1.005	1.001
122	1.257	1.113	1.033	1.005	1.001
123	1.256	1.112	1.033	1.004	1.001
124	1.256	1.112	1.032	1.004	1.001
125	1.255	1.111	1.031	1.003	1.001
126	1.254	1.110	1.031	1.002	1.001
127	1.253	1.109	1.030	1.002	1.001
128	1.252	1.108	1.029	1.001	1.001
129	1.250	1.107	1.027	1.000	1.001
130	1.249	1.105	1.026	1.000	1.001
131	1.248	1.104	1.025	1.001	1.001
132	1.246	1.102	1.023	1.002	1.001
133	1.250	1.101	1.022	1.002	1.001
134	1.254	1.100	1.023	1.003	1.001
135	1.255	1.099	1.024	1.003	1.001
136	1.255	1.099	1.024	1.003	1.001
137	1.255	1.099	1.024	1.003	1.001
138	1.255	1.099	1.024	1.003	1.001
139	1.255	1.099	1.024	1.002	1.001
140	1.254	1.098	1.024	1.002	1.001
141	1.254	1.098	1.024	1.002	1.001
142	1.254	1.098	1.023	1.002	1.001
143	1.254	1.098	1.023	1.001	1.000
144	1.254	1.097	1.023	1.001	1.000
145	1.253	1.097	1.022	1.001	1.000
146	1.252	1.096	1.021	1.000	1.000
147	1.251	1.095	1.021	1.000	1.000
148	1.249	1.094	1.020	1.000	1.000
149	1.248	1.092	1.018	1.000	1.000
150	1.246	1.091	1.017	1.001	1.000
151	1.249	1.090	1.016	1.001	1.000
152	1.250	1.088	1.017	1.001	1.000
153	1.251	1.086	1.017	1.001	1.000
154	1.250	1.085	1.017	1.001	1.000
155	1.250	1.085	1.017	1.001	1.000
156	1.250	1.084	1.016	1.001	1.000
157	1.250	1.084	1.016	1.001	1.000
158	1.250	1.084	1.016	1.001	1.000
159	1.249	1.084	1.016	1.000	1.000
160	1.250	1.084	1.016	1.000	1.000
161	1.250	1.084	1.016	1.000	1.000
162	1.249	1.084	1.016	1.000	1.000
163	1.249	1.084	1.016	1.000	1.000
164	1.249	1.084	1.015	1.000	1.000
165	1.249	1.084	1.015	1.000	1.000
166	1.248	1.083	1.015	1.001	1.001
167	1.249	1.083	1.014	1.001	1.001
168	1.248	1.082	1.014	1.001	1.001
169	1.249	1.081	1.013	1.001	1.001
170	1.251	1.080	1.013	1.001	1.001
171	1.251	1.078	1.013	1.001	1.001
172	1.251	1.077	1.013	1.002	1.001
173	1.251	1.076	1.013	1.002	1.001
174	1.250	1.075	1.013	1.002	1.001
175	1.249	1.074	1.012	1.002	1.001
176	1.249	1.074	1.012	1.002	1.001
177	1.248	1.073	1.011	1.001	1.001
178	1.247	1.073	1.011	1.001	1.001
179	1.248	1.073	1.011	1.001	1.001
180	1.247	1.072	1.010	1.001	1.001
181	1.247	1.072	1.010	1.001	1.001
182	1.247	1.072	1.010	1.001	1.001
183	1.247	1.072	1.010	1.001	1.001
184	1.247	1.072	1.010	1.001	1.001
185	1.247	1.072	1.010	1.001	1.001
186	1.247	1.072	1.009	1.002	1.001
187	1.248	1.072	1.010	1.002	1.001
188	1.250	1.071	1.010	1.002	1.001
189	1.251	1.071	1.011	1.002	1.001
190	1.251	1.070	1.011	1.002	1.001
191	1.251	1.069	1.011	1.002	1.001
192	1.250	1.068	1.011	1.002	1.001
193	1.249	1.067	1.010	1.002	1.001
194	1.249	1.066	1.010	1.002	1.001
195	1.247	1.066	1.009	1.002	1.001
196	1.247	1.065	1.009	1.002	1.001
197	1.246	1.064	1.008	1.002	1.001

198	1.244	1.063	1.008	1.002	1.001
199	1.243	1.063	1.007	1.002	1.001
200	1.243	1.062	1.007	1.002	1.001

2.10.11 Impact Limiter Dynamic Verification Testing

This appendix provides a description of the scale model dynamic test program performed to demonstrate that the impact limiter design meets all the requirements for transportation. The validity of the force-deflection curves and the resultant deceleration and displacement responses developed in Appendix 2.10.9 have been confirmed by performing a series of static and dynamic tests using 1/4 scale models of the impact limiters. This appendix describes the dynamic test program and its results; Appendix 2.10.12 provides the details of the static test program. Test articles were constructed as exact 1/4 scale duplicates of the full size limiters shown in Appendix 1.3.2. The measured test data is compared to the predictions using the as-tested materials, and the methodology and analytical tools described in Appendix 2.10.9.

2.10.11.1 Test Objectives

The goals for the dynamic test program were to provide confirmatory support for the structural design analysis for the NUHOMS®-MP187. A series of dynamic and static tests were selected to demonstrate the design meets the performance based requirements of 10CFR71. Therefore, the dynamic test program objectives are:

A. Verify that the impact limiters are structurally adequate to survive the hypothetical accident drops of 30 feet onto an unyielding surface in critical orientations.

B. Provide crush depth data for use in validating the dynamic prediction methodologies in Appendix 2.10.9.

C. Verify that the impact limiter measured damage from 40 inch drops onto a scale puncture bar are less than the predicted damage used in the Chapter 3.0, Thermal Analysis. Also, that the impact limiter remains attached to the cask.

2.10.11.2 Test Acceptance Criteria

The tests will be acceptable if the following conditions are met:

A. No "bottom-out" of the impact limiter for the 30 ft. drop tests.

B. Impact limiters do not separate from the dummy cask model.

C. Limiter deformations and measured damage are consistent with the analytical predictions, upon which the structural analysis is based.

2.10.11.3 Test Configuration

2.10.11.3.1 1/4 Scale Impact limiters

As shown in Figure 2.10.11-1 thru Figure 2.10.11-4, the 1/4 scale model impact limiters duplicate the dimensions, fabrication details, and features of the full size limiter required for the top of the cask. Each block of honeycomb manufactured for the scale models was tested statically and dynamically. The dynamic tests were performed at an impact velocity of 44 fps and temperatures of -20°F, room temperature, and 200°F to ensure that the material complied with the design requirements of Note 2, Figure 2.10.11-4. Similarly, the foam material was poured and tested in accordance with the procedures used for the full size limiter to ensure compliance with the specified properties of Appendix 2.10.8.

The trunnion cutouts and asymmetric bolt pattern required for the bottom impact limiter are minor deviations from the top limiter and were not modeled. These cutouts are less than the thickness of the neutron shield and do not impinge on the minimum required crush depth. The omission of the cutouts therefore does not affect the conclusion that the test models accurately represent the full size impact limiter behavior. Also, the external surface is not painted as the affects of insolation are not a test parameter.

2.10.11.3.2 Simulated Cask

As shown in Figure 2.10.11-5 the external surfaces of the impact limiters were stripped with contrasting tape colors to assist in identify each limiter and measuring impact limiter displacements from the high speed film. The simulated "dummy" cask is fabricated from 22 inch diameter, 2 inch thick pipe, internally reinforced with welded steel plates and partially filled with tightly packed lead shot to ensure that the scaled size, weight and mass moment of inertia are correctly modeled from the full size package. The cask/limiter interface was carefully modeled to exactly model the welding details, torsion blocks, necked bolt detail and scaled bolt torques from the full size values.

THIS SECTION CONTAINS
PROPRIETARY INFORMATION

Figure 2.10.11-1

1/4 Scale Impact Limiter-Sheet 1

THIS SECTION CONTAINS
PROPRIETARY INFORMATION

Figure 2.10.11-2
1/4 Scale Impact Limiter-Sheet 2

THIS SECTION CONTAINS
PROPRIETARY INFORMATION

Figure 2.10.11-3
1/4 Scale Impact Limiter-Sheet 3

THIS SECTION CONTAINS
PROPRIETARY INFORMATION

Figure 2.10.11-4
1/4 Scale Honeycomb Block Construction

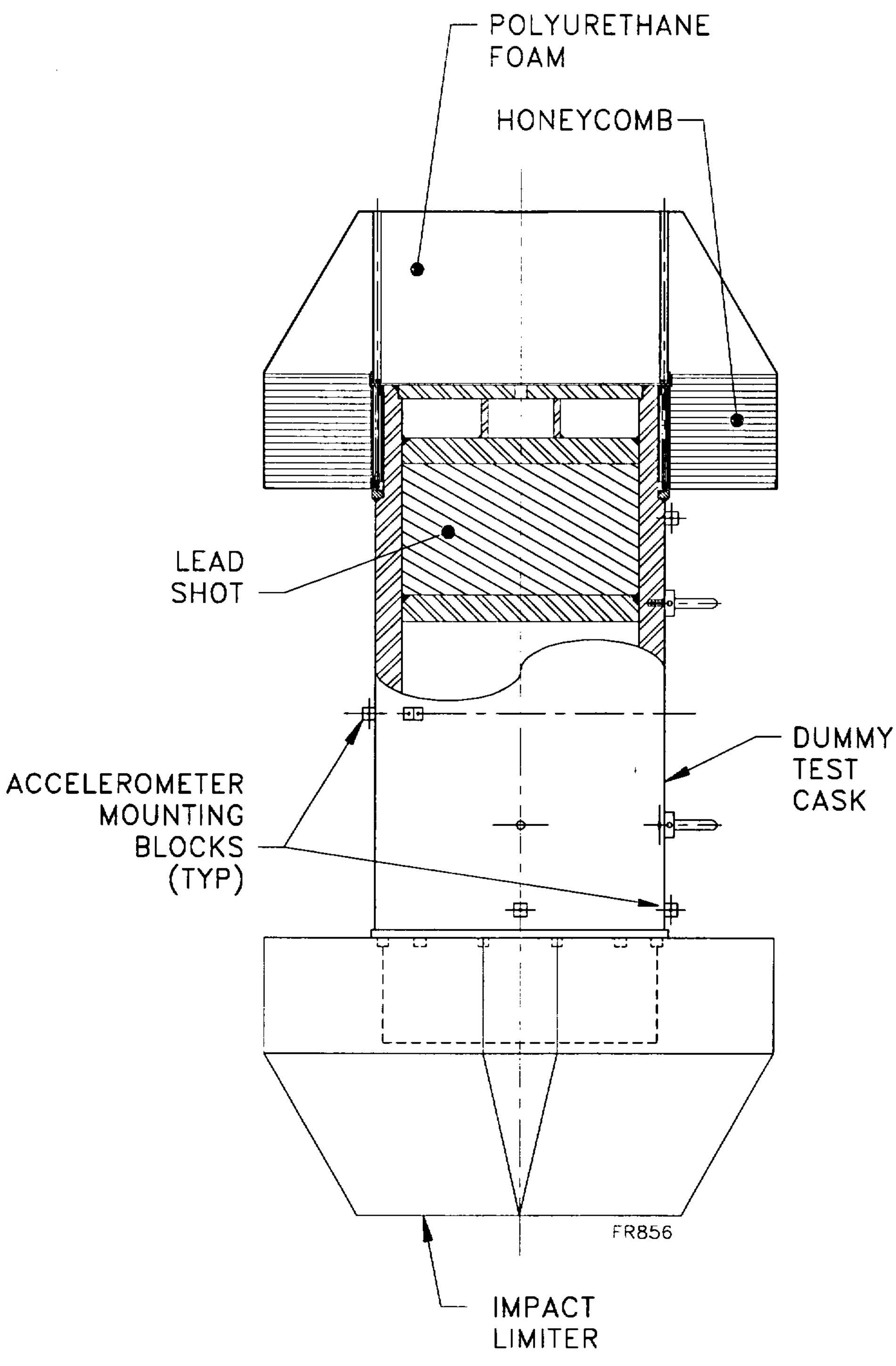

Figure 2.10.11-5

MP187 Test Package

2.10.11.3.3 Test Facility

The facilities for the test were provided by the Sacramento Municipal Utility District at the shut down Rancho Seco Nuclear Power Station. The unyielding target for the drop tests is an 80,000 lb., 3 foot thick reinforced concrete pad with a one inch steel plate grouted on the top surface to prevent spalling during drop testing. The mass of the 12 ft.-6 in. square pad is approximately twenty times that of the scale model package; this easily exceeds the IAEA Safety Series 37 [2.26] requirement for a factor of ten on the mass of the package for an unyielding surface. The test pad was serviced by the Rancho Seco 135 ton Turbine Building gantry crane. The 30 ton auxiliary hook, equipped with a remotely controlled quick release, was used to control the test article during the drop test program.

2.10.11.3.4 Installation of Impact Limiters

Impact limiters were installed onto the dummy cask so that flat faces are in the same plane and were seated to engage the torsion lugs located on the neutron shield top and bottom rings. The impact limiter attachment bolts were torqued to the specified quarter scale value for the first test. It was not possible to retorque the bolts following each test as distortion of the bolt tubes prevented access to the attachment bolts. The distortions in the tubes were small, and did not have a measurable affect on subsequent test results.

2.10.11.3.5 Accelerometers

The primary goal of the dynamic drop tests was to confirm that the analytical methodology of Appendix 2.10.9 conservatively predicts measured impact limiter displacements. The primary method of determining package deformations was the high speed film. As a backup to the film, and as direct confirmation of Appendix 2.10.9 methodology, eight accelerometers were mounted to the package to measure rigid body accelerations. As shown in Figure 2.10.11-6, the accelerometers were installed on the package at the cg and at each end adjacent to the impact limiters, close to the location of the "critical" spacer discs for the full scale package. Deltron Model 4395 isolated base accelerometers were used for the preoperational tests performed to demonstrate satisfactory behavior of the test equipment. These accelerometers proved to be fragile and were replaced with Model 4398 accelerometers for the certification tests. The accelerometers signals were processed through a DYTRAN Model 4121 current source and recorded on an HBM LABPLUS® system with a Sony 12 channel DAT recorder used as a backup in case the main DAS did not trigger or lost test data.

FIGURE WITHHELD UNDER 10 CFR 2.390

2.10.11.4 Certification Test Program

As described in Table 2.10.11-1, the certification tests included both static and dynamic tests performed at ambient temperature conditions. The dynamic test program is shown in Figure 2.10.11-7 and is described below. The static test program is described in Appendix 2.10.12. The dynamic test matrix was developed using two 1/4 scale prototypical impact limiters, in multiple uses, in different drop orientations. The test sequence was as follows:

1. A 30 foot drop with the cask axis inclined at 30° to the horizontal and the 90° azimuth at the top. Primary impact was on the large flat facet at 270° azimuth on impact limiter "a" with a secondary impact (slapdown) onto impact limiter "b".

2. A 30 foot drop with the cask cg over corner and the cask axis inclined at 72° to the horizontal and rotated in plan so that impact will occur on a diagonal corner of impact limiter "a".

In addition to the two 30 foot drop tests the impact limiter quarter scale models were subjected to a side puncture (limiter "b") and an end puncture (limiter "a") event (40 inch end drop onto a 1.5 inch diameter pin) to establish the behavior of the honeycomb and foam materials and the integrity of the impact limiter. These two tests were performed using the same impact limiter models as tests 1 and 2. The exact impact points for the puncture tests were chosen to maximize the potential impact limiter damage.

2.10.11.5 Photometric Equipment

High speed cameras provided 400 and 2,000 frames per second coverage during all four dynamic tests. As shown in Figure 2.10.11-6, the cameras were placed parallel and perpendicular to the cask impact zone to provide optimum viewing for measurement of the dynamic deformation in the impact limiters. Photometric coverage also included real-time color video and still shots. Painted backboards 12 ft.-0 in. wide by 8 ft.-0 in. high, with a 12 inch lined grid, were placed behind the drop pad to provide a contrasting background to assist in measurement of the dynamic deformation of the limiters from the film. Following film processing the total impact limiter deformations were determined using a film comparitor with the capability of resolving displacements to a 1/10th of an inch.

Table 2.10.11-1

NUHOMS®-MP187 Impact Limiter Certification Test Matrix

Section	Orientation	Certification Tests	
	Degrees from	Static Crush Test	Dynamic Drop Test
Definition	Horizontal	2 Prototype Limiters c & d (test #, limiter #)	2 Prototype Limiters a & b (test #, limiter #)
Thru	0 (side)	(5,c)	
Flats	30 (large facet)	(7,d)	(1,a)
Thru	30 (corner facet)	(8,d)	
Diagonal	0 (side)	(6,c)	
Special Cases			
a) Slapdown	Thru Flats		(1,b)
b) cg Over Corner	72° thru diagonal	(9,d)[2]	(2,a)
c) Puncture	45 thru flats		(3,b)
	90 (end)		(4,a)

Notes:

1 The above table describes nine separate certification tests to be performed on a total of four (a-d) impact limiters. For example test No. 7,d is a static test, with the test load oriented perpendicular to the large facet, using limiter "d".

2 Test 9,d was performed with the limiter oriented at 60° to the horizontal through the diagonal.

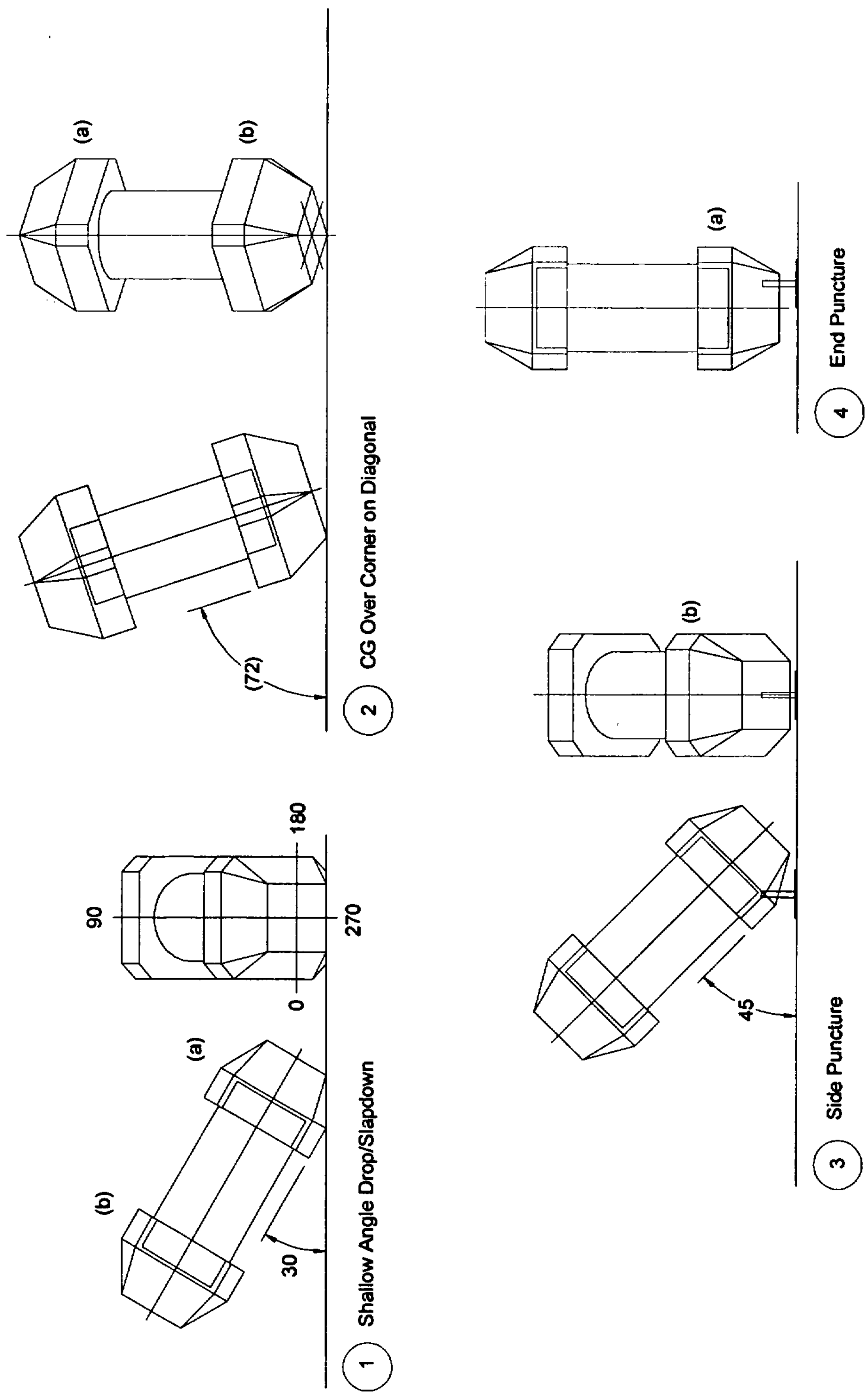

Figure 2.10.11-7

Impact Limiter Test Series - Certification Tests

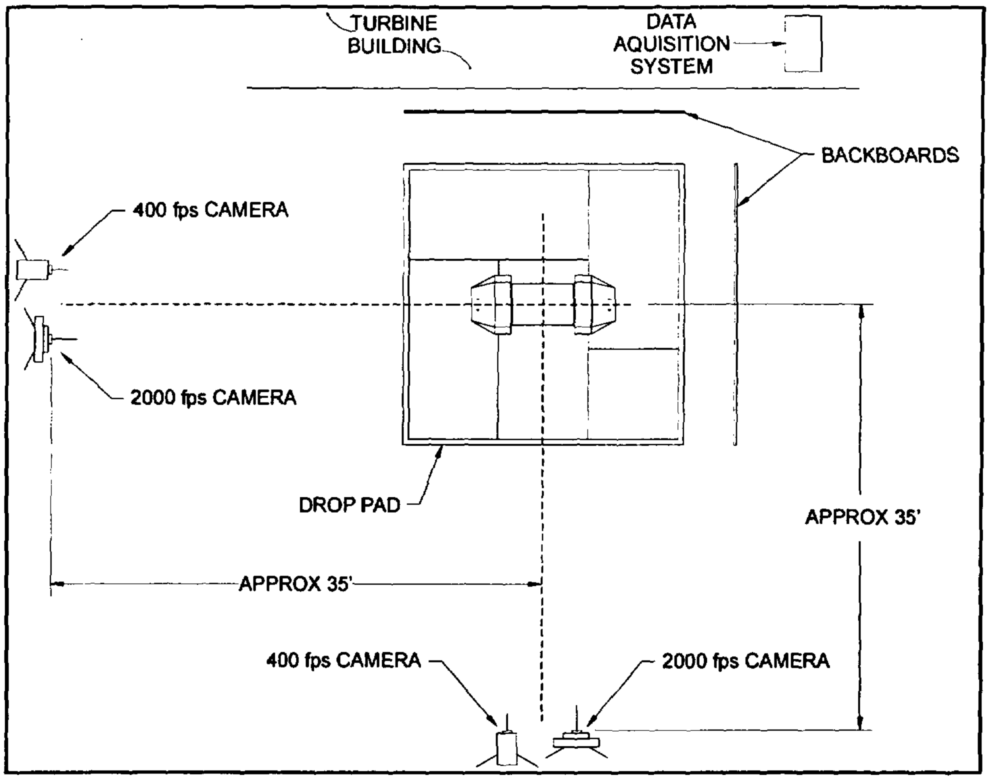

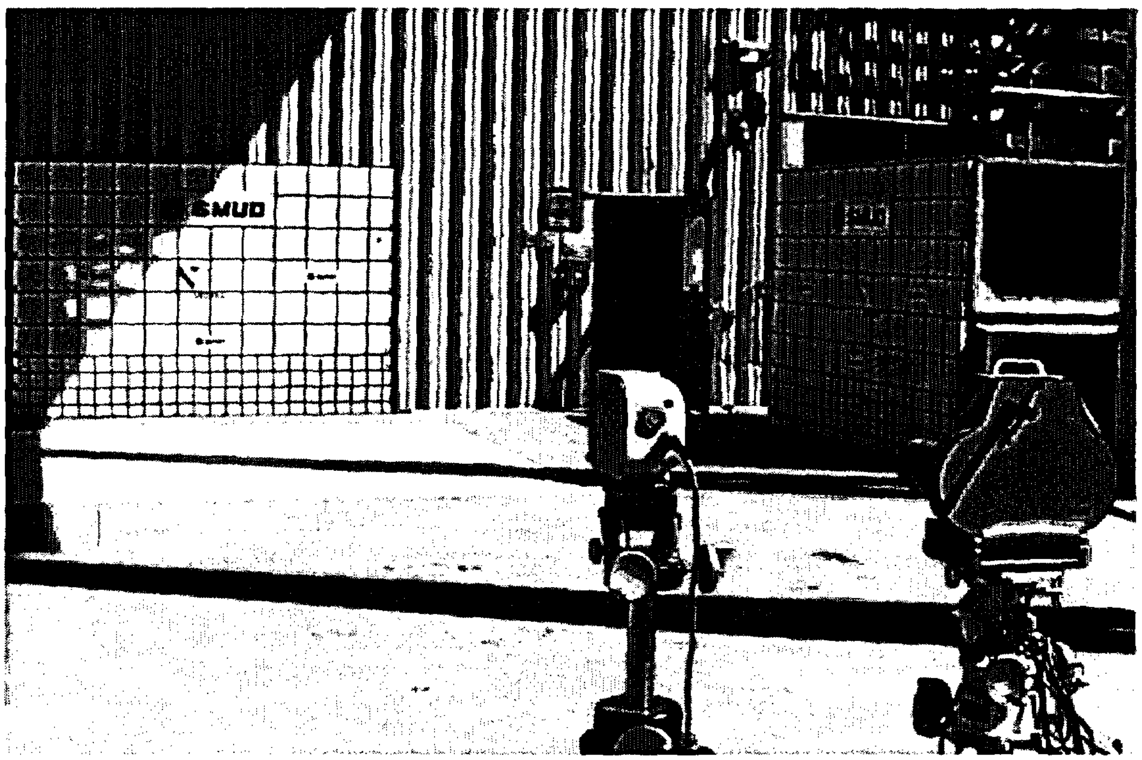

Figure 2.10.11-8

Camera Placement

2.10.11.6 Test Preparation

The overall certification test requirements are summarized in Table 2.10.11-2. Steps defined for Test Article Configuration and Pretest Observations precede the drop tests. Each test commenced with a check off of the test article configuration, followed by the pretest observation requirements, discussed below:

(A) Test Article Configuration Verification Procedures:

1. Prior to the first certification test, the 1/4 scale model impact limiters were striped on their exterior surfaces with a set of coordinate axes in the vertical and horizontal directions. Contrasting colors were used on each end (a = red, b = blue) to provide positive identification of each limiter from the test photography records.

2. Obtain pre-drop measurements of the impact limiters.

3. Install the impact limiters on the dummy cask. Verify that the impact limiters are properly installed and bolts torqued.

(B) Pretest Observation Procedures:

1. All impact limiter surfaces were visually inspected for cracks, gouges, dents or other damage.

2. Document the test set up and package with photographic records.

Table 2.10.11-2

Test Matrix for Dynamic Tests

	Slapdown Test 1	End Corner Drop Test 2	Side Puncture Test 3	End Puncture Test 4
TEST CONFIGURATION				
Impact Orientation				
- Impact Surface Azimuth	270°	135°	90°	N/A
- Angle (w/respect to horizontal)	30°±1°	72°±1°	45°±1°	90°±1°
Drop Height	30' +3" -0"	30' +3" -0"	40" +2" -0"	40" +2" -0"
PRETEST STEPS				
Torque Impact Limiter Bolts (if possible)	Yes	Yes	No	No
Dimensional Survey	Yes	Yes	Yes	Yes
Instrument Locations	Yes	Yes	Yes	Yes
DROP STEPS				
Visual Check	Yes	Yes	Yes	Yes
Instrumentation Check	Yes	Yes	Yes	Yes
Height & Orientation Check	Yes	Yes	Yes	Yes
Punch Pin Location Check	No	No	Yes	Yes
Drop	Yes	Yes	Yes	Yes
Document & Record	Yes	Yes	Yes	Yes
POST TEST STEPS				
Dimensional Survey of Damage	Yes	Yes	Yes	Yes
100% Visual Inspection	Yes	Yes	Yes	Yes
Remove Impact Limiters	No	No	No	Yes
Are Limiters Acceptable for Next Drop	Yes/No?	Yes/No?	Yes/No?	N/A

(C) Drop Test:

Before proceeding from one test to the next in the series, the impact limiters were visually inspected for damage that might invalidate subsequent test results.

All free drops were conducted at a height of 30 ft. +3 in./-0 in., measured from the unyielding impact surface (drop pad) to the lowest point of the suspended package. All puncture events were conducted at a height of 40 in. +2 in./-0 in., measured from the point of impact on the package to the top of the puncture spike.

With the test package suspended from the crane in the correct drop configuration, the package was free-dropped onto the target. The drop release was accomplished using a quick acting device. The drop test configurations are as follows:

Oblique Drop - TEST 1

Prior to the drop, the package was oriented with the cask axis at 30° to horizontal, centered above the drop pad. (See Figure 2.10.11-7, Test 1.)

C.G. Over Corner Drop - TEST 2

The package was oriented with the cask axis at an inclined angle, of 72° to horizontal, with a diagonal corner of the impact limiter centered above the drop pad, prior to drop. (See Figure 2.10.11-7, Test 2.)

Side Puncture Event - TEST 3

The package was oriented at 45° to the vertical on limiter "b", with the punch located as shown in Figure 2.10.11-7, Test 3. The quarter-scale, cylindrical puncture spike was mild steel, with a diameter of 1.50 in. +0/-0.01 in., a top edge radius of .06 in. +0/-0.008 in., and a projected length of 16.0 inches, or 28.0 inches above the surface of the drop pad.

End Puncture Event - TEST 4

The end puncture event was performed on impact limiter "a" as shown in Figure 2.10.11-7, Test 4. The quarter-scale, cylindrical puncture spike is similar to that described for test 3.

(D) Post Test Observations and Measurements:

1. All accessible impact limiter surfaces were visually inspected for cracks, gouges, dents, or other damage.

2. A visual inspection of the impact limiters documented with photographic records. All regions exhibiting damage deformation were identified and carefully characterized.

3. Impact limiter deformations for each drop event were documented by photographic means. Following the completion of the certification test program, both impact limiters were sectioned and the cross-sections documented by photographic means.

4. High-speed film records of each drop event were evaluated, using a film comparator to determine the total impact limiter displacements during impact.

5. Recorded time histories were reviewed for each accelerometer to determine that package accelerations were within the anticipated range. Exceeding predicted peak accelerations was a warning to review data before continuing with the test program. However, high peak g-levels were not used to stop the program provided the measured displacements were in the expected range.

6. A detailed record of the impact limiter external shape was established prior to, and after each test.

2.10.11.7 Comparison of Analytical and Test Results

As-manufactured material properties established by static and dynamic tests of the test materials at test temperature were used, in conjunction with the methodologies of Appendix 2.10.9, to develop predictions for the certification test impact decelerations and displacements.

2.10.11.7.1 30 Foot Drop Tests

As described in Appendix 2.10.9 the analytical predictions of the rigid body response were developed for the 1/4 scale test article using the analysis code SLAPDOWN; developed by Sandia National Laboratories. The predictions were compared to the measured response at each accelerometer location to demonstrate the performance of the impact limiters and benchmark the programs described in Appendix 2.10.9. The peak accelerations are taken directly from the measured acceleration time histories presented in Figure 2.10.11-9 thru Figure 2.10.11-20. These figures show the measured data with the data filtered at 500 Hz. There is very little difference in the peak g-levels for measured or 500 Hz filtered data. The predicted and measured values for peak accelerations and displacements are documented in Table 2.10.11-3. The displacement measurements were developed from a frame by frame review of each of the four high speed cameras used to record the event. Displacements and angular rotations were measured using a film comparator with a resolution of .1 inch.

Table 2.10.11-3

Comparison of Measured and Predicted Data for 30 Foot Drop

		Displacement (inches)		Peak Accelerations (g)[4]			
				Measured		Predicted	
		Measured	Predicted	Longitudinal	Transverse	Longitudinal	Transverse
TEST 1 (30° Oblique Drop)	Primary	2.4	2.4	66 (PT. 1)[1]	185 (PT 2)[1]	57	187
				63 (PT 4)[2]	90 (PT 5)[2]		
	Secondary	2.5	2.6	29 (PT 6)[1]	335/(210) (PT 7)[1,3]	18	203
				23 (PT 4)[2]	225/(141) (PT 5)[2,3]		
TEST 2	C.G Over Corner Drop	7.1	6.6	110 (PT 1)[1]	52 (PT 2)[1]	110	40
				110 (PT 4)[2]	30 (PT 5)[2]		

Note:

1. Measured accelerometer g loads at the locations adjacent to impact limiters
2. Measured accelerometer g loads at the C.G.
3. Measured g loads from the flat side slapdown are amplified by dynamic "ringing" in the cask 1/4 scale model, the rigid body response g loads, shown in (#), are obtained by dividing the measured g loads by the dynamic load factors (DLF = 1.6) as described in Appendix 2.10.9.
4. Predicted loads are developed for C.G. of package. Comparision of measured vs. predicted must be at C.G. location. Higher g loads at the locations adjacent to the impact limiters are due to package rotation in the impact event.

THIS SECTION CONTAINS
PROPRIETARY INFORMATION

Figure 2.10.11-9

30°, Primary Impact Acceleration History - Point 1

THIS SECTION CONTAINS
PROPRIETARY INFORMATION

Figure 2.10.11-10

30°, Primary Impact Acceleration History - Point 2

THIS SECTION CONTAINS
PROPRIETARY INFORMATION

Figure 2.10.11-11
30° , Primary Impact Acceleration History - Point 4

THIS SECTION CONTAINS
PROPRIETARY INFORMATION

Figure 2.10.11-11a
30° , Secondary Impact Acceleration History - Point 4

THIS SECTION CONTAINS
PROPRIETARY INFORMATION

Figure 2.10.11-12
30°, Primary Impact Acceleration History - Point 5

THIS SECTION CONTAINS
PROPRIETARY INFORMATION

Figure 2.10.11-13
30°, Secondary impact Acceleration History - Point 5

THIS SECTION CONTAINS
PROPRIETARY INFORMATION

Figure 2.10.11-14
30°, Primary Impact Acceleration History - Point 6

THIS SECTION CONTAINS
PROPRIETARY INFORMATION

Figure 2.10.11-14a
30°, Secondary Impact Acceleration History - Point 6

THIS SECTION CONTAINS
PROPRIETARY INFORMATION

Figure 2.10.11-15
30°, Secondary Impact Acceleration History - Point 7

THIS SECTION CONTAINS
PROPRIETARY INFORMATION

Figure 2.10.11-16
72° Drop Acceleration History - Point 1

THIS SECTION CONTAINS
PROPRIETARY INFORMATION

Figure 2.10.11-17
72° Drop Acceleration History - Point 2

THIS SECTION CONTAINS
PROPRIETARY INFORMATION

Figure 2.10.11-18
72° Drop Acceleration History - Point 4

THIS SECTION CONTAINS
PROPRIETARY INFORMATION

Figure 2.10.11-19
72° Drop Acceleration History - Point 5

THIS SECTION CONTAINS
PROPRIETARY INFORMATION

Figure 2.10.11-20
72° Drop Acceleration History - Point 6

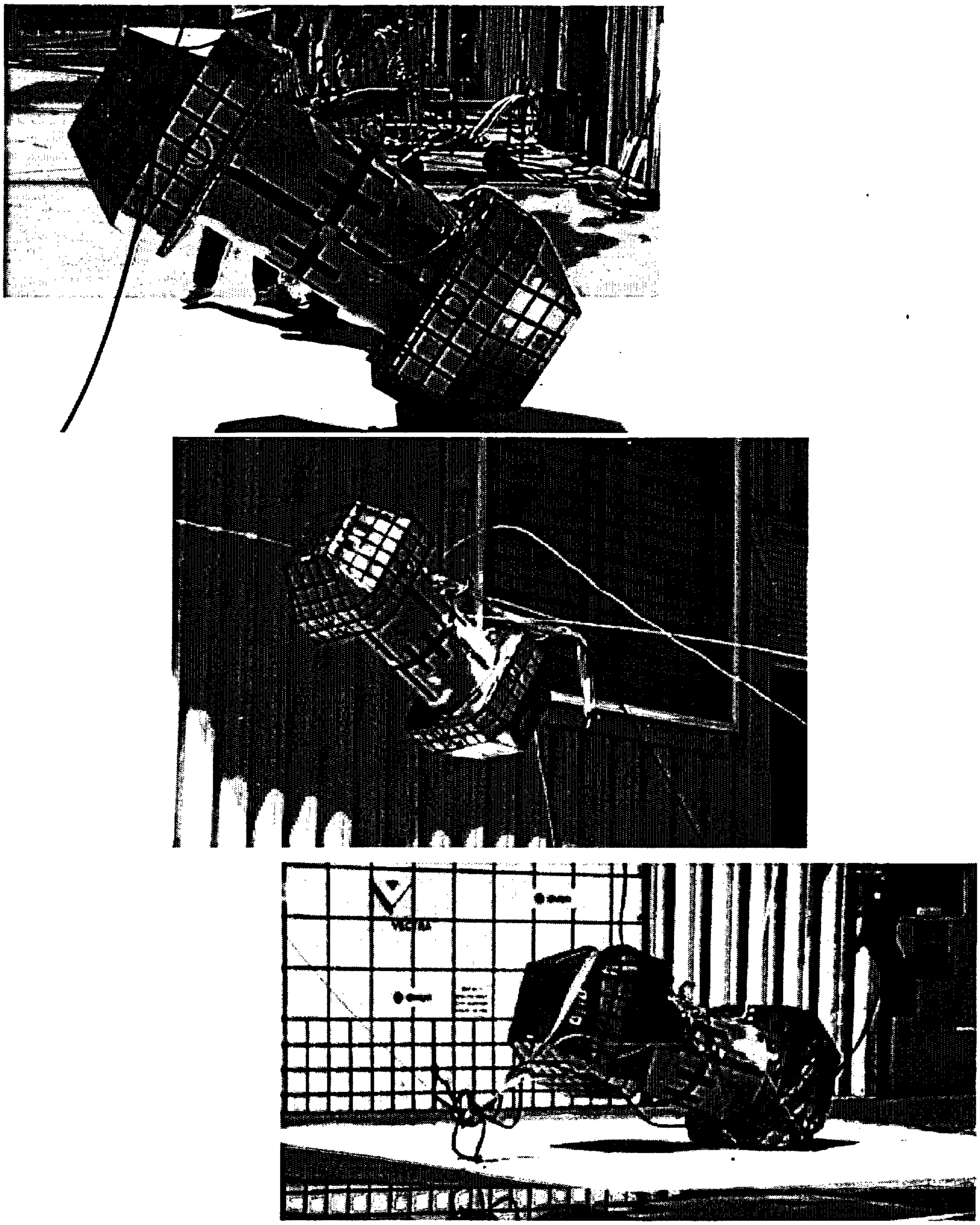

Figure 2.10.11-21

Test 1: Set Up And Drop Sequence

Figure 2.10.11-22

Test 2: Setup And Drop Sequence

Test 1 is shown in Figure 2.10.11-21. Shortly after the cable was released the lifting slings wrapped around the remote release cable which is used for the quick disconnect. The affect of this was to slightly alter the angle of the test article so that impact occurred at 32° to the horizontal compared to the preset 30°. This minor deviation in angle has no effect on the predictions for displacement and acceleration. The longitudinal and tangential measured acceleration time histories from Test 1 are provided in Figure 2.10.11-9 thru Figure 2.10.11-16 and are reported in Table 2.10.11-3.

Test 2 is shown in Figure 2.10.11-22. Photographs are provided for the pretest setup, initial impact and the rebound. The cask rebound rotated the cask 360° with the secondary impact on the same limiter as the initial impact. The measured longitudinal and tangential acceleration time histories for Test 2 are provided in Figure 2.10.11-16 through Figure 2.10.11-20.

2.10.11.7.2 Preoperational Tests

Prior to performing the certification test program a series of five preoperational drop tests were performed, using two 1/4 scale models to demonstrate that the equipment and DAS were working correctly. The preoperational test models were identical to the certification limiters with the exception of the honeycomb material. For the preoperational tests the honeycomb was replaced with foam of similar density and crush strength; all other details were identical. The preoperational drops conducted with these limiters were:

Test 1: 30 ft.-0 in. drop with cask axis at 30° to horizontal, impact onto small diagonal facet with slapdown onto opposite limiter;

Test 2: 30 ft.-0 in. drop with cask axis at 30° to horizontal, impact onto large flat facet with slapdown onto opposite limiter;

Test 3: 30 ft.-0 in. flat side drop with impact on large flat sides;

Test 4: 30 ft.-0 in. vertical drop;

Test 5: 30 ft.-0 in. flat side drop with impact onto diagonal corners of the limiters to impart the maximum rotational energy to the test article.

The preoperational tests clearly demonstrated that the impact limiter attachment bolts, and cask attachments, were robust and capable of sustaining the design basis drop loads and keep the limiters securely attached to the cask for multiple design basis drops.

2.10.11.7.3 Simulated Cask

Table 2.10.11-3 shows excellent agreement between the predicted data and the test results with the exception of the flat side slapdown accelerations from Test 1. The peak rigid body acceleration predicted at the slapdown end of the package was approximately 60% of the measured peak response. This discrepancy is due to the behavior of the dummy cask.

Examination of both the preoperational and certification acceleration test data showed a ringing signature at approx. 350 Hz for the flat side slapdown drop. This is significant as the one constant between the preoperational and certification tests is the dummy cask. This response indicated that the test article included a significant non rigid body response. The apparent ringing frequency is lower than analytically predicted and, is probably due to the interaction between the lead shot, steel pipe and stiffener plates that had not been included in the simplified analytical model. Two additional drops of the dummy cask without impact limiters (Figure 2.10.11-23) were conducted to determine the natural response of the bare cask. The cask was instrumented the same as the certification tests and dropped from heights of 12 and 40 inches. These drops both measured a natural frequency at the same frequency as the ringing tone (approximately 350 Hz). Additional analyses were conducted to include the response of the dummy cask and define the rigid body response.

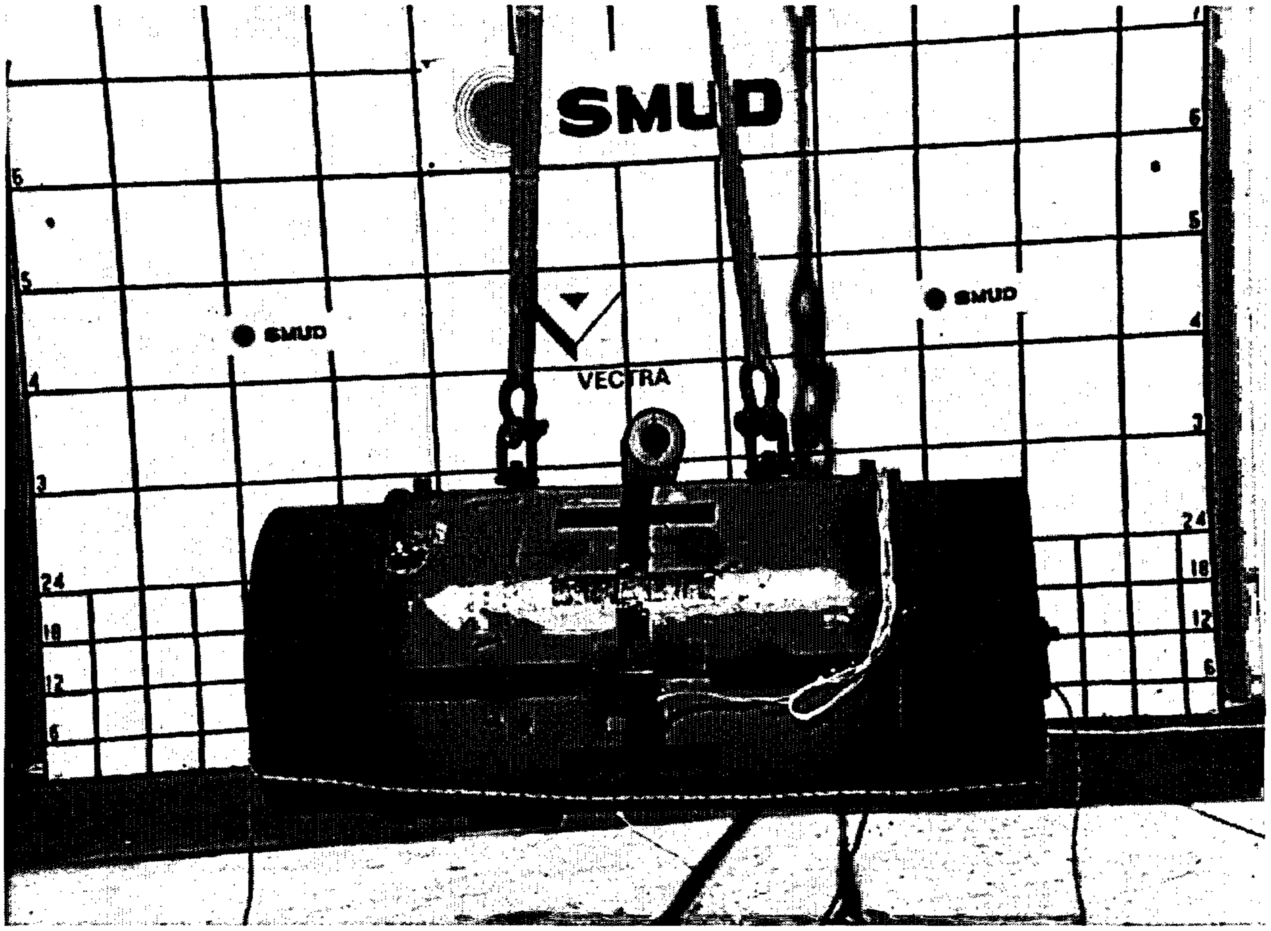

Figure 2.10.11-23
Set Up for Bare Cask Drop

Using the methods described in Appendix 2.10.9 the Dynamic Load Factor (DLF) was determined for a range of frequencies for a damping ratio of 6%. The damping ratio was calculated as the logarithmic decrement from the filtered drop acceleration time histories. The predicted rigid body response for the flat side slapdown drop was used as the forcing function for the DLF calculation. This analysis produced a predicted DLF of 1.6.

Applying the calculated DLF of 1.6 to the measured peak accelerations produces the rigid body response reported in Table 2.10.11-3. This clearly demonstrates that the difference between the peak rigid body response and the peak measured response is attributable to the dynamic amplification from the dummy test cask.

2.10.11.7.4 Puncture Pin Test Results

As shown in the photographic sequence of Figure 2.10.11-24, the 45° drop puncture spike cleanly punched through the stainless steel impact limiter shell and foam until it impacted the reinforcing ring at the inner shell. The internal reinforcing ring deflected the pin to follow the inner cylindrical shell; no puncture of the inner shell occurred and the pin was stopped 1.5 in. short of the cask attachment ring by a highly compacted wedge of honeycomb. The total penetration into the limiter was approximately 11.5 inches. With the vertical motion of the test article stopped by the limiter, the package toppled, and bent the pin through a 45° angle without tearing any of the material from the limiter. After the opposite (red) limiter contacted the ground, the test article rolled sideways and the pin was then bent approximately 90° to the initial bend without any evidence of any material tearing from the limiter. Internal damage to the limiter is restricted to the broken foam and crushed honeycomb material at the entry point. The maximum gap is 3 in. at the foam/honeycomb interface where the initial 45° rotation of the pin occurred; there were no other damaged areas which have any impact on the integrity of the limiter.

For Test 4, the test article was vertical and the puncture pin penetrated 13.0 inches to the inner steel shell while being deflected sideways approximately 4 inches to impact on the reinforcing ring at the outer edge of the inner shell. Figure 2.10.11-25, and the slow motion film shows that the test article stops with the pin completely embedded in the limiter and then slowly topples, bending the puncture pin at approximately 60°. After the test article has rotated about 60° the bottom edge of the impaled limiter contacted the test stand, the impact point on the bottom of the limiter was raised vertically, and the pin pulled up and out of the stand. Damage to the limiter was confined to the puncture entry point and the slightly curved path taken to the impact point on the inner shell. The stainless steel outer shell and foam had sufficient strength to totally restrain the pin and bend it through 60° plus extract it from the test stand.

The puncture pin tests clearly demonstrated that the limiter design is inherently very tough, and resistant to significant sections being removed during a puncture type event.

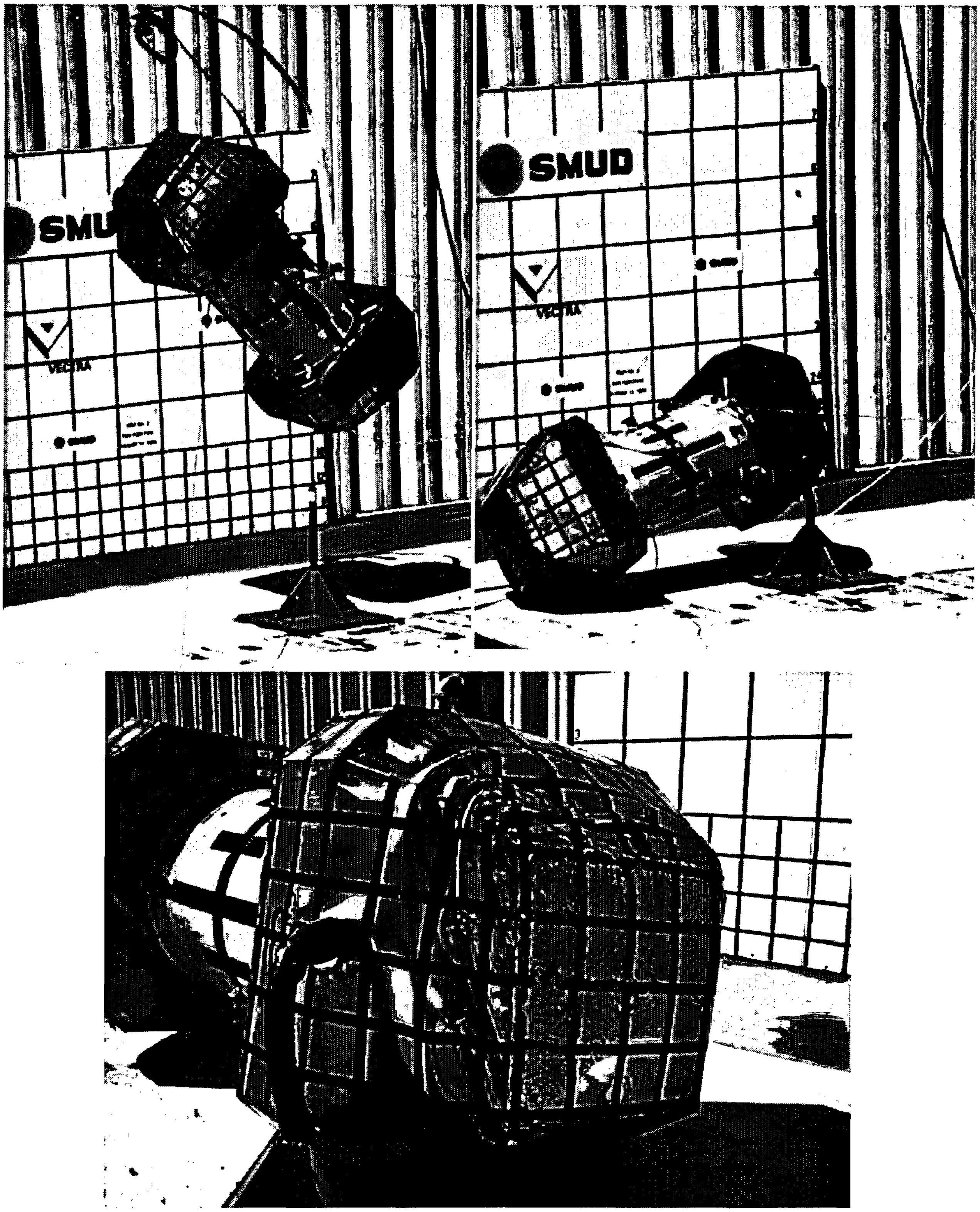

Figure 2.10.11-24

Test 3: 45° Puncture Pin Drop

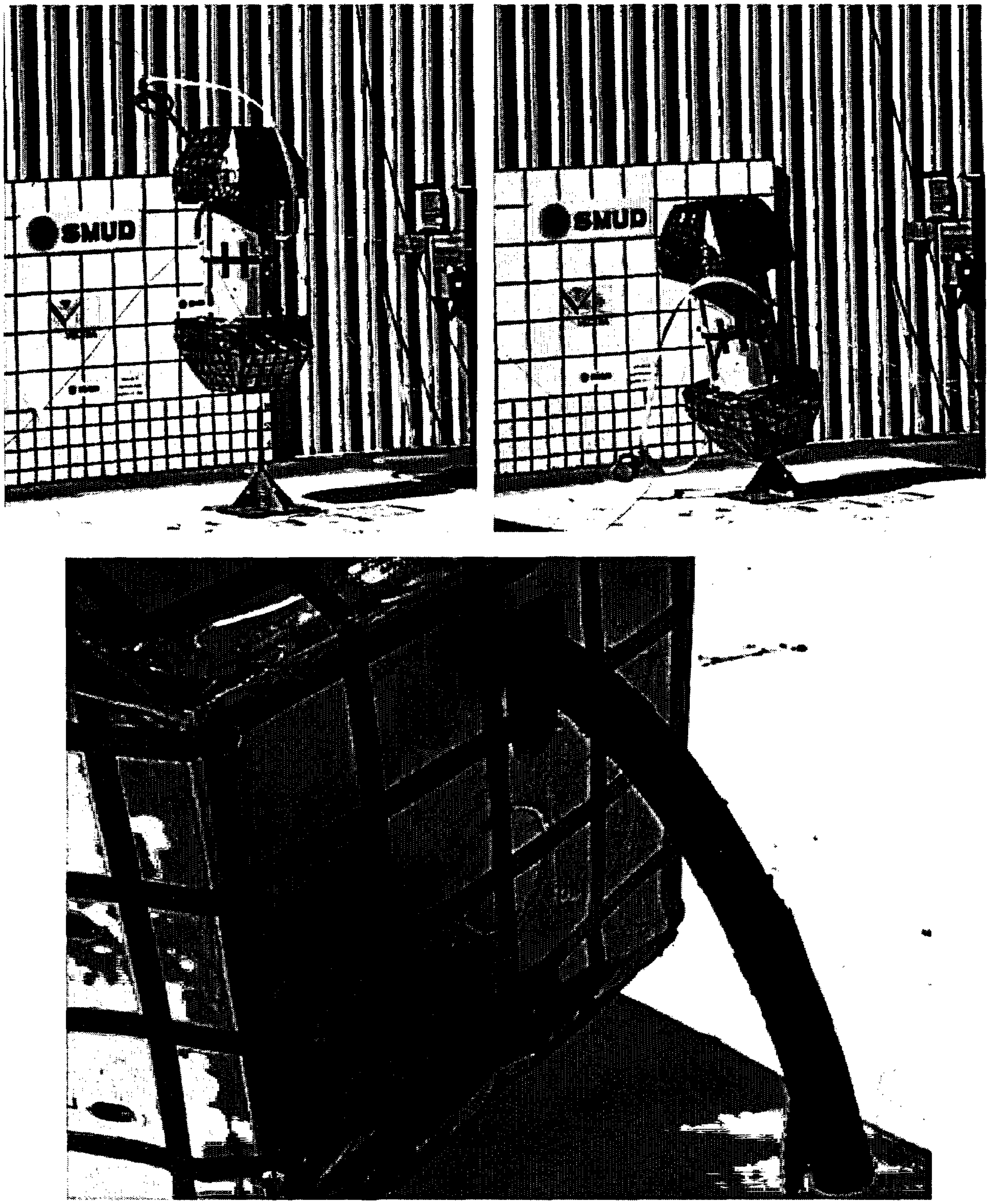

Figure 2.10.11-25

Test 4: Vertical Puncture Pin Drop

2.10.11.7.5 Conclusions

The dynamic test program has demonstrated that the methodology presented in Appendix 2.10.9 accurately predicts the impact limiter and package behavior. The measured displacements and accelerations exhibited excellent agreement with the analytical predictions with no bottoming out of the system. It also clearly demonstrated that the impact limiter attachments would take a multiple series of drops and preserve their integrity. The impact limiter design presented in Section 1.3.2 will safely protect the NUHOMS®-MP187 Cask and contents for all hypothetical drop accident conditions while limiting accelerations and displacements to within the design basis limits.

2.10.12 Impact Limiter Static Verification Testing

As discussed in Appendix 2.10.9 the validity of the analytically derived force-deflection curves has been confirmed by a series of static and dynamic tests. Appendix 2.10.8 describes the bench testing and scale models used to determine the basic material properties; Appendix 2.10.11 describes the dynamic test program; and this appendix provides the details for the static test verification program. The measured static test data are presented in the form of force-deflection curves for each of the five critical orientations. These curves are compared to analytical predictions using as-tested material properties, configurations and the methodology and analytical tools described in Appendix 2.10.9. The static tests were performed at the U.C. Berkeley, Structural Research Laboratory using the 4,000,000 lb. Universal Testing Machine (UTM).

2.10.12.1 Test Objectives

The objective for the static test program was to verify the analytically predicted static force-deflection curves developed for the impact limiters in Appendix 2.10.9. The five orientations selected, discussed in Section 2.10.12.4, match the Appendix 2.10.9 analytical cases which provide the design basis loadings for the package.

2.10.12.2 Test Acceptance Criteria

A. Measured impact limiter force-deflection curves consistent with predicted values.

B. Impact limiter does not separate from the test fixture and seams remain intact.

2.10.12.3 Test Configuration

As described in Appendix 2.10.11 the ¼ scale model impact limiters utilized for the static and dynamic test programs duplicated the dimensions, fabrication details, and features of the full size limiter required for the top of the cask. The trunnion cutouts and asymmetric bolt pattern required for the bottom impact limiter are minor deviations from the top limiter and were not modeled. Also, the external surface is not painted as the affects of insolation are not a test parameter. The impact limiter is mounted to a static test fixture and positioned in the universal test machine.

The static test fixture is a rigid frame, fabricated from pipe, plate, and rolled steel sections to ensure that it provides a rigid test platform simulating the end of the package. The fixture/limiter interface was modeled to include the torsion blocks, necked bolt detail and scaled bolt torques from the full size values.

Prior to each test, the impact limiter attachment bolts are torqued down. The bolt torques are measured and visual imspections are made to confirm that the impact limiter is seated correctly and engaged with the torsion lugs located on the test fixture mandrel.

2.10.12.4 Certification Test Program

As described in Table 2.10.11-1, the certification tests included both static and dynamic tests performed at ambient temperature conditions. The static test program is shown and described below. The static test program was developed using two ¼ scale model impact limiters for multiple tests in different loading orientations. The total crush deflections imposed for each test were larger than the maximum predicted deflection expected to occur under the bounding loading conditions. The static tests are numbered sequentially from test 5 to 9 and follow the dynamic tests (Tests 1 through 4, Appendix 2.10.11). Details of the test program, starting at Test Number 5 are:

5. A static test with the load applied to the 45° azimuth flat surface of the honeycomb portion of the limiter.

6. A static test, on the same impact limiter, with the load applied to the 180° azimuth large flat honeycomb facet.

7. Starting with a new impact limiter the static load was applied at 30° to the cask longitudinal axis to the 180° azimuth large flat side of the limiter.

8. A static load was applied at 30° to the cask longitudinal axis. through the 40° azimuth small corner facet.

9. A third static test was performed on the second impact limiter. For this test the load was applied at 60° to the cask longitudinal axis to the 325° azimuth diagonal corner of the impact limiter.

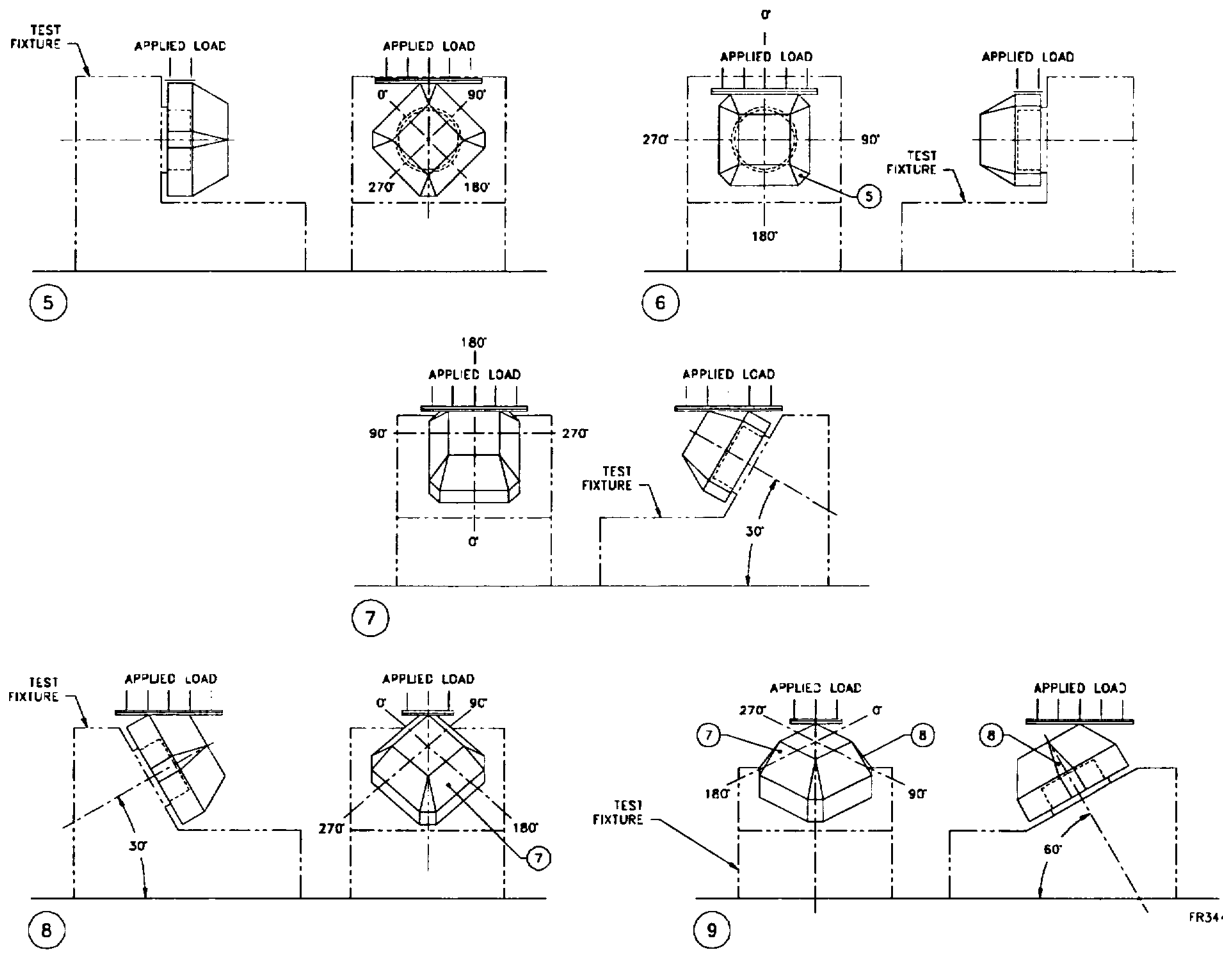

Figure 2.10.12-1

Impact Limiter Test Series - Certification Tests

2.10.12.5 Instrumentation and Data Acquisition

The instrumentation used for these tests consisted of displacement and load transducers. The deflection of the specimen was measured with two wire potentiometers (wirepots), one on each side of the special loading plates installed under the UTM head. The average of these two measurements was used to characterize the deflection corresponding to the applied load. Another displacement transducer was used to measure the deflection of the lower part of the impact limiter. In addition, the displacement of the UTM head (stroke), measured via an internal transducer, was also recorded for data verification purposes. The applied load was measured by a pressure transducer installed inside the control panel of the UTM. All instruments were calibrated prior to the testing program. Table 2.10.12-1 summarizes the instrumentation used.

The data acquisition consisted of a Metrabyte DAS 1601 card installed in a 50-Mhz 486 PC running under the QNX operating system. A specialized program was generated using the Automet Command Language to control the data acquisition and data logging processes. All data channels were scanned 10 times per second, converted to engineering units, and logged to disk. The following information was recorded in internal binary format (LDF) after each data scan: Date & Time Stamp, Test Number, PC Clock, Load, Avg Top Displacement = (Displacemnt #1(Disp1) + Displacement #2(Disp2))/2.0, Stroke, Disp1, Disp2, Disp3, and the Raw Channel Data in Volts.

Data in engineering units was computed as EU = (Cal. Fact. * Volts) - Offset, where the offsets were input manually before each test to achieve zero initial displacements.

Table 2.10.12-1

Instrumentation List

Channel Number	Channel ID	Engineering Units	Instrument Type	Calibration Factor[1]	Measurement Description
1	Disp1	in	Wirepot	-0.998	Top Displ.
2	Disp2	in	Wirepot	-0.999	Top Displ.
3[2]	Disp3	in	LVDT	+0.020	Bottom Displ.
3[2]	Disp3	in	Wirepot	-0.020	Bottom Displ.
5	Stroke	in	Temposonic	3.000	Head Stroke
16	Load	kip	Pressure Xdr	-399.44	Applied Load

[1] The calibration factor is used to convert the instrument output in Volts into the appropriate engineering units.

[2] A 0.4 inch LVDT was used to measure bottom displacement during test (5). Due to its limited range, it was replaced by a wirepot with a 4.0 inch range for all subsequent tests (6) through (9).

2.10.12.6 Test Procedure

The overall test requirements are summarized in Table 2.10.12-2. The tests were conducted in the sequence indicated in Section 2.10.12.4. Steps defined for Test Article Configuration and Pretest Observations preceding each test are described in the following sections. Each test commenced with a check off of the test article configuration requirements.

2.10.12.6.1 Test Article Configuration:

A. Obtain as-built measurements of the impact limiters to show they meet drawing requirements; document any variance from design drawings.

B. Install the impact limiters on the static test fixture madrel. Verify that the impact limiters are properly installed and bolts torqued.

Table 2.10.12-2

Static Test Matrix

	0° Small Facet (5)	0° Large Facet (6)	30° Large Facet (7)	30°Small Facet (8)	60° Corner (9)
TEST CONFIGURATION					
Orientation					
• Top Surface Az. for Applied Load	45°	0°	180°	45°	325°
• Angle (w/respect to horizontal)	0° ± 1°	0° ± 1°	30° ± 1°	3° ± 1°	60° ± 1°
PRETEST STEPS					
Torque Impact Limiter Bolts (if possible)	Yes	Yes	Yes	Yes	Yes
Sample Correctly Installed in Test Machine	Yes	Yes	Yes	Yes	Yes
STATIC CRUSH TEST					
Visual Check	Yes	Yes	Yes	Yes	Yes
Force-Deflection Instrumentation	Yes	Yes	Yes	Yes	Yes
Document & Record	Yes	Yes	Yes	Yes	Yes
POST TEST STEPS					
Dimensional Survey of Crushed Surface	Yes	Yes	Yes	Yes	Yes
100% Viaual Inspection	Yes	Yes	Yes	Yes	Yes
Remove Impact Limiters	No	Yes	No	No	Yes

2.10.12.6.2 Pretest Observations:

A. Visually inspect all impact limiter surfaces for cracks, gouges, dents or other damage.

B. Document the test set up and package with photographic records.

2.10.12.6.3 Static Test Performance:

Prior to proceeding from one test to the next in the series, the impact limiters were visually inspected for damage that might invalidate subsequent tests.

THIS SECTION CONTAINS
PROPRIETARY INFORMATION

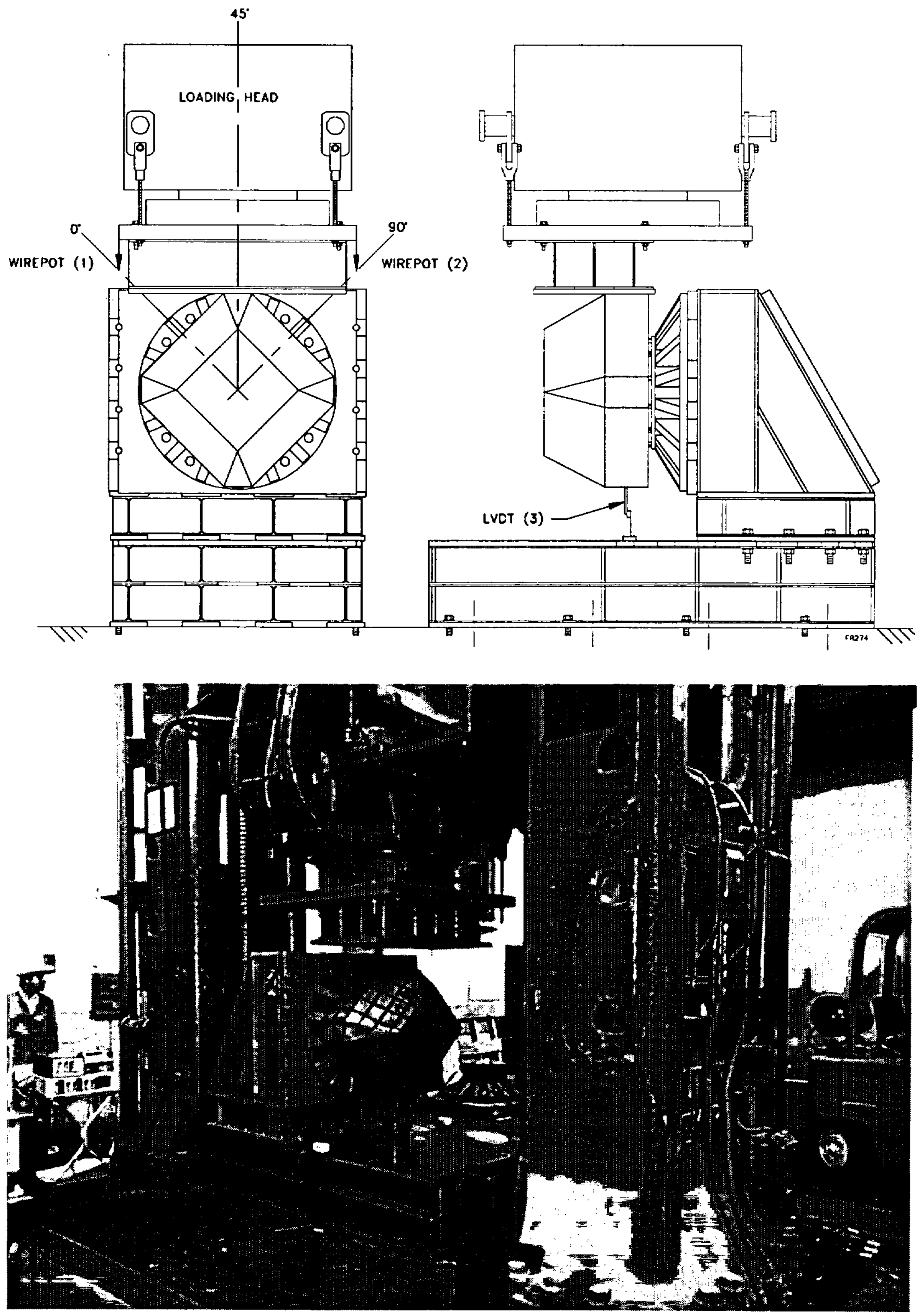

Figure 2.10.12-2

Configuration for Test No. 5

THIS SECTION CONTAINS
PROPRIETARY INFORMATION

Figure 2.10.12-3

Transnuclear Impact Limiters Static Tests - Test No. 5

THIS SECTION CONTAINS
PROPRIETARY INFORMATION

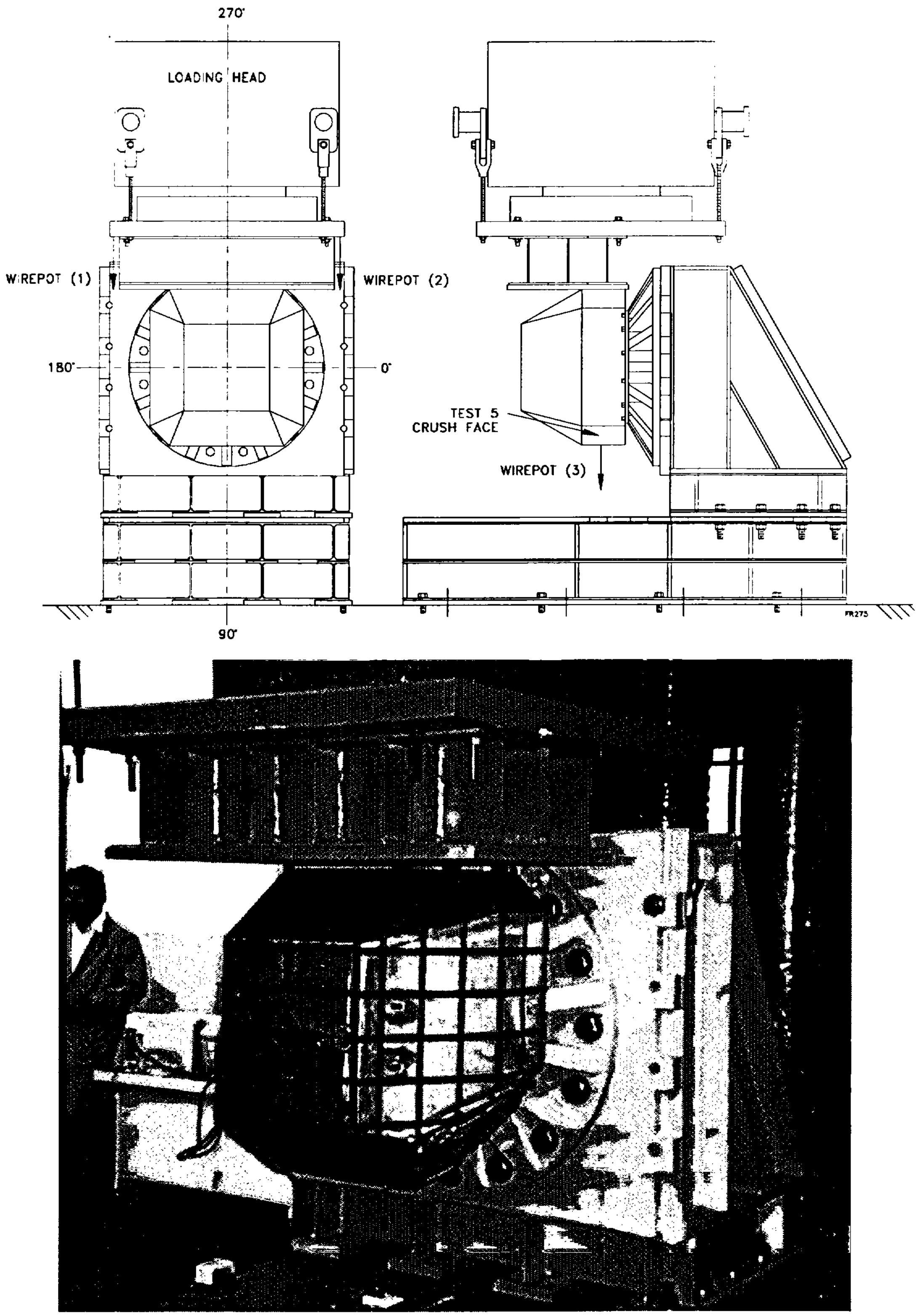

Figure 2.10.12-4

Configuration for Test No. 6

THIS SECTION CONTAINS
PROPRIETARY INFORMATION

Figure 2.10.12-5

Transnuclear Impact Limiters Static Tests - Test No. 6

THIS SECTION CONTAINS
PROPRIETARY INFORMATION

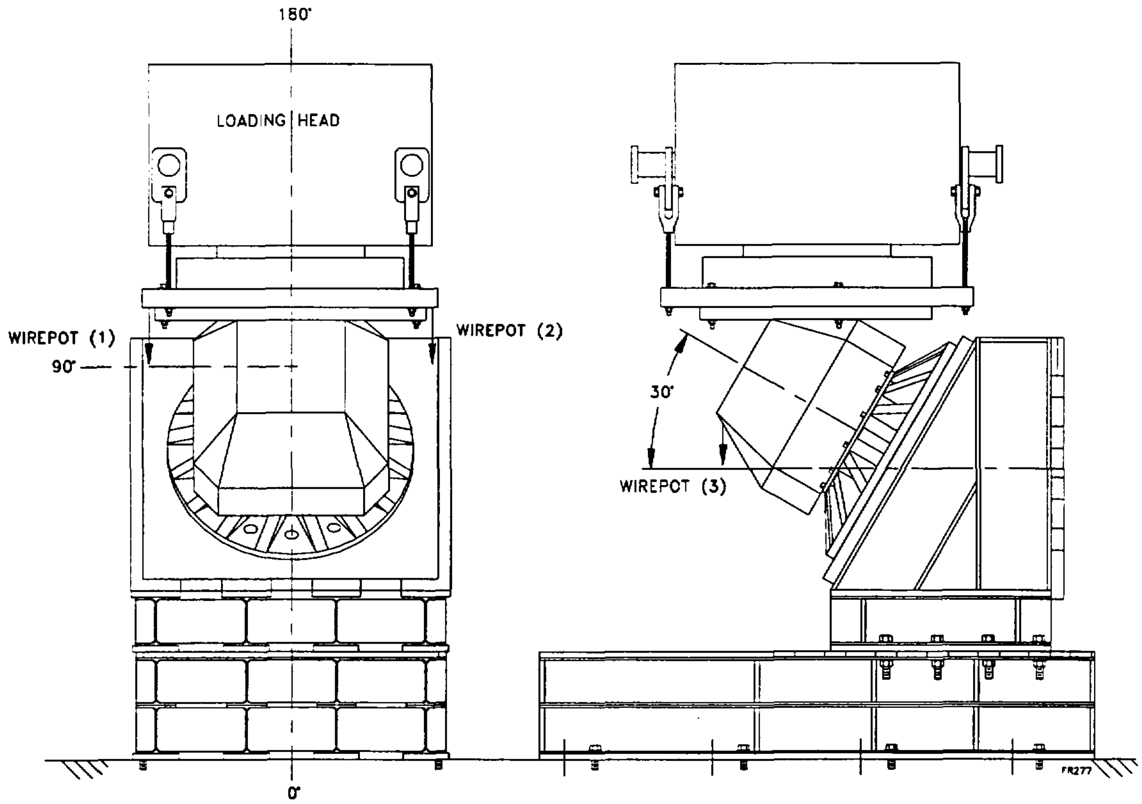

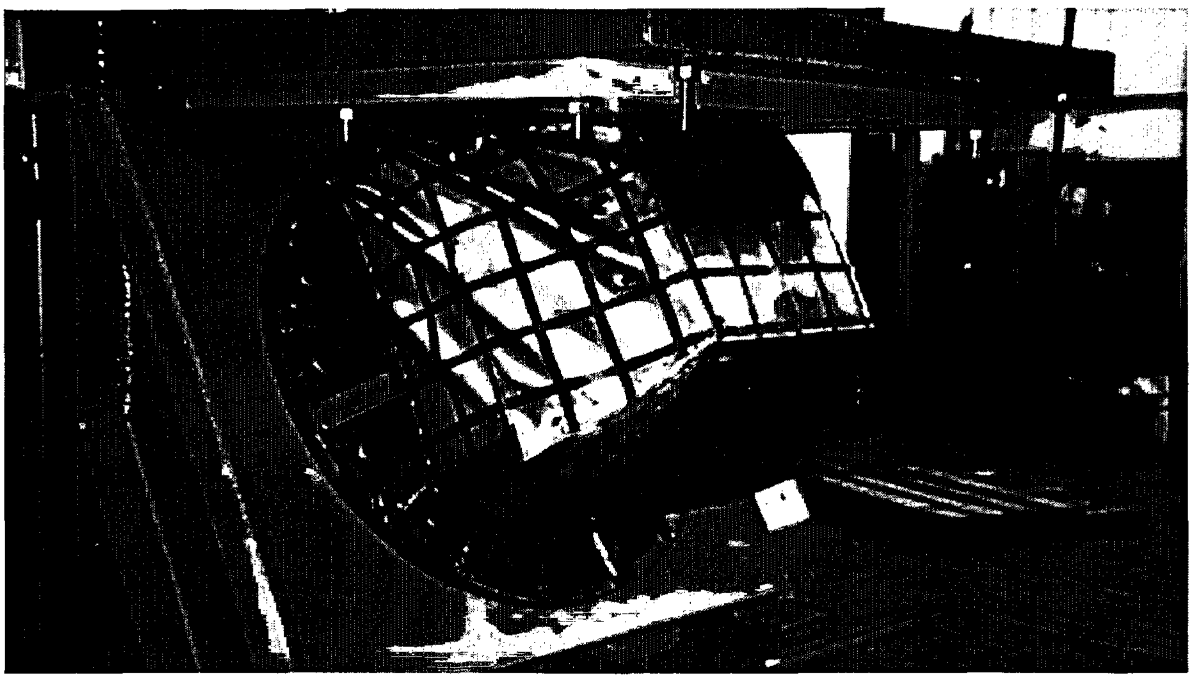

Figure 2.10.12-6

Configuration for Test No. 7

THIS SECTION CONTAINS
PROPRIETARY INFORMATION

Figure 2.10.12-7
Transnuclear mpact Limiters Static Tests - Test No. 7

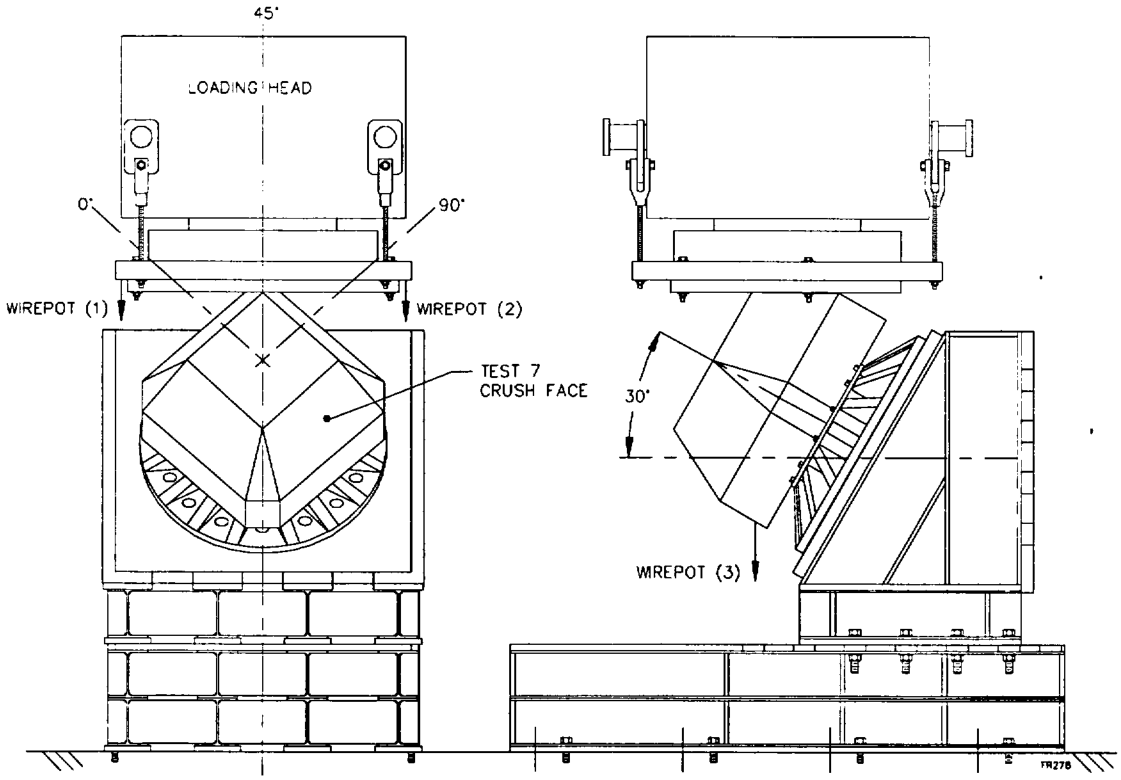

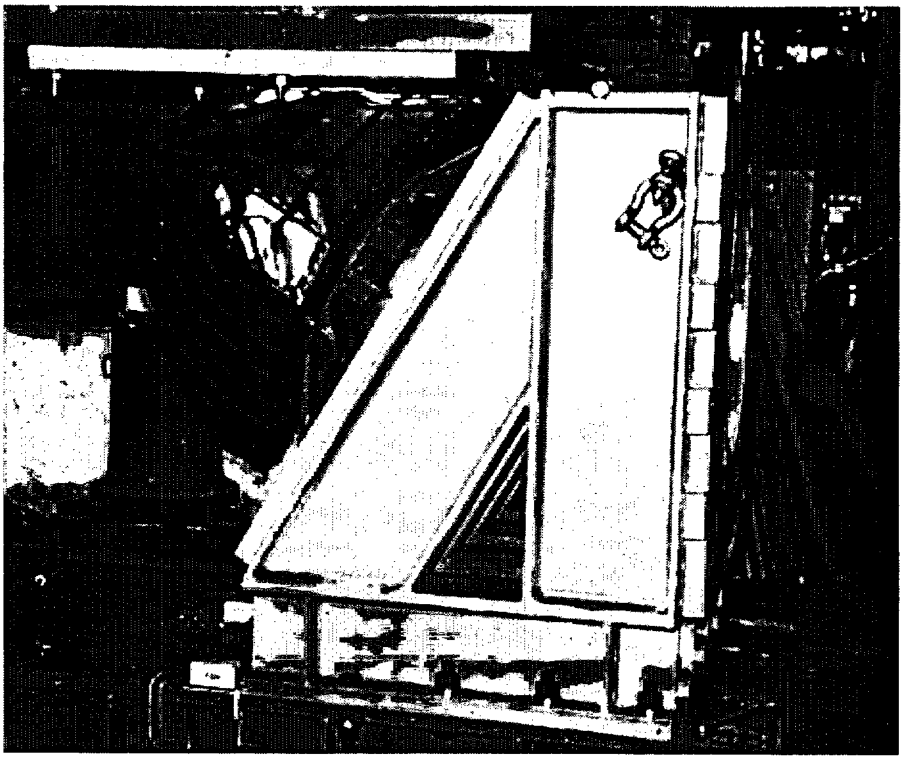

Figure 2.10.12-8

Configuration for Test No. 8

THIS SECTION CONTAINS
PROPRIETARY INFORMATION

Figure 2.10.12-9

Transnuclear Impact Limiters Static Tests - Test No. 8

Test 9 was performed after preparing the test fixture to orient the specimen at a 60° angle with respect to the horizontal. The load was applied to the 315° corner, as shown in Figure 2.10.12-10.

The limit event was a displacement of 9.6 inches. This displacement was achieved with a load of 484 kips. It was then decided to load the specimen further, as this was the last test of the program. The peak load achieved was 700 kips, at a deflection of 10.74 inches. The peak deflection was 10.90 inches, measured after the test was paused, and the load had dropped to 648 kips. The permanent deflection after unloading was 9.06 inches.

Figure 2.10.12-11 shows the measured static force-deflection curve and Figure 2.10.12-16 the predicted static force-deflection curve for this crush orientation.

2.10.12.7 Comparison of Analytical and Test Results

The as-manufactured material properties for the honeycomb and foam were determined by performing a series of static and dynamic tests in accordance with the criteria provided in Appendix 2.10.8. These measured properties were used as the input into the analytical methodology described in Appendix 2.10.9. The resulting force-deflection curves showed excellent agreement with the measured results for tests 5 through 8. For test 9 the analytical results under predicted the measured results. Minor modifications were made to the analytical methodology to provide a better prediction of the initial conditions by accounting for the stiffness of the impact limiter shell and its affect on the foam for this crush orientation.

Using the as built material properties, and the revised analytical methodology, the force-deflection predicted curves shown in through were developed. For comparison purposes the measured force-deflection curves are overlaid onto the predicted curves. These curves demonstrate that the methodology provides good correlation between measured and predicted values. As described in Appendix 2.10.11 the methodology was applied to the preoperational all foam test models and the certification test drop limiters to demonstrate that the dynamic accelerations are conservatively predicted.

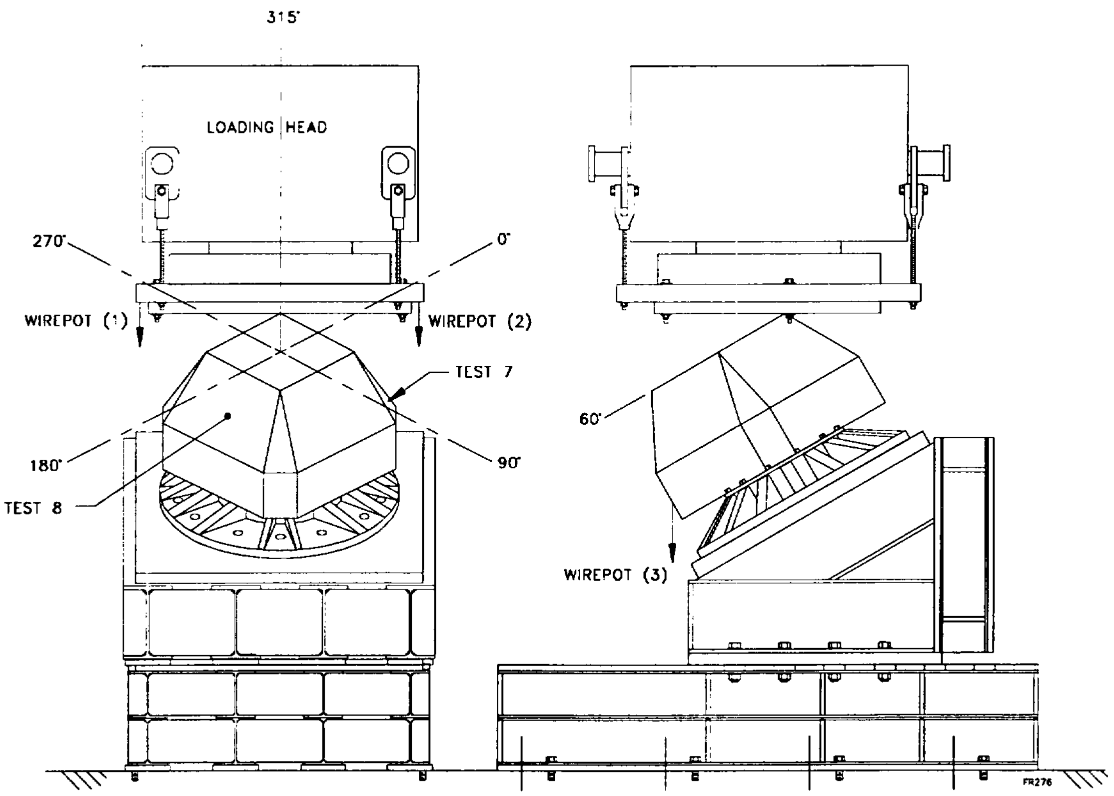

Figure 2.10.12-10

Configuration for Test No. 9

THIS SECTION CONTAINS
PROPRIETARY INFORMATION

Figure 2.10.12-11

Measured Static F-δ Curve - Test No. 9

THIS SECTION CONTAINS
PROPRIETARY INFORMATION

Figure 2.10.12-12

Comparison of Measured and Predicted Static F-δ Curves - Test No. 5

THIS SECTION CONTAINS
PROPRIETARY INFORMATION

Figure 2.10.12-13

Comparison of Measured and Predicted Static F-δ Curves - Test No. 6

THIS SECTION CONTAINS
PROPRIETARY INFORMATION

Figure 2.10.12-14

Comparison of Measured and Predicted Static F-δ Curves - Test No. 7

THIS SECTION CONTAINS
PROPRIETARY INFORMATION

Figure 2.10.12-15

Comparison of Measured and Predicted Static F-δ Curves - Test No. 8

THIS SECTION CONTAINS
PROPRIETARY INFORMATION

Figure 2.10.12-16

Comparison of Measured and Predicted Static F-δ Curves - Test No. 9

2.10.13 Evaluation of the Type XM-19 Basket Design Option for the FF-DSC

2.10.13.1 Introduction

This appendix is provided to address the XM-19 basket design option for the FF-DSC. This alternate basket design modifies the basket assembly material and includes other modifications to the FF-DSC configuration, which are presented in the general arrangement drawings in Section 1.3.2. The modifications to the FF-DSC considered in this appendix are:

- Use of ASME SA-240, Type XM-19 stainless steel for the spacer discs and support plates. (The design presented in the main body uses ASME SA-537 Class 2 carbon steel.)
- Relocation of the top spacer disc 3 inches toward the bottom of the basket.
- Removal of the two-plate option for fabrication of the support plates (leaving only the single 4-inch thick plate option).
- Alternate spacer disc to support plate weld configurations.
- Increase in length of the basket-to-shell shear key.

The evaluations presented in this appendix consider the effect of the alternate Type XM-19 basket material on thermal stresses, thermal expansion and allowable stresses. The relocation of the top spacer disc affects stresses in the spacer disc, support plates and fuel can body under basket lateral loading. The relocation of the top disc also increases the unsupported length of the top span of the support plate which affects the allowable axial stress. The single 4-inch support plate section is considered in the evaluation of end drop loading herein. The optional weld configurations for the connection of the spacer discs to the support plates affect the boundary conditions applicable to out-of-plane loading on the spacer discs. The modified basket-to-shell shear key results in a greater length between the face of the spacer disc and the weld of the key to the DSC shell. This increase in unwelded length results in higher key and weld stresses.

The evaluations presented in this appendix are applicable only to the controlling load conditions. Therefore, results for non-controlling load combinations such as vibration + thermal are not provided.

2.10.13.2 XM-19 Basket Assembly Material

This section addresses the use of ASME SA-240, Type XM-19 as an alternate material for the FF basket. All analyses presented in the main body of the SAR were performed using properties of ASME SA-537 Class 2 material. As shown in Section 2.10.13.2.2.1, the stress acceptance criteria for the spacer discs have increased. Section 2.10.13.2.2.2 discusses the effect of the slightly lower elastic modulus and demonstrates that no negative affects are induced. The largest effect caused by this material change is to the thermal properties, which is discussed in Section 2.10.13.2.2.3.

Properties for the ASME SA-240, Type XM-19 material are presented in this appendix and are compared to the values for the analysis material SA-537, Class 2. These are designated the 'alternate material' and the 'analysis material', respectively.

2.10.13.2.1 Material Properties

The structural material properties for both the SA-537, Class 2 and SA-240, Type XM-19 materials are listed in Table 2.10.13-1 through Table 2.10.13-5.

Table 2.10.13-1

Allowable Stress Intensities (S_m)

Material	Temperature					
	-20°F to 100°F	200°F	300°F	400°F	500°F	600°F
SA-537, Class 2	26.7 ksi	26.7 ksi	26.7 ksi	26.4 ksi	26.4 ksi	26.4 ksi
SA-240, Type XM-19	33.3 ksi	33.2 ksi	31.4 ksi	30.2 ksi	29.7 ksi	29.2 ksi

Notes:
(1) ASME B&PV Code [2.2], Section II, Part D, Table 2A

Table 2.10.13-2

Yield Stress Values (S_y)

Material	Temperature					
	-20°F to 100°F	200°F	300°F	400°F	500°F	600°F
SA-537, Class 2	60.0 ksi	55.0 ksi	52.2 ksi	50.0 ksi	47.6 ksi	46.0 ksi
SA-240, Type XM-19	55.0 ksi	47.0 ksi	43.4 ksi	40.8 ksi	38.8 ksi	37.3 ksi

Notes:
(1) ASME B&PV Code [2.2], Section II, Part D, Table Y-1

Table 2.10.13-3

Ultimate Stress Values (S_u)

Material	Temperature					
	-20°F to 100°F	200°F	300°F	400°F	500°F	600°F
SA-537, Class 2	80.0 ksi	80.0 ksi	80.0 ksi	79.3 ksi	79.3 ksi	79.3 ksi
SA-240, Type XM-19	100.0 ksi	99.5 ksi	94.3 ksi	90.7 ksi	89.1 ksi	87.8 ksi
E308	75.0 ksi	71.0 ksi	66.0 ksi	64.4 ksi	63.5 ksi	63.5 ksi

Notes:
(1) ASME B&PV Code [2.2], Section II, Part D, Table U
(2) The temperature dependent ultimate strength of the E308 weld filler material is based on SA-240, Type 304.

Table 2.10.13-4

Moduli of Elasticity (E)

Temperature (°F)	E (psi x 10^6)	
	SA-537, Class 2 (1)	SA-240 Type XM-19 (2)
-100	30.2	29.1
70	29.5	28.3
200	28.8	27.6
300	28.3	27.0
400	27.7	26.5
500	27.3	25.8
600	26.7	25.3

Notes:

(1) SA-537, Class 2 is a carbon steel with C≤ 0.30% material in ASME B&PV Code [2.2], Section II, Part D, Table TM-1

(2) SA-240, Type XM-19 is a high alloy steel with 22Cr-13Ni-5Mn, in ASME B&PV Code [2.2], Section II, Part D, Table TE-1

Table 2.10.13-5

Thermal Expansion Coefficient (α) (3)

Temperature (°F)	α (in/in°F x 10^{-6})	
	SA-537, Class 2 (1)	SA-240 Type XM-19 (2)
-20	4.83	8.08
70	5.42	8.24
100	5.53	8.30
150	5.71	8.40
200	5.89	8.48
250	6.09	8.57
300	6.26	8.65
350	6.43	8.73
400	6.61	8.79
450	6.77	8.86
500	6.91	8.92
550	7.06	8.98
600	7.17	9.03

Notes:

(1) SA-537, Class 2 is a carbon steel Group C material, in ASME B&PV Code [2.2], Section II, Part D, Table TE-1 [Ref. 2.68]

(2) SA-240, Type XM-19 is a high alloy steel with 22Cr-13Ni-5Mn, in ASME B&PV Code [2.2], Section II, Part D, Table TE-1

(3) Values shown are for the mean coefficient of thermal expansion in going from 70°F to the indicated temperature, with exception of the value for the value at 70°F, which is the instantaneous value.

2.10.13.2.2 Impact of Changes

The impacts of differences in the basket material properties on the results of the structural analyses are addressed in this section.

2.10.13.2.2.1 Allowable Stress Values

As shown by Table 2.10.13-1 and Table 2.10.13-3 (S_m, and S_u, respectively), the alternate material is stronger than the analysis material at all temperatures. Thus, since the allowable stresses are only dependent on S_m and S_u designations, the allowable stresses for the alternate material are greater than the allowable stress for the analysis material. The allowable spacer disc stresses for all service conditions for both materials are summarized in Table 2.10.13-6, which shows an increase in the allowable stress for each stress category and for both cold and warm temperatures. Although Table 2.10.13-2 reflects a lower yield stress for alternate material, this has no impact except for the support plate buckling analysis, which uses the 'linear-type' support analysis methodology from Appendix F of [2.2]. In Section 2.10.13.4, the support plate is re-evaluated using allowable stresses based upon the alternate, Type XM-19 material.

Table 2.10.13-6

Comparison of Allowable Stresses (ksi)

Service Level	Temperature	SA-537, Class 2	SA-240, Type XM-19
Level A (1)	-20°F	P_m: 26.7 P_m+P_b: 40.1 P_m+P_b+Q: 80.1	P_m: 33.3 P_m+P_b: 50.0 P_m+P_b+Q: 99.9
	400°F	P_m: 26.4 P_m+P_b: 39.6 P_m+P_b+Q: 79.2	P_m: 30.2 P_m+P_b: 45.3 P_m+P_b+Q: 90.6
Level D (2)	-20°F	P_m: 56.0 P_m+P_b: 72.0	P_m: 70.0 P_m+P_b: 100.0
	400°F	P_m: 55.5 P_m+P_b: 71.4	P_m: 63.5 P_m+P_b: 90.7

Notes:

(1) For Service Level A, the allowable stresses are found as:
$P_m \leq S_m$
P_m (or P_l) $+P_b \leq 1.5S_m$
P_m (or P_l) $+P_b+Q \leq 3.0S_m$

(2) For Service Level D, the allowable stresses are found as:

Carbon Steel Components	Austenitic Steel Components
$P_m \leq 0.7\ S_u$	$P_m \leq \min(2.4S_m, 0.7S_u)$
P_m (or P_l) $+P_b \leq 1.0S_u$	P_m (or P_l) $+P_b \leq \min(3.6S_m, 1.0S_u)$

2.10.13.2.2.2 Elastic Modulus

The elastic modulus impacts the structural analysis when calculating the overall structural stiffness and the relative stiffnesses between structural components. For mechanical loading of the spacer discs, all in-plane loads (from fuel and self weight) are carried by the discs. Out-of-plane loads consist only of self weight (of the disc) factored by gravitational or drop accelerations. These loads are carried through the disc to the support plates. Since all of the analyses are performed using elastic-only material properties, there are no significant alternate load paths for either in-plane or out-of-plane loads. Small changes in the elastic modulus (disc stiffness) will have insignificant effects on the analysis results.

2.10.13.2.2.3 Thermal Properties

Thermal expansion coefficients (α) and thermal conductivity both vary with temperature for the SA-537, Class 2 and SA-240, Type XM-19 materials. The effect of the different thermal properties is estimated based on (1) temperature distributions calculated in Appendix 2.10.4, (2) thermal expansion coefficients listed in Table 2.10.13-5, and (3) basic stress formulas.

Thermal stress results from differential thermal expansion (i.e., constraint of free expansion). The maximum temperatures occur at the center of the disc with the minimum temperatures at the edge of the disc. Thus, the center of the disc wants to expand more than the edge, resulting in constraint of free expansion and thermal stresses. The thermal stress is proportional to the differences in thermal growth between the center and edges of the disc.

The relative thermal stresses in the disc(s) (for the different materials) are estimated by assuming that the temperature distribution across the discs are similar for the different materials. Thus, the thermal stress for any material is proportional to the product $E \cdot \alpha \cdot \Delta T$ (e.g., see Article 15.6, Items 10 - 12) of [2.56]:

$$\sigma_{THERMAL} \propto (E \cdot \alpha \cdot \Delta T)$$

For the spacer discs, the thermal stress is related to the differential displacement between the inner and outer portions of the disc. The thermal stress is then proportional to:

$$\sigma_{THERMAL} \propto \left[(E \cdot \alpha \cdot \Delta T)_{MAX} - (E \cdot \alpha \cdot \Delta T)_{MIN}\right]$$

Where the maximum values are at the center (maximum temperature) of the disc and the minimum values are at the edge (minimum temperature) of the disc.

For any material (designated SA-__ in the following equations), the equation is written as (where σ_{EQ} denotes that the value is not the actual stress in the disc):

$$\sigma_{EQ}^{SA-} = \left[(E\cdot\alpha\cdot\Delta T)_{MAX} - (E\cdot\alpha\cdot\Delta T)_{MIN}\right]$$

Using an average value of E, the equation becomes:

$$\begin{aligned}\sigma_{EQ}^{SA-} &= E_{AVG}\left[(\alpha\cdot\Delta T)_{MAX} - (\alpha\cdot\Delta T)_{MIN}\right] \\ &= E_{AVG}\left[(\alpha_{MAX}\cdot(T_{MAX}-70)) - (\alpha_{MIN}\cdot(T_{MIN}-70))\right]\end{aligned}$$

This equation will be used to estimate the magnitude of thermal stress in a spacer disc of each material. It considers both differences in thermal gradients (different T_{MAX} and T_{MIN} resulting from different conductivities) and differences in expansion (α).

The change in thermal stress, $\Delta\sigma_{THERMAL}$, for the SA-240 Type XM-19 relative to the SA-537 Class 2 is determined as shown below:

$$\Delta\sigma_{THERMAL} = \sigma_{EQ}^{SA-240,\ XM\text{-}19} \Big/ \sigma_{EQ}^{SA-537,\ Class2}$$

Temperature data is listed in Table 2.10.13-7 (-20°F and 100°F ambient conditions).

Stress increase ratios are calculated in Table 2.10.13-8 (-20°F & 100°F ambient conditions) using temperature data from Table 2.10.13-7. As shown in Table 2.10.13-8, the maximum stress increase ratio is 1.32. As shown in Table 2.6.13-71 , the maximum P_l+P_b+Q stress is 33.9 ksi. Conservatively assuming that the stress ratio applies to the entire stress state and not just the thermal component, the resulting maximum stress in the Spacer Disc is 44.7 ksi. The allowable primary plus bending plus secondary stress for SA-240, Type XM-19 at a conservative temperature of 500°F, is 89.1 ksi. Therefore, based on the conservative assumptions presented above, the minimum margin of safety is +0.99.

2.10.13.2.2.4 Mechanical Interface

Thermal expansion of the XM-19 basket design option is evaluated below for interferences with the FF-DSC shell. The evaluation of the spacer discs and support plates is based on nominal dimensions in the same manner as in Sections 2.6.12.1.1 and 2.6.12.1.3 .

FF Spacer Disc Thermal Expansion

The diametral thermal growth of an FF-DSC spacer disc is conservatively calculated using an above average temperature and assuming free diametral thermal growth of the spacer disc. This neglects the restraining effect that the cooler outer perimetric portion of the spacer disc has on the hotter inner portion. A conservative above average temperature of 400°F is used to calculate the diametral thermal growth of the Type XM-19 FF-DSC spacer disc:

$$\delta_{bask\text{-}hot} = \alpha_{basket}\, D_{basket\text{-}cold}\, \Delta T_{basket}$$

$$= (8.79\text{x}10^{-6}\ \text{in/in-°F})(65.50\ \text{in})(400°\text{F} - 70°\text{F}) = 0.19\ \text{inches}$$

The maximum diametrical thermal growth of the FF spacer disc is less than the 0.44 inch nominal diametrical gap between the FF-DSC spacer disc and the DSC shell. Therefore the FF-DSC spacer discs will expand freely under normal thermal conditions.

Support Plate Thermal Expansion

The maximum temperature for the FF-DSC support plates is 380°F for the 100°F ambient condition. The nominal length of the support plates is 172.5 inches. The coefficient of thermal expansion of the Type XM-19 support plate material at 380°F is $8.76\text{x}10^{-6}$ in/in°F. The free thermal growth of the support plates is:

$$\delta_t = \alpha \cdot L \cdot \Delta T$$

$$= (8.76 \times 10^{-6} \text{ in/in°F})\ (172.5 \text{ in})(380°F - 70°F)$$

$$= 0.47 \text{ inches}$$

From Section 2.6.12.1.3, the average FF-DSC shell temperature for the 100°F ambient condition is 348°F. The free axial thermal growth of the FF-DSC shell is:

$$\delta_t = \alpha \cdot L \cdot \Delta T$$

$$= (9.63 \times 10^{-6} \text{ in/in°F})\ (173.0 \text{ in})(348°F - 70°F)$$

$$= 0.47 \text{ inches}$$

The differential growth between the support plate and the DSC shell is (0.47 - 0.47) = 0.0 inches which is less than the nominal gap of 0.50 inches. Therefore the support plates will expand freely under normal thermal conditions.

Table 2.10.13-7

Results of Thermal Analysis with Alternate Material

Condition	Maximum Temperature (°F)	Minimum Temperature (°F)	Maximum Gradient (°F)	Materials
For -20°F Ambient Temperature Case(1)	370	141	229	SA-537, Class 2
	386	152	234	SA-240, XM-19
For 100°F Ambient Temperature Case(2)	433	214	219	SA-537, Class 2
	459	252	207	SA-240, XM-19

Notes:

(1) The maximum and minimum temperatures analyzed for the SA-537, Class 2 materials are taken from Appendix 2.10.4, Figure 2.10.4-2. The maximum and minimum temperatures for the SA-240, Type XM-19 material are taken from SAR Table 3.6-5a.

(2) The maximum and minimum temperatures analyzed for the SA-537, Class 2 materials are taken from Appendix 2.10.4, Figure 2.10.4-1. The maximum and minimum temperatures for the SA-240, Type XM-19 material are taken from SAR Table 3.6-4a.

Table 2.10.13-8

Effect of Thermal Properties on Disc Thermal Stress

Material	$E^{(2)}$ ($\times 10^6$ psi)	$\Delta T_{max}^{(3)}$ (°F)	α_{max} ($\times 10^{-6}$ in/in°F)	$\Delta T_{min}^{(3)}$ (°F)	α_{min} ($\times 10^{-6}$ in/in°F)	$\Delta\sigma_{thermal}^{(1)}$
For -20°F Ambient Temperature Case						
SA-537, Class 2	28.5	300	6.50	71	5.68	1.32
SA-240, XM-19	27.9	316	8.77	82	8.39	
For 100°F Ambient Temperature Case						
SA-537, Class 2	28.2	363	6.72	144	5.95	1.15
SA-240, XM-19	27.3	389	8.86	182	8.57	

Notes:

(1) The ratio of the SA-240, Type XM-19 stress divided by the SA-537, Class 2 stress.

(2) The elastic modulus for the SA-537, Class 2 material is based on the bulk average temperature. The elastic modulus for the SA-240, Type XM-19 is conservatively based on the minimum temperature.

(3) Based on an ambient temperature of 70°F.

2.10.13.2.3 Conclusions of Material Evaluation

This section has presented the material properties for the alternate material for the FF spacer discs. The largest effect is caused by the change in the thermal expansion coefficient, which causes thermal stress to increase. Due to the increase in material strength afforded by the SA-240, Type XM-19, large existing margins of safety, and an engineering analysis of the change in thermal stresses, use of the alternate material is structurally acceptable.

2.10.13.3 Spacer Disc Evaluation for Relocation

The 3-inch downward shift of the top spacer disc increases the tributary load on the top spacer disc. The spacer disc has the highest stress ratio for the corner slapdown event. This analysis is performed in the manner of the one foot side drop. (See Section 2.10.4.1.1.2).

The 1' drop analysis is performed for the single spacer disc which supports the largest total tributary weight of the fuel assemblies and fuel can assemblies, in addition to its own self weight. The maximum weight of a single PWR fuel assembly is 1,530 pounds [2.8]. The weight distribution of a B&W 15X15 Mark B (PWR) fuel assembly over the four major axial regions are summarized in Table 2.10.4-1. The fuel assembly tributary weights are determined by multiplying the fuel region line loads by the respective tributary widths.

Each fuel can assembly consists of a fuel can body (tube), top lid subassembly, and bottom lid subassembly. The weight of the fuel can body tributary to each spacer disc is calculated by multiplying the fuel can body line load by the spacer disc tributary widths. The line weight of a single fuel can body, w_{tube}, is:

$$w_{tube} = (9.5^2 - 9.0^2)(0.2853)$$

$$= 2.64 \text{ lb/in}$$

The weights of the remaining fuel can assembly components are distributed to the spacer discs based on location. The weights of the other fuel can assembly components are:

Fuel can top lid subassembly	=	70 lb
Fuel can bottom lid subassembly	=	18.39 lb

The weight of the support plates tributary to each spacer disc is calculated by multiplying the support plate line load by the spacer disc tributary widths. The support plate line load, w_{supt}, is:

$$w_{supt} = 4x(12.0 \times 4.0)(0.2835)$$

$$= 54.4 \text{ lb/in}$$

The tributary widths of the spacer discs are calculated as follows:

$$b_{\#1} \text{ (bottom)} = 8.00 + (11.25/2)$$

$$= 13.63 \text{ inches}$$

$$b_{\#2\text{-}\#13} = 11.25 \text{ inches}$$

$$b_{\#14} = (11.25 + 6.50)/2$$

$$= \quad 8.88 \text{ inches}$$

$$b_{\#15}(\text{top}) = (6.50/2) + (172.50 - 160.75)$$

$$= \quad 15.00 \text{ inches}$$

With the relocation of the top spacer disc, spacer disc #15 (top end disc) supports the largest tributary weight. Note that prior to the disc relocation, the bottom disc (#1) controlled. Therefore, the spacer disc drop analysis will be evaluated for the top end spacer disc.

$$W_{15} = [(2.64)(15.00) + 70 + (2.68)(15.0 - 4.0 - 3.73) + (6.36)(3.73)](13) + (54.4)(15.0)$$

$$= 2{,}803 \text{ lb}$$

As the original analysis was performed with a tributary weight of 2,509 lb, the stresses resulting from the original analysis are ratioed by the factor 2,803/2,509 = 1.12. There is a degree of conservatism in the ratio applied to the weight of the spacer disc in addition to the tributary loading of the fuel can and support bars. The resulting stress intensity from the original analysis (see Section 2.7.7.1.1 , accident slapdown drop) was 72.8 ksi. The revised stress intensity is therefore:

$$\text{S.I.} = 72.8\ (1.12)$$

$$= 81.5 \text{ ksi}$$

The original analysis was based on ASME SA-537, Class 2 carbon steel, the present design uses Type XM-19 Stainless Steel. The allowable stress is S_u at 500°F, 89.1 ksi. The minimum margin of safety is 0.09 (9%).

The lowest factor of safety against buckling occurs in the flatside impact (Section 2.7.7.2). This factor was 4.6. The relocated spacer disc has a loading increase of 3% and the XM-19 material has a lower elastic modulus: (25.8 x 10^6 psi vs. 27.3 x 10^6 psi for SA-537 carbon steel, both at 500°F). As the ratio of the elastic modulus does not change significantly with temperature, the reduced factor of safety on buckling may be estimated as:

Buckling Factor of Safety = 4.6 / (1.03)(27.3/25.8)

= 4.2

The required factor of safety on buckling is 1.5, therefore, the revised spacer disc location meets the acceptance criteria for buckling.

2.10.13.4 Support Plate Evaluation for Spacer Disc Relocation

The support plate is evaluated below for a conservative bounding 75g end drop considering the material change to Type XM-19 and the 3-inch increase in span length caused by the shift in location of the top spacer disc. The calculation follows the methodology used in Section 2.7.7.3.1.1 of the SAR main body except that a single 4-inch thick support plate is evaluated. The two-plate option discussed in Section 2.7.7.3.1.1 is excluded from the FF basket design option evaluated in this appendix. The support plates are evaluated for the end drop using ASME criteria of F-1334.5 [2.2] for linear type components subjected to combined compression and bending loads.

The support plates support their own weight in addition to the weight of the 15 spacer discs for the postulated 30-foot end drop condition. The maximum uniform compressive stress in the support plates is:

$$f_a = P/A$$

$$= WG/A$$

where;

W = [(15 x 1065) + (8 x 1181)]/(4 x 1000), Tributary weight of a support plate

= 6.4 kips

G = 75g, End drop equivalent static acceleration

A = 48 in^2, Cross-section area of a single 4-inch thick support plate therefore,

f_a = (6.4 x 75)/48

= 10.0 ksi

The bending stress in the support plate, due to the moment reaction at the spacer disc locations, is:

f_b = M/S

where;

M = Moment reaction from spacer disc end drop Finite Element Analysis (Section 2.10.13.6)

= 150 in-kips (Section 2.10.13.6)

S = $bh^2/6$, Section modulus of support plate

= $(12)(4.0)^2/6$

= 32.0 in^3

therefore,

f_b = 150.0 / 32.0

= 4.7 ksi

The allowable compressive stress, F_a, is calculated as follows:

F_a = P/A_g

where P is determined in accordance with F-1334.3 and A_g is the gross area of the support plate (48 in^2), as follows:

P/P_y = $(1-\lambda^2/4)/[1.11 + 0.50\lambda + 0.17\lambda^2 - 0.28\lambda^3]$

where;

λ = $(KL/r)(1/\pi)(S_y/E)^{1/2}$

P_y = S_yA

K = 2.0, Factor for fixed-free boundary conditions

L = 10.75 in, Free distance at top end (increased 3inches due to spacer disc shift)

I = $(12 \times 4^3)/12$, Moment of Inertia of support plate

= 64.0 in^4

A = 48.0 in^2, Area of a support plates

r = $(64.0/48.0)^{1/2}$, Radius of gyration of support plate

= 1.15 inches

S_y = 40.8 ksi, Yield strength of Type XM-19 at 400°F per Table 2.10.13-2

E = 26.5×10^6 psi, Elastic modulus of Type XM-19 at 400°F per Table 2.10.13-4

KL/r = (2.0)(10.75)/1.15

= 18.6

Therefore,

λ = $(18.6)(1/\pi)(40{,}800/26.5 \times 10^6)^{1/2}$

= 0.23

P = $(40{,}800 \times 48)(1-0.23^2/4)/[1.11 + 0.50(0.23) + 0.17(0.23)^2 - 0.28(0.23)^3]$

= 1570 kips

$$F_a = 1570 / 48$$
$$= 32.7 \text{ ksi}$$

The value of F'_e is determined in accordance with F-1334.5(b) as follows:

$$F'_e = \pi^2 E/[1.30(Kl/r)^2]$$
$$= \pi^2(26.5 \times 10^6)/[1.30(18.6)^2]$$
$$= 581 \text{ kips}$$

The allowable bending stress, F_b, determined in accordance with F-1334.4(b) for compact sections, is equal to fS_y, where f is the plastic section factor for a rectangular section (=1.50) [2.7]. Therefore, the allowable bending stress is:

$$F_b = 1.5(40.8)$$
$$= 61.2 \text{ ksi}$$

Per ASME B&PV Code, F-1334.5, equations (20), (21), and (22) of NF-3322.1(e)(1) must be satisfied to demonstrate structural adequacy. Equation (20) is satisfied as follows:

$$f_a/F_a + C_{mx}f_{bx}/[(1-f_a/F'_{ex})F_{bx}] + C_{mY}f_{bY}/[(1-f_a/F'_{eY})F_{bY}] \leq 1.0$$
$$(10.0/32.7) + 1.0(4.7)/[(1-(10.0/581))(61.2)] + 0 = 0.38 < 1.0$$

Equation (21) is satisfied as follows:

$$f_a/0.6S_y + f_{bx}/F_{bx} + f_{bY}/F_{bY} \leq 1.0$$
$$10.0/(0.6 \times 40.8) + 4.7/61.2 + 0 = 0.49 < 1.0$$

Equation (22) is satisfied as follows:

$$f_a/F_a + f_{bx}/F_{bx} + f_{bY}/F_{bY} < 1.0$$
$$10.0/32.7 + 4.7/61.2 + 0 = 0.38 \leq 1.0$$

Therefore, the support plates satisfy the appropriate design criteria for a bounding 75g end drop in consideration of the material change to Type XM-19 and the increase in cantilevered span length by 3inches.

2.10.13.5 Fuel Can Evaluation for Spacer Disc Relocation

The fuel can is evaluated for the increased cantilever length resulting from the 3-inch relocation of the top spacer disc for this basket design option. The evaluations follow the methodology used in Section 2.6.12.3.3 (1-ft side drop) and Section 2.7.7.5.1.3 (30-ft oblique drop) of the SAR main body.

Fuel Can Body One Foot Side Drop

The evaluation of the fuel can panel bending presented in Section 2.6.12.3.3 is not affected by the 3-inch shift in spacer disc location. The affected top cantilever span of the can supports only the top and plenum regions of the fuel assembly which are significantly lighter and more rigid than the active fuel region.

The FF-DSC fuel can bodies are analyzed using hand calculations to determine the moments and shears induced by the fuel can body self weight and the PWR failed fuel assembly in the top cantilever section for the 1' side drop loading.

The fuel can bodies are 9.5 × 9.5 × 0.25 inch thick square tubes made of SA-240 Type 304 stainless steel. The fuel can assembly design temperature is 407°F. They are loaded by the acceleration of their own mass plus the mass of the failed fuel assembly for the side drop conditions. The maximum stress will occur at the top end cantilever section. Conservatively assuming that the basket assembly has slid to the bottom end of the DSC cavity and the fuel can is at the top of the DSC gives the maximum moment arm. The bending stress in the fuel can due to the dead weight load is:

$$\sigma_b = Mc/I$$

Moment due to top lid assembly and fuel can body is:

M_l = $[P_L e_L + P_c e_c]$ x Side Drop g-load

where:

L = Original Top end cantilever length

= 173.0 - 7 - 146.25 - 9.5 - 2

= 8.25 inches

Adding 3 inches:

$L_{revised}$ = 8.25 + 3

= 11.25 inches

P_L = Top lid assembly load

= 70 lb

e_L = Original top lid assembly moment arm.

= 8.25 - 4 + 1.05

= 5.3 inches

Adding 3 inches:

$e_{L\text{-revised}}$ = 5.3 + 3

= 8.3 inches

P_c = Fuel can load

= $(11.25 - 1)(9.5^2 - 9.0^2) \times 0.2853$

= $10.25 \times 9.25 \times 0.2853$ lb/in^3

= 27.1 lb

e_c = FF fuel can moment arm

= (11.25 - 1)/2

= 5.125 inches

Therefore:

M_1 = [(70)(8.3) + (27.1)(5.125)] × 25.1

(Conservatively, a side drop g load of 25.1g assumed for the fuel can)

= 18,070 in-lb

Moment due to fuel is:

M_2 = $[P_T e_T + P_P e_P]$ × Side Drop g-load

where:

P_T = Fuel top region load (6.36 lb/in, 3.73 inches long)

= 23.72 lb

e_T = 11.25 - 4 - (3.73/2)

= 5.39 inches

P_p = Plenum fuel region load (2.68 lb/in, 3.52 inches long)

= 9.43 lb

e_p = 11.25 - 4 - 3.73 - (0.52/2)

= 3.26 inches

Therefore:

M_2 = [(23.72)(5.39) + (9.43)(3.26)] 25.1

= 3981 in-lb

Total Moment

$$M = 18{,}070 + 3981$$
$$= 22{,}051 \text{ in-lb}$$

$$I_z = bd^3/12 - b_i d_i^3/12$$
$$= 9.5(9.5)^3/12 - 9(9)^3/12$$
$$= 132 \text{ in}^4$$

where i denotes inner can dimensions.

$$c = d/2 = 4.75 \text{ inches}$$

For the 25.1g side drop load, the maximum can bending stress is:

$$\sigma_b = [22.05\ (4.75)]/132$$
$$= 0.79 \text{ ksi}$$

The maximum can shear stress is defined as:

$$\tau_{max} = 3/2\ (V/A_{web})$$

where:

$$V = [P_L + P_C + P_T + P_P] \times \text{g-load}$$
$$= [70 + 27.1 + 23.72 + 9.43] \times 25.1$$
$$= 3{,}269 \text{ lb}$$

Therefore:

$$\tau_{max} = 3/2(3.269/\ (0.5 \times 9.0))$$
$$= 1.09 \text{ ksi}$$

The maximum primary membrane stress intensity is equal to twice the peak shear, or 2.18 ksi. Conservatively assuming that the maximum shear and bending stresses occur in the same location, the fuel can body side drop maximum stress intensities are:

P_m = 2.18 ksi $< S_m = 17.5$ ksi (SA-240 at 500°F is used)

P_l+P_b = $2[(.79/2)^2 + (1.09)^2]^{1/2}$

= 2.31 ksi $< 1.5\ S_m = 26.3$ ksi

Fuel Can Body 30' Oblique Drop Stress Analysis

The FF-DSC fuel cans are evaluated for the 30' drop condition using bounding longitudinal and tangential accelerations of 45g's and 93g's, respectively. The stresses in the fuel cans due to the 45g longitudinal load, calculated in Section 2.7.7.5.1.1 of the SAR main body, are:

f_a = 2.54 ksi

f_b = 0 ksi

The fuel can stresses due to the 93g tangential load are determined by scaling the stresses calculated above due to the 25.1g, 1 foot side drop by the ratio of 3.71 (= 93/25.1). Therefore, the fuel can stresses due to the 93g tangential load are:

f_b = 0.66 x 3.71 = 2.45 ksi

f_v = 0.94 x 3.71 = 3.50 ksi

Therefore, the combined fuel can stresses for the bounding oblique drop loads are:

f_a = 2.54 ksi

f_b = 0 + 2.45 = 2.45 ksi

f_v = 3.50 ksi

Using the allowable stresses from Section 2.7.7.5.1.3, checking Equations (20), (21), and (22) of NF-3322.1(e)(1) gives:

Eq. 20: $$\frac{2.54}{11.1}+\frac{1.0(2.45)}{[1-(2.54/24.1)](22.5)}=0.35\le 1.0$$

Eq. 21: $$\frac{2.54}{2x0.60(19.4)}+\frac{2.45}{22.5}=0.22\le 1.0$$

Eq. 22: $$\frac{2.54}{11.1}+\frac{2.45}{22.5}=0.34\le 1.0$$

The allowable shear stress is $0.42S_u$, or 26.7 ksi at 500°F for the fuel can material. The maximum shear stress in the fuel can resulting from the bounding oblique drop impact load is 3.5 ksi. Therefore, the fuel can shear stress is within the shear stress limit.

2.10.13.6 Spacer Disc Evaluation for Alternate Weld Patterns

The drawings in Section 1.3.2 note 5 options for the weld of the spacer discs to the support plates for the XM-19 basket design option for the FF-DSC.

ANSYS run *ffsdend_01b.out* provides the results of an elastic analysis for the 75g end drop (which envelops both the Part 71 and Part 72 end drop loads), where nodes representing the welds between the support plate and spacer disc are restrained in all directions. The ANSYS model is based on the same models evaluated in Appendix 2.10.4 except that the location of the support plate weld is modeled accurately for the weld options associated with the XM-19 basket design option evaluated here. Load Step 2 is used to evaluate the option where the support plates are welded to both sides of the spacer discs at only the 4-inch sides of the support plates. The boundary conditions for Load Step 2 are shown in Figure 2.10.13-1. Load Step 3 is used to evaluate the option where the support plates are welded to both sides of the spacer discs at the 4-inch sides and the 12-inch side of the support plates. The boundary conditions for Load Step 3 are shown in Figure 2.10.13-2. The corresponding stress intensity plots are shown in

Figure 2.10.13-3 and Figure 2.10.13-4. Figure 2.10.13-5 shows the node numbers for the possible weld locations.

The spacer disc maximum $P_L + P_b$ stress intensity (which governs over the P_m stress intensity) is 37,806 psi (see Figure 2.10.13-3). This occurs for the support plate weld options where the support plates are welded to both sides of the spacer discs at only the 4-inch sides of the support plates (Load Step 2). The allowable $P_m + P_b$ stress intensity at 500°F (see Table 2.10.13-3) is 89,100 psi for XM-19 material (lesser of 3.6 S_m or 1.0 S_u, S_m = 29,700 psi and S_u = 89,100 psi based on Table 2.10.13-1 and Table 2.10.13-3, respectively). Therefore, the maximum ratio of stress intensity to allowable is 37,806 / 89,100 = 0.424 and is acceptable (margin = 1.36).

Reactions at the weld locations are used in the support plate evaluation in Section 2.10.13.4 and are as follows:

Option	$F_{vertical}$ (lbs)	$M_{tangential}$ (in-lb)	M_{radial} (in-lb)
2-Sided Weld	19,250	143,000	10,400
3-Sided Weld	19,250	150,000	14,300

The ANSYS model used in the side drop and corner drop spacer disc stress and stability evaluations provided in Appendix 2.10.4 (Figure 2.10.4-9) conservatively represent the support plate restraint as a single pinned point. This assumed boundary condition is not affected by the different weld options, and further evaluation of the side drop is not required.

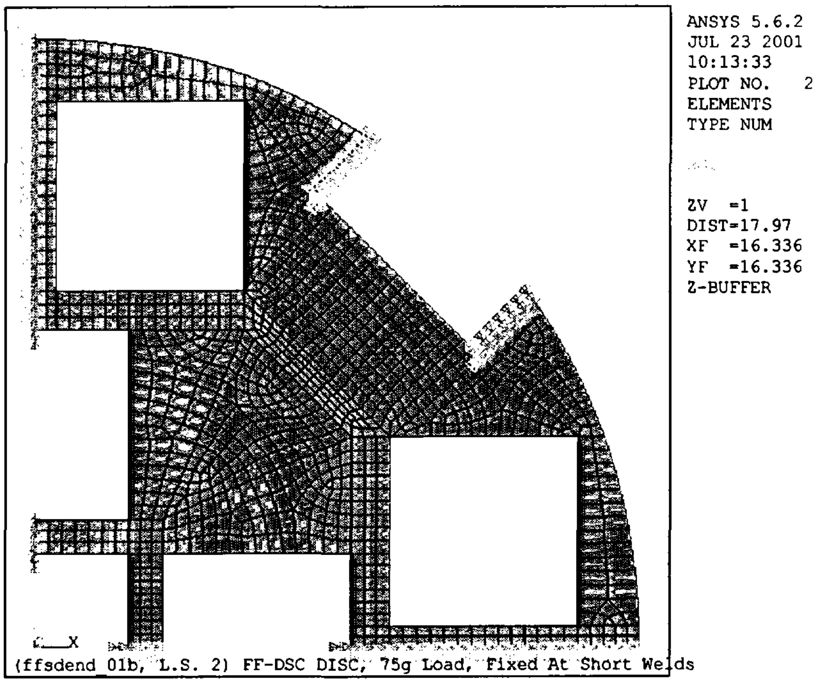

Figure 2.10.13-1. Boundary Conditions (Support Plate Welded on 2 Short Sides)

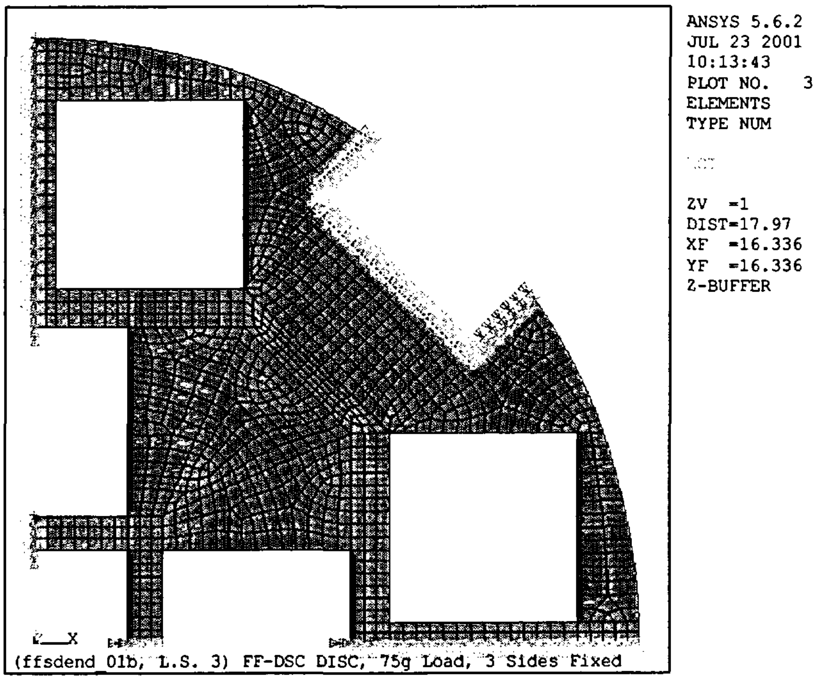

Figure 2.10.13-2. Boundary Conditions (Support Plate Welded on 3 Sides)

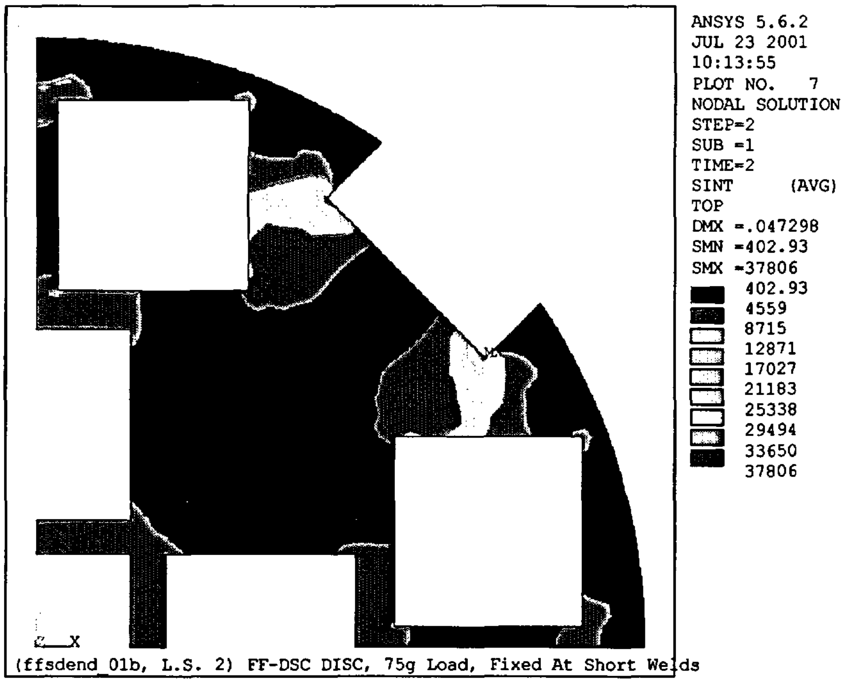

Figure 2.10.13-3. 75g End Drop P_m+P_b Stress Int. (2 Support Plate Welds)

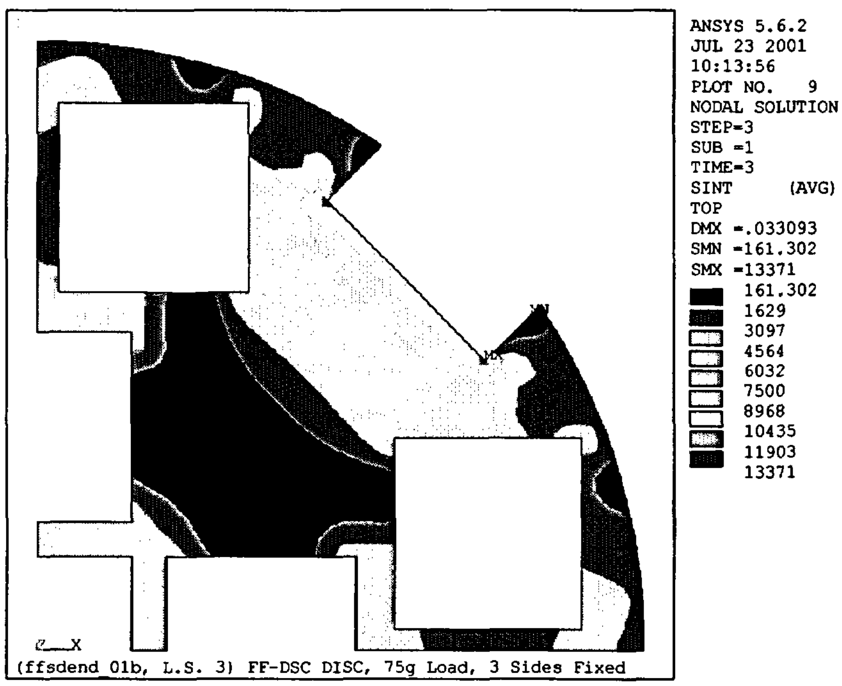

Figure 2.10.13-4. 75g End Drop P_m+P_b Stress Int. (psi) (3 Support Plate Welds)

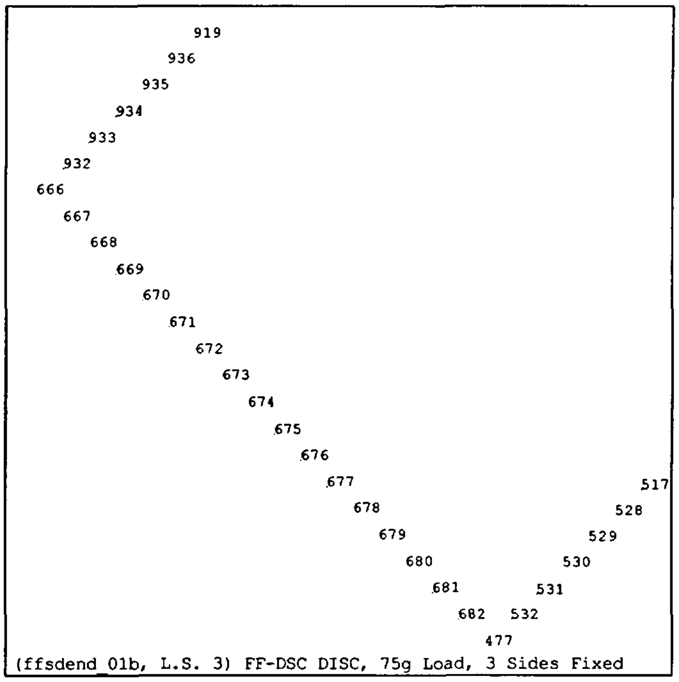

Figure 2.10.13-5. Weld Node Numbers

2.10.13.7 FF-DSC Anti-Rotation Key Analyses

The following analysis of the DSC shell-to-basket basket key follows that of Section 2.6.11.3.4, with the exception of the loading. The original analysis used a bounding loading from the FC DSC; this analysis is done only for the loading associated with the FF-DSC.

The key is welded to the inner wall of the DSC shell and mates with a slot on the outer circumference of the top spacer disc. For each DSC, two keys of this type are provided, spaced at 180 degrees. This pair of keys prevents rotation of the basket assembly within the DSC. Material properties and allowables below are used for the evaluation of stress in the keys. The maximum DSC shell temperature under normal conditions of transport is 400 °F.

For SA-240 Type 304 (or SA-479 Type 304) at 400°F:

$$S_Y = 20.7 \text{ ksi}$$

$$S_U = 64.4 \text{ ksi}$$

Allowable Shear Stress per NF-3320:

$$F_v = 0.4S_Y$$
$$= 8.3 \text{ ksi}$$

Allowable Plate Bending Stress per NF-3320:

$$F_b = 0.75S_Y$$
$$= 15.5 \text{ ksi}$$

Allowable Bearing Stress per NF-3320:

$$F_p = 0.9S_Y$$
$$= 18.6 \text{ ksi}$$

The welds are analyzed to the criteria of subsection NF. For fillet welds, Table NF-3324.5(a)-1 [2.2] provides the allowable stresses in the weld material and the base metal.

Therefore, S_U (weld metal) = 70 ksi [Table NF-3324.5(a)-1]

$$F_W \text{ (weld)} = 0.3\,S_U \text{ (weld metal)}$$

$$= 0.3(70) = 21 \text{ ksi}$$

$$F_W \text{ (base)} = 0.4\,S_Y$$

$$= 0.4(20.7) = 8.3 \text{ ksi}$$

The rotational moment of the FF-DSC:

The total weight of the fuel, W_{FF} = 19,946 lb (20 kip)

$$M_{FF} = 10\%(W_{FF})(2\text{ g})(CG_{FF})$$

$$= 0.1(20)(2)(13.34)$$

$$= 53.4 \text{ in-kip}$$

The two basket shear keys are located on the inside wall of the DSC shell, spaced 180 degrees apart. The keys mate with slots in the top spacer disc. The configuration of the basket key for the FF-DSC is 2-inches thick. The spacing diameter between the two keys is

$$d = 67.19 - 2(0.625) - 0.75$$

$$= 65.19 \text{ inches}$$

The shear reaction at each key to restrain rotation,

$$V_{FF} = M_{FF} / d$$

$$= 53.4 / 65.19$$

$$= 0.82 \text{ kip}$$

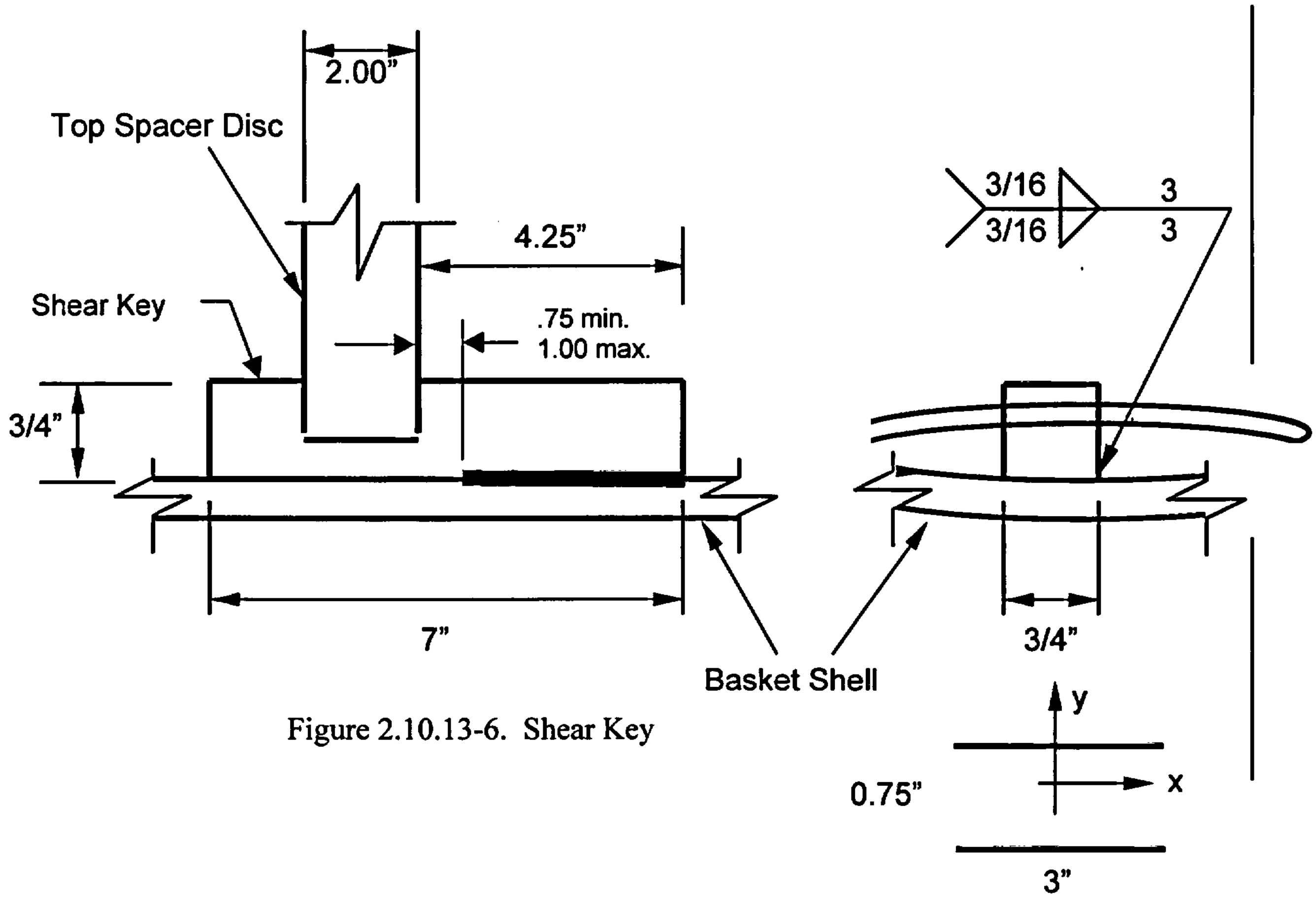

Figure 2.10.13-6. Shear Key

The welds have the highest stress ratio and therefore is the only portion evaluated.

A = 2(3) = 6 inches

S_x = 3(0.75) = 2.25 in^2

J = $[(3)^3 + 3(3)(0.75)^2]/6$ = 5.34 in^3

Shear, V = 0.82 kip

Moment, M = 0.82(0.75) (conservative moment arm)

= 0.62 in-kip

Torsion, T = 0.82(0.25 + 1.0 + 1.5) Conservatively taken from the mid-point of the weld to the shear reaction point taken as ¼ inch into the spacer disc from the face of the disc.

= 2.26 in-kip

Weld stresses,

$f_x = T(0.375)/J = 0.159$ kip/in

$f_y = V/A + T(1.5)/J = 0.771$ kip/in

$f_z = M/S_x = 0.276$ kip/in

$f_w = (f_x^2 + f_y^2 + f_z^2)^{1/2} = 0.83$ kip/in

Allowable stress,

$F_w = 0.4(20.7)(3/16) = 1.55$ kip/in (base metal, controls)

$= 0.3(70)(0.707)(3/16) = 2.78$ kip/in (weld metal)

Stress ratio, $f_w/F_w = 0.54 < 1.0$ ∴ ok

The bending stress in the key is determined by taking the bending arm as the distance from the start of the weld to the reaction point ¼ inch into the spacer disc from the face of the spacer disc.

$M_b = (0.82)(1.0 + 0.25) = 1.025$ in-kip

S (section modulus) $= b(t)^2/6$

$= (0.75)(0.75)^2/6$

$= 0.0703$ in^3

$$F_b = M_b/S$$

$$= 1.025/0.0703$$

$$= 14.6 \text{ ksi}$$

The allowable stress is 15.5 ksi which is greater than 14.6 ksi $\therefore$ ok

2.10.13.8 Finite Element Analysis Input Files

THIS SECTION CONTAINS
PROPRIETARY INFORMATION

3. THERMAL EVALUATION

Thermal analyses for the 10CFR71 [3.1] normal conditions of transport and hypothetical accident conditions are presented for the NUHOMS®-MP187 Package.

The purpose of the thermal analyses presented herein is to demonstrate that the NUHOMS®-MP187 Cask with the NUHOMS® DSC provides suitable heat dissipation under the 10CFR71 [3.1] normal conditions of transport and hypothetical accident conditions.

3.1 Discussion

The thermal cases considered include the extreme ambient conditions with enveloping solar heat flux, and the sustained fire and post-fire equilibrium conditions. The 10CFR71 normal conditions of transport and hypothetical accident transient analyses are performed using the HEATING7.2 computer program [3.2, 3.16]. The resulting temperatures for the NUHOMS®-MP187 Package components are used in Chapter 2 for the structural evaluation, and in this Chapter to confirm that the fuel clad temperatures are within the acceptable limits.

The thermal analyses results show that the maximum temperatures and pressures of the NUHOMS®-MP187 Package are within allowable material temperature and pressure limits.

3.1.1 Thermal Load Case Definition

The following heat transfer cases are considered. Details of the normal and hypothetical accident condition analyses are presented in Sections 3.4 and 3.5, respectively.

A) Steady state analysis at an ambient temperature of 100°F with solar insolation and payload decay heat load. (Note: An additional case for pre-fire conditions is evaluated at 100°F with payload decay heat load without solar insolation per 10CFR71.73(c)(3)[3.1]).

B) Steady state analysis at an ambient temperature of -40°F with payload decay heat load without solar insolation.

C) A free cask drop and puncture (crushed impact limiter with a 12 inch segment over the cask top seal area torn) followed by a 30 minute exposure to a 1475°F fire thermal radiation environment having an emissivity of 0.9 with payload decay heat load.

D) A free cask drop and puncture (the foam and honeycomb portions of impact limiter detached from the cask and only the impact limiter inner shell present) followed by a 30 minute exposure to a 1475°F fire thermal radiation environment having an emissivity of 0.9 with payload decay heat load.

E) Undamaged impact limiter followed by a 30 minute exposure to a 1475°F fire thermal radiation environment having an emissivity of 0.9 with payload decay heat load.

The fire accident boundary conditions initiate at steady state conditions without solar insolation. After 30 minutes the thermal boundary is returned to a 100°F ambient air condition as specified in 10CFR71.73(c)[3.1]. The transient is then continued for a time sufficient to determine maximum values for all temperatures within the cask and DSC. The cask is allowed to reach steady state after the post-fire case to obtain the final steady state thermal conditions.

3.1.2 Thermal Design Criteria

During shipment, the NUHOMS®-MP187 Cask contains one of the three DSC types described in Chapter 1. The FO-DSC and the FC-DSC each contain 24 intact PWR fuel assemblies. The FF-DSC contains 13 potentially damaged fuel assemblies. The maximum design basis decay heat utilized in the thermal analysis per DSC containing 24 intact fuel assemblies including the control components is 13.5 kW. The fuel assemblies in the FO-DSC do not have the control components, so their decay heat is bounded by the decay heat of the FC-DSC. The maximum design basis decay heat utilized in the thermal analysis per DSC containing 13 potentially damaged fuel assemblies is 9.93 kW. Other fuel having varied thermal characteristics will be licensed by amendment to the certificate of compliance for this package.

Using a peaking factor of 1.2 to account for axial power peaking during irradiation [3.3], the total decay heat per DSC considered is 13.5*1.2 = 16.2 kW for the DSC containing 24 intact fuel assemblies and 9.93*1.2 = 11.9 kW for the DSC containing 13 potentially damaged fuel assemblies.

The maximum fuel cladding temperature criteria for the design basis PWR fuel is 570°C which provides sufficient margin to ensure that cladding failure by creep rupture will not occur for all design basis conditions. This 570°C temperature limit is based on the data presented in Figure 3.1-1 [3.3]. Section 3.3 describes the technical specification limits for NUHOMS®-MP187 Package materials. Table 3.5-5 compares the design criteria of the MP187 package with the calculated values.

The maximum normal conditions of operation internal pressure (MNOP) in the cask internal cavity with 100% of fuel rods ruptured is 46.2 psia as discussed in Section 3.4.4. The design pressure of the MP187 Cask cavity is 64.7 psia (50.0 psig).

3.1.3 Results of Design Basis Thermal Analyses

The analytical results obtained from evaluating the design basis conditions are summarized in Table 3.1-1. The normal conditions of transport (NOC), 30-minute fire transient (FIRE), 10-hour postfire transient (POSTFIRE), and postfire equilibrium (final steady state) conditions are included in Table 3.1-1.

Table 3.1-1

Design Basis Thermal Analysis Results

Maximum Parameter Value	NOC	30-Minute Fire	10-Hour Postfire	Final Steady State	Material Temperature Limit (NOC/HAC)
Ambient Temp., (°F)	100	1475	100	100	n/a
DSC Shell Temp., (°F)	400	368	401	564	2552/2552
Fuel Clad Temp., (°F)	669	<790	<790	790	1058/1058
Cask Inner Shell Temp., (°F)	302	260	340	508	2552/2552
Cask Outer Surface Temp., (°F)(1)	207	1291	252	296	2552/2552
Neutron Shield Temp., (°F)	258	1284	320	481	n/a/n/a
Cask Lead Temp., (°F)	300	320	339	506	621/621
Foam Temp., (°F)	285	1460	273	435	300/n/a
Honeycomb Temp., (°F)	191	1375	286	404	1221/n/a
Top Closure Seal Temp., (°F)	254	243	289	352	600/600
Ram Closure Seal Temp., (°F)	283	246	271	445	600/600
Drain Port Seal Temp., (°F)	249	444	284	417	700/700
Cask Internal Pressure, Intact Fuel Rods, (Psia)	22.5	21.5	23.0	27.6	64.7/64.7
Cask Internal Pressure With All Rods Rupture, (Psia)	46.2	44.0	47.3	56.7	64.7/64.7

n/a: See Table 3.5-5 for hypothetical accident condition (HAC) limits.

(1) Neutron shield jacket surface temperature.

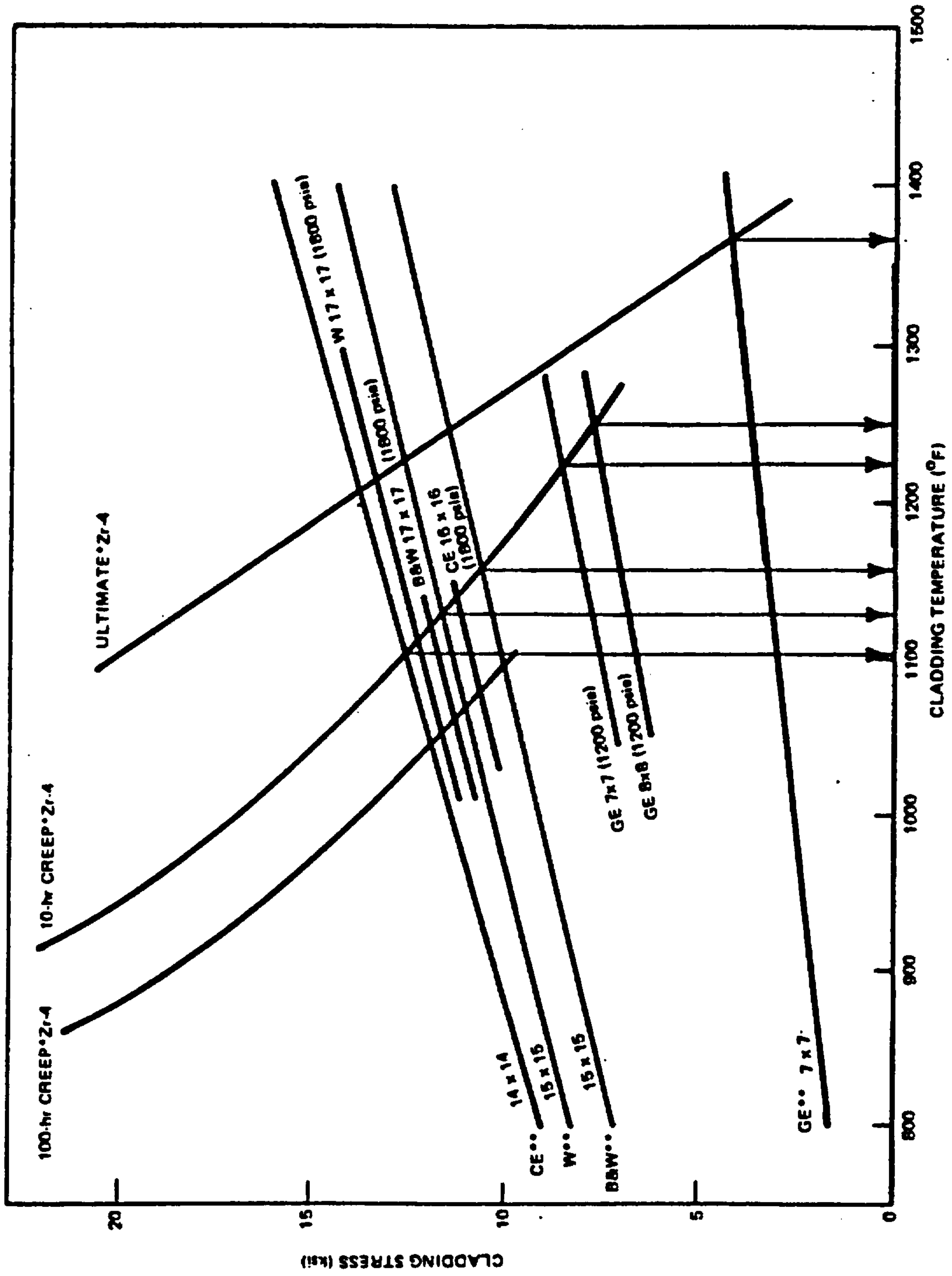

Figure 3.1-1

Zircaloy Cladding Perforation Temperatures [3.3]

3.2 Summary of Thermal Properties of Materials

The NUHOMS®-MP187 Cask is fabricated primarily of stainless steel, lead, and borated cementitious neutron shielding material. The impact limiter materials are polyurethane foam and aluminum honeycomb. The void spaces within the DSC are filled with inert gas (helium, although no credit is taken for heat removal by helium). Air is assumed to fill the annulus between the DSC outer shell and cask inner shell during transportation. Table 3.2-1 documents the thermal properties used in the analytic models.

3.2.1 Thermophysical Properties of Materials

The thermal properties of stainless steel types utilized in the cask are very similar. Therefore, the thermal properties of stainless steel Type 304 are used for these materials in the thermal analysis. The thermal properties of carbon steel types which may be utilized in the cask as optional spacer disk materials are very similar. Therefore, the thermal properties of carbon steel ASME SA-537 CL2 [3.4] are used for these materials in the thermal analysis.

3.2.1.1 Impact Limiter Foam

3.2.1.1.1 Uncrushed Foam

The foam density used in the thermal analysis of the impact limiter material is 15.0 lbm/ft^3 (pcf). Minor changes in the foam density, and hence the thermal conductivity, will have negligible impact on the thermal analysis results because of the large difference between the thermal conductivity of the foam and the other cask components. The thermal conductivity and specific heat corresponding to this foam density are 0.0273 Btu/hr-ft-°F and 0.375 Btu/lbm-°F, respectively [3.9, 3.11].

3.2.1.1.2 Crushed Foam

The maximum crush depth of the impact limiter material is assumed to be 75% for the worst drop conditions. Therefore, the accident condition thermal analysis is based on the conservative assumption of damage to the impact limiter due to both the side drop and end drop conditions. Even though the maximum damage to the impact limiter materials is only expected to occur on the impacted portion of the impact limiter, to be conservative during the fire transient, the entire impact limiter is assumed to sustain this damage. Also, to be conservative during the fire transient, this damage is assumed for both the top end and bottom end impact limiters. The density of the crushed foam based on the maximum drop damage is 45 pcf. The thermal conductivity corresponding to this crushed foam density is 0.052 Btu/hr-ft-°F [3.9]. The specific heat for the crushed foam is assumed to be the same as the pre-crushed value.

The impact limiter foam portion has 12 stainless steel tubes to accommodate the impact limiter attachment bolts. The total volume of the stainless steel in these tubes is 0.38 ft^3 based on 2.5 in. o.d., 52.125 in. length and 0.14 in. thickness. The volume of the crushed foam is calculated to be 51 ft^3. Using a volume average, the effective thermal conductivity of the crushed foam with tubes is 0.13 Btu/hr-ft-°F.

The charring of the foam starts at a temperature of approximately 500°F [3.9, 3.10]. The foam weight loss data during fire testing shows that there is very little foam weight loss up to 500°F, 55 percent foam weight loss up to 750°F, and 65 percent foam weight loss up to 1000°F [3.9]. In the transient thermal analysis for fire conditions, the density of the foam is reduced accordingly. The temperatures in the foam during the 30 minute fire transient are calculated assuming the thermal conductivity of uncharred foam. This is conservative because charring blocks heat flow to the cask via heat absorbed in change of phase and also due to lower thermal conductivity of charred compared with that of uncharred foam. During the post-fire transient in the thermal models the thermal conductivity of uncharred foam is used up to a temperature of 500°F and the thermal conductivity of air is used for charred foam at a temperature of 1000°F assuming that the charring is complete at a temperature of 1000°F. The thermal conductivity of the charred foam is assumed to be 0.032 Btu/hr-ft-°F based on the thermal conductivity of the air from Reference [3.6].

3.2.1.2 2 w/o B_4C/NS-3 with Stiffeners During NOC and HAC

3.2.1.2.1 2 w/o B_4C/NS-3 with Stiffeners During NOC

In the thermal analysis during NOC, to be conservative, no credit is taken for the heat removed by the 2 w/o B_4C/NS-3. It is assumed to be replaced by air throughout the NOC.

The neutron shield cavity contains 24 stiffeners made from 0.12 in. Stainless Steel Type 304, and 1/8 in. aluminum. The effective thermal conductivity of 2 w/o B_4C/NS-3 with stiffeners during NOC is calculated using the "series and parallel conductors" analogy from electrical resistors method. No contact is assumed between the aluminum stiffeners and the cask outer shell. The stainless steel stiffeners are welded to the neutron shield jacket. However, in the thermal analysis no credit is taken for the presence of the welds. No contact is assumed between the neutron shield jacket and stainless steel/aluminum stiffeners. The geometry assumed for calculating the effective thermal conductivity of material in the neutron shield cavity is shown in Figure 3.2-1. The results are summarized in Table 3.2-1.

3.2.1.2.2 2 w/o B_4C/NS-3 with Stiffeners During 30-Minute FIRE Transient

From Reference [3.12], when NS-3 material was heated in a furnace to a temperature of 1300°F ± 100°F (50 minutes to get to 1300°F) for a period of one hour, the weight loss from NS-3 was 41 percent. A white smoke started to come out of the furnace at a temperature of 600°F and continued for the duration of the test. At the end of the test, the NS-3 was solid (consisting of inorganic constituents), it did not burn, and was brittle with no mechanical strength.

The effective thermal conductivity of 2 w/o B_4C/NS-3 with stiffeners during 30-minute FIRE transient is calculated using the "series and parallel conductors" analogy from electrical resistors method similar to the NOC method described in Section 3.2.1.2.1 except air is now replaced with 2 w/o B_4C/NS-3. During the 30-minute FIRE transient, to be conservative, 2 w/o B_4C/NS-3 is assumed to be unaffected . This results in more heat input from the fire into the package. The effective thermal conductivity, density, and specific heat of 2 w/o B_4C/NS-3 are calculated as shown below.

A) 2 w/o B_4C/NS-3

The effective thermal conductivity of 2 w/o B_4C/NS-3 is calculated based on the volume percentage. The effective thermal conductivity of the NS-3 with 2 w/o B_4C is calculated using the values given in Table 3.2-1. The thermal conductivity, density, and specific heat of B_4C are 16 Btu/hr-ft-°F, 157.25 lbm/ft^3, and 0.22 Btu/lbm-°F respectively [3.13].

Volume fractions for thermal conductivity and density calculations and weight fractions for specific heat calculation are used.

$V_1 + V_2 = 1.0$ where V_1 and V_2 are the volume fractions of pure NS-3 and 2 w/o B_4C, respectively.

$110V_1 = 0.98W$ and $157.2V_2 = 0.02W$, where W is the total weight of 1 ft^3 of 2 w/o B_4C/NS-3.

Solving for W gives W = 110.665 lbm.

Solving for V_1 and V_2 gives $V_1 = 0.986\%$ and $V_2 = 0.014\%$.

The effective thermal conductivity of 2 w/o B_4C/NS-3 is given by:

$$K_{eff} = 0.986 * (0.4885) + 0.014 * 16.0 = 0.706$$

To calculate the effective specific heat and effective density of 2 w/o B_4C/NS-3 weight fraction and volume fraction averaged method is used which results in effective specific heat of 0.1485 Btu/lbm-°F and effective density of 110.66 lbm/ft^3.

The effective thermal conductivity of 2 w/o B_4C/NS-3 with stiffeners during the 30-minute FIRE transient is calculated using the "series and parallel conductors" analogy from electrical resistors method similar to the NOC method described in Section 3.2.1.2.1 except air is now replaced with 2 w/o B_4C/NS-3. The effective density and specific heat are calculated as shown below.

B) Effective Density and Specific Heat of 2w/o B_4C/NS-3 and SS304/Aluminum Stiffeners

Total volume of the 24 stainless steel stiffeners in the neutron shield cavity is calculated as:

Volume = 3.0 ft^3.

Therefore, the weight of stainless steel stiffeners = 3.0 ft^3 * 493 lbm/ft^3 = 1476 lbs.

Total volume of the 24 Aluminum stiffeners in the neutron shield cavity is calculated as:

Volume = 2.955 ft^3.

Therefore, the weight of Aluminum stiffeners = 2.955 ft^3 * 169.3 lbm/ft^3 = 500 lbs.

The total volume of the neutron shield cavity is calculated as:

$$V = \pi(46.065^2 - 41.75^2)133.5 = 1.589E5\ in^3 = 91.97\ ft^3$$

The volume of 2 w/o B_4C/NS-3 = 91.97 - 3.0- 2.95 = 86.02 ft^3.

Therefore, the weight of B_4C/NS-3 is = 86.02 ft^3 * 110.66 lbm/ft^3 = 9519 lbs.

The Volume fraction of stiffeners = 6.5% and volume fraction of 2 w/o B_4C/NS-3 is 93.5%.

Similarly the weight fractions of Aluminum stiffeners = 4.35%, weight fractions of Stainless Steel stiffeners = 12.8% and weight fraction of 2 w/o B_4C/NS-3 is 82.8%.

A method similar to 2 w/o B_4C/NS-3 is used to calculate the effective density and specific heat of B_4C/NS-3 with stiffeners. The weight fraction averaged method is used which results in effective specific heat of 0.149 Btu/lbm-°F. The volume fraction averaged method is used which results in effective density of 124.4 lbm/ft^3.

In the thermal analysis during the 30 minute fire transient, to be conservative, the thermal conductivity of NS-3 is assumed to be unaffected throughout the 30 minute fire transient. Similarly, during the fire transient, the density of NS-3 is assumed the pre-fire value up to 500°F and then at 1200°F it is assumed to be equal to the density of decomposed NS-3.

3.2.1.2.3 2 w/o B_4C/NS-3 with Stiffeners During POSTFIRE Transient

During postfire conditions even though some portions of NS-3/ B_4C will be present in the neutron shield cavity, to be conservative all of the NS-3/ B_4C is replaced with air and thermal conductivity of air is assumed for NS-3/B_4C. Similarly, aluminum stiffeners will be partially melted, but to be conservative, all of the aluminum stiffeners are assumed melted and replaced with air and the thermal conductivity of air is assumed for aluminum stiffeners. The effective thermal conductivity of material in the neutron shield cavity is calculated using the "series and parallel conductors" analogy from electrical resistors method similar to the NOC method described in Section 3.2.1.2.1 to account for the presence of only the stainless steel stiffeners present in the neutron shield cavity. The results are summarized in Table 3.2-1.

3.2.1.3 Impact Limiter Aluminum Honeycomb

3.2.1.3.1 Uncrushed Aluminum Honeycomb

The density of the uncrushed aluminum honeycomb used in the thermal analysis is 18 lbm/ft^3. Minor changes in the aluminum honeycomb density will have negligible impact on the thermal analysis results. The volume occupied by the aluminum honeycomb portion of the impact limiter is calculated to be 141 ft^3. The weight of the aluminum in this volume occupied by the aluminum honeycomb is 2538 lbs. The volume of the aluminum in the honeycomb is 2538 lbs/169 lbm/ft^3 = 15.0 ft^3. Using volume average, the effective thermal conductivity of the aluminum honeycomb is (15.02 ft^3 * 117 Btu/hr-ft-°F)/141 ft^3 = 12.46 Btu/hr-ft-°F.

3.2.1.3.2 Crushed Aluminum Honeycomb

The maximum crush depth of the impact limiter material is assumed to be 75% for the worst drop conditions. Therefore, the accident condition thermal analysis is based on the conservative assumption of 75% damage to the impact limiter due to worst drop conditions. Even though the maximum damage to the impact limiter materials is only expected to occur on the impacted portion of the impact limiter, to be conservative during fire transient, the entire impact limiter is assumed to have this damage. Also, to be conservative during the fire transient this damage is assumed for the impact limiter on both ends of the cask.

Based on the above assumptions, the volume of the crushed aluminum honeycomb is 29.9 ft^3. Therefore, the density of the crushed aluminum honeycomb based on the maximum drop damage is 2538 lbm/29.86 ft^3 = 85.0 pcf. with the aluminum volume of 15.0 ft^3. The effective thermal conductivity of the crushed aluminum honeycomb is (15.0 ft^3 * 117 Btu/hr-ft-°F)/29.86 ft^3 = 58.85 Btu/hr-ft-°F. In the thermal analysis during the 30 minute fire transient, to be conservative, the crushed aluminum is assumed to be unaffected throughout the 30 minute fire transient. The specific heat for the crushed aluminum honeycomb is assumed to be the same as the pre-crushed value.

During postfire conditions, even though some portions of the aluminum honeycomb will be present in the impact limiters, to be conservative all of the aluminum honeycomb is replaced with air and the thermal conductivity of air is assumed to be that of the air with closed cavity convection [3.14].

3.2.2 Emissivities

The effective emissivity between parallel stainless steel surfaces is given by:

$$\varepsilon_{eff} = \frac{1}{\left(\frac{1}{\varepsilon_1}\right) + \left(\frac{1}{\varepsilon_2}\right) - 1}$$

A) The effective emissivity of the gap between the DSC outer surface and the cask inner surface in the radial and axial directions is given by:

$$\varepsilon_1 = \varepsilon_2 = 0.587 \qquad [3.15]$$

$$\therefore \quad \varepsilon_{eff} = \frac{1}{\dfrac{1}{0.587} + \dfrac{1}{0.587} - 1} = 0.4154$$

$$\therefore \quad \sigma * \varepsilon = 0.4154 * 1.984E\text{-}13 = 8.2412E\text{-}14 \; \frac{Btu}{\text{min-}inch^2 \; {}^\circ R^4}$$

where σ is the Stephen Boltzman constant.

B) The effective emissivity between the impact limiter outside surfaces and ambient (all conditions except 30-minute fire transient) is calculated by assuming all thermal radiation from impact limiter external surfaces is between a small body within a large body. The impact limiter outer surfaces are painted with white paint having an emissivity of 0.9 and an absorptivity of 0.3. The effective emissivity is given by:

$$\varepsilon_1 = 0.9, \varepsilon_{ambient} = 1.0$$

$$\therefore \quad \varepsilon_{eff} = \frac{1}{\dfrac{1}{0.9} + \dfrac{1}{1.0} - 1} = 0.9$$

$$\therefore \quad \sigma * \varepsilon = 0.9 * 1.984E\text{-}13 = 1.786E\text{-}13 \; \frac{Btu}{\text{min-}inch^2 \; {}^\circ R^4}$$

C) The effective emissivity between the crushed impact limiter outside surfaces and ambient for all conditions except 30-minute fire transient is given by:

$$\varepsilon_1 = 0.587, \varepsilon_{ambient} = 1.0 \qquad [3.15]$$

$$\therefore \ \varepsilon_{eff} = \frac{1}{\frac{1}{0.587} + \frac{1}{1.0} - 1} = 0.587$$

$$\therefore \ \sigma * \varepsilon = 0.587 * 1.984E\text{-}13 = 1.1645E\text{-}13 \ \frac{Btu}{\text{min-}inch^2 \ {}^\circ R^4}$$

D) The effective emissivity between the cask outside surfaces and personnel barrier for all conditions except 30-minute fire transient is given by:

$$\varepsilon_1 = \varepsilon_2 = 0.587 \qquad [3.15]$$

$$\therefore \ \varepsilon_{eff} = \frac{1}{\frac{1}{0.587} + \frac{1}{0.587} - 1} = 0.4154$$

$$\therefore \ \sigma * \varepsilon = 0.4154 * 1.984E\text{-}13 = 8.2412E\text{-}14 \ \frac{Btu}{\text{min-}inch^2 \ {}^\circ R^4}$$

E) The effective emissivity between the crushed impact limiter surfaces and ambient for 30-minute fire transient is given by:

$$\varepsilon_1 = \varepsilon_2 = 0.90 \qquad [3.1]$$

$$\therefore \ \varepsilon_{eff} = \frac{1}{\frac{1}{0.9} + \frac{1}{0.9} - 1} = 0.818$$

$$\therefore \ \sigma * \varepsilon = 0.818 * 1.984E\text{-}13 = 1.623E\text{-}13 \ \frac{Btu}{\text{min-}inch^2 \ {}^\circ R^4}$$

3.2.3 Natural Convection Coefficient

Natural Convection from the cask and impact limiter external surfaces is based on standard natural convection relations for horizontal cylinders and vertical heated flat plates as given below [3.6]:

$$h_{cyl} = 0.18\,(\Delta\, T)^{1/3}$$

$$h_{plate} = 0.19\,(\Delta\, T)^{1/3}$$

These correlations are used in the HEATING7.2 [3.2, 3.16] analytical models to calculate the natural convection coefficients.

3.2.4 Forced Convection Coefficient

Forced Convection is considered during the fire conditions under 10CFR71 requirements during the hypothetical accident conditions. It is assumed that the flame velocity during fire produces significant forced convection heat transfer from the fire to the package. Churchill and Bernstein [3.26] have proposed a single comprehensive equation for the forced convection heat transfer that covers the entire range of Reynolds numbers, Re_D, and a wide range of Prandtl numbers (Pr). The equation is recommended for all $Re_D\,Pr > 0.2$, where all properties are evaluated at the film temperature. The equation for the forced convection heat transfer coefficient (h_c) is:

$$Nu_D = \frac{h_c \cdot D}{K} = \frac{0.62 \cdot {Re_D}^{1/2} \cdot Pr^{1/3}}{\left[1+\left(\frac{0.4}{Pr}\right)^{2/3}\right]^{1/4}} \cdot \left[1+\left(\frac{Re_D}{282{,}000}\right)^{1/2}\right] \qquad [3.26]$$

where, $Re_D = \frac{V \cdot D}{\nu}$. The parameter, V, is defined as the flame speed velocity which is conservatively assumed to be 15 meters per second per Reference [3.28]. D is the diameter of the MP187 Cask. A diameter of 83.50 inches is used as the diameter of the package which corresponds to the cask structural shell region. Conservatively, no credit for the neutron shielding material jacket and impact limiters is assumed. Parameters ν and K are kinematic viscosity and thermal conductivity, respectively.

When calculating the heat transfer coefficient, all properties are evaluated conservatively at surface temperature. The results of the calculations are summarized in Table 3.2-3. The values of forced convection heat transfer coefficient as a function of temperature is used during the 30 minute fire transient to account for heat transfer due to flame velocities to the package.

The thermal properties of air used in the calculations for the forced convection heat transfer coefficient are given in Table 3.2-2 [3.27].

Table 3.2-1

Thermal Properties of Materials

MATERIAL	TEMPERATURE (°F)	DENSITY (LBS./IN^3)	SPECIFIC HEAT, C_p (Btu/lb.°F)	THERMAL CONDUCTIVITY, K (Btu/min.in.°F)
ASME SA-240 Type 304 Stainless Steel [3.4, 3.5]	70	0.2853	0.125	0.0119
	100	-	-	0.0121
	150	-	-	0.0125
	200	-	-	0.0129
	250	-	-	0.0133
	300	-	-	0.0136
	350	-	-	0.0140
	400	-	-	0.0144
	450	-	-	0.0147
	500	-	-	0.0151
	550	-	-	0.0154
	600	-	-	0.0157
	650	-	-	0.0161
	700	-	-	0.0164
	750	-	-	0.0164
	800	-	-	0.0169
	850	-	-	0.0174
	900	-	-	0.0176
	950	-	-	0.0179
	1000	-	-	0.0183
	1050	-	-	0.0186
	1100	-	-	0.0189
	1150	-	-	0.0192
	1200	-	-	0.0194
	1250	-	-	0.0199
	1300	-	-	0.0201
	1350	-	-	0.0204
	1400	-	-	0.0207
	1450	-	-	0.0210
	1500	-	-	0.0213
Lead [3.6]	32	0.411	0.032	0.028
	212	-	-	0.027
	572	-	-	0.024

Table 3.2-1

Thermal Properties of Materials

(continued)

MATERIAL	TEMPERATURE (°F)	DENSITY (LBS./IN^3)	SPECIFIC HEAT, C_p (Btu/lb.°F)	THERMAL CONDUCTIVITY, K (Btu/min.in.°F)
Carbon Steel [3.5]	70	0.2853	0.125	0.0328
	100	-	-	0.0332
	150	-	-	0.0336
	200	-	-	0.0339
	300	-	-	0.0339
	400	-	-	0.0336
	500	-	-	0.0329
	600	-	-	0.0321
	700	-	-	0.0311
	800	-	-	0.0301
	900	-	-	0.0290
	1000	-	-	0.0278
Air [3.6]	0	4.977E-5	0.239	1.847E-5
	32	4.688E-5	0.240	1.944E-5
	100	4.109E-5	0.240	2.139E-5
	200	3.472E-5	0.241	2.417E-5
	300	3.009E-5	0.243	2.681E-5
	400	2.662E-5	0.245	2.944E-5
	500	2.384E-5	0.247	3.208E-5
	1000	1.568E-5	0.262	4.431E-5
Al Honeycomb [3.6]	-	0.01042	0.21	0.01733
Crushed Al Honeycomb [Section 3.2.1.1]	100	0.049	0.21	0.082
	300	0.049	0.21	0.082
	400	0.049	0.21	0.082
	500	0.049	0.21	0.082
	1221	0.049	0.21	0.082
Foam [3.9]	-	0.0087	0.375	3.792E-5
Crushed Foam [3.9, Section 3.2.1.1]	100	0.026	0.375	1.810E-4
	300	0.026	0.375	1.810E-4
	500	0.026	0.375	1.810E-4
	750	0.0117	0.375	1.810E-4
	1000	0.0091	0.375	1.810E-4
	1200	0.0091	0.375	1.810E-4

Table 3.2-1

Thermal Properties of Materials

(continued)

MATERIAL	TEMPERATURE (°F)	DENSITY (LBS./IN^3)	SPECIFIC HEAT, C_p (Btu/lb.°F)	THERMAL CONDUCTIVITY, K (Btu/min.in.°F)
Helium [3.17]	45	N/A	N/A	1.1535E-4
	80	-	-	1.2032E-4
	98	-	-	1.2281E-4
	152	-	-	1.2996E-4
	206	-	-	1.3710E-4
	260	-	-	1.4408E-4
	296	-	-	1.4874E-4
	350	-	-	1.5628E-4
	404	-	-	1.6423E-4
	458	-	-	1.7258E-4
	495	-	-	1.7820E-4
	549	-	-	1.8703E-4
	603	-	-	1.9505E-4
	657	-	-	2.0388E-4
	693	-	-	2.0950E-4
	747	-	-	2.1592E-4
	801	-	-	2.2315E-4
	855	-	-	2.3037E-4
	891	-	-	2.3438E-4
	909	-	-	2.3679E-4
	945	-	-	2.4161E-4
	1017	-	-	2.5044E-4
	1071	-	-	2.5766E-4
	1125	-	-	2.6408E-4
	1197	-	-	2.7291E-4
	1251	-	-	2.8014E-4
	1341	-	-	2.9138E-4
	1431	-	-	3.0181E-4
	1520	-	-	3.1225E-4
Aluminum [3.4] and [3.25]	32	0.18715	0.098	0.23
	70	0.18486	-	-
	100	0.18306	-	-
	150	0.18056	-	-
	200	0.17847	-	-
	250	0.17681	-	-
	300	0.17528	-	-

Table 3.2-1

Thermal Properties of Materials

(concluded)

MATERIAL	TEMPERATURE (°F)	DENSITY (LBS./IN^3)	SPECIFIC HEAT, C_p (Btu/lb.°F)	THERMAL CONDUCTIVITY, K (Btu/min.in.°F)
NS-3 with B_4C NOC [Section 3.2.1.2]	32	0.012	0.152	1.19E-03
	70	0.012	0.152	1.21E-03
	100	0.012	0.152	1.23E-03
	150	0.012	0.152	1.27E-03
	200	0.012	0.152	1.30E-03
	250	0.012	0.152	1.33E-03
	300	0.012	0.152	1.36E-03
NS-3 with B_4C FIRE [Section 3.2.1.2]	32	0.072	0.149	3.38E-03
	70	0.072	0.149	3.36E-03
	100	0.072	0.149	3.35E-03
	150	0.072	0.149	3.33E-03
	200	0.072	0.149	3.31E-03
	250	0.072	0.149	3.30E-03
	300	0.072	0.149	3.29E-03
	500	0.072	0.149	3.29E-03
	1200	0.072	0.149	3.29E-03
NS-3 with B_4C POSTFIRE [Section 3.2.1.2]	32	0.0093	0.125	1.77E-04
	70	0.0093	0.125	1.81E-04
	100	0.0093	0.125	1.85E-04
	150	0.0093	0.125	1.92E-04
	200	0.0093	0.125	1.99E-04
	250	0.0093	0.125	2.05E-04
	300	0.0093	0.125	2.11E-04
	500	0.0093	0.125	2.11E-04
	1200	0.0093	0.125	2.11E-04
FUEL [3.20]	400	0.397	0.055	2.222E-3
	500	-	-	2.917E-3
	600	-	-	3.610E-3
	700	-	-	4.440E-3
	800	-	-	5.417E-3
	900	-	-	6.258E-3
AIR With Convection [3.14]	-	2.900E-5	0.24	1.389E-4

N/A = not required for steady state analysis

Table 3.2-2

Thermal Properties of Air Used for Forced Convection

Coefficient Calculations

Material	Temperature (°F)	Kinematic Viscosity (m^2/s)	Conductivity (W/m-K)	Pr
Air [3.27]	44	1.39E-05	2.45E-02	0.721
	62	1.48E-05	2.52E-02	0.72
	80	1.57E-05	2.59E-02	0.719
	98	1.67E-05	2.65E-02	0.719
	116	1.76E-05	2.72E-02	0.719
	134	1.86E-05	2.79E-02	0.719
	152	1.96E-05	2.85E-02	0.719
	170	2.06E-05	2.92E-02	0.719
	188	2.16E-05	2.98E-02	0.719
	206	2.27E-05	3.04E-02	0.719
	224	2.38E-05	3.11E-02	0.719
	242	2.49E-05	3.17E-02	0.719
	260	2.60E-05	3.23E-02	0.719
	278	2.72E-05	3.30E-02	0.719
	296	2.83E-05	3.36E-02	0.719
	314	2.95E-05	3.42E-02	0.718
	332	3.07E-05	3.48E-02	0.718
	350	3.19E-05	3.55E-02	0.718
	368	3.30E-05	3.61E-02	0.718
	386	3.42E-05	3.67E-02	0.718
	404	3.55E-05	3.73E-02	0.718
	422	3.68E-05	3.79E-02	0.718
	440	3.81E-05	3.85E-02	0.718
	476	4.07E-05	3.98E-02	0.718
	512	4.33E-05	4.10E-02	0.718
	548	4.62E-05	4.22E-02	0.718
	584	4.90E-05	4.34E-02	0.718
	620	5.17E-05	4.46E-02	0.718
	656	5.46E-05	4.58E-02	0.718
	692	5.77E-05	4.70E-02	0.718
	728	6.08E-05	4.82E-02	0.717
	764	6.39E-05	4.95E-02	0.717
	800	6.70E-05	5.07E-02	0.717
	836	7.04E-05	5.19E-02	0.716
	872	7.36E-05	5.31E-02	0.716
	908	7.69E-05	5.44E-02	0.716
	944	8.04E-05	5.56E-02	0.716
	980	8.38E-05	5.68E-02	0.716
	1016	8.73E-05	5.80E-02	0.715
	1052	9.09E-05	5.92E-02	0.715
	1088	9.45E-05	6.03E-02	0.715

Table 3.2-2

Thermal Properties of Air Used for Forced Convection

Coefficient Calculations

(concluded)

Material	Temperature (°F)	Kinematic Viscosity (m^2/s)	Conductivity (W/m-K)	Pr
	1124	9.82E-05	6.15E-02	0.715
	1160	1.02E-04	6.27E-02	0.715
	1196	1.06E-04	6.39E-02	0.715
	1232	1.09E-04	6.50E-02	0.714
	1268	1.13E-04	6.62E-02	0.714
	1304	1.17E-04	6.73E-02	0.714
	1340	1.21E-04	6.84E-02	0.714
	1430	1.31E-04	7.11E-02	0.714
	1520	1.42E-04	7.38E-02	0.715

Table 3.2-3

Forced Convection Heat Transfer Coefficient as a function of Temperature

Temperature (°F)	Reynolds Number $Re_{,D}$	Nusselt Number $Nu_{,D}$	Forced Convection Heat Transfer Coefficient, h_c (Btu/min-in^2 °F)
44	2.29E+06	2849.2	6.71E-04
62	2.15E+06	2695.1	6.53E-04
80	2.02E+06	2554.5	6.36E-04
98	1.91E+06	2426.9	6.18E-04
116	1.81E+06	2319.7	6.06E-04
134	1.71E+06	2210.7	5.93E-04
152	1.62E+06	2109.7	5.78E-04
170	1.54E+06	2024.4	5.68E-04
188	1.47E+06	1944.9	5.57E-04
206	1.40E+06	1863.2	5.44E-04
224	1.34E+06	1794.0	5.36E-04
242	1.28E+06	1728.8	5.27E-04
260	1.23E+06	1667.7	5.18E-04
278	1.17E+06	1604.4	5.09E-04
296	1.12E+06	1550.4	5.01E-04
314	1.08E+06	1498.6	4.93E-04
332	1.04E+06	1450.4	4.85E-04
350	9.98E+05	1404.8	4.79E-04
368	9.65E+05	1366.0	4.74E-04
386	9.30E+05	1324.8	4.67E-04
404	8.96E+05	1285.7	4.61E-04
422	8.65E+05	1248.5	4.55E-04
440	8.35E+05	1213.1	4.49E-04
476	7.83E+05	1150.8	4.40E-04
512	7.35E+05	1093.5	4.31E-04
548	6.89E+05	1038.6	4.21E-04
584	6.50E+05	990.5	4.13E-04
620	6.16E+05	948.6	4.07E-04
656	5.83E+05	907.8	4.00E-04
692	5.52E+05	869.6	3.93E-04
728	5.23E+05	833.7	3.86E-04
764	4.98E+05	801.0	3.81E-04
800	4.75E+05	772.0	3.76E-04
836	4.52E+05	742.7	3.70E-04
872	4.32E+05	717.6	3.66E-04
908	4.14E+05	693.6	3.63E-04
944	3.95E+05	669.7	3.58E-04
980	3.79E+05	648.7	3.54E-04

Table 3.2-3

Forced Convection Heat Transfer Coefficient as a function of Temperature

(Concluded)

Temperature (°F)	Reynolds Number $Re_{,D}$	Nusselt Number $Nu_{,D}$	Forced Convection Heat Transfer Coefficient, h_c (Btu/min-in^2 °F)
1016	3.64E+05	628.3	3.50E-04
1052	3.50E+05	609.3	3.47E-04
1088	3.37E+05	591.6	3.43E-04
1124	3.24E+05	574.5	3.40E-04
1160	3.12E+05	558.4	3.36E-04
1196	3.01E+05	544.2	3.34E-04
1232	2.91E+05	529.2	3.31E-04
1268	2.80E+05	515.2	3.28E-04
1304	2.71E+05	502.0	3.25E-04
1340	2.62E+05	490.1	3.22E-04
1430	2.42E+05	461.5	3.15E-04
1520	2.24E+05	436.8	3.10E-04

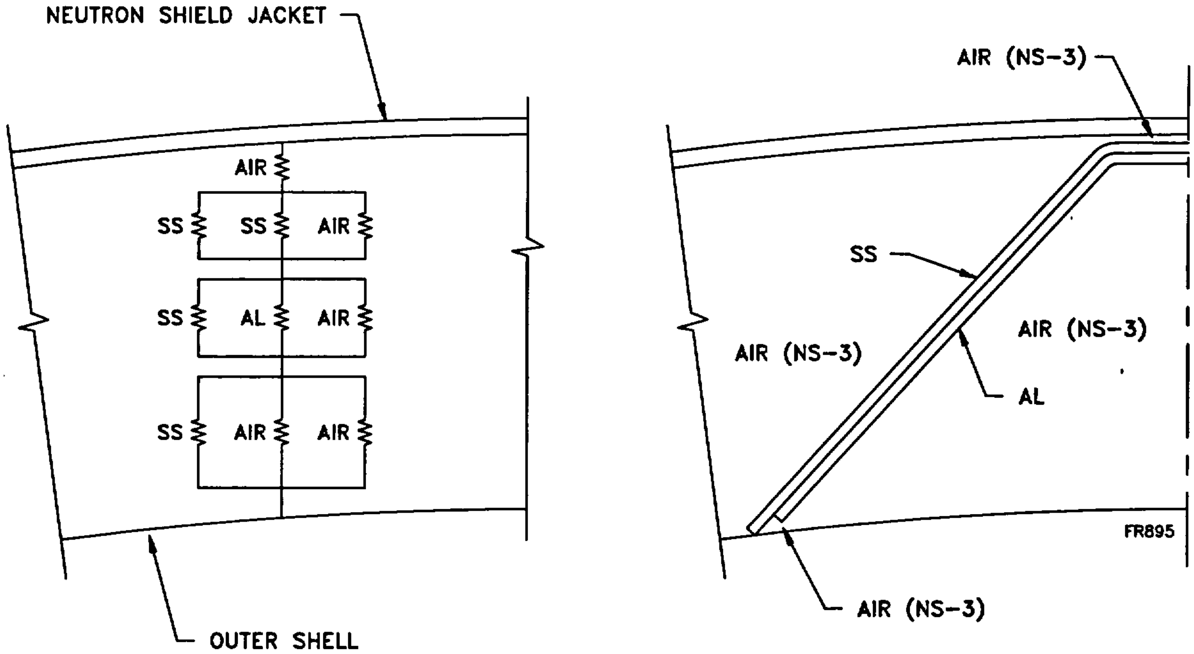

Figure 3.2-1

Series and Parallel Conductors Geometry Used for NS-3/B_4C with Stiffeners

3.3 Technical Specifications for Components

The materials used in the NUHOMS®-MP187 Package which are considered to be temperature sensitive are the metallic O-ring seals, neutron shielding material, aluminum stiffeners in the neutron shield cavity and the polyurethane foam and aluminum honeycomb used in the impact limiters. The metallic O-rings have an allowable temperature range of -450°F to 600°F for the Ram Closure Plate and Top Closure Plate Seal Material [3.23], and -450°F to 700°F for the drain and vent port seal material [3.21]. Manufacturer's recommendations for the neutron shielding material indicate acceptability of long term exposures at temperatures up to 250°F as well as short term excursions to 300°F. Low temperatures are considered to be of little consequence for the cementitious neutron shielding material. The recommended temperature range for the polyurethane foam used for the impact limiter is -30°F to 300°F and charring of foam will start at approximately 500°F, per manufacturer's recommendations [3.9, 3.10]. In addition, temperature excursions to -40°F for the foam will not permanently degrade its properties. The aluminum honeycomb material and aluminum stiffeners in the neutron shield cavity have a melting point of 1221°F [3.17].

Other Cask/DSC materials are stainless steel, lead, and carbon steel. The melting point for these materials are 2552°F, 621°F, and 2606°F, respectively [3.17]. The maximum fuel rod cladding temperature criteria for the PWR fuel is 1058°F/570°C [3.3]. The neutron absorbing material in the basket has a short term recommended temperature limit of 1000°F and a long term temperature limit of 850°F [3.24].

The neutron shield cavity is equipped with rupture disc devices designed to have a minimum bursting pressure of 34 psig as described in Section 2.6.1.3.4.

Using these technical specifications for the cask, DSC, and impact limiter materials, Sections 3.4.6 and 3.5.6 describe the package performance under normal conditions of transport and hypothetical accident conditions, respectively.

3.4 Thermal Evaluation for Normal Conditions of Transport

This section presents the thermal analysis of the NUHOMS®-MP187 Package for normal conditions of transport. The thermal conditions considered are those specified in 10CFR71.71 [3.1] and as described by Section 3.1.1. For case "a" identified in Section 3.1.1, the solar heat input to the exterior cask and impact limiter surfaces is in accordance with 10CFR71.71(c)(1). The DSC contains 24 intact fuel assemblies with the design basis heat load described in Section 3.1.2. The thermal analysis of the NUHOMS®-MP187 Cask containing a FF-DSC which contains 13 potentially damaged fuel assemblies is described in Appendix 3.6.5.

The cask is mounted on the skid in its normal position (horizontal orientation) with natural convection heat transfer on the cask side surface and impact limiter outside surfaces. Heat dissipation is by conduction, convection, and radiation from the fuel to the DSC shell; conduction, and radiation through the DSC shell to the cask body; conduction across the cask body; and a combination of natural convection and radiation from the cask and impact limiter exterior surfaces to the environment and the skid. The analytical models used in the thermal evaluation during normal conditions of transport are described in Section 3.4.1.

3.4.1 Thermal Model

The thermal analysis is performed using the HEATING7.2 computer program [3.2, 3.16] specifically developed by Oak Ridge National Laboratories for such shipping cask evaluations. The resulting temperatures for the various cask and DSC components are used in Chapter 2 for the structural evaluation.

The HEATING7.2 computer code is the most recent version of the HEATING series of computer programs. HEATING is an acronym for Heat Engineering and Transfer in Nine Geometries. The HEATING computer program series was designed to be a functional module within the SCALE system of computer programs for performing standardized analysis for licensing evaluations of nuclear systems. Thus their features were designed to perform thermal analyses on problems arising in licensing evaluations such as for transportation packages.

HEATING7.2 solves steady-state and/or transient heat conduction problems in one-, two-, or three-dimensional cartesian, cylindrical, or spherical coordinates. The thermal conductivity, density, and specific heat may be both spatial and temperature-dependent. In addition, the thermal conductivity may be anisotropic. Selected materials may undergo a change of phase for transient calculations involving one of the explicit procedures. The heat generation rates may be dependent on time, temperature and position. Boundary temperatures may be dependent on time and position. Boundary conditions which may be applied along surfaces of an analytical model include specified temperatures or any combination of prescribed heat flux, forced convection, natural convection, and radiation. In addition, one may specify radiative heat transfer across gaps or regions which are embedded in the model. The boundary condition parameters may be time- and/or temperature-dependent. The mesh spacing may be variable along each axis.

3.4.1.1 Heat

10CFR71.71(c)(1) regulations require that the transportation cask be subjected to an ambient temperature of 100°F in still air, and insolation. A thermal analysis of the NUHOMS®-MP187 Package is performed to determine the effect of the 100°F ambient temperature with solar heat load and internal heat generation on the cask parameters which influence the DSC response. The cask parameters of greatest importance to its suitability for transportation of an intact DSC are:

A) The average temperature of the impact limiter foam and aluminum honeycomb in the region of crush is of primary importance since it effects the foam and aluminum honeycomb force-deflection properties used in the cask drop analyses.

B) The fuel cladding temperatures must be within the allowable limits.

C) The temperature in the region of the seals must be shown to be within the limits of the seal material to ensure that the transportation cask remains leak tight.

D) The maximum pressures in the NUHOMS®-MP187 Cask must be within the design pressures for the cask components.

E) The thermal stress intensities in the transportation cask and DSC components must be shown to be within code allowables.

F) The temperature of the other cask materials must be within their allowable temperature limits.

The NUHOMS®-MP187 Cask is analyzed for the 100°F ambient condition using the axisymmetric HEATING7.2 model of the cask and DSC shown in Figure 3.4-1. The location of the grid lines were chosen to achieve an accurate determination of the temperature distribution in the major cask and DSC components. The analysis of the cask and DSC for the 100°F ambient condition is performed in 2 parts: 1) a steady-state thermal analysis is performed to determine the thermal distribution in the cask and DSC shell resulting from the 100°F ambient condition, and 2) the DSC shell temperatures are used to determine the maximum clad temperatures and temperatures of the DSC internals as shown in Appendix 3.6.3. The cask and DSC temperature distribution is used in Chapter 2 to determine the stresses resulting from the thermal distribution.

The analytical model used to perform the steady-state thermal analysis consists of various material regions with appropriate boundary conditions. The cylindrical shipping cask and DSC shells were modeled as long composite cylinders with the cross section configuration as shown in Figure 3.4-1. Due to symmetry, the cask/DSC were modeled as half cylinders with an insulated boundary condition at the axis of symmetry. Regions 1, 2, and 3 correspond to the DSC shell in the radial direction. Regions 4, 7, 24, and 25 correspond to air gaps between the DSC and cask. Regions 8, 10, 20, and 23 correspond to cask inner and outer shells. Region 9 is the lead in the cask. Region 94 corresponds to air gap between the lead and cask outer shell. Region 11 corresponds to neutron shielding. Regions 12, 57, and 90 correspond to the neutron shielding jacket and support ring. Regions 13, 14, 15, 17, 18, and 19 correspond to the DSC top and bottom shield plugs and cover plates. Region 16 corresponds to the heat generating region containing spent fuel assemblies. Regions 5, 6, 21, and 22 correspond to cask top and bottom closure plates. Regions 26, 59, 37, 70, 38, and 71 correspond to the impact limiter backing plates. Regions 36, 69, 96, and 97 correspond to the air gaps between the impact limiter backing plates and cask outside surfaces. Regions 39, 72, 100, and 101 correspond to the air gaps between the impact limiter backing plate and honeycomb impact limiter material. Regions 43, and 76 correspond to air gaps between the honeycomb material and outside skin of the impact limiter. Regions 27 through 34, and 60 through 67 correspond to the foam part of impact limiter. Regions 40 through 42, 73 through 75, 92, and 93 correspond to aluminum honeycomb part of the impact limiter. Regions 35, 68, 44 through 56, 58, 91, and 77 through 89 correspond to the impact limiter outer skin.

The thermal material properties used in the analytical model are listed in Table 3.2-1. The decay heat from the fuel assemblies is modeled as a volumetric heat density in HEATING7.2 models.

Volumetric Heat Density is calculated as follows:

$$\dddot{Q} = \frac{(13.5 \cdot 1.2kW)\dfrac{3412(Btu/hr)}{kW} \cdot \dfrac{hr}{60\,\text{min}}}{\pi(33)^2 inch^2 \cdot 173 inch}$$

where 33 in. and 173 in. are the DSC cavity internal radius and length respectively.

$$\therefore\ \dddot{Q} = 1.56E\text{-}3\ \frac{Btu}{\text{min-}inch^3}$$

The design basis volumetric decay heat density is applied evenly over the entire inner cavity of the DSC.

The heat load due to solar radiation is applied to the exposed external surfaces of the cask and impact limiters. The solar heat flux data from 10CFR71 is used. From 10CFR71 the solar heat flux for curved surfaces is 123 Btu/hr-ft^2 and for flat surfaces not horizontal is 61 Btu/hr-ft^2. The NUHOMS®-MP187 Cask body (impact limiter surfaces excluded) is covered with a personnel barrier during the transportation conditions. The personnel barrier has 50% open area which results in only 50% of the solar insolation being incident on the cask surface. The cask side surface between the top and bottom impact limiter is the only portion of the package with this 50% solar insolation. The heat load due to solar radiation is applied to the exposed external surfaces of the cask and impact limiters as solar transient. The 100°F transient thermal analysis is performed using an "explicit solution" technique in the HEATING7.2 code. The transient analysis is carried out for a sufficient period to estimate maximum temperatures and temperature distributions during normal conditions of transport. The -40°F steady state thermal analysis is performed using a "direct solution" technique in the HEATING7.2 code with a maximum of 20 iterations to allow the solution to converge. The results show that all the steady state analyses converge in less than 20 iterations.

The estimated steady state temperature distribution resulting from the 100°F ambient condition is shown in Appendix 3.6.2, Run Number NRCNOC25.OUT. The results are summarized in Table 3.4-1. The results are plotted in Figure 3.4-2. The maximum temperatures on the outer surface of the DSC, cask inner shell, and cask lead are 400°F (at r = 33.60 in., and z = 99.62 in.), 302°F (at r = 34.00 in., and z = 99.62 in.), 300°F (at r = 35.25 in., and z = 99.62 in.), respectively.

The results from Appendix 3.6.2, Run Number NRCNOC25.OUT show that the maximum and minimum foam temperatures are 285°F (at r = 0.00 in., and z = 202.13 in.) and 103°F (at r = 35.50 in., and z = 254.50 in.), respectively. Similarly, the maximum and minimum aluminum honeycomb temperatures are 191°F (at r = 42.38 in., and z = 31.75 in.) and 158°F (at r = 63.00 in., and z = 205.50 in.), respectively. The maximum NS-3 and the neutron shield jacket (cask outer surface) temperatures are 258 °F and 207°F, respectively.

The maximum temperatures in the region of the top closure plate O-ring, ram closure plate O-ring, and drain port seal O-rings are 254°F (at r = 35.25 in., and z = 195.00 in.), 283°F (at r = 8.50 in., and z = 4.00 in.), and 249°F (at r = 39.25 in., and z = 2.00 in.), respectively (Appendix 3.6.2, Run Number NRCNOC25.OUT). The temperature of the vent port seal is also the same as the drain port seal (249°F at r = 39.75 in., and z = 194.00 in.). The results are plotted in Figure 3.4-3.

3.4.1.1.1 Maximum Fuel Cladding Temperature

The NUHOMS®-MP187 Package analytical model calculates the DSC surface temperatures. The maximum DSC shell temperature for normal conditions of transport from Appendix 3.6.2, Run Number NRCNOC25.OUT is 400°F. The DSC shell temperatures are used to determine the maximum clad temperatures and temperatures of the DSC internals as shown in Appendix 3.6.3. The maximum fuel clad temperature is 669°F (354°C) for normal conditions of transport from Appendix 3.6.3. This maximum fuel clad temperature is considerably lower than the clad temperature limit of 1058°F (570°C) [3.3] used for this analysis. The maximum temperature of the neutron absorbing material in the basket is assumed to be equal to clad temperature which is below the 850°F limit for this material [3.24]. Note that the cladding and neutron absorber temperatures during some loading operations, including vacuum drying, may briefly exceed those reported herein. The temperatures for all conditions, however, remain below the short term allowables of 1058°F for the fuel cladding and 1000°F for the neutron absorbing material.

3.4.1.2 Cold

10CFR71.71(c)(2) regulations require that the transportation cask be subjected to an ambient temperature of -40°F in still air and shade. The temperatures of the foam and aluminum honeycomb impact limiters and the O-rings due to the -40°F ambient condition are bounded by those resulting from the 100°F ambient condition discussed in Section 3.4.1.1.

The NUHOMS®-MP187 Package is analyzed for the -40°F ambient thermal load condition using the same axisymmetric HEATING7.2 model of the cask and DSC described in Section 3.4.1.1 and shown in Figure 3.4-1. A steady-state thermal analysis is performed to determine the temperature distribution resulting from the -40°F ambient condition with the design basis heat load described in Section 3.1.2. The temperature dependent material properties used in the steady-state thermal analysis are the same as those described in Section 3.2.1.

The temperature distribution in the NUHOMS®-MP187 Cask for the -40°F ambient condition is illustrated in Appendix 3.6.2 Run Number NRCNOC3.OUT and summarized in Table 3.4-2.

The maximum temperature on the outer surface of the DSC is 317 °F (at r = 33.60 in., and z = 99.62 in.).

The results from Appendix 3.6.2, Run Number NRCNOC3.OUT also show that the maximum and minimum foam temperatures are 173°F (at r = 0.00 in., and z = 202.12 in.) and -40°F (at r = 35.50 in., and z = 254.50 in.), respectively.

The maximum temperature in the region of the top closure plate seal, ram closure plate seal, and drain port seal are 141°F (at r = 35.25 in., and z = 195.00 in.), 172°F (at r = 8.50 in., and z = 4.00 in.), and 136°F (at r = 39.75 in., and z = 2.00 in.), respectively (Appendix 3.6.2, Run Number NRCNOC3.OUT). The temperature of the vent port seal is also the same as the drain port seal (136°F at r = 39.75 in., and z = 194.00 in.). Therefore, the temperatures of the O-ring material for the -40°F ambient condition are bounded by those due to the 100°F ambient condition.

The steady state thermal distribution for the -40°F and -20°F ambient condition, shown in Appendix 3.6.2, Run Number NRCNOC3.OUT and NRCNOC4.OUT, are used in Chapter 2 to calculate thermal stresses. The maximum stress intensities in the transportation cask components due to the -40°F and -20°F ambient thermal condition are reported in Chapter 2.

3.4.1.2.1 Maximum Fuel Cladding Temperature

The maximum DSC shell temperature is higher for the 100°F ambient case than the -40°F ambient case. Therefore, the maximum cladding temperature for 100°F ambient also bounds the -40°F ambient case. The maximum fuel clad temperature of 669°F (354°C) from the 100°F ambient temperature condition is conservatively used for the normal conditions of transport at -40°F ambient. This maximum fuel clad temperature is considerably lower than the clad temperature limit of 1058°F (570°C) used for this analysis.

3.4.2 Maximum Temperatures

The maximum DSC shell temperature under all normal conditions of transport is 400°F as reported in Table 3.4-1. The maximum fuel cladding temperature is 669°F (354°C). The maximum temperatures of the other cask components are summarized in Table 3.4-1.

3.4.3 Minimum Temperatures

The minimum temperature distribution for the NUHOMS®-MP187 Package will occur with no decay heat load (empty DSC) and an ambient temperature of -40°F (per 10CFR71.71(c)(2)). Since the steady state analysis of these conditions represents a trivial case, no computerized thermal calculations were performed. Instead, it is assumed that all NUHOMS®-MP187 Cask components would reach the -40°F temperature under steady state conditions.

3.4.4 Maximum Internal Pressures

The maximum normal conditions of operation pressure in the cask internal cavity with all fuel rods intact and intact DSC is 22.5 psia. In the unlikely event of a leaking DSC, the DSC gaseous atmosphere will be discharged to the cask internal cavity. The maximum normal conditions of operation pressure (MNOP) in the cask internal cavity with 100% of fuel rods ruptured is 46.2 psia. This is considerably below the design pressure of 64.7 psia. The average temperature of neutron shielding material in the neutron shield cavity is (258 + 183)/2 = 221°F. At this temperature, the maximum pressure buildup in the Neutron shielding material will be less than 21 psig [3.22]. The neutron shield cavity is equipped with rupture disc devices designed to have a minimum bursting pressure of 34 psig as described in Section 2.6.1.3.4. Therefore, there is considerable margin in the neutron shield cavity pressures such that the neutron shield cavity remains sealed during normal conditions of transport.

3.4.5 Maximum Thermal Stresses

Maximum thermal stresses in the NUHOMS®-MP187 Package are calculated in Chapter 2.

3.4.6 Evaluation of Package Performance for Normal Conditions of Transport

The component temperatures associated with the more extreme normal thermal conditions presented in Section 3.4.2 and 3.4.3 are all within allowable limits for the respective materials as shown in Table 3.5-5. The minimum temperature for any cask component is -40°F (-20°F when combined with other load cases), and the maximum temperatures are summarized in Table 3.4-1.

The maximum normal operating internal pressure for the cask inner cavity is 46.2 psia. This is considerably below the design pressure of 64.7 psia. The maximum pressure in the neutron shield cavity is less than 21 psig which is considerably below the rupture disk minimum bursting pressure of 34 psig.

Table 3.4-1

Cask/DSC Temperatures, Normal Conditions of Transport, 100°F Ambient

Parameter, Units	Value
Ambient Air Temperature, °F	100
Max. DSC Shell Temperature, °F	400
Max. Cask Inner Shell Temperature ,°F	302
Max. Cask Outer Shell Temperature, °F	262
Max. Lead Temperature, °F	300
Max./Min. Neutron Shielding Temperature, °F	258/183
Max. Cask Outer Surface Temperature, °F	207
Max. Top Closure Seal Temperature, °F	254
Max. Ram Closure Seal Temperature, °F	283
Max. Drain Port Seal Temperature, °F	249
Max./Min. Polyurethane Foam Temperature, °F	285/103
Max./Min. Honeycomb Temperature, °F	191/158
Max. Impact Limiter Foam Surface Temperature, °F	121
Max. Impact Limiter Honeycomb Surface Temp. °F	174
Max. Fuel Cladding Temperature, °F	669

Table 3.4-2

Cask/DSC Temperatures Normal Conditions of Transport -40°F Ambient(1)

Parameter, Units	Value
Ambient Air Temperature, °F	-40
Max. DSC Shell Temperature, °F	317
Max. Cask Inner Shell Temperature ,°F	184
Max. Cask Outer Shell Temperature, °F	136
Max. Lead Temperature, °F	182
Max./Min. Neutron Shielding Temperature, °F	132/49
Max. Cask Outer Surface Temperature, °F	74
Maximum Top Closure Seal Temperature, °F	141
Maximum Ram Closure Seal Temperature, °F	172
Maximum Drain Port Seal Temperature, °F	136
Max./Min. Polyurethane Foam Temperature, °F (2)	173/-40
Max./Min. Honeycomb Temperature, °F (2)	63/-40
Max. Impact Limiter Foam Surface Temperature, °F	2
Max. Impact Limiter Honeycomb Surface Temp. °F	52
Max. Fuel Cladding Temperature, °F	<669

Note

1. Assumes design basis payload decay heat.
2. The minimum temperatures correspond to the stainless steel skin of the Impact Limiter.

THIS SECTION CONTAINS
PROPRIETARY INFORMATION

Figure 3.4-1
Heat Transfer Thermal Model for the Cask and DSC, NOC

THIS SECTION CONTAINS
PROPRIETARY INFORMATION

Figure 3.4-1
Heat Transfer Thermal Model for the Cask and DSC, NOC
(Continued)

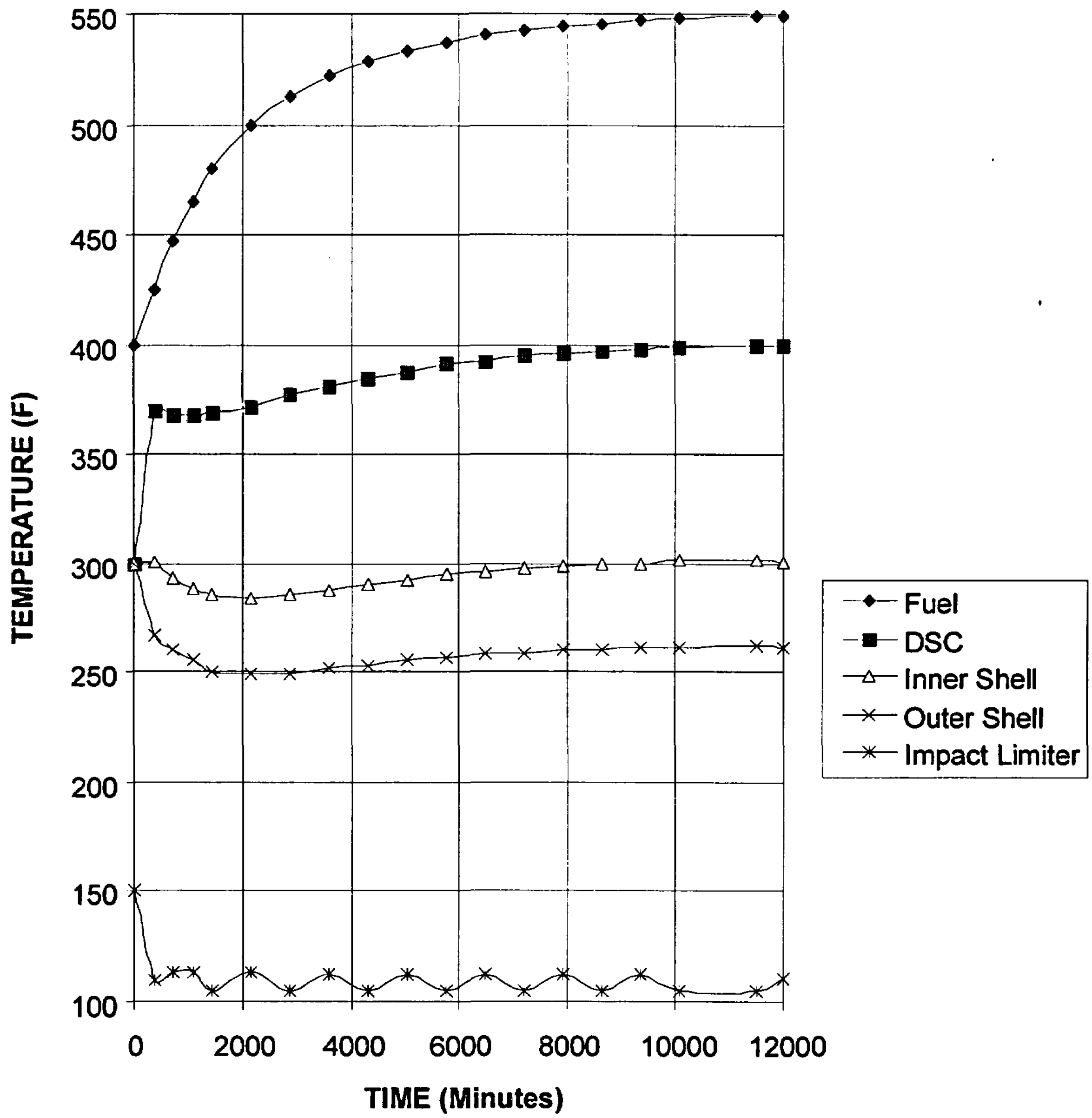

Figure 3.4-2

Cask/DSC Temperature Distribution 100°F Ambient NOC

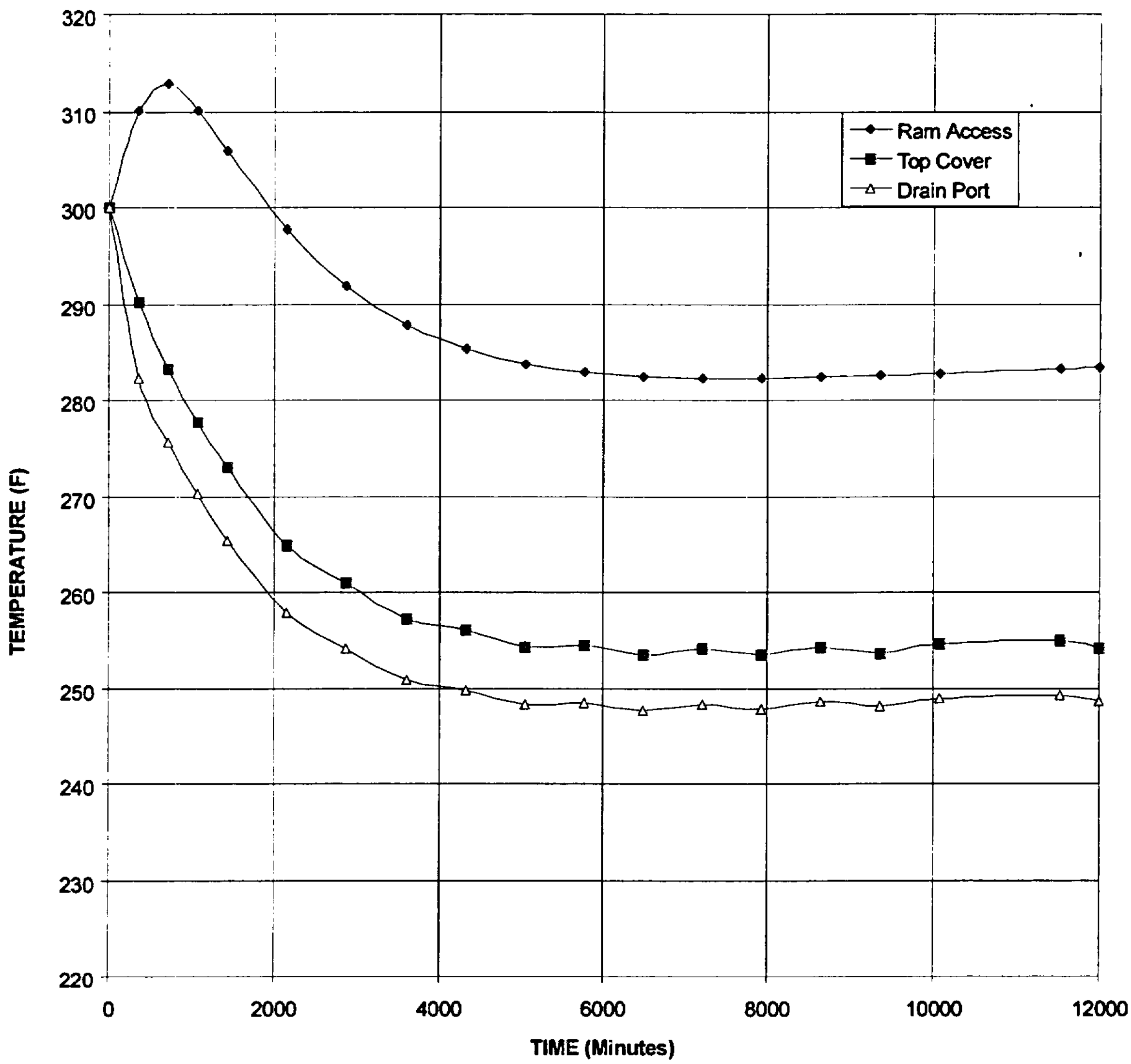

Figure 3.4-3

Seal Temperature Distribution 100°F NOC

3.5 Hypothetical Accident Thermal Evaluation

This section presents the thermal analyses of the NUHOMS®-MP187 Package for the hypothetical thermal accident condition specified in 10CFR71.73(c) [3.1]. The cask is assumed to be separated from the skid and the personnel barrier. To determine the effect of the hypothetical thermal accident condition, the following accident sequences are considered:

a) A free cask drop and puncture (crushed impact limiter with a 12 inch segment over the cask top seal area torn) followed by a 30 minute exposure to a 1475°F fire thermal radiation environment having an emissivity of 0.9.

b) A free cask drop and puncture (the foam and honeycomb portions of impact limiter detached from the cask and only the impact limiter inner shell present) followed by a 30 minute exposure to a 1475°F fire thermal radiation environment having an emissivity of 0.9.

c) Undamaged impact limiter followed by a 30 minute exposure to a 1475°F fire thermal radiation environment having an emissivity of 0.9.

After 30 minutes the thermal boundary is returned to a 100°F ambient air condition similar to the pre-fire condition with the addition of a solar insolation boundary present as specified in 10CFR71.73(c) [3.1]. The transient is then continued for a time sufficient to determine maximum values for all temperatures within the cask and DSC. The cask and the DSC are allowed to reach steady state after the postfire condition to obtain the final steady state thermal conditions following the drop and exposure to the fire. The analytical models used in the thermal evaluation during hypothetical accident conditions described above are given in Section 3.5.2.

3.5.1 Bounding Condition for Accident Transients

The accident sequences described in Section 3.5 are considered to determine the bounding condition for the accident transients. The accident sequence "c" of Section 3.5 which starts with undamaged impact limiters in the beginning of the fire transient is not expected to produce the bounding temperatures for the cask and DSC internals because the impact limiter and neutron shielding materials (foam and aluminum honeycomb in impact limiters and neutron shielding material in neutron shield cavity) will act as insulators during the fire and prevent excessive heat input to the cask, DSC, and impact limiters. The postfire and steady state temperatures will be higher than the normal conditions of transport because of the decomposed neutron shielding material and melted aluminum stiffeners in the neutron shield cavity and slightly charred foam in the top foam layer, but they will be bounded by the accident sequence “a” of Section 3.5.

The accident sequence “b” of Section 3.5 which starts with the foam and honeycomb portions of impact limiter detached from the cask and only the impact limiter inner shell present in the beginning of the fire transient is also not expected to produce the bounding temperatures for the cask and DSC internals because the gaps between the impact limiter inner shell and the cask body, and neutron shielding material in the neutron shield cavity will act as insulators during the fire and prevent excessive heat input to the cask and DSC. The thermal masses of the cask and DSC are sufficient to prevent excessive temperatures during the 30-minute fire transient. Also the cooldown of the cask following the fire (postfire and final steady state conditions) is faster and hence less severe, because insulating effects of the impact limiter materials (foam and honeycomb) are absent. The temperatures will be higher than the normal conditions of transport because of the decomposed neutron shielding material and melted aluminum stiffeners in the neutron shield cavity, but they will be bounded by the accident sequence “a” of Section 3.5.

The accident sequence “a” of Section 3.5 which starts with a free cask drop and puncture (crushed impact limiter with a 12 inch segment over the cask top seal area torn) in the beginning of the fire transient is expected to produce bounding temperatures for the cask and DSC internals because the crushed foam and aluminum honeycomb materials of the impact limiters have significantly higher thermal conductivity than the uncrushed materials. Also, the gap between the impact limiter material and outer impact limiter skin is assumed to be absent due to the drop and a 12 inch segment of the impact limiter portion over the cask top seal is assumed to be torn. This portion of the model is also representative of the shear key region of the cask since it allows direct heat input to the cask shell over a surface area greater than that of the shear key. All these conditions will increase the heat input to the impact limiters, cask, and DSC during the 30-minute fire transient compared to the intact limiter accident sequence "c" of Section 3.5. The thermal mass of the cask is again sufficient to prevent excessive temperatures during 30-minute fire transient. The cooldown of the cask following the fire, i.e. postfire and final steady state conditions, is slower and hence more severe, than the case of the accident sequence "b" of Section 3.5 with only the impact limiter inner shell present because of the insulating effect of the impact limiter materials. The final steady state temperatures will be bounding due to the charred foam and also because the neutron shielding material, aluminum stiffeners and aluminum honeycomb are assumed lost and replaced with air.

3.5.2 Thermal Model

The analytical model used to evaluate accident conditions is identical to those described in Sections 3.4.1 except, damage conditions, such as pin puncture and all drop indentations of the impact limiters are also considered. The HEATING7.2 model during accident conditions of the NUHOMS®-MP187 Package is shown in Figure 3.5-1. The analytical model boundary conditions are the same as described in Section 3.4.1, except as described below. As specified in 10CFR71.73(c)(3) [3.1], solar radiation heat loads are considered during the accident fire thermal conditions.

The ambient temperature is changed to 1,475°F during the fire event. After the fire, the ambient air temperature is returned to 100°F similar to the pre-fire condition with the addition of solar insolation. The emissivity of the cask and impact limiters is set to 0.9 [3.1] and 0.587 [3.15], respectively during the 30-minute fire and postfire transient.

The maximum crush depth of the impact limiter material is assumed to be 75 percent for the worst drop conditions. Therefore, the accident condition thermal analysis is based on the conservative assumption of damage to the impact limiter due to both the side drop and end drop. Even though the maximum damage to the impact limiter materials will only be on the impacted portion of the impact limiter, the entire impact limiter is conservatively assumed to have this damage during the fire transient. Also, to be conservative during the fire transient, this damage is assumed for both the top and bottom end impact limiters. The thermal properties of the crushed foam and crushed honeycomb are taken from Section 3.2.1.

A steady state analysis without solar insolation is run prior to the 30-minute fire transient condition. These temperature results are used as initial temperatures for 30-minute fire conditions and are presented in Table 3.5-1 for the cask and DSC components of significance.

The temperature distributions during PREFIRE, FIRE, POSTFIRE and FINAL STEADY STATE conditions are summarized in Table 3.5-1 through Table 3.5-4, respectively.

Input files prepared for the HEATING7.2 model of the accident sequence described above are included in Appendix 3.6.3. The HEATING7.2 results at the end of the 30-minute FIRE transient are also included in Appendix 3.6.3 and summarized in Table 3.5-2. The temperature of the DSC shell slightly increases during the 30-minute fire transient. The results show that crushed foam and honeycomb and neutron shielding material act as a thermal radiation barrier, thus limiting the heat input to the cask and DSC body from the fire.

The maximum cask inner shell temperature at the end of the 30-minute FIRE transient is 260°F (at r = 34.00 in., and z = 99.62 in.). The maximum DSC shell centerline temperature and the maximum lead temperature at the end of the 30-minute FIRE transient are 368°F (at r = 33.60 in., and z = 99.62 in.) and 320°F (at r = 39.19 in., and z = 195.00 in.), respectively.

The maximum temperatures in the region of top closure plate O-rings and ram closure plate O-rings are 243°F (at r = 35.25 in., and z = 195.00 in.) and 246°F (at r = 8.50 in., and z = 4.00 in.), respectively. The maximum temperature in the region of the vent/or drain port seal is 444°F which is estimated from the temperature shown in the output at r = 41.75 in., and z = 195.00 in. due to the assumed location of the puncture damage from the drop (Appendix 3.6.3, Run Number FIRECON2.OUT).

The most limiting thermal conditions experienced by the cask internals are in the period following the 30-minute fire. The impact limiter and neutron shielding materials, which act as a barrier to external thermal radiation during the fire, act as an insulator to internal heat dissipation after the fire.

The HEATING7.2 results for the POSTFIRE sequence are summarized in Table 3.5-3. The postfire transient is evaluated for a period of approximately 10 hours to determine peak transient temperatures in the cask inner cavity. Normally, the peak transient temperatures in the cask inner cavity are observed during the first few hours into the post accident transient (1 to 3 hours based on the results of other transportation packages [3.3]). The results for the NUHOMS®-MP187 Package show that the heatup rate of the cask inner cavity (DSC shell) is very slow (3°F to 4°F per hour initially in the postfire transient for the first five hours, falling to less than 3.0°F per hour after five hours, and falling to less than 2.5°F per hour after ten hours due to the large thermal mass of the cask internals). Hence the maximum temperatures are obtained during the final steady state conditions. The maximum cask inner shell temperatures at the end of 600 minutes in the transient is 340°F (at r = 34.00 in., and z = 99.62 in.). The maximum DSC shell temperature at 600 minutes into the transient is 401°F (at r = 33.60 in., and z = 99.62 in.). The maximum lead, neutron shield and neutron shield jacket surface (cask outer surface) temperatures at this time are 339°F (at r = 35.25 in., and z = 99.62 in.), 320°F (at r = 41.75 in., and z = 99.62 in.) and 252°F (at r = 46.06 in., and z = 167.50 in.), respectively. The maximum temperatures in the region of the top closure plate seal, ram closure plate seal, and drain port seal are 289°F (at r = 35.25 in., and z = 195.00 in.), 271°F (at r = 8.50 in., and z = 4.00 in.), and 284°F (at r = 40.50 in., and z = 2.00 in.), respectively (Appendix 3.6.3, Run Number POSTCON2.OUT). The temperature at the vent port seal location (at r = 41.75 in., and z = 195.00 in.) is 284°F.

The HEATING7.2 results at 90 minutes and 600 minutes into the FIRE transient are shown in Appendix 3.6.3. The temperature transient results are plotted in Table 3.5-2 through Table 3.5-4.

The temperature distribution at the end of the 600 minutes postfire transient is used as an input to calculate the final steady state thermal conditions following the drop and exposure to fire.

The HEATING7.2 results for the final steady state sequence are summarized in Table 3.5-4. The results of the final steady state temperature distribution for the post-accident conditions are included in Appendix 3.6.3. The results show that the maximum DSC shell surface temperature is 564°F (at r = 33.60 in., and z = 99.62 in.), and the maximum cask inner shell temperature is 508°F (at r = 34.00 in., and z = 99.62 in.). The maximum neutron shield temperature is 481°F (at r = 41.75 in., and z = 99.62 in.) with a maximum neutron shield jacket surface (cask outer surface) temperature of 296°F (at r = 45.50 in., and z = 33.00 in.). The maximum temperatures in the region of the top closure plate seal, ram closure plate seal, and drain port seal are 352°F (at r = 35.25 in., and z = 195.00 in.), 445°F (at r = 8.50 in., and z = 4.00 in.), and 417 °F (at r = 40.50 in., and z = 2.00 in.), respectively. The maximum temperature at the vent port location is 341°F (Appendix 3.6.3, Run Number FINLCON2.OUT).

3.5.3 Maximum Internal Pressures

It is expected that no fuel rods will rupture during hypothetical accident condition. However, for the worst case accident it is conservatively assumed that 100 percent of the fuel rods from all the 24 fuel assemblies rupture and that 100 percent of the fill gas and 30 percent of the fission gases in the fuel rods are released into the DSC cavity. In the unlikely event of a leaking DSC, the DSC gaseous atmosphere will be discharged in the annulus between the cask and DSC (i.e., cask internal cavity). The maximum pressure in the cask cavity during accident conditions is 29.1 psia due to fission and fill gas in the fuel rods and 27.6 psia due to gases in the annulus for a total maximum pressure of 56.7 psia as calculated in Appendix 3.6.5.2. This is the maximum internal pressure for the NUHOMS®-MP187 Package during the accident conditions.

3.5.4 Maximum Temperatures

The maximum temperatures noted for accident fire transient conditions (PREFIRE, FIRE, POSTFIRE, FINAL STEADY STATE) are presented in Table 3.5-1 through Table 3.5-4 for the Cask and DSC components.

3.5.4.1 Maximum Fuel Cladding Temperature

The results of the cask analysis show that the maximum DSC shell temperature during all the accident transient conditions is 564°F corresponding to postfire final steady state condition. Fróm Appendix 3.6.3 the maximum cladding temperature for all of the accident conditions is 790°F (421°C). This maximum fuel clad temperature is considerably lower than the clad temperature limit of 1058°F (570°C) used for this analysis.

3.5.5 Maximum Thermal Stresses

The maximum thermal stresses in the NUHOMS®-MP187 Package due to hypothetical accident transients are calculated in Chapter 2.

3.5.6 Evaluation of Package Performance for Accident Conditions

This section includes descriptions of the performance of the NUHOMS®-MP187 Package for the hypothetical accident conditions

The NUHOMS®-MP187 Cask with DSC is assumed to be separated from the skid. The neutron shield jacket surrounding the neutron shielding material is assumed to be in place but punctured due to the cask drop accident. The cask inner cavity remains sealed due to the integrity of the closure. The neutron shielding material is assumed to be decomposed but still present in the neutron shield cavity and the aluminum stiffeners in the neutron shield cavity may be partially melted, although no credit for them is taken in the thermal analysis. Similarly the aluminum honeycomb may be partially melted but the thermal analysis during postfire conditions conservatively assumes its complete loss. The foam may be charred but the charring only affects the foam on the top surface and no detrimental effect on the cask and DSC components is expected.

The primary importance for the NUHOMS®-MP187 Cask are the temperatures of the various seal materials, lead, neutron shielding material, aluminum stiffeners in the neutron shielding cavity, and the fuel cladding temperatures. The above damage conditions result in increased component temperatures. None of the temperatures except the neutron shielding material and aluminum stiffeners, foam and honeycomb noted from the hypothetical accident transient analysis exceed temperature limitations of the respective materials as defined in Table 3.5-5 and Section 3.3. The highest lead temperature of 506°F is well below the melting point of 621°F. The maximum seal temperature is 445°F for the ram closure. At no time during the transient, do the temperatures of the seals exceed 450°F which is considerably below the limit of seal material. The seals are metallic and the maximum temperature limit for the Ram Closure seal and Top Closure Plate seal material is 600°F, and the Drain and vent Port seal material is 700°F. The NUHOMS® DSC fuel basket contains stainless steel and carbon steel with transition temperatures of 2552°F and 2797°F, respectively [3.2]. The stainless steel and carbon steel temperatures are well below this limit. The temperature of the neutron absorber material is less than the fuel temperature of 790°F which is also considerably below the material temperature limit of 850°F.

The maximum fuel rod cladding temperature limit of 1058°F (570°C) [3.3] is the temperature at which cladding failure by creep rupture would be predicted. The temperatures resulting from 10CFR71 [3.1] normal and accident conditions fall well within the above temperature limits.

In the fire transient, the polyurethane foam and aluminum honeycomb impact limiter materials experience temperatures in excess of their recommended temperature limits, but they will still perform their function as an insulator. The softening and melting temperatures of polyurethane foam and aluminum honeycomb are 500°F and 1221°F, respectively [3.9, 3.17]. The foam and honeycomb temperatures resulting from 10CFR71 [3.1] accident conditions exceed these temperature limits causing the foam to char and aluminum honeycomb to melt. The structural analysis, containment analysis, and criticality analysis documented in other sections of this SAR confirm that the charred foam, decomposed neutron shielding material, melted aluminum stiffeners, and melted honeycomb during accident conditions cause no safety hazard and all the 10CFR71 requirements are satisfied. The maximum internal pressure of the NUHOMS®-MP187 Package is 56.7 psia which is less than the design internal pressure of 64.7 psia.

Table 3.5-1

Cask/DSC Temperatures PREFIRE Condition

Parameter, Units	Value
Ambient Air Temperature, °F	100
Max. DSC Shell Temperature, °F	368
Max. Cask Inner Shell Temperature ,°F	257
Max. Cask Outer Shell Temperature, °F	216
Max. Lead Temperature, °F	254
Max./Min. Neutron Shielding Temperature, °F	209/171
Max. Cask Outer Surface Temperature, °F	186
Max. Top Closure Seal Temperature, °F	220
Max. Ram Closure Seal Temperature, °F	246
Max. Vent/Drain Port Seal Temperature, °F	215
Max./Min. Polyurethane Foam Temperature, °F	241/107
Max./Min. Honeycomb Temperature, °F	176/132
Max. Impact Limiter Foam Surface Temperature, °F	139
Max. Impact Limiter Honeycomb Surface Temperature, °F	171
Max. Fuel Cladding Temperature, °F	<790

Table 3.5-2

Cask/DSC Temperatures 30 Minute FIRE Transient

Parameter, Units	Value
Ambient Air Temperature, °F	1475
Max. DSC Shell Temperature, °F	368
Max. Cask Inner Shell Temperature ,°F	260
Max. Cask Outer Shell Temperature, °F	639
Max. Lead Temperature, °F	320
Max./Min. Neutron Shielding Temperature, °F	1284/359
Max. Cask Outer Surface Temperature, °F	1291
Max. Top Closure Seal Temperature, °F	243
Max. Ram Closure Seal Temperature, °F	246
Max. Vent/Drain Port Seal Temperature, °F	444
(1)Max./Min. Polyurethane Foam Temperature, °F	1460/125
(1)Max./Min. Honeycomb Temperature, °F	1375/746
Max. Impact Limiter Foam Surface Temperature, °F	1462
Max. Impact Limiter Honeycomb Surface Temperature, °F	1380
Max. Fuel Cladding Temperature, °F	<790

NOTES:

(1) Temperatures are reported for the stainless steel skin of impact limiter. Actual impact limiter material temperatures are lower due to the lower thermal conductivity of the material.

Table 3.5-3

Cask/DSC Temperatures POSTFIRE Transient at 600 Minutes

Parameter, Units	Value
Ambient Air Temperature, °F	100
Max. DSC Shell Temperature, °F	401
Max. Cask Inner Shell Temperature ,°F	340
Max. Cask Outer Shell Temperature, °F	321
Max. Lead Temperature, °F	339
(1)(3)Max./Min. Neutron Shielding Temperature, °F	320/197
Max. Cask Outer Surface Temperature, °F	252
Max. Top Closure Seal Temperature, °F	289
Max. Ram Closure Seal Temperature, °F	271
Max. Vent/Drain Port Seal Temperature, °F	284
Max./Min. Polyurethane Foam Temperature, °F	273/155
(1)(2)Max./Min. Honeycomb Temperature, °F	286/155
Max. Impact Limiter Foam Surface Temperature, °F	190
Max. Impact Limiter Honeycomb Surface Temperature, °F	221
Max. Fuel Cladding Temperature, °F	<790

NOTES:

(1) Material is assumed to be lost and replaced with air at the start of postfire transient.

(2) The minimum temperature reported corresponds to stainless steel impact limiter skin.

(3) The minimum temperature reported corresponds to neutron shield jacket.

Table 3.5-4

Cask/DSC Temperatures Final Steady State Conditions

Parameter, Units	Value
Ambient Air Temperature, °F	100
Max. DSC Shell Temperature, °F	564
Max. Cask Inner Shell Temperature ,°F	508
Max. Cask Outer Shell Temperature, °F	484
Max. Lead Temperature, °F	506
(1)(3)Max./Min. Neutron Shielding Temperature, °F	481/222
Max. Cask Outer Surface Temperature, °F	296
Max. Top Closure Seal Temperature, °Fp	352
Max. Ram Closure Seal Temperature, °F	445
Max. Vent/Drain Port Seal Temperature, °F	417
Max./Min. Polyurethane Foam Temperature, °F	435/153
(1)(2)Max./Min. Honeycomb Temperature, °F	404/153
Max. Impact Limiter Foam Surface Temperature, °F	190
Max. Impact Limiter Honeycomb Surface Temperature, °F	245
Max. Fuel Cladding Temperature, °F	790

NOTES:

(1) Material is assumed to be lost and replaced with air at the start of postfire transient.

(2) The minimum temperature reported corresponds to stainless steel impact limiter skin.

(3) The minimum temperature reported corresponds to neutron shield jacket.

Table 3.5-5

Material Temperature Limits

Material	Maximum Material Temperature NOC (°F)	Maximum Material Temperature Accident (°F)	Material Temperature Limit (°F)
Stainless Steel	400	1462	2552
Carbon Steel	<669	<790	2797
Lead	300	506	621
Neutron Shielding	n/a	1284(1)	250
Polyurethane Foam	285	1460(3,4)	300/500(5)
Honeycomb	191	1375(2,3)	1221
Metallic Seal-Aluminum Jacketed	283	445	600
Metallic Seal Silver Plated	249	444	700
Neutron Absorber Sheets	669	790	1000
Fuel Cladding	669	790	1058

NOTES:

n/a- No credit is taken for neutron shielding material for heat removal during NOC.

(1) Neutron shielding material decomposes and aluminum stiffeners are partially melted and they are assumed to be replaced with air for evaluation of postfire transients.

(2) Honeycomb is assumed to be melted and replaced with air for evaluation of postfire transients.

(3) Temperature reported for stainless steel skin of impact limiter. Actual foam/honeycomb temperatures are lower.

(4) Temperature reported for the top foam layer which chars. The remaining foam temperatures are lower than the charring limit.

(5) Foam starts to char at a temperature of 500°F.

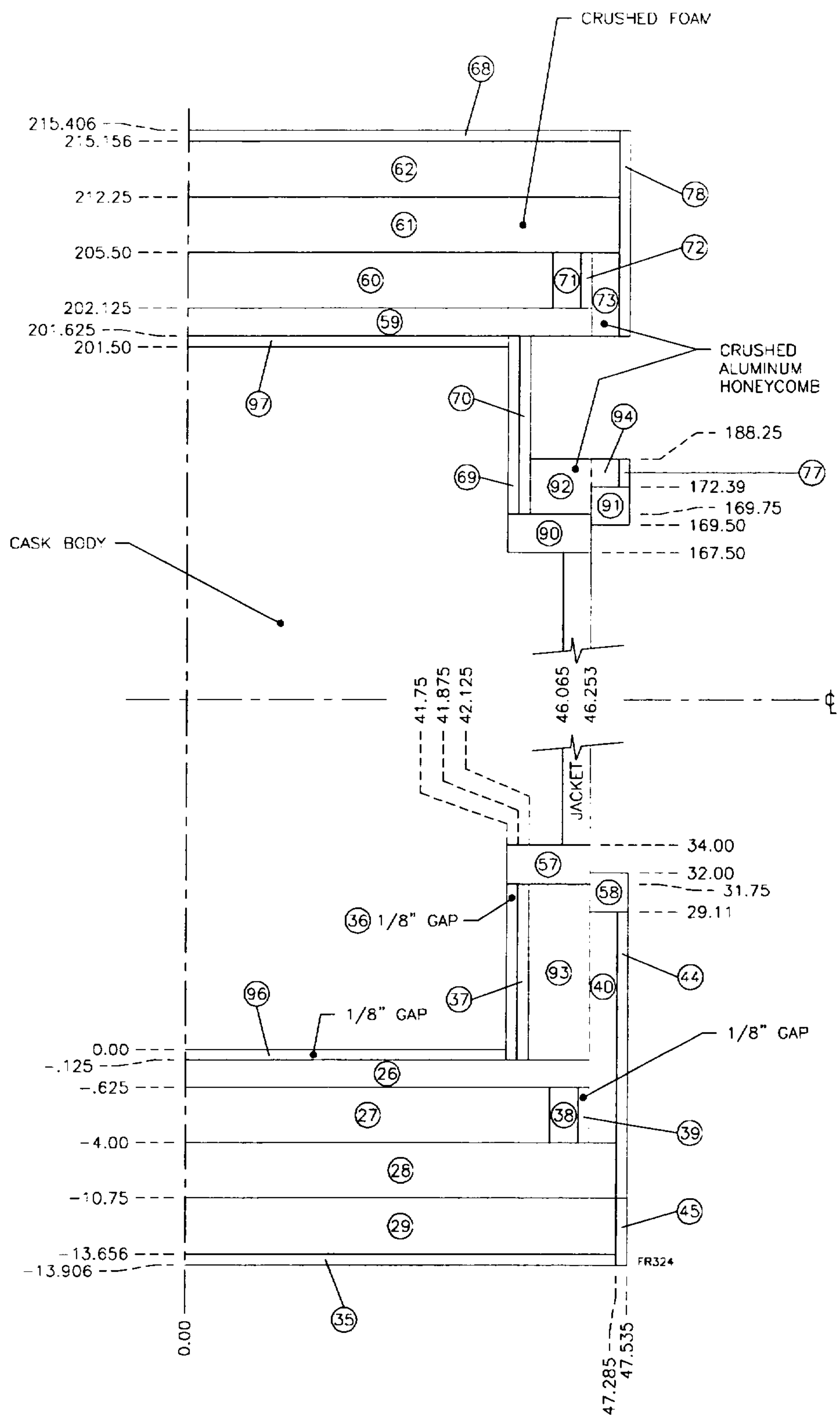

Figure 3.5-1

Heat Transfer Thermal Model for the Cask/DSC, Accident Conditions

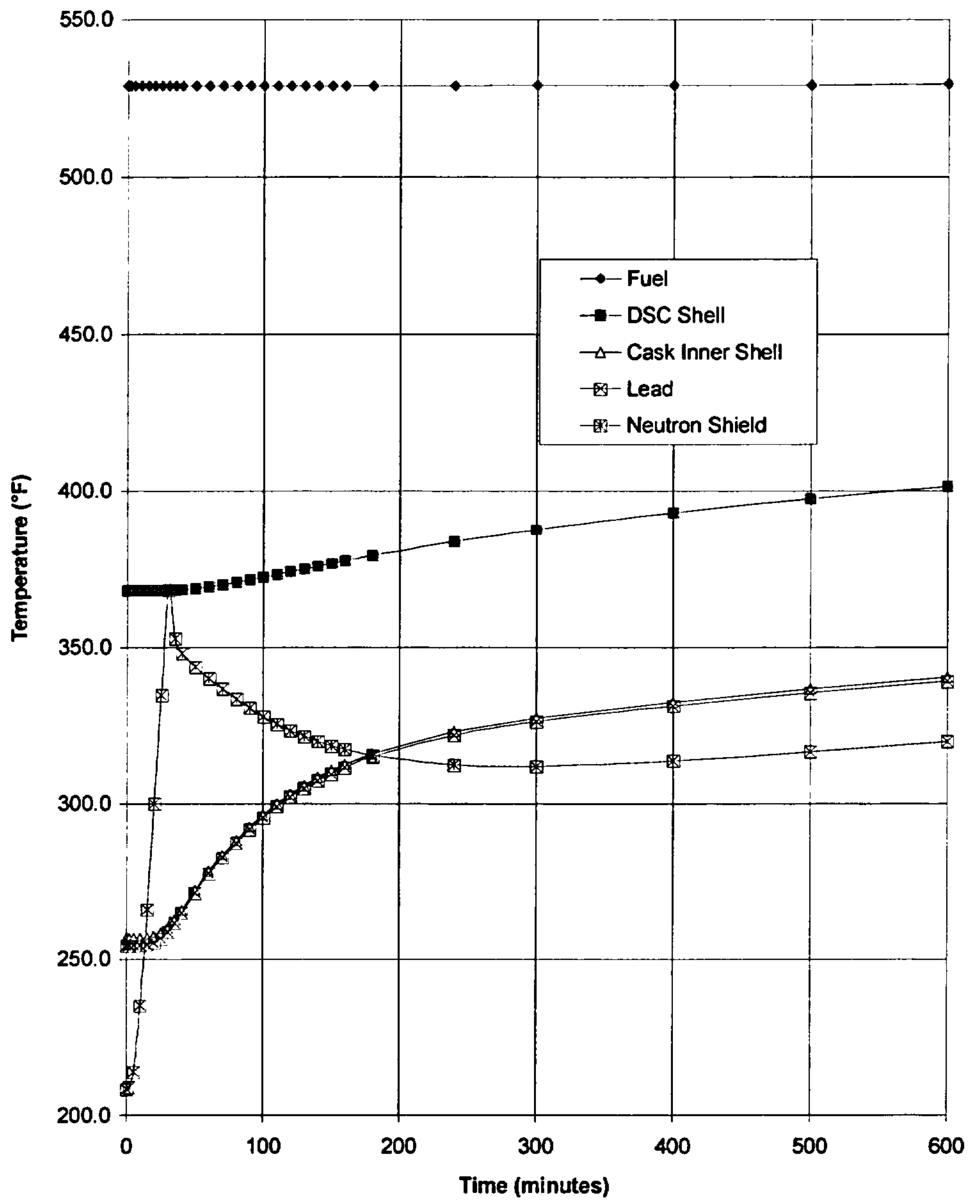

Figure 3.5-3

Temperature Transient Crushed Impact Limiter FIRE Case Plot 2

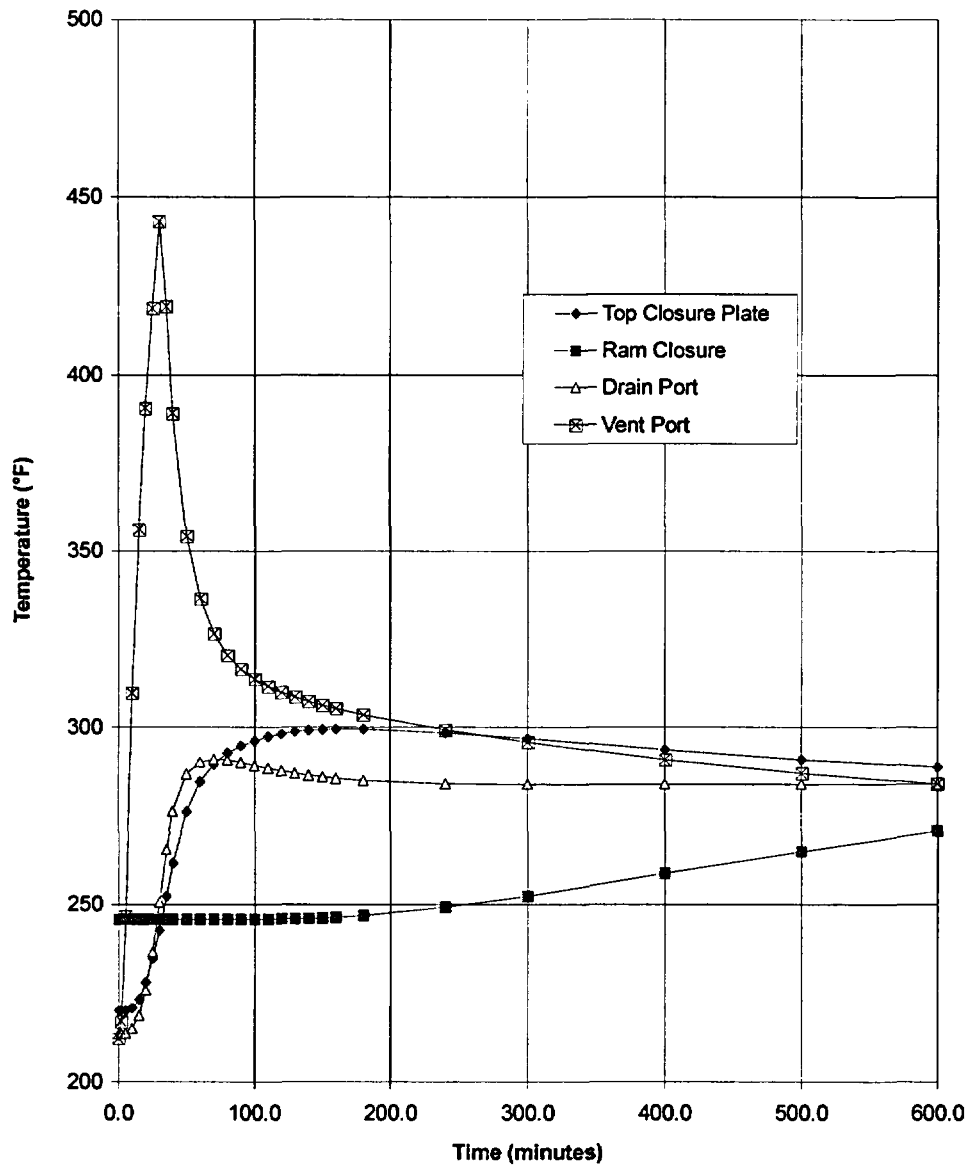

Figure 3.5-4

Temperature Transient Crushed Impact Limiter Seal Temperatures FIRE Case

3.6 Appendix

3.6.1 References

3.1 "Packaging and Transportation of Radioactive Materials," Title 10, Code of Federal Regulations, Part 71 (10CFR71), USNRC, 1/1/91.

3.2 Computer Code: "HEATING7.2b, Multidimensional, Finite-Difference Heat Conduction Analysis", PSR-199, Oak Ridge National Laboratory, March 1993, Transnuclear West File Number QA040.221.

3.3 "Consolidated Safety Analysis Report for IF-300 Shipping Cask," NEDO-10084-3, Volumes 1 & 2, General Electric Company, Docket No. 71-9001, May 1985.

3.4 "ASME Boiler and Pressure Vessel Code, Section II, Part D, Section III, Division 1, Subsection NG and Appendices," 1992 Edition with 1993 Addendum.

3.5 "CRC Handbook of Tables for Applied Science," 2nd Edition, R. E. Bolz and G. L. Tuve, Chemical Rubber Co., (1973).

3.6 "Principles of Heat Transfer," Third Edition, Frank Krieth, Harper and Row Publishers.

3.7 Technical Data Sheet, "NS-3" Castable Neutron and/or Gamma Shielding Material, BISCO Products, Inc., Elk Grove Village, Illinois.

3.8 "Basic Heat Transfer," M. Necati Özisik, McGraw-Hill Book Company, 1977.

3.9 "LAST-A-FOAM® FR-3700 for Crash and Fire Protection of Nuclear Material Shipping Containers," General Plastics Manufacturing company, Tacoma, WA. Initial Issue 4/91, Reprinted 12/93.

3.10 "Impact Limiter Polyurethane Foam High Temperature Structural Performance Test Results Final Report", NUPAC Report No. IL-001-NP, Prepared by Nuclear Packaging Inc., Federal Way, WA September 28, 1989.

3.11 Letter from Floyd Henry (General Plastics) to I.D. McInnes (TNW), Dated July 22,1993, PNFS File Number NUH005.0019.

3.12 "Effects of 1300°F on Unfilled NS-3", Bisco Products Technical Report No. NS-3-020, Revision 0, Bisco Products (A Dow Corning Affiliate), Elk Grove Village, Il. 11/20/1984.

3.13 Safety Analysis Report for the NUPAC 125-B Fuel Shipping Cask", NRC Docket Number 71-9200, Revision 0, Nuclear Packaging Inc., Federal Way, WA., April 1991.

3.14 "HTAS1: A Two Dimensional Heat Transfer Analysis of Fuel Casks" NUREG/CR-0200, Volume 1, Section H1, ORNL/NUREG/CSD-2/V1/R3, Oak Ridge National Laboratory, December 1984.

3.15 "Scoping Design Analyses for Optimized Shipping Casks Containing 1-, 2-, 3-, 5-, 7- or 10-Year-Old PWR Spent Fuel", J. A. Bucholz, ORNL/CSD/TM-149 TTC-9316, January 1983.

3.16 Computer Code, HEATING7, Version 7.2c, "A Multidimensional Heat Conduction Analysis with the Finite Difference Formulation," NUREG/CR-0200, Volume 2, Revision 4, Section F10, ORNL/NUREG/CSD-2/V2, 1993, Transnuclear West File Number QA040.221.0001.

3.17 "CRC Handbook of Chemistry and Physics", 60th Edition, R. C. Weast Editor, Chemical Rubber Co., (1981).

3.18 Characteristics of Spent Fuel, High Level Waste, and Other Radioactive Wastes Which May Require Long-Term Isolation, DOE/RW-0184-R1, U.S. Department of Energy, Office of Civilian Radioactive Waste Management, July 1992.

3.19 "Extended Fuel Burnup Demonstration Program", Final Report, DOE/ET/34014-10, Nuclear Assurance Corporation, September 1983.

3.20 Westinghouse Electric Corporation, "Spent Fuel Dry Storage Testing at E-MAD (March 1978 - March 1982)", PNL-4533, September 1983.

3.21 "Helicoflex® Metallic O-Rings Product Data Sheets", LeCarbone-Lorraine, Columbia, South Carolina.

3.22 "Determination of Weight Loss and Off-gassing of NS-3 and R-1528 After Heat Aging", Technical Report No. NS-3-033, Bisco Products Inc., Revision 0, June 26, 1989.

3.23 "Helicoflex® High Performance Sealing Product Data Sheets", LeCarbone-Lorraine, Columbia, South Carolina.

3.24 "Standard Specification for BORAL Composite Sheet", Specification Number BPS-9000-04, AAR Advanced Structures, Livonia Michigan.

3.25 Annual Book of ASTM Standards, Section 2, "Nonferrous Metal Products," Volume 02.02, 1994.

3.26 "A Correlating Equation for Forced Convection From Gases and Liquids to a Circular Cylinder in Crossflow", S.W. Churchill and M. Bernstein, Transactions of the ASME Journal of Heat Transfer, Vol.99, May 1977.

3.27 "Handbook of Single-Phase Convective Heat Transfer," S. Kakac, R. K. Shaw, and W. Aung, Wiley, 1987.

3.28 "Methods for Reviewing Safety Analysis Reports", Thermal Analysis, DOE Training Course Session 2, Fission Energy and Systems Safety Program, LLNL, March 6-17, 1995.

3.6.2 NOC Results

NUHOMS®-MP187 Package thermal model HEATING7.2 input, and temperature distribution for the Normal Condition of Transport is included in this appendix.

3.6.2.1 HEATING7.2 INPUT FILE NAME: NRCNOC25.INP

THIS SECTION CONTAINS
PROPRIETARY INFORMATION

3.6.2.2 HEATING7.2 INPUT FILE NAMES: NRCNOC3.INP and NRCNOC4.INP

THIS SECTION CONTAINS
PROPRIETARY INFORMATION

3.6.2.3 HEATING7.2 OUTPUT FILE NAME: NRCNOC25.OUT

NOC,100F,50%ENC,TRAN SOLAR,NRCNOC2,NO NS3 CREDIT,0.12"SS,1/8"AL STIFF Fri Oct 13 16:07:17 1995

Transient Temperature Distribution at Time 1.1520E+04

65	254.50	104.51	104.50	104.49	104.39	104.06	103.74	103.65	103.58	103.34	103.33				
64	254.25	104.52	104.52	104.50	104.41	104.07	103.75	103.66	103.59	103.35	103.34				
63	247.50	125.86	125.73	125.33	122.88	116.52	112.85	111.21	109.87	104.14	104.13	104.00	103.82	103.81	103.44
62	247.25	126.53	126.40	125.99	123.47	116.93	113.19	111.52	110.15	104.22	104.15	104.01	103.83	103.82	103.45
61	240.50	142.83	142.61	141.95	137.96	128.13	124.14	123.28	122.71	120.87	120.50	117.84	114.51	114.36	105.77
60	240.25	143.44	143.23	142.56	138.52	128.60	124.58	123.74	123.17	121.36	121.00	118.28	114.88	114.72	105.96
59	233.50	160.53	160.27	159.46	154.58	142.66	137.62	136.54	135.81	133.46	132.98	129.35	125.60	125.47	120.05
58	233.25	161.20	160.94	160.12	155.22	143.22	138.16	137.07	136.33	133.96	133.48	129.82	126.04	125.91	120.51
57	226.50	180.22	179.92	178.99	173.39	159.78	153.90	152.62	151.74	148.92	148.34	143.88	139.17	139.01	132.27
56	226.25	180.99	180.69	179.75	174.12	160.45	154.54	153.25	152.37	149.53	148.95	144.47	139.73	139.57	132.79
55	219.50	203.49	203.13	202.03	195.47	180.01	173.36	171.91	170.93	167.76	167.11	162.13	156.88	156.70	149.25
54	219.25	204.41	204.05	202.94	196.35	180.81	174.12	172.67	171.68	168.50	167.84	162.84	157.57	157.39	149.90
53	212.50	231.72	231.28	229.94	222.12	204.38	196.60	194.90	193.75	190.03	189.27	183.44	177.39	177.19	168.88
52	212.25	232.84	232.40	231.05	223.18	205.39	197.55	195.85	194.68	190.93	190.16	184.28	178.17	177.96	169.56
51	205.50	265.79	265.28	263.73	254.88	235.93	226.69	224.58	223.12	218.29	217.28	209.27	200.44	200.14	187.43
50	202.12	284.56	284.04	282.45	273.58	255.98	247.21	245.08	243.58	238.44	237.31	227.78	215.20	214.70	190.17
49	201.62	284.58	284.06	282.48	273.61	256.02	247.28	245.15	243.65	238.54	237.40	227.91	215.39	214.89	190.41
48	201.50	287.51	287.00	285.47	277.02	262.10	257.03	256.02	255.35	253.27	252.86	249.92	247.17	247.08	243.87
47	199.33	287.95	287.43	285.90	277.48	262.65	257.66	256.68	256.03	254.06	253.67	251.00	248.63	248.56	246.02
46	197.17	288.92	288.41	286.88	278.46	263.65	258.43	257.38	256.69	254.70	254.33	251.81	249.64	249.57	247.27
45	195.00	290.43	289.92	288.39	279.97	265.16	259.45	257.98	256.90	254.92	254.57	252.29	250.21	250.14	247.79
44	194.50	343.62	343.15	341.75	334.28	322.81	319.79	319.11	256.36	254.84	254.54	252.38	250.30	250.23	247.79
43	192.25	345.68	345.20	343.80	336.27	324.71	321.93	321.30	255.91	254.56	254.38	252.81	250.75	250.36	247.13
42	188.25	348.75	348.26	346.81	339.02	326.65	322.82	322.17	257.11	255.88	255.76	254.90	254.20	241.60	240.02
41	187.50	349.35	348.85	347.39	339.54	327.02	322.34	321.80	257.34	256.14	256.02	255.23	254.60	240.15	238.65
40	169.75	477.29	475.64	470.64	441.35	378.44	352.95	352.10	260.49	258.64	258.45	257.00	255.43	209.32	204.22
39	169.50	478.36	476.70	471.67	442.24	378.99	353.36	352.50	260.65	258.79	258.60	257.15	255.58	209.31	201.57
38	167.50	486.36	484.64	479.41	448.89	383.21	356.59	355.70	262.01	260.11	259.92	258.47	256.92	211.53	203.94
37	165.25	494.38	492.60	487.18	455.57	387.65	360.09	359.19	263.73	261.79	261.60	260.17	258.73	218.88	215.43
36	143.38	532.02	530.00	523.90	488.56	415.79	385.22	384.24	285.89	283.81	283.60	282.15	280.83	247.61	244.33
35	121.50	545.59	543.53	537.28	501.21	427.85	397.44	396.43	298.36	296.22	296.01	294.49	293.11	258.89	255.41
34	99.62	549.04	546.97	540.70	504.53	431.19	400.88	399.86	302.07	299.92	299.70	298.17	296.76	262.08	258.52
33	77.75	545.08	543.02	536.78	500.75	427.42	397.01	396.00	297.93	295.79	295.58	294.07	292.69	258.50	255.01
32	55.88	530.46	528.46	522.39	487.22	414.69	384.21	383.23	285.03	282.95	282.75	281.30	279.97	246.42	243.13
31	34.00	489.46	487.73	482.48	451.79	385.33	358.33	357.43	263.48	261.56	261.37	259.89	258.31	212.91	208.26
30	32.00	481.58	479.92	474.85	445.29	381.21	355.12	354.26	262.58	260.71	260.52	259.07	257.49	211.17	203.59
29	31.75	480.53	478.87	473.84	444.43	380.68	354.71	353.85	262.48	260.62	260.43	258.98	257.41	211.23	205.53
28	21.25	421.33	420.15	416.58	396.00	354.44	335.54	334.86	261.00	259.59	259.45	258.48	257.60	234.78	232.94
27	14.50	352.85	352.24	350.48	341.61	328.33	324.25	323.75	259.46	258.25	258.14	257.35	256.73	241.95	240.45
26	13.75	351.45	350.86	349.11	340.43	327.63	324.46	323.84	259.25	258.04	257.92	257.13	256.51	242.79	241.30
25	10.25	348.84	348.23	346.44	338.08	326.02	323.35	322.71	258.16	256.88	256.75	255.76	255.02	247.01	245.43
24	8.50	347.39	346.75	344.74	336.47	324.54	321.62	320.92	257.99	256.49	256.32	254.80	253.09	250.29	247.63
23	8.00	340.06	337.09	285.88	278.54	265.49	260.52	259.24	258.29	256.53	256.28	254.57	252.01	251.66	248.10
22	6.00	311.91	308.04	284.25	276.99	263.99	259.41	258.48	257.87	256.11	255.78	253.54	251.27	251.19	248.56
21	4.00	286.48	285.72	283.25	275.84	262.87	258.52	257.66	257.09	255.36	255.03	252.65	250.46	250.39	247.97
20	2.00	285.37	284.66	282.58	275.09	262.08	257.76	256.89	256.32	254.54	254.19	251.67	249.34	249.27	246.69
19	.00	284.90	284.21	282.26	274.73	261.61	257.16	256.25	255.65	253.75	253.37	250.60	247.92	247.84	244.61
18	-.12	281.77	281.20	279.57	271.55	255.55	247.19	245.13	243.67	238.66	237.55	228.15	215.66	215.16	190.59
17	-.38	281.76	281.19	279.55	271.53	255.52	247.15	245.08	243.62	238.59	237.48	228.05	215.51	215.01	190.39
16	-.62	281.75	281.18	279.55	271.53	255.51	247.13	245.06	243.60	238.57	237.45	228.02	215.46	214.96	190.32
15	-4.00	263.33	262.83	261.34	253.19	235.41	226.42	224.34	222.91	218.15	217.14	209.20	200.40	200.09	187.35
14	-10.75	231.18	230.76	229.48	222.04	204.88	197.17	195.49	194.34	190.63	189.86	184.03	177.95	177.75	169.37
13	-11.00	230.09	229.68	228.40	220.99	203.88	196.22	194.55	193.41	189.72	188.97	183.19	177.17	176.97	168.69
		.00	4.25	8.50	19.25	30.00	33.00	33.60	34.00	35.25	35.50	37.34	39.19	39.25	41.75
		1	2	3	4	5	6	7	8	9	10	11	12	13	14

NOC,100F,50%ENC,TRAN SOLAR,NRCNOC2,NO NS3 CREDIT,0.12"SS,1/8"AL STIFF Fri Oct 13 16:07:17 1995

Transient Temperature Distribution at Time 1.1520E+04

65	254.50														
64	254.25														
63	247.50	103.40	103.39												
62	247.25	103.39	103.39												
61	240.50	104.06	104.05	104.04	104.02	104.01	103.48	103.39	103.28	103.27					
60	240.25	104.16	104.08	104.05	104.03	104.02	103.49	103.40	103.27	103.27					
59	233.50	119.44	118.82	118.50	118.18	118.01	109.41	107.11	104.00	104.00	103.58	103.58			
58	233.25	119.90	119.27	118.95	118.62	118.45	109.69	107.32	104.09	104.01	103.59	103.58			
57	226.50	131.57	130.86	130.51	130.15	129.97	121.83	120.42	118.66	117.86	104.58	104.57	103.82	103.81	
56	226.25	132.09	131.38	131.02	130.67	130.49	122.35	120.94	119.17	118.37	104.69	104.58	103.83	103.82	
55	219.50	148.49	147.73	147.35	146.97	146.78	138.46	137.28	135.89	135.29	127.07	126.16	105.25	105.23	104.64
54	219.25	149.14	148.38	148.00	147.62	147.43	139.11	137.93	136.55	135.95	127.82	126.90	105.39	105.25	104.65
53	212.50	168.06	167.26	166.86	166.45	166.25	157.90	156.79	155.50	154.95	147.93	147.22	133.28	132.30	108.10
52	212.25	168.74	167.93	167.52	167.12	166.92	158.53	157.43	156.15	155.60	148.70	148.00	134.36	133.37	108.30
51	205.50	186.24	185.07	184.49	183.92	183.63	172.65	172.63	172.58	170.19	169.28	169.17	166.35	166.20	163.12
50	202.12	187.11	184.10	182.54	181.08	180.39	173.06	172.78	172.44	171.45	169.68	169.51	166.46	166.30	163.43
49	201.62	187.04	184.40	181.74	180.25	179.63	173.32	172.78	172.14	171.79	169.73	169.55	166.47	166.32	163.47
48	201.50	186.93	186.55	179.53	179.41	179.32	173.35	172.78	172.13	171.86	169.75	169.56	166.48	166.32	163.49
47	199.33	197.08	196.92	175.70	175.65	175.63	172.84	172.47	172.05	171.87	169.83	169.64	166.54	166.39	163.67
46	197.17	201.42	201.25	174.20	174.15	174.12	172.27	172.00	171.68	171.55	169.76	169.59	166.58	166.43	163.80
45	195.00	203.09	202.92	173.52	173.46	173.43	171.87	171.64	171.37	171.25	169.65	169.49	166.57	166.43	163.86
44	194.50	203.28	203.11	173.41	173.35	173.32	171.81	171.58	171.31	171.20	169.62	169.47	166.56	166.42	163.86
43	192.25	203.36	203.19	173.13	173.06	173.03	171.60	171.39	171.14	171.03	169.53	169.38	166.52	166.38	163.84
42	188.25	201.31	201.16	173.11	173.06	173.03	171.62	171.41	171.16	171.05	169.52	169.36	166.38	166.23	163.61
41	187.50	200.91	200.76	173.21	173.15	173.12	171.70	171.48	171.22	171.11	169.54	169.38	166.34	166.19	163.53
40	169.75	194.24	193.98	186.36	186.24	186.17	180.27	179.42	178.42	177.99	172.40	171.90	164.26	163.93	158.75
39	169.50	197.26	193.52	191.55	189.83	189.03	180.74	179.79	178.67	178.17	172.07	171.57	163.97	163.63	158.49
38	167.50	201.44	199.04	197.89	196.78	196.23	183.67	182.68	181.77	181.64					
37	165.25	212.96	210.53	209.32	208.13	207.53	183.63	180.33	176.45	176.27					
36	143.38	241.17	238.03	236.46	234.90	234.11	201.44	196.98	191.79	191.57					
35	121.50	251.99	248.58	246.88	245.19	244.34	208.82	203.98	198.32	198.07					
34	99.62	255.02	251.54	249.81	248.08	247.21	210.88	205.92	200.13	199.88					
33	77.75	251.60	248.21	246.52	244.83	243.98	208.56	203.73	198.09	197.84					
32	55.88	240.00	236.89	235.34	233.79	233.01	200.70	196.29	191.15	190.93					
31	34.00	205.78	203.39	202.23	201.11	200.55	184.17	182.17	179.89	179.72					
30	32.00	199.81	196.47	194.71	193.15	192.42	182.14	180.93	179.58	179.03	171.61	171.02	162.70	162.35	157.15
29	31.75	197.10	196.75	190.08	189.92	189.82	181.78	180.68	179.40	178.85	171.94	171.35	162.99	162.63	157.41
28	21.25	198.95	198.82	174.11	174.06	174.04	172.40	172.13	171.80	171.66	169.62	169.41	165.52	165.33	162.19
27	14.50	201.33	201.17	172.59	172.53	172.50	171.12	170.91	170.67	170.56	169.07	168.92	166.00	165.85	163.26
26	13.75	201.62	201.47	172.54	172.48	172.45	171.08	170.87	170.63	170.52	169.06	168.91	166.03	165.89	163.33
25	10.25	203.03	202.86	172.60	172.54	172.51	171.10	170.90	170.65	170.55	169.10	168.95	166.17	166.03	163.54
24	8.50	203.42	203.25	172.79	172.73	172.69	171.24	171.03	170.77	170.66	169.17	169.02	166.22	166.08	163.58
23	8.00	203.43	203.26	172.86	172.80	172.77	171.30	171.08	170.82	170.71	169.20	169.05	166.23	166.09	163.59
22	6.00	202.98	202.81	173.28	173.22	173.19	171.59	171.35	171.07	170.95	169.32	169.16	166.26	166.12	163.57
21	4.00	201.16	201.00	174.05	173.99	173.96	172.02	171.74	171.41	171.27	169.44	169.27	166.27	166.12	163.50
20	2.00	196.78	196.62	175.60	175.56	175.53	172.59	172.20	171.76	171.58	169.51	169.32	166.24	166.08	163.38
19	.00	187.13	186.76	179.33	179.21	179.12	173.07	172.48	171.81	171.53	169.42	169.23	166.18	166.02	163.21
18	-.12	187.13	184.74	181.41	179.99	179.43	173.05	172.49	171.82	171.47	169.41	169.22	166.17	166.02	163.20
17	-.38	187.20	184.11	182.34	180.78	180.04	172.95	172.50	171.87	171.31	169.38	169.20	166.16	166.01	163.18
16	-.62	187.20	184.07	182.49	180.97	180.25	172.80	172.54	172.24	171.09	169.35	169.18	166.16	166.00	163.15
15	-4.00	186.15	184.97	184.39	183.81	183.52	172.41	172.38	172.33	169.86	168.96	168.85	166.06	165.90	162.85
14	-10.75	168.56	167.74	167.34	166.94	166.73	158.37	157.26	155.98	155.44	148.56	147.87	134.30	133.31	108.37
13	-11.00	167.88	167.07	166.67	166.27	166.07	157.74	156.63	155.34	154.79	147.80	147.09	133.22	132.24	108.18
		42.00	42.25	42.38	42.50	42.56	45.25	45.62	46.06	46.25	48.75	49.00	53.75	54.00	58.75
		15	16	17	18	19	20	21	22	23	24	25	26	27	28

NOC,100F,50%ENC,TRAN SOLAR,NRCNOC2,NO NS3 CREDIT,0.12"SS,1/8"AL STIFF Fri Oct 13 16:07:17 1995

Transient Temperature Distribution at Time 1.1520E+04

65	254.50				
64	254.25				
63	247.50				
62	247.25				
61	240.50				
60	240.25				
59	233.50				
58	233.25				
57	226.50				
56	226.25				
55	219.50	104.64			
54	219.25	104.64			
53	212.50	108.09	110.66	110.75	110.77
52	212.25	108.13	110.69	110.88	110.87
51	205.50	162.93	159.51	132.27	132.12
50	202.12	163.28	161.01	133.96	133.82
49	201.62	163.33	161.15	134.12	133.98
48	201.50	163.34	161.18	134.16	134.02
47	199.33	163.54	161.60	134.60	134.46
46	197.17	163.67	161.83	134.85	134.70
45	195.00	163.73	161.94	134.98	134.84
44	194.50	163.74	161.96	135.00	134.86
43	192.25	163.71	161.95	135.07	134.93
42	188.25	163.48	161.71	135.23	135.09
41	187.50	163.41	161.62	135.35	135.21
40	169.75	158.52	155.43	150.37	150.16
39	169.50	158.26	154.89	152.46	151.08
38	167.50				
37	165.25				
36	143.38				
35	121.50				
34	99.62				
33	77.75				
32	55.88				
31	34.00				
30	32.00	156.92	153.58	151.92	150.92
29	31.75	157.18	154.01	150.59	150.38
28	21.25	162.05	160.16	135.13	135.00
27	14.50	163.14	161.37	134.83	134.69
26	13.75	163.21	161.45	134.83	134.69
25	10.25	163.42	161.67	134.87	134.73
24	8.50	163.46	161.71	134.87	134.73
23	8.00	163.47	161.71	134.86	134.72
22	6.00	163.45	161.67	134.80	134.66
21	4.00	163.38	161.54	134.67	134.53
20	2.00	163.25	161.31	134.44	134.30
19	.00	163.07	160.92	134.02	133.88
18	-.12	163.06	160.89	133.99	133.85
17	-.38	163.03	160.82	133.91	133.77
16	-.62	163.01	160.74	133.83	133.69
15	-4.00	162.66	159.26	132.17	132.03
14	-10.75	108.20	110.91	111.10	111.09
13	-11.00	108.16	110.87	110.98	111.02
		59.00	63.00	63.12	63.38
		29	30	31	32

NOC,100F,50%ENC,TRAN SOLAR,NRCNOC2,NO NS3 CREDIT,0.12"SS,1/8"AL STIFF Fri Oct 13 16:07:17 1995

Transient Temperature Distribution at Time 1.1520E+04

12	-17.75	203.45	203.10	202.03	195.66	180.45	173.83	172.39	171.41	168.25	167.60	162.63	157.39	157.21	149.76
11	-18.00	202.55	202.20	201.14	194.81	179.66	173.07	171.64	170.66	167.52	166.87	161.92	156.70	156.52	149.10
10	-24.75	180.50	180.21	179.29	173.77	160.25	154.37	153.09	152.22	149.39	148.81	144.35	139.63	139.47	132.71
9	-25.00	179.75	179.45	178.54	173.05	159.59	153.74	152.46	151.59	148.78	148.20	143.77	139.07	138.91	132.19
8	-31.75	160.99	160.73	159.92	155.06	143.13	138.08	137.00	136.26	133.90	133.41	129.76	125.99	125.87	120.48
7	-32.00	160.33	160.07	159.27	154.43	142.57	137.55	136.47	135.74	133.40	132.92	129.30	125.56	125.43	120.03
6	-38.75	143.36	143.15	142.48	138.46	128.56	124.55	123.71	123.14	121.34	120.98	118.27	114.87	114.71	105.96
5	-39.00	142.75	142.54	141.88	137.90	128.10	124.11	123.26	122.68	120.85	120.48	117.83	114.50	114.35	105.77
4	-45.75	126.51	126.38	125.97	123.45	116.92	113.19	111.52	110.15	104.22	104.15	104.01	103.83	103.82	103.45
3	-46.00	125.83	125.71	125.31	122.86	116.51	112.85	111.20	109.86	104.14	104.13	104.00	103.82	103.81	103.44
2	-52.75	104.52	104.52	104.50	104.41	104.07	103.75	103.65	103.59	103.35	103.34				
1	-53.00	104.51	104.50	104.49	104.39	104.06	103.74	103.64	103.58	103.34	103.33				
		.00	4.25	8.50	19.25	30.00	33.00	33.60	34.00	35.25	35.50	37.34	39.19	39.25	41.75
		1	2	3	4	5	6	7	8	9	10	11	12	13	14

NOC,100F,50%ENC,TRAN SOLAR,NRCNOC2,NO NS3 CREDIT,0.12"SS,1/8"AL STIFF Fri Oct 13 16:07:17 1995

Transient Temperature Distribution at Time 1.1520E+04

12	-17.75	149.00	148.24	147.86	147.48	147.29	139.00	137.83	136.45	135.85	127.75	126.84	105.39	105.25	104.67
11	-18.00	148.35	147.59	147.21	146.83	146.64	138.36	137.18	135.79	135.19	127.01	126.11	105.25	105.23	104.66
10	-24.75	132.01	131.31	130.95	130.60	130.42	122.31	120.90	119.14	118.34	104.69	104.58	103.83	103.82	
9	-25.00	131.50	130.80	130.44	130.09	129.91	121.80	120.38	118.63	117.83	104.58	104.57	103.82	103.81	
8	-31.75	119.87	119.25	118.92	118.60	118.43	109.68	107.31	104.09	104.01	103.59	103.58			
7	-32.00	119.42	118.80	118.48	118.15	117.99	109.40	107.10	104.00	104.00	103.58	103.58			
6	-38.75	104.16	104.08	104.05	104.03	104.02	103.49	103.40	103.27	103.27					
5	-39.00	104.06	104.05	104.04	104.02	104.01	103.48	103.39	103.28	103.27					
4	-45.75	103.39	103.39												
3	-46.00	103.40	103.39												
2	-52.75														
1	-53.00														
		42.00	42.25	42.38	42.50	42.56	45.25	45.62	46.06	46.25	48.75	49.00	53.75	54.00	58.75
		15	16	17	18	19	20	21	22	23	24	25	26	27	28

NOC,100F,50%ENC,TRAN SOLAR,NRCNOC2,NO NS3 CREDIT,0.12"SS,1/8"AL STIFF Fri Oct 13 16:07:17 1995

Transient Temperature Distribution at Time 1.1520E+04

12	-17.75	104.66			
11	-18.00	104.65			
10	-24.75				
9	-25.00				
8	-31.75				
7	-32.00				
6	-38.75				
5	-39.00				
4	-45.75				
3	-46.00				
2	-52.75				
1	-53.00				
		59.00	63.00	63.12	63.38
		29	30	31	32

3.6.2.4 HEATING7.2 OUTPUT FILE NAME NRCNOC3.OUT

NOC,-40F,NO SOLAR,NRCNOC3,NO CREDIT FOR NS3,1/8"SS,1/8"AL STIFFNERS Fri Oct 13 17:53:08 1995

Steady-State Temperature Distribution at Time 0.0000E+00

65	254.50	-39.00	-39.01	-39.05	-39.22	-39.52	-39.57	-39.58	-39.58	-39.59	-39.59				
64	254.25	-39.00	-39.01	-39.04	-39.22	-39.52	-39.57	-39.58	-39.58	-39.59	-39.59				
63	247.50	-24.42	-24.58	-25.08	-27.87	-33.69	-36.58	-37.27	-37.74	-39.32	-39.32	-39.38	-39.43	-39.44	-39.48
62	247.25	-23.85	-24.02	-24.53	-27.41	-33.40	-36.36	-37.07	-37.57	-39.30	-39.32	-39.38	-39.43	-39.44	-39.48
61	240.50	-7.53	-7.83	-8.75	-13.82	-23.35	-26.89	-27.63	-28.13	-29.72	-30.03	-32.40	-34.90	-34.99	-38.78
60	240.25	-6.87	-7.18	-8.10	-13.25	-22.91	-26.48	-27.23	-27.73	-29.33	-29.65	-32.07	-34.64	-34.73	-38.69
59	233.50	12.63	12.21	10.93	3.85	-9.11	-13.78	-14.76	-15.43	-17.56	-18.00	-21.30	-24.75	-24.87	-29.79
58	233.25	13.44	13.01	11.72	4.57	-8.51	-13.22	-14.22	-14.89	-17.04	-17.48	-20.82	-24.30	-24.42	-29.40
57	226.50	37.40	36.86	35.27	26.39	10.05	4.11	2.85	2.00	-.73	-1.29	-5.55	-10.05	-10.21	-16.72
56	226.25	38.39	37.85	36.24	27.31	10.86	4.87	3.60	2.74	-.02	-.58	-4.87	-9.40	-9.56	-16.12
55	219.50	67.92	67.30	65.45	55.08	35.55	28.34	26.82	25.79	22.49	21.82	16.72	11.42	11.24	3.76
54	219.25	69.13	68.51	66.65	56.24	36.61	29.35	27.81	26.77	23.45	22.77	17.64	12.31	12.12	4.60
53	212.50	105.12	104.46	102.46	91.19	68.93	60.09	58.21	56.93	52.82	51.98	45.65	39.15	38.93	30.12
52	212.25	106.58	105.92	103.92	92.64	70.32	61.41	59.51	58.22	54.07	53.22	46.81	40.22	40.00	31.07
51	205.50	149.49	148.85	146.91	135.92	112.95	101.99	99.50	97.78	92.11	90.92	81.58	71.38	71.03	56.69
50	202.12	173.36	172.76	170.95	160.73	139.80	129.11	126.52	124.70	118.49	117.13	105.75	91.03	90.45	62.62
49	201.62	173.39	172.79	170.98	160.76	139.85	129.19	126.61	124.79	118.61	117.25	105.91	91.24	90.67	62.87
48	201.50	177.50	176.93	175.22	165.80	149.18	143.64	142.55	141.83	139.60	139.17	136.08	133.27	133.18	130.04
47	199.33	177.99	177.42	175.71	166.32	149.83	144.36	143.30	142.60	140.48	140.07	137.25	134.81	134.74	132.23
46	197.17	179.06	178.49	176.79	167.42	150.95	145.20	144.05	143.31	141.15	140.74	138.07	135.82	135.75	133.46
45	195.00	180.73	180.16	178.46	169.09	152.61	146.29	144.66	143.46	141.28	140.90	138.47	136.30	136.24	133.87
44	194.50	256.35	255.87	254.45	246.83	235.15	232.01	231.28	142.82	141.15	140.82	138.53	136.37	136.30	133.82
43	192.25	258.57	258.09	256.66	248.98	237.21	234.38	233.69	142.06	140.57	140.39	138.78	136.68	136.26	132.85
42	188.25	261.64	261.14	259.66	251.72	239.16	235.28	234.59	143.03	141.68	141.57	140.72	140.04	125.65	124.11
41	187.50	262.25	261.75	260.26	252.26	239.54	234.79	234.20	143.21	141.89	141.78	141.01	140.42	123.85	122.40
40	169.75	401.23	399.20	393.09	358.97	294.41	269.00	268.11	144.48	142.52	142.34	140.96	139.47	83.31	77.94
39	169.50	402.61	400.58	394.42	360.03	294.99	269.45	268.55	144.61	142.64	142.46	141.08	139.59	83.24	75.08
38	167.50	412.94	410.86	404.51	368.05	299.48	272.95	272.03	145.74	143.73	143.55	142.16	140.68	85.23	77.27
37	165.25	423.21	421.07	414.56	376.26	304.18	276.73	275.79	147.20	145.16	144.97	143.60	142.21	92.60	88.94
36	143.38	470.35	468.01	460.88	418.80	333.50	302.65	301.61	167.86	165.64	165.43	164.03	162.76	121.54	118.11
35	121.50	487.38	485.01	477.79	435.43	346.55	314.65	313.58	180.09	177.80	177.59	176.13	174.80	132.82	129.21
34	99.62	491.79	489.41	482.20	439.88	350.19	318.05	316.98	183.85	181.55	181.34	179.86	178.51	136.07	132.39
33	77.75	486.87	484.50	477.29	434.95	346.19	314.33	313.26	179.81	177.52	177.31	175.85	174.52	132.53	128.92
32	55.88	468.78	466.45	459.34	417.40	332.58	301.86	300.82	167.38	165.16	164.96	163.56	162.27	120.55	117.11
31	34.00	418.04	415.94	409.53	372.38	302.04	275.08	274.15	147.71	145.69	145.50	144.08	142.57	86.61	81.70
30	32.00	408.14	406.09	399.84	364.60	297.62	271.54	270.64	147.01	145.04	144.86	143.47	141.96	85.26	77.16
29	31.75	406.81	404.77	398.55	363.58	297.05	271.09	270.19	146.94	144.98	144.80	143.41	141.91	85.39	79.32
28	21.25	336.33	335.09	331.34	310.37	268.58	249.46	248.74	146.56	145.04	144.90	143.96	143.12	115.68	113.85
27	14.50	266.28	265.64	263.79	254.71	241.22	237.01	236.47	145.57	144.25	144.13	143.37	142.77	125.73	124.28
26	13.75	264.79	264.16	262.33	253.44	240.45	237.24	236.57	145.41	144.08	143.96	143.18	142.60	126.86	125.42
25	10.25	262.23	261.59	259.69	251.10	238.84	236.10	235.41	144.51	143.10	142.97	141.97	141.24	132.34	130.78
24	8.50	260.78	260.09	257.88	249.38	237.23	234.20	233.43	144.48	142.81	142.63	141.07	139.32	136.27	133.50
23	8.00	250.70	246.78	175.19	167.20	152.85	147.36	145.92	144.86	142.89	142.62	140.86	138.23	137.85	134.09
22	6.00	211.55	206.36	173.38	165.50	151.20	146.18	145.16	144.50	142.59	142.23	139.87	137.52	137.45	134.77
21	4.00	175.43	174.67	172.24	164.23	149.96	145.23	144.30	143.70	141.84	141.49	138.99	136.74	136.67	134.26
20	2.00	174.31	173.59	171.50	163.39	149.07	144.39	143.47	142.86	140.97	140.60	137.97	135.59	135.52	132.97
19	.00	173.82	173.13	171.14	162.97	148.52	143.70	142.73	142.09	140.08	139.68	136.80	134.09	134.00	130.85
18	-.12	169.69	169.09	167.33	158.25	139.19	128.95	126.44	124.67	118.60	117.26	106.03	91.39	90.81	62.91
17	-.38	169.68	169.07	167.31	158.23	139.15	128.90	126.38	124.60	118.52	117.18	105.91	91.23	90.65	62.70
16	-.62	169.67	169.06	167.30	158.22	139.14	128.87	126.35	124.58	118.49	117.14	105.87	91.17	90.59	62.63
15	-4.00	146.41	145.80	143.98	133.89	112.29	101.59	99.14	97.45	91.85	90.67	81.39	71.19	70.84	56.42
14	-10.75	104.51	103.88	101.98	91.26	69.71	60.94	59.06	57.78	53.68	52.84	46.47	39.92	39.70	30.79
13	-11.00	103.08	102.45	100.55	89.83	68.32	59.63	57.76	56.50	52.43	51.60	45.31	38.85	38.63	29.84
		.00	4.25	8.50	19.25	30.00	33.00	33.60	34.00	35.25	35.50	37.34	39.19	39.25	41.75
		1	2	3	4	5	6	7	8	9	10	11	12	13	14

NOC,-40F,NO SOLAR,NRCNOC3,NO CREDIT FOR NS3,1/8"SS,1/8"AL STIFFNERS Fri Oct 13 17:53:08 1995

Steady-State Temperature Distribution at Time 0.0000E+00

65	254.50														
64	254.25														
63	247.50	-39.48	-39.48												
62	247.25	-39.48	-39.48												
61	240.50	-39.18	-39.18	-39.19	-39.19	-39.19	-39.29	-39.29	-39.30	-39.30					
60	240.25	-39.16	-39.18	-39.18	-39.19	-39.19	-39.29	-39.29	-39.30	-39.30					
59	233.50	-30.29	-30.80	-31.05	-31.30	-31.43	-37.00	-37.82	-38.80	-38.80	-38.88	-38.88			
58	233.25	-29.91	-30.42	-30.68	-30.93	-31.06	-36.81	-37.69	-38.77	-38.80	-38.88	-38.88			
57	226.50	-17.40	-18.09	-18.43	-18.78	-18.96	-26.78	-27.94	-29.32	-29.92	-38.18	-38.19	-38.38	-38.38	
56	226.25	-16.80	-17.50	-17.84	-18.19	-18.37	-26.25	-27.42	-28.83	-29.44	-38.13	-38.18	-38.37	-38.38	
55	219.50	3.00	2.23	1.84	1.46	1.26	-7.21	-8.43	-9.87	-10.48	-18.89	-19.75	-36.95	-36.96	-36.33
54	219.25	3.84	3.06	2.68	2.29	2.10	-6.40	-7.61	-9.05	-9.67	-18.07	-18.95	-36.88	-36.95	-36.32
53	212.50	29.27	28.42	27.99	27.57	27.36	18.64	17.47	16.10	15.52	7.99	7.22	-8.35	-9.33	-31.25
52	212.25	30.21	29.35	28.93	28.50	28.29	19.56	18.40	17.05	16.47	9.07	8.31	-7.00	-8.00	-31.11
51	205.50	55.43	54.22	53.63	53.06	52.77	43.76	43.74	43.70	41.74	40.92	40.82	38.22	38.07	35.21
50	202.12	59.27	55.99	54.30	52.73	51.99	44.57	44.28	43.95	43.02	41.37	41.21	38.39	38.25	35.61
49	201.62	59.15	56.28	53.39	51.81	51.17	44.86	44.32	43.70	43.36	41.43	41.26	38.42	38.28	35.67
48	201.50	58.99	58.60	51.07	50.95	50.86	44.90	44.33	43.70	43.43	41.45	41.27	38.43	38.29	35.68
47	199.33	70.57	70.42	47.15	47.11	47.09	44.42	44.07	43.66	43.50	41.58	41.41	38.55	38.41	35.94
46	197.17	76.00	75.85	45.64	45.59	45.56	43.88	43.63	43.34	43.21	41.57	41.41	38.65	38.52	36.15
45	195.00	78.33	78.17	44.98	44.93	44.90	43.53	43.32	43.08	42.97	41.51	41.37	38.72	38.59	36.29
44	194.50	78.62	78.46	44.88	44.83	44.80	43.47	43.27	43.03	42.93	41.51	41.37	38.74	38.61	36.32
43	192.25	78.95	78.80	44.66	44.61	44.58	43.34	43.15	42.93	42.83	41.50	41.36	38.78	38.66	36.39
42	188.25	76.84	76.70	44.82	44.77	44.74	43.52	43.34	43.11	43.01	41.65	41.51	38.83	38.69	36.35
41	187.50	76.40	76.27	44.94	44.90	44.87	43.63	43.44	43.21	43.11	41.70	41.56	38.83	38.69	36.32
40	169.75	67.29	67.02	59.00	58.88	58.82	53.15	52.34	51.39	50.99	45.73	45.26	38.04	37.73	32.86
39	169.50	70.50	66.54	64.47	62.67	61.82	53.61	52.70	51.65	51.18	45.44	44.97	37.78	37.46	32.62
38	167.50	74.68	72.20	71.00	69.85	69.29	56.52	55.53	54.62	54.49					
37	165.25	86.42	83.94	82.70	81.48	80.87	56.52	53.17	49.25	49.08					
36	143.38	114.95	111.80	110.23	108.66	107.88	75.14	70.70	65.52	65.29					
35	121.50	125.81	122.43	120.74	119.06	118.21	82.87	78.06	72.45	72.20					
34	99.62	128.92	125.47	123.75	122.03	121.17	85.07	80.15	74.42	74.17					
33	77.75	125.53	122.16	120.47	118.79	117.95	82.67	77.87	72.27	72.03					
32	55.88	113.96	110.84	109.28	107.73	106.95	74.50	70.09	64.96	64.74					
31	34.00	79.13	76.67	75.47	74.31	73.74	57.03	55.02	52.74	52.57					
30	32.00	73.10	69.53	67.65	66.00	65.22	54.97	53.80	52.50	51.98	44.93	44.36	36.41	36.07	31.13
29	31.75	70.20	69.83	62.70	62.54	62.45	54.60	53.54	52.31	51.79	45.22	44.65	36.67	36.33	31.36
28	21.25	73.47	73.35	46.08	46.04	46.02	44.57	44.33	44.03	43.91	42.04	41.85	38.27	38.10	35.24
27	14.50	76.71	76.56	44.17	44.13	44.10	42.91	42.73	42.51	42.42	41.10	40.96	38.33	38.20	35.89
26	13.75	77.06	76.91	44.09	44.04	44.02	42.83	42.65	42.43	42.34	41.04	40.91	38.33	38.20	35.92
25	10.25	78.60	78.44	44.00	43.95	43.92	42.70	42.52	42.30	42.21	40.92	40.79	38.30	38.17	35.95
24	8.50	78.88	78.73	44.12	44.07	44.04	42.77	42.59	42.36	42.26	40.93	40.80	38.27	38.14	35.92
23	8.00	78.84	78.68	44.18	44.13	44.10	42.81	42.62	42.39	42.29	40.94	40.80	38.26	38.13	35.90
22	6.00	78.02	77.86	44.55	44.50	44.47	43.05	42.84	42.58	42.47	40.99	40.85	38.21	38.09	35.80
21	4.00	75.51	75.36	45.29	45.25	45.22	43.44	43.18	42.87	42.74	41.05	40.89	38.15	38.01	35.66
20	2.00	70.05	69.91	46.87	46.83	46.81	43.98	43.61	43.19	43.01	41.07	40.89	38.06	37.92	35.46
19	.00	59.05	58.67	50.69	50.56	50.47	44.42	43.84	43.19	42.92	40.94	40.76	37.94	37.80	35.22
18	-.12	59.10	56.49	52.86	51.37	50.79	44.40	43.84	43.19	42.85	40.92	40.75	37.93	37.79	35.21
17	-.38	59.20	55.83	53.92	52.23	51.45	44.29	43.83	43.23	42.69	40.89	40.73	37.92	37.78	35.18
16	-.62	59.20	55.80	54.08	52.45	51.67	44.12	43.85	43.56	42.47	40.86	40.70	37.91	37.76	35.15
15	-4.00	55.16	53.93	53.34	52.76	52.47	43.31	43.29	43.26	41.22	40.41	40.31	37.73	37.59	34.75
14	-10.75	29.93	29.07	28.65	28.22	28.01	19.29	18.13	16.78	16.21	8.83	8.07	-7.14	-8.13	-31.04
13	-11.00	28.99	28.14	27.72	27.30	27.09	18.38	17.21	15.85	15.27	7.76	6.99	-8.48	-9.45	-31.18
		42.00	42.25	42.38	42.50	42.56	45.25	45.62	46.06	46.25	48.75	49.00	53.75	54.00	58.75
		15	16	17	18	19	20	21	22	23	24	25	26	27	28

NOC,-40F,NO SOLAR,NRCNOC3,NO CREDIT FOR NS3,1/8"SS,1/8"AL STIFFNERS Fri Oct 13 17:53:08 1995

Steady-State Temperature Distribution at Time 0.0000E+00

65	254.50				
64	254.25				
63	247.50				
62	247.25				
61	240.50				
60	240.25				
59	233.50				
58	233.25				
57	226.50				
56	226.25				
55	219.50	-36.33			
54	219.25	-36.32			
53	212.50	-31.25	-26.12	-25.96	-25.89
52	212.25	-31.21	-26.09	-25.76	-25.76
51	205.50	35.03	31.71	1.91	1.77
50	202.12	35.47	33.40	2.62	2.50
49	201.62	35.54	33.57	2.71	2.59
48	201.50	35.56	33.60	2.73	2.61
47	199.33	35.82	34.11	3.04	2.92
46	197.17	36.04	34.43	3.27	3.15
45	195.00	36.18	34.62	3.45	3.33
44	194.50	36.21	34.66	3.49	3.37
43	192.25	36.28	34.75	3.66	3.53
42	188.25	36.24	34.70	4.10	3.98
41	187.50	36.21	34.66	4.31	4.19
40	169.75	32.65	29.79	24.84	24.65
39	169.50	32.40	29.28	26.90	25.56
38	167.50				
37	165.25				
36	143.38				
35	121.50				
34	99.62				
33	77.75				
32	55.88				
31	34.00				
30	32.00	30.91	27.78	26.15	25.19
29	31.75	31.14	28.19	24.85	24.64
28	21.25	35.11	33.45	4.57	4.45
27	14.50	35.78	34.25	3.48	3.36
26	13.75	35.81	34.29	3.43	3.31
25	10.25	35.85	34.33	3.31	3.19
24	8.50	35.81	34.29	3.25	3.13
23	8.00	35.80	34.27	3.23	3.10
22	6.00	35.70	34.14	3.12	3.00
21	4.00	35.55	33.94	2.98	2.85
20	2.00	35.34	33.63	2.77	2.65
19	.00	35.10	33.16	2.49	2.37
18	-.12	35.08	33.12	2.47	2.35
17	-.38	35.05	33.04	2.43	2.31
16	-.62	35.01	32.95	2.39	2.27
15	-4.00	34.57	31.28	1.71	1.57
14	-10.75	-31.15	-25.92	-25.59	-25.59
13	-11.00	-31.18	-25.95	-25.78	-25.70
		59.00	63.00	63.12	63.38
		29	30	31	32

NOC,-40F,NO SOLAR,NRCNOC3,NO CREDIT FOR NS3,1/8"SS,1/8"AL STIFFNERS Fri Oct 13 17:53:08 1995

Steady-State Temperature Distribution at Time 0.0000E+00

12	-17.75	67.77	67.17	65.37	55.31	36.12	28.95	27.43	26.40	23.11	22.44	17.35	12.05	11.87	4.39
11	-18.00	66.57	65.98	64.19	54.16	35.07	27.95	26.44	25.42	22.15	21.48	16.43	11.17	10.99	3.55
10	-24.75	37.49	36.97	35.40	26.68	10.50	4.58	3.32	2.47	-.26	-.82	-5.08	-9.58	-9.73	-16.25
9	-25.00	36.52	36.00	34.44	25.77	9.70	3.82	2.58	1.73	-.98	-1.53	-5.76	-10.22	-10.38	-16.85
8	-31.75	12.86	12.44	11.18	4.16	-8.74	-13.41	-14.40	-15.07	-17.20	-17.64	-20.94	-24.40	-24.52	-29.46
7	-32.00	12.07	11.65	10.40	3.45	-9.34	-13.96	-14.94	-15.60	-17.72	-18.15	-21.42	-24.85	-24.97	-29.85
6	-38.75	-7.21	-7.51	-8.42	-13.50	-23.04	-26.58	-27.32	-27.82	-29.41	-29.73	-32.12	-34.68	-34.77	-38.69
5	-39.00	-7.87	-8.16	-9.06	-14.06	-23.48	-26.99	-27.72	-28.22	-29.79	-30.11	-32.45	-34.94	-35.03	-38.79
4	-45.75	-24.01	-24.18	-24.68	-27.53	-33.45	-36.39	-37.09	-37.59	-39.31	-39.32	-39.38	-39.44	-39.44	-39.48
3	-46.00	-24.58	-24.74	-25.22	-27.98	-33.74	-36.61	-37.29	-37.76	-39.32	-39.32	-39.39	-39.44	-39.44	-39.48
2	-52.75	-39.01	-39.02	-39.05	-39.23	-39.52	-39.58	-39.58	-39.59	-39.59	-39.59				
1	-53.00	-39.01	-39.02	-39.05	-39.23	-39.52	-39.58	-39.58	-39.59	-39.59	-39.59				
		.00	4.25	8.50	19.25	30.00	33.00	33.60	34.00	35.25	35.50	37.34	39.19	39.25	41.75
		1	2	3	4	5	6	7	8	9	10	11	12	13	14

NOC,-40F,NO SOLAR,NRCNOC3,NO CREDIT FOR NS3,1/8"SS,1/8"AL STIFFNERS Fri Oct 13 17:53:08 1995

Steady-State Temperature Distribution at Time 0.0000E+00

12	-17.75	3.63	2.86	2.48	2.09	1.90	-6.55	-7.76	-9.19	-9.81	-18.17	-19.04	-36.88	-36.95	-36.30
11	-18.00	2.79	2.03	1.65	1.26	1.07	-7.37	-8.58	-10.01	-10.62	-18.99	-19.84	-36.95	-36.96	-36.31
10	-24.75	-16.93	-17.62	-17.96	-18.31	-18.49	-26.32	-27.49	-28.88	-29.49	-38.14	-38.19	-38.38	-38.38	
9	-25.00	-17.53	-18.21	-18.55	-18.90	-19.07	-26.85	-28.00	-29.38	-29.97	-38.19	-38.19	-38.38	-38.38	
8	-31.75	-29.97	-30.48	-30.73	-30.99	-31.12	-36.82	-37.70	-38.78	-38.80	-38.89	-38.89			
7	-32.00	-30.35	-30.85	-31.10	-31.35	-31.48	-37.02	-37.84	-38.80	-38.81	-38.89	-38.89			
6	-38.75	-39.16	-39.18	-39.19	-39.19	-39.20	-39.29	-39.30	-39.30	-39.30					
5	-39.00	-39.19	-39.19	-39.19	-39.20	-39.20	-39.29	-39.30	-39.30	-39.30					
4	-45.75	-39.48	-39.48												
3	-46.00	-39.48	-39.48												
2	-52.75														
1	-53.00														
		42.00	42.25	42.38	42.50	42.56	45.25	45.62	46.06	46.25	48.75	49.00	53.75	54.00	58.75
		15	16	17	18	19	20	21	22	23	24	25	26	27	28

NOC,-40F,NO SOLAR,NRCNOC3,NO CREDIT FOR NS3,1/8"SS,1/8"AL STIFFNERS Fri Oct 13 17:53:08 1995

Steady-State Temperature Distribution at Time 0.0000E+00

12	-17.75	-36.31			
11	-18.00	-36.31			
10	-24.75				
9	-25.00				
8	-31.75				
7	-32.00				
6	-38.75				
5	-39.00				
4	-45.75				
3	-46.00				
2	-52.75				
1	-53.00				
		59.00	63.00	63.12	63.38
		29	30	31	32

3.6.2.5 HEATING7.2 OUTPUT FILE NAME NRCNOC4.OUT

NOC,-20F,NO SOLAR,NRCNOC4,NO CREDIT FOR NS3,1/8"SS,1/8"AL STIFFNERS Fri Oct 13 17:53:18 1995

Steady-State Temperature Distribution at Time 0.0000E+00

65	254.50	-19.11	-19.12	-19.15	-19.31	-19.58	-19.63	-19.64	-19.64	-19.65	-19.65				
64	254.25	-19.11	-19.12	-19.14	-19.30	-19.58	-19.63	-19.64	-19.64	-19.64	-19.65				
63	247.50	-4.90	-5.06	-5.54	-8.26	-13.92	-16.73	-17.40	-17.86	-19.39	-19.39	-19.45	-19.51	-19.51	-19.55
62	247.25	-4.35	-4.51	-5.00	-7.81	-13.63	-16.51	-17.20	-17.69	-19.37	-19.39	-19.45	-19.50	-19.51	-19.55
61	240.50	11.55	11.25	10.36	5.42	-3.87	-7.31	-8.03	-8.52	-10.06	-10.37	-12.67	-15.11	-15.20	-18.89
60	240.25	12.19	11.89	10.99	5.97	-3.44	-6.91	-7.64	-8.13	-9.69	-10.00	-12.35	-14.86	-14.95	-18.79
59	233.50	31.19	30.77	29.53	22.62	9.98	5.43	4.47	3.82	1.74	1.32	-1.90	-5.26	-5.38	-10.17
58	233.25	31.97	31.55	30.30	23.32	10.56	5.97	5.00	4.34	2.25	1.82	-1.43	-4.83	-4.94	-9.79
57	226.50	55.32	54.80	53.24	44.57	28.62	22.82	21.59	20.76	18.09	17.54	13.39	9.01	8.85	2.51
56	226.25	56.28	55.76	54.19	45.46	29.40	23.55	22.32	21.48	18.79	18.24	14.05	9.64	9.48	3.09
55	219.50	85.07	84.47	82.66	72.52	53.43	46.39	44.89	43.89	40.66	40.00	35.03	29.85	29.67	22.36
54	219.25	86.26	85.65	83.83	73.65	54.46	47.36	45.86	44.84	41.60	40.93	35.92	30.71	30.53	23.18
53	212.50	121.36	120.72	118.76	107.72	85.95	77.30	75.45	74.20	70.18	69.36	63.15	56.78	56.56	47.92
52	212.25	122.79	122.14	120.18	109.13	87.30	78.58	76.72	75.45	71.39	70.56	64.28	57.82	57.60	48.84
51	205.50	164.67	164.05	162.14	151.35	128.88	118.17	115.74	114.06	108.51	107.34	98.19	88.17	87.83	73.71
50	202.12	187.99	187.40	185.62	175.56	155.08	144.66	142.14	140.37	134.32	132.99	121.89	107.50	106.94	79.60
49	201.62	188.02	187.43	185.64	175.60	155.13	144.74	142.23	140.46	134.43	133.10	122.04	107.71	107.15	79.85
48	201.50	191.95	191.39	189.70	180.39	163.96	158.47	157.39	156.67	154.47	154.04	150.96	148.16	148.07	144.92
47	199.33	192.43	191.87	190.18	180.90	164.60	159.18	158.13	157.43	155.33	154.93	152.12	149.69	149.61	147.10
46	197.17	193.49	192.93	191.25	181.99	165.70	160.01	158.87	158.13	155.99	155.59	152.93	150.69	150.62	148.33
45	195.00	195.14	194.58	192.90	183.64	167.34	161.09	159.47	158.29	156.13	155.75	153.34	151.18	151.12	148.76
44	194.50	267.41	266.93	265.51	257.88	246.19	243.06	242.33	157.66	156.01	155.68	153.40	151.25	151.18	148.72
43	192.25	269.61	269.13	267.70	260.01	248.24	245.40	244.72	156.93	155.46	155.28	153.68	151.58	151.16	147.78
42	188.25	272.68	272.19	270.71	262.76	250.19	246.30	245.62	157.93	156.60	156.48	155.63	154.95	140.81	139.26
41	187.50	273.29	272.79	271.31	263.30	250.56	245.81	245.23	158.11	156.81	156.69	155.92	155.33	139.06	137.60
40	169.75	411.82	409.85	403.86	369.66	304.95	279.50	278.60	159.59	157.65	157.47	156.08	154.58	100.00	94.69
39	169.50	413.16	411.18	405.16	370.72	305.53	279.93	279.04	159.72	157.78	157.59	156.20	154.71	99.94	91.87
38	167.50	423.14	421.11	414.94	378.72	309.97	283.39	282.47	160.88	158.89	158.71	157.31	155.83	101.96	94.08
37	165.25	433.08	431.00	424.66	386.93	314.63	287.13	286.19	162.37	160.34	160.15	158.77	157.38	109.29	105.68
36	143.38	479.13	476.84	469.87	428.88	343.65	312.80	311.77	183.14	180.94	180.74	179.33	178.05	138.09	134.69
35	121.50	495.84	493.52	486.46	445.16	356.66	324.78	323.72	195.37	193.10	192.89	191.43	190.10	149.33	145.76
34	99.62	499.96	497.63	490.55	449.10	360.51	328.34	327.27	199.15	196.87	196.66	195.17	193.82	152.58	148.94
33	77.75	495.38	493.06	486.01	444.74	356.29	324.45	323.39	195.07	192.81	192.60	191.14	189.81	149.04	145.47
32	55.88	477.64	475.35	468.41	427.55	342.75	312.02	310.99	182.62	180.42	180.22	178.82	177.53	137.08	133.68
31	34.00	428.22	426.18	419.97	383.00	312.49	285.49	284.56	162.79	160.78	160.59	159.16	157.64	103.33	98.47
30	32.00	418.64	416.65	410.58	375.24	308.12	281.99	281.09	162.06	160.11	159.93	158.53	157.02	101.93	93.94
29	31.75	417.36	415.38	409.33	374.22	307.55	281.55	280.65	161.99	160.04	159.86	158.47	156.96	102.06	96.06
28	21.25	347.15	345.92	342.18	321.18	279.36	260.24	259.53	161.48	159.97	159.83	158.89	158.05	131.28	129.46
27	14.50	277.20	276.56	274.72	265.64	252.15	247.96	247.42	160.43	159.12	159.01	158.24	157.64	140.92	139.46
26	13.75	275.71	275.09	273.27	264.39	251.40	248.19	247.52	160.26	158.95	158.83	158.05	157.46	142.00	140.56
25	10.25	273.15	272.51	270.62	262.04	249.78	247.05	246.37	159.34	157.95	157.82	156.83	156.09	147.31	145.76
24	8.50	271.69	271.01	268.83	260.33	248.19	245.17	244.41	159.30	157.65	157.48	155.92	154.17	151.16	148.41
23	8.00	262.02	258.24	189.70	181.79	167.57	162.14	160.72	159.68	157.73	157.46	155.70	153.09	152.71	148.97
22	6.00	224.50	219.51	187.92	180.11	165.95	160.97	159.97	159.31	157.41	157.06	154.71	152.37	152.30	149.63
21	4.00	190.00	189.25	186.80	178.85	164.73	160.03	159.12	158.51	156.67	156.32	153.84	151.59	151.52	149.11
20	2.00	188.89	188.17	186.07	178.02	163.85	159.21	158.29	157.68	155.81	155.44	152.82	150.45	150.38	147.82
19	.00	188.40	187.71	185.71	177.62	163.30	158.53	157.57	156.93	154.93	154.54	151.67	148.96	148.87	145.71
18	-.12	184.42	183.82	182.07	173.12	154.48	144.52	142.07	140.35	134.44	133.13	122.18	107.87	107.30	79.92
17	-.38	184.40	183.80	182.06	173.11	154.45	144.46	142.01	140.28	134.35	133.05	122.06	107.71	107.15	79.70
16	-.62	184.39	183.79	182.05	173.10	154.43	144.44	141.99	140.26	134.32	133.01	122.02	107.66	107.09	79.63
15	-4.00	161.67	161.07	159.28	149.37	128.24	117.79	115.39	113.74	108.26	107.10	98.01	88.00	87.66	73.46
14	-10.75	120.76	120.15	118.28	107.79	86.71	78.13	76.29	75.04	71.02	70.19	63.96	57.53	57.32	48.58
13	-11.00	119.37	118.75	116.89	106.39	85.36	76.84	75.02	73.78	69.80	68.99	62.83	56.49	56.27	47.66
		.00	4.25	8.50	19.25	30.00	33.00	33.60	34.00	35.25	35.50	37.34	39.19	39.25	41.75
		1	2	3	4	5	6	7	8	9	10	11	12	13	14

NOC,-20F,NO SOLAR,NRCNOC4,NO CREDIT FOR NS3,1/8"SS,1/8"AL STIFFNERS Fri Oct 13 17:53:18 1995

Steady-State Temperature Distribution at Time 0.0000E+00

65	254.50														
64	254.25														
63	247.50	-19.55	-19.55												
62	247.25	-19.55	-19.55												
61	240.50	-19.27	-19.27	-19.28	-19.28	-19.28	-19.38	-19.39	-19.39	-19.39					
60	240.25	-19.25	-19.27	-19.27	-19.28	-19.28	-19.38	-19.39	-19.39	-19.39					
59	233.50	-10.66	-11.14	-11.39	-11.64	-11.76	-17.18	-17.98	-18.93	-18.93	-19.02	-19.02			
58	233.25	-10.28	-10.78	-11.03	-11.28	-11.41	-16.99	-17.86	-18.91	-18.93	-19.02	-19.02			
57	226.50	1.84	1.17	.84	.50	.33	-7.29	-8.42	-9.76	-10.34	-18.38	-18.38	-18.59	-18.59	
56	226.25	2.42	1.75	1.41	1.07	.90	-6.78	-7.92	-9.28	-9.88	-18.33	-18.38	-18.59	-18.59	
55	219.50	21.62	20.87	20.49	20.12	19.93	11.65	10.47	9.07	8.46	.27	-.57	-17.30	-17.30	-16.77
54	219.25	22.43	21.68	21.30	20.92	20.73	12.44	11.26	9.86	9.25	1.06	.21	-17.23	-17.29	-16.77
53	212.50	47.08	46.25	45.83	45.42	45.21	36.66	35.51	34.17	33.60	26.23	25.48	10.28	9.32	-12.06
52	212.25	48.00	47.16	46.74	46.32	46.11	37.55	36.41	35.08	34.52	27.27	26.53	11.58	10.60	-11.93
51	205.50	72.47	71.27	70.69	70.12	69.83	60.84	60.82	60.79	58.83	58.01	57.91	55.30	55.16	52.30
50	202.12	76.28	73.03	71.36	69.80	69.06	61.66	61.37	61.04	60.10	58.46	58.30	55.48	55.33	52.69
49	201.62	76.17	73.32	70.45	68.88	68.24	61.95	61.41	60.79	60.45	58.52	58.35	55.50	55.36	52.75
48	201.50	76.02	75.63	68.15	68.02	67.93	61.98	61.42	60.79	60.52	58.54	58.36	55.51	55.37	52.77
47	199.33	87.38	87.23	64.25	64.21	64.19	61.52	61.16	60.76	60.59	58.67	58.49	55.63	55.49	53.02
46	197.17	92.63	92.48	62.75	62.71	62.68	60.98	60.73	60.44	60.31	58.65	58.50	55.73	55.59	53.21
45	195.00	94.85	94.69	62.10	62.05	62.02	60.63	60.42	60.17	60.07	58.60	58.46	55.80	55.67	53.35
44	194.50	95.13	94.97	62.01	61.95	61.93	60.58	60.37	60.13	60.03	58.59	58.45	55.81	55.68	53.38
43	192.25	95.42	95.26	61.79	61.73	61.71	60.44	60.25	60.03	59.93	58.58	58.45	55.85	55.72	53.44
42	188.25	93.30	93.16	61.93	61.88	61.85	60.62	60.43	60.20	60.10	58.72	58.58	55.89	55.75	53.40
41	187.50	92.87	92.74	62.06	62.01	61.98	60.72	60.53	60.29	60.19	58.78	58.64	55.88	55.75	53.36
40	169.75	84.18	83.92	75.97	75.86	75.79	70.14	69.33	68.38	67.98	62.72	62.25	55.04	54.73	49.87
39	169.50	87.36	83.45	81.40	79.61	78.78	70.60	69.69	68.64	68.16	62.43	61.95	54.78	54.46	49.62
38	167.50	91.52	89.06	87.88	86.75	86.19	73.52	72.54	71.65	71.51					
37	165.25	103.19	100.74	99.52	98.31	97.71	73.68	70.38	66.50	66.33					
36	143.38	131.57	128.46	126.91	125.37	124.59	92.24	87.85	82.72	82.50					
35	121.50	142.40	139.06	137.39	135.72	134.89	99.94	95.17	89.62	89.38					
34	99.62	145.51	142.10	140.39	138.69	137.84	102.13	97.26	91.58	91.33					
33	77.75	142.11	138.77	137.11	135.45	134.61	99.73	94.98	89.43	89.19					
32	55.88	130.57	127.49	125.95	124.41	123.64	91.59	87.23	82.15	81.93					
31	34.00	95.94	93.49	92.32	91.17	90.60	74.07	72.09	69.83	69.66					
30	32.00	89.94	86.42	84.57	82.94	82.17	71.98	70.81	69.51	68.99	61.94	61.37	53.43	53.10	48.17
29	31.75	87.08	86.71	79.68	79.52	79.43	71.61	70.55	69.32	68.80	62.24	61.67	53.69	53.36	48.40
28	21.25	90.09	89.97	63.19	63.15	63.12	61.66	61.42	61.12	60.99	59.12	58.93	55.34	55.17	52.29
27	14.50	93.19	93.05	61.31	61.26	61.24	60.03	59.85	59.63	59.53	58.20	58.06	55.41	55.28	52.96
26	13.75	93.54	93.39	61.23	61.18	61.16	59.95	59.77	59.55	59.46	58.15	58.01	55.41	55.28	52.99
25	10.25	95.06	94.90	61.15	61.10	61.07	59.83	59.65	59.43	59.33	58.04	57.90	55.39	55.26	53.03
24	8.50	95.37	95.21	61.27	61.22	61.19	59.91	59.71	59.49	59.39	58.04	57.91	55.36	55.24	53.00
23	8.00	95.33	95.17	61.33	61.28	61.25	59.94	59.75	59.52	59.42	58.05	57.91	55.36	55.23	52.98
22	6.00	94.57	94.41	61.70	61.65	61.62	60.18	59.96	59.71	59.60	58.11	57.96	55.31	55.18	52.89
21	4.00	92.18	92.02	62.44	62.39	62.36	60.57	60.30	60.00	59.86	58.17	58.01	55.25	55.12	52.75
20	2.00	86.89	86.75	64.00	63.96	63.93	61.10	60.73	60.31	60.13	58.18	58.01	55.16	55.02	52.56
19	.00	76.10	75.72	67.79	67.66	67.57	61.54	60.96	60.31	60.03	58.05	57.88	55.05	54.91	52.33
18	-.12	76.14	73.55	69.94	68.47	67.89	61.51	60.95	60.30	59.97	58.04	57.86	55.04	54.90	52.31
17	-.38	76.24	72.90	71.00	69.32	68.54	61.40	60.95	60.34	59.81	58.00	57.84	55.03	54.89	52.28
16	-.62	76.24	72.86	71.16	69.54	68.76	61.24	60.97	60.68	59.59	57.97	57.81	55.02	54.87	52.26
15	-4.00	72.21	71.00	70.41	69.84	69.55	60.42	60.40	60.37	58.34	57.53	57.43	54.85	54.70	51.87
14	-10.75	47.73	46.89	46.48	46.06	45.85	37.29	36.15	34.83	34.27	27.04	26.30	11.44	10.48	-11.87
13	-11.00	46.82	45.99	45.57	45.16	44.95	36.41	35.26	33.93	33.36	26.01	25.26	10.15	9.20	-12.00
		42.00	42.25	42.38	42.50	42.56	45.25	45.62	46.06	46.25	48.75	49.00	53.75	54.00	58.75
		15	16	17	18	19	20	21	22	23	24	25	26	27	28

NOC,-20F,NO SOLAR,NRCNOC4,NO CREDIT FOR NS3,1/8"SS,1/8"AL STIFFNERS Fri Oct 13 17:53:18 1995

Steady-State Temperature Distribution at Time 0.0000E+00

65	254.50				
64	254.25				
63	247.50				
62	247.25				
61	240.50				
60	240.25				
59	233.50				
58	233.25				
57	226.50				
56	226.25				
55	219.50	-16.77			
54	219.25	-16.77			
53	212.50	-12.06	-7.25	-7.09	-7.03
52	212.25	-12.03	-7.22	-6.90	-6.90
51	205.50	52.12	48.84	19.80	19.66
50	202.12	52.56	50.48	20.68	20.56
49	201.62	52.62	50.65	20.78	20.66
48	201.50	52.64	50.68	20.81	20.69
47	199.33	52.90	51.17	21.15	21.03
46	197.17	53.10	51.48	21.39	21.27
45	195.00	53.24	51.67	21.57	21.44
44	194.50	53.27	51.70	21.60	21.48
43	192.25	53.33	51.79	21.76	21.63
42	188.25	53.29	51.73	22.17	22.04
41	187.50	53.25	51.69	22.36	22.23
40	169.75	49.65	46.80	41.88	41.69
39	169.50	49.41	46.29	43.93	42.59
38	167.50				
37	165.25				
36	143.38				
35	121.50				
34	99.62				
33	77.75				
32	55.88				
31	34.00				
30	32.00	47.95	44.83	43.21	42.25
29	31.75	48.18	45.24	41.92	41.72
28	21.25	52.17	50.50	22.55	22.43
27	14.50	52.85	51.30	21.59	21.46
26	13.75	52.88	51.34	21.54	21.42
25	10.25	52.93	51.40	21.44	21.32
24	8.50	52.89	51.36	21.38	21.26
23	8.00	52.88	51.34	21.36	21.24
22	6.00	52.78	51.22	21.26	21.14
21	4.00	52.64	51.02	21.11	20.99
20	2.00	52.44	50.72	20.89	20.77
19	.00	52.20	50.26	20.58	20.46
18	-.12	52.19	50.22	20.56	20.44
17	-.38	52.15	50.15	20.51	20.39
16	-.62	52.12	50.06	20.46	20.34
15	-4.00	51.69	48.43	19.60	19.46
14	-10.75	-11.97	-7.05	-6.73	-6.73
13	-11.00	-12.00	-7.08	-6.91	-6.84
		59.00	63.00	63.12	63.38
		29	30	31	32

NOC,-20F,NO SOLAR,NRCNOC4,NO CREDIT FOR NS3,1/8"SS,1/8"AL STIFFNERS Fri Oct 13 17:53:18 1995
Steady-State Temperature Distribution at Time 0.0000E+00

12	-17.75	84.92	84.34	82.58	72.74	53.98	46.97	45.49	44.48	41.27	40.61	35.64	30.46	30.28	22.98
11	-18.00	83.76	83.18	81.42	71.62	52.96	46.00	44.53	43.53	40.33	39.68	34.75	29.60	29.43	22.16
10	-24.75	55.41	54.90	53.37	44.85	29.05	23.27	22.04	21.21	18.55	18.00	13.85	9.47	9.32	2.96
9	-25.00	54.46	53.95	52.43	43.96	28.27	22.54	21.32	20.50	17.85	17.31	13.19	8.84	8.69	2.38
8	-31.75	31.41	31.00	29.77	22.92	10.33	5.78	4.82	4.17	2.09	1.67	-1.55	-4.92	-5.04	-9.85
7	-32.00	30.64	30.23	29.01	22.23	9.76	5.25	4.30	3.65	1.59	1.17	-2.02	-5.36	-5.47	-10.23
6	-38.75	11.86	11.57	10.68	5.73	-3.57	-7.01	-7.73	-8.22	-9.76	-10.07	-12.41	-14.89	-14.98	-18.80
5	-39.00	11.22	10.93	10.06	5.18	-3.99	-7.41	-8.12	-8.61	-10.14	-10.44	-12.72	-15.14	-15.23	-18.89
4	-45.75	-4.50	-4.66	-5.15	-7.92	-13.68	-16.54	-17.22	-17.71	-19.38	-19.39	-19.46	-19.51	-19.51	-19.55
3	-46.00	-5.05	-5.21	-5.68	-8.37	-13.97	-16.76	-17.42	-17.88	-19.40	-19.40	-19.46	-19.51	-19.51	-19.55
2	-52.75	-19.11	-19.12	-19.15	-19.31	-19.58	-19.63	-19.64	-19.64	-19.65	-19.65				
1	-53.00	-19.12	-19.13	-19.15	-19.31	-19.58	-19.63	-19.64	-19.64	-19.65	-19.65				
		.00	4.25	8.50	19.25	30.00	33.00	33.60	34.00	35.25	35.50	37.34	39.19	39.25	41.75
		1	2	3	4	5	6	7	8	9	10	11	12	13	14

NOC,-20F,NO SOLAR,NRCNOC4,NO CREDIT FOR NS3,1/8"SS,1/8"AL STIFFNERS Fri Oct 13 17:53:18 1995
Steady-State Temperature Distribution at Time 0.0000E+00

12	-17.75	22.23	21.48	21.11	20.73	20.54	12.29	11.11	9.72	9.12	.97	.12	-17.23	-17.29	-16.75
11	-18.00	21.42	20.68	20.30	19.93	19.74	11.51	10.33	8.93	8.33	.18	-.65	-17.29	-17.30	-16.76
10	-24.75	2.30	1.63	1.29	.96	.78	-6.84	-7.98	-9.34	-9.93	-18.34	-18.38	-18.59	-18.59	
9	-25.00	1.72	1.06	.72	.39	.22	-7.36	-8.48	-9.81	-10.39	-18.38	-18.39	-18.59	-18.59	
8	-31.75	-10.34	-10.84	-11.09	-11.33	-11.46	-17.01	-17.87	-18.91	-18.94	-19.02	-19.03			
7	-32.00	-10.71	-11.20	-11.44	-11.69	-11.81	-17.20	-18.00	-18.94	-18.94	-19.03	-19.03			
6	-38.75	-19.25	-19.27	-19.28	-19.28	-19.29	-19.38	-19.39	-19.39	-19.39					
5	-39.00	-19.28	-19.28	-19.28	-19.29	-19.29	-19.38	-19.39	-19.39	-19.39					
4	-45.75	-19.55	-19.55												
3	-46.00	-19.55	-19.55												
2	-52.75														
1	-53.00														
		42.00	42.25	42.38	42.50	42.56	45.25	45.62	46.06	46.25	48.75	49.00	53.75	54.00	58.75
		15	16	17	18	19	20	21	22	23	24	25	26	27	28

NOC,-20F,NO SOLAR,NRCNOC4,NO CREDIT FOR NS3,1/8"SS,1/8"AL STIFFNERS Fri Oct 13 17:53:18 1995
Steady-State Temperature Distribution at Time 0.0000E+00

12	-17.75	-16.75			
11	-18.00	-16.76			
10	-24.75				
9	-25.00				
8	-31.75				
7	-32.00				
6	-38.75				
5	-39.00				
4	-45.75				
3	-46.00				
2	-52.75				
1	-53.00				
		59.00	63.00	63.12	63.38
		29	30	31	32

3.6.3 Accident Condition Results

The NUHOMS®-MP187 Package thermal model HEATING7.2 input, and temperature distribution for the 30-minute fire, Postfire and Final Steady State accident conditions are included in this appendix.

HEATING7.2 Input file Name: FIRECON2.INP

THIS SECTION CONTAINS
PROPRIETARY INFORMATION

3.6.3.1 HEATING7.2 OUTPUT FILE NAME: FIRECON2.OUT

FIRE,CRUSHED IL,1/8"AL,1/8"SS STIFFNERS,WITH NS3, Forced Convection Mon Dec 9 19:47:21 1996

Transient Temperature Distribution at Time 3.0000E+01

58	215.41	1439.74	1439.74	1439.73	1439.70	1439.65	1439.59	1439.49	1439.42	1439.41	1439.40	1439.40	1439.37	1439.36	1439.32
57	215.16	1437.71	1437.71	1437.70	1437.67	1437.62	1437.55	1437.45	1437.38	1437.36	1437.35	1437.35	1437.32	1437.31	1437.27
56	214.43	785.11	785.03	784.79	784.23	783.35	782.07	780.23	778.88	778.59	778.49	778.38	777.73	777.59	776.55
55	213.70	335.69	335.59	335.30	334.62	333.56	332.02	329.82	328.20	327.84	327.71	327.59	326.79	326.62	325.35
54	212.98	184.96	184.84	184.47	183.64	182.32	180.41	177.67	175.64	175.18	175.03	174.87	173.85	173.64	172.00
53	212.25	145.57	145.42	144.98	143.96	142.38	140.07	136.76	134.28	133.72	133.53	133.34	132.08	131.82	129.79
52	208.88	173.51	173.25	172.46	170.66	167.87	163.82	157.99	153.53	152.50	152.15	151.79	149.45	148.96	145.07
51	205.50	206.95	206.58	205.46	202.94	199.06	193.53	185.67	179.55	178.12	177.62	177.12	173.79	173.08	167.40
50	204.66	215.47	215.07	213.87	211.18	207.05	201.21	192.95	186.56	185.08	184.57	184.05	180.65	179.94	174.49
49	203.81	224.05	223.62	222.35	219.48	215.12	208.98	200.40	193.99	192.64	192.19	191.75	189.10	188.67	186.80
48	202.97	232.69	232.25	230.89	227.86	223.27	216.86	208.19	203.31	203.29	203.40	203.58	206.48	207.82	226.45
47	202.12	241.41	240.94	239.51	236.32	231.50	224.93	217.67	224.03	231.38	234.45	237.87	267.58	276.53	373.86
46	201.62	241.50	241.02	239.60	236.40	231.58	225.01	217.78	224.25	231.63	234.72	238.14	267.94	276.90	374.16
45	201.50	249.57	249.09	247.66	244.48	239.78	233.61	226.69	226.23	227.79	228.47	229.23	236.19	238.32	262.10
44	195.00	253.06	252.58	251.14	247.95	243.25	237.07	230.24	230.87	233.18	234.16	235.27	242.89	245.15	270.11
43	194.50	315.10	314.65	313.31	310.40	306.29	301.25	295.81	293.14	292.60	263.57	239.45	244.58	246.55	270.35
42	192.25	317.26	316.81	315.46	312.53	308.38	303.30	297.83	295.36	294.87	271.24	247.25	251.84	253.23	270.90
41	188.25	320.33	319.87	318.47	315.44	311.13	305.76	299.67	296.29	295.72	266.74	237.07	238.66	239.12	243.63
40	187.50	320.93	320.46	319.05	316.00	311.65	306.22	300.00	295.90	295.42	265.67	235.17	236.25	236.60	239.51
39	172.39	443.85	442.21	437.24	425.86	407.91	382.01	347.84	324.31	323.52	279.88	234.53	233.96	234.03	234.97
38	169.75	456.55	454.83	449.60	437.60	418.64	390.86	353.91	328.87	328.04	283.24	236.63	236.32	236.47	238.65
37	169.50	457.65	455.92	450.67	438.61	419.57	391.64	354.45	329.28	328.46	283.53	236.78	236.47	236.63	238.84
36	167.50	465.90	464.11	458.68	446.21	426.51	397.58	358.62	332.52	331.67	285.63	237.66	237.25	237.39	239.33
35	165.25	474.10	472.25	466.64	453.76	433.41	403.62	362.95	335.94	335.06	287.63	238.15	237.46	237.53	238.59
34	148.84	507.26	505.18	498.86	484.44	461.92	429.54	383.90	353.63	352.65	301.27	247.48	246.32	246.32	246.80
33	132.44	521.51	519.34	512.78	497.82	474.58	441.36	394.92	363.26	362.25	309.77	254.80	253.54	253.53	253.95
32	116.03	527.58	525.39	518.75	503.62	480.15	446.71	400.11	367.92	366.89	314.13	258.87	257.58	257.57	257.96
31	99.62	529.17	526.97	520.31	505.15	481.64	448.15	401.53	369.21	368.17	315.37	260.06	258.76	258.74	259.13
30	83.22	527.14	524.95	518.31	503.20	479.74	446.31	399.71	367.56	366.53	313.78	258.53	257.24	257.23	257.62
29	66.81	520.40	518.24	511.69	496.77	473.57	440.39	393.98	362.43	361.41	308.99	254.07	252.82	252.81	253.23
28	50.41	504.76	502.69	496.43	482.11	459.74	427.53	382.06	352.03	351.06	299.90	246.36	245.22	245.22	245.72
27	34.00	467.99	466.20	460.77	448.25	428.37	399.11	359.51	333.10	332.24	285.74	237.27	236.71	236.81	238.19
26	33.00	464.03	462.28	456.94	444.64	425.09	396.26	357.47	331.48	330.64	284.62	236.69	236.13	236.23	237.68
25	32.00	459.83	458.11	452.88	440.81	421.61	393.27	355.35	329.82	328.98	283.47	236.07	235.50	235.59	237.02
24	31.75	458.74	457.03	451.82	439.82	420.71	392.50	354.81	329.39	328.56	283.17	235.91	235.33	235.42	236.82
23	30.43	452.71	451.05	445.99	434.33	415.72	388.30	351.86	327.09	326.27	281.55	235.02	234.36	234.42	235.52
22	29.11	446.16	444.55	439.65	428.37	410.30	383.84	348.76	324.70	323.90	279.88	234.10	233.34	233.38	234.09
21	21.25	393.83	392.62	388.98	380.84	368.52	351.14	326.97	308.75	308.09	269.63	229.86	228.98	228.96	229.08
20	14.50	324.76	324.16	322.39	318.80	313.84	307.84	301.28	297.19	296.69	262.58	227.45	226.89	226.92	227.37
19	13.75	323.33	322.73	320.99	317.47	312.63	306.82	300.58	297.41	296.79	262.57	227.33	226.85	226.89	227.49
18	10.25	320.71	320.10	318.31	314.90	310.26	304.74	299.00	296.30	295.67	261.84	227.06	227.07	227.23	229.11
17	8.50	319.21	318.57	316.53	313.16	308.57	303.12	297.43	294.53	293.84	256.99	226.19	226.73	227.00	230.94
16	8.00	310.67	306.43	248.68	246.06	241.90	236.37	229.59	225.94	225.63	225.58	225.57	226.21	226.55	230.98
15	4.00	248.64	247.97	245.77	243.08	238.94	233.46	226.84	223.51	223.27	223.23	223.22	223.78	224.14	229.62
14	2.00	247.43	246.80	244.96	242.16	238.01	232.54	225.95	222.78	222.63	222.62	222.65	223.56	224.03	230.75
13	.00	246.77	246.16	244.44	241.61	237.46	231.97	225.37	222.32	222.28	222.34	222.43	223.90	224.56	233.63
12	-.12	238.70	238.21	236.79	233.90	229.61	223.66	215.84	213.69	215.93	217.00	218.25	230.88	235.49	292.85
11	-.62	238.62	238.13	236.71	233.82	229.53	223.58	215.74	213.50	215.69	216.74	217.98	230.45	235.02	292.06
10	-2.31	221.63	221.21	219.98	217.40	213.52	208.06	200.40	194.62	193.38	192.97	192.56	190.09	189.69	187.88
9	-4.00	204.90	204.54	203.49	201.22	197.78	192.91	186.03	180.78	179.58	179.17	178.76	176.03	175.46	171.09
8	-6.25	182.95	182.67	181.84	180.01	177.21	173.22	167.60	163.44	162.51	162.20	161.88	159.81	159.38	156.11
7	-8.50	161.46	161.25	160.63	159.26	157.16	154.15	149.94	146.92	146.26	146.04	145.81	144.36	144.07	141.82
6	-10.75	146.43	146.29	145.89	145.00	143.62	141.65	138.94	137.05	136.65	136.51	136.38	135.50	135.33	133.99
		.00	4.25	8.50	13.88	19.25	24.62	30.00	33.00	33.60	33.80	34.00	35.25	35.50	37.34
		1	2	3	4	5	6	7	8	9	10	11	12	13	14

FIRE,CRUSHED IL,1/8"AL,1/8"SS STIFFNERS,WITH NS3, Forced Convection Mon Dec 9 19:47:21 1996

Transient Temperature Distribution at Time 3.0000E+01

58	215.41	1439.33	1439.33	1439.33	1439.75	1439.85	1440.07	1448.20	1450.53	1452.34	1457.29	1460.85	1461.67
57	215.16	1437.27	1437.27	1437.28	1437.70	1437.80	1438.04	1446.54	1449.06	1451.02	1456.42	1460.32	1460.91
56	214.43	775.52	775.51	775.50	775.09	775.73	777.26	871.61	958.93	1029.46	1238.47	1455.03	1456.06
55	213.70	324.01	323.99	323.97	322.55	322.92	323.89	410.82	562.61	690.97	1071.00	1448.33	1449.87
54	212.98	170.24	170.21	170.18	167.97	168.25	169.03	251.87	410.71	546.83	990.67	1443.05	1444.89
53	212.25	127.58	127.54	127.50	124.56	124.80	125.48	206.55	366.71	503.84	960.42	1439.38	1441.38
52	208.88	140.76	140.68	140.61	134.57	134.76	135.40	226.55	384.37	519.68	965.90	1432.73	1434.91
51	205.50	161.00	160.90	160.81	156.08	161.02	173.42	1108.87	1125.17	1357.72	1365.51	1375.14	1380.31
50	204.66	169.51	169.47	169.43	171.55	177.28	191.34	1149.77	1154.02	1360.57	1363.87	1367.49	1373.10
49	203.81	192.17	192.41	192.66	229.12	236.48	253.67	1195.13	1198.37	1359.59	1361.95	1364.67	1370.28
48	202.97	278.88	280.25	281.64	444.42	455.90	480.21	1249.52	1252.01	1357.27	1359.66	1362.49	1368.23
47	202.12	562.58	566.87	571.19	1013.63	1035.80	1072.85	1306.90	1319.73	1350.03	1356.77	1361.15	1367.31
46	201.62	562.05	566.34	570.66	1016.47	1058.83	1082.66	1306.93	1329.04	1349.15	1358.26	1363.73	1371.24
45	201.50	309.77	310.83	311.90	423.91	1121.40	1135.00						
44	195.00	320.04	321.18	322.33	444.31	1247.63	1259.19						
43	194.50	318.83	319.99	321.15	443.15	1248.83	1260.38						
42	192.25	305.65	309.14	312.63	432.31	1244.15	1255.80						
41	188.25	248.85	284.00	317.93	387.44	1150.21	1160.31	1192.52	1195.44	1197.71	1204.34	1212.12	1227.79
40	187.50	242.58	279.20	314.49	379.06	1134.90	1144.80	1181.76	1184.67	1186.89	1193.12	1199.52	1213.11
39	172.39	236.61	262.52	287.74	332.55	903.00	909.77	966.60	971.19	974.70	985.77	996.89	1018.77
38	169.75	243.83	343.04	433.70	615.10	755.61	790.60	923.93	930.65	935.45	992.47	1041.08	1062.38
37	169.50	244.10	345.30	437.63	638.93	675.06	736.29	914.97	925.24	933.03	1011.29	1060.27	1080.90
36	167.50	243.68	322.40	395.51	518.74	537.46	573.90	911.60	938.09	948.82			
35	165.25	240.70	276.20	310.45	366.53	387.41	429.95	1180.22	1245.02	1253.64			
34	148.84	248.33	277.40	305.63	359.49	381.69	426.92	1221.53	1281.32	1288.87			
33	132.44	255.44	283.79	311.33	364.78	386.90	431.95	1223.32	1282.77	1290.27			
32	116.03	259.43	287.28	314.36	367.56	389.63	434.57	1224.06	1283.35	1290.83			
31	99.62	260.59	288.30	315.24	368.37	390.42	435.33	1224.27	1283.52	1291.00			
30	83.22	259.09	286.99	314.10	367.33	389.40	434.35	1224.00	1283.30	1290.79			
29	66.81	254.73	283.15	310.76	364.24	386.37	431.45	1223.17	1282.65	1290.15			
28	50.41	247.26	276.43	304.74	358.65	380.83	426.01	1219.70	1279.75	1287.35			
27	34.00	241.04	289.95	336.56	410.91	432.62	475.34	1030.22	1099.73	1112.29			
26	33.00	241.04	307.27	369.44	513.82	531.05	566.53	944.11	952.26	954.32			
25	32.00	240.54	314.19	382.90	576.70	621.05	693.86	910.87	922.53	932.06	1008.09	1059.78	1080.75
24	31.75	240.28	312.84	380.59	562.04	691.44	746.01	907.23	915.90	922.27	988.50	1040.84	1062.52
23	30.43	238.11	287.40	334.35	415.71	803.14	809.11	908.81	913.32	916.41	955.25	996.78	1018.66
22	29.11	235.59	260.35	284.48	324.77	848.36	854.48	920.38	925.50	929.40	941.63	953.75	977.47
21	21.25	229.70	243.04	256.18	294.59	936.71	944.10	987.64	991.59	994.63	1003.33	1012.53	1033.63
20	14.50	228.29	245.16	261.73	303.17	968.54	976.36	1018.30	1022.05	1024.95	1033.22	1041.95	1061.87
19	13.75	228.55	245.55	262.23	304.00	971.00	978.85	1020.77	1024.51	1027.39	1035.63	1044.32	1064.15
18	10.25	231.64	247.37	262.84	306.64	979.81	987.77	1029.93	1033.63	1036.49	1044.62	1053.19	1072.66
17	8.50	239.52	246.56	253.55	304.04	982.71	990.73	1033.54	1037.25	1040.11	1048.23	1056.76	1076.08
16	8.00	244.96	245.75	246.54	303.05	983.31	991.35	1034.50	1038.22	1041.08	1049.20	1057.72	1077.01
15	4.00	246.01	246.47	246.94	303.92	984.29	992.36	1041.27	1045.15	1048.12	1056.44	1064.96	1083.98
14	2.00	249.67	250.17	250.69	311.84	977.15	985.19	1046.46	1051.04	1054.47	1063.76	1072.60	1091.39
13	.00	258.64	259.30	259.97	338.91	951.05	965.49	1053.79	1062.71	1069.47	1083.39	1093.41	1111.62
12	-.12	439.62	443.46	447.34	878.48	919.04	963.70	1053.60	1063.43	1073.93	1086.73	1096.39	1114.43
11	-.62	438.90	442.73	446.61	876.09	901.29	946.98	1051.72	1059.57	1094.86	1102.09	1109.99	1127.23
10	-2.31	193.31	193.56	193.82	232.04	237.64	250.40	879.51	883.67	1148.02	1151.79	1157.97	1173.08
9	-4.00	166.87	166.82	166.78	166.38	169.66	177.81	785.08	797.66	1170.83	1179.25	1193.29	1208.06
8	-6.25	152.80	152.74	152.69	149.07	149.45	150.49	249.59	400.55	530.80	954.28	1399.85	1402.92
7	-8.50	139.52	139.49	139.45	136.65	136.89	137.58	217.52	374.53	509.07	957.38	1432.18	1434.38
6	-10.75	132.65	132.63	132.61	131.06	131.36	132.18	214.66	374.18	510.74	964.48	1439.46	1441.45
		39.19	39.22	39.25	41.75	41.88	42.12	45.81	46.06	46.25	46.77	47.28	47.53
		15	16	17	18	19	20	21	22	23	24	25	26

FIRE,CRUSHED IL,1/8"AL,1/8"SS STIFFNERS,WITH NS3, Forced Convection Mon Dec 9 19:47:21 1996

Transient Temperature Distribution at Time 3.0000E+01

5	-11.48	184.64	184.53	184.20	183.46	182.32	180.70	178.48	176.96	176.63	176.52	176.41	175.72	175.58	174.53
4	-12.20	335.26	335.17	334.91	334.31	333.40	332.10	330.33	329.14	328.89	328.81	328.72	328.19	328.08	327.29
3	-12.93	784.74	784.66	784.45	783.96	783.20	782.12	780.66	779.69	779.49	779.42	779.35	778.92	778.83	778.21
2	-13.66	1437.69	1437.69	1437.68	1437.65	1437.61	1437.55	1437.47	1437.42	1437.41	1437.41	1437.40	1437.38	1437.38	1437.36
1	-13.91	1439.73	1439.72	1439.71	1439.69	1439.65	1439.59	1439.52	1439.47	1439.46	1439.45	1439.45	1439.43	1439.43	1439.41
		.00	4.25	8.50	13.88	19.25	24.62	30.00	33.00	33.60	33.80	34.00	35.25	35.50	37.34
		1	2	3	4	5	6	7	8	9	10	11	12	13	14

FIRE,CRUSHED IL,1/8"AL,1/8"SS STIFFNERS,WITH NS3, Forced Convection Mon Dec 9 19:47:21 1996

Transient Temperature Distribution at Time 3.0000E+01

5	-11.48	173.49	173.48	173.46	172.40	172.74	173.63	257.91	416.40	552.23	993.66	1443.18	1445.02
4	-12.20	326.55	326.54	326.53	326.05	326.46	327.53	415.81	567.64	695.67	1073.38	1448.46	1449.99
3	-12.93	777.69	777.69	777.68	778.09	778.76	780.37	875.29	962.12	1032.21	1239.91	1455.14	1456.16
2	-13.66	1437.39	1437.39	1437.39	1437.86	1437.96	1438.20	1446.71	1449.22	1451.17	1456.54	1460.41	1461.00
1	-13.91	1439.44	1439.44	1439.44	1439.90	1440.00	1440.23	1448.36	1450.67	1452.48	1457.40	1460.94	1461.75
		39.19	39.22	39.25	41.75	41.88	42.12	45.81	46.06	46.25	46.77	47.28	47.53
		15	16	17	18	19	20	21	22	23	24	25	26

3.6.3.2 HEATING7.2 INPUT FILE NAME: POSTCON2.INP

THIS SECTION CONTAINS
PROPRIETARY INFORMATION

3.6.3.3 HEATING7.2 OUTPUT FILE NAME: POSTCON2.OUT

POSTFIRE,CRUSHED IL,NO NS3,NO AL,ONLY 1/8"SS STIFFNERS, with Solar Tue Dec 10 09:44:59 1996

Transient Temperature Distribution at Time 9.0000E+01

58	215.41	303.36	303.34	303.29	303.18	303.00	302.74	302.38	302.15	302.11	302.09	302.08	302.02	302.01	302.02
57	215.16	304.02	304.00	303.95	303.84	303.66	303.40	303.04	302.80	302.76	302.75	302.73	302.67	302.66	302.67
56	214.43	368.51	368.46	368.32	367.99	367.48	366.73	365.66	364.87	364.70	364.65	364.59	364.22	364.15	363.63
55	213.70	348.38	348.30	348.06	347.50	346.63	345.35	343.53	342.18	341.88	341.77	341.67	341.00	340.87	339.85
54	212.98	279.56	279.45	279.10	278.32	277.10	275.31	272.75	270.83	270.41	270.26	270.11	269.16	268.96	267.47
53	212.25	205.96	205.81	205.38	204.38	202.83	200.56	197.30	194.87	194.32	194.13	193.94	192.71	192.46	190.52
52	208.88	176.66	176.40	175.61	173.81	171.02	166.97	161.15	156.71	155.69	155.35	155.00	152.70	152.22	148.56
51	205.50	207.10	206.73	205.61	203.09	199.21	193.71	186.06	180.72	179.64	179.29	178.94	176.82	176.45	174.37
50	204.66	215.51	215.11	213.91	211.22	207.11	201.45	194.54	192.14	192.24	192.33	192.44	193.84	194.34	200.44
49	203.81	224.06	223.63	222.36	219.51	215.23	209.79	205.66	210.04	212.39	213.30	214.27	221.84	223.76	242.29
48	202.97	232.70	232.25	230.90	227.93	223.69	219.59	223.01	240.07	245.74	247.81	249.97	265.46	269.02	300.05
47	202.12	241.42	240.95	239.55	236.57	233.01	233.02	251.80	284.15	292.41	295.28	298.21	317.70	321.78	353.39
46	201.62	241.50	241.03	239.64	236.65	233.11	233.14	251.97	284.29	292.52	295.39	298.30	317.73	321.79	353.24
45	201.50	249.57	249.11	247.72	244.80	241.49	241.59	256.23	277.31	282.17	283.82	285.48	296.15	298.28	313.73
44	195.00	253.07	252.59	251.20	248.27	244.94	244.89	258.79	278.97	283.73	285.37	287.02	294.76	296.17	305.49
43	194.50	315.10	314.66	313.33	310.49	306.64	302.47	299.42	298.96	298.88	294.64	292.27	296.42	297.41	305.58
42	192.25	317.27	316.82	315.49	312.63	308.73	304.44	301.01	300.21	300.15	300.43	300.74	302.21	302.56	306.66
41	188.25	320.34	319.87	318.49	315.51	311.38	306.65	302.47	301.32	301.25	300.38	299.53	300.43	300.62	302.48
40	187.50	320.93	320.46	319.07	316.06	311.87	307.02	302.64	301.34	301.30	300.20	299.10	299.96	300.14	301.80
39	172.39	443.85	442.21	437.24	425.86	407.92	382.07	348.69	329.43	329.01	311.16	293.10	293.92	294.17	296.63
38	169.75	456.55	454.83	449.60	437.60	418.65	390.91	354.72	333.82	333.35	313.02	292.40	293.13	293.37	295.89
37	169.50	457.65	455.92	450.67	438.61	419.57	391.70	355.26	334.22	333.75	313.18	292.32	293.04	293.28	295.79
36	167.50	465.90	464.11	458.68	446.21	426.51	397.63	359.41	337.32	336.81	314.37	291.57	292.18	292.41	294.81
35	165.25	474.10	472.25	466.64	453.76	433.41	403.67	363.71	340.57	340.02	315.49	290.52	291.00	291.20	293.36
34	148.84	507.26	505.18	498.86	484.44	461.92	429.57	384.45	356.88	356.13	320.00	282.79	282.28	282.34	283.09
33	132.44	521.51	519.34	512.78	497.82	474.58	441.39	395.46	366.41	365.60	327.21	287.59	286.84	286.86	287.40
32	116.03	527.58	525.39	518.75	503.62	480.16	446.74	400.66	371.10	370.27	331.50	291.49	290.69	290.71	291.21
31	99.62	529.17	526.97	520.31	505.15	481.64	448.18	402.08	372.40	371.57	332.75	292.68	291.88	291.89	292.38
30	83.22	527.14	524.95	518.31	503.20	479.75	446.34	400.26	370.73	369.91	331.15	291.15	290.36	290.37	290.87
29	66.81	520.40	518.24	511.69	496.77	473.57	440.42	394.52	365.57	364.77	326.46	286.94	286.21	286.23	286.78
28	50.41	504.76	502.69	496.43	482.11	459.74	427.56	382.62	355.33	354.59	318.98	282.34	281.87	281.93	282.74
27	34.00	467.99	466.20	460.77	448.25	428.38	399.16	360.27	337.72	337.19	313.28	288.96	289.40	289.60	291.91
26	33.00	464.03	462.28	456.94	444.64	425.09	396.30	358.22	336.04	335.51	311.95	287.99	288.45	288.65	290.94
25	32.00	459.83	458.11	452.88	440.81	421.61	393.32	356.08	334.28	333.76	310.51	286.87	287.34	287.55	289.81
24	31.75	458.74	457.03	451.82	439.82	420.71	392.55	355.53	333.83	333.31	310.14	286.57	287.05	287.25	289.51
23	30.43	452.71	451.05	445.99	434.33	415.72	388.35	352.55	331.39	330.89	308.07	284.89	285.38	285.58	287.78
22	29.11	446.16	444.55	439.65	428.37	410.30	383.88	349.42	328.85	328.36	305.90	283.08	283.58	283.78	285.89
21	21.25	393.83	392.62	388.98	380.84	368.53	351.18	327.48	311.94	311.54	291.43	271.04	271.50	271.68	273.24
20	14.50	324.76	324.16	322.40	318.82	313.94	308.19	302.44	299.78	299.54	283.78	267.86	268.28	268.42	269.76
19	13.75	323.33	322.74	321.00	317.50	312.75	307.23	301.88	299.78	299.45	283.66	267.72	268.16	268.31	269.73
18	10.25	320.71	320.10	318.32	314.94	310.40	305.23	300.45	298.70	298.35	282.77	267.07	267.94	268.15	270.58
17	8.50	319.21	318.57	316.54	313.19	308.71	303.62	299.03	297.34	296.98	277.79	262.98	266.18	266.70	271.86
16	8.00	310.67	306.43	248.70	246.17	242.50	239.53	243.24	254.20	257.38	258.51	259.68	265.02	265.95	272.16
15	4.00	248.64	247.98	245.79	243.18	239.56	236.71	240.74	251.47	254.27	255.24	256.23	262.77	264.13	274.48
14	2.00	247.43	246.80	244.98	242.26	238.65	235.87	240.26	251.70	254.74	255.81	256.90	264.22	265.76	277.77
13	.00	246.77	246.17	244.46	241.71	238.10	235.36	240.14	252.49	255.84	257.01	258.21	266.36	268.09	281.76
12	-.12	238.70	238.21	236.80	233.99	230.24	227.91	239.23	268.71	277.29	280.34	283.49	305.26	310.02	349.02
11	-.62	238.62	238.13	236.72	233.91	230.16	227.81	239.10	268.65	277.26	280.33	283.49	305.36	310.15	349.37
10	-2.31	221.63	221.21	219.98	217.41	213.58	208.54	203.94	206.45	208.22	208.91	209.67	215.74	217.34	233.21
9	-4.00	204.94	204.58	203.53	201.26	197.83	192.99	186.42	182.29	181.60	181.38	181.17	180.09	179.97	180.11
8	-6.25	183.55	183.27	182.44	180.61	177.82	173.83	168.22	164.14	163.25	162.95	162.65	160.72	160.34	157.58
7	-8.50	169.57	169.36	168.75	167.38	165.27	162.26	158.06	155.05	154.39	154.17	153.95	152.51	152.22	150.07
6	-10.75	218.47	218.34	217.94	217.07	215.72	213.79	211.13	209.28	208.89	208.75	208.62	207.76	207.59	206.33
		.00	4.25	8.50	13.88	19.25	24.62	30.00	33.00	33.60	33.80	34.00	35.25	35.50	37.34
		1	2	3	4	5	6	7	8	9	10	11	12	13	14

POSTFIRE,CRUSHED IL,NO NS3,NO AL,ONLY 1/8"SS STIFFNERS, with Solar Tue Dec 10 09:44:59 1996

Transient Temperature Distribution at Time 9.0000E+01

58	215.41	302.31	302.32	302.33	303.68	303.79	304.03	308.69	307.96	307.35	305.51	303.94	303.34
57	215.16	302.96	302.97	302.98	304.34	304.45	304.69	309.46	308.71	308.08	306.16	304.56	304.14
56	214.43	363.41	363.42	363.43	366.26	366.98	368.56	414.60	405.89	397.65	365.09	308.26	307.66
55	213.70	339.19	339.20	339.22	343.57	344.88	347.81	437.86	428.69	419.49	380.74	310.98	310.33
54	212.98	266.39	266.40	266.42	271.97	273.81	277.92	409.27	405.43	400.29	372.44	312.28	311.66
53	212.25	189.03	189.05	189.06	195.43	197.67	202.71	367.66	370.39	370.46	357.69	312.87	312.30
52	208.88	145.53	145.54	145.55	153.43	156.32	162.82	372.28	375.73	376.09	363.45	319.08	318.49
51	205.50	177.30	177.56	177.82	222.37	230.08	246.94	673.09	671.04	625.37	495.55	342.80	341.83
50	204.66	215.15	215.61	216.08	277.09	284.61	300.80	668.78	668.15	609.80	474.93	338.17	337.37
49	203.81	272.13	272.81	273.50	349.31	356.08	370.37	655.89	655.25	595.68	463.22	332.91	332.15
48	202.97	340.33	341.11	341.89	416.36	421.71	432.78	632.57	631.94	576.33	449.49	326.97	326.24
47	202.12	385.04	385.55	386.06	424.29	426.81	432.78	596.24	597.12	595.23	427.74	320.40	319.76
46	201.62	384.68	385.18	385.68	422.72	423.07	430.09	594.69	593.57	591.10	340.81	316.22	316.09
45	201.50	326.94	327.13	327.31	338.55	413.25	413.05						
44	195.00	312.78	312.87	312.96	316.67	285.49	285.09						
43	194.50	312.56	312.65	312.74	316.58	282.45	282.05						
42	192.25	312.56	313.07	313.58	319.47	279.87	279.45						
41	188.25	304.65	326.00	346.90	348.98	311.45	310.74	209.62	209.02	209.23	214.12	240.01	240.01
40	187.50	303.79	328.23	352.10	354.40	338.21	338.11	252.94	250.40	248.74	245.24	242.86	242.68
39	172.39	300.13	346.26	390.45	396.58	412.55	412.60	375.07	372.17	369.96	367.45	360.89	360.00
38	169.75	299.69	351.74	401.33	411.85	414.29	414.72	416.11	411.07	404.37	399.43	395.13	393.49
37	169.50	299.59	351.79	401.53	412.74	413.52	414.84	416.28	413.31	411.11	398.96	394.07	392.40
36	167.50	298.48	349.05	397.30	408.82	410.21	412.75	415.78	412.72	411.84			
35	165.25	296.53	339.15	380.09	385.11	383.69	380.71	308.80	296.79	296.46			
34	148.84	284.42	304.04	323.28	325.28	323.86	320.97	261.72	252.25	252.04			
33	132.44	288.59	306.92	324.91	326.76	325.32	322.37	261.25	251.68	251.47			
32	116.03	292.37	310.28	327.87	329.67	328.15	325.04	261.69	251.98	251.77			
31	99.62	293.54	311.31	328.77	330.56	329.01	325.85	261.83	252.07	251.86			
30	83.22	292.04	309.98	327.61	329.41	327.90	324.80	261.65	251.95	251.74			
29	66.81	287.98	306.39	324.46	326.32	324.90	321.97	261.22	251.67	251.46			
28	50.41	284.15	304.78	325.00	327.11	325.71	322.84	263.92	254.39	254.18			
27	34.00	295.64	347.22	396.37	402.80	403.02	403.34	385.42	375.16	374.43			
26	33.00	294.62	345.68	394.36	402.43	402.68	403.09	392.65	391.78	391.56			
25	32.00	293.40	343.37	391.06	400.19	400.93	402.06	394.13	391.70	389.82	382.44	378.69	377.22
24	31.75	293.07	342.66	389.99	398.92	401.15	401.85	394.12	390.89	387.22	383.21	379.75	378.29
23	30.43	291.16	338.00	382.82	389.64	400.26	400.30	382.45	380.57	379.12	378.09	375.75	374.45
22	29.11	289.07	332.79	374.73	380.47	396.78	396.83	373.16	371.90	370.98	368.74	362.02	361.11
21	21.25	275.26	302.87	329.73	333.79	358.41	358.48	292.90	288.07	284.41	274.19	263.69	263.43
20	14.50	271.40	293.55	315.21	318.84	346.96	347.03	278.42	273.76	270.25	260.60	250.93	250.71
19	13.75	271.38	292.27	312.72	316.35	345.70	345.78	277.83	273.19	269.71	260.13	250.53	250.31
18	10.25	272.84	285.50	297.99	302.20	340.37	340.47	277.87	273.38	269.98	260.58	251.10	250.88
17	8.50	277.61	281.89	286.16	294.05	341.12	341.26	281.63	276.96	273.39	263.43	253.30	253.07
16	8.00	280.79	281.14	281.48	292.27	342.22	342.37	283.60	278.79	275.12	264.81	254.27	254.04
15	4.00	284.61	284.77	284.92	295.03	367.42	367.66	317.00	309.58	303.71	286.45	268.20	267.91
14	2.00	289.58	289.76	289.94	302.37	402.92	403.28	384.57	370.82	359.41	323.55	284.42	284.03
13	.00	295.65	295.87	296.09	312.38	461.13	462.36	555.76	539.61	520.80	415.30	306.42	305.79
12	-.12	393.16	393.93	394.71	459.91	463.24	469.63	572.55	571.88	570.68	423.30	307.54	306.89
11	-.62	393.81	394.58	395.36	461.07	464.38	470.98	573.88	573.97	572.03	437.58	311.65	310.96
10	-2.31	260.43	261.08	261.73	334.19	340.40	353.46	608.02	607.47	551.59	436.38	320.56	319.87
9	-4.00	185.61	185.88	186.15	227.85	234.35	248.51	610.87	609.98	565.95	454.86	326.75	325.93
8	-6.25	156.19	156.24	156.29	168.81	172.05	179.29	401.17	400.19	396.80	372.82	317.63	317.01
7	-8.50	148.56	148.58	148.61	155.96	158.42	163.94	344.64	350.45	352.98	347.60	311.01	310.47
6	-10.75	205.65	205.68	205.71	212.94	215.13	220.03	377.80	378.81	377.48	360.60	311.47	310.88
		39.19	39.22	39.25	41.75	41.88	42.12	45.81	46.06	46.25	46.77	47.28	47.53
		15	16	17	18	19	20	21	22	23	24	25	26

POSTFIRE,CRUSHED IL,NO NS3,NO AL,ONLY 1/8"SS STIFFNERS, with Solar Tue Dec 10 09:44:59 1996

Transient Temperature Distribution at Time 9.0000E+01

5	-11.48	285.73	285.63	285.32	284.63	283.57	282.05	279.97	278.53	278.22	278.12	278.02	277.36	277.23	276.28
4	-12.20	350.88	350.81	350.59	350.10	349.34	348.26	346.79	345.78	345.57	345.50	345.42	344.97	344.88	344.25
3	-12.93	369.33	369.28	369.16	368.87	368.42	367.79	366.93	366.35	366.23	366.20	366.16	365.92	365.87	365.58
2	-13.66	304.16	304.14	304.10	304.00	303.85	303.63	303.35	303.18	303.16	303.15	303.14	303.12	303.12	303.20
1	-13.91	303.49	303.48	303.44	303.34	303.19	302.97	302.69	302.52	302.50	302.49	302.49	302.47	302.47	302.55
		.00	4.25	8.50	13.88	19.25	24.62	30.00	33.00	33.60	33.80	34.00	35.25	35.50	37.34
		1	2	3	4	5	6	7	8	9	10	11	12	13	14

POSTFIRE,CRUSHED IL,NO NS3,NO AL,ONLY 1/8"SS STIFFNERS, with Solar Tue Dec 10 09:44:59 1996

Transient Temperature Distribution at Time 9.0000E+01

5	-11.48	275.85	275.87	275.90	282.28	284.10	288.18	416.14	411.17	405.12	374.53	311.47	310.84
4	-12.20	344.05	344.08	344.10	349.08	350.40	353.34	441.91	432.08	422.36	382.01	310.54	309.89
3	-12.93	365.62	365.64	365.66	368.85	369.57	371.16	416.55	407.54	399.04	365.72	308.06	307.46
2	-13.66	303.56	303.57	303.58	304.99	305.10	305.33	309.80	309.00	308.33	306.29	304.55	304.12
1	-13.91	302.91	302.92	302.93	304.33	304.44	304.66	309.02	308.25	307.60	305.63	303.94	303.33
		39.19	39.22	39.25	41.75	41.88	42.12	45.81	46.06	46.25	46.77	47.28	47.53
		15	16	17	18	19	20	21	22	23	24	25	26

POSTFIRE,CRUSHED IL,NO NS3,NO AL,ONLY 1/8"SS STIFFNERS, with Solar Tue Dec 10 09:44:59 1996

Transient Temperature Distribution at Time 6.0000E+02

58	215.41	156.76	156.73	156.64	156.45	156.16	155.83	155.63	155.88	155.99	156.04	156.08	156.41	156.49	157.21
57	215.16	156.82	156.79	156.70	156.50	156.22	155.88	155.69	155.94	156.05	156.09	156.13	156.47	156.55	157.27
56	214.43	168.29	168.24	168.07	167.70	167.16	166.45	165.80	165.91	166.05	166.11	166.17	166.67	166.80	168.07
55	213.70	178.65	178.57	178.33	177.79	177.00	175.95	174.87	174.87	175.04	175.11	175.19	175.86	176.05	177.85
54	212.98	187.54	187.44	187.13	186.44	185.41	184.05	182.61	182.53	182.74	182.83	182.93	183.78	184.01	186.35
53	212.25	194.78	194.66	194.28	193.45	192.21	190.59	188.85	188.75	189.01	189.12	189.24	190.28	190.57	193.44
52	208.88	206.22	206.02	205.44	204.19	202.44	200.37	198.56	199.21	199.80	200.04	200.30	202.40	202.94	208.23
51	205.50	222.63	222.54	222.30	221.89	221.64	221.91	223.36	225.87	226.74	227.06	227.40	229.85	230.42	235.46
50	204.66	230.30	230.29	230.30	230.42	230.89	231.93	233.88	236.09	236.78	237.03	237.29	239.15	239.57	243.18
49	203.81	239.62	239.71	240.01	240.75	241.98	243.74	245.91	247.47	247.88	248.02	248.17	249.16	249.37	251.03
48	202.97	250.79	250.99	251.60	252.94	254.88	257.15	259.14	259.65	259.67	259.67	259.67	259.56	259.51	258.77
47	202.12	263.97	264.27	265.14	266.99	269.41	271.83	273.11	272.21	271.77	271.60	271.42	270.02	269.67	266.26
46	201.62	264.09	264.39	265.27	267.12	269.54	271.97	273.24	272.34	271.90	271.73	271.55	270.16	269.80	266.40
45	201.50	274.85	275.17	276.12	278.08	280.58	283.09	284.81	284.92	284.84	284.80	284.76	284.41	284.31	283.39
44	195.00	278.16	278.47	279.36	281.21	283.57	285.98	287.86	288.50	288.60	288.64	288.67	288.60	288.55	287.75
43	194.50	328.92	328.79	328.39	327.50	326.23	324.61	322.67	321.41	321.07	303.81	289.56	289.23	289.14	288.31
42	192.25	330.89	330.74	330.29	329.31	327.90	326.12	324.04	322.86	322.55	307.68	292.70	292.14	292.07	291.18
41	188.25	333.47	333.30	332.79	331.68	330.10	328.09	325.74	324.34	324.05	310.63	297.12	296.55	296.48	295.99
40	187.50	333.93	333.76	333.24	332.11	330.49	328.44	326.03	324.40	324.18	311.11	297.94	297.38	297.32	296.87
39	172.39	445.61	444.13	439.67	429.81	415.43	396.95	375.21	360.60	360.12	337.26	314.03	313.03	312.92	312.17
38	169.75	457.69	456.11	451.35	440.79	425.33	405.37	381.33	365.54	365.03	340.94	316.43	315.36	315.25	314.41
37	169.50	458.75	457.16	452.37	441.75	426.20	406.11	381.88	365.99	365.47	341.27	316.66	315.58	315.47	314.62
36	167.50	466.70	465.04	460.06	448.98	432.73	411.69	386.03	369.40	368.87	343.88	318.45	317.34	317.22	316.35
35	165.25	474.67	472.95	467.77	456.23	439.28	417.30	390.31	372.95	372.39	346.65	320.44	319.30	319.18	318.33
34	148.84	507.63	505.65	499.69	486.39	466.70	440.92	409.53	389.43	388.81	361.06	332.74	331.54	331.42	330.61
33	132.44	521.86	519.79	513.56	499.65	478.99	451.80	418.50	397.31	396.65	367.59	337.90	336.64	336.51	335.67
32	116.03	527.94	525.84	519.53	505.42	484.46	456.79	422.75	401.08	400.40	370.52	339.99	338.69	338.57	337.70
31	99.62	529.53	527.43	521.10	506.95	485.93	458.15	423.93	402.10	401.41	371.25	340.42	339.11	338.98	338.11
30	83.22	527.50	525.41	519.10	504.99	484.04	456.37	422.29	400.55	399.87	369.86	339.18	337.88	337.75	336.88
29	66.81	520.75	518.68	512.47	498.57	477.93	450.72	417.29	395.90	395.24	365.77	335.67	334.39	334.27	333.42
28	50.41	505.11	503.14	497.22	483.98	464.33	438.46	406.65	386.26	385.63	357.08	327.93	326.70	326.58	325.76
27	34.00	468.43	466.75	461.69	450.36	433.54	411.39	384.09	366.62	366.05	339.78	312.99	311.84	311.72	310.81
26	33.00	464.53	462.88	457.92	446.83	430.34	408.62	381.99	364.89	364.34	338.52	312.21	311.08	310.96	310.07
25	32.00	460.40	458.79	453.94	443.09	426.96	405.70	379.81	363.10	362.56	337.23	311.43	310.34	310.22	309.36
24	31.75	459.33	457.73	452.91	442.12	426.08	404.95	379.25	362.64	362.11	336.91	311.24	310.15	310.04	309.18
23	30.43	453.42	451.87	447.20	436.77	421.26	400.81	376.19	360.16	359.64	335.16	310.24	309.19	309.08	308.27
22	29.11	447.04	445.54	441.05	431.01	416.08	396.40	372.98	357.57	357.06	333.36	309.25	308.24	308.13	307.37
21	21.25	396.99	395.95	392.85	386.13	376.65	364.81	350.29	339.74	339.37	321.40	303.23	302.50	302.43	301.94
20	14.50	335.47	335.14	334.20	332.38	330.01	327.33	324.60	323.20	323.03	310.03	296.93	296.43	296.38	296.07
19	13.75	334.29	333.97	333.06	331.32	329.07	326.54	324.00	322.83	322.58	309.43	296.19	295.70	295.65	295.36
18	10.25	332.00	331.68	330.76	329.16	327.13	324.87	322.62	321.49	321.18	306.88	292.47	292.07	292.03	291.87
17	8.50	330.60	330.26	329.17	327.64	325.73	323.63	321.54	320.37	320.04	303.07	289.73	289.99	290.03	290.14
16	8.00	323.32	320.11	274.08	274.81	277.14	280.44	284.43	287.20	287.91	288.16	288.43	289.36	289.50	289.72
15	4.00	270.04	270.26	270.91	272.14	274.70	278.17	282.07	284.06	284.39	284.49	284.59	285.11	285.20	285.53
14	2.00	268.89	269.11	269.78	271.20	273.81	277.32	281.15	282.94	283.22	283.31	283.39	283.84	283.91	284.21
13	.00	268.15	268.37	269.04	270.52	273.16	276.67	280.47	282.19	282.46	282.54	282.62	283.03	283.09	283.36
12	-.12	257.34	257.55	258.21	259.76	262.33	265.78	269.53	271.13	271.35	271.41	271.46	271.69	271.71	271.42
11	-.62	257.22	257.43	258.09	259.64	262.20	265.65	269.40	271.01	271.22	271.28	271.34	271.57	271.59	271.31
10	-2.31	234.78	234.79	234.88	235.25	236.29	238.32	241.78	244.99	245.84	246.14	246.45	248.56	249.02	252.80
9	-4.00	219.57	219.45	219.10	218.51	218.11	218.38	220.32	223.65	224.75	225.15	225.57	228.58	229.28	235.35
8	-6.25	208.32	208.12	207.55	206.39	204.92	203.47	203.03	205.06	205.97	206.32	206.68	209.49	210.18	216.49
7	-8.50	202.54	202.36	201.84	200.72	199.13	197.23	195.62	196.34	196.91	197.14	197.39	199.35	199.86	204.71
6	-10.75	191.90	191.78	191.43	190.65	189.52	188.07	186.65	186.84	187.16	187.28	187.42	188.59	188.89	191.90
		.00	4.25	8.50	13.88	19.25	24.62	30.00	33.00	33.60	33.80	34.00	35.25	35.50	37.34
		1	2	3	4	5	6	7	8	9	10	11	12	13	14

POSTFIRE,CRUSHED IL,NO NS3,NO AL,ONLY 1/8"SS STIFFNERS, with Solar Tue Dec 10 09:44:59 1996

Transient Temperature Distribution at Time 6.0000E+02

58	215.41	158.18	158.20	158.22	159.92	160.03	160.24	164.23	164.84	165.32	166.81	168.48	168.69
57	215.16	158.24	158.26	158.28	160.00	160.10	160.31	164.30	164.91	165.39	166.89	168.78	168.98
56	214.43	169.87	169.90	169.94	172.62	172.71	172.88	173.09	172.91	172.77	172.31	171.77	171.79
55	213.70	180.46	180.50	180.55	184.16	184.24	184.35	180.81	179.90	179.17	176.95	174.45	174.45
54	212.98	189.74	189.80	189.85	194.37	194.43	194.51	187.52	185.98	184.74	181.00	176.88	176.87
53	212.25	197.59	197.66	197.73	203.14	203.20	203.24	193.31	191.23	189.56	184.55	179.07	179.05
52	208.88	215.52	215.64	215.76	225.06	225.17	225.27	209.40	206.02	203.29	195.06	186.16	186.10
51	205.50	241.30	241.39	241.47	246.83	246.75	246.49	226.72	226.42	220.08	204.93	190.01	189.93
50	204.66	246.98	247.03	247.08	249.28	249.10	248.65	228.46	228.40	215.39	203.02	190.02	189.95
49	203.81	252.17	252.17	252.17	250.34	250.04	249.39	230.37	230.32	216.06	203.19	189.99	189.92
48	202.97	256.73	256.68	256.62	249.86	249.42	248.54	232.45	232.40	218.92	204.63	189.91	189.84
47	202.12	260.73	260.61	260.49	247.84	247.17	245.99	234.82	234.54	234.21	207.63	189.70	189.62
46	201.62	260.88	260.76	260.64	247.85	246.72	245.86	234.91	234.47	234.12	198.83	189.38	189.35
45	201.50	282.08	282.05	282.03	279.81	245.36	245.06						
44	195.00	286.39	286.37	286.34	283.76	237.56	237.25						
43	194.50	286.89	286.86	286.83	284.13	237.67	237.36						
42	192.25	289.55	289.38	289.22	285.81	239.37	239.07						
41	188.25	295.53	291.61	287.69	286.07	249.04	248.63	187.01	185.60	184.71	183.06	184.17	184.16
40	187.50	296.48	292.11	287.72	286.38	260.88	260.77	200.47	197.52	195.39	189.87	184.63	184.60
39	172.39	311.47	303.38	295.23	293.88	285.94	285.89	231.29	227.45	224.55	223.37	221.05	220.82
38	169.75	313.55	302.55	291.44	286.48	284.09	283.55	251.19	247.30	242.38	239.17	236.95	236.34
37	169.50	313.75	302.61	291.35	285.72	284.88	283.29	251.34	248.99	247.42	239.33	236.70	236.06
36	167.50	315.47	304.22	292.86	287.34	286.21	283.97	253.51	252.11	251.79			
35	165.25	317.53	308.29	298.98	297.32	294.80	289.77	217.22	211.56	211.46			
34	148.84	329.95	322.97	315.95	314.65	311.17	304.23	204.27	197.56	197.48			
33	132.44	334.95	327.32	319.63	318.23	314.62	307.42	204.39	197.51	197.43			
32	116.03	336.95	328.96	320.92	319.49	315.83	308.55	204.60	197.66	197.58			
31	99.62	337.35	329.31	321.22	319.77	316.11	308.81	204.66	197.70	197.62			
30	83.22	336.14	328.22	320.25	318.82	315.18	307.94	204.47	197.56	197.48			
29	66.81	332.71	325.18	317.61	316.24	312.68	305.59	204.03	197.24	197.16			
28	50.41	325.08	317.90	310.68	309.38	306.06	299.45	204.14	197.69	197.62			
27	34.00	309.86	297.90	285.80	282.85	281.16	277.97	242.59	238.81	238.59			
26	33.00	309.14	297.16	285.04	279.58	278.76	277.02	244.47	243.79	243.61			
25	32.00	308.46	296.89	285.18	279.69	278.75	277.07	243.30	240.55	238.57	231.38	228.72	228.11
24	31.75	308.30	296.89	285.37	280.34	278.17	277.28	243.18	239.40	235.15	231.28	228.92	228.33
23	30.43	307.46	297.35	287.15	284.65	279.32	279.28	233.24	228.90	225.50	224.94	224.04	223.64
22	29.11	306.64	297.88	289.05	287.66	280.80	280.76	228.22	224.57	221.82	220.76	218.52	218.29
21	21.25	301.55	297.29	293.02	292.30	284.29	284.24	216.85	212.42	209.10	200.02	190.97	190.91
20	14.50	295.84	293.49	291.13	290.62	282.70	282.65	213.34	208.81	205.42	196.18	187.02	186.96
19	13.75	295.14	293.00	290.85	290.36	282.42	282.37	213.12	208.60	205.21	195.98	186.83	186.78
18	10.25	291.71	290.59	289.46	288.98	280.81	280.76	212.52	208.07	204.73	195.61	186.58	186.53
17	8.50	289.81	289.44	289.08	288.31	279.74	279.68	212.55	208.13	204.81	195.76	186.78	186.73
16	8.00	289.16	289.13	289.10	288.08	279.37	279.32	212.63	208.22	204.91	195.87	186.89	186.84
15	4.00	285.47	285.46	285.46	284.94	275.35	275.29	214.97	210.55	207.20	197.92	188.59	188.53
14	2.00	284.16	284.15	284.15	283.57	271.72	271.66	222.49	217.54	213.66	202.34	190.57	190.51
13	.00	283.25	283.24	283.24	282.46	265.67	265.53	244.70	240.89	236.82	215.31	193.10	193.00
12	-.12	270.12	270.08	270.04	265.74	265.41	264.70	246.76	246.27	245.93	216.59	193.19	193.09
11	-.62	270.01	269.97	269.93	265.62	265.28	264.56	246.66	246.40	245.92	218.41	193.43	193.32
10	-2.31	256.64	256.69	256.75	259.32	259.17	258.80	240.29	240.24	224.33	208.95	192.85	192.77
9	-4.00	242.46	242.57	242.68	250.21	250.25	250.25	235.36	235.22	226.47	209.04	192.09	192.00
8	-6.25	224.57	224.70	224.83	234.49	234.58	234.65	216.61	212.62	209.37	199.56	189.01	188.94
7	-8.50	211.32	211.43	211.53	219.89	219.98	220.07	205.46	202.42	199.98	192.69	184.78	184.74
6	-10.75	196.11	196.18	196.25	201.72	201.78	201.84	192.64	190.67	189.09	184.35	179.17	179.14
		39.19	39.22	39.25	41.75	41.88	42.12	45.81	46.06	46.25	46.77	47.28	47.53
		15	16	17	18	19	20	21	22	23	24	25	26

POSTFIRE,CRUSHED IL,NO NS3,NO AL,ONLY 1/8"SS STIFFNERS, with Solar Tue Dec 10 09:44:59 1996

Transient Temperature Distribution at Time 6.0000E+02

5	-11.48	185.20	185.10	184.81	184.18	183.24	182.04	180.86	181.02	181.27	181.37	181.49	182.43	182.67	185.10
4	-12.20	176.89	176.81	176.59	176.11	175.39	174.47	173.60	173.77	173.97	174.06	174.15	174.88	175.07	176.93
3	-12.93	167.12	167.07	166.92	166.59	166.10	165.49	164.98	165.20	165.36	165.42	165.49	166.03	166.17	167.47
2	-13.66	156.22	156.20	156.12	155.94	155.69	155.41	155.29	155.58	155.70	155.75	155.79	156.14	156.22	156.96
1	-13.91	156.17	156.14	156.06	155.88	155.63	155.35	155.24	155.53	155.65	155.69	155.74	156.09	156.17	156.91
		.00	4.25	8.50	13.88	19.25	24.62	30.00	33.00	33.60	33.80	34.00	35.25	35.50	37.34
		1	2	3	4	5	6	7	8	9	10	11	12	13	14

POSTFIRE,CRUSHED IL,NO NS3,NO AL,ONLY 1/8"SS STIFFNERS, with Solar Tue Dec 10 09:44:59 1996

Transient Temperature Distribution at Time 6.0000E+02

5	-11.48	188.52	188.58	188.64	193.17	193.24	193.33	186.93	185.49	184.32	180.80	176.92	176.90
4	-12.20	179.55	179.59	179.64	183.25	183.33	183.46	180.35	179.51	178.83	176.76	174.44	174.43
3	-12.93	169.28	169.31	169.34	172.03	172.13	172.30	172.78	172.64	172.53	172.16	171.73	171.74
2	-13.66	157.95	157.97	157.99	159.73	159.84	160.05	164.16	164.78	165.27	166.79	168.70	168.91
1	-13.91	157.89	157.91	157.93	159.66	159.77	159.98	164.09	164.71	165.20	166.71	168.40	168.61
		39.19	39.22	39.25	41.75	41.88	42.12	45.81	46.06	46.25	46.77	47.28	47.53
		15	16	17	18	19	20	21	22	23	24	25	26

3.6.3.4 HEATING7.2 INPUT FILE NAME: FINLCON2.INP

THIS SECTION CONTAINS
PROPRIETARY INFORMATION

3.6.3.5 HEATING7.2 OUTPUT FILE NAME: FINLCON2.OUT

```
FINAL STEADY STATE,CRUSHED IL,NO NS3,NO AL,ONLY 1/8"SS STIFFNERS                                  Mon Dec 30 21:55:59 1996
                              Steady-State Temperature Distribution at Time 6.0000E+02

  58  215.41 |  155.85  155.81  155.71  155.48  155.11  154.57  153.84  153.41  153.33  153.31  153.29  153.16  153.14  153.06
  57  215.16 |  155.91  155.87  155.77  155.54  155.17  154.63  153.89  153.46  153.38  153.36  153.33  153.21  153.19  153.11
  56  214.43 |  167.74  167.68  167.49  167.06  166.38  165.38  163.95  162.96  162.76  162.69  162.62  162.20  162.12  161.54
  55  213.70 |  179.58  179.49  179.22  178.60  177.61  176.15  174.03  172.48  172.15  172.03  171.92  171.19  171.04  169.95
  54  212.98 |  191.42  191.31  190.95  190.14  188.85  186.94  184.12  182.02  181.55  181.39  181.23  180.20  179.98  178.36
  53  212.25 |  203.29  203.14  202.70  201.71  200.12  197.75  194.25  191.59  190.99  190.78  190.58  189.23  188.95  186.79
  52  208.88 |  258.61  258.34  257.53  255.68  252.75  248.41  241.88  236.67  235.45  235.03  234.60  231.79  231.20  226.46
  51  205.50 |  314.61  314.23  313.07  310.44  306.35  300.39  291.52  284.23  282.48  281.88  281.26  277.14  276.26  269.11
  50  204.66 |  328.76  328.35  327.11  324.30  319.96  313.66  304.38  296.75  294.90  294.26  293.61  289.23  288.28  280.55
  49  203.81 |  342.98  342.54  341.22  338.23  333.64  327.05  317.44  309.54  307.62  306.95  306.26  301.66  300.66  292.38
  48  202.97 |  357.27  356.80  355.40  352.24  347.42  340.56  330.69  322.62  320.65  319.96  319.25  314.49  313.44  304.70
  47  202.12 |  371.63  371.13  369.65  366.33  361.28  354.19  344.14  336.01  334.01  333.31  332.60  327.75  326.68  317.63
  46  201.62 |  371.75  371.26  369.77  366.45  361.40  354.32  344.28  336.17  334.18  333.48  332.77  327.94  326.87  317.86
  45  201.50 |  380.88  380.39  378.91  375.64  370.80  364.36  356.32  351.19  350.12  349.76  349.40  347.13  346.67  343.22
  44  195.00 |  384.93  384.44  382.96  379.69  374.88  368.55  360.76  355.83  354.80  354.45  354.11  352.25  351.87  348.99
  43  194.50 |  435.37  434.90  433.50  430.46  426.15  420.85  415.03  411.81  411.08  379.91  354.32  352.77  352.43  349.68
  42  192.25 |  437.78  437.30  435.89  432.82  428.48  423.14  417.29  414.33  413.65  385.63  357.08  355.66  355.46  353.34
  41  188.25 |  441.40  440.90  439.44  436.26  431.74  426.13  419.72  416.05  415.41  389.64  363.42  362.17  362.03  360.95
  40  187.50 |  442.06  441.56  440.09  436.88  432.33  426.65  420.14  415.79  415.27  390.19  364.68  363.46  363.33  362.37
  39  172.39 |  552.62  551.34  547.47  538.64  524.86  505.11  477.45  457.10  456.30  424.72  392.43  390.77  390.58  389.20
  38  169.75 |  565.03  563.67  559.55  550.16  535.52  514.56  485.39  464.22  463.39  431.02  397.90  396.16  395.96  394.43
  37  169.50 |  566.13  564.76  560.62  551.19  536.47  515.41  486.12  464.88  464.05  431.62  398.44  396.68  396.48  394.95
  36  167.50 |  574.49  573.07  568.77  558.98  543.73  521.95  491.82  470.17  469.32  436.46  402.83  401.04  400.83  399.26
  35  165.25 |  583.07  581.60  577.15  567.02  551.26  528.82  497.97  476.00  475.13  441.95  408.00  406.18  405.97  404.44
  34  148.84 |  624.81  623.21  618.38  607.41  590.55  567.08  535.84  514.34  513.43  482.04  449.99  448.17  447.96  446.57
  33  132.44 |  649.34  647.74  642.94  632.08  615.48  592.45  562.10  541.46  540.55  510.94  480.83  479.01  478.80  477.38
  32  116.03 |  663.53  661.96  657.23  646.56  630.29  607.82  578.18  558.11  557.21  528.73  499.81  497.99  497.77  496.33
  31   99.62 |  669.54  667.99  663.29  652.72  636.62  614.41  585.10  565.29  564.38  536.39  507.97  506.15  505.94  504.47
  30   83.22 |  667.97  666.41  661.71  651.12  635.00  612.72  583.34  563.47  562.56  534.44  505.89  504.07  503.86  502.40
  29   66.81 |  658.55  656.98  652.25  641.57  625.27  602.67  572.84  552.59  551.69  522.81  493.48  491.66  491.45  490.00
  28   50.41 |  639.61  638.06  633.37  622.75  606.41  583.59  553.24  532.40  531.49  501.23  470.41  468.58  468.36  466.90
  27   34.00 |  604.89  603.52  599.34  589.83  575.01  553.90  524.85  504.15  503.28  472.02  440.11  438.23  438.00  436.17
  26   33.00 |  601.62  600.27  596.17  586.83  572.29  551.53  522.90  502.44  501.58  470.68  439.15  437.29  437.07  435.27
  25   32.00 |  598.18  596.86  592.85  583.71  569.46  549.09  520.92  500.73  499.88  469.39  438.28  436.46  436.24  434.49
  24   31.75 |  597.30  595.99  592.00  582.90  568.73  548.47  520.42  500.30  499.46  469.07  438.07  436.26  436.05  434.31
  23   30.43 |  592.46  591.19  587.32  578.51  564.76  545.08  517.75  498.04  497.21  467.45  437.09  435.34  435.13  433.48
  22   29.11 |  587.30  586.07  582.34  573.83  560.56  541.53  515.01  495.76  494.96  465.88  436.24  434.54  434.34  432.79
  21   21.25 |  548.86  547.97  545.26  539.15  529.70  516.16  496.87  481.93  481.29  457.46  433.29  431.97  431.82  430.77
  20   14.50 |  497.95  497.39  495.78  492.40  487.66  481.86  475.45  471.51  471.05  450.88  430.48  429.39  429.27  428.46
  19   13.75 |  496.63  496.08  494.48  491.17  486.54  480.91  474.79  471.63  471.05  450.70  430.12  429.03  428.91  428.10
  18   10.25 |  493.69  493.14  491.53  488.35  483.94  478.64  473.05  470.38  469.79  449.15  428.29  427.16  427.03  426.10
  17    8.50 |  492.08  491.51  489.75  486.65  482.32  477.09  471.59  468.77  468.14  444.94  427.41  426.28  426.12  424.80
  16    8.00 |  486.57  483.74  447.56  445.39  441.96  437.50  432.11  428.64  427.87  427.61  427.35  426.13  425.93  424.46
  15    4.00 |  447.37  446.76  444.71  442.41  439.02  434.63  429.34  426.11  425.47  425.26  425.05  423.74  423.48  421.63
  14    2.00 |  446.00  445.42  443.76  441.37  437.98  433.59  428.29  425.04  424.38  424.16  423.94  422.56  422.29  420.27
  13     .00 |  445.12  444.58  443.03  440.63  437.24  432.83  427.47  424.12  423.43  423.20  422.96  421.49  421.19  418.97
  12    -.12 |  435.57  435.13  433.87  431.45  427.95  423.18  416.61  411.38  410.10  409.65  409.19  406.07  405.38  399.54
  11    -.62 |  435.43  434.98  433.73  431.31  427.81  423.04  416.46  411.21  409.92  409.47  409.01  405.88  405.18  399.32
  10   -2.31 |  399.16  398.79  397.72  395.56  392.36  387.86  381.29  375.78  374.40  373.92  373.43  370.09  369.36  363.18
   9   -4.00 |  363.13  362.82  361.92  360.02  357.15  353.00  346.69  341.23  339.87  339.39  338.90  335.60  334.87  328.82
   8   -6.25 |  315.39  315.15  314.45  312.92  310.56  307.02  301.47  296.57  295.34  294.91  294.47  291.50  290.84  285.39
   7   -8.50 |  267.92  267.75  267.23  266.10  264.31  261.58  257.21  253.34  252.37  252.04  251.69  249.36  248.85  244.59
   6  -10.75 |  220.64  220.53  220.21  219.49  218.33  216.56  213.70  211.22  210.61  210.40  210.19  208.73  208.42  205.83
             +-----------------------------------------------------------------------------------------------------------------
                  .00    4.25    8.50   13.88   19.25   24.62   30.00   33.00   33.60   33.80   34.00   35.25   35.50   37.34
                    1       2       3       4       5       6       7       8       9      10      11      12      13      14
```

FINAL STEADY STATE,CRUSHED IL,NO NS3,NO AL,ONLY 1/8"SS STIFFNERS Mon Dec 30 21:55:59 1996

Steady-State Temperature Distribution at Time 6.0000E+02

58	215.41	153.21	153.22	153.22	154.08	154.16	154.34	158.90	159.57	160.10	161.71	163.46	163.70
57	215.16	153.25	153.26	153.27	154.12	154.21	154.39	158.95	159.62	160.15	161.77	163.75	163.97
56	214.43	161.10	161.10	161.09	160.99	161.02	161.08	163.48	163.92	164.27	165.35	166.63	166.66
55	213.70	168.91	168.89	168.88	167.76	167.72	167.66	167.70	167.88	168.03	168.53	169.14	169.16
54	212.98	176.70	176.67	176.64	174.46	174.36	174.16	171.71	171.63	171.58	171.47	171.43	171.44
53	212.25	184.49	184.45	184.41	181.14	180.98	180.65	175.65	175.29	175.01	174.27	173.56	173.56
52	208.88	221.09	220.99	220.90	212.50	212.03	211.08	194.49	192.54	191.00	186.50	181.85	181.82
51	205.50	260.85	260.71	260.56	248.25	247.69	246.59	233.93	233.66	225.57	207.09	189.69	189.60
50	204.66	271.37	271.21	271.04	256.75	256.08	254.77	237.88	237.83	221.86	206.43	190.35	190.28
49	203.81	282.22	282.04	281.85	265.13	264.34	262.79	242.52	242.47	224.56	207.92	190.87	190.79
48	202.97	293.57	293.35	293.14	273.41	272.48	270.63	247.82	247.76	230.28	211.04	191.21	191.12
47	202.12	305.63	305.39	305.15	281.60	280.37	278.15	253.95	253.43	252.99	216.28	191.23	191.13
46	201.62	305.91	305.67	305.43	281.73	279.82	278.08	254.18	253.49	252.99	205.11	190.91	190.87
45	201.50	339.74	339.69	339.63	335.15	277.97	277.45						
44	195.00	345.78	345.72	345.66	340.96	270.47	269.98						
43	194.50	346.43	346.37	346.31	341.43	270.71	270.22						
42	192.25	350.04	349.74	349.44	343.41	273.21	272.71						
41	188.25	359.95	352.35	344.71	341.89	286.75	286.10	192.76	190.63	189.29	186.80	188.44	188.44
40	187.50	361.50	353.03	344.49	342.14	305.19	305.03	213.26	208.78	205.53	197.12	189.14	189.09
39	172.39	387.81	373.31	358.63	356.17	344.50	344.43	261.09	255.22	250.78	248.96	245.38	245.01
38	169.75	392.76	373.93	354.79	346.76	343.20	342.39	292.22	286.25	278.73	273.85	270.51	269.62
37	169.50	393.27	374.23	354.86	345.75	344.46	342.03	292.44	288.85	286.45	274.14	270.17	269.24
36	167.50	397.56	378.39	358.91	349.51	347.59	343.82	295.73	293.53	293.01			
35	165.25	402.90	387.14	371.17	368.22	364.02	355.68	239.76	230.69	230.54			
34	148.84	445.40	435.43	425.38	423.21	416.86	404.20	226.30	214.18	214.04			
33	132.44	476.18	466.59	456.94	454.67	447.48	433.16	231.64	217.99	217.83			
32	116.03	495.08	485.40	475.66	473.29	465.62	450.34	235.16	220.61	220.45			
31	99.62	503.20	493.47	483.67	481.26	473.37	457.68	236.67	221.74	221.56			
30	83.22	501.13	491.40	481.60	479.20	471.37	455.78	236.28	221.45	221.28			
29	66.81	488.76	478.98	469.13	466.78	459.28	444.34	233.99	219.76	219.60			
28	50.41	465.60	454.74	443.79	441.41	434.64	421.16	231.69	218.72	218.56			
27	34.00	434.05	412.15	389.82	383.87	380.57	374.31	304.41	296.64	296.18			
26	33.00	433.19	411.07	388.54	377.61	376.00	372.56	308.56	307.21	306.87			
25	32.00	432.47	410.97	389.08	378.02	376.17	372.83	306.73	301.60	297.94	284.69	279.85	278.77
24	31.75	432.31	411.11	389.51	379.39	375.06	373.29	306.52	299.48	291.60	284.46	280.16	279.12
23	30.43	431.64	412.72	393.50	388.36	378.63	378.55	288.15	279.82	273.32	272.29	270.68	269.99
22	29.11	431.12	414.60	397.85	394.89	382.83	382.74	278.70	271.47	266.03	263.97	259.57	259.11
21	21.25	429.81	421.07	412.27	410.67	397.22	397.12	258.83	249.74	242.92	224.30	205.72	205.60
20	14.50	427.81	422.46	417.08	415.89	402.42	402.31	254.77	245.14	237.94	218.28	198.80	198.69
19	13.75	427.47	422.51	417.54	416.37	402.80	402.70	254.64	244.99	237.76	218.05	198.52	198.41
18	10.25	425.42	422.54	419.65	418.48	404.03	403.92	254.82	245.09	237.81	217.96	198.30	198.19
17	8.50	423.40	422.41	421.43	419.53	403.85	403.74	255.40	245.67	238.37	218.47	198.73	198.63
16	8.00	422.40	422.32	422.24	419.71	403.62	403.50	255.70	245.96	238.66	218.72	198.94	198.83
15	4.00	419.84	419.81	419.78	417.74	398.28	398.16	260.94	251.04	243.55	222.83	202.04	201.92
14	2.00	418.31	418.28	418.24	415.85	390.39	390.24	276.10	265.07	256.47	231.46	205.56	205.42
13	.00	416.69	416.65	416.61	413.48	375.41	375.03	321.35	313.03	304.23	257.81	209.87	209.66
12	-.12	391.74	391.58	391.42	375.88	374.84	372.82	325.51	324.39	323.67	260.48	209.97	209.76
11	-.62	391.47	391.31	391.15	375.53	374.50	372.38	325.16	324.51	323.53	264.06	210.16	209.93
10	-2.31	355.24	355.08	354.93	340.43	339.57	337.80	305.08	304.98	275.08	241.95	207.57	207.40
9	-4.00	321.26	321.12	320.98	308.21	307.58	306.32	290.38	290.17	272.34	237.20	204.05	203.88
8	-6.25	278.50	278.36	278.23	265.66	264.86	263.21	230.07	224.85	220.61	208.04	194.93	194.84
7	-8.50	239.18	239.08	238.98	229.06	228.43	227.15	202.11	199.56	197.58	191.91	186.09	186.04
6	-10.75	202.65	202.59	202.53	196.99	196.66	196.00	183.90	182.92	182.18	180.09	178.00	177.99
		39.19	39.22	39.25	41.75	41.88	42.12	45.81	46.06	46.25	46.77	47.28	47.53
		15	16	17	18	19	20	21	22	23	24	25	26

FINAL STEADY STATE,CRUSHED IL,NO NS3,NO AL,ONLY 1/8"SS STIFFNERS Mon Dec 30 21:55:59 1996
Steady-State Temperature Distribution at Time 6.0000E+02

5	-11.48	205.40	205.32	205.05	204.47	203.53	202.08	199.76	197.76	197.28	197.11	196.94	195.80	195.55	193.55
4	-12.20	190.17	190.11	189.91	189.46	188.74	187.62	185.85	184.36	184.00	183.88	183.76	182.93	182.76	181.34
3	-12.93	174.95	174.91	174.77	174.46	173.96	173.19	171.97	170.99	170.77	170.69	170.61	170.10	170.00	169.18
2	-13.66	159.73	159.71	159.64	159.47	159.19	158.76	158.11	157.64	157.55	157.52	157.48	157.29	157.26	157.03
1	-13.91	159.66	159.64	159.56	159.39	159.12	158.69	158.04	157.58	157.48	157.45	157.42	157.23	157.19	156.97
		.00	4.25	8.50	13.88	19.25	24.62	30.00	33.00	33.60	33.80	34.00	35.25	35.50	37.34
		1	2	3	4	5	6	7	8	9	10	11	12	13	14

FINAL STEADY STATE,CRUSHED IL,NO NS3,NO AL,ONLY 1/8"SS STIFFNERS Mon Dec 30 21:55:59 1996
Steady-State Temperature Distribution at Time 6.0000E+02

5	-11.48	191.14	191.10	191.05	187.03	186.81	186.34	178.45	177.91	177.51	176.40	175.33	175.33
4	-12.20	179.73	179.70	179.67	177.18	177.05	176.80	173.04	172.91	172.83	172.67	172.59	172.59
3	-12.93	168.35	168.34	168.33	167.34	167.31	167.26	167.48	167.77	168.01	168.77	169.71	169.73
2	-13.66	156.97	156.97	156.97	157.45	157.51	157.65	161.64	162.31	162.85	164.51	166.57	166.79
1	-13.91	156.91	156.91	156.91	157.39	157.46	157.60	161.58	162.25	162.79	164.43	166.25	166.49
		39.19	39.22	39.25	41.75	41.88	42.12	45.81	46.06	46.25	46.77	47.28	47.53
		15	16	17	18	19	20	21	22	23	24	25	26

3.6.4 Calculation of Maximum Clad Temperatures

This appendix contains calculations of maximum cladding temperatures of the design basis fuel assemblies inside the package during 10CFR71 [3.1] transportation conditions. Both normal conditions of transport and accident conditions are considered.

3.6.4.1 Thermal Model of the NUHOMS® DSC

The HEATING7.2 computer program [3.2, 3.16] is used to perform the thermal analysis of the DSC internal basket assembly and spent fuel assembly regions. To calculate the maximum clad temperature, the internal basket assembly of the DSC is modeled in detail. Even though the DSC is initially filled with helium, during transportation conditions air is conservatively assumed within the DSC. A three -dimensional portion of the DSC and fuel cross sections is modeled. The cross-section at z = 0.00 in. corresponds to the location in between the two spacer disks in the middle of the active fuel region of fuel assemblies. In the z direction, two spacer disks are included in the model. Insulated boundary conditions are conservatively assumed at z = 0.00 in. and z = 13.50 in. The HEATING7.2 model constructed of the FO/FC DSC basket is shown in Figure 3.6-1.

Regions 1 to 6 correspond to the fuel assemblies. Regions 13 to 36 correspond to the guide sleeves around fuel assemblies. Regions 70 to 79 correspond to the DSC shell. Regions 200 to 217 correspond to the neutron absorber plates. Regions 300 to 317 correspond to the over sleeves surrounding the neutron absorber plates. Regions 402, 411, 414, 417, 421, 425, 429, 432, 435, 440, 444, and 448 correspond to the gaps (assumed filled with air) between the adjacent oversleeves of the fuel assemblies where heat transfer is mainly due to radiation and conduction. Regions 403, 412, 413, 415, 416, 418, 420, 422, 424, 426, 430, 431, 433, 434, 436, 439, 443 and 447 correspond to the gaps (assumed filled with air) between the guide sleeves and the neutron absorber plates. These gaps are conservatively assumed due to fabrication tolerances where heat transfer is mainly due to radiation and conduction. The remaining regions between 400 to 448 correspond to the gaps between the DSC shell and the outer fuel assemblies where heat transfer is mainly due to radiation, natural convection, and conduction. Note that no credit is taken for heat removed by convection thereby maximizing the fuel assembly temperatures. Regions 500 to

517 correspond to the gaps (assumed filled with air) between the neutron absorber plates and the over sleeves. These gaps are conservatively assumed due to fabrication tolerances where heat transfer is mainly due to radiation and conduction. Regions 525 to 536 and 560 to 571 correspond to spacer disks #1 and #2, respectively. Regions 540 to 551 and regions 580 to 591 correspond to air gap regions between spacer disk #1 and #2, and between spacer disk #2 and #3, respectively.

3.6.4.1.1 Decay Heat Generation

The decay heat from the fuel assemblies is modeled as a volumetric heat density in HEATING7.2 models. Volumetric Heat Density ($\ddot{Q}$) is calculated assuming all the heat is generated in the active fuel portion of the fuel assemblies and a peaking factor of 1.2 to account for axial power peaking during irradiation [3.3].

$$\ddot{Q} = \frac{(0.764*1.2)\,kW * \dfrac{3412\ (Btu/hr)}{kW} * \dfrac{hr}{60\ \text{min}}}{(8.9)^2\ inch^2 * 141.8\ inch}$$

$$\therefore \ddot{Q} = 0.004642\ \frac{Btu}{\text{min-}inch^3}$$

Note that the fuel clad temperatures are calculated assuming 0.764*24 = 18.34 kW of total decay heat inside the cask inner cavity even though the maximum design basis heat load allowed is only 13.5 kW. This assumption is conservative because it will result in higher clad temperatures.

3.6.4.1.2 Material Properties

An effective thermal conductivity for the fuel region inside the DSC guide sleeve which accounts for the different materials (UO_2, zircaloy and helium) and includes the combined effects of radiation, conduction, and convection is taken from Reference [3.20]. The thermal conductivity and emissivity values used for the materials are the same as those of the Section 3.2.1. The neutron absorber material has a minimum thermal conductivity of 44.38 Btu/hr-ft-°F

[3.24]. To be conservative, stainless steel thermal conductivity values which are lower than this are used for the neutron absorber material.

3.6.4.1.3 Maximum Cladding Temperature

The maximum steady state outer surface temperatures for the DSC are calculated in Sections 3.4 and 3.5 for normal conditions of transport and hypothetical accident conditions respectively. The results for the normal conditions of transport show that the maximum DSC surface temperatures are 400°F and 317°F for the 100°F and -40°F ambient temperature cases, respectively. Similarly, the maximum DSC shell temperatures are 368°F, 368°F, 401°F, and 564°F for the prefire, fire, postfire and final steady state conditions, respectively.

The DSC surface temperatures of 400°F, and 564°F are used as a constant temperature boundary condition for the normal conditions of transport and bounding accident cases, respectively, based on the DSC thermal analysis. The HEATING7.2 input and output files DSC-100F.IN2 and DSC-100F.OU2, respectively, are included for the 100°F case.

The results of the calculations described above show maximum fuel clad temperatures of 669°F (354°C) and 790°F (421°C) for the normal conditions of transport, and accident conditions respectively. These maximum fuel clad temperatures are still considerably lower than the clad temperature limit of 1058°F (570°C) used for this analysis [3.3]. The neutron absorbing material in the basket is conservatively assumed to have the same temperature as the fuel clad. Therefore, the maximum temperature of the basket neutron absorber material is 790°F during normal conditions of operation or hypothetical accident conditions. This is still below the material temperature limit of 850°F [3.24].

3.6.4.1.4 Maximum Spacer Disc Temperature Distribution

The results at z = 3.375 in. gives the maximum temperature distribution for the spacer disk because this spacer disk is located approximately in the middle of the active fuel region inside the DSC. The results are included in Table 3.6-2 for the -20°F ambient case. Using the similar method for the 100°F and -40°F ambient cases, the maximum spacer disk gradients are 269°F and 295°F, respectively. These gradients are used in the thermal stress analysis documented in Chapter 2.

3.6.4.1.5 Maximum Guide Sleeve and Support Rod Temperatures

Table 3.6-1a represents the maximum Guide Sleeve and Support Rod temperatures for both the normal and hypothetical accident conditions. The Support Rod centerline is located at x=24.00 in. and y=13.67 in. The hottest Guide Sleeve and Support Rod were conservatively chosen to give maximum temperature at z=0.0. Table 3.6-1a is used in thermal stress analysis documented in Chapter 2.

Table 3.6-1

FO/FC DSC Maximum Clad Temperatures

THIS SECTION CONTAINS
PROPRIETARY INFORMATION

Table 3.6-1a

Maximum Guide Sleeve and Support Rod Temperatures

THIS SECTION CONTAINS
PROPRIETARY INFORMATION

THIS SECTION CONTAINS
PROPRIETARY INFORMATION

Figure 3.6-1
HEATING7.2 Model of NUHOMS® DSC Basket

THIS SECTION CONTAINS
PROPRIETARY INFORMATION

Figure 3.6-1
HEATING7.2 Model of NUHOMS® DSC Basket
(Concluded)

Table 3.6-2

Spacer Disk Temperature Distribution for FO/FC DSC, -20°F NOC

THIS SECTION CONTAINS
PROPRIETARY INFORMATION

Table 3.6-2

Spacer Disk Temperature Distribution for FO/FC DSC, -20°F NOC

(Continued)

THIS SECTION CONTAINS
PROPRIETARY INFORMATION

Table 3.6-2

Spacer Disk Temperature Distribution for FO/FC DSC, -20°F NOC

(Concluded)

THIS SECTION CONTAINS
PROPRIETARY INFORMATION

3.6.4.2 HEATING7.2 INPUT FILE: DSC-100F.IN2

THIS SECTION CONTAINS
PROPRIETARY INFORMATION

3.6.4.3 HEATING7.2 OUTPUT FILE: DSC-100F.OU2

SMUD-FC-BSKT,100F AMB,AIR,DSC-100F.in2 Mon Dec 23 11:52:00 1996

Steady-State Temperature Distribution at Time 0.0000E+00

Z = 0.0000E+00

41	33.62	400.00	400.00	400.00	400.00	400.00	400.00	400.00	400.00	400.00	400.00				
40	33.00	400.35	400.42	400.42	400.42	400.44	400.44	400.46	400.42	400.26	400.26				
39	31.85	413.08	413.95	413.98	413.99	414.13	414.18	414.39	413.49	402.18	400.00	400.00	400.00	400.00	400.00
38	31.23	418.12	421.11	421.23	421.27	421.94	422.14	423.02	421.54	407.29	401.59	401.58	401.56	401.56	401.55
37	30.41	417.02	425.86	427.06	427.49	434.58	437.43	437.54	433.76	426.03	426.00	425.29	423.24	423.11	422.73
36	30.30	428.38	437.96	437.96	438.09	438.09	437.65	437.65	433.85	426.11	426.10	425.76	424.65	424.58	424.37
35	26.48	479.49	479.77	479.77	479.80	479.80	480.43	480.45	473.50	454.96	454.93	454.67	453.84	453.78	453.62
34	25.86	486.43	486.32	486.32	486.34	486.34	486.89	486.90	479.11	459.54	459.52	459.26	458.44	458.38	458.22
33	21.41	541.76	527.44	527.44	527.00	526.98	526.07	526.07	511.00	489.27	489.24	489.19	489.02	489.01	488.97
32	21.30	541.69	531.75	531.56	531.50	530.62	530.17	526.16	511.10	489.36	489.36	491.54	492.55	492.58	492.65
31	21.27	541.76	532.66	532.49	532.43	531.65	531.47	532.85	519.54	496.90	496.86	494.50	493.61	493.58	493.50
30	21.19	542.15	535.55	535.42	535.37	534.73	534.52	532.91	519.61	496.96	496.94	497.35	496.55	496.49	496.31
29	21.19	542.19	535.75	535.61	535.57	534.94	534.74	534.65	521.90	498.97	498.82	497.66	496.75	496.69	496.50
28	21.17	542.29	536.31	536.19	536.15	535.55	535.38	534.67	521.92	498.98	498.83	498.46	497.35	497.28	497.06
27	20.34	557.43	563.22	563.32	563.36	563.84	563.97	564.44	560.95	535.09	534.75	533.03	527.46	527.09	526.03
26	20.33	557.53	563.79	563.90	563.94	564.48	564.64	564.45	560.97	535.10	534.77	533.75	527.79	527.37	526.15
25	20.32	557.57	563.99	564.10	564.14	564.70	564.88	566.21	563.27	537.23	537.15	534.04	527.91	527.47	526.19
24	20.24	557.98	566.92	567.09	567.15	567.95	568.12	566.28	563.35	537.30	537.25	534.96	529.97	528.96	526.43
23	20.21	558.05	567.84	568.03	568.10	569.03	569.55	573.96	573.28	547.24	547.02	534.51	534.31	526.34	526.17
22	20.10	558.00	572.15	572.15	572.61	572.62	574.06	574.08	573.41	547.37	547.22	535.02	534.92	532.14	532.13
21	15.66	605.38	605.58	605.58	605.60	605.61	606.18	606.20	602.31	584.90	584.79	576.95	576.88	575.03	575.02
20	11.22	635.64	627.97	627.97	627.71	627.71	627.30	627.30	619.73	604.68	604.60	599.99	599.96	598.97	598.96
19	11.11	635.36	630.13	630.04	630.01	629.60	629.39	627.35	619.79	604.72	603.98	603.28	601.54	601.41	601.04
18	11.08	635.34	630.59	630.51	630.48	630.13	630.07	630.90	624.01	607.58	604.40	603.76	601.97	601.84	601.48
17	11.00	635.38	632.03	631.98	631.96	631.72	631.64	630.94	624.06	607.60	605.59	605.07	603.37	603.25	602.92
16	10.99	635.39	632.13	632.07	632.06	631.83	631.76	631.93	625.28	608.30	605.68	605.16	603.46	603.35	603.01
15	10.98	635.41	632.41	632.36	632.34	632.14	632.09	631.94	625.29	608.30	605.95	605.43	603.74	603.63	603.30
14	10.01	643.37	646.39	646.44	646.45	646.64	646.68	646.76	643.46	624.82	622.94	622.50	621.00	620.90	620.60
13	10.00	643.39	646.68	646.73	646.74	646.97	647.03	646.77	643.47	624.83	623.39	622.90	621.31	621.20	620.89
12	9.99	643.39	646.77	646.83	646.84	647.08	647.16	647.78	644.74	626.25	623.55	623.04	621.42	621.31	620.99
11	9.91	643.42	648.23	648.32	648.35	648.78	648.87	647.82	644.78	626.30	625.74	625.09	623.01	622.87	622.45
10	9.88	643.40	648.69	648.79	648.83	649.35	649.64	652.07	650.18	631.76	626.81	625.73	623.50	623.34	622.89
9	9.77	643.10	650.83	650.83	651.11	651.12	652.13	652.14	650.26	631.84	631.76	626.22	626.16	624.73	624.72
8	5.33	665.05	665.26	665.26	665.29	665.29	665.82	665.83	663.18	650.04	649.96	644.45	644.40	643.10	643.09
7	.89	669.08	669.15	669.15	669.16	669.17	669.48	669.48	665.71	651.76	651.69	647.36	647.32	646.28	646.27
6	.78	669.09	669.16	669.17	669.17	669.23	669.28	669.48	665.70	651.74	649.21	648.42	646.67	646.55	646.19
5	.75	669.09	669.16	669.16	669.17	669.22	669.23	669.16	665.16	650.71	648.91	648.33	646.60	646.48	646.14
4	.67	669.10	669.15	669.15	669.15	669.16	669.17	669.15	665.16	650.70	648.38	647.89	646.35	646.25	645.95
3	.66	669.10	669.15	669.15	669.15	669.16	669.16	669.14	665.13	650.42	648.34	647.86	646.33	646.23	645.94
2	.65	669.10	669.15	669.15	669.15	669.15	669.15	669.14	665.13	650.42	648.23	647.76	646.28	646.18	645.89
1	.00	669.10	669.10	669.09	669.09	669.09	669.09	669.07	664.92	642.52	642.83	642.85	642.82	642.82	642.80
		.00	.65	.66	.67	.75	.78	.89	5.33	9.77	9.88	9.91	9.99	10.00	10.01
		1	2	3	4	5	6	7	8	9	10	11	12	13	14

SMUD-FC-BSKT,100F AMB,AIR,DSC-100F.in2 Mon Dec 23 11:52:00 1996

Steady-State Temperature Distribution at Time 0.0000E+00

Z = 0.0000E+00

41	33.62														
40	33.00														
39	31.85	400.00	400.00	400.00	400.00	400.00	400.00	400.00	400.00	400.00					
38	31.23	401.16	401.16	401.16	401.13	401.13	401.09	400.77	400.48	400.48					
37	30.41	413.24	413.12	413.08	412.48	412.30	411.49	405.06	400.21	400.00	400.00				
36	30.30	414.75	414.62	414.57	413.92	413.73	412.85	405.66	400.19	400.00	400.00				
35	26.48	445.17	445.04	444.99	444.36	444.16	443.28	423.71	400.82	400.00	400.00	400.00	400.00	400.00	400.00
34	25.86	449.84	449.71	449.67	449.03	448.84	447.95	427.14	401.83	400.29	400.29	400.27	400.27	400.27	400.16
33	21.41	482.11	482.00	481.96	481.36	481.18	480.34	456.47	435.09	434.49	434.36	433.94	433.91	433.83	429.64
32	21.30	483.45	483.30	483.25	482.54	482.32	481.32	457.56	436.32	435.66	435.52	435.06	435.03	434.94	430.48
31	21.27	483.74	483.59	483.54	482.79	482.57	481.53	457.80	436.59	435.92	435.77	435.30	435.27	435.18	430.67
30	21.19	484.68	484.51	484.45	483.62	483.37	482.22	458.58	437.48	436.75	436.60	436.09	436.06	435.96	431.26
29	21.19	484.74	484.57	484.51	483.68	483.42	482.27	458.64	437.54	436.81	436.65	436.15	436.11	436.02	431.30
28	21.17	484.92	484.75	484.69	483.84	483.58	482.41	458.79	437.72	436.98	436.82	436.30	436.27	436.17	431.42
27	20.34	493.71	493.39	493.29	491.77	491.30	489.23	467.41	447.76	445.59	445.26	444.49	444.44	444.30	437.62
26	20.33	493.69	493.45	493.37	491.94	491.38	489.33	467.60	448.02	445.23	444.97	444.57	444.54	444.47	437.74
25	20.32	493.69	493.47	493.40	492.01	491.40	489.37	467.66	448.11	445.10	444.86	444.59	444.58	444.52	437.79
24	20.24	493.44	493.93	494.14	493.46	491.42	489.89	468.60	449.47	442.26	442.90	444.98	445.09	445.41	438.43
23	20.21	493.19	493.29	495.75	495.75	490.12	490.04	468.90	449.93	439.71	442.29	445.25	445.39	445.77	438.62
22	20.10	497.52	497.51	496.18	496.14	490.32	490.24	469.04	450.04	450.03	449.61	448.41	448.33	448.10	439.55
21	15.66	544.45	544.44	542.62	542.56	536.07	535.99	511.34	478.15	478.12	477.75	476.56	476.48	476.24	465.51
20	11.22	577.76	577.74	576.08	576.02	570.25	570.18	537.75	500.36	500.32	500.02	499.07	499.00	498.81	488.59
19	11.11	580.00	579.49	579.31	576.85	575.67	570.25	537.82	500.39	501.17	501.09	500.53	500.49	500.36	489.46
18	11.08	580.52	580.06	579.90	577.56	576.84	576.02	543.86	502.94	501.62	501.45	500.89	500.85	500.72	489.66
17	11.00	582.26	581.89	581.76	579.88	579.30	576.08	543.91	502.96	502.76	502.63	502.12	502.08	501.96	490.29
16	10.99	582.38	582.01	581.89	580.04	579.48	577.72	545.58	503.54	502.85	502.72	502.21	502.17	502.05	490.33
15	10.98	582.72	582.37	582.25	580.51	579.98	577.73	545.59	503.55	503.11	502.98	502.47	502.43	502.31	490.46
14	10.01	602.80	602.51	602.41	600.93	600.47	598.34	573.71	530.31	529.35	528.98	527.47	527.36	527.03	499.11
13	10.00	603.12	602.83	602.73	601.28	600.83	598.35	573.72	530.33	530.55	529.98	528.22	528.09	527.70	499.25
12	9.99	603.24	602.95	602.85	601.40	600.95	599.29	575.43	532.89	530.98	530.32	528.48	528.35	527.94	499.30
11	9.91	604.88	604.60	604.51	603.13	602.63	599.32	575.49	532.97	537.83	535.09	532.53	532.22	531.44	500.05
10	9.88	605.38	605.11	605.01	603.75	603.31	603.77	582.82	542.90	542.80	534.61	534.52	532.52	532.50	500.31
9	9.77	607.69	607.69	606.95	606.93	603.89	603.85	582.92	543.03	542.91	534.64	534.57	532.71	532.70	500.43
8	5.33	624.42	624.41	623.15	623.11	618.74	618.68	600.61	571.07	570.94	561.36	561.28	559.08	559.06	521.72
7	.89	631.11	631.10	630.09	630.05	626.41	626.35	604.83	572.61	572.50	564.92	564.86	563.14	563.13	534.01
6	.78	631.26	630.92	630.80	629.19	628.50	626.35	604.82	572.60	568.17	566.77	563.58	563.35	562.69	534.70
5	.75	631.32	630.99	630.88	629.26	628.72	626.78	604.26	571.23	567.67	566.61	563.42	563.20	562.57	534.87
4	.67	631.52	631.23	631.13	629.62	629.14	626.79	604.26	571.22	566.77	565.84	562.88	562.68	562.10	535.44
3	.66	631.54	631.25	631.15	629.65	629.17	627.05	604.23	570.77	566.71	565.78	562.84	562.64	562.07	535.49
2	.65	631.59	631.30	631.20	629.73	629.26	627.05	604.23	570.77	566.52	565.62	562.73	562.54	561.97	535.60
1	.00	634.66	634.63	634.63	634.59	634.60	634.89	604.05	556.90	556.93	556.86	556.45	556.42	556.31	541.46
		10.98	10.99	11.00	11.08	11.11	11.22	15.66	20.10	20.21	20.24	20.32	20.33	20.34	21.17
		15	16	17	18	19	20	21	22	23	24	25	26	27	28

3.6.5 FF-DSC Temperature Distribution

This appendix calculates the temperature distribution in the FF-DSC inside a NUHOMS®-MP187 Cask during transportation conditions. The temperatures of the DSC shell are used to calculate the maximum temperature gradients across spacer disks constructed of either carbon steel or XM-19 stainless steel.

The thermal model of the NUHOMS®-MP187 Cask and the FF-DSC is the same as that described in Section 3.4 with the following changes.

a. The volumetric heat generation is changed to 1.145E-3 Btu/min-in^3 to account for the lower heat load in the FF-DSC (9.93 kW vs. 13.5 kW from Section 3.1.2).

b. The air gap between the DSC outer shell and cask inner shell is changed to 0.40 in. to simulate the DSC in a horizontal position and to calculate the maximum DSC shell temperature at the top portion of the FF-DSC. To calculate the temperature of the FF-DSC bottom portion the gap is replaced by the stainless steel material (i.e., contact of the DSC outer shell and cask inner shell). All the other input parameters in the HEATING7.2 [3.2] model are the same as Section 3.4. The results are summarized in Table 3.6-3.

3.6.5.1 FF-DSC Basket Temperature Distribution, NOC

The temperatures of the DSC shell calculated in Section 3.6.5 are used to calculate the temperature distribution in the FF-DSC basket.

The analytical model of the FF-DSC basket using the HEATING7.2 [3.2] code to determine the DSC basket temperature distribution is shown in Figure 3.6-2. The HEATING7.2 model corresponds to the case when the loaded FF- DSC is in the NUHOMS®-MP187 Cask in a horizontal position. The DSC basket thermal analysis is performed for the 100°F, -20°F, and -40°F ambient conditions using the corresponding DSC shell temperatures as described in

Section 3.6.5. Even though the DSC is initially filled with helium, during transport conditions air is conservatively assumed within the DSC.

3.6.5.1.1 HEATING7.2 Model

The HEATING7.2 model constructed is shown in the Figure 3.6-2. A three-dimensional portion of the DSC and fuel cross-section is modeled. The cross-section at z = 0.00 in. corresponds to the location between the two spacer disks in the middle of the active fuel region. In the z-direction, two spacer disks are included in the model. An insulated boundary condition is conservatively assumed at z = 0.00 in. and z = 22.50 in. Regions 1 to 8 correspond to the fuel assemblies. Regions 11 to 39 correspond to the fuel assembly canisters. Regions 100 to 113 correspond to the DSC shell. Regions 45, 46, 50,52, 53, 54, 56, 60, and 61 correspond to the air gap between fuel assemblies where heat transfer is mainly due to radiation and conduction.

The other remaining regions between 40 to 65 correspond to the air surrounding the central fuel assemblies and the region between the DSC shell and the outer fuel assemblies where heat transfer is mainly due to radiation, natural convection and conduction. Note that no credit is taken for heat removed by convection, thereby maximizing the fuel assembly temperatures and gradients. Regions 140 to 166 and 340 to 366 correspond to spacer disk #1 and #2, respectively. Regions 240 to 266 and 440 to 466 correspond to air gap regions between spacer disk #1 and #2 and between spacer disk #2 and #3, respectively. The FF-DSC basket was evaluated with carbon steel spacer disks and with XM-19 spacer disks.

3.6.5.1.2 Decay Heat Generation

The decay heat from the fuel assemblies is modeled as a volumetric heat density. Volumetric heat density ($\dddot{Q}$) is calculated assuming all the heat is generated in the active fuel portion of the fuel assemblies and includes a peaking factor of 1.2 to account for axial power peaking during irradiation [3.3].

$$\dddot{Q} = \frac{(0.764*1.2)\ kW * \frac{3412\ (Btu/hr)}{kW} * \frac{hr}{60\ \min}}{(9.0)^2\ in^2 * 141.8\ in}$$

$$\dddot{Q} = 0.00454\ \frac{Btu}{\min\text{-}inch^3}$$

3.6.5.1.3 Material Properties

The DSC, fuel, failed fuel can and carbon steel thermal conductivity and emissivity values used for the materials are the same as those of Section 3.2. The XM-19 conductivity and emissivity values are given in Table 3.6-3a, below.

Table 3.6-3a

Thermal Properties of XM-19 Stainless Steel

Temperature (°F)	Conductivity (Btu/min-in-°F) [3.4]	Emissivity [3.15]
100.0	0.00917	0.587
200.0	0.00986	
300.0	0.01070	
400.0	0.01140	
500.0	0.01220	
600.0	0.01290	
700.0	0.01380	

3.6.5.1.4 Calculation of Maximum Spacer Disc Temperature Gradient

Table 3.6.4 shows the temperature distribution in a carbon steel spacer disc located mid-length at z = 5.625 in. along the axis of the DSC. Table 3.6.4a shows the temperature distribution in an XM-19 spacer disk at the same location. This location gives the maximum temperature distribution for a spacer disk because the spacer disk is located approximately in the middle of the active fuel region.

Table 3.6-3

FF-DSC Shell Temperatures when Inside NUHOMS®-MP187 Cask, NOC

AMBIENT TEMPERATURE (°F)	DSC SHELL TEMPERATURE AT TOP (°F)	DSC SHELL TEMPERATURE AT BOTTOM (°F)	ESTIMATED DSC SHELL TEMPERATURE AT SIDE (°F)
100	348	252	300
-20	263	152	208
-40	251	136	194

Table 3.6-4

FF-DSC Carbon Steel Spacer Disk Temperature Distribution, 100°F, NOC

THIS SECTION CONTAINS
PROPRIETARY INFORMATION

Table 3.6-4

FF-DSC Carbon Steel Spacer Disk Temperature Distribution, 100°F, NOC

(Concluded)

THIS SECTION CONTAINS
PROPRIETARY INFORMATION

Table 3.6-4a

FF-DSC XM-19 Spacer Disk Temperature Distribution, 100°F, NOC

THIS SECTION CONTAINS
PROPRIETARY INFORMATION

Table 3.6-4a

FF-DSC XM-19 Spacer Disk Temperature Distribution, 100°F, NOC

(Cooncluded)

THIS SECTION CONTAINS
PROPRIETARY INFORMATION

Table 3.6-5

FF-DSC Carbon Steel Spacer Disk Temperature Distribution, -20°F, NOC

THIS SECTION CONTAINS
PROPRIETARY INFORMATION

Table 3.6-5

FF-DSC Carbon Steel Spacer Disk Temperature Distribution, -20°F, NOC

(Concluded)

THIS SECTION CONTAINS PROPRIETARY INFORMATION

Table 3.6-5a

FF-DSC XM-19 Spacer Disk Temperature Distribution, -20°F, NOC

THIS SECTION CONTAINS
PROPRIETARY INFORMATION

Table 3.6-5a

FF-DSC XM-19 Spacer Disk Temperature Distribution, -20°F, NOC

(Concluded)

THIS SECTION CONTAINS
PROPRIETARY INFORMATION

THIS SECTION CONTAINS
PROPRIETARY INFORMATION

Figure 3.6-2
HEATING7.2 Model of FF-DSC Basket

THIS SECTION CONTAINS
PROPRIETARY INFORMATION

Figure 3.6-2
HEATING7.2 Model of FF-DSC Basket
(Concluded)

3.6.5.2 HEATING7.2 Input and Output Listings for the FF-DSC

3.6.5.2.1 HEATING7.2 Input File Name: FF-NOC3.INP

THIS SECTION CONTAINS
PROPRIETARY INFORMATION

3.6.5.2.2 HEATING7.2 Output File Name: FF-NOC3.OUT

NOC,-40F,FF-NOC3,NO NS3 CREDIT,1/8"AL,1/8"SS STIFFNERS 14-OCT-95 14:47:39

Steady-State Temperature Distribution at Time 0.0000E+00

71	254.50	-39.21	-39.22	-39.25	-39.38	-39.62	-39.66	-39.67	-39.67	-39.67	-39.67	-39.67			
70	254.25	-39.21	-39.22	-39.24	-39.38	-39.62	-39.66	-39.67	-39.67	-39.67	-39.67	-39.67			
69	247.50	-27.91	-28.03	-28.42	-30.59	-35.10	-37.34	-37.87	-38.24	-38.84	-39.46	-39.46	-39.56	-39.56	-39.58
68	247.25	-27.46	-27.59	-27.99	-30.23	-34.87	-37.16	-37.71	-38.10	-38.74	-39.45	-39.46	-39.56	-39.56	-39.58
67	240.50	-14.81	-15.05	-15.75	-19.69	-27.09	-29.83	-30.41	-30.80	-31.41	-32.03	-32.28	-36.00	-36.07	-37.50
66	240.25	-14.30	-14.53	-15.25	-19.25	-26.74	-29.52	-30.10	-30.49	-31.11	-31.73	-31.98	-35.79	-35.86	-37.34
65	233.50	0.83	0.50	-0.49	-5.99	-16.04	-19.66	-20.42	-20.94	-21.76	-22.59	-22.93	-28.16	-28.25	-30.13
64	233.25	1.45	1.12	0.12	-5.43	-15.57	-19.23	-20.00	-20.52	-21.35	-22.19	-22.53	-27.81	-27.90	-29.80
63	226.50	20.03	19.62	18.38	11.49	-1.18	-5.79	-6.76	-7.42	-8.47	-9.54	-9.98	-16.75	-16.87	-19.35
62	226.25	20.80	20.39	19.14	12.20	-0.56	-5.20	-6.18	-6.85	-7.91	-8.99	-9.42	-16.25	-16.37	-18.87
61	219.50	43.71	43.23	41.79	33.74	18.58	12.99	11.81	11.01	9.74	8.46	7.93	-0.13	-0.27	-3.13
60	219.25	44.65	44.17	42.72	34.64	19.40	13.77	12.58	11.77	10.50	9.20	8.67	0.55	0.41	-2.46
59	212.50	72.57	72.06	70.51	61.75	44.43	37.57	36.10	35.11	33.53	31.93	31.28	21.27	21.11	17.72
58	212.25	73.71	73.19	71.64	62.87	45.50	38.58	37.11	36.10	34.51	32.89	32.24	22.10	21.93	18.50
57	205.50	107.00	106.51	105.01	96.48	78.51	69.93	67.98	66.64	64.47	62.22	61.29	46.08	45.81	40.36
56	202.13	125.52	125.06	123.67	115.77	99.36	90.86	88.81	87.36	84.98	82.42	81.34	61.59	61.14	51.21
55	201.63	125.54	125.08	123.69	115.79	99.40	90.92	88.87	87.44	85.06	82.51	81.43	61.75	61.30	51.40
54	201.50	129.00	128.57	127.27	120.10	107.43	103.22	102.39	101.85	101.00	100.17	99.84	95.37	95.30	94.06
53	199.33	129.38	128.94	127.65	120.50	107.95	103.79	102.98	102.45	101.64	100.85	100.54	96.54	96.49	95.47
52	197.17	130.20	129.77	128.47	121.35	108.81	104.45	103.57	103.00	102.15	101.35	101.04	97.32	97.27	96.33
51	195.00	131.47	131.04	129.75	122.63	110.10	105.31	104.08	103.18	102.24	101.45	101.16	97.72	97.67	96.68
50	194.50	198.57	198.22	197.17	191.54	182.89	180.51	179.94	102.60	102.02	101.38	101.12	97.80	97.74	96.67
49	192.25	200.26	199.90	198.85	193.19	184.48	182.36	181.84	102.13	101.58	101.00	100.87	98.21	97.88	96.08
48	188.25	202.48	202.12	201.03	195.19	185.93	183.06	182.53	102.87	102.35	101.84	101.75	100.56	89.19	88.63
47	187.50	202.93	202.57	201.47	195.59	186.21	182.69	182.24	103.01	102.49	101.99	101.91	100.86	87.77	87.23
46	169.75	306.06	304.60	300.21	275.69	228.99	210.50	209.83	104.01	103.28	102.54	102.41	100.30	55.26	53.32
45	169.50	307.07	305.61	301.18	276.48	229.45	210.86	210.19	104.11	103.38	102.64	102.51	100.40	55.21	52.94
44	167.50	314.79	313.24	308.56	282.45	232.98	213.72	213.03	105.04	104.29	103.54	103.41	101.29	56.19	53.75
43	165.25	322.66	321.02	316.08	288.54	236.69	216.82	216.11	106.25	105.49	104.72	104.59	102.52	61.22	59.65
42	154.31	349.90	347.97	342.17	310.00	251.20	229.58	228.82	114.06	113.24	112.44	112.30	110.38	76.81	75.48
41	143.38	366.66	364.57	358.30	323.67	261.31	238.74	237.95	121.25	120.40	119.57	119.43	117.49	85.08	83.76
40	132.44	377.07	374.90	368.38	332.44	268.15	245.04	244.23	126.86	126.00	125.15	125.00	123.02	90.30	88.95
39	121.50	383.38	381.16	374.51	337.86	272.53	249.11	248.30	130.78	129.90	129.04	128.89	126.88	93.67	92.29
38	110.56	386.75	384.52	377.80	340.81	274.96	251.39	250.57	133.06	132.18	131.32	131.16	129.12	95.59	94.19
37	99.63	387.77	385.53	378.79	341.71	275.71	252.09	251.27	133.79	132.91	132.05	131.89	129.85	96.21	94.80
36	88.69	386.58	384.35	377.64	340.67	274.87	251.30	250.49	133.01	132.13	131.27	131.12	129.08	95.55	94.15
35	77.75	382.99	380.78	374.14	337.56	272.33	248.93	248.12	130.69	129.81	128.96	128.81	126.79	93.58	92.20
34	66.81	376.35	374.19	367.70	331.88	267.79	244.73	243.93	126.76	125.89	125.05	124.90	122.92	90.12	88.77
33	55.88	365.38	363.31	357.09	322.71	260.72	238.25	237.46	121.19	120.34	119.52	119.37	117.43	84.66	83.33
32	44.94	347.63	345.73	340.02	308.34	250.25	228.83	228.08	114.26	113.45	112.65	112.51	110.55	75.51	74.14
31	34.00	318.56	316.98	312.22	285.62	235.12	215.64	214.94	107.45	106.70	105.95	105.81	103.62	56.78	54.72
30	32.00	311.10	309.61	305.10	279.88	231.65	212.75	212.07	106.77	106.03	105.29	105.16	103.01	56.31	53.96
29	31.75	310.12	308.64	304.16	279.13	231.20	212.38	211.71	106.69	105.96	105.23	105.09	102.95	56.43	54.29
28	21.25	258.27	257.37	254.64	239.41	208.90	194.83	194.28	106.05	105.47	104.89	104.79	103.47	81.21	80.40
27	14.50	206.60	206.12	204.75	198.02	188.04	184.91	184.50	105.22	104.70	104.20	104.11	103.06	89.43	88.88
26	13.75	205.47	205.00	203.63	197.05	187.45	185.08	184.56	105.09	104.57	104.07	103.98	102.90	90.33	89.81
25	10.25	203.64	203.15	201.72	195.34	186.25	184.21	183.68	104.37	103.84	103.30	103.21	101.77	94.68	94.21
24	8.50	202.58	202.06	200.35	194.03	185.01	182.73	182.13	104.26	103.69	103.03	102.90	100.51	97.95	96.74
23	8.00	193.72	190.34	127.43	121.42	110.59	106.46	105.39	104.60	103.78	103.07	102.86	99.97	99.68	97.35
22	6.00	159.24	154.77	126.03	120.12	109.32	105.52	104.75	104.25	103.49	102.78	102.51	99.05	98.99	97.78
21	4.00	127.38	126.85	125.14	119.15	108.36	104.78	104.08	103.61	102.90	102.21	101.94	98.35	98.30	97.31
20	2.00	126.58	126.07	124.57	118.50	107.67	104.12	103.42	102.96	102.25	101.54	101.26	97.45	97.39	96.37
19	0.00	126.22	125.73	124.30	118.18	107.23	103.58	102.84	102.36	101.60	100.84	100.54	96.29	96.23	95.00
		0.00	4.25	8.50	19.25	30.00	33.00	33.60	34.00	34.63	35.25	35.50	39.19	39.25	40.50
		1	2	3	4	5	6	7	8	9	10	11	12	13	14

NOC,-40F,FF-NOC3,NO NS3 CREDIT,1/8"AL,1/8"SS STIFFNERS 14-OCT-95 14:47:39

Steady-State Temperature Distribution at Time 0.0000E+00

71	254.50														
70	254.25														
69	247.50	-39.59	-39.59	-39.59											
68	247.25	-39.59	-39.59	-39.59											
67	240.50	-39.04	-39.35	-39.35	-39.36	-39.36	-39.36	-39.43	-39.44	-39.44	-39.44				
66	240.25	-38.97	-39.33	-39.35	-39.35	-39.36	-39.36	-39.43	-39.44	-39.44	-39.44				
65	233.50	-32.06	-32.45	-32.84	-33.03	-33.23	-33.33	-37.65	-38.29	-39.04	-39.04	-39.11	-39.11		
64	233.25	-31.75	-32.15	-32.55	-32.75	-32.95	-33.05	-37.50	-38.19	-39.02	-39.04	-39.10	-39.10		
63	226.50	-21.93	-22.45	-22.98	-23.25	-23.52	-23.66	-29.72	-30.62	-31.69	-32.15	-38.55	-38.55	-38.69	-38.69
62	226.25	-21.46	-21.99	-22.52	-22.79	-23.06	-23.20	-29.30	-30.21	-31.30	-31.77	-38.51	-38.55	-38.68	-38.68
61	219.50	-6.05	-6.64	-7.23	-7.53	-7.83	-7.98	-14.53	-15.47	-16.58	-17.06	-23.56	-24.22	-37.54	-37.54
60	219.25	-5.39	-5.99	-6.58	-6.88	-7.18	-7.33	-13.89	-14.83	-15.94	-16.42	-22.92	-23.60	-37.48	-37.53
59	212.50	14.38	13.73	13.07	12.75	12.42	12.26	5.55	4.64	3.59	3.15	-2.65	-3.25	-15.25	-16.01
58	212.25	15.12	14.46	13.80	13.47	13.15	12.98	6.26	5.37	4.33	3.88	-1.82	-2.40	-14.20	-14.97
57	205.50	35.08	34.10	33.16	32.70	32.25	32.03	25.06	25.05	25.02	23.55	22.93	22.86	20.91	20.80
56	202.13	39.31	36.76	34.27	33.00	31.81	31.25	25.67	25.45	25.21	24.50	23.27	23.15	21.04	20.94
55	201.63	39.46	36.65	34.48	32.30	31.11	30.62	25.89	25.48	25.02	24.76	23.32	23.19	21.07	20.96
54	201.50	93.01	36.52	36.23	30.55	30.46	30.39	25.91	25.49	25.01	24.81	23.33	23.20	21.07	20.97
53	199.33	94.67	45.29	45.18	27.58	27.55	27.53	25.54	25.28	24.98	24.86	23.43	23.30	21.17	21.07
52	197.17	95.59	49.50	49.39	26.43	26.39	26.37	25.13	24.95	24.73	24.64	23.41	23.30	21.25	21.15
51	195.00	95.93	51.36	51.24	25.93	25.89	25.87	24.86	24.71	24.53	24.45	23.38	23.27	21.31	21.21
50	194.50	95.89	51.60	51.48	25.85	25.82	25.80	24.82	24.67	24.50	24.42	23.37	23.27	21.32	21.22
49	192.25	95.12	51.90	51.79	25.69	25.65	25.63	24.72	24.58	24.42	24.35	23.37	23.27	21.36	21.26
48	188.25	88.08	50.34	50.24	25.81	25.77	25.76	24.87	24.73	24.56	24.49	23.49	23.39	21.41	21.31
47	187.50	86.71	50.01	49.91	25.91	25.87	25.85	24.95	24.81	24.64	24.56	23.53	23.43	21.41	21.31
46	169.75	51.38	42.67	42.46	36.42	36.34	36.29	32.12	31.53	30.83	30.53	26.65	26.30	20.95	20.72
45	169.50	48.08	44.80	41.94	40.42	39.10	38.49	32.47	31.80	31.02	30.67	26.43	26.08	20.76	20.53
44	167.50	49.77	47.88	46.07	45.20	44.36	43.95	34.69	33.99	33.35	33.26				
43	165.25	58.41	56.56	54.74	53.85	52.96	52.52	35.45	33.09	30.32	30.19				
42	154.31	74.29	72.09	69.89	68.80	67.72	67.17	44.69	41.66	38.13	37.98				
41	143.38	82.51	80.15	77.80	76.63	75.46	74.87	50.54	47.24	43.41	43.25				
40	132.44	87.66	85.19	82.73	81.51	80.29	79.68	54.19	50.74	46.72	46.55				
39	121.50	90.97	88.43	85.91	84.65	83.39	82.76	56.52	52.96	48.82	48.64				
38	110.56	92.85	90.27	87.71	86.43	85.15	84.51	57.84	54.22	50.01	49.83				
37	99.63	93.45	90.86	88.28	87.00	85.72	85.07	58.26	54.62	50.39	50.20				
36	88.69	92.81	90.23	87.67	86.39	85.12	84.47	57.81	54.19	49.98	49.80				
35	77.75	90.88	88.34	85.82	84.56	83.31	82.68	56.45	52.90	48.76	48.58				
34	66.81	87.48	85.01	82.56	81.34	80.12	79.51	54.06	50.61	46.60	46.43				
33	55.88	82.08	79.73	77.38	76.21	75.05	74.46	50.22	46.94	43.12	42.96				
32	44.94	72.94	70.76	68.60	67.53	66.46	65.92	43.93	40.96	37.50	37.35				
31	34.00	52.40	50.49	48.67	47.79	46.94	46.53	35.63	34.50	33.29	33.17				
30	32.00	49.31	46.44	43.89	42.53	41.35	40.79	33.58	32.74	31.79	31.39	26.12	25.70	19.78	19.53
29	31.75	51.90	44.54	44.26	39.02	38.90	38.83	33.25	32.48	31.58	31.20	26.33	25.91	19.97	19.72
28	21.25	79.84	47.74	47.65	26.81	26.78	26.77	25.71	25.54	25.32	25.23	23.86	23.72	21.07	20.95
27	14.50	88.35	50.33	50.22	25.38	25.34	25.32	24.45	24.32	24.16	24.09	23.12	23.02	21.08	20.98
26	13.75	89.27	50.60	50.50	25.31	25.28	25.26	24.39	24.26	24.10	24.04	23.08	22.98	21.07	20.98
25	10.25	93.64	51.77	51.66	25.24	25.20	25.19	24.29	24.16	24.00	23.93	22.98	22.89	21.04	20.95
24	8.50	95.88	51.96	51.85	25.33	25.29	25.28	24.35	24.21	24.04	23.97	22.99	22.89	21.01	20.92
23	8.00	96.34	51.92	51.80	25.38	25.34	25.32	24.38	24.24	24.07	23.99	22.99	22.89	21.00	20.91
22	6.00	96.94	51.24	51.12	25.66	25.62	25.60	24.56	24.40	24.21	24.13	23.03	22.92	20.97	20.87
21	4.00	96.54	49.25	49.14	26.23	26.19	26.18	24.86	24.66	24.43	24.34	23.08	22.96	20.91	20.81
20	2.00	95.55	45.02	44.91	27.43	27.40	27.39	25.27	24.99	24.68	24.55	23.09	22.96	20.84	20.74
19	0.00	93.93	36.66	36.38	30.34	30.24	30.17	25.61	25.18	24.69	24.48	23.00	22.86	20.75	20.65
		41.75	42.00	42.25	42.38	42.50	42.56	45.25	45.63	46.06	46.25	48.75	49.00	53.75	54.00
		15	16	17	18	19	20	21	22	23	24	25	26	27	28

NOC,-40F,FF-NOC3,NO NS3 CREDIT,1/8"AL,1/8"SS STIFFNERS　　14-OCT-95 14:47:39

Steady-State Temperature Distribution at Time 0.0000E+00

71	254.50					
70	254.25					
69	247.50					
68	247.25					
67	240.50					
66	240.25					
65	233.50					
64	233.25					
63	226.50					
62	226.25					
61	219.50	-37.00	-37.00			
60	219.25	-37.00	-37.00			
59	212.50	-32.91	-32.91	-28.80	-28.67	-28.62
58	212.25	-32.80	-32.88	-28.78	-28.51	-28.51
57	205.50	18.65	18.52	16.01	-6.82	-6.93
56	202.13	18.96	18.86	17.30	-6.34	-6.43
55	201.63	19.01	18.91	17.43	-6.27	-6.36
54	201.50	19.02	18.92	17.46	-6.26	-6.35
53	199.33	19.22	19.13	17.85	-6.03	-6.12
52	197.17	19.38	19.30	18.10	-5.86	-5.95
51	195.00	19.50	19.42	18.25	-5.72	-5.81
50	194.50	19.52	19.44	18.28	-5.69	-5.78
49	192.25	19.58	19.50	18.36	-5.55	-5.64
48	188.25	19.57	19.49	18.34	-5.17	-5.26
47	187.50	19.55	19.47	18.31	-5.00	-5.10
46	169.75	17.11	16.95	14.83	11.15	11.01
45	169.50	16.93	16.77	14.45	12.68	11.69
44	167.50					
43	165.25					
42	154.31					
41	143.38					
40	132.44					
39	121.50					
38	110.56					
37	99.63					
36	88.69					
35	77.75					
34	66.81					
33	55.88					
32	44.94					
31	34.00					
30	32.00	15.85	15.68	13.35	12.14	11.42
29	31.75	16.02	15.86	13.66	11.17	11.02
28	21.25	18.82	18.73	17.49	-4.71	-4.80
27	14.50	19.27	19.19	18.05	-5.63	-5.73
26	13.75	19.28	19.21	18.07	-5.68	-5.77
25	10.25	19.30	19.22	18.09	-5.79	-5.88
24	8.50	19.26	19.18	18.05	-5.85	-5.94
23	8.00	19.25	19.17	18.03	-5.87	-5.96
22	6.00	19.17	19.09	17.93	-5.95	-6.04
21	4.00	19.05	18.97	17.77	-6.06	-6.15
20	2.00	18.90	18.81	17.53	-6.22	-6.31
19	0.00	18.71	18.62	17.16	-6.42	-6.51
		58.75	59.00	63.00	63.13	63.38
		29	30	31	32	33

NOC,-40F,FF-NOC3,NO NS3 CREDIT,1/8"AL,1/8"SS STIFFNERS 14-OCT-95 14:47:39

Steady-State Temperature Distribution at Time 0.0000E+00

18	-0.13	122.85	122.40	121.09	114.13	99.17	91.00	89.00	87.59	85.25	82.74	81.67	62.03	61.58	51.63
17	-0.38	122.84	122.39	121.07	114.11	99.14	90.95	88.95	87.53	85.19	82.67	81.60	61.91	61.46	51.48
16	-0.63	122.83	122.38	121.07	114.10	99.12	90.93	88.93	87.51	85.17	82.64	81.58	61.87	61.42	51.43
15	-4.00	104.81	104.35	102.95	95.15	78.22	69.82	67.90	66.57	64.43	62.19	61.28	46.07	45.80	40.31
14	-10.75	72.27	71.79	70.31	61.99	45.18	38.36	36.90	35.90	34.32	32.72	32.06	21.96	21.79	18.37
13	-11.00	71.16	70.68	69.20	60.88	44.11	37.34	35.89	34.90	33.34	31.75	31.11	21.13	20.97	17.59
12	-17.75	43.73	43.27	41.87	34.04	19.12	13.55	12.37	11.57	10.30	9.02	8.50	0.42	0.28	-2.58
11	-18.00	42.80	42.34	40.95	33.15	18.30	12.77	11.60	10.81	9.55	8.27	7.76	-0.26	-0.40	-3.25
10	-24.75	20.21	19.80	18.59	11.80	-0.77	-5.37	-6.34	-7.01	-8.06	-9.13	-9.56	-16.35	-16.47	-18.95
9	-25.00	19.45	19.05	17.84	11.10	-1.39	-5.95	-6.92	-7.58	-8.62	-9.68	-10.11	-16.85	-16.97	-19.43
8	-31.75	1.08	0.75	-0.23	-5.69	-15.71	-19.34	-20.10	-20.62	-21.44	-22.28	-22.62	-27.87	-27.96	-29.85
7	-32.00	0.46	0.14	-0.84	-6.24	-16.18	-19.77	-20.53	-21.04	-21.85	-22.68	-23.02	-28.21	-28.31	-30.18
6	-38.75	-14.52	-14.75	-15.46	-19.40	-26.83	-29.58	-30.15	-30.54	-31.16	-31.78	-32.03	-35.81	-35.88	-37.36
5	-39.00	-15.03	-15.26	-15.95	-19.84	-27.17	-29.89	-30.47	-30.85	-31.46	-32.08	-32.32	-36.02	-36.09	-37.52
4	-45.75	-27.57	-27.70	-28.09	-30.30	-34.90	-37.18	-37.73	-38.11	-38.75	-39.45	-39.46	-39.56	-39.56	-39.58
3	-46.00	-28.01	-28.13	-28.51	-30.66	-35.13	-37.36	-37.88	-38.25	-38.85	-39.46	-39.46	-39.56	-39.56	-39.58
2	-52.75	-39.22	-39.22	-39.25	-39.39	-39.62	-39.66	-39.67	-39.67	-39.67	-39.67	-39.67			
1	-53.00	-39.22	-39.23	-39.25	-39.39	-39.62	-39.66	-39.67	-39.67	-39.67	-39.67	-39.67			
		0.00	4.25	8.50	19.25	30.00	33.00	33.60	34.00	34.63	35.25	35.50	39.19	39.25	40.50
		1	2	3	4	5	6	7	8	9	10	11	12	13	14

NOC,-40F,FF-NOC3,NO NS3 CREDIT,1/8"AL,1/8"SS STIFFNERS 14-OCT-95 14:47:39

Steady-State Temperature Distribution at Time 0.0000E+00

18	-0.13	39.59	36.71	34.73	31.98	30.86	30.41	25.59	25.17	24.68	24.43	22.98	22.86	20.75	20.64
17	-0.38	39.45	36.79	34.23	32.78	31.51	30.91	25.51	25.17	24.71	24.31	22.96	22.84	20.74	20.63
16	-0.63	39.41	36.80	34.21	32.91	31.67	31.08	25.39	25.18	24.97	24.15	22.94	22.82	20.73	20.62
15	-4.00	34.98	33.99	33.03	32.57	32.11	31.89	24.79	24.77	24.74	23.21	22.60	22.52	20.59	20.49
14	-10.75	14.99	14.32	13.66	13.34	13.01	12.84	6.11	5.22	4.18	3.74	-1.96	-2.54	-14.28	-15.05
13	-11.00	14.25	13.59	12.94	12.61	12.29	12.12	5.40	4.50	3.45	3.00	-2.79	-3.38	-15.32	-16.08
12	-17.75	-5.50	-6.10	-6.69	-6.99	-7.28	-7.43	-13.97	-14.91	-16.02	-16.49	-22.97	-23.65	-37.48	-37.53
11	-18.00	-6.16	-6.74	-7.33	-7.63	-7.93	-8.08	-14.61	-15.54	-16.65	-17.13	-23.61	-24.27	-37.53	-37.54
10	-24.75	-21.53	-22.06	-22.59	-22.86	-23.13	-23.27	-29.34	-30.25	-31.33	-31.80	-38.51	-38.55	-38.68	-38.68
9	-25.00	-22.00	-22.52	-23.05	-23.32	-23.58	-23.72	-29.75	-30.65	-31.71	-32.17	-38.55	-38.55	-38.69	-38.69
8	-31.75	-31.79	-32.18	-32.58	-32.78	-32.98	-33.08	-37.51	-38.19	-39.03	-39.04	-39.11	-39.11		
7	-32.00	-32.09	-32.48	-32.87	-33.06	-33.26	-33.36	-37.66	-38.30	-39.05	-39.05	-39.11	-39.11		
6	-38.75	-38.98	-39.34	-39.35	-39.36	-39.36	-39.36	-39.43	-39.44	-39.44	-39.44				
5	-39.00	-39.04	-39.35	-39.35	-39.36	-39.36	-39.36	-39.44	-39.44	-39.44	-39.44				
4	-45.75	-39.59	-39.59	-39.59											
3	-46.00	-39.59	-39.59	-39.59											
2	-52.75														
1	-53.00														
		41.75	42.00	42.25	42.38	42.50	42.56	45.25	45.63	46.06	46.25	48.75	49.00	53.75	54.00
		15	16	17	18	19	20	21	22	23	24	25	26	27	28

NOC,-40F,FF-NOC3,NO NS3 CREDIT,1/8"AL,1/8"SS STIFFNERS 14-OCT-95 14:47:39

Steady-State Temperature Distribution at Time 0.0000E+00

18	-0.13	18.70	18.61	17.13	-6.44	-6.52
17	-0.38	18.68	18.58	17.07	-6.46	-6.55
16	-0.63	18.66	18.56	17.01	-6.49	-6.58
15	-4.00	18.35	18.21	15.72	-6.95	-7.06
14	-10.75	-32.74	-32.82	-28.63	-28.37	-28.37
13	-11.00	-32.85	-32.85	-28.66	-28.52	-28.46
12	-17.75	-36.98	-36.98			
11	-18.00	-36.99	-36.99			
10	-24.75					
9	-25.00					
8	-31.75					
7	-32.00					
6	-38.75					
5	-39.00					
4	-45.75					
3	-46.00					
2	-52.75					
1	-53.00					
		58.75	59.00	63.00	63.13	63.38
		29	30	31	32	33

3.6.5.2.3 HEATING7.2 Input File Name: FFD-40F.INP

THIS SECTION CONTAINS
PROPRIETARY INFORMATION

3.6.5.2.4 HEATING7.2 Output File Name: FFD-40F.OUT

FF DSC,P71 CONDITIONS,-40F AMB,3-D MODEL,AIR,FFD-40F Fri Nov 3 16:54:47 1995

Steady-State Temperature Distribution at Time 0.0000E+00

Z = 0.0000E+00

41	33.62	251.00	251.00	251.00	251.00	251.00	251.00								
40	33.00	251.04	251.10	251.15	251.18	251.10	251.00	251.00	251.00	251.00	251.00	251.00	251.00		
39	32.38	255.13	255.22	255.22	255.03	253.08	251.21	251.19	251.18	251.18	251.15	251.07	251.00	251.00	251.00
38	31.75	259.25	259.43	259.43	259.21	257.72	257.38	256.69	256.28	256.17	255.25	252.33	251.04	251.01	251.00
37	29.25	275.51	277.57	277.60	278.48	278.37	278.28	277.72	276.87	276.61	274.07	270.48	270.36	258.26	251.71
36	29.00	276.56	277.66	277.69	278.60	278.49	278.40	277.84	276.98	276.72	274.18	270.52	270.44	258.87	251.78
35	19.50	296.87	295.61	295.63	296.30	295.15	294.86	293.63	291.94	291.44	286.82	280.90	280.78	274.82	255.79
34	19.25	300.21	295.69	295.65	296.27	295.08	294.72	293.59	291.90	291.40	286.79	280.97	280.94	279.21	265.47
33	18.63	299.36	297.30	296.86	292.58	262.95	242.12	278.80	286.64	287.45	284.49	279.40	278.93	274.92	260.53
32	17.00	303.46	302.98	302.78	300.71	297.45	297.17	290.27	287.15	286.43	281.17	275.97	275.33	269.09	263.39
31	16.75	303.52	303.05	302.85	300.77	297.47	297.39	291.30	287.29	286.41	280.82	275.58	274.93	268.45	263.82
30	11.25	311.15	310.34	309.99	306.13	299.70	299.55	294.04	289.47	288.44	281.83	276.19	275.47	268.09	261.49
29	11.00	311.15	310.34	309.99	306.14	299.74	299.59	294.14	289.61	288.58	282.03	276.43	275.72	268.36	261.71
28	7.25	307.36	306.79	306.55	303.90	299.76	299.62	295.38	292.03	291.28	286.66	282.44	281.87	275.53	268.86
27	7.00	307.32	306.75	306.51	303.87	299.76	299.30	295.37	292.21	291.51	287.19	283.13	282.58	276.33	269.63
26	5.00	307.55	307.10	306.91	304.87	301.96	301.51	295.20	293.67	293.65	292.51	290.08	289.69	284.29	277.91
25	4.75	307.59	307.14	306.95	304.91	302.00	301.91	296.13	293.71	293.69	292.57	290.15	289.76	284.35	277.95
24	3.12	309.89	309.38	309.15	306.71	302.72	302.65	297.93	294.75	294.76	295.01	293.12	292.75	286.95	278.56
23	1.50	310.01	309.44	309.19	306.49	302.10	302.02	297.41	294.21	294.23	295.07	293.51	293.16	287.17	277.85
22	1.25	309.84	309.26	309.01	306.29	301.86	301.79	297.17	293.96	293.97	294.86	293.33	292.99	286.99	277.62
21	.00	308.24	307.65	307.39	304.62	300.11	300.04	295.28	292.01	292.02	292.97	291.52	291.18	285.29	275.95
20	-1.25	305.46	304.89	304.64	301.92	297.49	297.41	292.26	288.92	288.93	289.69	288.17	287.83	282.23	273.25
19	-1.50	304.78	304.21	303.96	301.27	296.88	296.80	291.46	288.18	288.20	288.87	287.32	286.99	281.47	272.63
18	-3.12	299.35	298.84	298.62	296.21	292.26	292.19	284.33	282.46	282.46	282.28	280.39	280.06	275.35	267.92
17	-4.75	292.66	292.23	292.05	290.10	287.42	287.33	263.14	275.95	275.90	273.80	271.37	271.05	267.77	262.42
16	-5.00	292.56	292.12	291.94	290.00	287.28	286.57	250.90	275.45	275.68	273.62	271.17	270.86	267.64	262.24
15	-7.00	276.46	275.90	275.65	273.02	269.01	268.73	263.71	263.25	262.97	259.76	256.43	256.00	251.54	245.90
14	-7.25	276.45	275.88	275.64	273.00	268.94	268.83	264.14	262.18	261.73	258.26	254.82	254.38	249.84	244.50
13	-11.00	270.45	269.72	269.41	265.99	260.49	260.38	254.24	249.34	248.25	241.68	236.82	236.27	231.88	230.51
12	-11.25	269.77	269.04	268.73	265.31	259.82	259.72	253.49	248.47	247.36	240.65	235.73	235.19	230.86	229.59
11	-16.75	246.50	246.11	245.97	244.51	242.29	242.24	234.50	228.74	227.48	220.14	215.24	214.85	214.46	208.49
10	-17.00	246.40	245.99	245.85	244.40	242.21	242.05	233.09	227.68	226.50	219.34	214.43	214.12	215.78	206.53
9	-18.63	235.32	230.34	229.76	227.93	217.28	210.18	220.13	220.50	220.19	214.47	209.08	209.42	230.22	193.30
8	-19.25	236.37	223.26	223.16	224.27	223.61	223.40	221.96	219.97	219.35	213.15	205.32	205.88	244.19	203.19
7	-19.50	227.40	223.04	223.08	224.25	223.60	223.36	221.93	219.89	219.26	213.06	205.04	204.87	223.43	157.12
6	-29.00	175.81	177.09	177.11	177.55	176.95	176.78	175.93	174.80	174.48	171.51	167.64	167.56	151.51	137.54
5	-29.25	174.11	176.96	176.99	177.41	176.81	176.65	175.80	174.67	174.35	171.38	167.58	167.44	150.10	137.37
4	-31.75	148.88	149.08	149.07	148.51	146.12	145.60	144.53	143.94	143.79	142.53	138.14	136.06	136.03	136.01
3	-32.38	142.46	142.54	142.53	142.12	139.10	136.23	136.21	136.20	136.19	136.17	136.08	136.00	136.00	136.00
2	-33.00	136.06	136.12	136.17	136.19	136.10	136.00	136.00	136.00	136.00	136.00	136.00	136.00		
1	-33.62	136.00	136.00	136.00	136.00	136.00	136.00								
		.00	1.25	1.50	3.12	4.75	5.00	6.00	7.00	7.25	9.12	11.00	11.25	14.00	16.75
		1	2	3	4	5	6	7	8	9	10	11	12	13	14

3.6.6 Calculation of Maximum Pressures

The purpose of this appendix is to determine the peak pressure in the NUHOMS®-MP187 Package during transportation conditions. The peak pressures are calculated for the normal conditions of transport and accident conditions.

3.6.6.1 Maximum Pressures in the Cask Cavity During Normal Conditions of Transport

The normal conditions of transport maximum pressures in the cask inner cavity (i.e., annulus between the DSC outer shell and cask inner shell) are calculated using the ideal gas law. The gas in the inner cavity is assumed to be initially at an atmospheric pressure and 70°F temperature. The gas pressure for various ambient temperatures is given by:

$$P_{gas} = P_1 T_2/T_1 = (14.7 \text{ psia}(T_2 + 460)/(460 + 70))$$

where T_2 is the average cavity gas temperature (°F) during various normal conditions.

The average cavity gas temperature is calculated by averaging the maximum DSC shell temperature and the maximum cask inner shell temperature. From Section 3.4 the maximum DSC shell temperatures are 400°F and 317°F, for the 100°F and -40°F ambient temperature cases, respectively. The corresponding maximum cask inner shell temperatures are 302°F and 184°F for the 100°F and -40°F ambient temperature cases, respectively. The calculations are summarized in Table 3.6-6.

Table 3.6-6

Cask Internal Cavity Normal Conditions of Transport Pressures

Case	Ambient Air Temperature (°F)	Average Cavity Temperature (°F)	Cavity(1) Pressure (psia)	Partial(2) Pressure Fission and Fill Gas (psia)	Design Basis Accident Pressure (psia)
1	-40	250.5	19.7	20.7	40.4
2	100	351	22.5	23.7	46.2

(1) Normal operating pressures with all fuel rods intact and intact DSC.

(2) Enveloping accident pressure increase due to 100% of fuel rod fill gas and 30% of fission gas assumed to be released and also leaking DSC as described in Section 3.6.6.2.

3.6.6.2 Maximum Pressures in the Cask Cavity During Hypothetical Accident Conditions

It is expected that no fuel rods will rupture during hypothetical accident conditions, however, for calculation of maximum cask cavity pressures, it is assumed that all of the fuel rods from all 24 fuel assemblies of a DSC rupture and that 100% of the fill gas and 30% of fission product residual gases in the fuel rods are released into the DSC cavity. It is further assumed that the DSC is in the cask and is leaking its contents into the cask inner cavity (i.e., annulus between the DSC outer shell and cask inner shell).

The methodology consists of calculating the free volume inside the FO-, FC- and FF-DSCs to select the bounding DSC for pressure calculations. Then, using the bounding DSC, the amount of gaseous mixture in the annulus between the cask and the DSC, the maximum temperatures for the various operating conditions, the maximum pressures inside the annulus between the cask and DSC are calculated. Both the cases of all the fuel rods intact and all the fuel rods ruptured are evaluated.

3.6.6.2.1 Calculation of Bounding DSC Free Volume

The calculations below show that the difference between the FO-DSC and FC-DSC free volumes is small (approximately 3% higher for the FC-DSC) and the pressures with the FF-DSC in the NUHOMS®-MP187 Cask are bounded by the FO-DSC or the FC-DSC inside the

NUHOMS®-MP187 Cask. So the FO-DSC cavity free volume is used for the subsequent pressure calculations.

(A) <u>FC-DSC Free Volume</u>

The FC-DSC cavity free volume is the volume of the DSC cavity minus the volume of DSC internals. The DSC internals consists of spacer discs, support rods, guide sleeves, fuel assemblies including the control components. The volumes of these components are calculated below:

Volume of the DSC cavity is calculated as:

$$V_{cavity} = \pi R^2 L$$

$$\therefore V_{cavity} = 590{,}791 \ inch^3$$

Volume of the spacer discs is calculated as:

$$V_{sp\ disk} = \pi R^2 L \ - \ volume\ of\ cutouts$$

$$V_{sp\ disk} = 1{,}469\, inch^3$$

The volume of one spacer disc = 1469 in^3. The DSC contains 26 spacer discs, the total volume occupied by all the spacer discs = 26*1469 = 38,194 $in.^3$

Volume of the support rods is calculated as:

$$V_{supp\ rod} = \pi R^2 L$$

$$\therefore V_{supp\ rods} = 4{,}877 \ inch^3$$

Volumes of the support structure (i.e., guide sleeves, outer support sleeves, and neutron absorber plates) are calculated as:

$$V_{support\ structure} = V_{guide\ sleeve} + V_{n\text{-}absorber\ plate} + V_{support\ sleeve}$$

The total volume of all the guide sleeves, poison plates, and poison support sleeves for 24 fuel assemblies is 3890 + 9965 + 3890 + 4982 + 3890 = 26617 in^3

Volume of fuel assemblies without control components is calculated by using the geometry of fuel assembly as:

- Fuel assembly weight w/o control components = 1530 lbs.

- Weight of control component = 135 lbs.

- Fuel rod length = 153.125 in.

- Number of fuel rods per assembly = 225.

- Fuel rod outside diameter = 0.43 in.

- Weight of Heavy metal per assembly = 1023 lbs.

- Weight of Oxygen in UO2 per assembly = 122 lbs.

Volume occupied by fuel rods is calculated as:

$$V_{fuel\ rods} = 5{,}003\ in^3$$

Weight of the fuel assembly skeleton which includes nozzles and other non fuel rod components of the fuel assembly is given by:

1530 - 1023 - 122 = 385 lbs.

Assuming that all the skeleton material is zircaloy (which is conservative for this calculation), the volume of the skeleton material = 385 /0.238 = 1618 in^3.

So the volume of the fuel assembly w/o control components is 5003 + 1618 = 6621 in^3. For 24 fuel assemblies the total volume will be 24 * 6621 = 158,904 $in^3 \approx$ 159,000 in^3.

Volume occupied by control components is calculated as:

- The control rod assembly weight = 135 lbs.
- The weight of burnable poison is = 95 lbs.
- The weight of other material of the control component

  = 135 - 95 = 40 lbs.

  Assuming that this material is all stainless steel, the volume is given by 40/0.2835 = 141 in^3

Volume of the poison material is calculated as:

$$V_{poison\ mat} = 256\ in^3$$

So the volume of the control component is 256 + 141 = 397 in^3. For 24 control components, the total volume will be 24 * 397 = 9,528 in^3.

The total free volume of the FC-DSC is then calculated as:

$V_{FC\text{-}DSC}$ = 590791 - 38194 - 4877 - 26617 - 159000 - 9528 = 352,575 in^3.

(B) FO-DSC Free Volume

The FO-DSC cavity free volume is the volume of the DSC cavity minus the volume of DSC internals. The DSC internals consists of spacer discs, support rods, guide sleeves, and fuel assemblies without the control components. Volume of these components are calculated below:

Volume of the DSC cavity is calculated as:

$$V_{cavity} = \pi R^2 * L$$

$$\therefore V_{cavity} = 570{,}301 \ in^3$$

The volume of the FO-DSC spacer discs is the same as FC-DSC spacer discs calculated in Section 3.6.6.2.1(a).

$$V_{sp\,disk} = 38194 \ in^3$$

The volume of the support rods is calculated as:

$$V_{supp\,rod} = \pi R^2 \cdot L$$

$$\therefore V_{supp\,rods} = 4{,}708 \ in^3$$

The volume of the FO-DSC guide sleeves, outer support sleeves, and neutron absorber plates is the same as FC-DSC calculated in Section 3.6.6.2.1(a).

$$V_{support\,structure} = 26{,}617 \ in^3$$

The volume of the fuel assemblies in the FO-DSC is the same as FC-DSC calculated in Section 3.6.6.2.1.

For 24 fuel assemblies without control component, the total volume will be 24 * 6621 = 158,904 $in^3 \approx 159{,}000\ in^3$.

The total free volume of the FO-DSC is then calculated as:

$$V_{FO\text{-}DSC} = 570301 - 38194 - 4708 - 26617 - 159000 = 341{,}782\ in^3.$$

(C) FF-DSC Free Volume

The FF-DSC cavity free volume is the volume of the DSC cavity minus the volume of DSC internals. The DSC internals consists of spacer discs, support plates, fuel assembly support canisters, and fuel assemblies without the control components.

The FF-DSC inner cavity length is the same as the FO-DSC and it contains only 13 fuel assemblies as compared to the 24 fuel assemblies for the FO-DSC or FC-DSC. The FF-DSC contains support plates instead of the support rods and also contains 11 less spacer discs than the FO-DSC or FC-DSC. Also the FF-DSC does not contain outer support sleeves and neutron absorber plates. So the free volume of the FF-DSC will be larger than the FO-DSC free volume.

Since the FF-DSC contains only 9.93 kW total decay heat due to a total of 13 fuel assemblies (Appendix 3.6.5.1.2) as compared to 13.5 kW total decay heat due to 24 fuel assemblies of the FC- or FO-DSC (Section 3.1.2), the package temperatures will be lower with the FF-DSC than the FC-DSC, or the FO-DSC in the NUHOMS®-MP187 Cask.

Since larger free volumes and lower temperatures will produce lower pressures, detailed calculations are not made for the FF-DSC. Instead it is conservatively assumed that the pressures calculated with the FO-DSC inside the NUHOMS®-MP187 Cask will also be applicable to the case of the FF-DSC inside the NUHOMS®-MP187 Cask.

3.6.6.2.2 Calculation of Gaseous Mixture in the Cask Internal Cavity

The quantity of total gaseous mixture in the cask internal cavity during accident conditions is the sum of DSC and fuel rod fill gas (helium), the fuel rod residual fission gas and the fill gas in the cask internal cavity (air).

(A) Quantity of Helium Fill Gas in the DSC cavity

Since the DSC is drained and vacuum dried before backfilling with helium, the amount of residual pool water vapor remaining in the DSC cavity is negligible. The fill gas in the DSC cavity is helium at 0 to 2.5 psig. The average helium temperature is assumed to be 400°F to account for the heatup during draining, drying, backfilling, and sealing operations.

Assuming ideal gas mixtures, the maximum quantity of helium in the DSC cavity is equal to:

$$\eta_{He} = \frac{(17.2\,psia)(6894.8\,Pa/psia)(341782\,in^3)(1.6387x\,10^{-5}\,\frac{m^3}{in^3})}{(8.314\,J/mol-K)(400°\,F\ +\ 460°\,R)(5/9\,K/°\,R)}$$

$$\therefore \eta_{He} = 167 gmoles$$

(B) Quantity of Helium Fill Gas in the Fuel Rods

The volume of fill gas in a B&W 15X15 fuel pin is 1.6 in^3 and there are 208 fueled pins in an assembly. The fill pressure is 415 psig (429.7 psia) and the fill temperature is assumed to be room temperature (80°F) [3.18]. The quantity of fill gas in 24 fuel assemblies is then given by:

$$\eta_{He} = \frac{(429.7psia)(6894.8\frac{Pa}{psia})(24\cdot 208\cdot 1.6\,in^3)(1.6387x\,10^{-5}\frac{m^3}{in^3})}{(8.314\frac{J}{mol\cdot K})(80°\,F + 460°\,R)(\frac{5\,K}{9\,R})}$$

$$\eta_{He} = 155\ gmoles$$

(C) Quantity of Fission Product Gases in the Fuel Rods

The B&W 15X15 fuel assembly used for the analysis has a maximum burnup of 38,268 MWD/MTU. The volume at STP (101,000 Pa and 273K) of fission product gases is 0.226 liter of tritium, 52.59 liters of Krypton-85, and 472.275 liters of Xenon-131m in each fuel assembly (linearly interpolated between 35 GWD/MTU and 45 GWD/MTU [3.19]). The total fission gas volume is then 525 liters = 0.525 m^3. The quantity of fission product gases in 24 fuel assemblies is:

$$\eta_{FissGas} = \frac{(0.3)(24)(101{,}000\ Pa)(0.525\ m^3)}{(8.314\ J/mol.K)(273°\ K)} = 168\ gmoles$$

(D) Quantity of Fill Gas (Air) in the Cask Internal Cavity

The volume of the cask internal cavity (annulus between cask and DSC)

$$= \pi(34.0^2 - 33.6^2)(187) + \pi(34^2)(1)$$

$$= 19{,}517\ in^3$$

The gas in the cask internal cavity is assumed to be initially at an atmospheric pressure at 70°F temperature. The quantity of gas in the cask internal cavity is then given by:

$$\eta_{air} = \frac{(14.7 psia)(6894.8\frac{Pa}{psia})(19517\ in^3)(1.6387x\ 10^{-5}\frac{m^3}{in^3})}{(8.314\frac{J}{mol \cdot K})(70°\ F + 459.7°\ R)(\frac{5\ K}{9\ R})}$$

$$\eta_{air} = 13\ gmoles$$

Therefore, the quantity of total gaseous mixture in the cask internal cavity during accident conditions is:

$$\eta_{DSC} = 167 + 155 + 168 + 13 = 503\ gmoles$$

The maximum accident pressure in the cask internal cavity, including fuel, fill, and fission gases is given by:

$$P_{acc} = \frac{(1.4504x\,10^{-4})(503mol)(8.314\frac{J}{mol \cdot K})(T + 459.7R)}{(341782 + 19517\,in^3)(1.6387x\,10^{-5}\frac{m^3}{in^3})(1.8\frac{°R}{K})}$$

where T is the average annulus gas temperature (°F) for the various accident conditions.

The average annulus temperature is calculated by averaging the maximum DSC shell temperature and the maximum cask inner shell temperature. From Section 3.5, the maximum DSC shell temperatures are 368°F, 368°F, 401°F, and 564°F for the prefire, fire, postfire and final steady state conditions respectively. The corresponding maximum cask inner shell temperatures are 257°F, 260°F, 340°F, and 508°F for the prefire, fire, postfire and final steady state conditions respectively. The calculations are summarized in Table 3.6-7.

Table 3.6-7

Cask Internal Cavity Accident Condition Pressures

Case	Accident Condition	Average Cavity Gas Temperature (°F)	Cavity Gas(1) Pressure (psia)	Partial(2) Pressure Fission and Fill Gas (psia)	Design Basis Accident Pressure (psia)
1	Prefire	312.5	21.4	22.5	43.9
2	Fire	314.0	21.5	22.5	44.0
3	Postfire	370.5	23.0	24.3	47.3
4	Final Steady State	536.0	27.6	29.1	56.7

Notes:

(1) Normal operating pressures with all fuel rods intact and intact DSC.

(2) Enveloping accident pressure increase due to 100% of fuel rod fill gas and 30% of fission gas assumed to be released and leaking DSC.

4. CONTAINMENT

4.1 Containment Boundary

The containment boundary for the package includes the cask inner shell, bottom forging, the ram closure plate port, the top end forging, top closure plate, the vent and drain ports and their associated seals. Each is described in more detail in the following sections.

4.1.1 Containment Vessel

The containment vessel consists of the 1.25-inch thick inner shell with a vent port located in the top forging, an 8-inch thick bottom forging with a drain plug, 5-inch thick ram closure plate, and a 6.5-inch thick top closure plate. All of the containment vessel components are fabricated from austenitic stainless steel. The containment boundary described herein is illustrated in the General Arrangement Drawings in Appendix 1.3.2.

4.1.2 Containment Penetrations

The only penetrations into the containment boundary are the drain and vent ports, ram closure plate, and the top closure plate. Each penetration is designed to maintain a leak rate not to exceed 1×10^{-7} standard cubic centimeters per second (atm-cm^3/sec), defined as "leak tight" per ANSI N14.5 1987, Section 3 [4.1]. To obtain these seal requirements, each penetration has an O-ring face seal type of closure.

4.1.3 Seals and Welds

4.1.3.1 Seals

Containment seals are located at the ram access port closure plate, the top closure plate, the drain plug and at the vent port. The inner seal in all cases is the primary containment seal. The outer seals facilitate leak testing of the inner seal for the ram closure plate and the top closure plate. The outer seals for the ram closure plate and the top closure plate serve as a secondary containment seal during a postulated hypothetical accident condition in which the closure bolt analysis (Section 2.10.5) has identified a potential for the momentary unloading of the inner seal. The test ports outer seals are non-containment seals for all normal & hypothetical accident conditions.

All the seals used in the NUHOMS®-MP187 Multi-Purpose Cask containment boundary are static face seals. The seal areas are designed for no significant plastic deformation under accident conditions as shown in Section 2. The bolts are torqued to maintain a seal load on the seals during all load conditions as shown in Appendix 2.10.5. The seals used for the ram access and top closure plates are metallic O-rings that are composed of an aluminum jacket, an Inconel liner and an Inconel spring. The seals used for the vent and drain ports are silver plated, stainless steel precompressed tubular O-rings. The metallic O-rings may be used for storage conditions and will also meet the transportation requirements. These metallic O-rings, as described in Appendix 4.4.2, are proven to be leak tight in accordance with Reference 4.1. These seals have the capability of limiting leakage in accordance with Reference 4.2 through all the specified normal and accident conditions. The selection of the materials is described in Appendix 4.4.2. The seals have to maintain leak tightness in a static environment. The controlling requirement for the seals is the operating temperature during and after both the normal and the accident conditions. The composite metallic O-ring, has a proven record of performing through a temperature range of -450°F to over 600°F per reference 4.5 which exceeds the expected temperature range derived in Section 3. The vent and drain port seals have an operating temperature range of cryogenic temperatures to over 700°F per Reference 4.6. All containment seals shall be replaced after each use.

A summary of seal testing prior to first use, during routine maintenance, and upon assembly for transportation is as follows:

4.1.3.1.1 Fabrication Verification Leak Test

The containment boundary shall be tested per the fabrication verification leak test, delineated in Section 8.1.3. This test verifies the structural adequacy of the package to a leak rate less than

1×10^{-7} std-cm^3/sec of helium. The leak rate for the ram closure plate and top closure outer seals is verified to be less than 7×10^{-3} std-cm^3/sec of air (verified by a pressure rise test for the volume betwiin the inner seal and outer seal).

4.1.3.1.2 Maintenance Verification Leak Test

After the third use, annually (i.e. within one year of use for transportation), or at the time of seal replacement, the cask shall be tested per the maintenance verification leak test, delineated in Section 8.2.2. This test verifies the sealing integrity of the package to a leak rate less than 1×10^{-7} std-cm^3/sec of helium. The leak rate for the ram closure plate and top closure outer seals is verified to be less than 7×10^{-3} std-cm^3/sec of air (verified by a pressure rise test for the volume betwiin the inner seal and outer seal).

4.1.3.1.3 Assembly Verification Leak Test

Prior to shipment of the loaded NUHOMS®-MP187 Multi-Purpose Cask, it shall be leak tested per the assembly verification leak test, delineated in Appendix 7.4.2. Since the seals are replaced after each use this test is basically the same as the maintenance verification test.

4.1.3.2 Welds

All containment boundary welds are full penetration bevel or groove welds to ensure structural and sealing integrity. These full penetration welds are designed per ASME III Subsection NB and are fully radiographically examined where possible. Where radiographical examination is not practical, multi-layer liquid penetrant examination is performed.

4.1.3.3 Closure

Closure of the cask top cover plate is accomplished by thirty-six (36), SA-320, Grade L43, 2 inch diameter bolts tightened to the value specified on the drawings in Appendix 1.3.2. Closure of the ram closure plate is accomplished by twelve (12) SA-320 Grade L43 1 inch diameter bolts tightened to the values shown on the drawings in Appendix 1.3.2. Closure of each of the vent and drain ports is accomplished by a single 3/4 inch diameter SA-320 Grade L43 bolt with seals under the head of the bolt tightened to the values shown on the drawings in Appendix 1.3.2. Calculation of the required bolt preloads to maintain the seal can be found in Appendix 2.10.5.

4.2 Requirements for Normal Conditions of Transport

4.2.1 Containment of Radioactive Material

The results of the structural and thermal analyses performed in Sections 2 and 3, respectively, verify that there is no release of radioactive materials under any of the normal conditions of transport as described in 10CFR71 [4.2].

4.2.2 Pressurization of Containment Vessel

As shown in Section 3.4.4, the maximum normal operating pressure of the NUHOMS®-MP187 Multi-Purpose Cask is less than the design pressure of 50 psig. The analyses in Section 2 and Section 3 demonstrate that the NUHOMS®-MP187 Multi-Purpose Cask effectively maintains containment integrity per Section 4.2.1 with an internal pressure of 50 psig.

4.2.3 Contamination Criteria

The external contamination limits for the loaded package are delineated in 49 CFR 173.443 [4.3]. Previously used, empty packages, are handled and shipped per the requirements of 49 CFR 173.427 [4.3] or those for LSA packages when the internal components meet the requirements of Low Specific Activity material per 10 CFR 71.4 [4.2].

4.3 Containment Requirements for Hypothetical Accident Conditions

4.3.1 Fission Gas Products

The total activity available for release in a hypothetical accident condition is:

- 10% of fission gases are available due to rupture of fuel rods [4.8, Fig. 8-3]
- Release fractions for fission gases released is taken as the most conservative of [4.8, Table 8.3] and [4.7].

Nuclide	Release Fraction	Reference
H-3	.3	[4.7]
Kr	.3a	[4.8]
Te	1.0	N/A
I	.1	[4.7]
Xe	1.0	N/A
Cs	2 x 10-4	[4.8]
Co-60	.15	[4.7]

4.3.2 Containment of Radioactive Material

The results of the structural and thermal analyses performed in Sections 2 and 3, respectively, verify that the package will meet the leakage criteria of 10CFR71 using the methodology of ANSI N14.5 [4.1] for the entire hypothetical accident scenario.

4.3.3 Containment Criteria

This package has been designed, and is verified by leak testing, to meet the leakage criteria of 10CFR71 established in ANSI N14.5 [4.1].

4.4 Appendix

4.4.1 References

4.1 ANSI N14.5-1987, American National Standard for Radioactive Materials - Leakage Tests on Packages for Shipment.

4.2 Title 10, Code of Federal Regulations, Part 71 (10 CFR 71), Packaging and Transportation of Radioactive Materials.

4.3 Title 49, Code of Federal Regulations, Part 173.400 (49 CFR 173.400), Radioactive Materials, March 10, 1993.

4.4 Safety Analysis Report for the NuPac 125-B Fuel Shipping Cask, Docket Number 71-9200.

4.5 "Seals for Ultra-Vacuum and Cryogenics," Le Carbone-Lorraine Helicoflex. Excerpts found in Appendix 4.4.3.

4.6 Helicoflex Company Metallic O-Rings. Excerpts found in Appendix 4.4.4.

4.7 "Standard Review Plan for Dry Cask Storage Systems", Final Report, NUREG-1536, USNRC, January 1997.

4.8 "Shipping Container Response to Severe Highway and Railway Accident Conditions", Main Report, NUREG/CR-4829, UCID-20733, Vol. 1, February 1987.

4.4.2 Seal Material

4.4.2.1 Introduction and Background

The NUHOMS®-MP187 Cask is a multi-purpose cask that is used to transfer fuel out of fuel pools to dry storage modules, store fuel on site in a metal cask, and transport fuel.

For transportation, a seal is provided for the cask body as part of the containment boundary since no credit is taken for the containment capability of the canisters described in Section 1. The seal must provide for both long term storage and the varying temperature and load conditions required for transportation.

4.4.2.2 Operating Requirements

The limiting condition for the seal is the operating temperature. Although the normal operating temperature for the seal is less than 300°F for the maximum thermal load as shown in Section 3, the lid seal temperatures increase for the post accident fire condition. In Section 3.5 the calculated seal temperature approaches 450°F. This high temperature occurs in the post accident time period when some of the heat transfer mechanisms are partially damaged and some of the insulation that protects the seals is destroyed. The drain port seals are shown to reach temperatures slightly above 400°F (less than 450°F) for less than 30 minutes during the fire transient. The seal must also maintain a seal at -40°F as per 10CFR71 [4.2]. The seal also must be able to be leak tested in accordance with ANSI N14.5 [4.1]. The criteria for leakage rate for normal conditions of transport is conservatively assumed to be a leak tight condition. A leak tight condition is defined by Reference 4.1 as a leak rate no greater than 1×10^{-7} std-cm^3/sec. To demonstrate this leakage rate a helium leak test is required. To adequately determine leak rate, the seals must have low enough permeability to retain the helium during the leak test. Failure to have the proper material can slightly increase exposure to personnel since, if a leak test fails, the lid has to be removed so the seals can be replaced with seals that are not saturated with helium.

4.4.2.3 Seal Material Selection

To satisfy the dual purpose of the seal, metallic O-rings were selected. The metallic seals were selected for the storage mode due to the lack of deterioration over time. Metallic seals used when the cask is in the storage mode have also been demonstrated to meet the leak tight standards from -450°F to over 600°F [4.3]. Typical metallic O-rings used for the top cover and the ram closure port are composite structure with an aluminum jacket, an Inconel lining and an Inconel spring. The spring provides a degree of resilience in the seal to maintain a seal force if any deformation to the seal surface or elongation of the bolts should occur. The vent and drain port seals are tubular 300 series O-rings coated with silver. These tubular O-rings have a temperature range from cryogenic temperatures to over 700°F. These seals when in a static application, are fully capable of maintaining a seal meeting the regulatory requirements for leak tightness for this package for a period of up to 50 years.

Accordingly, if a cask which has been used for storage with metallic seals is to be transported and the seals maintain their leak tightness as demonstrated by the required leak test for transportation, it should not be necessary to replace the metallic seals in accordance with the periodic replacement requirements of ANSI N14.5 [4.1]. Exemption from the periodic replacement requirements of ANSI N14.5 [4.1] in this situation would avoid the radiation exposure associated with seal replacement without jeopardizing seal integrity.

4.4.3 Excerpts (8 pages) From "Seal for Ultra-Vacuum and Cryogenics" [4.5]

Contents

Mission Statement

We the employees of the Helicoflex Company, shall strive to use all available human and physical resources in our commitment to **Customer Satisfaction.**

Customer Satisfaction is attained through continuously improving the Quality of our people, our products, our processes, our service, and our vendors in order to provide quality products on time at a fair price.

Customer Satisfaction requires employee satisfaction; therefore, we strive to treat one another with respect and work as a team to achieve quality in our work life.

Customer Satisfaction and quality in our work life result in growth, security, pride, and opportunity for ourselves and our company.

FOREWORD

Today's sealing requirements for Ultra-High Vacuum and Cryogenics are more demanding than ever before:

- High sealing power
- Low outgasing
- Ultra-high vacuum cleanliness
- Bakeability
- Resistance to cryogenic temperatures
- Resistance to radiation
- Long-life expectancy
- Remote handling
- Chemical compatibility

These rigorous sealing requirements have rendered traditional gaskets such as Conflat®, elastomer and solid metal seals obsolete.

Through extensive research, Helicoflex Co. has developed an advanced metal seal called Helicoflex® and sealing systems to meet these tough sealing requirements.

HELICOFLEX®

CEA-CEFILAC patented system

DESCRIPTION

This design concept makes the HELICOFLEX seal unique in sealing technology.

Its exceptional compression and elastic recovery properties enable it, while retaining the quality of metal seals, to approach those of elastomer seals.

The HELICOFLEX seal is composed of a close-wound helical spring surrounded by two metal linings. It can be fitted with an internal or external compression limiter.

HELICOFLEX SEALING PRINCIPLE

The sealing principle of the HELICOFLEX seal is based upon the plastic deformation of a lining of greater ductility than the flange materials. This occurs between the sealing face of a flange and an elastic core composed of a close-wound helical spring.

The spring is selected to have a specific compression resistance. During compression, the resulting specific pressure forces the lining to yield and ensures positive contact with the flange sealing faces.

Each coil of the helical spring acts independently and allows the seal to conform to surface irregularities on the flange surface.

The choice of a close-wound helical spring as an elastic core ensures, by the individual action of the coils, the relative total independence during compression.

TECHNICAL DATA

Dimensions: .157 in. to 400 in. (4mm to 10 meters)
Temperature: – 458 to 1472°F
- 271 to 800°C
+ 1.8 to 427°K
Helium sealing level: $Q \leq 10^{-13}$ atm cm³/s
Pressure: up to 45,000 psi (3000 bars)
Resistant to radiation
Can be produced in all metal materials:
ALUMINUM, SILVER, COPPER, SOFT IRON, NICKEL, STAINLESS STEEL, INCONEL, etc.

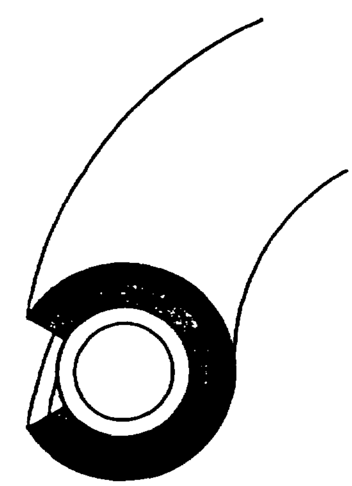

HELICOFLEX CHARACTERISTIC CURVE

Compression and decompression cycle

The compression and decompression cycle of the HELICOFLEX seal is characterized by gradual flattening of the compression curve. The decompression curve is distinct from the compression curve as the result of a hysteresis phenomenon to which is added a permanent dual deformation (spring deformation and lining creep).

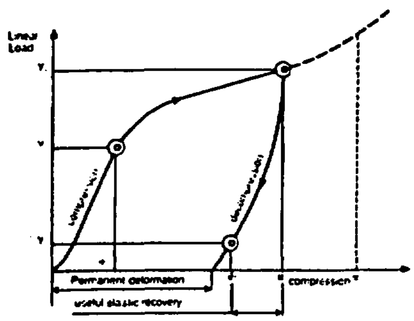

Definition

- Y_0 = tightening load per linear cm of seal necessary to obtain sealing to chosen criterion.
- Y_2 = tightening load per linear cm of seal corresponding to compression e_2 chosen as operating point.
- Y_1 = tightening load per linear cm of seal at which the sealing obtained at Y_0 is lost. Y_1 is always lower than Y_0 because of the hysteresis in the decompression cycle.
- e_2 = optimum compression.
- e_c = critical compression beyond which there is risk of damaging the seal.

The HELICOFLEX seal has the most flexible design capability for vacuum applications.

A RESILIENT METAL SEAL

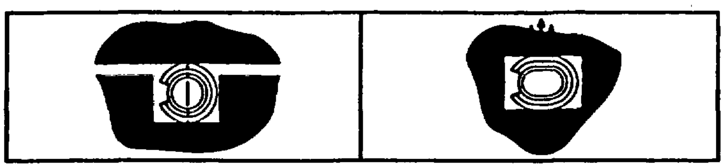

HN 200

HL 200

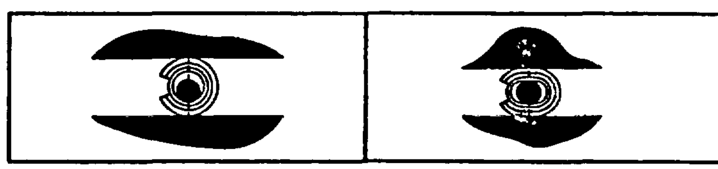

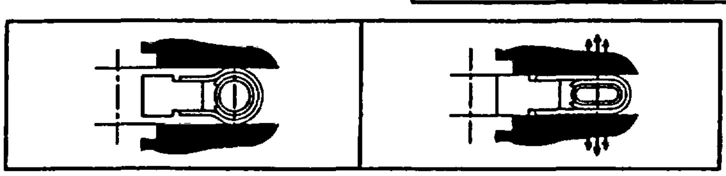

HN 208 A

HNDE 290 C

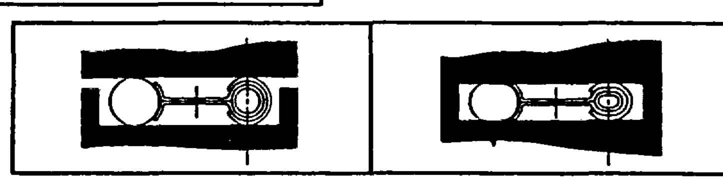

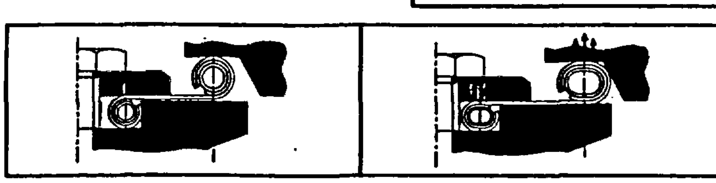

HND 229

HN 290 PM

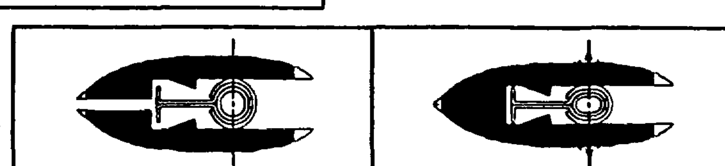

Characteristic Values Helicoflex Seal

	Cross Section C.S		Compression e2		Helium Sealing Y2		Helium Sealing Y1		Maximum Temperature	
			e2+/-0.004	e2 +/-0.1						
	inch	mm	inch	mm	lb/in	daN/cm	lb/in	daN/cm	°F	°C
ALUMINIUM	0.079	[illegible]	0.028	[illegible]	914	[illegible]	114	[illegible]	302	[illegible]
	0.102	[illegible]	0.028	[illegible]	999	[illegible]	114	[illegible]	428	[illegible]
	0.130	[illegible]	0.031	[illegible]	1056	[illegible]	143	[illegible]	482	[illegible]
	0.157	[illegible]	0.035	[illegible]	1142	[illegible]	143	[illegible]	536	[illegible]
	0.189	[illegible]	0.035	[illegible]	1199	[illegible]	143	[illegible]	536	[illegible]
	0.220	[illegible]	0.035	[illegible]	1313	[illegible]	171	[illegible]	608	[illegible]
	0.264	[illegible]	0.039	[illegible]	1399	[illegible]	200	[illegible]	644	[illegible]

	Cross Section C.S		Compression e2		Helium Sealing Y2		Helium Sealing Y1		Maximum Temperature	
			e2+/-0.004	e2 +/-0.1						
	inch	mm	inch	mm	lb/in	daN/cm	lb/in	daN/cm	F	C
SILVER	0.075	[illegible]	0.024	[illegible]	1256	[illegible]	171	[illegible]	464	[illegible]
	0.102	[illegible]	0.028	[illegible]	1370	[illegible]	257	[illegible]	536	[illegible]
	0.130	[illegible]	0.031	[illegible]	1485	[illegible]	286	[illegible]	572	[illegible]
	0.157	[illegible]	0.031	[illegible]	1713	[illegible]	314	[illegible]	662	[illegible]
	0.189	[illegible]	0.031	[illegible]	1827	[illegible]	343	[illegible]	698	[illegible]
	0.220	[illegible]	0.031	[illegible]	2056	[illegible]	371	[illegible]	752	[illegible]
	0.264	[illegible]	0.035	[illegible]	2284	[illegible]	400	[illegible]	842	[illegible]

	Cross Section C.S		Compression e2		Helium Sealing Y2		Helium Sealing Y1		Maximum Temperature	
			e2+/-0.004	e2 +/-0.1						
	inch	mm	inch	mm	lb/in	daN/cm	lb/in	daN/cm	F	°C
[illegible]	0.075	[illegible]	0.024	[illegible]	1599	[illegible]	286	[illegible]	662	[illegible]
	0.102	[illegible]	0.028	[illegible]	1827	[illegible]	400	[illegible]	716	[illegible]
	0.130	[illegible]	0.028	[illegible]	1999	[illegible]	457	[illegible]	716	[illegible]
	0.157	[illegible]	0.031	[illegible]	2455	[illegible]	514	[illegible]	788	[illegible]
	0.189	[illegible]	0.031	[illegible]	2684	[illegible]	571	[illegible]	842	[illegible]
	0.220	[illegible]	0.031	[illegible]	3141	[illegible]	685	[illegible]	896	[illegible]
	0.264	[illegible]	0.035	[illegible]	3597	[illegible]	799	[illegible]	968	[illegible]

	Cross Section C.S		Compression e2		Helium Sealing Y2		Helium Sealing Y1		Maximum Temperature	
			e2+/-0.004	e2 +/-0.1						
	inch	mm	inch	mm	lb/in	daN/cm	lb/in	daN/cm	°F	°C
[illegible]	0.075	[illegible]	0.020	[illegible]	1999	[illegible]	457	[illegible]	716	[illegible]
	0.102	[illegible]	0.024	[illegible]	2570	[illegible]	571	[illegible]	842	[illegible]
	0.130	[illegible]	0.024	[illegible]	2912	[illegible]	628	[illegible]	896	[illegible]
	0.157	[illegible]	0.028	[illegible]	3654	[illegible]	799	[illegible]	1022	[illegible]
	0.189	[illegible]	0.028	[illegible]	3997	[illegible]	857	[illegible]	1112	[illegible]
	0.220	[illegible]	0.028	[illegible]	4854	[illegible]	1142	[illegible]	1202	[illegible]

Other materials are available on request: Stainless Steel, Inconel, Tantalum, Gold...

Note: Minimum temperature is 1.8°K / −271°C. Maximum temperatures shown in the tables only relate to the characteristics of the seal and are to be checked for every type of fluid.

Groove Design Helicoflex Seal

	Cross Section		Depth		Recommended Width		Mini Width		Clearance OD seal OD groove		Recommended Surface Finish	
	inch	mm	inch	mm	inch	mm	inch	mm	inch	mm	RMS	Ra in µm
	0.079		0.051		0.195		0.100		0.020		32 to 125	
	0.102		0.075		0.220		0.130		0.020		32 to 125	
	0.130		0.098		0.250		0.165		0.030		32 to 125	
	0.157		0.122		0.280		0.195		0.030		32 to 125	
	0.189		0.154		0.320		0.225		0.035		32 to 125	
	0.220		0.185		0.350		0.260		0.040		32 to 125	
	0.264		0.224		0.395		0.310		0.040		32 to 125	

	Cross Section		Depth		Recommended Width		Mini Width		Clearance OD seal OD groove		Recommended Surface Finish	
	inch	mm	inch	mm	inch	mm	inch	mm	inch	mm	RMS	Ra in µm
	0.075		0.051		0.195		0.100		0.020		32 to 125	
	0.102		0.075		0.220		0.130		0.020		32 to 125	
	0.130		0.098		0.250		0.165		0.020		32 to 125	
	0.157		0.126		0.280		0.190		0.025		32 to 125	
	0.189		0.157		0.320		0.220		0.030		32 to 125	
	0.220		0.189		0.350		0.255		0.030		32 to 125	
	0.264		0.228		0.395		0.300		0.035		32 to 125	

	Cross Section		Depth		Recommended Width		Mini Width		Clearance OD seal/OD groove		Recommended Surface Finish	
	inch	mm	inch	mm	inch	mm	inch	mm	inch	mm	RMS	Ra in µm
	0.075		0.051		0.195		0.100		0.020		32 to 125	
	0.102		0.075		0.220		0.130		0.020		32 to 125	
	0.130		0.102		0.250		0.160		0.020		32 to 125	
	0.157		0.126		0.280		0.190		0.025		32 to 125	
	0.189		0.157		0.320		0.220		0.025		32 to 125	
	0.220		0.189		0.350		0.250		0.025		32 to 125	
	0.264		0.228		0.395		0.300		0.030		32 to 125	

	Cross Section		Depth		Recommended Width		Mini Width		Clearance OD seal/OD groove		Recommended Surface Finish	
	inch	mm	inch	mm	inch	mm	inch	mm	inch	mm	RMS	Ra in µm
	0.075		0.055		0.195		0.100		0.020		32 to 63	
	0.102		0.079		0.220		0.130		0.020		32 to 63	
	0.130		0.106		0.250		0.155		0.020		32 to 63	
	0.157		0.130		0.280		0.185		0.025		32 to 63	
	0.189		0.161		0.320		0.220		0.025		32 to 63	
	0.220		0.193		0.350		0.250		0.025		32 to 63	

These groove designs are only applicable for vacuum and low pressure (up to 300 psi/20 bar). For higher pressure applications, please consult our engineering staff.

Groove Design Helicoflex Seal

	Cross Section		Depth		Recommended Width		Min Width		Clearance		Recommended Surface Finish	
	[illegible]	[illegible]	[illegible]	[illegible]	[illegible]	[illegible]	[illegible]	[illegible]	[illegible]	[illegible]	[illegible]	0.8 to 3.2
	[illegible]	[illegible]	[illegible]	[illegible]	[illegible]	[illegible]	[illegible]	[illegible]	[illegible]	[illegible]	[illegible]	0.8 to 3.2
	[illegible]	[illegible]	[illegible]	[illegible]	[illegible]	[illegible]	[illegible]	[illegible]	[illegible]	[illegible]	[illegible]	0.8 to 3.2
	[illegible]	[illegible]	[illegible]	[illegible]	[illegible]	[illegible]	[illegible]	[illegible]	[illegible]	[illegible]	[illegible]	0.8 to 3.2
	[illegible]	[illegible]	[illegible]	[illegible]	[illegible]	[illegible]	[illegible]	[illegible]	[illegible]	[illegible]	[illegible]	0.8 to 3.2
	[illegible]	[illegible]	[illegible]	[illegible]	[illegible]	[illegible]	[illegible]	[illegible]	[illegible]	1.0	[illegible]	0.8 to 3.2
	[illegible]	[illegible]	[illegible]	[illegible]	[illegible]	[illegible]	[illegible]	[illegible]	[illegible]	1.0	[illegible]	0.8 to 3.2

	Cross Section		Depth		Recommended Width		Min Width		Clearance		Recommended Surface Finish	
	[illegible]	[illegible]	[illegible]	[illegible]	[illegible]	[illegible]	0.100	[illegible]	[illegible]	[illegible]	[illegible]	0.8 to 3.2
	[illegible]	[illegible]	[illegible]	[illegible]	0.220	[illegible]	0.130	[illegible]	[illegible]	[illegible]	[illegible]	0.8 to 3.2
	[illegible]	[illegible]	[illegible]	[illegible]	0.250	[illegible]	0.165	[illegible]	[illegible]	0.5	[illegible]	0.8 to 3.2
	[illegible]	[illegible]	[illegible]	[illegible]	[illegible]	[illegible]	0.190	[illegible]	0.025	0.8	[illegible]	0.8 to 3.2
	[illegible]	[illegible]	[illegible]	[illegible]	[illegible]	[illegible]	0.220	[illegible]	[illegible]	0.8	[illegible]	0.8 to 3.2
	[illegible]	[illegible]	[illegible]	[illegible]	[illegible]	[illegible]	0.255	[illegible]	0.030	[illegible]	[illegible]	0.8 to 3.2
	[illegible]	[illegible]	[illegible]	[illegible]	[illegible]	[illegible]	0.300	[illegible]	.035	0.8	[illegible]	0.8 to 3.2

	Cross Section		Depth		Recommended Width		Min Width		Clearance		Recommended Surface Finish	
	[illegible]	[illegible]	[illegible]	[illegible]	[illegible]	[illegible]	[illegible]	[illegible]	[illegible]	0.5	[illegible]	0.8 to 3.2
	[illegible]	[illegible]	[illegible]	1.9	[illegible]	[illegible]	[illegible]	[illegible]	[illegible]	[illegible]	[illegible]	0.8 to 3.2
	[illegible]	[illegible]	[illegible]	2.6	[illegible]	[illegible]	[illegible]	[illegible]	[illegible]	[illegible]	[illegible]	0.8 to 3.2
	[illegible]	[illegible]	[illegible]	3.2	[illegible]	[illegible]	[illegible]	[illegible]	0.025	[illegible]	[illegible]	0.8 to 3.2
	[illegible]	[illegible]	[illegible]	4.0	[illegible]	[illegible]	[illegible]	[illegible]	[illegible]	[illegible]	[illegible]	0.8 to 3.2
	[illegible]	[illegible]	[illegible]	4.8	[illegible]	[illegible]	[illegible]	[illegible]	[illegible]	[illegible]	[illegible]	0.8 to 3.2
	[illegible]	[illegible]	[illegible]	[illegible]	[illegible]	10.0	[illegible]	[illegible]	[illegible]	[illegible]	[illegible]	0.8 to 3.2

	Cross Section		Depth		Recommended Width		Min Width		Clearance		Recommended Surface Finish	
	[illegible]	[illegible]	[illegible]	1.4	[illegible]	[illegible]	[illegible]	[illegible]	[illegible]	[illegible]	[illegible]	0.8 to 1.6
	0.102	[illegible]	[illegible]	[illegible]	[illegible]	[illegible]	[illegible]	[illegible]	[illegible]	[illegible]	[illegible]	0.8 to 1.6
	0.130	[illegible]	[illegible]	[illegible]	[illegible]	[illegible]	[illegible]	[illegible]	[illegible]	[illegible]	[illegible]	0.8 to 1.6
	0.157	[illegible]	[illegible]	[illegible]	[illegible]	[illegible]	[illegible]	[illegible]	[illegible]	[illegible]	[illegible]	0.8 to 1.6
	0.189	[illegible]	[illegible]	[illegible]	[illegible]	[illegible]	[illegible]	[illegible]	[illegible]	[illegible]	[illegible]	0.8 to 1.6
	0.220	[illegible]	[illegible]	[illegible]	[illegible]	[illegible]	[illegible]	[illegible]	[illegible]	[illegible]	[illegible]	0.8 to 1.6

These groove designs are only applicable for vacuum and low pressure (up to 300 psi/20 bar). For higher pressure applications, please consult our engineering staff

The sealing level has been determined through intensive tests.

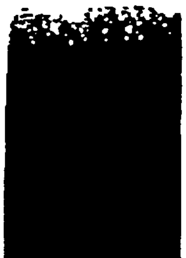

Wall Thickness	T	M	H	T	M	H	T	M	H	T	M	H
0.035"	■	■		■	■		■			■		
0.063"	■	■	■	■	■		■	■		■		
0.093"	■	■	■	■	■		■	■		■	■	
0.125"	■	■		■	■		■	■		■		
0.156"	■	■		■	■		■	■		■		
0.188"	■	■		■	■		■	■		■		
0.250"	■			■			■					
0.375"		■	■		■	■		■	■		■	■
0.500"		■	■		■	■		■	■		■	■
0.625"		■			■			■			■	

Wall Thickness	T	M	H	T	M	H	T	M	H	T	M	H
0.035"		▲	▲		▲	▲		▲	▲	▲	▲	▲
0.063"		▲	▲		▲	▲		▲	▲	▲	▲	▲
0.093"			▲			▲			▲		▲	▲
0.125"		▲	▲		▲	▲	●	▲	▲		▲	▲
0.156"	■	▲	▲	■	▲	▲	■	▲	▲	■	▲	▲
0.188"	■		▲	■		▲			▲		▲	▲
0.250"	▲	▲	▲	▲	▲	▲	▲	▲	▲	▲	▲	▲
0.375"			▲			▲			▲			▲
0.500"			▲			▲			▲			▲
0.625"												

Wall Thickness	T	M	H	T	M	H	T	M	H	T	M	H
0.035"			▲			▲			▲	▲	▲	▲
0.063"			▲			▲			▲	▲	▲	▲
0.093"	■		▲	■		▲			▲	▲	▲	▲
0.125"	■		▲	■	●	▲			▲	▲	▲	▲
0.156"	■		▲	■	●	▲	■		▲	■	▲	▲
0.188"	■		▲	■	●	▲	■	●	▲	▲	▲	▲
0.250"			▲		●	▲			▲	▲	▲	▲
0.375"		●	▲		●	▲		●	▲			▲
0.500"		●	▲		●	▲		●	▲		●	▲
0.625"								●			●	

Wall Thickness	T	M	H	T	M	H	T	M	H	T	M	H
0.035"	■			■		●	■		●			▲
0.063"	■	■		■		●	■	●	●			
0.093"	■	■		■	■	●	■	■		■		
0.125"	■		●	■		●	■			■		▲
0.156"	■	●	●	■	●	●	■			■		▲
0.188"	■	■		■	■	●	■		●	■		▲
0.250"	■	●	●		●	●	●		▲			▲
0.375"		■			■	●		■			■	
0.500"		■			■	●		■			■	
0.625"								■			■	

■ Low Sealing Level $Q > 10^{-5}$ Torr liter s^{-1}

Bubble Sealing Level $10^{-5} < Q < 10^{-9}$ Torr liter.s^{-1}

▲ Helium Sealing Level $Q < 10^{-9}$ Torr.liter.s^{-1}

Q= Leak rate

4.4.4 Excerpts (9 pages) From "Helicoflex Company Metallic O-Rings" [4.6]

Hēlicoflex company

Metallic O-Rings

The World Leader in High Performance Sealin

Mission Statement

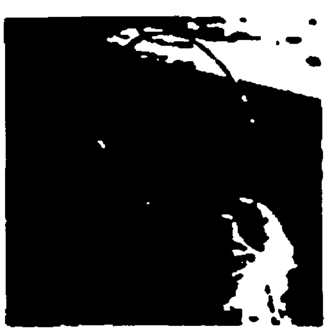

We the employees of the Helicoflex Company. shall strive to use all available human and physical resources in our commitment to **Customer Satisfaction**

Customer Satisfaction is attained through continuously improving the Quality of our people. our products. our processes. our service. and our vendors in order to provide quality products on time at a fair price.

Customer Satisfaction requires employee satisfaction: Therefore. we strive to treat one another with respect and work as a team to achieve quality in our work life.

Customer Satisfaction and quality in our work life result in growth. security. pride. and opportunity for ourselves and our company.

History and Profile

HISTORY

HELICOFLEX COMPANY is a subsidiary of Carbone Lorraine North America, a company with a world wide reputation in the graphite industry. By contributing to the development of sealing technologies for more than a century HELICOFLEX COMPANY associated with its sister company LCL CEFILAC ETANCHEITE, has proven to be the world leader in high performance sealing.

HELICOFLEX COMPANY offers customer service and engineering support dedicated to solving sealing problems and has unique Research and Development capability to develop seals and specially engineered sealing systems.

PROFILE

Specializing in metallic seals and servicing all types of industries including Nuclear, Aerospace, Vacuum, Petrochemical, Chemical Process Industry, etc. HELICOFLEX COMPANY offers the following product lines suited to most sealing needs:

STATIC SEALING

- Helicoflex® seals
- Metal O-Rings
- Metal C-Rings
- Metal V-Rings
- OFHC copper gaskets
- Vitaflex® spiral wound gaskets
- Cefilair® inflatable seals
- Papyex® flexible graphite

DYNAMIC SEALING

- GPA® mechanical seals
- Gulliver® mechanical seals
- Fargraf® graphite packing

SEALING SYSTEMS

- Quick disconnect systems
- Bolted flange assemblies
- Heat exchangers
- Mechanical engineering

Contents

Helicoflex Metallic O-Rings

METALLIC O-RING, THE VERSATILE SEAL

GENERAL INFORMATION

Helicoflex Metallic O-Rings are designed to provide a high sealing level under adverse working conditions whether the medium is gas or liquid
Helicoflex Metallic O-Rings are manufactured from stainless steel or high temperature alloy tubing or wire

SEALING CONCEPT

The sealing concept of Metallic O-Rings is based on the elastic deformation of the tube which during the compression cycle gives a contact point on each sealing surface
The tube characteristics determine the compressive load of the seal This load combined with an accurate compression rate results in a specific pressure which is directly related to the sealing level obtained A certain specific pressure is necessary to make the seal flow into the flange imperfections A softer surface treatment is available to increase the plasticity of the seal and reduce the specific pressure necessary to reach the desired sealing level
Metallic O-Rings require a controlled compression by some mechanical method such as a custom machined groove or a limiter of appropriate thickness

GENERAL CHARACTERISTICS

- Wide range of applications:
  - Dimensional: Diameters from 0 250 inches(6 3 mm) to 300 inches(7 6 m)
    Cross sections from 0 031 inches(0.8 mm) to 0.625 inches(15 9mm)
  - Temperature: Cryogenic to 1800 degrees F (982 degrees C)
  - Pressure: Ultra High Vacuum to 60000 PSI (4100 bars)
- Excellent resilience (Springback)
- Adaptable to a majority of standard flanges
- Available in many shape configurations, rectangular oval, oblong etc..
- Suited to different types of assemblies
  - metal metal with groove
  - flat flanges with a retainer
  - 3 face contact
- Extended shelf life
- Extended service life
- Excellent resistance to corrosion and radiation
- Minimum relaxation

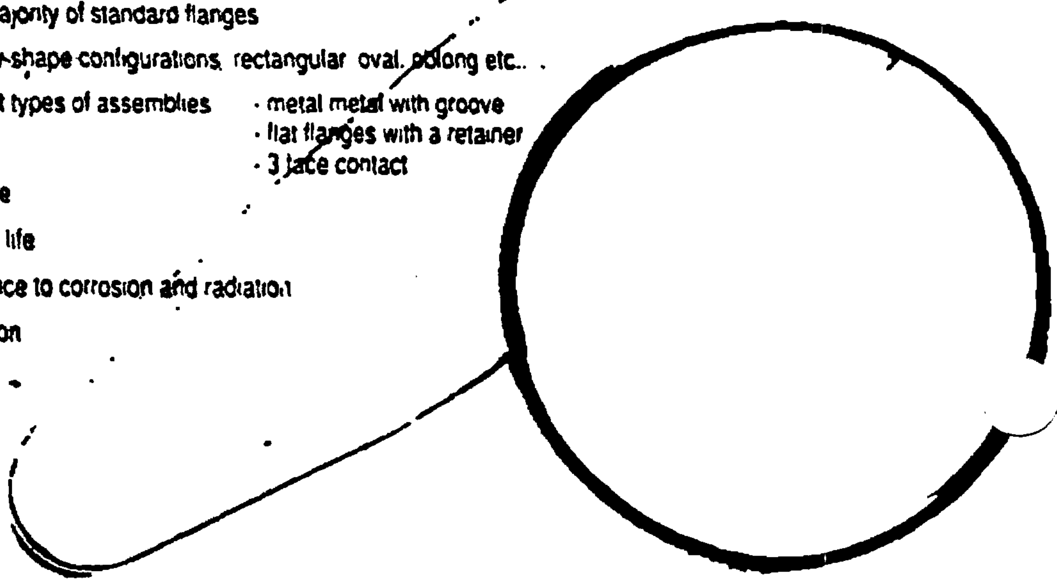

Seal Characteristics

MATERIALS

Helicoflex Metallic O-Rings can be manufactured using different materials such as 300 series Stainless Steel Alloy 600. Alloy X750. Alloy 718 or other special alloys The temperature. the pressure and the corrosive aspects of the media determine which material is best suited for the application

HEAT TREATMENT

Since tensile strength and resilience of the seal are determined in part by metal temper. Helicoflex Company offers a choice of heat treatment (age hardening or annealing) according to AMS. MIL. ASTM or customer specification

SURFACE TREATMENT

Sealing capability can be improved by surface treatments such as Teflon[1] coating or electroplating with silver. nickel or other malleable metals. These specialized surface treatments are recommended when sealing gaseous media. The coating or plating increases the seal plasticity and yields during installation. filling minor surface imperfections and creating a positive seal

When service conditions allow. silver is the preferred surface treatment.

DIFFERENT TYPES OF SEALS

PLAIN Type: NP

The plain seal type NP (Not self energized or Pressure filled) is made of metal tubing (or wire) available in most metal alloys This type is the most economical O-Ring. It is designed for low to moderate pressure and vacuum applications

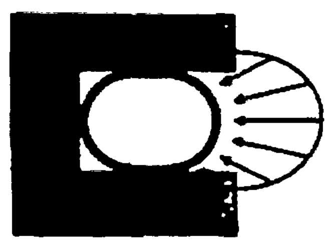

SELF-ENERGIZING Type: SE

The surface exposed to the highest pressure. usually the inner periphery. is vented by small holes or slots. Self-Energizing seal type SE is recommended for high pressure applications This feature allows the system pressure to enter the O-Rings. creating maximum specific pressure and reducing the pressure differential across the seal. For media other than high viscosity. one hole is sufficient.

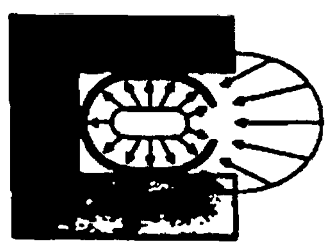

PRESSURE FILLED Type:PF

Pressure Filled O-Rings are designed for a temperature range of 800 to 2000 degrees F (425-1093 degrees C). The rings are filled with an inert gas at 600 PSI (41 bars) At elevated temperatures. gas pressure increases to offset the loss of strength in the tubing and specific pressure

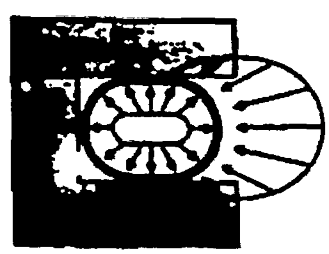

WHATEVER YOUR REQUIREMENTS, WE HAVE THE SEALING SOLUTION

O RING TYPE SELECTION

TYPE NP for working conditions from vacuum to 100 PSI (7 bars)
TYPE SE for pressure above 100 PSI (7 bars) and temperature up to 1800° F (982°C)
TYPE PF for high pressure and high temperature from 800° F (426°C) to 2000° F (1093°C)

MATERIAL SELECTION

Temperature and media to be sealed determine the type of O-Ring material

[redacted]

The welding characteristics of Alloy 718 make it especially resistant to post weld cracking above 1100° F exceeding that of Alloy X 750.

O-RING SIZE SELECTION

Tubing diameter is determined by ring outside diameter, available space and sealing level required (See table on page 7). For each cross section, we have selected 3 different wall thicknesses. Thin(T), Medium(M) and Heavy(H) which give the appropriate specific pressure according to the required sealing level (See table on page 5)

SURFACE TREATMENT

Different coatings or platings are available to provide better plasticity which yields and conforms to the microscopic groove or flange irregularities.
The recommended surface treatments are:

SURFACE TREATMENT	TEMPERATURE
Teflon®	Cryogenic to 500° F (260° C)
Silver	Cryogenic to 1200°F (649° C)
Nickel	Cryogenic to 2200° F (1204° C)

SURFACE FINISH REQUIREMENTS

Surface Treatment	NONE	TEFLON	SILVER	NICKEL
Recommended Surface Finish	< 16 RMS	16 to 32 RMS	16 to 63 RMS	16 to 32 RMS

5. SHIELDING EVALUATION

The shielding analysis of the NUHOMS®-MP187 Cask is described in this chapter. During shipment, the NUHOMS®-MP187 Cask contains one of the three DSC designs described in Chapter 1. The FO-DSC and the FC-DSC each contain 24 intact PWR spent fuel assemblies. The FF-DSC contains 13 potentially failed PWR spent fuel assemblies. The design basis fuel parameters evaluated herein include a maximum burnup of 40,000 megawatt days per metric ton uranium (MWd/MTU), initial ^{235}U enrichments ranging from 2.38% to 3.19% by weight (w/o), a minimum post-irradiation cooling time of at least five years, a maximum assembly decay heat of 0.764 kW, and a maximum cask decay heat of 13.5 kW. Fuel assemblies with initial enrichments greater than those used for this analysis, up to the maximum allowable initial enrichment of 3.43 w/o ^{235}U, will have source terms bounded by those used herein. Other fuel having varied characteristics will be licensed by amendment to the certificate of compliance for this package.

The packaging is shown in the following sections to provide adequate shielding to ensure compliance with the external dose rate requirements specified in 10 CFR Part 71.47, 10 CFR Part 71.51 [5.1], and 49 CFR Part 173.441 [5.2] for the fuel parameters stated above. As stated in Chapter 7, the dose rates surrounding the package are measured prior to each shipment and verified to be in compliance with 10 CFR Part 71.47 and 49 CFR 173.441. The MP187 shielding evaluation results presented in Table 5.1-1 show that the predicted dose rates with the least margin relative to the regulatory limits are those for normal conditions of transport. A package that meets the dose rate limits of 10 CFR Part 71.47 and 49 CFR 173.441 for normal conditions of transport will also, therefore, meet the limits of 10 CFR 71.51 after sustaining damage from the hypothetical accident conditions. The shielding evaluation presented herein is thus intended to describe the expected shielding performance of the packaging and to show that the dose rates observed during normal conditions of transport represent the bounding case.

5.1 Discussion and Results

The packaging provides neutron and gamma-ray radiation shielding for up to 24 PWR spent fuel assemblies. Gamma-ray shielding is provided by lead and stainless steel shells that make up the cask wall. Neutron shielding is provided by a cementitious castable material contained within a stainless steel jacket surrounding the cylindrical portion of the cask body. Gamma shielding in the cask ends is provided by stainless steel and the top and bottom end assemblies of the DSC.

The FO-DSC and FC-DSC transported in the cask contain 24 intact PWR fuel assemblies. The FC-DSC also contains 24 PWR control components and therefore represents the design basis source term. The design basis payload neutron and gamma-ray sources, based on the FC-DSC, are 4.640×10^9 neutrons/sec and 3.162×10^{16} MeV(γ)/sec, respectively as derived in Sections 5.2.2 (neutron) and 5.2.1.5 (gamma). The FF-DSC contains 13 PWR fuel assemblies that may have experienced gross cladding failure prior to shipment.

The NUHOMS®-MP187 package will be transported by exclusive use shipment, inside a closed transport vehicle (enclosure provided by the personnel barrier). The applicable 10 CFR Part 71.47 external radiation requirements for normal conditions during shipment include [5.1]:

1. Radiation levels must not exceed 10 mSv/hr (1000 mrem/hr) on the external surface of the package.

2. Radiation levels must not exceed 2 mSv/hr (200 mrem/hr) at any point on the outer surface of the transport vehicle.

3. Radiation levels must not exceed 0.1 mSv/hr (10 mrem/hr) at any point two meters from the outer lateral surfaces of the vehicle or, in the case of a flat-bed style vehicle, at any point two meters from the vertical planes projected by the outer edges of the vehicle and on the lower external surface of the vehicle.

4. Radiation levels must not exceed 0.02 mSv/hr (2 mrem/hr) in any normally occupied space.

In the shielding evaluations, the external surface of the packaging is defined as the radial surface of the cask neutron shield panel and the surfaces of the impact limiters. The outer surface of the vehicle is bounded by the impact limiters and the personnel barrier, which is mounted on the skid and extends to the same radius as the impact limiters as shown on the drawings provided in Section 1.3.2. The 10 CFR Part 71.51 external radiation requirements after the 10 CFR Part 71.73 hypothetical accident conditions are that there shall be [5.1],

> ". . . no external radiation dose rate exceeding 10 mSv/h (1 rem/hr) at one meter from the external surface of the package."

During the hypothetical accident conditions defined in 10 CFR Part 71.73, the cask is assumed to be separated from the skid. The cask neutron shield and neutron shield jacket are assumed to be lost during the accident, as are the impact limiters. The cask lead shielding is assumed to have slumped, producing relatively unshielded gaps in the cask wall. The suitability of the cask cavity closure during the hypothetical accident conditions is documented in Chapters 2 and 4.

The results of the shielding evaluation performed for the NUHOMS®-MP187 Cask are summarized in Table 5.1-1. The values in Table 5.1-1 are described in detail in Section 5.4.2. The bounding dose rate for the MP187 Package is the two meter dose rate along the package side. The reported value of 9.94 mrem per hour is just below the 10CFR71.47 limit. This result is acceptable because:

(1) The methodology used to calculate the package dose rates is based on a series of conservative assumptions which provide assurance that the actual package dose rates will be below the applicable limits. Conservative assumptions in the analysis include:

- Impact limiter thickness assumed equal to the minimum thickness with no credit taken for the actual rectangular cross-section.

- Worst case nuclear data used for source term calculations.

- Source terms used in shielding analysis based on total cask heat load of 14.3 kW, which exceeds maximum allowable heat load by 6%.
- No credit taken for shielding of control components by fuel rods (worth about 14% of the total dose rate for the FC-DSC).
- Conservative neutron shield properties used including a 10% reduction in hydrogen and a 50% reduction in boron
- The methodology used to perform the shielding calculations has been thoroughly benchmarked against measured data and shown to provide significantly conservative (factor of two or more) results as documented in Reference [5.15].

(2) All package dose rates are measured immediately prior to shipment and the package will not be shipped if the 10CFR71 limits are exceeded.

Because the dose rates at the top and bottom ends of the package are less than two mrem/hr, the radiation level in occupied positions of the vehicle will also be less than two mrem/hr. The cask meets all of the applicable external radiation criteria as documented in the remainder of this chapter.

Table 5.1-1

Summary of Maximum Dose Rates

(mrem/hr)

5.2 Source Specification

The NUHOMS®-MP187 Cask is designed to transport any one of the three DSCs described in Chapter 1. Each DSC can hold 24 PWR fuel assemblies (13 in the FF-DSC). The neutron and gamma-ray radiological source strengths and the gamma-ray source spectrum for the design basis fuel assembly are determined using the ORIGEN2 computer code [5.3]. Section 1.2.3 defines two sets of fuel assembly parameters (described below) which are suitable for transportation in the MP187 Cask. Selection and placement of assemblies are controlled by the specifications in Section 1.2.3 and the procedures in Section 7 of this SAR. Type I assemblies, which have the larger sources, may be placed only in an FF-DSC (any fuel cell) or in the interior four fuel cells of an FO-DSC or FC-DSC. Type II assemblies, which have the smaller sources, may be placed in any fuel cell of any DSC type. Design basis sources for both Type I and Type II assemblies are developed in this section. Gamma-ray source strengths are also developed for the design basis control components that will be shipped with the fuel assemblies in the FC-DSC.

The design basis payload neutron and gamma-ray sources are 4.640×10^9 neutrons/sec and 3.162×10^{16} MeV(γ)/sec, respectively. The fuel parameters used to develop the design basis source are taken from Section 1.2.3. These parameters include a maximum burnup of 40,000 MWd/MTU and a minimum cooling time of five years. Type I assemblies are limited to a maximum decay heat of 0.764 kW. Type II assemblies are limited to 0.563 kW, with a total cask maximum decay heat not to exceed 13.5 kW. The PWR fuel assembly chosen as the design basis radiological source is a Babcock and Wilcox (B&W) 15x15 assembly, with its associated B&W control components. The control component with the largest gamma source is an axial power shaping rod assembly (APSRA). Other fuel having varied radiological characteristics will be licensed by amendment to the certificate of compliance for this package.

The ORIGEN2 computer code [5.3] is used to calculate the gamma and neutron sources for the Type I and Type II assemblies described above. The design basis source term for the NUHOMS®-MP187 Cask shielding analysis is represented by 4 Type I assemblies and 20 Type II assemblies, including control components, with the design basis neutron and gamma source terms described below. The ORIGEN2 results were then mapped from the ORIGEN2 energy structure to the CASK-81 [5.4] energy structure for the external dose rate calculations.

For the acceptable fuel parameters defined in Section 1.2.3, the source calculations described below determine bounding neutron and gamma-ray sources. The process used to develop the design basis source is shown in Figure 5.2-1. The bounding sources are calculated by preparing several ORIGEN models of the design basis assembly and, for each case, calculating the required cooling times to meet the Type I and Type II allowable decay heats per assembly. The neutron and gamma sources that correspond to the burnup, enrichment, and cooling time for each case are then input to 1-D cask shielding calculations to determine which case maximizes the cask surface dose rates.

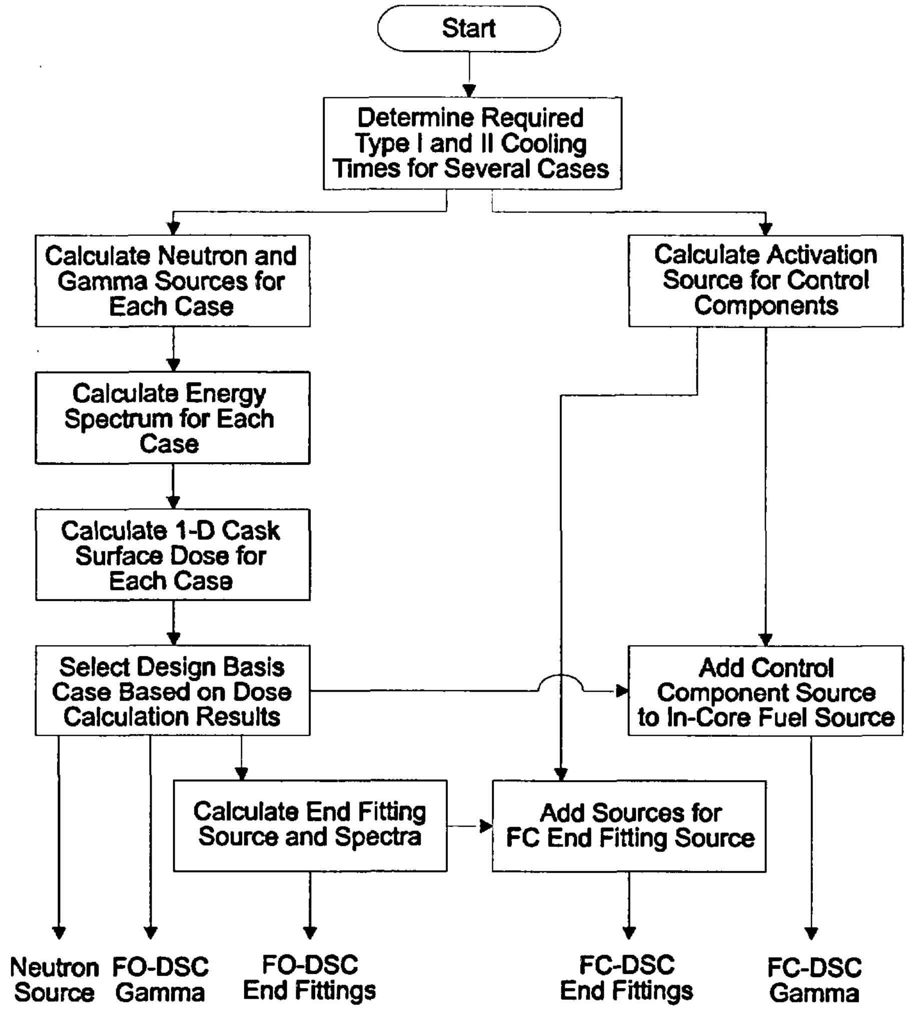

Figure 5.2-1

Source Term Calculation Flow Chart

Acceptable fuel burnups range from 0 MWd/MTU to 40,000 MWd/MTU. Acceptable fuel cooling times are greater than or equal to five years, such that the decay heat criteria are met. The initial enrichments of the fuel assemblies vary according to the burnup of the assembly. The choice of initial enrichment for each case has a significant effect on the neutron source (lower enrichments produce greater sources). To select an appropriate enrichment for a given burnup, a statistical evaluation was performed for 2615 B&W 15x15 fuel assemblies from five reactors. The average enrichment and standard deviation were calculated as a function of burnup and the design basis initial enrichment is then defined as the average enrichment minus one standard deviation. This choice of enrichment will result in bounding sources for about 84% of the fuel inventory. This is considered a reasonable design value for shielding calculations because actual dose rates are measured and must meet 10CFR71.47 and 49CFR173.441 prior to each shipment.

Five ORIGEN cases are run to bound the minimum cooling time and maximum burnup specifications listed above. For each ORIGEN case, the cooling time required to meet the assembly decay heat limits of 0.764 kW (Type I) and 0.563 kW (Type II) is calculated. The gamma and neutron sources for each case are extracted from the ORIGEN output and used to develop the design basis sources discussed below. A summary of the ORIGEN cases is provided in Table 5.2-1. As will be shown below, the case that results in the largest dose rates around the cask, for both Type I and Type II assemblies is a burnup of 40,000 MWd/MTU and an initial enrichment of 3.19 w/o ^{235}U. The corresponding cooling time for Type I assemblies is 9 years and for Type II assemblies is 17 years.

Table 5.2-1

ORIGEN2 Input Cases for Shielding Evaluation

Case	Burnup (MWd/MTU)	Initial Enrichment (w/o ^{235}U)	Type I Required Cooling Time (years)	Type II Required Cooling Time (years)	Type II Decay Heat (kW/assy)
I	23,200	2.38	5	5	0.5600
II	25,000	2.49	5	6	0.5206
III	30,000	2.76	5	8	0.5329
IV	35,000	2.99	7	11	0.5590
V	40,000	3.19	9	17	0.5536

5.2.1 Gamma Source

ORIGEN2 [5.3] is used to calculate both the neutron and gamma-ray source terms for the NUHOMS®-MP187 Cask. A description of the fuel assembly models and data reduction is provided in this section. Data reduction that applies specifically to the neutron source is described in Section 5.2.2. The ORIGEN2 code computes the radioactivity of fuel assemblies that have undergone irradiation in a nuclear reactor and subsequent decay after removal from the reactor core. It has the ability to compute the isotopic fractions, radioactivity, decay thermal power, toxicity, neutron absorption, neutron emission, and photon emission for various isotopes in the fuel assembly. ORIGEN2 results are used in spent fuel shipping package analyses to develop neutron and gamma ray radioactive decay source strengths and to develop decay thermal powers. ORIGEN2 is an industry standard code that is distributed by Oak Ridge National Laboratory's Radiation Shielding Information Center (ORNL/RSIC).

5.2.1.1 Description of Fuel Assembly ORIGEN Models

The assumed fuel assembly material weights used in the ORIGEN2 models are shown in Table 5.2-2. The detailed material compositions and impurities are given in the sample input files reproduced in Section 5.5.2. The fuel assembly ORIGEN2 model is split into four distinct regions: in-core, plenum, top nozzle, and bottom nozzle. Additional ORIGEN2 runs are made to calculate the activation source term in the design basis control components.

The power irradiation in ORIGEN2 is performed for the fuel assembly materials in the active fuel region. A flux irradiation is then performed on the top nozzle, plenum, bottom nozzle, and control component regions. The assumed operating histories are listed in the ORIGEN2 input files. The fractions of the in-core flux that are applied to the top nozzle, plenum, and bottom nozzle zones for the calculation of activation products in these zones are taken from Reference 5.5.

Table 5.2-2

Summary of Fuel Assembly Material Weights Used in Source Term Calculations

Region	Component(s)	Material	Weight (kg) [5.6]
In-Core	Fuel	UO_2	525.9
	Cladding	Zircaloy-4	107.14
	Guide/Inst. Tubes	Zircaloy-4	7.972
	Grid Spacers	Inconel-718	4.90
	Grid Supports	Zircaloy-4	0.64
	APSRA (FC)	SS-304	9.009
	APSRA Poison (FC)	Inconel-718	15.36
Gas Plenum	Cladding	Zircaloy-4	8.976
	Guide/Inst. Tubes	Zircaloy-4	0.668
	Grid Spacer	Inconel-718	1.04
	Support Spacers	Zircaloy-4	3.925
	APSRA (FC)	SS-304	0.764
Top Nozzle	Top Nozzle	SS-304	8.96
	Holddown Spring	Inconel-718	1.80
	APSRA (FC)	SS-304	2.50
Above Top Nozzle	APSRA (FC)	SS-304	1.136
Bottom Nozzle	Bottom Nozzle	SS-304	8.31
	Grid Spacer	Inconel-718	1.30
	Support Spacers	Zircaloy-4	3.925

A sample ORIGEN2 input file for the design basis fuel assembly is reproduced in Section 5.5.2. After the assembly is irradiated in the manner described above, the materials in the assembly are decayed for 5 to 17 years, depending on the irradiation parameters assumed, until the assembly decay heat reaches the cask average decay heat of 0.563 kW/assy. The ORIGEN2 33,000 MWd/MTU burnup, PWR data library is used in this calculation for burnup cases less than 33,000 MWd/MTU (Cases I through III). The ORIGEN2 50,000 MWd/MTU burnup, PWR data library is used for burnup cases greater than 33,000 MWd/MTU (Cases IV and V). In this way, the most conservative library is used for actual burnups between those used to generate the libraries.

5.2.1.2 Description of Control Component ORIGEN Models

The B&W axial power shaping rod assembly was selected as the design basis control component. The APSRA was selected due to its significant mass, which increases the amount of activated material, and its presence in the core during reactor operation. Control rod assemblies, while more massive than the APSRAs, are withdrawn from the core during full power operation. Orifice rods and burnable poison rods contain significantly less material than the APSRAs.

Both black and gray APSRAs are modeled using the ORIGEN code. The black and gray APSRAs differ primarily in the poison material used. The black APSRA uses a silver-indium-cadmium poison while the gray APSRA uses Inconel. The APSRA materials used in the ORIGEN runs are listed in Table 5.2-3. Each APSRA is assumed to be irradiated for five cycles. Each irradiation cycle is identical to those used for the fuel assembly source calculation. Each control component is assumed to have cooled for at least 8 years prior to placement in the cask.

As discussed in detail in Section 5.2.1.5, the gray APSRA will result in larger dose rates on the surface of the cask. This was determined using a 1-D shielding model of the MP187 Cask with both of the calculated control component source terms. The derivation of the cask source term is discussed in detail below.

Table 5.2-3

Control Component Regional Weights

Region	Material	Black APSRA (kg)	Gray APSRA (kg)
Above Top	SS304	1.182	1.136
Top Nozzle	SS304	2.632	2.500
Gas Plenum	SS304	0.891	0.764
In-Core	SS304	10.57	9.009
In-Core	Poison(1)	10.64	15.36

1) Black APSRA poison material is Ag-In-Cd, Gray poison material is Inconel.

5.2.1.3 Selection of Design Basis Fuel Parameters

As stated in Section 5.2, five burnup/enrichment/cooling time cases were modeled for both Type I and Type II fuel assemblies in order to determine the case that will result in the largest cask surface dose rates. This determination was made by performing one-dimensional shielding calculations using the neutron and gamma-ray sources taken from the five ORIGEN runs. The discrete-ordinates code ANISN [5.13] was used for this calculation. The ANISN models are similar to the shielding models described in Section 5.4. The results of the ANISN runs are used only to compare the dose rates due to each of the five source cases and are not used in the final shielding calculations. The two-dimensional code DORT-PC is used to perform the final shielding calculations for the design basis source term as described in Section 5.4.

The 1-D ANISN dose rate results are multiplied by peaking factors (PF for gammas and $(PF)^4$ for neutrons) to account for axial peaking in the assemblies. The peaking factor for an assembly (equal to the peak axial burnup divided by the assembly average burnup) decreases as the burnup is increased. Previous revisions of this SAR conservatively used a peaking factor of 1.2 for all fuel burnups. However, because this section of the SAR determines which combination of fuel parameters results in the highest cask surface dose rates, it is a relatively simple matter to incorporate the variation in axial peaking factors. Figure 4-4 of Reference [5.14], portions of which are included as an Appendix to this Chapter, provides the normalized axial burnup profile as a function of burnup for PWR fuel assemblies. Based on this data, an appropriate peaking factor for the 23.2 GWd/MTU case is 1.17 and for the remaining cases is 1.12.

The results of the 1-D dose rate comparison for the five source cases are shown in Figure 5.2-2 (assuming 24 Type I assemblies) and in Figure 5.2-3 (assuming 24 Type II assemblies). The total cask gamma source strength and spectrum are shown in Table 5.2-4 and Table 5.2-5 for each of the five burnup cases, assuming the presence of 24 Type I and Type II assemblies, respectively. These tables provide sources for 24 assemblies because the 1-D dose rate comparisons are performed for both Type I and Type II assemblies to verify that the same assembly parameters are bounding for each case. In both cases, for a given decay heat, the cask surface dose rate increases as a function of burnup. Case V, the 40,000 MWd/MTU model, represents the worst case for the shielding evaluation. The ORIGEN results from Case V are used to develop the design basis source terms in the next section and in Section 5.2.2.

5.2.1.4 Design Basis Gamma Source for FO-DSC

The gamma source strengths and energy spectra for the top nozzle (including the top nozzle and plenum sources), in-core, and bottom nozzle regions and for the whole assembly are shown in Table 5.2-6 and Table 5.2-7 for the design basis Type I and Type II sources, respectively. The maximum source in an FO-DSC, as discussed above, is based on 4 Type I and 20 Type II assemblies. Table 5.2-8 and Table 5.2-9 provide the total FO-DSC source. The energy structure is that used by the CASK-81 cross-section library. The total design basis gamma source strength in the package containing 24 PWR fuel assemblies (4 Type I and 20 Type II) in an FO-DSC is

8.429×10^{16} photons per second (2.723×10^{16} MeV/sec). This design basis source, when used with the design basis neutron source described below, bounds that of B&W 15x15 assemblies that meet the acceptance criteria listed in Section 1.2.3.

The 18 group gamma ray energy spectra shown in Table 5.2-4 through Table 5.2-9 have been converted from that used by the ORIGEN2 code. The energy spectrum used in the shielding calculations is that of the CASK-81 22 neutron group, 18 gamma ray group cross section set [5.4]. To map the ORIGEN2 energy structure into the CASK-81 energy structure, the particles in each group are assumed to be evenly distributed in logarithmic energy space. The total number of particles and the total gamma power (MeV/sec) are conserved. Logarithmic mapping is a common practice and is considered reasonable for this application. The formulae used to map the ORIGEN2 energy structure into the CASK-81 gamma-ray energy group structure are shown in Table 5.2-10.

Table 5.2-4

In-Core FO-DSC Gamma Source Strength and Energy Spectrum for Each Burnup Case for Type I Fuel

Figure 5.2-2

Determination of Bounding Type I Assembly Source

Table 5.2-5

In-Core FO-DSC Gamma Source Strength and Energy Spectrum for Each Burnup Case for Type II Fuel

Figure 5.2-3

Determination of Bounding Type II Assembly Source

Table 5.2-6

Type I Assembly Design Basis Gamma Source Strength and Energy Spectrum

Table 5.2-7

Type II Assembly Design Basis Gamma Source Strength and Energy Spectrum

Table 5.2-8

FO-DSC Design Basis Gamma Source Strength and Energy Spectrum

Table 5.2-9

FO-DSC Design Basis Gamma Power and Energy Spectrum

Table 5.2-10

Formulae for Mapping Gamma Source from ORIGEN2 to CASK-81 Energy Groups

ORIGEN2 Group	ORIGEN2 E_{mean} (MeV)	CASK-81 Group	CASK-81 E_{upper} (MeV)	Formula ORIGEN2 → CASK-81
a	9.500	23	10.000	a
b	7.000	24	8.000	0.722b
c	5.000	25	6.500	0.278b + 0.450c
d	3.500	26	5.000	0.550c
e	2.750	27	4.000	d
f	2.250	28	3.000	e
g	1.750	29	2.500	f
h	1.250	30	2.000	0.648g
i	0.850	31	1.660	0.352g + 0.297h
j	0.575	32	1.330	0.703h
k	0.375	33	1.000	0.626i
l	0.225	34	0.800	0.374i + 0.349j
m	0.125	35	0.600	0.651j + 0.290k
n	0.085	36	0.400	0.710k
o	0.058	37	0.300	0.585l
p	0.038	38	0.200	0.415l + m
q	0.025	39	0.100	n + 0.762o
r	0.010	40	0.050	0.238o + p + q + r

5.2.1.5 Design Basis Gamma Source for FC-DSC

The payload of the FC-DSC differs from that of the FO-DSC only by the addition of control components. As discussed in Section 5.2.1.2, ORIGEN2 was used to calculate sources for both black and gray APSRAs, which represent the bounding control components, after 8-years cooling. The calculated source per component for both the in-core and top nozzle regions is provided in Table 5.2-11 (energy group mapping per Table 5.2-10). As shown in Table 5.2-11, it is not obvious which control component would produce the greatest cask dose rates. The black APSRA has the highest total source while the gray APSRA has the highest source in the specific energy groups that contribute the most to the cask dose rates. The effect of the two types of APSRA on the cask dose rates is assessed using two additional ANISN runs. The Type I assembly, Case V ANISN runs described in Section 5.2.1.3 were modified to include the control component sources from Table 5.2-11. The calculated gamma dose rates with the black and gray APSRAs (neglecting axial peaking) are 25.4 mrem/hr and 35.6 mrem/hr, respectively. Based on these results, the gray APSRA is considered the design basis control component.

The gamma source strengths and energy spectra for the top nozzle (including the top nozzle and plenum sources), in-core, and bottom nozzle regions and for the whole assembly are shown in Table 5.2-12 and Table 5.2-13 for the design basis Type I and Type II sources, respectively, with control components. These sources were calculated by summing the contributions from the design basis FO sources and control components, group-by-group, for the in-core and top-nozzle regions. Because the APSRA does not extend into the bottom nozzle region, the bottom nozzle source for the FO-DSC and FC-DSC are identical.

The maximum source in an FC-DSC, as discussed above, is based on 4 Type I and 20 Type II assemblies. Table 5.2-14 and Table 5.2-15 provide the total FC-DSC source. The energy spectrum is that used by the CASK-81 cross-section library. The total design basis gamma source strength in the package containing 24 PWR fuel assemblies (4 Type I and 20 Type II) in an FC-DSC is 8.794×10^{16} photons per second (3.162×10^{16} MeV/sec). This design basis source, when used with the design basis neutron source described below, bounds that of B&W 15x15 assemblies with control components that meet the acceptance criteria listed in Section 1.2.3.

Table 5.2-11

Design Basis Control Component Source Terms

Table 5.2-12

Type I Assembly w/ Control Component

Design Basis Gamma Source Strength and Energy Spectrum

Table 5.2-13

Type II Assembly w/ Control Component

Design Basis Gamma Source Strength and Energy Spectrum

Table 5.2-14

FC-DSC Design Basis Gamma Source Strength and Energy Spectrum

Table 5.2-15

FC-DSC Design Basis Gamma Power and Energy Spectrum

Table 5.2-16

FC-DSC Gamma Source Strength and Energy Spectrum for Each Burnup Case for Type I Fuel

Table 5.2-17

FC-DSC Gamma Source Strength and Energy Spectrum for Each Burnup Case for Type II Fuel

5.2.2 Neutron Source

The neutron source strength for the design basis fuel assembly is calculated using the same ORIGEN2 runs as were used to calculate the gamma source. All input parameters and assumptions are the same as those used for the gamma ray calculations described above.

The neutron source results from spontaneous fission and (α,n) reactions in the active fuel region. The total neutron sources for the design basis case are 2.455×10^8 neutrons/sec per Type I assembly and 1.829×10^8 neutrons/sec per Type II assembly (4.640×10^9 neutrons/sec/cask assuming 4 Type I assemblies and 20 Type II assemblies) as calculated by the ORIGEN2 code.

The spectrum for spontaneous fission neutrons from ^{244}Cm is assumed for the neutron source in this analysis [5.7]. The ^{244}Cm spontaneous fission spectrum was chosen because it represents more than 90% of the total neutron source in the package. The ^{244}Cm spectrum group fractions for the CASK-81 energy structure are then multiplied by the total source strength to determine the groupwise source strengths for the cask to be used in the shielding calculations. The total neutron source strength and energy spectrum for each of the five burnup cases is shown in Table 5.2-18 and Table 5.2-19 for Type I and Type II assemblies, respectively.

Table 5.2-18

Design Basis Neutron Source Strength and Energy Spectrum for Type I Fuel

Table 5.2-19

Design Basis Neutron Source Strength and Energy Spectrum for Type II Fuel

Upper Energy (MeV)	Case I 23.2 GWd/MTU (n/sec/cask)	Case II 25 GWd/MTU (n/sec/cask)	Case III 30 GWd/MTU (n/sec/cask)	Case IV 35 GWd/MTU (n/sec/cask)	Case V 40 GWd/MTU (n/sec/cask)
1.492E+01	2.274E+05	2.739E+05	4.450E+05	7.149E+05	8.858E+05
1.220E+01	1.291E+06	1.556E+06	2.527E+06	4.060E+06	5.030E+06
1.000E+01	5.038E+06	6.069E+06	9.860E+06	1.584E+07	1.963E+07
8.180E+00	1.992E+07	2.400E+07	3.899E+07	6.263E+07	7.761E+07
6.360E+00	4.695E+07	5.656E+07	9.190E+07	1.476E+08	1.829E+08
4.960E+00	6.356E+07	7.657E+07	1.244E+08	1.998E+08	2.476E+08
4.060E+00	1.349E+08	1.625E+08	2.640E+08	4.240E+08	5.254E+08
3.010E+00	1.084E+08	1.305E+08	2.121E+08	3.406E+08	4.221E+08
2.460E+00	2.542E+07	3.062E+07	4.975E+07	7.992E+07	9.903E+07
2.350E+00	1.383E+08	1.666E+08	2.706E+08	4.347E+08	5.386E+08
1.830E+00	2.378E+08	2.864E+08	4.653E+08	7.474E+08	9.262E+08
1.110E+00	2.021E+08	2.435E+08	3.956E+08	6.355E+08	7.875E+08
5.500E-01	1.282E+08	1.545E+08	2.510E+08	4.031E+08	4.995E+08
1.110E-01	1.466E+07	1.766E+07	2.869E+07	4.609E+07	5.711E+07
3.350E-03	7.386E+04	8.898E+04	1.446E+05	2.322E+05	2.877E+05
5.830E-04	5.369E+03	6.468E+03	1.051E+04	1.688E+04	2.092E+04
1.010E-04	3.531E+02	4.254E+02	6.912E+02	1.110E+03	1.376E+03
2.900E-05	5.101E+01	6.145E+01	9.984E+01	1.604E+02	1.987E+02
1.010E-05	1.100E+01	1.325E+01	2.152E+01	3.457E+01	4.284E+01
3.060E-06	1.714E+00	2.065E+00	3.354E+00	5.388E+00	6.677E+00
1.120E-06	3.778E-01	4.551E-01	7.395E-01	1.188E+00	1.472E+00
4.140E-07	1.091E-01	1.314E-01	2.135E-01	3.430E-01	4.250E-01
Total	1.127E+09	1.357E+09	2.205E+09	3.542E+09	4.390E+09

5.3 Model Specification

The shielding analysis described below was performed to verify that the packaging containing 24 PWR fuel assemblies meets the shielding criteria specified in 10 CFR Part 71 [5.1] and 49 CFR Part 173 [5.2]. Analytical models of the package were developed to determine the dose rates around the package for both normal and hypothetical accident conditions. The 2-D discrete ordinates code DORT-PC [5.9] was used to calculate the neutron and gamma-ray dose rates as described in Section 5.4.

5.3.1 Description of the Radial and Axial Shielding Configuration

The radial and axial shielding configuration of the package is shown in Figure 5.3-1, and Figure 5.3-2 through Figure 5.3-5. Figure 5.3-1 is a scale drawing of the package that shows the overall package dimensions for both the FO-DSC and the FC-DSC. The FF-DSC shielding configuration is identical to that of the FC-DSC. The DORT-PC model for the FC-DSC is shown in Figure 5.3-2 and Figure 5.3-3 (not to scale). The model for the FO-DSC is similar and is shown in Figure 5.3-4 and Figure 5.3-5. The cask is modeled symmetrically in cylindrical coordinates and nominal dimensions were used to generate the model. A single model is used to calculate radial and axial, neutron and gamma-ray dose rates around the NUHOMS®-MP187 Cask containing an FC-DSC as defined in Chapter 1. A separate model is used to calculate dose rates around the cask containing an FO-DSC. The FF-DSC contains only 13 fuel assemblies and its source is therefore bounded by that of the FC-DSC.

The DORT-PC model of the package includes irregularities in the lead shielding to represent the tapered ends of the lead column. Minor discontinuities in the cask components due to fabrication details which do not significantly affect the cask shielding performance have been neglected in the models. Significant penetrations are addressed as described below. The impact limiters have a square cross-section that cannot be modeled accurately in cylindrical coordinates. The impact limiter geometry is therefore approximated using cylinders with radii such that they would be completely enclosed by the actual impact limiter geometry. The trunnions and the drain, vent, and test ports have been neglected. Because the upper trunnions extend through the neutron shield, the dose rates around these trunnions are evaluated separately as described in Section 5.4.1.8. The cask drain, vent and test ports contain steel plugs during shipment and do not represent a shine path. The support rods in the DSC have also been neglected. The spacer discs are neglected in the homogenized fuel region, but are explicitly modeled in the gap between the fuel region and the DSC shell. A gap is modeled in the cask bottom cover. This gap is not currently shown on the cask drawings, but represents a conservatism in the shielding calculations. The package shielding normal operation materials are shown for the FC-DSC in Figure 5.3-6. The FO-DSC materials are identical except for the use of carbon steel shield plugs rather than lead.

The neutron shielding and neutron shield jacket are assumed to be lost during the hypothetical accident conditions due to the postulated cask drop and subsequent fire. This assumption is made purely for conservatism as the neutron shield is expected to at least partially survive the hypothetical accident. The impact limiters are assumed to be lost during the hypothetical accident as well, even though there is no physical mechanism that could remove the impact limiter inner shells. The cask lead shielding is assumed to slump 2.5 inches at each end during the postulated drop, producing air gaps in the cask shielding. The suitability of the cask cavity closure during the hypothetical accident conditions is documented in Chapters 2 and 4. During the accident, the DSC is assumed to slide to the top of the cask cavity, and the fuel is assumed to slide to the top of the DSC cavity. These assumptions are made to maximize the streaming through the lead slump gap at the top of the DSC. The package shielding materials for the hypothetical accident conditions are shown in Figure 5.3-7.

Neutron and gamma ray dose rates were calculated in various locations, radially and axially, around the package. These locations include the package surface, the surface of the transport vehicle, and two meters from the surface of the transport vehicle along its top, bottom, and sides. The maximum dose rates reported in Table 5.1-1 are the maximum dose rates observed at any location, radially and axially, along the surface, for any of the three DSC designs. The package surface is defined by the surface of the impact limiters and the neutron shield during normal conditions of transport. The package surface is defined by the cask structural shell after the hypothetical accident. The outer surface of the vehicle is defined by the impact limiters and the personnel barrier, which is mounted on the skid and extends to the same radius as the impact limiters as shown on the drawings provided in Section 1.3.2.

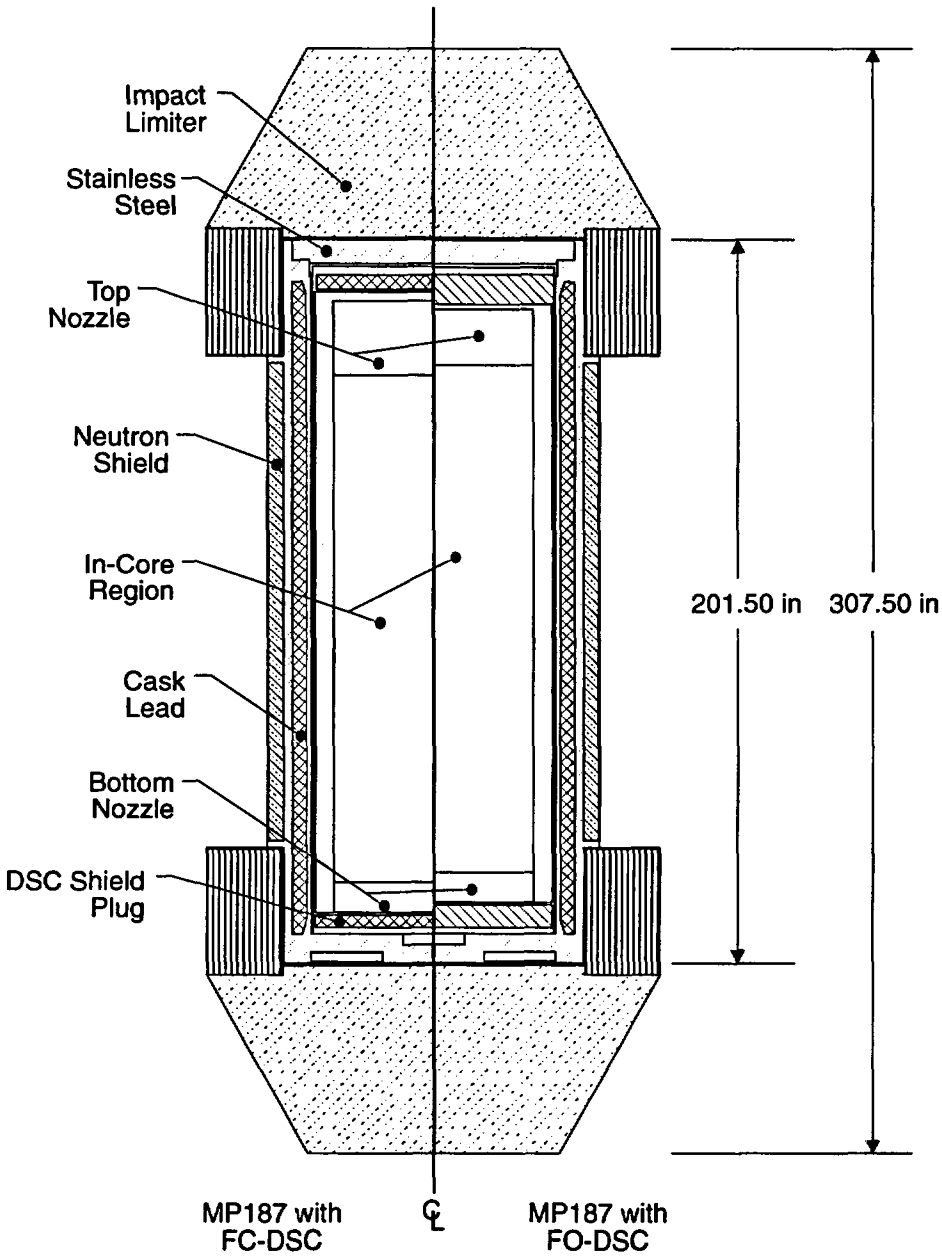

Figure 5.3-1

NUHOMS®-MP187 Cask Configuration

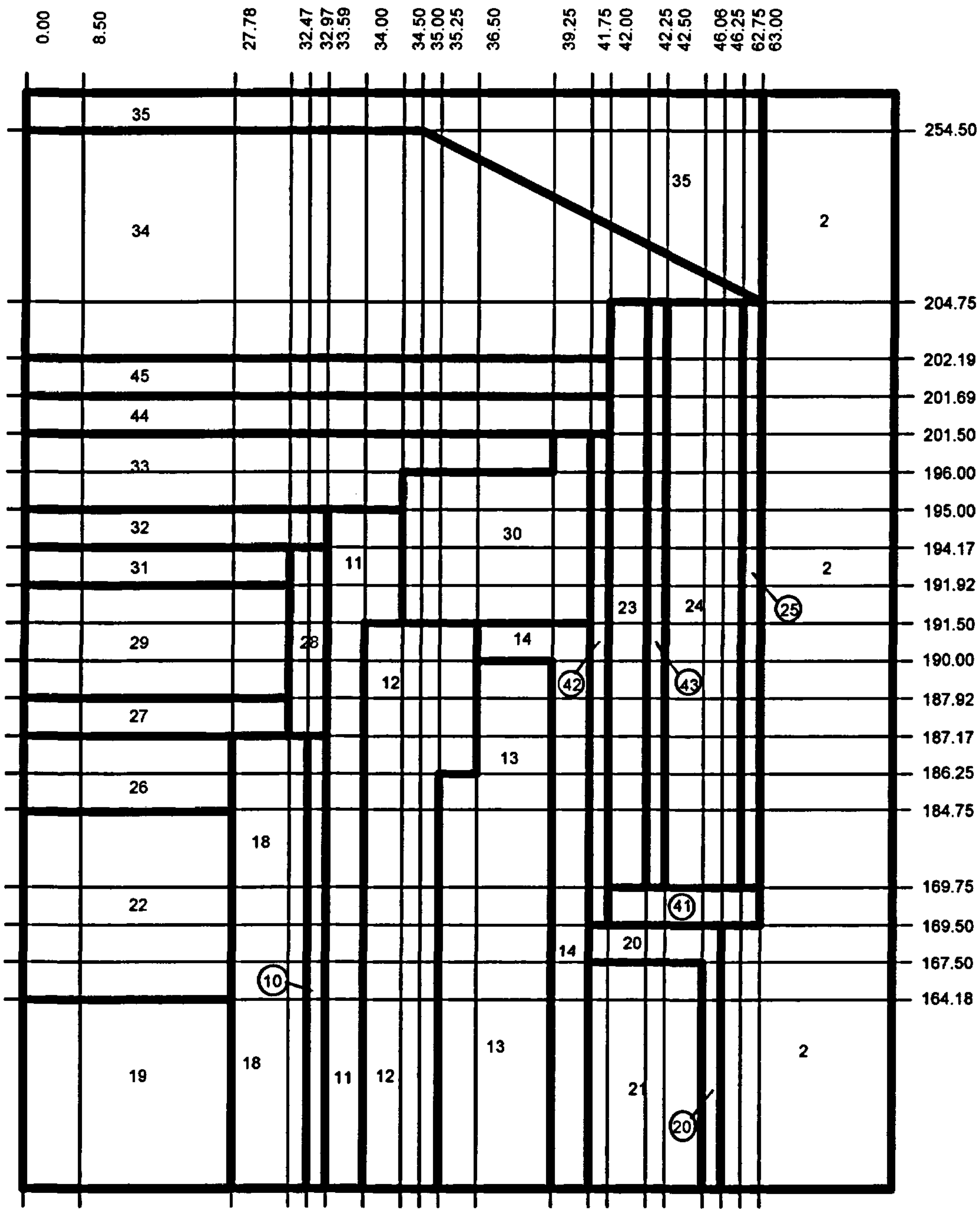

Figure 5.3-2

NUHOMS®-MP187 Normal Operations DORT-PC FC-DSC Top End Model

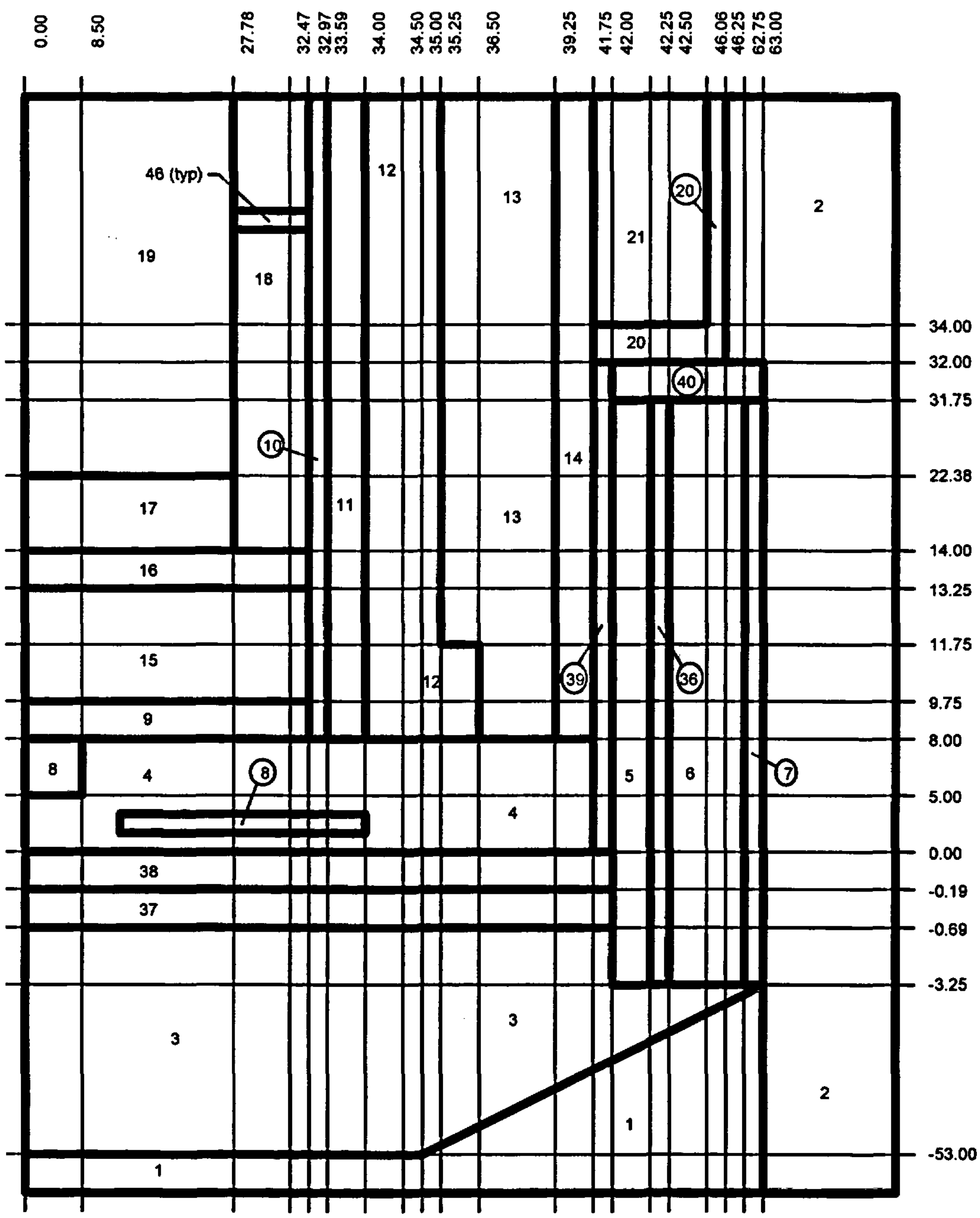

Figure 5.3-3

NUHOMS®-MP187 Normal Operations DORT-PC FC-DSC Bottom End Model

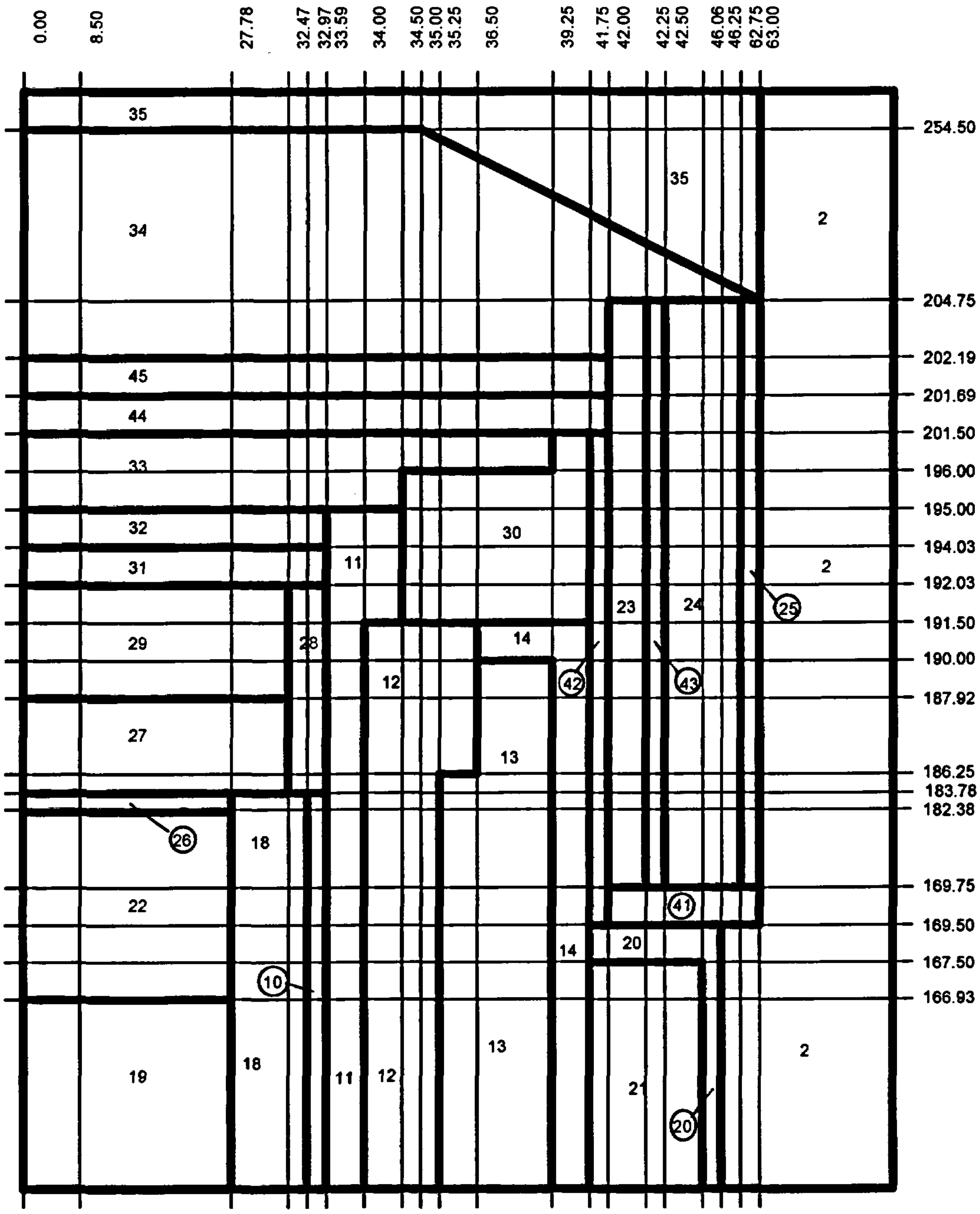

Figure 5.3-4

NUHOMS®-MP187 Normal Operations DORT-PC FO-DSC Top End Model

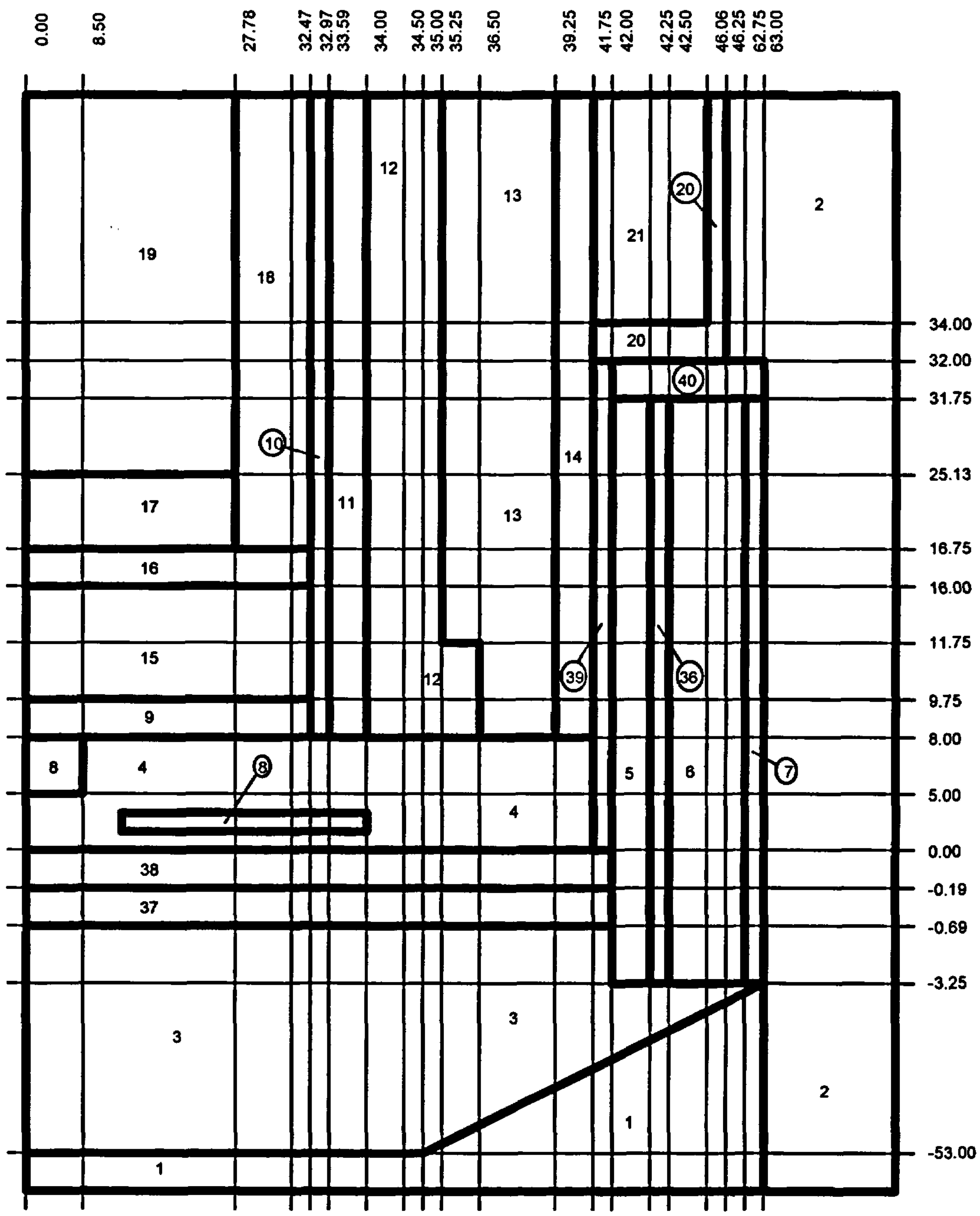

Figure 5.3-5

NUHOMS®-MP187 Normal Operations DORT-PC FO-DSC Bottom End Model

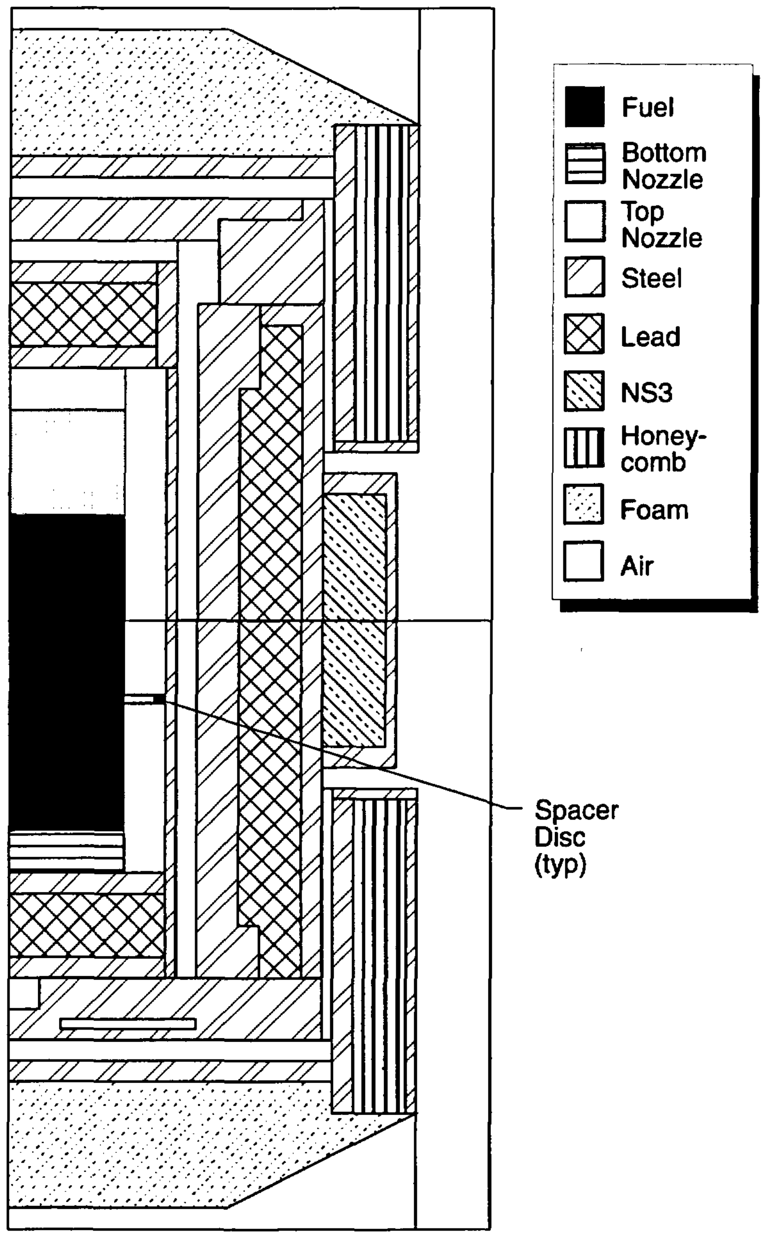

Figure 5.3-6

NUHOMS®-MP187 Normal Operation Shielding Materials

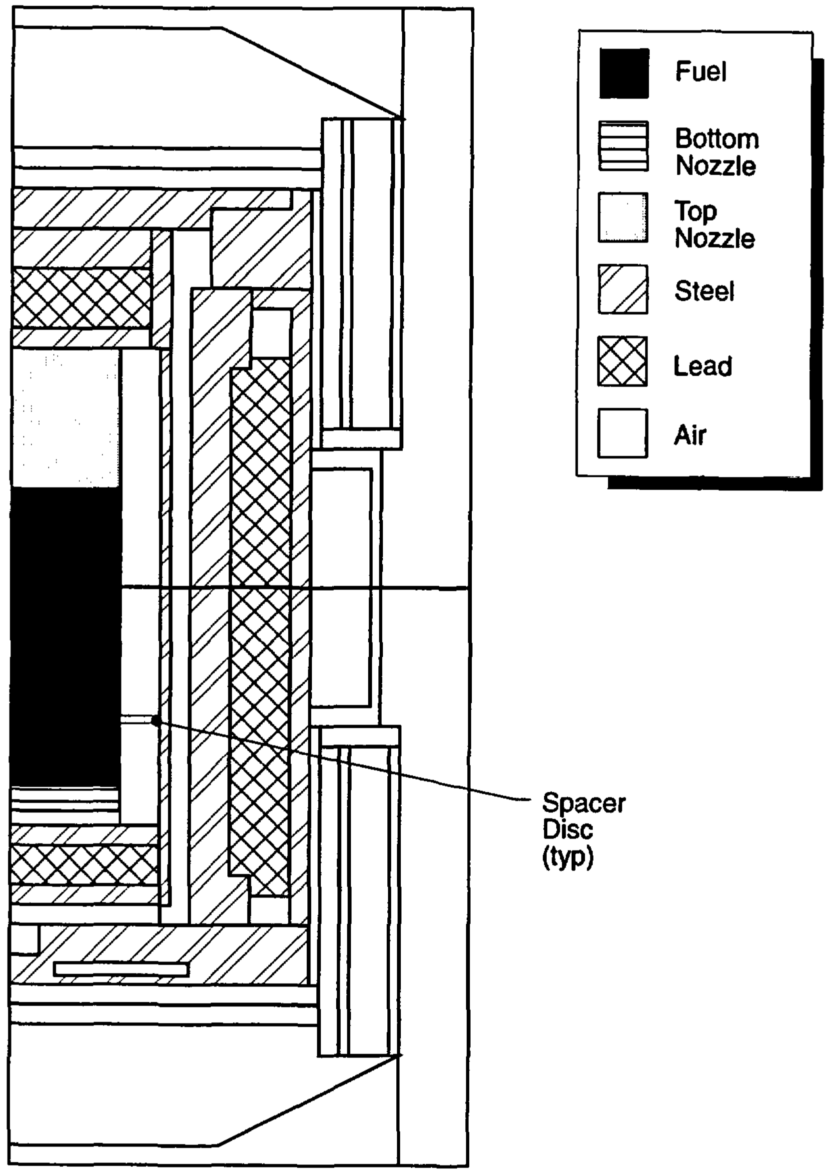

Figure 5.3-7

NUHOMS®-MP187 Hypothetical Accident Condition Shielding Materials

5.3.2 Shield Regional Densities

The mass densities (grams/cc) and atomic number densities (atoms/barn·cm) for all of the constituent nuclides in the materials used in the analytical models of the package are given in this section. Shield regional densities for the in-core, top nozzle, and bottom nozzle regions are calculated using the material weights given in Table 5.2-2. The materials in these regions are assumed to be evenly distributed over the entire volume of the region (smeared). This is a common modeling technique for shielding calculations.

The basket assembly support rods are not assumed to provide any shielding. The DSC guide sleeves and neutron absorber plates are assumed to completely cover the active fuel region in the model. The top nozzle and bottom nozzle regions are assumed to be uncovered. Minor impurities in the fuel, DSC, and the cask materials have been neglected.

The fissile nuclides present in significant quantities in the fuel, ^{235}U, ^{239}Pu, and ^{241}Pu, are included in the homogenized fuel region to provide a source for subcritical multiplication. Subcritical multiplication accounts for only about 5% of the total cask surface dose rates reported in Table 5.1-1. Because the fixed neutron source (spontaneous fission and (α,n) reactions) produces the majority of the neutron dose rate on the package surface, the overall neutron dose rates are thus maximized by using the largest possible fixed neutron source. This occurs at the greatest fuel burnup allowed by the package design. The fissile content in the fuel is significantly depleted at these high burnups and use of the initial enrichment for subcritical multiplication is, therefore, unnecessarily conservative.

The ORIGEN2 runs described above calculate fuel weight fractions of 0.635% ^{235}U, 0.579% ^{239}Pu, and 0.111% ^{241}Pu for the design basis, 40 GWd/MTU case. For simplicity, the quantities of the two Pu isotopes are summed and modeled as ^{239}Pu. An extra margin of safety is included to account for uncertainties in the quantities calculated by ORIGEN2 such that a weight fraction of 0.75% is used for both ^{235}U and ^{239}Pu. Additional margin is provided by: (1) Not taking credit for the buildup of other actinides which would serve as neutron poisons; and (2) Not taking credit for the buildup of fission products which would serve as neutron poisons. It is therefore concluded that using the burned fuel enrichment, including fissile plutonium, represents a more realistic while still conservative methodology to account for subcritical multiplication in the MP187 Cask than using the initial enrichment.

The neutron shield density and material composition are shown in Table 5.3-1. Variations in the composition of the neutron shield over the life of the package are accounted for by neglecting 10% of the hydrogen weight and 50% of the boron weight. Variations in the actual neutron shield boron loading have only a small impact on the cask dose rates. A 50% reduction in the boron weight conservatively bounds any depletion that may occur during the life of the package.

The neutron shield is completely encased in a sealed, stainless-steel annulus. When the neutron shield is exposed to high temperatures, some steam can be evolved from the material. Because the neutron shield is completely encased in a sealed, stainless-steel annulus, none of this steam is released from the cask and the total neutron shield weight remains constant. A 10% loss of hydrogen is assumed, however, to account for stratification of steam released by the solid material. Long term thermal testing of the neutron shield has been performed as discussed in Reference 5.8. Blocks of neutron shield material were held at a constant temperature of 250°F for an extended period of time. The test results show that the neutron shield material weight stabilized after a two month period and that the total reduction in hydrogen weight is less than 9.3 percent. The maximum neutron shield temperature during normal operation in the NUHOMS®-MP187 Cask is less than 250°F as documented in Chapter 3. The assumed hydrogen loss of 10 weight percent, therefore, results in conservative material properties for the shielding calculations.

The mass and atom densities of the remaining materials used in the shielding calculations are given in Table 5.3-1.

Table 5.3-1

Summary of NUHOMS®-MP187 Cask Shielding Material Densities

(atoms/b·cm, g/cc)

Element	Stainless Steel	Carbon Steel	Lead	Neutron Shield[1]	Aluminum Honeycomb	Foam	Air
H	-	-	-	4.180×10^{-2} (0.070)	-	1.004×10^{-2} (0.017)	-
B	-	-	-	7.131×10^{-4} (0.013)	-	-	-
C	-	-	-	7.871×10^{-3} (0.157)	-	7.220×10^{-3} (0.144)	-
N	-	-	-	-	-	8.255×10^{-4} (0.019)	3.587×10^{-5} (8.343×10^{-4})
O	-	-	-	3.442×10^{-2} (0.915)	-	2.168×10^{-3} (0.058)	9.534×10^{-6} (2.533×10^{-4})
Al	-	-	-	8.528×10^{-3} (0.382)	6.428×10^{-3} (0.288)	-	-
Si	-	-	-	1.155×10^{-3} (0.054)	-	-	-
Ca	-	-	-	1.351×10^{-3} (0.090)	-	-	-
Cr	1.728×10^{-2} (1.492)	-	-	6.104×10^{-4} (0.053)	-	-	-
Fe	6.073×10^{-2} (5.632)	8.465×10^{-2} (7.85)	-	2.242×10^{-3} (0.208)	-	-	-
Ni	7.447×10^{-3} (0.726)	-	-	2.631×10^{-4} (0.026)	-	-	-
Pb	-	-	3.296×10^{-2} (11.34)	-	-	-	-

(1) Neutron shield material densities include an assumed 10% hydrogen loss and a 50% reduction in boron. Neutron shield material densities include the stainless steel and aluminum stiffeners present in the neutron shield annulus.

Table 5.3-1

Summary of NUHOMS®-MP187 Cask Shielding Material Densities

(atoms/b·cm, g/cc)

(concluded)

Element	FO Top Nozzle	FC Top Nozzle	FO Active Fuel	FC Active Fuel	Bottom Nozzle
B	-	-	8.137×10^{-4} (1.461×10^{-2})	8.137×10^{-4} (1.461×10^{-2})	-
C	-	-	2.033×10^{-4} (4.055×10^{-3})	2.033×10^{-4} (4.055×10^{-3})	-
O	-	-	9.992×10^{-3} (2.655×10^{-1})	9.992×10^{-3} (2.655×10^{-1})	-
Al	-	-	8.656×10^{-4} (3.878×10^{-2})	8.656×10^{-4} (3.878×10^{-2})	-
Cr	1.412×10^{-3} (1.219×10^{-1})	1.344×10^{-3} (1.161×10^{-1})	8.658×10^{-4} (7.476×10^{-2})	1.094×10^{-3} (9.449×10^{-2})	2.244×10^{-3} (1.937×10^{-1})
Fe	4.731×10^{-3} (4.387×10^{-1})	4.552×10^{-3} (4.221×10^{-1})	2.923×10^{-3} (2.711×10^{-1})	3.347×10^{-3} (3.104×10^{-1})	7.345×10^{-3} (6.812×10^{-1})
Ni	7.873×10^{-4} (7.676×10^{-2})	7.138×10^{-4} (6.959×10^{-2})	4.648×10^{-4} (4.532×10^{-2})	8.504×10^{-4} (8.290×10^{-2})	1.379×10^{-3} (1.344×10^{-1})
Zr	2.489×10^{-3} (3.770×10^{-1})	1.869×10^{-3} (2.831×10^{-1})	3.255×10^{-3} (4.931×10^{-1})	3.255×10^{-3} (4.931×10^{-1})	-
^{235}U	-	-	3.795×10^{-5} (1.481×10^{-2})	3.795×10^{-5} (1.481×10^{-2})	-
^{238}U	-	-	4.921×10^{-3} (1.945×10^{0})	4.921×10^{-3} (1.945×10^{0})	
^{239}Pu	-	-	3.731×10^{-5} (1.481×10^{-2})	3.731×10^{-5} (1.481×10^{-2})	-

5.4 Shielding Evaluation

The neutron and gamma-ray dose rates for the package are estimated using the DORT-PC computer code [5.9]. The DORT-PC input parameters and results are discussed in the following sections.

5.4.1 DORT-PC Input Parameters

5.4.1.1 The DORT-PC Computer Code

DORT-PC determines the fluence of particles throughout one-dimensional or two-dimensional geometric systems by solving the Boltzmann transport equation using either the method of discrete ordinates or a diffusion theory approximation. Particles can be generated by either particle interaction with the transport medium or extraneous sources incident upon the system. Anisotropic cross-sections can be expressed in a Legendre expansion of arbitrary order. DORT-PC is an industry standard code distributed by ORNL/RSIC.

The DORT-PC code implements the discrete ordinates method as its primary mode of operation. Balance equations are solved for the flow of particles moving in a set of discrete directions in each cell of a space mesh and in each group of a multigroup energy structure. Iterations are performed until all implicitness in the coupling of cells, directions, groups, and source regeneration has been resolved.

DORT-PC was chosen for this application because of its ability to solve two dimensional, cylindrical, deep penetration, radiation transport problems. The package has thick multilayered shields which are difficult to analyze with point-kernel codes. The cask geometry is too complicated to be treated adequately with a one-dimensional discrete ordinates code.

5.4.1.2 Source Distribution

Four DORT-PC runs were made for each case, normal operating and hypothetical accident, to account for the contributions from the three different source regions and for neutron and gamma sources. In the first two runs, the gamma and neutron sources were placed throughout the active fuel region of the DORT-PC model. The remaining runs accounted for the gamma contributions from the top nozzle and bottom nozzle regions. The results of these four runs were then summed to determine the total neutron and gamma-ray dose rates around the package.

Figure 5.4-1 shows the arrangement of the Type I and Type II assemblies in an FO-DSC or FC-DSC. Type I assemblies are placed only in the interior four fuel cells and are radially shielded by the remaining 20 Type II assemblies. The Type II source, therefore, will dominate the cask surface dose rates. The DORT-PC models described in this calculation use cylindrical source regions with volumetric Type II assembly sources from Table 5.2-7 (FO gamma), Table 5.2-13 (FC gamma), and Table 5.2-19 (neutron). Volumetric sources are calculated by multiplying the assembly sources by 24 (assemblies) and dividing by the regional volumes. The volume of the active fuel region assumed in this analysis is 5,633,674 cm^3, the volume of the top nozzle region is 817,439 cm^3 (FC) and the volume of the bottom nozzle region is 332,736 cm^3.

In order to conservatively account for the effect of the four Type I assemblies on the cask dose rates, including streaming effects, two 3-D MCNP [5.7] models of the DSC were generated. MCNP is a multi-purpose neutron, photon, and electron monte-carlo transport code. Each model includes a 1/8 symmetric (on the x, y, and z-axes), pin-by-pin representation of the fuel assemblies in the basket including the cladding, fuel, and guide sleeves as shown in Figure 5.4-1. The first model calculates the dose rate on the DSC surface as a function of angle assuming all 24 fuel cells contain a Type II fuel assembly. The second model includes the Type I assemblies in the four innermost fuel cells. The MCNP input files are provided in Appendix 5.5.3.

The purpose of the MCNP models is to calculate a conservative factor by which the dose rates calculated using only the Type II assembly sources can be multiplied to account for the presence of the Type I assemblies. As shown in Figure 5.4-1, dose rate ratios from the two MCNP models are calculated for both neutrons and gammas in 10° increments along the DSC surface. The maximum ratio is 1.029, calculated for neutrons in the 40°-50° segment. All dose rates, neutron and gamma, calculated by the DORT-PC models are then multiplied by 1.03 to bound any source/streaming from the Type I assemblies.

Dose rates are calculated on the DSC surface instead of the cask surface to improve the statistics of the monte-carlo simulation. This is expected to produce a conservative result since scattering in the cask layers will tend to "smooth" the dose rate ratios. The resulting DORT-PC dose rate calculations will be conservative because the worst case ratio (as a function of angle) is applied over the entire DSC/cask. An additional conservatism is introduced by using a single bounding factor for both neutron and gamma dose rate calculations. This represents a 2% conservatism in the gamma dose rate calculations. Although this method will slightly underpredict the cask top and bottom dose rates, the dose rates at these locations are well below the limits for transportation (see Table 5.1-1).

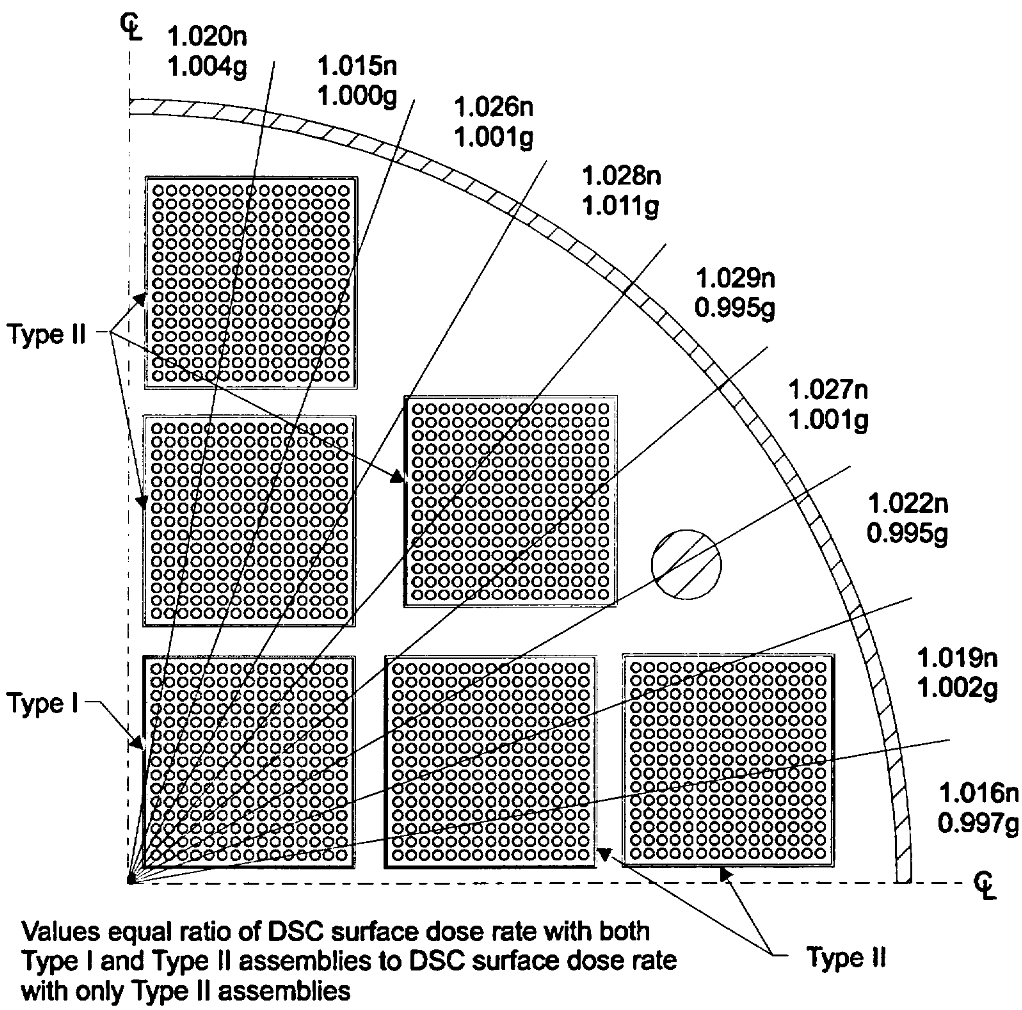

Figure 5.4-1

DSC Dose Rate Ratios as a Function of Angle

The Watt ^{235}U fission spectrum [5.10] is input into the 1* array of the DORT-PC input file to account for subcritical multiplication, increasing the neutron source in the active fuel region. Axial peaking is accounted for in the active fuel region by inputting a relative flux factor at each node in the 97* array. As discussed in Section 5.2.1.3, the flux factor data is taken from Figure 4-4 of Reference [5.14] for PWR fuel. The appropriate flux factor for the design basis case is 1.12 for gamma-rays, assumed to vary linearly with fuel burnup. The flux factors for neutrons have been raised to the fourth power to account for the variation of neutron sources with fuel burnup. Differences between PWR fuel designs, including the locations of the grid spacers and associated hardware, is accounted for by applying the maximum peaking factor of 1.12 across the entire middle section of the active fuel region. The flux factor data used in this analysis is shown in Table 5.4-1. Note that because the length-averaged flux factor shown in Table 5.4-1 is greater than 1.0, the total source present in the in-core region is greater than that discussed in Section 5.2.

Table 5.4-1

PWR Fuel Assembly Axial Flux Distribution

Midpoint of Fuel Segment (in)	Average Gamma Factor in Fuel Segment[1]	Average Neutron Factor in Segment	Product of Segment Length and γ Flux Factor (in)
0.43	0.50	0.06	0.22
1.15	0.54	0.09	0.39
2.40	0.60	0.13	0.75
4.00	0.65	0.18	1.04
5.10	0.68	0.21	0.75
6.10	0.70	0.24	0.70
6.75	0.74	0.30	0.48
7.87	0.79	0.39	0.89
9.50	0.84	0.50	1.37
10.62	0.88	0.60	0.99
11.32	0.90	0.66	0.63
12.94	0.94	0.78	1.53
15.00	0.96	0.85	1.97
16.55	0.98	0.92	1.52
18.92	1.01	1.04	2.40
21.00	1.03	1.13	2.14
23.15	1.05	1.22	2.26
25.02	1.06	1.26	1.99
26.12	1.07	1.31	1.18
27.50	1.10	1.46	1.51
29.37	1.11	1.52	2.08
71.79	1.12	1.57	91.94
114.15	1.11	1.52	2.91
115.00	1.10	1.46	0.94
117.75	1.08	1.36	2.97
120.37	1.05	1.22	2.76
121.50	1.03	1.13	1.16
124.75	0.99	0.96	3.22
128.00	0.94	0.78	3.06
130.20	0.90	0.66	1.98
132.82	0.82	0.45	2.15
134.50	0.76	0.33	1.27
135.80	0.72	0.27	0.94
137.09	0.65	0.18	0.84
138.80	0.60	0.13	1.02
140.50	0.58	0.11	0.99
141.26	0.56	0.10	0.43
141.60	0.55	0.09	0.18
	Total →		145.58

(1) The length-average flux factor for gammas is (145.58/141.80)=1.027.

5.4.1.3 Model Geometry

The package geometry shown in Figure 5.3-2 through Figure 5.3-5 is used in the DORT-PC computer models. The package is modeled in cylindrical (R-Z) coordinates and one model is used for both radial and axial dose rates. A total of 46 zones are defined by a mesh of 86 intervals in the radial direction and 193 intervals in the axial direction. A reflective boundary condition is placed on the central axis of the cask (left boundary). The boundary conditions on the remaining boundaries are voids.

A total of twelve DORT-PC runs were made to calculate the normal operation (for both FO-DSCs and FC-DSCs) and hypothetical accident (for FC-DSCs only) dose rates around the package. The first two runs for each case include the in-core region gamma and neutron sources, respectively. The third run for each case includes only the top nozzle source. The final run includes only the bottom nozzle source. Each run includes the full cask geometry. The normal operation case materials are as shown in Figure 5.3-6 and the hypothetical accident case materials are as shown in Figure 5.3-7.

5.4.1.4 Cross Section Data

The cross section data used in this analysis is taken from the CASK-81 22 neutron, 18 gamma-ray energy group, coupled cross-section library [5.4]. CASK-81 is an industry standard cross section library compiled for the purpose of performing calculations of spent fuel shipping casks and is distributed by ORNL/RSIC. The cross section data allows coupled neutron/gamma-ray runs to be made that account for secondary gamma radiation (n,γ).

Microscopic P_3 cross sections were taken from the CASK-81 library and mixed using the GIP-PC computer program distributed with DORT-PC [5.9] to provide macroscopic cross sections for the materials in the cask model. The GIP input file is reproduced in Section 5.5.4. The material compositions used in the GIP input file are listed in Table 5.3-1.

An additional element and material, "fluxdosium," is included in the cross section data and mixing table in the GIP input file. Fluxdosium is used to provide flux-to-dose rate conversion factors as described below for use in activity calculations. The presence of fluxdosium in the cross-section data does not impact the actual flux calculations.

5.4.1.5 Flux-to-Dose Rate Conversion Factors

The flux distribution calculated by the DORT-PC code is converted to dose rates using the flux-to-dose rate conversion factors provided in ANSI/ANS-6.1.1-1977 [5.11]. The gamma-ray and neutron flux-to-dose rate conversion factors for the CASK–81 energy groups are shown in Table 5.4-2 and Table 5.4-3 respectively.

The dose rate at each node in the DORT-PC model is calculated using the activity calculation feature of DORT-PC. The "cross section" data for one material in the input file contains only flux-to-dose rate conversion factors. This material, "fluxdosium," is then specified for activity calculations which determines the gamma and neutron dose rate at each node.

Table 5.4-2

Gamma-Ray Flux-to-Dose Rate Factors

Energy Group	E_{Lower} (MeV)	E_{Upper} (MeV)	Flux-to Dose Factor (ORem/hr)/(γ/s/cm^2)
23	8.00e+00	1.00e+01	8.7716
24	6.50e+00	8.00e+00	7.4785
25	5.00e+00	6.50e+00	6.3748
26	4.00e+00	5.00e+00	5.4136
27	3.00e+00	4.00e+00	4.6221
28	2.50e+00	3.00e+00	3.9596
29	2.00e+00	2.50e+00	3.4686
30	1.66e+00	2.00e+00	3.0192
31	1.33e+00	1.66e+00	2.6276
32	1.00e+00	1.33e+00	2.2051
33	8.00e-01	1.00e+00	1.8326
34	6.00e-01	8.00e-01	1.5228
35	4.00e-01	6.00e-01	1.1725
36	3.00e-01	4.00e-01	0.87594
37	2.00e-01	3.00e-01	0.63061
38	1.00e-01	2.00e-01	0.38338
39	5.00e-02	1.00e-01	0.26693
40	1.00e-02	5.00e-02	0.93477

Table 5.4-3

Neutron Flux-to-Dose Rate Factors

Energy Group	E_{Lower} (MeV)	E_{Upper} (MeV)	Flux-to Dose Factor (ORem/hr)/(n/s/cm^2)
1	12.2e+01	1.49e+01	194.49
2	1.00e+01	1.22e+01	159.71
3	8.18e+00	1.00e+01	147.06
4	6.36e+00	8.18e+00	147.73
5	4.96e+00	6.36e+00	153.39
6	4.06e+00	4.96e+00	150.62
7	3.01e+00	4.06e+00	138.92
8	2.46e+00	3.01e+00	128.43
9	2.35e+00	2.46e+00	125.27
10	1.83e+00	2.35e+00	126.32
11	1.11e+00	1.83e+00	128.94
12	5.50e-01	1.11e+00	116.85
13	1.11e-01	5.50e-01	65.209
14	3.35e-03	1.11e-01	9.1878
15	5.83e-04	3.35e-03	3.7134
16	1.01e-04	5.83e-04	4.0086
17	2.90e-05	1.01e-04	4.2946
18	1.07e-05	2.90e-05	4.4761
19	3.06e-06	1.01e-05	4.5673
20	1.12e-06	3.06e-06	4.5355
21	4.14e-07	1.12e-06	4.3701
22	1.00e-08	4.14e-07	3.7142

5.4.1.6 Quadrature Data

The DORT-PC runs use a 402 direction radially biased set based on the half-symmetric S_{10} set and the 210 direction upward biased set discussed in Reference 5.12. In two-dimensional systems such as that which is used to describe the package, the discrete ordinates method can lead to solutions with flux distortions. This is particularly true in poorly scattering media (such as air and the impact limiter materials) that contain isolated sources. Because the cask structural shell directly adjacent to the top and bottom end fittings exhibits localized high dose rates, flux oscillations could be observed at the one and two meter distances required for this evaluation. The potential for flux oscillations is reduced by using a more detailed, radially biased quadrature set in the top and bottom nozzle source runs. The quadrature data is provided in the DORT-PC input files listed in Section 5.5.4.

5.4.1.7 DORT-PC Input Files

The DORT-PC input files are included in Section 5.5.4. The DORT-PC input parameters are discussed in the preceding sections for the twelve normal operation and hypothetical accident runs. DORT-PC is run using the quadrature sets described above and a P_3 order of scattering.

5.4.1.8 Evaluation of Cask Penetrations

Several penetrations exist through the NUHOMS®-MP187 Cask shielding. These include the upper and lower trunnions, the shear key, the test ports, and the drain and vent ports. An evaluation of the impact of these penetrations on the shielding effectiveness of the cask is provided in this section.

5.4.1.8.1 Upper Trunnions

The NUHOMS®-MP187 cask upper trunnion sleeve extends through the neutron shield and partially into the lead gamma shield as shown in Figure 5.4-2. The trunnion sleeve contains a plug during transportation that provides gamma and neutron shielding. The effect of the trunnion on the cask shielding analysis is assessed as described below.

The computer program ANISN-ORNL [5.13] is used to calculate the dose rate on the surface of the cask neutron shield panel in the center of the in-core region. ANISN is run using the same cross-section and flux-to-dose data as was used in the DORT-PC runs. The ANISN results are used as a "base case" for the evaluations and to provide information regarding the angular distribution of the neutrons and gamma-rays as they exit the cask surface.

Two additional ANISN-ORNL runs are made to estimate the dose rates on the face of the trunnion. The geometries used in these runs are shown in Figure 5.4-2. Models have been generated for both the trunnion sleeve and the trunnion plug. Although the skid is present during all normal operating transport conditions, no credit has been taken for shielding of the trunnions by the skid. Table 5.4-4 summarizes the results of the ANISN runs.

Table 5.4-4

ANISN Results for Trunnion Models

Case	Neutron (mrem/hr)	Gamma (mrem/hr)
Base	18.32	24.24
Sleeve	95.20	3.406
Plug	15.42	11.31

The dose rates on the surface of the trunnion are calculated for both the FC-DSC and FO-DSC in the following manner: (1) The neutron and gamma dose rates on the cask surface at each interval are taken from the DORT results; (2) These dose rates are scaled by the ratio of the ANISN results (see Table 5.4-4) for the case evaluated to the results from the base case; (3) The neutron and gamma dose rates are summed to calculate the total surface dose rate; and (4) Manual calculations are performed as described below to calculate dose rates on the transport vehicle outer surface and 2 meters from that surface. Because the surface dose rate is calculated at each interval in the trunnion region, axial variations in both source and geometry have been considered.

Table 5.4-5 shows the neutron and gamma dose rates calculated at the surface of the trunnions for the FC-DSC payload. The "interval" and "midpoint" refer to the axial location of the interval in the DORT model of the cask. For both neutrons and gammas, the DORT calculated dose rate on the package surface is listed. The sleeve and plug dose rates are calculated by multiplying the

DORT dose by the result from the appropriate ANISN run (Table 5.4-4) and dividing by the base case dose. The maximum surface dose rate on the trunnion is 160.2 mrem/hr at interval 128. Similar results for the FO-DSC are shown in Table 5.4-6 (FO-DSC peak is 237.1 mrem/hr).

Table 5.4-5

FC-DSC Trunnion Surface Dose Rates

Interval	Midpoint (cm)	Neutron (mrem/hr) DORT	Sleeve	Plug	Gamma (mrem/hr) DORT	Sleeve	Plug
117	381.96	16.820	87.383		13.442	1.889	
118	387.03	15.982	83.031		12.585	1.769	
119	393.70	15.155	78.732	12.754	11.807	1.659	5.508
120	398.47	14.769	76.729	12.430	11.281	1.585	5.263
121	401.96	14.666	76.194	12.343	10.731	1.508	5.006
122	405.45	14.784	76.807	12.442	10.162	1.428	4.741
123	409.58	15.075	78.318	12.687	9.556	1.343	4.458
124	413.71	15.614	81.119	13.141	9.098	1.279	4.245
125	416.16	16.185	84.084	13.621	8.696	1.222	4.057
126	418.06	17.338	90.074	14.591	8.294	1.166	3.869
127	420.69	20.889	108.524		7.465	1.049	
128	423.86	30.688	159.434		5.790	0.814	

Table 5.4-6

FO-DSC Trunnion Surface Dose Rates

Interval	Midpoint (cm)	Neutron (mrem/hr) DORT	Sleeve	Plug	Gamma (mrem/hr) DORT	Sleeve	Plug
116	380.69	20.026	104.039		6.317	0.888	
117	388.94	18.829	97.820		5.907	0.830	
118	394.53	18.003	93.531	15.151	5.534	0.778	2.582
119	401.20	17.510	90.971	14.737	5.254	0.738	2.451
120	405.45	17.494	90.886	14.723	5.146	0.723	2.401
121	408.75	17.656	91.725	14.859	5.043	0.709	2.353
122	412.05	17.914	93.070	15.077	4.965	0.698	2.316
123	416.37	19.502	101.319	16.413	4.788	0.673	2.234
124	420.69	24.111	125.261		4.449	0.625	
125	422.64	29.001	150.666		4.118	0.579	
126	423.50	32.775	170.273		3.776	0.531	
127	424.37	38.613	200.606		3.387	0.476	
128	425.09	45.555	236.671		3.002	0.422	

To calculate the contributions from the trunnions to the vehicle surface and 2 meter dose rates, cosine power functions, $Cos^n(\theta)$, are fit to the neutron and gamma ray angular data. As shown in Figure 5.4-3, the neutron angular flux distribution can be approximated by a $Cos(\theta)$ function and the gamma-ray angular flux distribution can be approximated by a $Cos^6(\theta)$ function. Note that the $Cos(\theta)$ fit for the neutron distribution is more sharply peaked than the data. This will result in a conservative estimate of the neutron dose rate two meters from the vehicle surface.

The neutron and gamma surface "delta dose" (the difference between the DORT calculated dose and the trunnion sleeve/plug dose at a radius of 46.25 in) is calculated for each trunnion interval. Negative delta doses result from DORT model results which exceed those of the trunnion sleeves and plugs. A point kernel approximation is used to calculate the delta dose at the vehicle surface and 2 meters from the vehicle surface. For a $Cos(\theta)$ angular distribution, the dose rate at a distance R from a source point is given by,

$$S = \frac{S_o \cdot Cos(\theta) \cdot A}{\pi R^2}$$

Where S_O is the surface delta dose, θ is the angle to the detector relative to the surface normal, and A is the area assigned to the source point. The corresponding equation for a $Cos^6(\theta)$ distribution is,

$$S = \frac{7S_o \cdot Cos^6(\theta) \cdot A}{2\pi R^2}$$

The trunnion sleeves are divided into rectangular regions corresponding to the DORT intervals as shown in Figure 5.4-4, which also shows the location of the trunnions relative to the active fuel region. The height of each region is equal to the difference in height between the sleeve radius (10 inches) and the plug radius (6 inches) at the midpoint of the interval. The contribution from each rectangular region to each trunnion interval (as reported in Table 5.4-5 and Table 5.4-6 for the FC-DSC and FO-DSC, respectively) at the vehicle surface and at a distance of 2 meters from the vehicle surface is calculated using the above equations and summed. Note that because the plug surface doses are less than those on the surface of the neutron shield, the plugs have been neglected from this calculation.

For each trunnion interval in the FC-DSC model, Table 5.4-7 shows the calculated vehicle surface dose rates, the delta dose due to the presence of the trunnions, and the total dose rate including both the DORT results and the trunnion contribution. Corresponding results for the 2-meter dose rates are provided in Table 5.4-8. The package surface, vehicle surface, and 2-meter dose rates, including the trunnion contributions, are included in the results presented in Section 5.4.2.

Table 5.4-7

Trunnion Dose Calculations on the Vehicle Surface

FC-DSC Results:

	Midpoint	Neutron (mrem/hr)			Gamma (mrem/hr)		
Interval	(cm)	DORT	Trunnion Δ	Total	DORT	Trunnion Δ	Total
117	381.96	17.237	9.779	27.016	7.528	-2.893	4.635
118	387.03	17.455	10.625	28.080	7.233	-3.226	4.007
119	393.70	18.524	11.461	29.985	6.770	-3.338	3.432
120	398.47	19.685	11.840	31.525	6.360	-3.232	3.128
121	401.96	19.994	11.997	31.991	6.050	-3.099	2.951
122	405.45	20.159	12.052	32.211	5.865	-2.942	2.923
123	409.58	20.289	11.980	32.269	5.637	-2.743	2.894
124	413.71	20.648	11.754	32.402	5.326	-2.527	2.799
125	416.16	20.324	11.545	31.869	4.939	-2.388	2.551
126	418.06	20.504	11.344	31.848	4.677	-2.273	2.404
127	420.69	20.590	11.013	31.603	4.499	-2.103	2.396
128	423.86	19.374	10.535	29.909	4.295	-1.879	2.416

FO-DSC Results:

	Midpoint	Neutron (mrem/hr)			Gamma (mrem/hr)		
Interval	(cm)	DORT	Trunnion Δ	Total	DORT	Trunnion Δ	Total
116	380.69	18.418	12.379	30.797	3.566	-1.620	1.946
117	388.94	19.406	13.757	33.163	3.450	-1.767	1.683
118	394.53	20.832	14.327	35.159	3.319	-1.723	1.596
119	401.20	21.885	14.625	36.510	3.092	-1.598	1.494
120	405.45	21.619	14.604	36.223	2.963	-1.510	1.453
121	408.75	22.189	14.473	36.662	2.988	-1.441	1.547
122	412.05	22.822	14.237	37.059	2.941	-1.369	1.572
123	416.37	22.377	13.765	36.142	2.673	-1.262	1.411
124	420.69	22.581	13.105	35.686	2.457	-1.131	1.326
125	422.64	21.824	12.750	34.574	2.405	-1.064	1.341
126	423.50	21.115	12.583	33.698	2.368	-1.033	1.335
127	424.37	20.897	12.407	33.304	2.328	-1.001	1.327
128	425.09	19.788	12.257	32.045	2.257	-0.973	1.284

Table 5.4-8

Trunnion Dose Calculations 2 Meters from the Vehicle Surface

FC-DSC Results:

	Midpoint	Neutron (mrem/hr)			Gamma (mrem/hr)		
Interval	(cm)	DORT	Trunnion Δ	Total	DORT	Trunnion Δ	Total
117	381.96	4.867	0.476	5.343	2.299	-0.198	2.101
118	387.03	4.939	0.478	5.417	2.235	-0.200	2.035
119	393.70	5.051	0.480	5.531	2.159	-0.201	1.958
120	398.47	5.095	0.481	5.576	2.109	-0.202	1.907
121	401.96	5.023	0.482	5.505	2.082	-0.202	1.880
122	405.45	4.877	0.482	5.359	2.065	-0.201	1.864
123	409.58	4.741	0.482	5.223	2.038	-0.200	1.838
124	413.71	4.678	0.481	5.159	2.005	-0.199	1.806
125	416.16	4.664	0.480	5.144	1.982	-0.198	1.784
126	418.06	4.632	0.480	5.112	1.962	-0.197	1.765
127	420.69	4.542	0.477	5.019	1.932	-0.196	1.736
128	423.86	4.441	0.477	4.918	1.899	-0.194	1.705

FO-DSC Results:

	Midpoint	Neutron (mrem/hr)			Gamma (mrem/hr)		
Interval	(cm)	DORT	Trunnion Δ	Total	DORT	Trunnion Δ	Total
116	380.69	4.921	0.588	5.509	1.060	-0.106	0.954
117	388.94	5.064	0.592	5.656	1.020	-0.107	0.913
118	394.53	5.148	0.594	5.742	0.993	-0.108	0.885
119	401.20	5.085	0.595	5.680	0.973	-0.108	0.865
120	405.45	4.916	0.595	5.511	0.966	-0.108	0.858
121	408.75	4.804	0.595	5.399	0.960	-0.107	0.853
122	412.05	4.761	0.594	5.355	0.955	-0.107	0.848
123	416.37	4.681	0.592	5.273	0.939	-0.106	0.833
124	420.69	4.543	0.590	5.133	0.917	-0.105	0.812
125	422.64	4.469	0.589	5.058	0.905	-0.104	0.801
126	423.50	4.448	0.589	5.037	0.899	-0.104	0.795
127	424.37	4.431	0.588	5.019	0.894	-0.104	0.790
128	425.09	4.410	0.588	4.998	0.891	-0.103	0.788

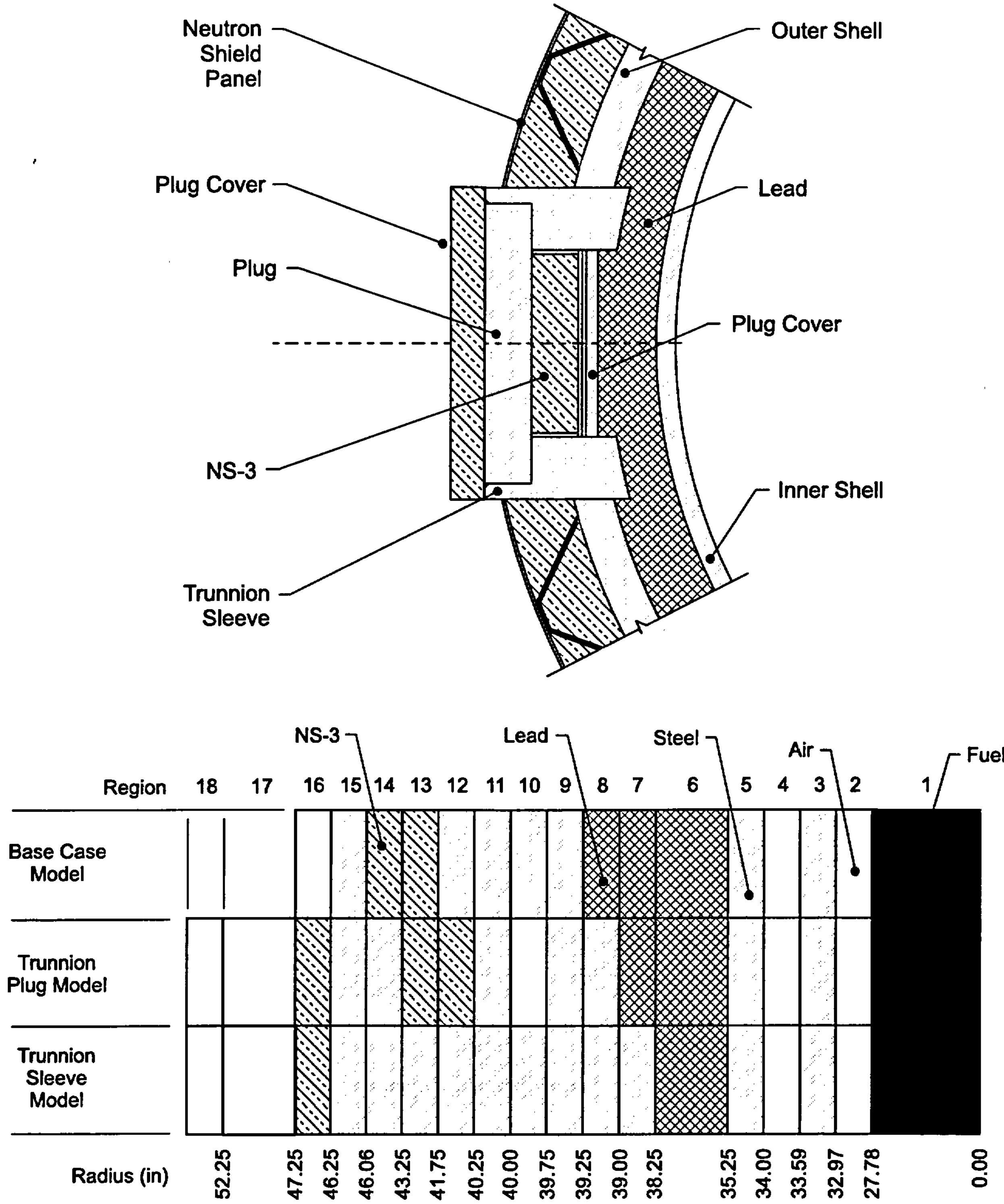

Figure 5.4-2

NUHOMS®-MP187 Cask Upper Trunnion Geometry

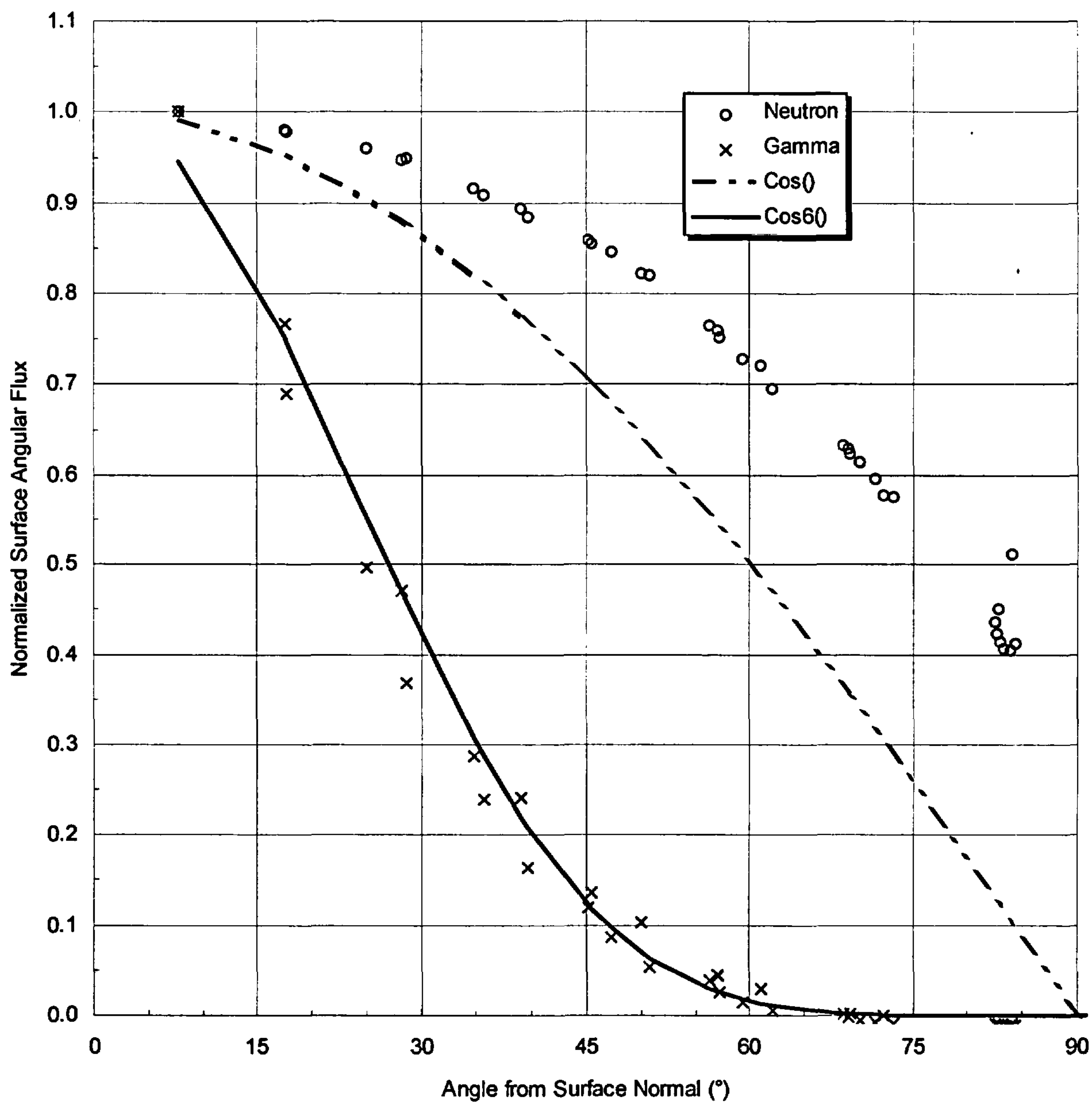

Figure 5.4-3

Neutron and Gamma-Ray Angular Distributions on the Cask Surface

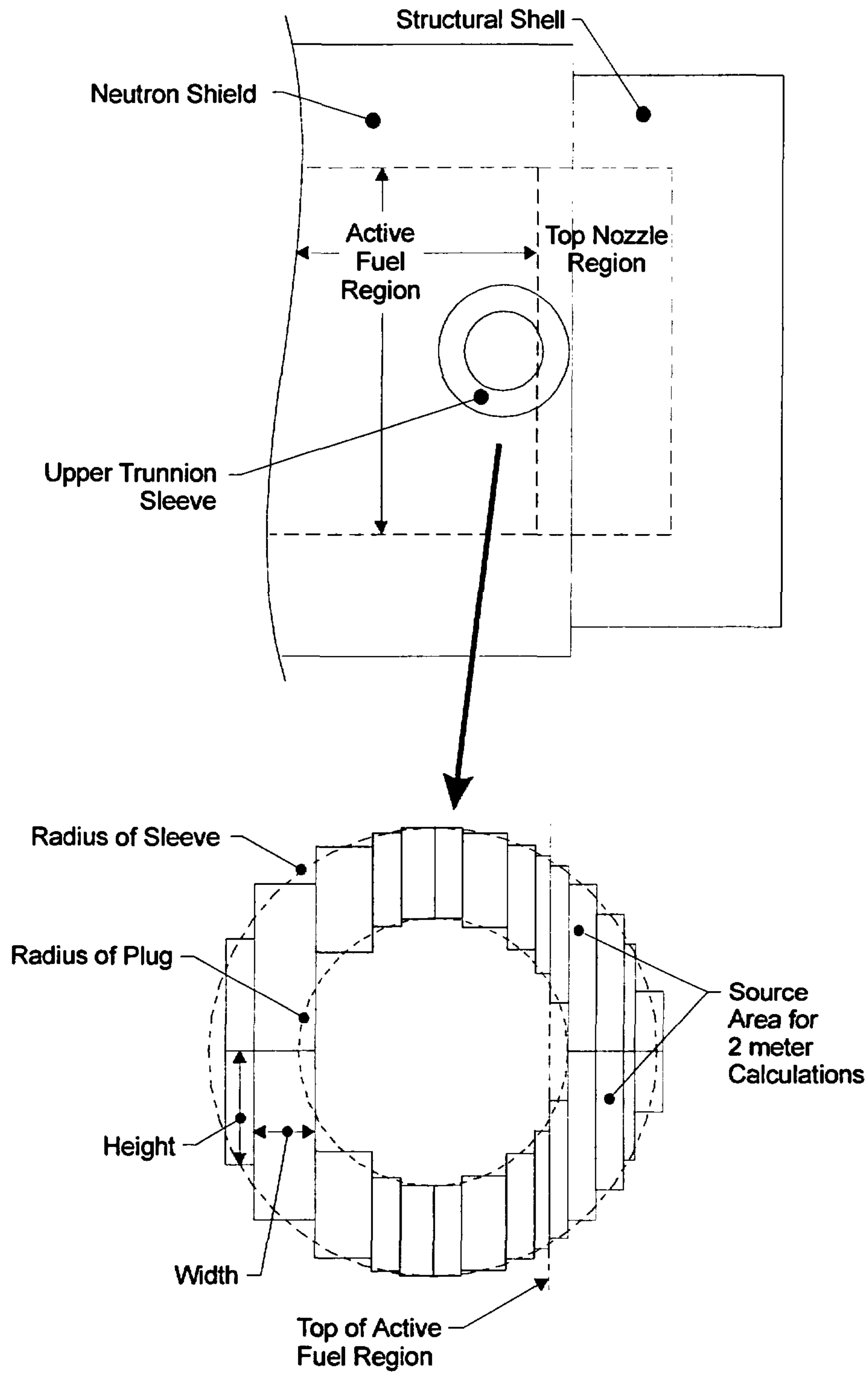

Figure 5.4-4

Source Geometry Used in Trunnion Manual Dose Calculations

5.4.1.8.2 Lower Trunnions

The lower trunnions are located below the cask neutron shield and displace only the impact limiter honeycomb. Because the lower trunnions provide shielding superior to that of the honeycomb, the lower trunnions serve to reduce the package dose rates.

5.4.1.8.3 Shear Key

The cask shear key opening extends through the cask neutron shield. The shear key opening is underneath the cask during transportation and is shielded by the shear key itself, the cask support skid, and the railcar. Although the dose rate on the underside of the vehicle is expected to be well below the applicable limits, an analysis similar to that performed for the upper trunnions is provided below to demonstrate compliance with the 200 mrem/hr limit of 10CFR71.47(b)(2).

The ANISN-ORNL [5.13] code is used to estimate the dose rates in the vicinity of the shear key. The models and assumptions are similar to those described in Section 5.4.1.8.1. The geometry in the region of the shear key, including the cask, skid, and shear key is shown in Figure 5.4-5. The base case model from Section 5.4.1.8.1 is used for comparison to the cask dose rates calculated in the DORT runs described in Section 5.4.1. Three additional ANISN runs, using the geometries shown in Figure 5.4-5, are used to estimate one-dimensional dose rates through the 1.5 inch thick plate, through the shear key sleeve, and through the shear key itself.

The ANISN models assume that the skid is directly adjacent to the neutron shield panels. The skid is composed of two plates, 1.5 inches thick, assembled as shown in Figure 5.4-5 with a total box thickness of 18 inches. The shear key fills the cask shear key opening with the exception of a 0.25 inch thick gap at the top. The shear key is located with its centerline 100.75 inches from the cask bottom and its axial thickness is six inches. No credit is taken for the railcar deck or structures.

The dose rates at the bottom of the skid in the vicinity of the shear key are calculated for each of the three models in the following manner: (1) The maximum neutron and gamma dose rates on the cask surface at the axial location of the shear key are taken from the DORT results; (2) These dose rates are scaled by the ratio of the ANISN results for the case evaluated to those from the base case; and (3) The neutron and gamma dose rates are summed to calculate the total dose rate. This calculation, therefore, accounts for axial variations in both source and geometry.

The results of the shear key analysis are shown in Table 5.4-9. The peak calculated dose rate, due to streaming through the shear key sleeve, is 190.3 mrem/hr, about 5% less than the limit of 200 mrem/hr. Note that there are several significant conservatisms in this calculation. The ANISN models are one-dimensional, assuming that the modeled geometry exists over 360° of the cask surface. The shear key sleeve is actually only three inches wide and as shown in Table 5.4-9, the dose rates on either side of the sleeve are only about 20 mrem/hr. The railcar is completely neglected in this calculation and the space between the cask and the skid has been ignored.

Table 5.4-9

Shear Key Dose Rate Results

	DORT Result (D) (mrem/hr)		Base Case (B) (mrem/hr)		ANISN Result (A) (mrem/hr)		Total (D*A/B)
Location	Neutron	Gamma	Neutron	Gamma	Neutron	Gamma	(mrem/hr)
Plate	28.85	18.26	18.32	24.24	13.46	0.58	21.63
Sleeve	28.85	18.26	18.32	24.24	120.6	0.51	190.3
Shear Key	28.85	18.26	18.32	24.24	10.48	0.058	16.55

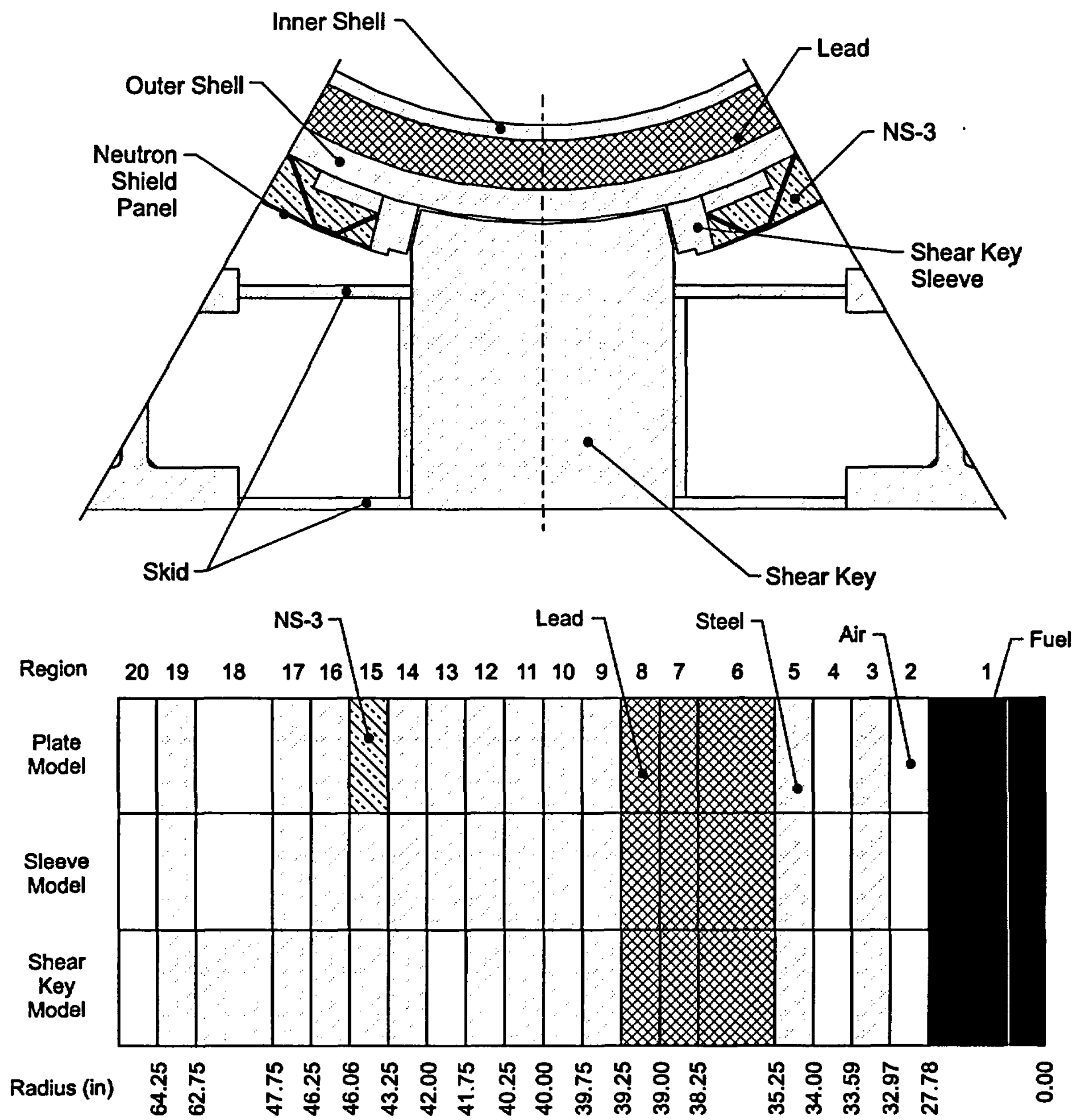

Figure 5.4-5

NUHOMS®-MP187 Cask Shear Key Geometry and ANISN Models

5.4.1.8.4 Cask Test and Drain/Vent Ports

The cask test, drain, and vent ports extend through the steel top and bottom covers and bottom forging. Because these ports are shielded by steel plugs that effectively fill the ports during shipment, no further analysis is required.

5.4.1.8.5 DSC Shield Plug Geometry

The geometry of the FC-DSC shield plug used in the shielding models differs from that shown on the drawings in Chapter 1. The differences include the thickness of the lead shielding, the steel plate thicknesses, and the addition of steel stiffeners in the lead. The FC-DSC DORT models described in Section 5.4.1.3 have been modified as described below to conservatively model these changes to the shield plug in order to demonstrate that the analysis presented in this Chapter remains bounding for the MP187 Package.

A comparison of the modeled geometry versus that shown on the drawings is provided in Table 5.4-10. The total thickness of both shield plugs is identical in the models and on the drawings. The total steel thickness in the bottom shield plug has been reduced from 2.50 inches to 2.25 inches, with a corresponding increase in the lead thickness of 0.25 inches. Similarly, the total steel thickness in the top shield plug has been reduced 0.12 inches with a 0.12 inch increase in the lead thickness. In both cases, however, stiffeners have been provided which extend through the lead shielding. As shown on the drawings, the stiffeners have been angled to eliminate direct shine paths through the plug but still represent a reduction in the effective lead thickness.

The FC-DSC DORT models have been modified to incorporate the thicknesses shown on the drawings. Additionally, a one inch thick portion of the lead shielding has been replaced with steel to account for the presence of the stiffeners (the actual axial thickness of the stiffeners is 0.86 inches) and a steel annulus representing the grappling ring has been included in the bottom shield plug. A sample modified DORT input file is provided in Section 5.5.4. Note that the DORT model conservatively assumes that the reduction in lead thickness occurs over the entire radius of the shield plug. The actual geometry of the stiffeners will limit this reduction to a few localized areas.

Table 5.4-10

FC-DSC Shield Plug Geometry Comparison

Parameter	Modeled Geometry (Section 5.4.1.3)	Drawing Geometry (Chapter 1)
DSC Bottom End		
Outer Cover Thickness	1.75 in	0.75 in
Lead Thickness	3.50 in	3.75 in
Inner Cover Thickness	0.75 in	1.50 in
Stiffeners	not modeled	included
Grapple Ring	not modeled	penetrates lead
DSC Top End		
Plug Bottom Casing	0.75 in	0.50 in
Lead Thickness	4.00 in	4.12 in
Plug Top Casing	0.25 in	0.38 in
Stiffeners	not modeled	included

The dose rates calculated by the modified DORT input files show an increase in the peak gamma dose rates on the cask ends, as is expected due to the reduction in lead shielding. The greatest increase occurs on the cask bottom surface in the grapple ring region. The gamma dose rate at this location increased from 0.64 mrem/hr to 0.75 mrem/hr. However, the peak total (neutron plus gamma) dose rates for the Package side, top, and bottom remain below those calculated using the geometry described in Section 5.4.1.3.

This result is consistent with expectations because: (1) The peak side dose rates are unaffected by changes in the shield plug design provided the total thickness is unchanged; (2) The neutron dose rate, which is the primary contributor to the peak top and bottom dose rates, is reduced by replacing lead with steel; and (3) The peak top and bottom dose rates occur outside the cask body radius and are due primarily to contributions from the cask side which are shielded only by the impact limiters. Because the peak dose rates on all Package surfaces are unchanged, the model described in Section 5.4.1.3 calculates dose rates which bound those for the shield plug design shown on the drawings. The average lead thickness specified on the drawing notes has been selected to correspond to the shielding analysis described in Section 5.4.1.3.

5.4.1.8.6 Shielding Uncertainty Evaluation

The purpose of this calculation is to evaluate the impact of several uncertainties present in the shielding calculations presented in this Chapter. This evaluation demonstrates that the overall impact of these uncertainties will not affect the conclusions of the shielding analysis presented in Section 5.4.2.

As stated in Section 5.3.1, the MP187 shielding calculations are based on nominal cask dimensions. This represents a potential non-conservatism in that shielding thicknesses less than those used in the analysis may exist in fabricated packages while still complying with the tolerances shown on the drawings. The 1-D discrete-ordinates computer code ANISN [5.13] is used to calculate the potential dose rate increase associated with assuming each shielding layer is at its minimum acceptable material thicknesses. This calculation is performed on the cask side surface during normal operations which is the location and configuration associated with the bounding dose rates for the MP187 cask.

There are also several conservatisms in the MP187 shielding calculations which are listed in Section 5.1. These include an overprediction of the quantity of ^{154}Eu present in the fuel assemblies, neglecting the shielding of control components by the fuel assemblies, and neglecting half of the boron in the neutron shield. The value of each of these conservatisms will be quantified by making modifications to the computer runs provided in the Appendices. By summing the effects of these conservatisms and the tolerance calculation, this evaluation shows that the analyses provided in this Chapter fully support the design, including tolerances, of the NUHOMS®-MP187 cask. Additional conservatisms in the shielding models remain and are listed below as well.

This calculation determines correction factors for both neutron and gamma-ray dose rates based on a 1-D radial slice through the cask midplane. These correction factors are assumed to apply to the neutron and gamma, package surface, vehicle surface and two meter, side doses reported in Section 5.4.2. The cask ends are not evaluated because the dose rates at these locations are at least an order of magnitude less than the applicable limit. For example, if the average lead thickness specified on the drawing notes are reduced by the allowed tolerance (0.06 inches), the increase in the dose rates at the ends of the cask are less than 10% assuming the half value layer for lead from a Co-60 source is 12 mm. Finally, because the peak accident dose rates result from gaps in the lead due to drop loads (lead slump), the cask tolerances (particularly the lead tolerance) will not significantly affect the accident dose rates.

(A) Tolerances

The effect of tolerances (i.e. minimum allowed shielding thicknesses) on the MP187 dose rates has been determined by performing a 1-D, radial shielding analysis through the cask neutron shield. This location was selected because the bounding dose rates (those closest to the 10CFR71.47 limits) occur on the cask side and because this cask section includes each of the cask layers. The base ANISN computer model described in Section 5.4.1.8.1 was modified to include the minimum material thicknesses as shown on the drawings provided in Chapter 1.

The modified ANISN computer run, provided in Section 5.5.5, calculates maximum MP187 dose rates based on the minimum dimensions allowed by the drawings. The neutron and gamma dose rates on the surface of the cask calculated by this run are shown in Table 5.4-11, as are the corresponding results from the base run and the fractional dose rate increases due to the minimum shielding dimensions.

Table 5.4-11

Tolerance Evaluation Results

	ANISN Base	ANISN Tolerance	Fractional Change (tol/base)
Neutron	18.32	18.85	1.029
Gamma	24.24	31.94	1.318

As shown below, there is sufficient margin in the FO-DSC calculations to support this potential increase with no additional analysis:

Package Surface: $(0.42\gamma)(1.318) + (236.7n)(1.029) = 244.1$ mrem/hr is less than 1000

Vehicle Surface: $(2.24\gamma)(1.318) + (40.2n)(1.029) = 44.3$ mrem/hr is less than 200

2 Meter: $(1.31\gamma)(1.318) + (6.34n)(1.029) = 8.3$ mrem/hr is less than 10

However, because there is little margin in the existing FC-DSC results, additional evaluations have been performed as described below to demonstrate that existing conservatisms in the calculations fully offset the increase in dose rates related to minimum material thicknesses.

(B) Photon Source Term

As described in Section 5.2, the ORIGEN2 code [5.3] was used to calculate all neutron and gamma source terms for the MP187 shielding analysis. The ORIGEN2 cross section libraries are based primarily on ENDF/B-IV data. More recent cross-section data (ENDF/B-VI) has significantly revised the production rate of ^{154}Eu - an important contributor to the gamma-ray dose rates. Several references have documented this overprediction of the ^{154}Eu inventory. Reference [5.16], Section 5.4 states (TN clarifications in brackets), "the percentage difference for isobar 154 (^{154}Sm+^{154}Eu+^{154}Gd) is 30.8% using ENDF/B-V Eu data [similar to the ORIGEN2 data for Eu] and -2.1% using ENDF/B-VI data. This change is due to comparable [relative to a similar change for isobar 155] structural variations [the addition of resonances in ENDF/B-VI that result in greater depletion of Eu during operation]in the ^{154}Eu data in the two libraries."

Reference [5.17], Section 5 states, "These Eu isotopes are important for both spent fuel source terms and burnup credit applications, and major updates were made in the ENDF/B-VI evaluation. The effect of these cross-section changes was enhanced ^{154}Eu capture and, hence, decreases of some 30 to 40% in the ^{154}Eu inventories in the spent fuel." To address the impact of this ^{154}Eu overprediction, an additional 1-D ANISN run was made, using a source term which reduces the contribution due to ^{154}Eu by 30%.

Table 5.4-12 lists the design basis (FO) in-core source term as well as the ^{154}Eu contribution to that source. The ^{154}Eu contribution is taken directly from the fission product photon data in the ORIGEN2 output. Following the methodology described in Section 5.2.1, the design basis control component source is added to the revised FO source and the result is converted to a volumetric source, in the CASK-81 format required by the ANISN model.

Table 5.4-12

Calculation of Corrected Assembly Source Term

ORIGEN Group	Mean Energy (MeV)	In-Core (γ/sec/assy)	^{154}Eu (γ/sec/assy)	30% ^{154}Eu (γ/sec/assy)	Revised In-Core (γ/sec/assy)
1	0.010	8.441E+14	1.227E+13	3.681E+12	8.404E+14
2	0.025	1.703E+14	1.810E+12	5.430E+11	1.697E+14
3	0.038	2.167E+14	1.669E+13	5.007E+12	2.117E+14
4	0.058	1.770E+14	4.478E+12	1.343E+12	1.756E+14
5	0.085	9.495E+13	0.000E+00	0.000E+00	9.495E+13
6	0.125	8.705E+13	2.728E+13	8.184E+12	7.887E+13
7	0.225	7.949E+13	5.637E+12	1.691E+12	7.779E+13
8	0.375	3.371E+13	8.982E+11	2.695E+11	3.344E+13
9	0.575	1.459E+15	0.000E+00	0.000E+00	1.459E+15
10	0.850	4.841E+13	3.191E+13	9.573E+12	3.883E+13
11	1.250	6.239E+13	3.533E+13	1.060E+13	5.179E+13
12	1.750	1.186E+12	1.059E+12	3.177E+11	8.684E+11
13	2.250	3.839E+08	0.000E+00	0.000E+00	3.839E+08
14	2.750	3.094E+08	0.000E+00	0.000E+00	3.094E+08
15	3.500	2.136E+07	0.000E+00	0.000E+00	2.136E+07
16	5.000	7.839E+06	0.000E+00	0.000E+00	7.839E+06
17	7.000	9.037E+05	0.000E+00	0.000E+00	9.037E+05
18	9.500	1.038E+05	0.000E+00	0.000E+00	1.038E+05
	Total	3.274E+15	1.374E+14	4.121E+13	3.233E+15

The modified ANISN computer run, provided in Section 5.5.5, calculates maximum MP187 dose rates based on the corrected source term provided in Table 5.4-12. The neutron and gamma dose rates on the surface of the cask calculated by this run are shown in Table 5.4-13, as are the corresponding results from the base run and the fractional dose rate decreases due to the corrected source term.

Table 5.4-13

Photon Source Evaluation Results

	ANISN Base	ANISN ^{154}Eu	Fractional Change (Eu/base)
Neutron	18.32	18.32	1.000
Gamma	24.24	22.89	0.944

(C) <u>FC-DSC Source Self-Shielding</u>

The shielding analysis described in Section 5.4 assumes a uniform, "smeared" source. This uniform source includes both the fuel assemblies as well as the control components stored within the assemblies. However, because the control components are stored inside the assemblies, the activated control component rods are shielded by two or more rows of fuel pins. The uniform source model, therefore, underpredicts the shielding of the control components by the fuel assemblies.

As shown in Section 5.4.2, the calculated peak surface gamma dose rate for the FC-DSC exceeds that of the FO-DSC by a factor of 2.15 (both peaks occur near the center of the active fuel region). The only difference between these two calculations is the inclusion of the control component source terms and number densities in the FC-DSC model. The large increase in dose rate for the FC-DSC is due primarily to the large control component source at 1.25 MeV, which is the photon energy group that contributes the greatest amount to the cask dose rates. The fuel source at 1.25 MeV is 6.24×10^{13} γ/s/assy while the gray APSRA source is 1.44×10^{14} γ/s/assy. The actual increase in dose rate due to the presence of control components is calculated below by modifying the MCNP [5.7] model described in Section 5.4.1.2.

One MCNP run is made to calculate the gamma dose rate on the surface of the DSC (the DSC is used rather than the cask surface to improve the monte-carlo statistics - this same technique was used in Section 5.4.1.2) using only the fuel pin source in each fuel assembly. A second run was made using only the control component source. This pin-by-pin model places the 16 control component rods in the appropriate locations in the 15x15 assembly array (for each assembly) to correctly calculate the dose rate contribution from the control components. These runs are provided in Section 5.5.3 and the model geometry is shown in Figure 5.4-6.

Figure 5.4-6
Source Self-Shielding Geometry

The calculated fuel-only dose rate on the surface of the DSC shell is 4.067×10^6 mrem/hr and the control component only dose rate on the surface of the DSC shell is 1.216×10^6 mrem/hr. The total (fuel plus APSRA) dose rate on the DSC shell is then:

$$4.067 \times 10^6 + 1.216 \times 10^6 = 5.283 \times 10^6 \text{ mrem/hr}$$

The FC-DSC gamma dose rate is, therefore, expected to exceed the FO-DSC gamma dose rate by a factor of $(5.283 \times 10^6)/(4.067 \times 10^6) = 1.299$. The gamma dose rates on the side of the MP187 cask, as calculated by DORT using a homogenized source, can be factored by $1.299/2.15 = 0.604$ to account for shielding of the control components by the fuel rods. Note that the FC-DSC control component analysis is based on gray axial power shaping rods. Although the analysis assumes 24 such components, B&W plants typically only have eight onsite.

(D) Neutron Shield Materials

As discussed in Section 0, the MP187 shielding calculations take credit for only 50% of the minimum acceptable boron concentration specified for the neutron shield. NRC practice for criticality analyses, which have a greater safety impact than shielding calculations, has been to allow 75% credit for boron in fixed neutron absorbers. This 75% value has been used for the absorber sheets in the MP187 criticality analysis as well. An additional ANISN run has been made to quantify the conservatism associated with using 50% of the boron loading rather than 75%.

The modified ANISN computer run, provided in Section 5.5.5, calculates maximum MP187 dose rates based on increasing the neutron shield boron loading by a factor of 1.5 (75%/50%) relative to the base model. The revised boron atom density is 1.070×10^{-3} atoms/b·cm. The neutron and gamma dose rates on the surface of the cask calculated by this run are shown in Table 5.4-14, as are the corresponding results from the base run and the fractional dose rate decreases due to the additional boron. These decreases will only be applied to dose rates adjacent to the neutron shield. Note that this result takes credit for only 75% of the boron in the neutron shield and only 90% of the hydrogen, providing additional conservatism.

Table 5.4-14

Neutron Shield Material Evaluation Results

	ANISN Base	ANISN Boron	Fractional Change (boron/base)
Neutron	18.32	18.01	0.983
Gamma	24.24	24.08	0.993

(E) Results and Conclusions

Using the correction factors described above, the revised package surface dose rates for the MP187 package containing an FC-DSC are (neutron and gamma doses at the location representing the peak surface dose rate from the DORT shielding models):

Neutron	(192.95)(1.029) =	198.55 mrem/hr
Gamma	(4.74)(1.318)(0.944)(0.604) =	3.56 mrem/hr
Total		202.11 mrem/hr < 1000 mrem/hr

The revised vehicle surface dose rates are:

Neutron	(51.26)(1.029) =	52.75 mrem/hr
Gamma	(4.30)(1.318)(0.944)(0.604) =	3.23 mrem/hr
Total		55.98 mrem/hr < 200 mrem/hr

The revised vehicle lower external surface dose rates are:

Neutron	(189.92)(1.029) =	195.43 mrem/hr
Gamma	(0.38)(1.318)(0.944)(0.604) =	0.29 mrem/hr
Total		195.72 mrem/hr < 200 mrem/hr

The revised two meter dose rates are:

Neutron	(6.94)(1.029)(0.983) =	7.02 mrem/hr
Gamma	(3.0)(1.318)(0.944)(0.604)(0.993) =	2.24 mrem/hr
Total		9.26 mrem/hr < 10 mrem/hr

As shown above, the package surface and vehicle surface dose rates increase slightly (<3%) while the peak 2 meter dose rate slightly decreases based on the evaluations performed herein. In both cases, the peak dose rate remains within the 10CFR71.47 acceptance criteria. Therefore, because the potential increase in dose rates due to components with below nominal thicknesses is sufficiently offset by the conservatisms in the shielding calculations to maintain dose rates within allowable levels, the MP187 shielding analysis fully supports the cask dimensions, including tolerances.

Additional conservatisms remain in the analysis, including minimum impact limiter thicknesses, minimum initial enrichments used to calculate neutron sources, conservative neutron shield material parameters, and a design basis source which corresponds to a cask heat of 14.3 kW (compared to a limit of 13.5 kW). Also, as discussed in References [5.15] and [5.17], the shielding calculations performed for this cask are expected to be conservative, particularly along the cask side, by 40% to 200% relative to measured doses.

5.4.2 NUHOMS®-MP187 Package Dose Rate Results

The DORT-PC computer run dose rate results are included in Section 5.5.5. The results of each of the four runs are summed node-by-node for both the normal operations and hypothetical accident cases. The dose rates calculated in Section 5.4.1.8.1 are then added, as appropriate, to the maximum normal operation, radial dose rates. The maximum gamma, neutron, and total dose rates at the package side, top, and bottom for the normal operations case are listed in Table 5.4-15. As shown in Table 5.4-15, with the exception of the surface dose rate, the cask dose rates with the FC-DSC bound those with the FO-DSC. Because the FO-DSC surface dose rate peak is due to the penetration of the neutron shield by the trunnion, and because the neutron shield is neglected in the hypothetical accident analysis, the FC-DSC is used in the hypothetical accident calculations as described below. Note that at some locations the sum of the maximum gamma-ray and neutron dose rates does not equal the maximum total dose rate. This implies that the maximum gamma, neutron, and total dose rates occur at different locations around the package. As shown in Table 5.4-15, the 10 CFR Part 71.47 [5.1] limits at the surface of the package, at the surface of the vehicle, and at a distance of two meters from the surface of the vehicle are not exceeded. The limit for occupied locations in the vehicle is met as well because the package top and bottom surface dose rates are less than the two mrem/hr requirement. The packaging therefore provides suitable shielding during normal operating conditions to ship 24 PWR fuel assemblies with sources bounded by those discussed in Section 5.2 in accordance with 10 CFR Part 71.

Table 5.4-15

Summary of Maximum Normal Operation Dose Rates

Package Surface	FC-DSC			FO-DSC		
	Side (mrem/hr)	Top (mrem/hr)	Bottom (mrem/hr)	Side (mrem/hr)	Top (mrem/hr)	Bottom (mrem/hr)
Normal Conditions						
Gamma	1.87E+1	2.18E-1	6.40E-1	8.71E+0	1.31E-1	2.82E-1
Neutron	1.93E+2	6.79E-1	1.31E+0	2.37E+2	6.60E-1	1.01E+0
Total	1.98E+2	8.47E-1	1.62E+0	2.37E+2	7.57E-1	1.18E+0
10 CFR 71 Limit	1.00E+3	1.00E+3	1.00E+3	1.00E+3	1.00E+3	1.00E+3
Vehicle Outer Surface	FC-DSC			FO-DSC		
	Side (mrem/hr)	Top (mrem/hr)	Bottom (mrem/hr)	Side (mrem/hr)	Top (mrem/hr)	Bottom (mrem/hr)
Normal Conditions						
Gamma	1.07E+1	2.18E-1	6.40E-1	4.86E+0	1.31E-1	2.82E-1
Neutron	5.13E+1	6.79E-1	1.31E+0	4.02E+1	6.60E-1	1.01E+0
Total	5.56E+1	8.47E-1	1.62E+0	4.24E+1	7.57E-1	1.18E+0
10 CFR 71 Limit	2.00E+2	2.00E+2	2.00E+2	2.00E+2	2.00E+2	2.00E+2
2 Meters from Vehicle Outer Surface	FC-DSC			FO-DSC		
	Side (mrem/hr)	Top (mrem/hr)	Bottom (mrem/hr)	Side (mrem/hr)	Top (mrem/hr)	Bottom (mrem/hr)
Normal Conditions						
Gamma	3.14E+0	6.46E-2	2.16E-1	1.35E+0	4.20E-2	9.76E-2
Neutron	7.04E+0	3.02E-1	5.39E-1	6.34E+0	2.94E-1	4.28E-1
Total	9.94E+0	3.37E-1	6.72E-1	7.65E+0	3.19E-1	4.97E-1
10 CFR 71 Limit	1.00E+1	1.00E+1	1.00E+1	1.00E+1	1.00E+1	1.00E+1

Note: Peak dose rate on the lower external surface of the vehicle is 190.3 mrem/hr located adjacent to the shear key. Applicable 10CFR71.47 limit is 200 mrem/hr.

The maximum gamma, neutron, and total dose rates at the package side, top, and bottom for the hypothetical accident case are listed in Table 5.4-16. As shown in Table 5.4-16, the 10 CFR Part 71.51 [5.1] limit at a distance of one meter from the surface of the package is not exceeded. The packaging therefore provides suitable shielding during the hypothetical accident conditions to ship 24 PWR fuel assemblies with sources bounded by that discussed in Section 5.2 in accordance with 10 CFR Part 71. Because the hypothetical accident dose rates are less than 50% of the limit while the maximum normal operation dose rates are at the allowable, the normal operation case is bounding for the NUHOMS®-MP187. Because the dose rates are surveyed prior to transport and verified to meet the 10CFR71 and 49CFR173 limits for normal operation, the package will meet all applicable dose limits under both normal and accident conditions.

Table 5.4-16

Summary of Maximum Hypothetical Accident Dose Rates

	Package Surface			1 Meter from Surface of Package		
	Side (mrem/hr)	Top (mrem/hr)	Bottom (mrem/hr)	Side (mrem/hr)	Top (mrem/hr)	Bottom (mrem/hr)
Accident Conditions						
Gamma	1.7E+3	1.2E+1	5.3E+0	1.8E+2	1.7E+0	1.8E+0
Neutron	1.0E+3	8.5E+1	1.6E+2	4.4E+2	3.6E+1	5.8E+1
Total	1.8E+3	8.6E+1	1.6E+2	4.8E+2	3.6E+1	5.9E+1
10 CFR Part 71 Limit	-	-	-	1.0E+3	1.0E+3	1.0E+3

Figure 5.4-7 and Figure 5.4-8 show the total dose rate along the length of the package for normal operations for the FC-DSC and FO-DSC, respectively. Neutron, gamma, and total dose rates are shown at the package surface and at a distance of two meters from the vehicle surface. The total dose rate is also shown along the vehicle surface. The peak dose rates are seen to occur just above and below the neutron shield during normal operations. Peaks which are due to the presence of the trunnions are visible at a height of 200 inches to 210 inches. The package surface dose rate peak for the FC-DSC occurs at the bottom end of the neutron shield, while the peak for the FO-DSC occurs at the upper trunnion. This difference is due to the fact that the active fuel region (neutron source) is closer to the trunnion with the FO-DSC than it is for the FC-DSC.

The dose rates in the vicinity of the shear key are not shown since they exist underneath the transport vehicle. The hypothetical accident dose rates are shown in Figure 5.4-9. The peak dose rates during the hypothetical accident occur due to streaming through the postulated gaps in the lead shielding.

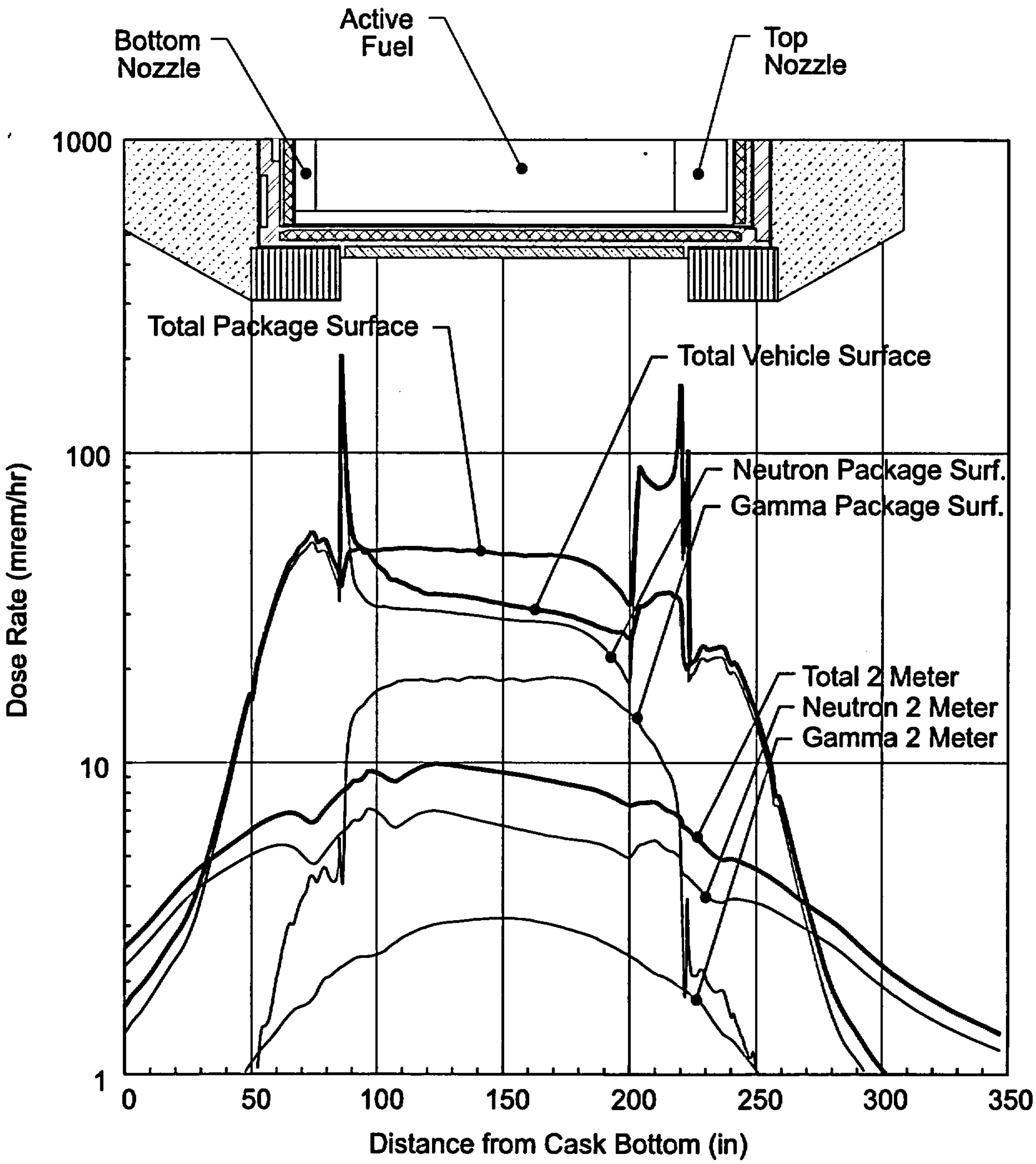

Figure 5.4-7

NUHOMS®-MP187 FC-DSC Normal Operation Dose Rate Distribution

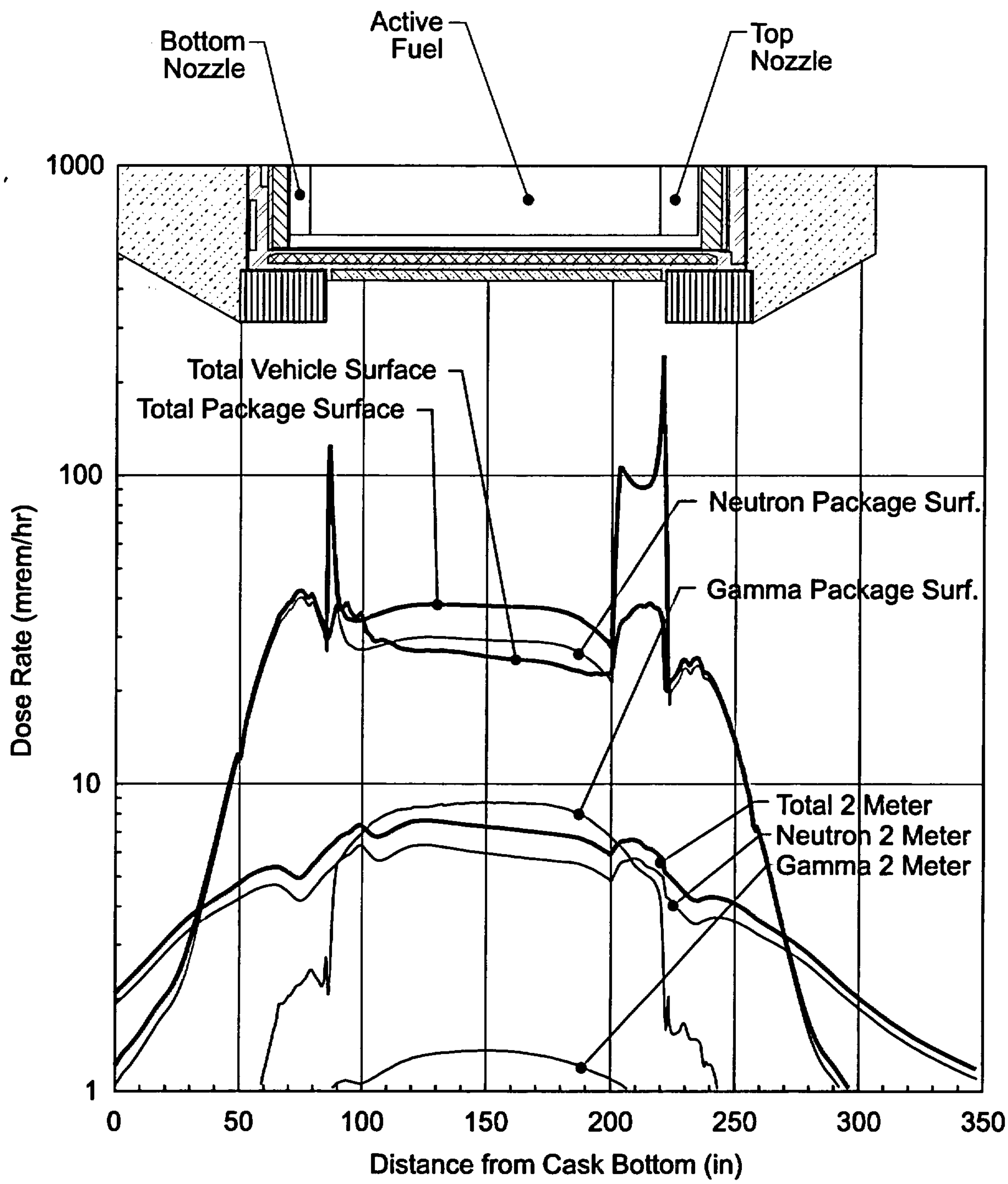

Figure 5.4-8

NUHOMS®-MP187 FO-DSC Normal Operation Dose Rate Distribution

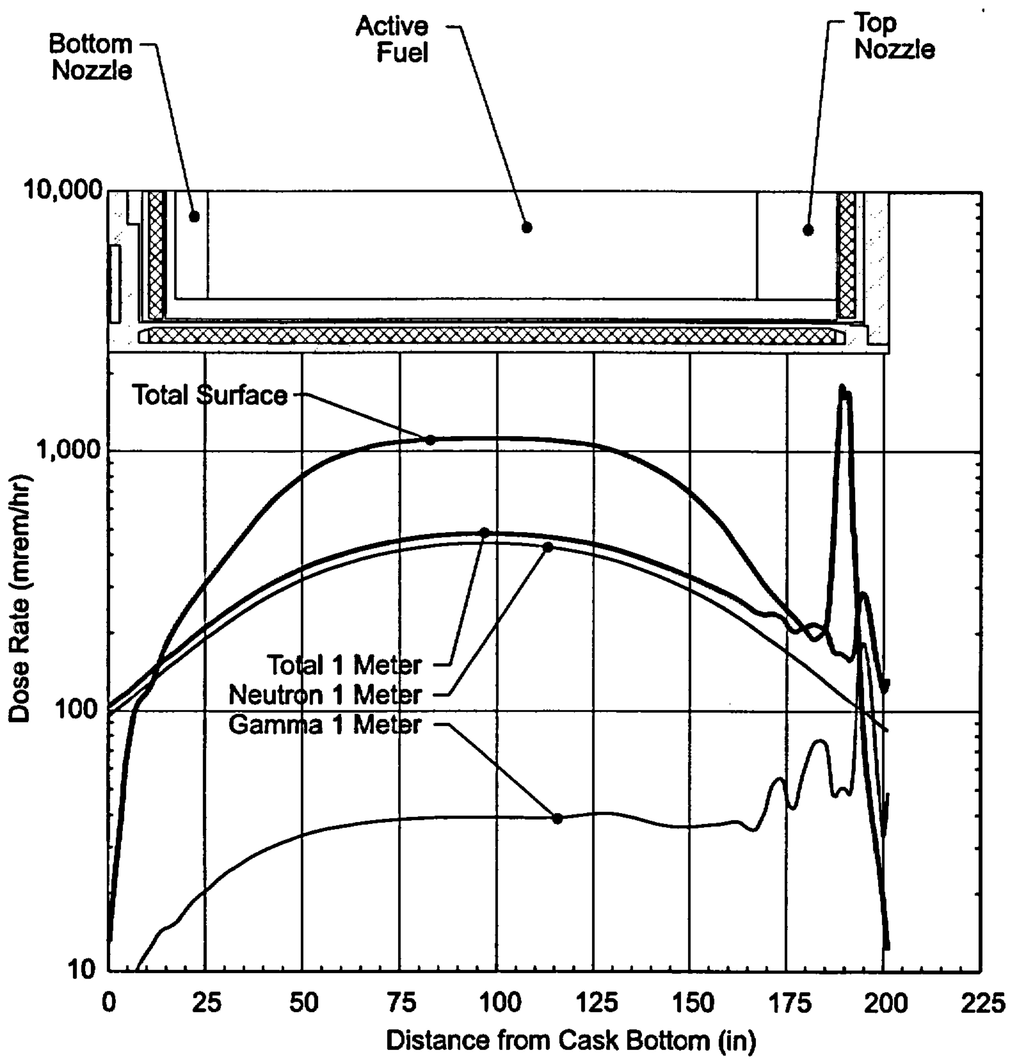

Figure 5.4-9

NUHOMS®-MP187 Hypothetical Accident Dose Rate Distribution

5.5 Appendix

5.5.1 References

5.1 U.S. Government, "Packaging and Transportation of Radioactive Material," Title 10 Code of Federal Regulations, Part 71, Office of the Federal Registrar, Washington DC.

5.2 U.S. Government, "Shippers – General Requirements for Shipments and Packagings," Title 49 Code of Federal Regulations, Part 173, Section 441, Office of the Federal Registrar, Washington DC.

5.3 "ORIGEN2.1 - Isotope Generation and Depletion Code - Matrix Exponential Method", CCC-371, Oak Ridge National Laboratory, RSIC Computer Code Collection, August 1991.

5.4 "CASK-81 - 22 Neutron, 18 Gamma-Ray Group, P_3, Cross Sections for Shipping Cask Analysis", DLC-23, Oak Ridge National Laboratory, RSIC Data Library Collection, June 1987.

5.5 Luksic, A., "Spent Fuel Assembly Hardware: Characterization and 10CFR61 Classification for Waste Disposal," Volume 1, Pacific Northwest Laboratory, PNL-6906, June 1989.

5.6 "Characteristics of Potential Repository Wastes", DOE/RW-0184-R1, Office of Civilian Radioactive Waste Management, July 1992.

5.7 "MCNP 4 - Monte Carlo Neutron and Photon Transport Code System", CCC-200A/B, Oak Ridge National Laboratory, RSIC Computer Code Collection, October 1991.

5.8 "Moderate Temperature (250°F) Weight Loss of NS-3," Technical Report No. NS-3-029, Bisco Products, Inc., Park Ridge, Illinois, Revision 0, April 1985 (Appendix 5.5.6).

5.9 "DORT-PC - Two-Dimensional Discrete Ordinates Transport Code System", CCC-532, Oak Ridge National Laboratory, RSIC Computer Code Collection, October 1991.

5.10 Watt, B. E., "Energy Spectrum of Neutrons and Thermal Fission of U^{235}," Phys. Rev 87, 1037 (1952).

5.11 "American National Standard Neutron and Gamma-Ray Flux-to-Dose-Rate Factors", ANSI/ANS-6.1.1-1977, American Nuclear Society, La Grange Park, Illinois, March 1977.

5.12 Jenal, J. P., P. J. Erickson, W. A. Rhoades, D. B. Simpson, and M. L. Williams, "The Generation of a Computer Library for Discrete Ordinates Quadrature Sets", ORNL/TM-6023, Oak Ridge National Laboratory, October 1977.

5.13 "ANISN-ORNL - One-Dimensional Discrete Ordinates Transport Code System with Anisotropic Scattering", CCC-254, Oak Ridge National Laboratory, RSIC Computer Code Collection, April 1991.

5.14 "Topical Report on Actinide-Only Burnup Credit for PWR Spent Nuclear Fuel Packages," DOE/RW-0472, Office of Civilian Radioactive Waste Management, Revision 0, May 1995.

5.15 Jones, K.B., and B.D. Thomas, "Dry Fuel Storage Cask Shielding Benchmarks," Proceedings of the Sixth Annual International High Level Radioactive Waste Management Conference, Las Vegas, Nevada, May 1995.

5.16 Hermann, O. W., and S. M. Bowman, M. C. Brady, and C. V. Parks, "Validation of the Scale System for PWR Spent Fuel Isotopic Composition Analysis," ORNL/TM-12667, Oak Ridge National Laboratory, March 1995.

5.17 "Evaluation of Shielding Analysis Methods in Spent Fuel Cask Environments", EPRI TR-104329, Electric Power Research Institute, May 1995.

5.5.2 ORIGEN2 Input Files

THIS SECTION CONTAINS
PROPRIETARY INFORMATION

5.5.3 MCNP Input Files

THIS SECTION CONTAINS PROPRIETARY INFORMATION

5.5.4 DORT-PC and GIP Input Files

THIS SECTION CONTAINS
PROPRIETARY INFORMATION

5.5.5 ANISN Input Files

THIS SECTION CONTAINS
PROPRIETARY INFORMATION

5.5.6 Moderate Temperature Weight Loss of NS-3

This Appendix contains Bisco Products, Inc. Report NS-3-029, "Moderate Temperature (250°F) Weight Loss of NS-3," Revision 0, April 1995 (8 pages).

bisco

bisco products, inc.
1125 howard st.
elk grove village, illinois 60007
(312) 640-1840

TECHNICAL REPORT

Number: NS-3-029

Subject: Moderate Temperature Weight Loss of NS-3

Date: April 10, 1985

By: Michael L. McCullar
Michael L. McCullar
Research Chemist

PURPOSE:

To determine the rate of weight loss of NS-3 when exposed to 250° F for an extended period of time. Assuming that water loss is the primary reason for weight loss, the worst case hydrogen stability of NS-3 can then be determined.

CONCLUSIONS:

It takes about 2 months at 250° F before the NS-3 weight reaches a s point.

2. The NS-3 loses about 4.2% weight during this time frame.

3. Under these conditions (250° F), the % hydrogen in NS-3 decreases from 5.1% to 4.6%.

PROCEDURE:

BISCO Procedure NS-3-03 Rev. 1 was followed (appendix).

RESULTS AND DISCUSSION:

A one inch thick slab of NS-3 was made with laboratory raw materials and cured in accordance with standard BISCO procedures. Two 1 inch cubes were cut from the slab for this test.

Table 1 contains the raw weight data for each cube, average weight loss, ar average percent weight loss for each time period. Graph 1 is a plot of average % weight loss versus time.

RESULTS AND DISCUSSION (cont.):

The justification for each conclusion is discussed:

1. The weight of both NS-3 cubes decreased steadily from day 1 to day 54. From day 54 to day 59, no change in weight was observed. Based on this data, it takes about 2 months for the NS-3 to stop losing weight.

2. The average percent weight loss at day 59 was 4.226%. See the data in Table 1.

3. The % hydrogen in properly formulated and cured NS-3 is 5.1%. The average % weight loss of the NS-3 was 4.226%. It is reasonable to assume that all of the weight loss was in the form of water since no other volatile materials are present in NS-3. Since water consists of 11.19% hydrogen (as H), the overall hydrogen loss = 11.19% times 4.226% = 0.473% Given the starting NS-3 hydrogen content (theoretical) of 5.1%, the worst case hydrogen stability at 250° F is 5.1% - 0.473% = 4.627%.

No visual changes were apparent in the heat treated NS-3 cubes, other than some minor darkening.

TABLE 1

NP-03

Raw Data For NS-3 Cubes Heated at 250° F

ime rame	Cube #13 Weight (gms)	Cube #14 Weight (gms)	Average Weight Loss (gms)	Average % Weight Loss
tart	21.9182	24.2544	0	
day	21.1194	23.4523	.8005	3.467
days	21.0863	23.4152	.8356	3.619
days	21.0762	23.4038	.8463	3.666
days	21.0698	23.3972	.8528	3.694
days	21.0670	23.3944	.8556	3.706
days	21.0672	23.3942	.8556	3.706
0 days	21.0471	23.3721	.8767	3.797
1 days	21.0479	23.3734	.8757	3.793
2 days	21.0454	23.3702	.8785	3.805
3 days	21.0462	23.3710	.8779	3.802
4 days	21.0438	23.3687	.8801	3.812
ays	21.0344	23.3587	.8898	3.854
8 days	21.0319	23.3556	.8926	3.866
9 days	21.0331	23.3568	.8914	3.861
0 days	21.0297	23.3529	.8950	3.877
1 days	21.0288	23.3520	.8959	3.881
4 days	21.0252	23.3485	.8995	3.896
5 days	21.0251	23.3480	.8998	3.897
7 days	21.0192	23.3413	.9061	3.925
1 days	21.0140	23.3359	.9114	3.948
5 days	21.0125	23.3328	.9137	3.958
8 days	20.9873	23.3032	.9411	4.076
9 days	20.9840	23.3022	.9432	4.086
0 days	20.9815	23.3000	.9456	4.096
2 days	20.9806	23.2982	.9469	4.102

TABLE 1

~~Time~~ rame	Cube #13 Weight (gms)	Cube #14 Weight (gms)	Average Weight Loss (gms)	Average Weight Loss
6 days	20.9649	23.2786	.9646	4.178
8 days	20.9558	23.2715	.9727	4.213
2 days	20.9659	23.2805	.9631	4.172
3 days	20.9557	23.2697	.9736	4.217
4 days	20.9530	23.2671	.9763	4.229
6 days	20.9540	23.2679	.9754	4.225
9 days	20.9537	23.2678	.9756	4.226

Moderature Temperature Weight Loss of N at 250F in Percent

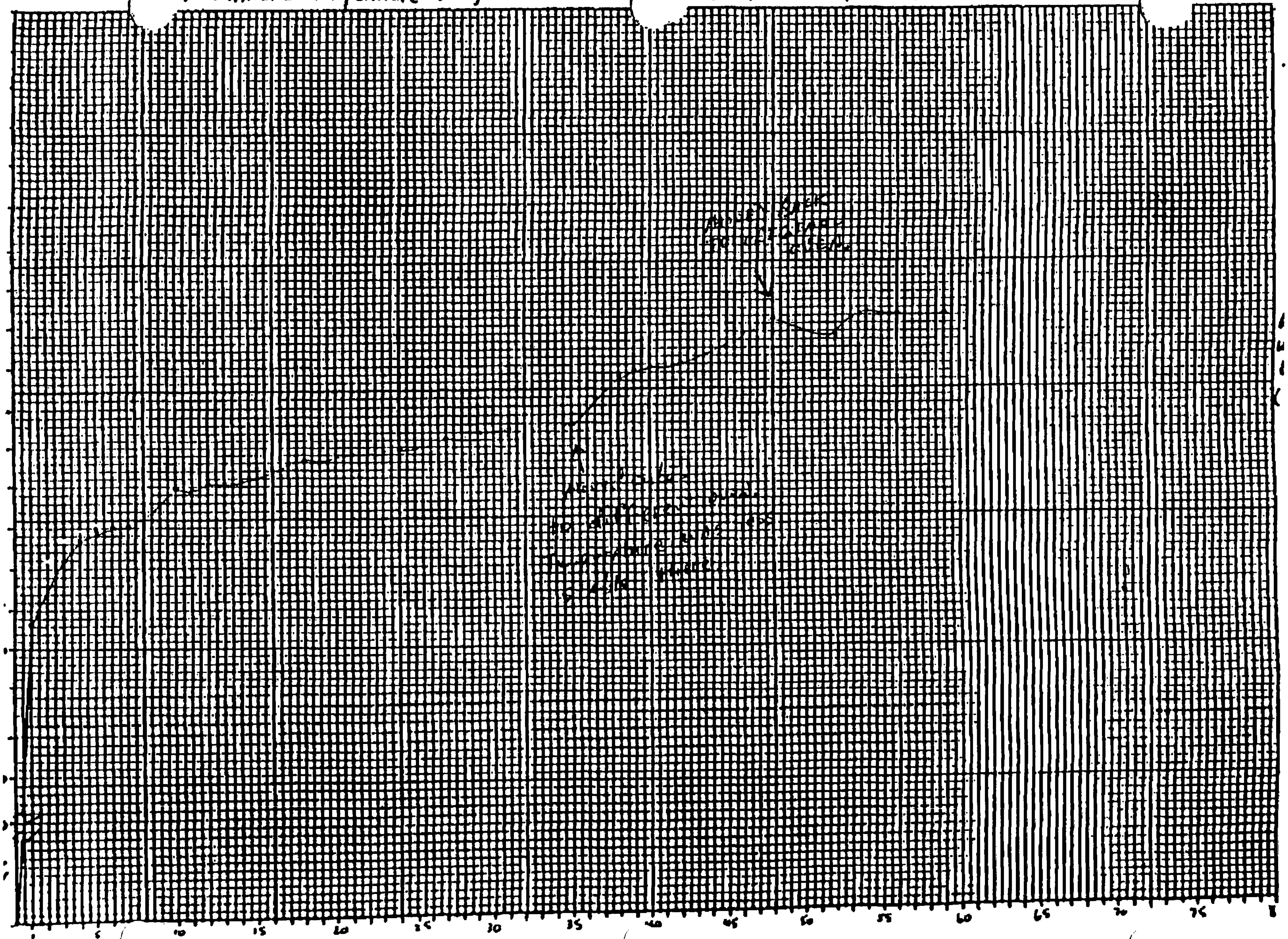

bisco

PROCEDURE

Procedure No. NS3-03

Project

Title: MODERATE TEMPERATURE WEIGHT LOSS OF NS-3

REV.	DATE	AUTHOR	TECH. REVIEW	Q.A. REVIEW	CORP. APPROVAL	SCOPE OF REVISION
0	5/15/84					Initial issue
1	1/20/85	MLM	[illegible]	4/17/85 [illegible]	[illegible]	Change from weighing cube in glassware to weighing cube alor change min. cube size to 20mm
2						
3						
4						
5						
6						

bisco products, inc.
1420 renaissance drive
park ridge, illinois 60068

one of the brand companies

bisco

Procedure No. NS3-03 Page 1 of 2

Title: MODERATE TEMPERATURE WEIGHT LOSS OF NS-3

Rev. 1

Date: January 20, 1985

DESCRIPTION

This test procedure describes the method to determine the weight loss of NS-3 when exposed to 250° F for an extended period of time. Data obtained from this test may be used to establish the worst case hydrogen stability of NS-3 at 250° F by considering that all weight loss is in the form of water and calculating the hydrogen equivalent loss as a fraction of total hydrogen.

MATERIALS

The test described is performed on NS-3 without additives, formulated and cured in accordance with standard BISCO procedures. The tests are performed in a static air oven with a temperature accuracy of ±5F. The samples are set in standard pyrex glassware while in the oven.

PROCEDURE

Two samples of NS-3, each sample not smaller than 20mm cubed, nor larger than 100mm cubed, shall be prepared, with each side of the cube machined smooth to prevent loose powder loss during the test. Each sample shall be wiped with a dry cloth and weighed to an accuracy obtainable on a Mettler type balance, then set in a clean dry glass container. The sample configuration shall be such that five sides of each sample are completely exposed. The container, with the cover removed, shall be placed in the oven and exposed to 250° F for a period of 24 hours. At the end of the exposure period gently remove each cube from the container using tongs, then weigh each cube within 15 minutes of removal. Following re-weighing, place the cubes back into the container and replace into the oven for further exposure. The cycle is to be repeated until the data indicates no further weight change is anticipated. The interval between weighings may be increased as deemed suitable by the shape of the weight loss curve.

REPORT

Following a completion of the test, a report shall be issued containing at least the following information:

1. A description of the samples including batch identification.
2. A summary of the data obtained.
3. An evaluation of worst case hydrogen stability as identified under "Description".
4. A list of observations.
5. A curve of showing the average weight loss of the samples as a function of time.
6. An appendix containing the test procedure and all data obtained.

End of Procedure

5.5.7 Fuel Assembly Axial Burnup Profiles

This Appendix contains portions of "Topical Report on Actinide-Only Burnup Credit for PWR Spent Nuclear Fuel Packages," DOE/RW-0472, Revision 0, May 1995 (3 pages). Note that Revision 1 of this report is scheduled to be issued in the near future. Transnuclear has reviewed the current draft of Revision 1 and verified that the axial burnup profiles used in the MP187 shielding analysis bound those provided in the revised report (maximum factor of 1.12 used herein, 1.108 used in Revision 1 of DOE/RW-0472).

Burnup credit analyses must consider the effects of moderator density from 0 to 1.0 g/cc within the spent fuel package. The moderator density effects must be evaluated with zero burnup at low enrichments (the maximum fresh fuel enrichment limit for the SNF package) and at high enrichments (the highest enrichment evaluated for the package) with the associated burnup from the burnup credit loading curve. If these evaluations indicate that a reactivity maximum exists at any density but 1.0 g/cc, then an optimum moderator density search is required at all enrichments evaluated for the burnup credit loading curve.

4.2.2 Axial Burnup Profile

The axial power peaking effect caused by neutron leakage from the ends of the finite-length fuel assembly produces an axial profile in the burnup. The effect of the burnup profile is to have less burnup in the fuel assembly ends than the average for the assembly, resulting in a local reactivity increase at the fuel ends and a decrease in the central region compared to the reactivity that would have existed if the assembly were uniformly burned to the average value. The axial burnup effect can be incorporated into burnup credit criticality safety analyses by dividing the assembly length into a number of zones of varying burnup. An evaluation was performed to determine the number of zones necessary to accurately model the reactivity effect of the axial burnup profile for two cases: 1) burned PWR fuel whose composition includes only the actinide isotopes validated in Chapter 2 of this topical report, and 2) burned fuel with a composition that also includes fission products. The fission product cases are provided as a basis of comparison for the end-effects with actinide-only credit.

4.2.2.1 Modeling of Fuel Ends

An example of the axial profile of spent fuel is illustrated by the measurement of Cs-137 as shown in Figure 4-3.[4-2] The shape of the burnup profile is a flattened cosine, with a peak from 1.1 to 1.2 times the average value of the burnup, and a burnup at the fuel rod ends that equals from 50 to 60% of the average value. Details of the calculational modeling approach used for the end effects are discussed below. The axial profile for each individual spent fuel assembly will vary somewhat from this profile depending on the specific power history of the assembly. Restrictions are placed upon the selection of candidate fuel assemblies in Section 6 to ensure that the profiles of assemblies loaded into an SNF package system with burnup credit do not differ significantly from the profile used as a basis for studies in this topical report, which are depicted in Figure 4-4.

A study was performed to evaluate the effect that the number of axial zones has upon the calculated reactivity of spent fuel.[4-1] The results of this evaluation are illustrated in Figure 4-5 (actinide plus fission product isotopes) and Figure 4-6 (actinide isotopes, without fission products). The results for actinide plus fission product isotopes showed that a higher k_{eff} results from incorporating the end effects for fuel that has attained the major portion of its burnup potential, as shown in Figure 4-5. For fuel that has a relatively low burnup (compared to the burnup that it could achieve in a PWR reactor if maintenance problems or fuel failures do not occur to cause the fuel to be prematurely discharged), a flat burnup profile (one uniform axial zone) results in a higher k_{eff}. Similar results were reported in independent studies of burnup credit.[4-3]

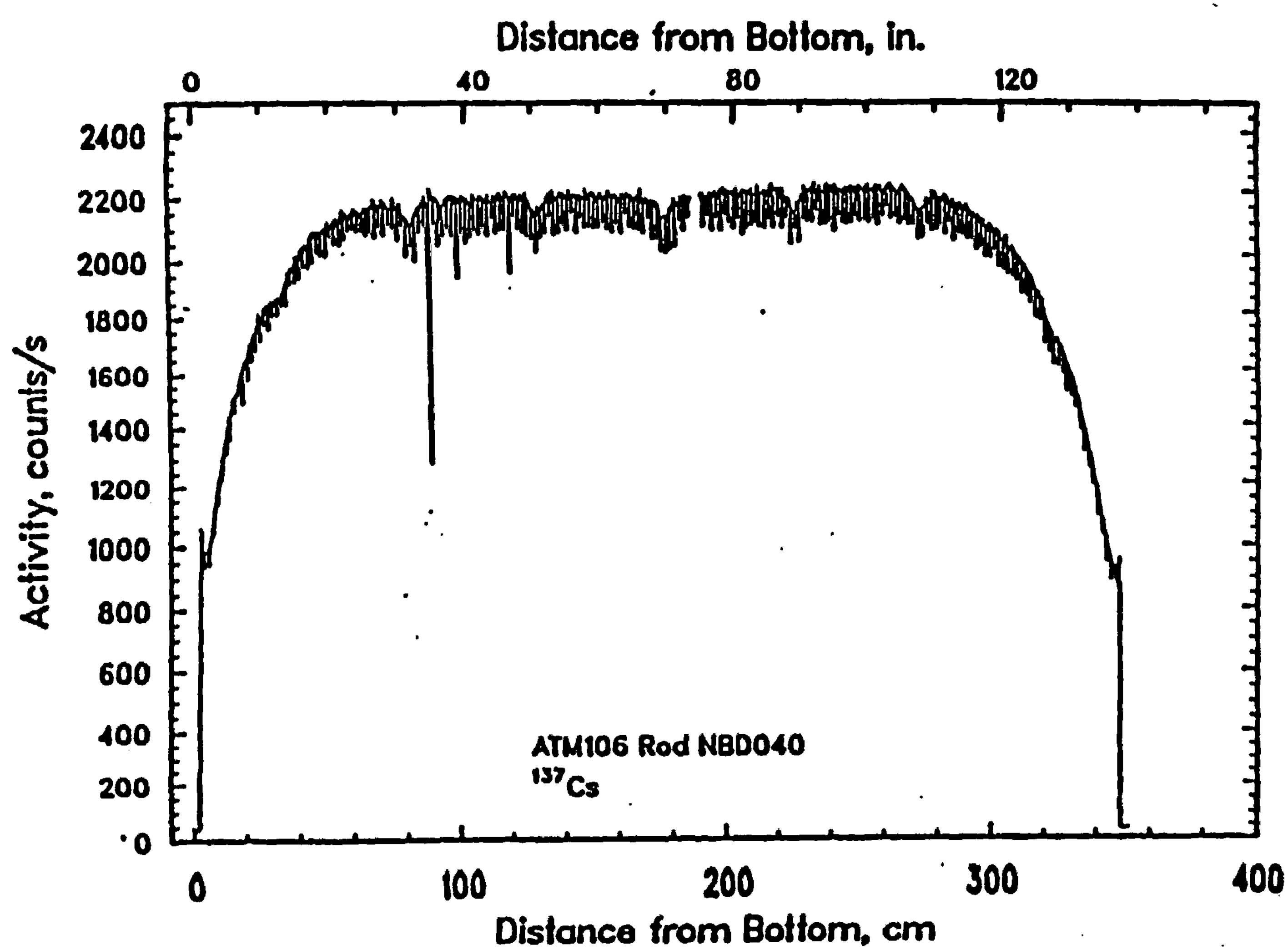

Figure 4-3. Burnup Profile Measurement by Gamma Scan

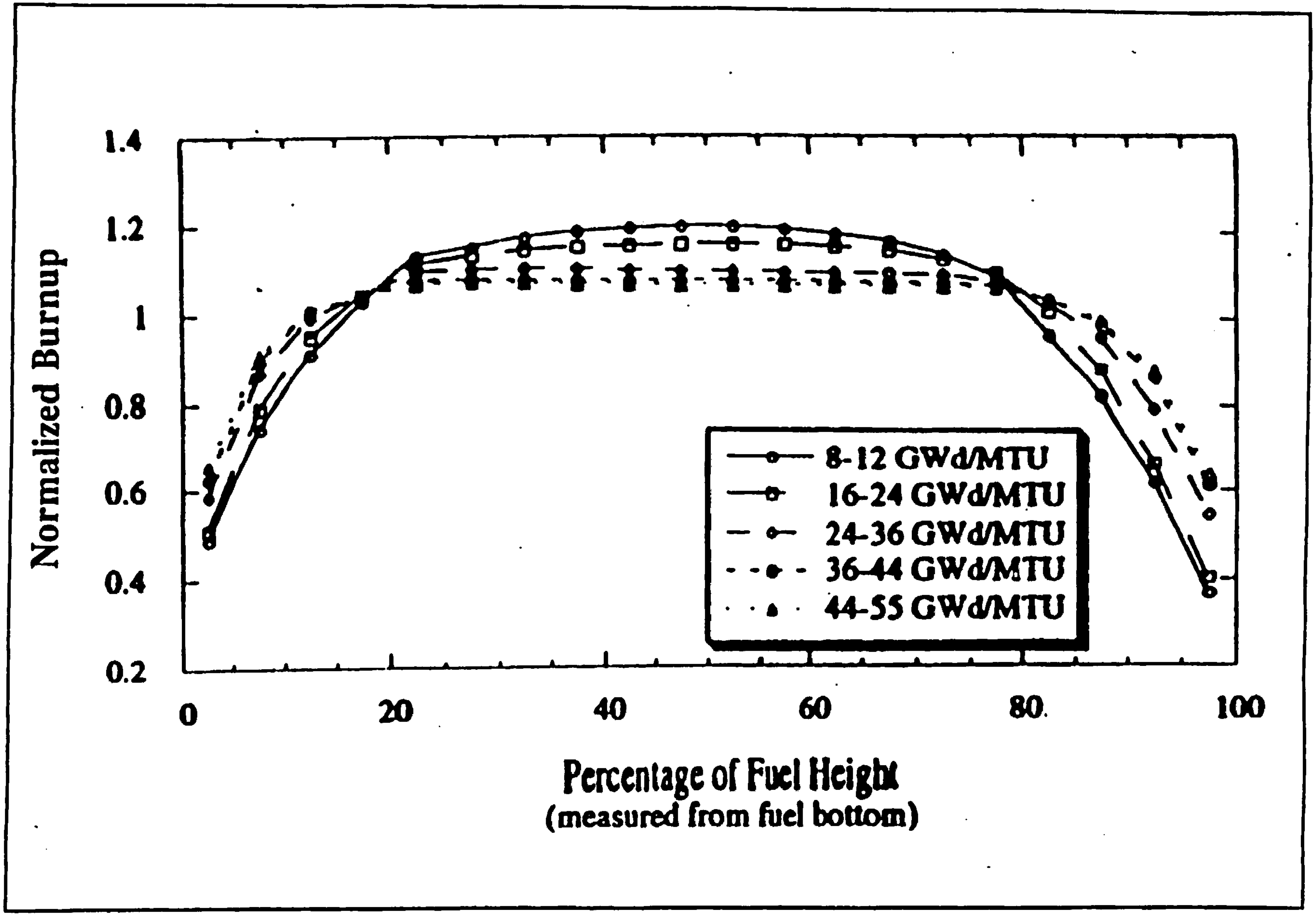

Figure 4-4. Normalized Axial Burnup Profiles

5.5.8 Alternate Fuel Parameters

This Appendix contains details of the analysis performed to generate the alternate fuel qualification criteria shown in Table 1.2-3. The intention of this table is to permit fuel assemblies with initial enrichments less than those permitted by Table 1.2-1 to be transported in the MP187 package, provided all other design criteria are satisfied. The fuel parameters shown in Table 1.2-3 are intended to supplement those in Table 1.2-1, and are not considered a replacement.

This is primarily a shielding evaluation, based on the fact that for a given burnup, the neutron source (and to a lesser extent the photon source) increases as the initial enrichment of the assembly decreases. The assembly decay heat also increases as the initial enrichment is decreased, but to a lesser extent than the radiological sources. Because only the maximum initial enrichment is important for criticality safety (limited to 3.43 w/o U-235), these low-enriched assemblies are bounded by the existing criticality analyses.

The low-enriched fuel assemblies will be qualified for loading in the MP187 cask in the following manner:

1. Three burnup/enrichment cases are modeled using the ORIGEN2 code [5.3]. The models are identical to those described in Section 5.2 to calculate the design basis MP187 source term. The ORIGEN2 code is used to calculate the decay heat, neutron source, photon source, and photon spectrum for each of the three cases.

2. The results of the three ORIGEN2 models are used to develop ANISN [5.13] source terms for each of the three cases, for both Type I and Type II fuel. The ANISN models are based on those described in Section 5.2.1.3 which determined the design basis fuel parameters. Source terms are developed using the same methodology as was used in the models described in Section 5.2.1.3.

3. The ANISN code calculates the neutron and gamma dose rates on the surface of the MP187 cask. These dose rates are multiplied by appropriate peaking factors and summed to calculate the total cask surface dose rate at the midpoint of the active fuel region. This duplicates the method used in Section 5.2.1.3 to determine the design bases burnup/enrichment case for the MP187 cask.

4. The DORT [5.9] code is used to calculate the dose rates at the package surface, vehicle outer surface, and two meters from the vehicle outer surface for the normal operating configuration. The DORT code is also used to calculate the dose rates one meter from the surface of the package for the hypothetical accident case. The DORT models duplicate those described in Section 5.4.1 of the SAR and include contributions from activated hardware in the end fittings, plenum, and control components.

5. Each of the three burnup/enrichment cases is qualified by demonstrating that:

    a) The total dose rate on the surface of the cask (as calculated by ANISN) for each case is bounded by that for the design basis case in the NUHOMS®-MP187 source term calculation (Section 5.2.1.3). For Type I assemblies the maximum dose rate is 61.5 mrem/hr and for Type II assemblies the maximum dose rate is 39.1 mrem/hr. This calculation ensures that both the Type I and Type II sources for each case are consistent with the criteria used to develop the MP187's design basis sources in Section 5.2.1.3.

    b) The maximum decay heat for a Type I assembly is limited to 0.764 kW and that for a Type II assembly is limited to 0.563 kW (Section 1.2.3).

    c) Because neutrons are the dominant contributor to the MP187 dose rates (at locations other than those modeled by ANISN), the neutron source term for each case must be bounded by the corresponding design basis neutron source term from Section 5.2.2. Because the primary neutron source for each case is the same (spontaneous fission of ^{244}Cm), the neutron spectrum for each case is the same and this provides assurance that all MP187 dose rates for the burnup/enrichment cases modeled herein will be bounded by those evaluated in Section 5.2.

d) The maximum total (neutron plus gamma for all assembly sources) dose rate on the package surface during normal operations is limited to 1000 mrem/hr per 10CFR71.47(b)(1). Compliance is demonstrated using the DORT models described above.

e) The maximum total (neutron plus gamma for all assembly sources) dose rate on the vehicle outer surface during normal operations is limited to 200 mrem/hr per 10CFR71.47(b)(2). Compliance is demonstrated using the DORT models described above.

f) The maximum total (neutron plus gamma for all assembly sources) dose rate two meters from the vehicle outer surface during normal operations is limited to 10 mrem/hr per 10CFR71.47(b)(3). Compliance is demonstrated using the DORT models described above.

g) The maximum total (neutron plus gamma for all assembly sources) dose rate one meter from the external surface of the package subsequent to the hypothetical accident conditions is limited to 1000 mrem/hr per 10CFR71.51(a)(2). Compliance is demonstrated using the DORT models described above.

h) Because the fuel design, maximum allowable initial enrichment, and uranium content are not being changed, no additional analyses are required for these parameters.

5.5.8.1 Calculations

5.5.8.1.1 Cases Addressed

The burnup/enrichment cases addressed in this calculation section are shown in Table 5.5.8-1 (DB refers to the design basis case from Section 5.2).

Table 5.5.8-1

Burnup/Enrichment Cases

Case	Enrichment (w/o U-235)	Burnup (MWd/MTU)
1	3.00	37,000
2	2.00	29,000
3	2.67	35,000
DB	3.19	40,000

5.5.8.1.2 Source Term Calculations

Source terms (neutron, photon, photon spectra, thermal) are calculated using the ORIGEN2 code with models based on those described in Section 5.2 (original ORIGEN2 models provided in Appendix 5.5.2). The alternate fuel source term models are described in the following sections.

(A) Case 1 - BW37-R0

The Case 1 ORIGEN2 model (37,000 MWd/MTU, 3 w/o U-235) is based on file BW40-R2A.INP from Appendix 5.5.2. All inputs are identical with the exception of: (1) The power irradiation was changed to account for the 37,000 MWd/MTU fuel burnup; (2) The decay times were changed as required for this calculation; and (3) The actinide composition was changed to account for the 3 w/o U-235 enrichment. The input cards which have been changed relative to those in Appendix 5.5.2 are shown below.

Specific Power: changed to 19.06 MW/assy which corresponds to a burnup of 37,000 MWd/MTU accumulated over 900 full power days (0.4636 MTU).

```
IRP      60.0  19.06  -6  1  4  2
IRP     120.0  19.06   1  1  4  0
IRP     180.0  19.06   1  1  4  0
IRP     240.0  19.06   1  1  4  0
IRP     300.0  19.06   1  1  4  0
DEC     380.0          1  1  4  0
IRP     440.0  19.06   1  1  4  0
IRP     500.0  19.06   1  1  4  0
IRP     560.0  19.06   1  1  4  0
IRP     620.0  19.06   1  1  4  0
IRP     680.0  19.06   1  1  4  0
DEC     760.0          1  1  4  0
IRP     820.0  19.06   1  1  4  0
IRP     880.0  19.06   1  1  4  0
```

```
IRP      940.0  19.06   1  1  4  0
IRP     1000.0  19.06   1  1  4  0
IRP     1060.0  19.06   1  1  4  0
```

Decay Time: Two decay times are addressed. Eight years cooling is assumed for Type I assemblies, and 14 years is assumed for Type II assemblies. The remainder of this Appendix will demonstrate that a 37,000 MWd/MTU, 3 w/o U-235 assembly cooled for these times satisfies the design criteria.

```
TIT      37,000 MWD/MTU AFTER 8.0 YEARS
DEC             8.000   -1         1         5        4
DEC             8.000   -2         2         5        4
DEC             8.000   -3         3         5        4
DEC             8.000   -4         4         5        4
HED             1 IN-CORE
HED             2 TOP
HED             3 PLENUM
HED             4 BOTTOM
OUT      -4    1    -1   0
TIT      37,000 MWD/MTU AFTER 14.0 YEARS
DEC             14.00   -1         1         5        4
DEC             14.00   -2         2         5        4
DEC             14.00   -3         3         5        4
DEC             14.00   -4         4         5        4
HED             1 IN-CORE
HED             2 TOP
HED             3 PLENUM
HED             4 BOTTOM
OUT      -4    1    -1   0
```

Actinide Composition: The U-235 mass (grams U-235 per MTU) has been changed to represent an initial enrichment of 3.0 w/o U-235. The U-238 mass has also been changed to maintain a total uranium weight of 1×10^6 grams per metric ton.

```
2    922340  240.00   922350   30000.00   922380   969760.00   0   0.0 FUEL
ACTINIDES
```

(B) Case 2 - BW29-R0

The Case 2 ORIGEN2 model (29,000 MWd/MTU, 2.0 w/o U-235) is based on that for 30,000 MWd/MTU fuel as described in Section 5.2.1.1. All inputs are identical with the exception of: (1) The power irradiation was changed to account for the 29,000 MWd/MTU fuel burnup; (2) The decay times were changed as required for this calculation; and (3) The actinide composition was changed to account for the 2 w/o U-235 enrichment. The input cards which have been changed relative to those in the original model are shown below.

Specific Power: changed to 14.94 MW/assy which corresponds to a burnup of 29,000 MWd/MTU accumulated over 900 full power days (0.4636 MTU).

```
IRP      60.0  14.94  -6  1  4  2
IRP     120.0  14.94   1  1  4  0
IRP     180.0  14.94   1  1  4  0
IRP     240.0  14.94   1  1  4  0
IRP     300.0  14.94   1  1  4  0
DEC     380.0          1  1  4  0
IRP     440.0  14.94   1  1  4  0
IRP     500.0  14.94   1  1  4  0
IRP     560.0  14.94   1  1  4  0
IRP     620.0  14.94   1  1  4  0
IRP     680.0  14.94   1  1  4  0
DEC     760.0          1  1  4  0
IRP     820.0  14.94   1  1  4  0
IRP     880.0  14.94   1  1  4  0
IRP     940.0  14.94   1  1  4  0
IRP    1000.0  14.94   1  1  4  0
IRP    1060.0  14.94   1  1  4  0
```

Decay Time: Two decay times are addressed. Six years cooling is assumed for Type I assemblies, and 10 years is assumed for Type II assemblies. The remainder of this Appendix will demonstrate that a 29,000 MWd/MTU, 2 w/o U-235 assembly cooled for these times satisfies the design criteria.

```
TIT      29,000 MWD/MTU AFTER   6.0 YEARS
DEC              6.00    -1      1        5        4
DEC              6.00    -2      2        5        4
DEC              6.00    -3      3        5        4
DEC              6.00    -4      4        5        4
HED              1 IN-CORE
HED              2 TOP
HED              3 PLENUM
HED              4 BOTTOM
OUT      -4    1    -1    0
TIT      29,000 MWD/MTU AFTER  10.0 YEARS
DEC             10.00    -1      1        5        4
DEC             10.00    -2      2        5        4
DEC             10.00    -3      3        5        4
DEC             10.00    -4      4        5        4
HED              1 IN-CORE
HED              2 TOP
HED              3 PLENUM
HED              4 BOTTOM
OUT      -4    1    -1    0
```

Actinide Composition: The U-235 mass (grams U-235 per MTU) has been changed to represent an initial enrichment of 2.0 w/o U-235. The U-238 mass has also been changed to maintain a total uranium weight of 1×10^6 grams per metric ton.

```
2       922340  240.00  922350 20000.0  922380  979760.00  0  0.0 FUEL
ACTINIDES
```

(C) Case 3 - BW35-R0

The Case 1 ORIGEN2 model (35,000 MWd/MTU, 2.67 w/o U-235) is based on file BW40-R2A.INP from Appendix 5.5.2. All inputs are identical with the exception of: (1) The power irradiation was changed to account for the 35,000 MWd/MTU fuel burnup; (2) The decay times were changed as required for this calculation; and (3) The actinide composition was changed to account for the 2.67 w/o U-235 enrichment. The input cards which have been changed relative to those in Appendix 5.5.2 are shown below.

Specific Power: changed to 18.03 MW/assy which corresponds to a burnup of 35,000 MWd/MTU accumulated over 900 full power days (0.4636 MTU).

```
IRP        60.0  18.03  -6  1  4  2
IRP       120.0  18.03   1  1  4  0
IRP       180.0  18.03   1  1  4  0
IRP       240.0  18.03   1  1  4  0
IRP       300.0  18.03   1  1  4  0
DEC       380.0          1  1  4  0
IRP       440.0  18.03   1  1  4  0
IRP       500.0  18.03   1  1  4  0
IRP       560.0  18.03   1  1  4  0
IRP       620.0  18.03   1  1  4  0
IRP       680.0  18.03   1  1  4  0
DEC       760.0          1  1  4  0
IRP       820.0  18.03   1  1  4  0
IRP       880.0  18.03   1  1  4  0
IRP       940.0  18.03   1  1  4  0
IRP      1000.0  18.03   1  1  4  0
IRP      1060.0  18.03   1  1  4  0
```

Decay Time: Two decay times are addressed. Seven years cooling is assumed for Type I assemblies, and 14 years is assumed for Type II assemblies. The remainder of this Appendix will demonstrate that a 2935,000 MWd/MTU, 2.67 w/o U-235 assembly cooled for these times satisfies the design criteria.

```
TIT       35,000 MWD/MTU AFTER 7.0 YEARS
DEC              7.00    -1       1         5         4
DEC              7.00    -2       2         5         4
DEC              7.00    -3       3         5         4
DEC              7.00    -4       4         5         4
HED             1 IN-CORE
HED             2 TOP
HED             3 PLENUM
HED             4 BOTTOM
```

```
OUT      -4   1    -1    0
TIT      35,000 MWD/MTU AFTER 14.0 YEARS
DEC             14.00    -1        1         5         4
DEC             14.00    -2        2         5         4
DEC             14.00    -3        3         5         4
DEC             14.00    -4        4         5         4
HED             1 IN-CORE
HED             2 TOP
HED             3 PLENUM
HED             4 BOTTOM
OUT      -4   1    -1    0
```

Actinide Composition: The U-235 mass (grams U-235 per MTU) has been changed to represent an initial enrichment of 2.67 w/o U-235. The U-238 mass has also been changed to maintain a total uranium weight of 1×10^6 grams per metric ton.

```
2    922340  240.00  922350  26700.00  922380  973060.00  0  0.0 FUEL
ACTINIDES
```

5.5.8.1.3 ORIGEN2 Results

The ORIGEN2 results for each case are summarized in Table 5.5.8-2. The values in the "Neutron" column are taken from the overall total portion of ORIGEN2's neutron table, summed across the four fuel assembly regions. The decay heat data shown in Table 5.5.8-2 is taken from the cumulative totals portion of ORIGEN2's thermal power table, again summed across the four assembly regions. The total gamma source for each assembly is equal to the sum of the source in each of ORIGEN2's 18 energy groups for the four assembly regions and three photon tables (activation products, actinides and daughters, and fission products). Data is provided in Table 5.5.8-2 for all three cases and for both Type I (shorter cooling) and Type II (longer cooling) fuel. The design basis data from Section 5.2 is provided as well (denoted "DB" and shown in italic). The values in Table 5.5.8-2 are all total source per assembly and include all contributions from the in-core region, top and bottom end fittings, and the gas plenum. Contributions from control components are not included in Table 5.5.8-2.

The results shown in Table 5.5.8-2 are suitable for determining compliance with the second and third acceptance criteria. The total decay heats for each case are below the decay heat limits for both Type I and Type II assemblies. Criterion (b) is, therefore, satisfied. The total neutron sources for each case, for both Type I and Type II assemblies, are less than those for the design basis case. Criterion (c) is, therefore, satisfied.

Table 5.5.8-2

ORIGEN2 Result Summary

Case	Enrichment (w/o U-235)	Burnup (MWd/MTU)	Type I Neutron (n/s/assy)	Type I Gamma (γ/s/assy)	Type II Neutron (n/s/assy)	Type II Gamma (γ/s/assy)	Decay Heat Type I (W/assy)	Decay Heat Type II (W/assy)
1	3.00	37,000	2.087E+08	4.658E+15	1.674E+08	3.344E+15	699.8	545.7
2	2.00	29,000	1.725E+08	4.544E+15	1.488E+08	3.071E+15	652.4	479.5
3	2.67	35,000	2.182E+08	4.872E+15	1.687E+08	3.138E+15	721.3	518.4
DB	*3.19*	*40,000*	*2.455E+08*	*4.672E+15*	*1.829E+08*	*3.280E+15*	*764.0*	*562.5*

The total in-core gamma source and spectrum is used to calculate the dose rates on the cask surface to determine compliance with acceptance criterion (a). This information is provided for each case in Table 5.5.8-3. The values in Table 5.5.8-3 are calculated by summing the activation product, actinide and daughter, and fission product source in the in-core region for each ORIGEN2 energy group and converting. Conversion of these spectra to an energy structure format useable in ANISN is (described in the next section and in Section 5.2.1.4). Contributions from the end fittings, gas plenum, and control components are not shown in Table 5.5.8-3.

Table 5.5.8-3

ORIGEN2 In-Core Gamma Results by Energy Group

Cask Group	E_{upper} (MeV)	Case 1 Type I	Case 1 Type II	Case 2 Type I	Case 2 Type II	Case 3 Type I	Case 3 Type II	Design Basis Type I	Design Basis Type II
		In-Core CASK Source (γ/s/assy)							
23	10.00	1.191E+05	9.507E+04	9.863E+04	8.485E+04	1.247E+05	9.584E+04	1.402E+05	1.038E+05
24	8.00	7.487E+05	5.975E+05	6.198E+05	5.333E+05	7.834E+05	6.024E+05	8.808E+05	6.525E+05
25	6.50	4.334E+06	3.460E+06	3.589E+06	3.088E+06	4.537E+06	3.489E+06	5.100E+06	3.779E+06
26	5.00	4.945E+06	3.948E+06	4.095E+06	3.523E+06	5.177E+06	3.980E+06	5.819E+06	4.311E+06
27	4.00	1.387E+09	3.884E+07	4.614E+09	3.100E+08	2.699E+09	3.865E+07	7.676E+08	2.136E+07
28	3.00	1.079E+10	4.176E+08	3.582E+10	2.429E+09	2.093E+10	3.978E+08	5.995E+09	3.094E+08
29	2.50	1.993E+11	1.993E+09	8.208E+11	3.223E+10	4.312E+11	1.934E+09	9.584E+10	3.839E+08
30	2.00	1.531E+12	8.690E+11	1.782E+12	9.254E+11	1.733E+12	8.276E+11	1.495E+12	7.686E+11
31	1.66	4.803E+13	2.380E+13	5.527E+13	3.248E+13	5.355E+13	2.313E+13	4.591E+13	1.895E+13
32	1.33	1.117E+14	5.523E+13	1.285E+14	7.569E+13	1.245E+14	5.369E+13	1.068E+14	4.386E+13
33	1.00	1.719E+14	4.334E+13	2.126E+14	7.202E+13	2.138E+14	4.091E+13	1.480E+14	3.030E+13
34	0.80	7.953E+14	5.405E+14	7.693E+14	5.139E+14	8.418E+14	5.111E+14	7.892E+14	5.274E+14
35	0.60	1.308E+15	9.702E+14	1.217E+15	8.886E+14	1.350E+15	9.174E+14	1.323E+15	9.598E+14
36	0.40	4.074E+13	2.515E+13	4.707E+13	2.504E+13	4.523E+13	2.332E+13	3.895E+13	2.393E+13
37	0.30	6.182E+13	4.688E+13	6.256E+13	4.054E+13	6.439E+13	4.336E+13	6.240E+13	4.650E+13
38	0.20	1.767E+14	1.249E+14	1.778E+14	1.142E+14	1.857E+14	1.165E+14	1.782E+14	1.200E+14
39	0.10	2.906E+14	2.294E+14	2.809E+14	1.946E+14	2.984E+14	2.137E+14	2.957E+14	2.298E+14
40	0.05	1.634E+15	1.276E+15	1.567E+15	1.100E+15	1.672E+15	1.186E+15	1.665E+15	1.273E+15
	Total	4.641E+15	3.336E+15	4.521E+15	3.058E+15	4.851E+15	3.130E+15	4.654E+15	3.274E+15

5.5.8.1.4 ANISN Source Term Generation

Derivation of source terms for use in the ANISN shielding models is performed in the following sections for neutrons and gammas. The ANISN models require volumetric source terms (particles per second per cubic centimeter) in the CASK-81 [5.4] energy group format. This calculation is performed in a manner identical to that described in Section 5.2.1.4.

The ANISN neutron source for each group is equal to the total neutron source per assembly (from Table 5.5.8-2) multiplied by 24 (the number of assemblies), divided by the active fuel volume (5,633,674 cm), and multiplied by the normalized group fraction. The results of these calculations for each case are shown in Table 5.5.8-4.

Table 5.5.8-4

Neutron Source Calculations

		CASK Grouped Volumetric Source (n/s/cm3)					
	^{244}Cm	Case 1		Case 2		Case 3	
Cask Group	Fraction	Type I	Type II	Type I	Type II	Type I	Type II
1	2.018E-04	1.794E-01	1.439E-01	1.483E-01	1.279E-01	1.876E-01	1.450E-01
2	1.146E-03	1.019E+00	8.173E-01	8.422E-01	7.265E-01	1.065E+00	8.236E-01
3	4.471E-03	3.975E+00	3.188E+00	3.286E+00	2.834E+00	4.156E+00	3.213E+00
4	1.768E-02	1.572E+01	1.261E+01	1.299E+01	1.121E+01	1.643E+01	1.271E+01
5	4.167E-02	3.705E+01	2.972E+01	3.062E+01	2.641E+01	3.873E+01	2.995E+01
6	5.641E-02	5.015E+01	4.023E+01	4.145E+01	3.576E+01	5.244E+01	4.054E+01
7	1.197E-01	1.064E+02	8.536E+01	8.796E+01	7.588E+01	1.113E+02	8.603E+01
8	9.616E-02	8.549E+01	6.858E+01	7.066E+01	6.096E+01	8.939E+01	6.911E+01
9	2.256E-02	2.006E+01	1.609E+01	1.658E+01	1.430E+01	2.097E+01	1.621E+01
10	1.227E-01	1.091E+02	8.750E+01	9.017E+01	7.778E+01	1.141E+02	8.818E+01
11	2.110E-01	1.876E+02	1.505E+02	1.551E+02	1.338E+02	1.961E+02	1.516E+02
12	1.794E-01	1.595E+02	1.279E+02	1.318E+02	1.137E+02	1.668E+02	1.289E+02
13	1.138E-01	1.012E+02	8.116E+01	8.363E+01	7.214E+01	1.058E+02	8.179E+01
14	1.301E-02	1.157E+01	9.278E+00	9.561E+00	8.247E+00	1.209E+01	9.350E+00
15	6.555E-05	5.828E-02	4.675E-02	4.817E-02	4.155E-02	6.093E-02	4.711E-02
16	4.765E-06	4.236E-03	3.398E-03	3.502E-03	3.021E-03	4.429E-03	3.425E-03
17	3.134E-07	2.786E-04	2.235E-04	2.303E-04	1.987E-04	2.913E-04	2.252E-04
18	4.527E-08	4.025E-05	3.228E-05	3.327E-05	2.870E-05	4.208E-05	3.253E-05
19	9.759E-09	8.677E-06	6.960E-06	7.172E-06	6.186E-06	9.072E-06	7.014E-06
20	1.521E-09	1.352E-06	1.085E-06	1.118E-06	9.642E-07	1.414E-06	1.093E-06
21	3.353E-10	2.981E-07	2.391E-07	2.464E-07	2.125E-07	3.117E-07	2.410E-07
22	9.683E-11	8.609E-08	6.905E-08	7.116E-08	6.138E-08	9.001E-08	6.959E-08
	Total	8.891E+02	7.131E+02	7.349E+02	6.339E+02	9.295E+02	7.187E+02

Gamma source terms for use in ANISN are calculated using the same methodology as is described in Section 5.2.1.4. The gamma sources shown in Table 5.5.8-3 are converted to volumetric sources (multiplied by 24 and divided by the volume: 5,633,674 cm) and mapped into the CASK-81 energy structure. The mapping functions are shown in Table 5.2-10. The resulting in-core gamma source terms are shown in Table 5.5.8-5. The results in Table 5.5.8-5 include the in-core gamma source contribution for each case. Table 5.5.8-5 does not include contributions from end fittings or control components. Activated hardware sources are provided in Table 5.5.8-8.

Table 5.5.8-5

Gamma Source Calculations

Cask Group	CASK Grouped Volumetric Source (γ/s/cm3)					
	Case 1		Case 2		Case 3	
	Type I	Type II	Type I	Type II	Type I	Type II
23	5.074E-01	4.050E-01	4.202E-01	3.615E-01	5.312E-01	4.083E-01
24	3.190E+00	2.546E+00	2.641E+00	2.272E+00	3.337E+00	2.566E+00
25	1.846E+01	1.474E+01	1.529E+01	1.316E+01	1.933E+01	1.486E+01
26	2.107E+01	1.682E+01	1.744E+01	1.501E+01	2.206E+01	1.696E+01
27	5.909E+03	1.655E+02	1.966E+04	1.321E+03	1.150E+04	1.647E+02
28	4.595E+04	1.779E+03	1.526E+05	1.035E+04	8.917E+04	1.695E+03
29	8.492E+05	8.490E+03	3.497E+06	1.373E+05	1.837E+06	8.240E+03
30	6.521E+06	3.702E+06	7.592E+06	3.942E+06	7.382E+06	3.525E+06
31	2.046E+08	1.014E+08	2.354E+08	1.384E+08	2.281E+08	9.854E+07
32	4.759E+08	2.353E+08	5.475E+08	3.224E+08	5.305E+08	2.287E+08
33	7.325E+08	1.846E+08	9.058E+08	3.068E+08	9.106E+08	1.743E+08
34	3.388E+09	2.303E+09	3.277E+09	2.189E+09	3.586E+09	2.177E+09
35	5.574E+09	4.133E+09	5.186E+09	3.785E+09	5.753E+09	3.908E+09
36	1.736E+08	1.071E+08	2.005E+08	1.067E+08	1.927E+08	9.935E+07
37	2.634E+08	1.997E+08	2.665E+08	1.727E+08	2.743E+08	1.847E+08
38	7.526E+08	5.323E+08	7.576E+08	4.866E+08	7.911E+08	4.965E+08
39	1.238E+09	9.774E+08	1.196E+09	8.289E+08	1.271E+09	9.102E+08
40	6.960E+09	5.436E+09	6.677E+09	4.686E+09	7.121E+09	5.053E+09
Total	1.977E+10	1.421E+10	1.926E+10	1.303E+10	2.067E+10	1.333E+10

5.5.8.1.5 ANISN Dose Rate Calculations

The ANISN discrete-ordinates computer code is used to calculate the dose rate on the surface of the NUHOMS®-MP187 cask. Because the ANISN code is one-dimensional, the model is representative only of the dose rate along the neutron shield. These ANISN models are similar to those described in Section 5.2.1.3 (which are provided in Appendix 5.5.5), the only differences being the neutron and gamma source terms. These are taken directly from Table 5.5.8-4 (neutrons) and Table 5.5.8-5 (gammas).

Six ANISN runs are used to calculate the dose rate for each case, for both Type I and Type II assemblies. The neutron and gamma dose rates on the surface of the cask (interval 72) are shown in Table 5.5.8-6, as are the corresponding design basis dose rates from Figure 5.2-2 and Figure 5.2-3 (denoted "DB" and shown in italic).

The dose rates calculated by ANISN are based on assembly average enrichment and burnup. Peaking factors of 1.12 are applied to the gamma dose rates and 1.12^4 are applied to the neutron dose rates to calculate the total centerline dose rates. This is identical to the methodology used in Section 5.2.1.3. These totals are shown in Table 5.5.8-7. Table 5.5.8-7 demonstrates compliance with acceptance criterion (a) because the total dose rate for each case is bounded by the total dose rate for the design basis case.

Table 5.5.8-6

ANISN Dose Rate Results

	ANISN Results (mrem/hr)			
	Type I		Type II	
Case	Neutron	Gamma	Neutron	Gamma
DB	*2.46E+01*	*2.04E+01*	*1.83E+01*	*9.21E+00*
1	2.09E+01	2.12E+01	1.68E+01	1.09E+01
2	1.73E+01	2.53E+01	1.49E+01	1.40E+01
3	2.18E+01	2.41E+01	1.69E+01	1.06E+01

Table 5.5.8-7

Total Dose Rate Results

	Peaked Results (mrem/hr)					
	Type I			Type II		
Case	Neutron	Gamma	Total	Neutron	Gamma	Total
DB	*3.87E+01*	*2.29E+01*	*6.15E+01*	*2.88E+01*	*1.03E+01*	*3.91E+01*
1	3.29E+01	2.37E+01	5.66E+01	2.64E+01	1.22E+01	3.86E+01
2	2.72E+01	2.84E+01	5.55E+01	2.34E+01	1.56E+01	3.91E+01
3	3.44E+01	2.70E+01	6.13E+01	2.66E+01	1.19E+01	3.85E+01

5.5.8.1.6 DORT Model Generation

DORT models have been generated for each of the three cases to calculate dose rates on the package surface, vehicle outer surface, and 2-meters from the vehicle outer surface. These models are identical to the FC-DSC models described in Section 5.4.1, with the exception of the source terms. The FC-DSC, which includes control components, was selected for this evaluation because:

1. The FC-DSC produces the bounding total dose rates for all locations on the vehicle outer surface and at 2-meters from the vehicle outer surface. The FC-DSC 2-meter dose rate of 9.94 mrem/hr is the design basis value with the least margin relative to the regulatory limits.

2. The FC-DSC produces the larger gamma dose rate at all locations. The three cases evaluated herein have larger gamma source terms than the original design basis case. Utilizing the FC-DSC model will, therefore, calculate the largest gamma dose rates. All neutron source terms calculated herein are less than those used in the design basis analysis.

3. The peak dose rate on the package surface, calculated for the FO-DSC, is due completely to the streaming of neutrons through the trunnion sleeve. Because the neutron source terms for all three cases included in this section are less than those used for the design basis evaluation, the FO-DSC package surface dose rate at this location will decrease.

As discussed in Section 5.4.1.2, there are four DORT models required for each case: neutron, in-core gamma, top end fitting gamma, and bottom end-fitting gamma. The neutron source terms for the DORT models are identical to those used in the ANISN models, listed above in Table 5.5.8-4. The in-core gamma source term for each case is equal to the sum of the data in Table 5.5.8-5 and the control component source. These contributions are added group-by-group. The design basis (gray APSRA) control component sources (per assembly) are listed in Table 5.2-11. The total FC-DSC gamma source for the in-core region is shown in Table 5.5.8-8 for each case. Top and bottom sources are also shown in Table 5.5.8-8. These sources were calculated in the same manner as were the in-core sources. The top source includes contributions from the plenum, top end fitting, and control components. The bottom source includes only the bottom end fitting. As with the design basis analysis, all dose rates are calculated using the Type II assembly source and are multiplied by 1.03 to account for the presence of Type I fuel assemblies in the inner four fuel cells. This correction factor was determined in Section 5.4.1.2 and was selected to bound both neutrons and gammas. However, because the factor calculated for neutrons is greater than that for gammas, use of the 1.03 factor herein is conservative.

Table 5.5.8-8

FC-DSC Gamma Source Terms for DORT Calculations

Cask	Case 1 (γ/s/cm³)			Case 2 (γ/s/cm³)			Case 3 (γ/s/cm³)		
Group	In-Core	Bottom	Top	In-Core	Bottom	Top	In-Core	Bottom	Top
23	4.050E-01	2.685E-11	3.779E-11	3.615E-01	2.377E-11	3.344E-11	4.083E-01	2.674E-11	3.764E-11
24	2.546E+00	1.701E-10	2.393E-10	2.272E+00	1.505E-10	2.117E-10	2.566E+00	1.695E-10	2.385E-10
25	1.474E+01	1.001E-09	1.409E-09	1.316E+01	8.843E-10	1.244E-09	1.486E+01	9.971E-10	1.403E-09
26	1.682E+01	1.143E-09	1.609E-09	1.501E+01	1.010E-09	1.421E-09	1.696E+01	1.139E-09	1.603E-09
27	1.655E+02	2.515E-07	3.540E-07	1.321E+03	3.444E-06	4.836E-06	1.647E+02	2.483E-07	3.492E-07
28	1.789E+03	4.477E+00	2.752E+00	1.036E+04	7.602E+00	4.034E+00	1.705E+03	4.458E+00	2.744E+00
29	1.174E+04	1.447E+03	8.892E+02	1.406E+05	2.457E+03	1.304E+03	1.149E+04	1.440E+03	8.867E+02
30	3.702E+06	3.188E-03	4.487E-03	3.942E+06	4.044E-03	5.690E-03	3.525E+06	3.174E-03	4.466E-03
31	2.836E+08	8.108E+07	4.983E+07	3.206E+08	1.377E+08	7.305E+07	2.807E+08	8.074E+07	4.969E+07
32	6.665E+08	1.919E+08	1.179E+08	7.537E+08	3.259E+08	1.729E+08	6.600E+08	1.911E+08	1.176E+08
33	1.855E+08	1.134E+05	1.255E+05	3.076E+08	1.621E+05	1.339E+05	1.751E+08	1.132E+05	1.254E+05
34	2.303E+09	1.586E+05	2.027E+05	2.190E+09	3.092E+05	3.785E+05	2.178E+09	1.579E+05	2.018E+05
35	4.133E+09	2.313E+05	3.226E+05	3.785E+09	5.388E+05	7.527E+05	3.908E+09	2.299E+05	3.206E+05
36	1.072E+08	1.514E+05	2.068E+05	1.067E+08	3.491E+05	4.795E+05	9.937E+07	1.505E+05	2.055E+05
37	1.998E+08	4.338E+04	4.244E+04	1.727E+08	8.637E+04	8.666E+04	1.848E+08	4.317E+04	4.223E+04
38	5.326E+08	1.554E+05	1.089E+05	4.869E+08	2.746E+05	1.804E+05	4.968E+08	1.548E+05	1.085E+05
39	9.795E+08	9.358E+05	5.782E+05	8.310E+08	1.591E+06	8.516E+05	9.123E+08	9.317E+05	5.765E+05
40	5.459E+09	1.024E+07	6.687E+06	4.708E+09	1.755E+07	1.037E+07	5.076E+09	1.020E+07	6.665E+06
Total	1.485E+10	2.850E+08	1.760E+08	1.367E+10	4.845E+08	2.592E+08	1.397E+10	2.838E+08	1.755E+08

(A) Case 1: 37,000 MWd/MTU

Four Case 1 DORT models were run to calculate the dose rates around the MP187 cask containing 37,000 MWd/MTU fuel assemblies. These runs are identical to those provided in Appendix 5.5.4, with the exception of the source terms. Source terms are given in Table 5.5.8-4 (neutron) and Table 5.5.8-8 (gamma).

The dose rate contributions from all of the models are summed node-by-node to calculate the total dose rate at each location around the cask. This was done in an identical manner to the DORT data reduction described in Section 5.4.2. Dose rates adjacent to the trunnions (DORT J-meshes 117-128) include contributions from the trunnion streaming analysis provided in Section

5.4.1.8.1. Trunnion contributions are added to each of the affected nodes for the package surface dose rates (per Table 5.4-5), vehicle surface dose rates (per Table 5.4-7), and 2-meter dose rates (Table 5.4-8).

The trunnion dose rates are based on the design basis source terms evaluated in Section 5.4.1.8.1. The trunnion evaluation concluded that the presence of the trunnions increases the neutron dose rates while decreasing the gamma dose rates. Because the design basis neutron source bounds the neutron sources calculated for the three cases addressed herein, the trunnion dose rates calculated in Section 5.4.1.8.1 may conservatively be used in this calculation.

The maximum neutron, gamma, and total dose rates along the side, top, and bottom of the package are shown in Table 5.5.8-9. Comparisons between Table 5.5.8-9 and the results presented in Table 5.4-15 show while the gamma doses have increased, all of the "total" dose rates calculated for Case 1 are bounded by those of the design basis case. Acceptance criteria numbers (d), (e), and (f) are satisfied for Case 1.

It should also be noted that the dose rate on the lower external surface of the vehicle calculated in 5.4.1.8.3 remains bounding for all of the cases addressed herein. The calculated dose rate at this location was 190.3 mrem/hr, of which 189.9 mrem/hr (99.8%) was due to neutrons. Because the design basis neutron source bounds those of the three cases evaluated herein, the maximum shear key dose rate will be unaffected by this calculation.

Table 5.5.8-9

Case 1 Dose Rate Results

	Package Surface		
	Side (mrem/hr)	Top (mrem/hr)	Bottom (mrem/hr)
Normal Conditions			
Gamma	1.97E+1	2.07E-1	6.72E-1
Neutron	1.77E+2	6.21E-1	1.20E+0
Total	1.82E+2	8.01E-1	1.53E+0
10 CFR71 Limit	1.00E+3	1.00E+3	1.00E+3
	Vehicle Outer Surface		
	Side (mrem/hr)	Top (mrem/hr)	Bottom (mrem/hr)
Normal Conditions			
Gamma	1.13E+1	2.07E-1	6.72E-1
Neutron	4.69E+1	6.21E-1	1.20E+0
Total	5.20E+1	8.01E-1	1.53E+0
10 CFR71 Limit	2.00E+2	2.00E+2	2.00E+2
	2 Meters from Vehicle Outer Surface		
	Side (mrem/hr)	Top (mrem/hr)	Bottom (mrem/hr)
Normal Conditions			
Gamma	3.35E+0	5.91E-2	2.25E-1
Neutron	6.44E+0	2.77E-1	4.93E-1
Total	9.56E+0	3.09E-1	6.33E-1
10 CFR71 Limit	1.00E+1	1.00E+1	1.00E+1

(B) Case 2: 29,000 MWd/MTU

Four Case 2 DORT models were run to calculate the dose rates around the MP187 cask containing 29,000 MWd/MTU fuel assemblies. These runs are identical to those provided in Appendix 5.5.4, with the exception of the source terms. Source terms are given in Table 5.5.8-4 (neutron) and Table 5.5.8-8 (gamma).

The dose rate contributions from all of the models are combined in the same manner as was described above for Case 1. The maximum neutron, gamma, and total dose rates along the side, top, and bottom of the package are shown in Table 5.5.8-10. Comparisons between Table 5.5.8-10 and the results presented in Table 5.4-15 show while the gamma doses have increased, all of the "total" dose rates calculated for Case 2 are bounded by those of the design basis case. Acceptance criteria numbers (d), (e), and (f) are satisfied for Case 2.

Table 5.5.8-10

Case 2 Dose Rate Results

	Package Surface		
	Side (mrem/hr)	Top (mrem/hr)	Bottom (mrem/hr)
Normal Conditions			
Gamma	2.16E+1	2.17E-1	7.87E-1
Neutron	1.57E+2	5.52E-1	1.06E+0
Total	1.63E+2	7.68E-1	1.46E+0
10 CFR71 Limit	1.00E+3	1.00E+3	1.00E+3
	Vehicle Outer Surface		
	Side (mrem/hr)	Top (mrem/hr)	Bottom (mrem/hr)
Normal Conditions			
Gamma	1.25E+1	2.17E-1	7.87E-1
Neutron	4.17E+1	5.52E-1	1.06E+0
Total	4.85E+1	7.68E-1	1.46E+0
10 CFR71 Limit	2.00E+2	2.00E+2	2.00E+2
	2 Meters from Vehicle Outer Surface		
	Side (mrem/hr)	Top (mrem/hr)	Bottom (mrem/hr)
Normal Conditions			
Gamma	3.75E+0	5.25E-2	2.61E-1
Neutron	5.73E+0	2.46E-1	4.38E-1
Total	9.26E+0	2.74E-1	6.01E-1
10 CFR71 Limit	1.00E+1	1.00E+1	1.00E+1

(C) Case 3: 35,000 MWd/MTU

Four Case 3 DORT models were run to calculate the dose rates around the MP187 cask containing 35,000 MWd/MTU fuel assemblies. These runs are identical to those provided in Appendix 5.5.4, with the exception of the source terms. Source terms are given in Table 5.5.8-4 (neutron) and Table 5.5.8-8 (gamma).

The dose rate contributions from all of the models are combined in the same manner as was described above for Case 1. The maximum neutron, gamma, and total dose rates along the side, top, and bottom of the package are shown in Table 5.5.8-11. Comparisons between Table 5.5.8-11 and the results presented in Table 5.4-15 show while the gamma doses have increased, all of the "total" dose rates calculated for Case 3 are bounded by those of the design basis case. Acceptance criteria numbers (d), (e), and (f) are satisfied for Case 3.

Table 5.5.8-11

Case 3 Dose Rate Results

	Package Surface		
	Side (mrem/hr)	Top (mrem/hr)	Bottom (mrem/hr)
Normal Conditions			
Gamma	1.95E+1	2.08E-1	6.73E-1
Neutron	1.78E+2	6.26E-1	1.21E+0
Total	1.83E+2	8.06E-1	1.54E+0
10 CFR71 Limit	1.00E+3	1.00E+3	1.00E+3
	Vehicle Outer Surface		
	Side (mrem/hr)	Top (mrem/hr)	Bottom (mrem/hr)
Normal Conditions			
Gamma	1.12E+1	2.08E-1	6.73E-1
Neutron	4.73E+1	6.26E-1	1.21E+0
Total	5.23E+1	8.06E-1	1.54E+0
10 CFR71 Limit	2.00E+2	2.00E+2	2.00E+2
	2 Meters from Vehicle Outer Surface		
	Side (mrem/hr)	Top (mrem/hr)	Bottom (mrem/hr)
Normal Conditions			
Gamma	3.32E+0	5.95E-2	2.26E-1
Neutron	6.49E+0	2.79E-1	4.97E-1
Total	9.58E+0	3.11E-1	6.37E-1
10 CFR71 Limit	1.00E+1	1.00E+1	1.00E+1

(D) Hypothetical Accident Conditions

The hypothetical accident condition DORT models provided in Appendix 5.5.4 have been revised to incorporate the Case 2 source terms defined above. Case 2 was selected because, as shown in Table 5.5.8-10, the Case 2 gamma dose rates bound those of Cases 1 and 3. The bounding gamma case was selected because a significant portion of the hypothetical accident dose rates is due to gamma streaming through the postulated lead-slump gap. Four hypothetical accident models were run to account for each of the source regions. The results of the runs were summed node-by-node and are summarized in Table 5.5.8-12.

Table 5.5.8-12

Hypothetical Accident Dose Rate Results

	Package Surface			1 Meter from Surface of Package		
Normal Conditions	Side (mrem/hr)	Top (mrem/hr)	Bottom (mrem/hr)	Side (mrem/hr)	Top (mrem/hr)	Bottom (mrem/hr)
Gamma (max)	3.01E+03	1.67E+01	9.99E+00	3.23E+02	2.28E+00	3.14E+00
Neutron (max)	8.53E+02	6.94E+01	1.29E+02	3.61E+02	2.91E+01	4.68E+01
Total (max)	3.10E+03	7.03E+01	1.38E+02	4.08E+02	2.99E+01	5.00E+01
10 CFR Part 71 Limit				1.00E+03	1.00E+03	1.00E+03

Comparisons between Table 5.5.8-12 and Table 5.4-16 show that while the gamma dose rates have nearly doubled for the Case 2 source, the total dose rates remain bounded by those calculated in Table 5.4-16. Acceptance criterion (g) is, therefore, satisfied.

5.5.8.1.7 <u>Conclusions</u>

As documented in Section 5.5.8.1.3, Table 5.5.8-2; and in Section 5.5.8.1.5, Table 5.5.8-7; and Section 5.5.8.1.6, Table 5.5.8-9, Table 5.5.8-10, Table 5.5.8-11, and Table 5.5.8-12, all of the acceptance criteria defined in Paragraph 5 of Section 5.5.5 have been satisfied for the three burnup/enrichment cases modeled herein. The following alternate fuel qualification table provided as Table 5.5.8-13 is, therefore, justified by this calculation. Table 5.5.8-14 provides a summary of the maximum calculated gamma, neutron, and total dose rates at the package surface, vehicle outer surface, two meters from the vehicle outer surface, and one meter from the surface of the package. This summary provides the bounding results from the design basis case and the three cases addressed in this Appendix.

Table 5.5.8-13

Alternate Cooling Times for Fuel Qualification

Maximum Burnup(1) (MWd/MTIHM)	Minimum Enrichment (w/o U-235)	Minimum Required Type I Cooling Time (years)	Minimum Required Type II Cooling Time (years)
29,000	2.00	6	10
35,000	2.67	7	14
37,000	3.00	8	14

(1) Actual fuel burnup shall be rounded up to the values shown in this column to determine applicable enrichment and cooling limits. For example, an assembly with a burnup of 29,300 MWd/MTIHM would have a minimum enrichment limit of 2.67 w/o U-235 and required cooling times of 7 years and 14 years for Type I and Type II, respectively.

Table 5.5.8-14

Summary of Maximum Package Dose Rates

	Package Surface		
	Side (mrem/hr)	Top (mrem/hr)	Bottom (mrem/hr)
Normal Conditions			
Gamma(1)	2.16E+1	2.18E-1	7.87E-1
Neutron(2)	1.93E+2	6.79E-1	1.31E+0
Total(2)	1.98E+2	8.47E-1	1.62E+0
10 CFR71 Limit	1.00E+3	1.00E+3	1.00E+3
	Vehicle Outer Surface		
	Side (mrem/hr)	Top (mrem/hr)	Bottom (mrem/hr)
Normal Conditions			
Gamma(1)	1.25E+1	2.18E-1	7.87E-1
Neutron(2)	5.13E+1	6.79E-1	1.31E+0
Total(2)	5.56E+1	8.47E-1	1.62E+0
10 CFR71 Limit	2.00E+2	2.00E+2	2.00E+2
	2 Meters from Vehicle Outer Surface		
	Side (mrem/hr)	Top (mrem/hr)	Bottom (mrem/hr)
Normal Conditions			
Gamma(1)	3.75E+0	6.46E-2	2.61E-1
Neutron(2)	7.04E+0	3.02E-1	5.39E-1
Total(2)	9.94E+0	3.37E-1	6.72E-1
10 CFR71 Limit	1.00E+1	1.00E+1	1.00E+1
	1 Meter from Surface of Package		
	Side (mrem/hr)	Top (mrem/hr)	Bottom (mrem/hr)
Hypothetical Accident Conditions			
Gamma(1)	3.23E+2	2.28E+0	3.14E+0
Neutron(3)	4.43E+2	3.57E+1	5.75E+1
Total(3)	4.83E+2	3.63E+1	5.93E+1
10 CFR71 Limit	1.00E+3	1.00E+3	1.00E+3

(1) Side and Bottom results taken from Case 2.
Top results per (2) and (3), below.
(2) Result taken from Table 5.4-15
(3) Result taken fromTable 5.4-16

6. CRITICALITY EVALUATION

This chapter describes the engineering/physics design elements of the NUHOMS®-MP187 Package which are important to safety and necessary to comply with the performance requirements specified in Sections 71.55 and 71.59 of 10 CFR Part 71 [6.1].

The results of detailed analyses are presented which demonstrate that the NUHOMS®-MP187 Package is critically safe, under normal and accident conditions, considering a variety of mechanical uncertainties. Sufficient detail has been included herein to permit reviewers to accomplish an independent evaluation of the criticality analyses. Much of this detail is available in the Appendix in which computer inputs have been provided for review.

6.1 Discussion and Results

6.1.1 NUHOMS®-MP187 Cask Design Features

The NUHOMS®-MP187 Package is designed to provide criticality control through a combination of mechanical and neutronic isolation of fuel assemblies. Unlike traditional spent fuel shipping packages, the NUHOMS®-MP187 Cask is designed to carry a payload of canisterized fuel. The dry shielded canisters (DSCs) are suitable for use in the NUHOMS®-24P dry storage system, and for transportation in the NUHOMS®-MP187 Cask. This SAR addresses three specific types of DSCs and one design basis fuel assembly type. Other fuel assembly types having varied characteristics will be licensed by amendment to the certificate of compliance for this package.

6.1.2 Fuel-Only (FO) DSC Design Features

The principal performance features of the NUHOMS®-MP187 Cask and FO-DSC as they relate to criticality control are:

A. The package is designed such that it would be subcritical if water were to leak into or out of the canister. No credit is taken for the containment capability of the canister to exclude moderator from the fuel matrix (10CFR71.55 b).

B. The criticality analyses have been performed with consideration for the most reactive credible configuration consistent with the chemical and physical form of the material (10CFR71.55b1), moderation by water to the most reactive credible extent (10CFR71.55b2), and close full reflection by water on all sides or such greater reflection of the containment system as may additionally be provided by the surrounding material of the packaging (10CFR71.55b3).

C. Any number of undamaged, or damaged (10CFR71.73) packages will remain subcritical in any arrangement with close full water reflection and optimum interspersed hydrogenous moderation. Therefore, the transport index for the package is zero (10CFR71.59b).

The FO-DSC support structure is composed of four axially oriented support rods and twenty-six spacer discs. This basket assembly provides positive location for twenty-four fuel assemblies under both normal operating condition (NOC) and post-hypothetical accident conditions (HAC). The basket assembly utilizes fixed neutron absorbers which isolate each fuel assembly. Guide sleeves are designed to permit unrestricted flooding and draining of fuel cells.

The absorber panel material was chosen due to its desirable neutron attenuation, low density, and minimal thickness. It has been used for applications and in environments comparable to those found in spent fuel storage and transportation since the early 1950s (the U.S. Atomic Energy Commission's AE-6 Water-Boiler Reactor). In the 1960s, it was used as a poison material to ship irradiated fuel rods from Canada's Chalk River laboratories to Savannah River. More than 12,000 British Nuclear Fuels, Ltd. (BNFL) flasks containing the material have been used to transport fuel to BNFL's reprocessing plant in Sellafield.

The neutron absorber panels are composed of boron carbide and 1100 alloy aluminum. Boron carbide provides the necessary content of the neutron absorbing B10 isotope in a chemically inert, heat resistant, highly crystalline and extremely hard form. Boron carbide contained in the panels does not react under these conditions. The boron carbide core is tightly held within an 1100 aluminum alloy matrix and further protected by solid 1100 aluminum alloy cladding plates. Although 1100 alloy aluminum is a chemically reactive material, it behaves much like an inert material when properly applied. Proper application includes due consideration to the formation of a highly protective aluminum oxide layer and allowance for creation of the reaction by-product hydrogen.

Aluminum reacts with water to produce hydrogen (H_2) and an impervious tightly adhering layer of hydrated aluminum oxide ($Al_2O_3 \bullet 3H_2O$) called bayerite which protects the surface from further attack.

$$2\ Al + 6\ H_2O \rightarrow Al_2O_3 \bullet 3H_2O + 6H^+ + 6\text{electrons}$$

Initially, the DSC basket will be submerged in the spent fuel pool. During this period, aluminum in the panels will react with water in the manner noted above to form a small amount of hydrogen gas and produce a stable bayerite layer on all surfaces of the panel. The bayerite layer formed on the panel during pool immersion persists through DSC drying, sealing, storage, and eventual shipping; preventing further corrosion or hydrogen production. A complete corrosion discussion for the package components is provided in Section 2.4.4

Leaching of the boron carbide along the unsealed edges of the panels is expected to occur to an insignificant degree. There are three reasons why this is anticipated to be insignificant. First, the panel core is a sintered Al/B_4C material. Only the boron carbide particles exposed by saw cut are available for leaching. Second, the immersion environment is relatively benign and the time is brief (a few hours or days). The material has been commonly used in U.S. spent fuel racks for many years and, in fact, has gained a reputation for not leaching, as other neutron absorbing materials have done. And third, direct experimental observations of accelerated aging tests performed at the University of Michigan [6.10] showed no indications of boron degradation. The test specimens were exposed to high neutron and gamma irradiation in a reactor pool environment for over nine years. Subsequent neutron radiography showed no signs of reduced neutron attenuation anywhere on the test specimens.

6.1.3 Fuel-Control Components (FC) DSC Design Features

The FC-DSC is designed with a longer internal cavity length to accommodate fuel control components. No credit is taken for the presence of control hardware, thus the FC-DSC is identical to the FO-DSC for the purpose of criticality analysis. Further references to the FO-DSC apply to this canister design also.

6.1.4 Failed Fuel (FF) DSC Design Features

The FF-DSC is different from the FO-DSC in its capacity, function, and design. The FF-DSC's capacity is thirteen fuel assemblies. The basket material can be either a carbon steel or SA240 Type XM-19 stainless steel material since there is not a statistically significant difference in regards to neutron cross-sections between these two materials. It is intended to package fuel with gross cladding defects which might be discovered during the plant defueling campaign. Fuel assemblies to be stored and/or transported are to be visually inspected to document that cladding damage is limited to no more than 15 fuel pins with known or suspected cladding damage greater than hairline cracks and pinhole leaks. The potential does exist, however, for individual pellets to escape the cladding during transportation. This material would still be confined by the 13 fuel cans. The fuel must not have damage that would preclude it from being handled in the ordinary manner. Each assembly is placed in a separate, removable can with a fixed mesh screen on the bottom and similarly screened lid on top. These cans have slightly larger interior dimensions than the FO-DSCs (9.00" vs. 8.90") to accommodate bowed or twisted fuel. Due to its smaller payload and the relatively massive nature of the FF-DSC cans, the FF-DSC does not require borated neutron absorbers. The fuel cans are designed to permit unrestricted flooding and draining of fuel cells.

The FF-DSC is analyzed using the same criteria as the FO-DSC, plus additional considerations arising from mechanical uncertainties of failed fuel after transport or hypothetical accident conditions.

6.1.5 Criticality Analysis Summary and Results

The calculated maximum k_{eff} for the NUHOMS®-MP187 Package is 0.94968 including all biases and uncertainties applicable to the calculational methodology and the design. The results are summarized in Table 6.1-1.

Table 6.1-1

Summary of Criticality Evaluation

	Required	Calculated
NORMAL CONDITIONS		
Number of undamaged packages calculated to be subcritical	∞	∞
Optimum interspersed hydrogenous moderation	yes	0.93740(2)
Closely and fully reflected by water	yes	yes
Package cavity size, cm^3	--	1.11E+07
ACCIDENT CONDITIONS		
Number of damaged packages calculated to be subcritical	∞	∞
Optimum interspersed hydrogenous moderation, optimum water reflection	yes	0.94968(3)
Package cavity size, cm^3	--	1.11E+07
Transport Index	--	0

Notes:

1 All K_{eff}s include 2σ uncertainty. See Section **Error! Reference source not found.** for summary details.

2 Maximum of the "FONXF" studies (refer to Section **Error! Reference source not found.**).

3 Maximum of FF DSC analysis (refer to Section **Error! Reference source not found.**).

The criticality analysis was performed in accordance with the requirements of:

- ANSI/ANS-8.1-1983, "Nuclear Criticality Safety in Operations with Fissionable Materials Outside Reactors." [6.2]
- ANSI/ANS-8.17-1984, "Criticality Safety Criteria for the Handling, Storage, and Transportation of LWR Fuel Outside Reactors." [6.3]
- USNRC Regulatory Guide 3.41, "Validation of Calculational Methods for Nuclear Criticality Safety," Revision 1, May, 1977. [6.4]
- ANSI N16.9-1975, "Validation of Calculational Methods for Nuclear Criticality Safety." [6.5]

Guidance has been taken from USNRC Regulatory Guide 1.13, "Spent Fuel Storage Facility Design Basis," Proposed Revision 2, December 1981 [6.6], as it applies to the calculation of k_{eff} for a transportation cask.

6.2 Package Fuel Loading

The NUHOMS®-MP187 Cask is designed to accommodate one of the three DSCs as described above. The design basis fuel is B&W 15x15 Mark B fuel with a maximum fuel enrichment of 3.43 w/o U235. The fuel loading parameters as they relate to criticality are summarized in Table 6.2-1. Since no credit for burnup was assumed in the criticality calculations, unirradiated fuel is qualified for shipment. Other fuel assembly types having varied characteristics will be licensed by amendment to the certificate of compliance for this package.

Table 6.2-1

Maximum Fuel Loading Parameters

Parameter	Value
Number of Assemblies, FO/FC-DSCs	≤ 24
Number of Assemblies, FF-DSC	≤ 13
Enrichment, w/o U235	≤ 3.43%
Minimum Burnup	0
Design Basis Fuel	B&W 15x15
Maximum Number of Failed Rods (FF-DSC only)	15/assy

The design properties of the reference fuel are given in Table 6.2-2.

Table 6.2-2

Design Basis Fuel Parameters for Criticality Analysis

Parameter	Value
Fuel Pellet Outside Diameter	0.3686 in
Fuel Clad Thickness	0.0265 in
Fuel Clad Outside Diameter	0.43 in
Fuel Rod Pitch	0.568 in
Active Fuel Height	141.8 in
Enrichment, w/o U-235	3.43%
UO2 Density, %Theoretical Dens.	95.0%
Rod Array (NxN Rods)	15
Fueled Rod Locations	208

6.3 Model Specification

6.3.1 Description of Calculational Model

The criticality calculations were done using full-cask KENO5A [6.8] models. They are described in detail below and in the Appendices.

The safety requirements of ANSI/ANS-8.17 [6.3] prescribe that all applicable biases and uncertainties must be investigated and statistically attached to the nominal case k_{eff}. Rather than a statistical approach, this criticality analysis models the system with all the important parameters concurrently in their worst-case state:

- Maximum fabrication thickness and minimum boron content for all the neutron absorber plates (this combination is the worst case since aluminum displaces moderator and is not a strong absorber),
- Minimum fabrication width for all the neutron absorber plates,
- Minimum fabrication thickness for all steel guide tubes and steel absorber wrappers,
- Only 75% credit taken for the boron in neutron absorber plates,
- Worst-case fuel assembly position (includes DSC fabrication tolerances and an allowance for fuel assembly bow and twist),
- Maximum enrichment (3.43 w/o U235) B&W 15x15 Mark B fuel.

6.3.2 NUHOMS®-MP187 Cask/FO-DSC Model

The KENO models consist of 560 axial layers stacked into an array. The layers consist of partial spacer disc and partial moderator regions inside and outside of the active fuel region. The very top and bottom of the model are the DSC steel cylinder. The length of the active fuel layers is equivalent to the greatest common denominator of the spacer disc and moderator region axial lengths. For example, five 0.25" layers of the spacer disc are stacked to make an equivalent 1.25" spacer disc region. The center to center spacing of the spacer disc intervals varies over a range starting at 0.0 and ending at 6.75 inches. However, some of these intervals occur in non-fuel areas. This axially finite arrangement is shown in Figure 6.3-1. By specifying specular reflection on the $\pm$x and $\pm$y directions of these array layers, the model represents an infinite array of casks.

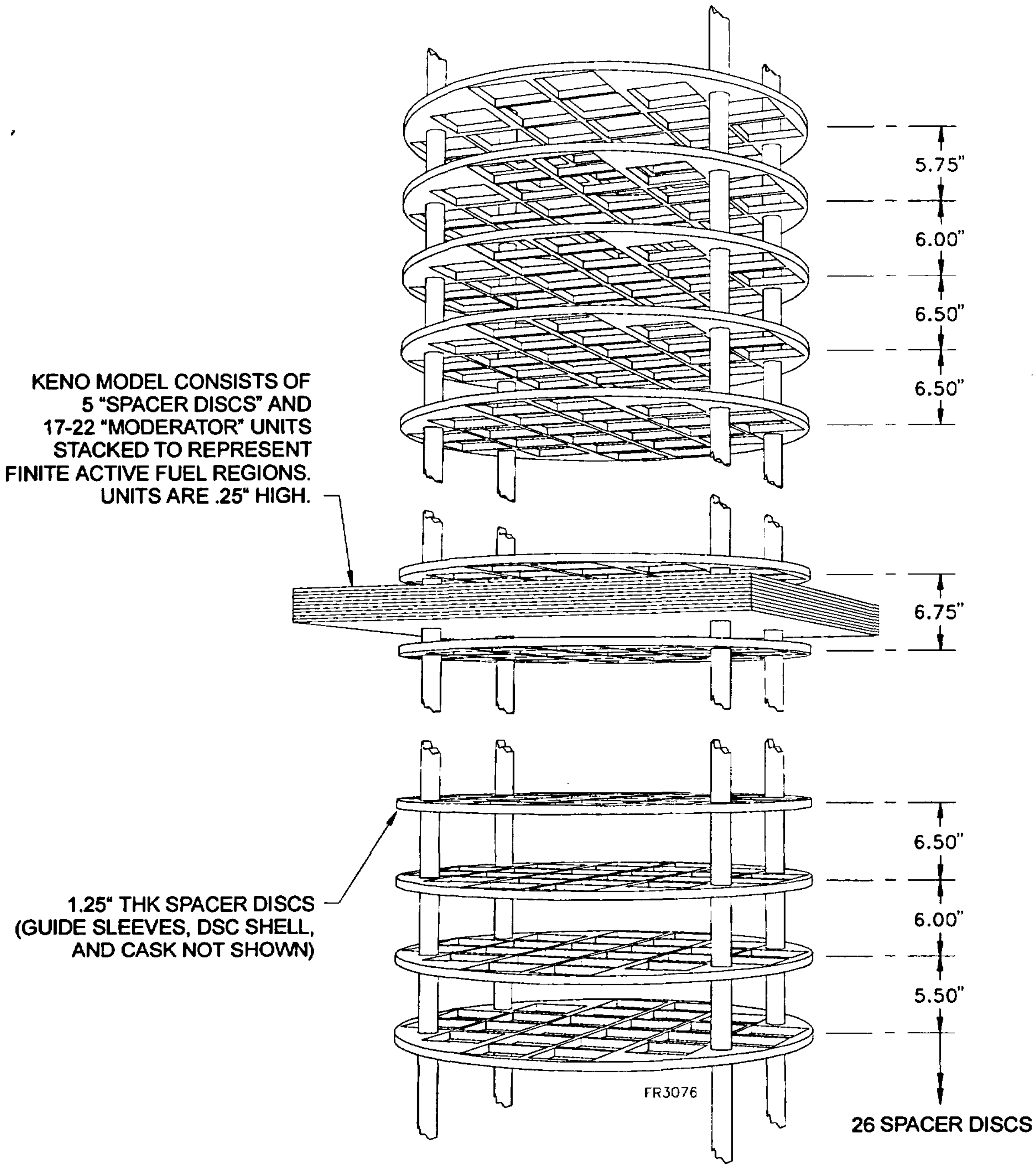

Figure 6.3-1

KENO Model and DSC Basket

Figure 6.3-2 shows the KENO model in an exploded view. UNIT 33 is a slice through the cask at the DSC spacer disc level. UNIT 34 is a similar slice, but in between the spacer discs.

Figure 6.3-3 shows the structure of UNITs 33 and 34: the cask slices. Note that the difference between the two UNITs is that UNIT 33 is a spacer disc (steel surrounding fuel assemblies) and UNIT 34 has steel support rods only (water surrounding fuel assemblies). Also, for the HAC cases, there is no guide sleeve deformation within the spacer disc (Unit 33) region. The fuel assemblies are identified in Figure 6.3-3 by the position numbers (1-24) used to refer to their unique locations. UNIT numbers 1-8 represent the active fuel assemblies in the spacer disc region and UNIT numbers 82-89 represent the active fuel assemblies in the moderator region. The fuel assemblies are inserted into the model using KENO5A's HOLE capability.

A detail of the guide sleeve assembly is shown in the enlarged section of Figure 6.3-3. These models include all major components of the guide sleeve assembly: the square tube, absorber sheets (4 per tube), and the over sleeves which hold the sheets in place. Note that the guide sleeves on the outer periphery of the basket (12 total) only have two absorber sheets per tube.

Figure 6.3-4 shows more closely the way in which UNITs 1-8 are constructed. Each HOLE is identified by UNIT number and its own particular coordinate origin.

UNIT 32 is a cross section of the design basis B&W 15x15 Mark B fuel assembly. It is illustrated in Figure 6.3-5 , which also shows the locations of the fuel assembly guide tubes, instrumentation tube, and the UNIT origin for insertion as a HOLE. The theoretical half width of the fuel (fifteen times half the rod pitch) is 4.26" (10.8204 cm).

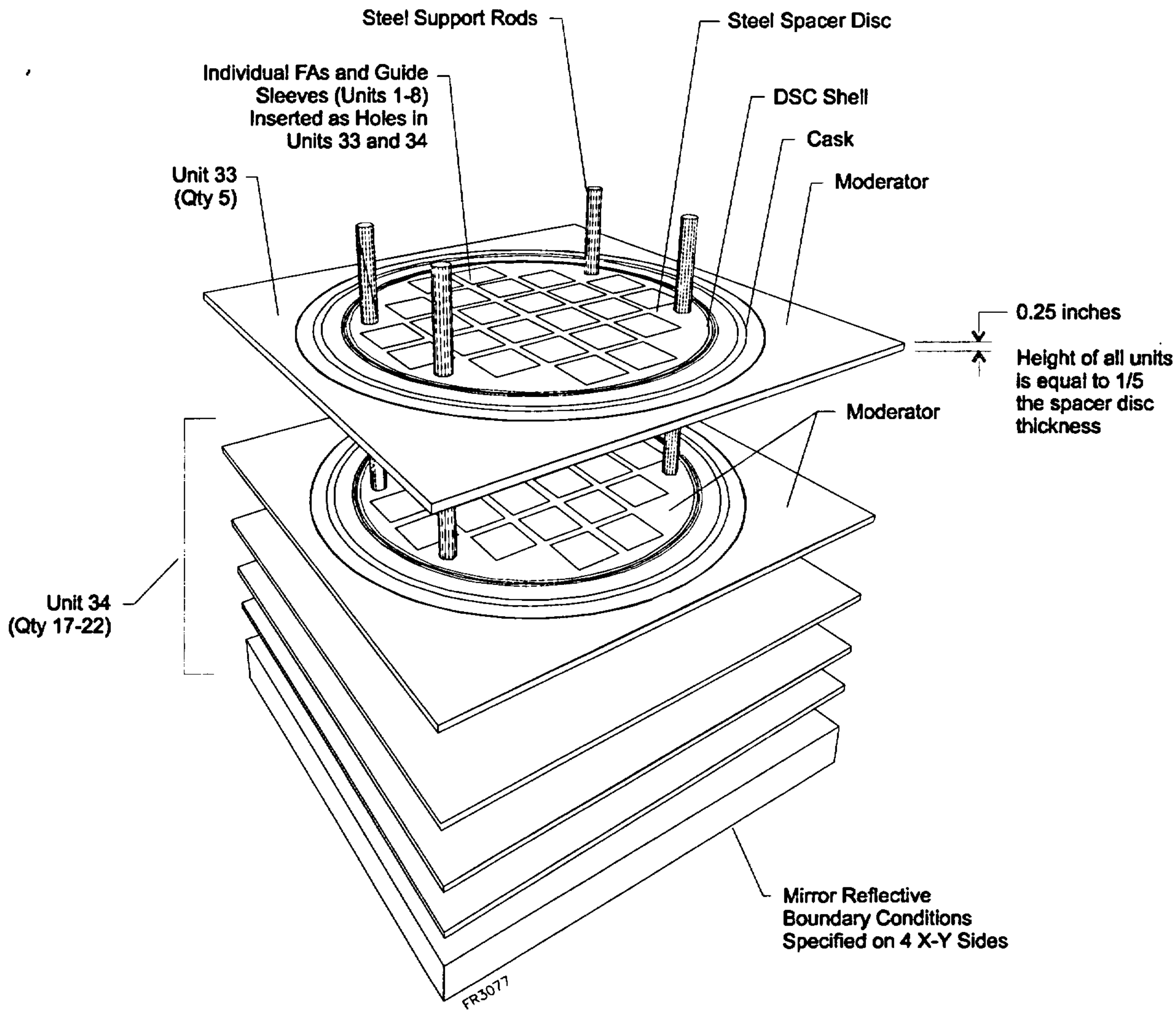

Figure 6.3-2

Exploded View of KENO Model

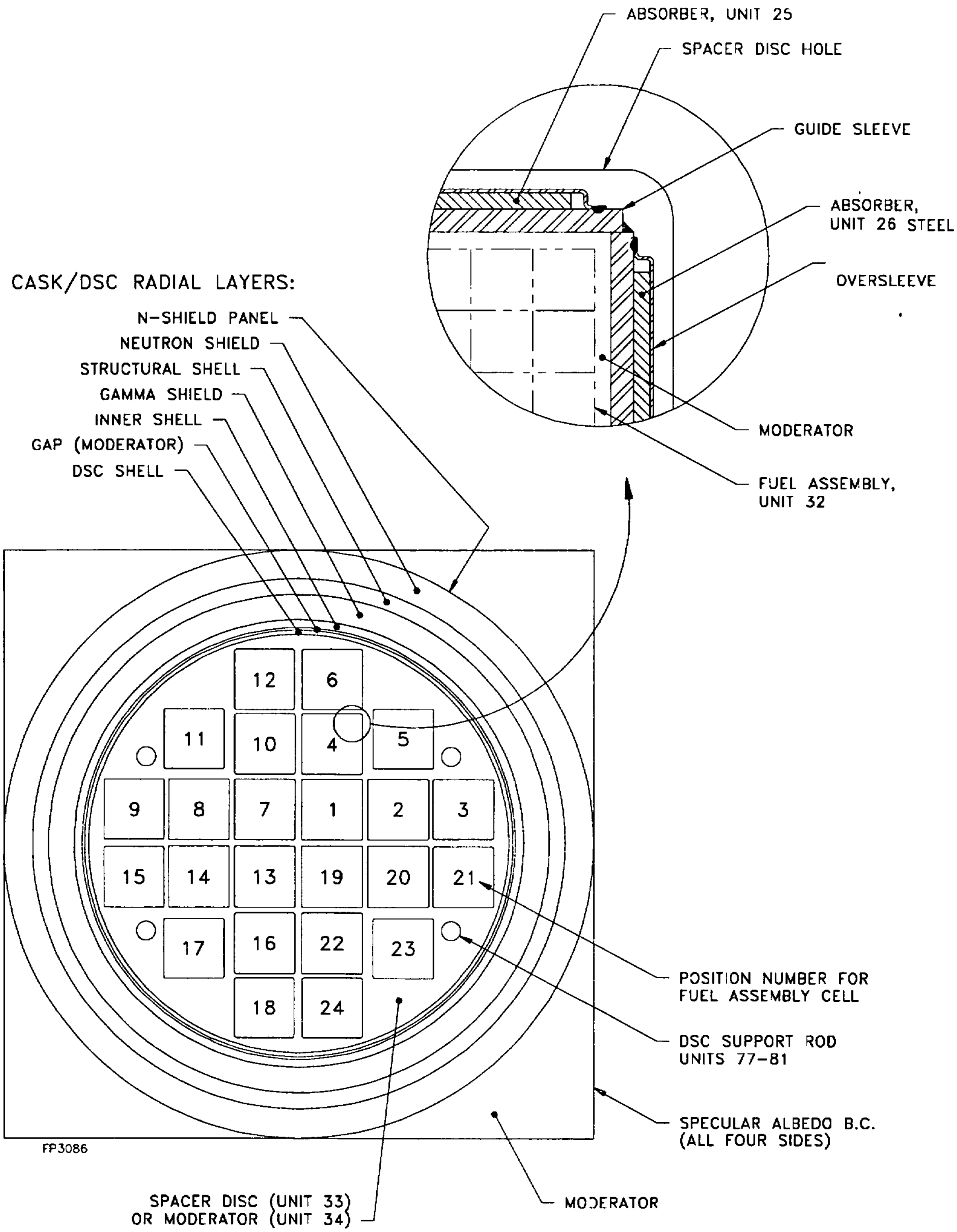

Figure 6.3-3

Structure of KENO Model UNITS 33 and 34

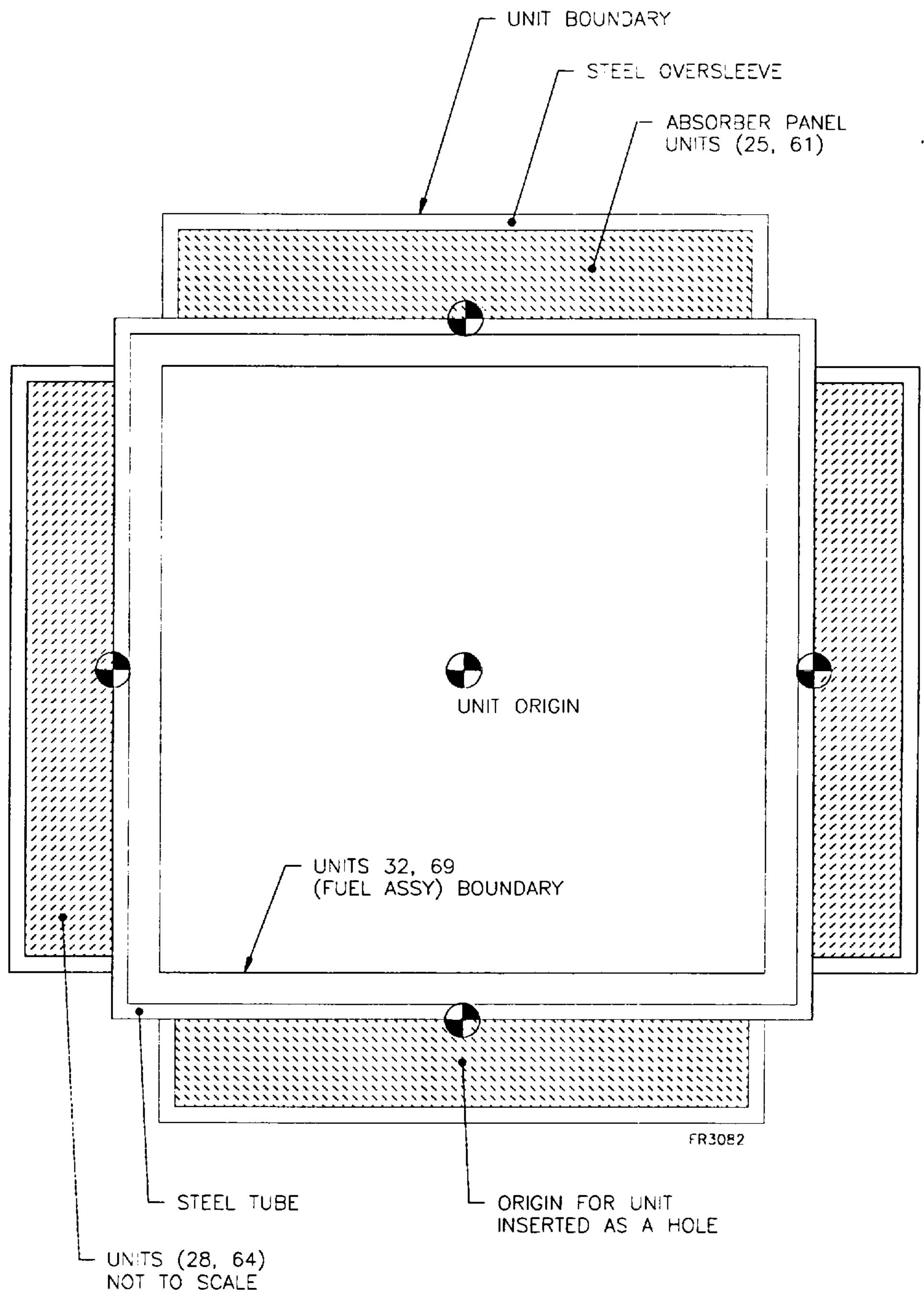

Figure 6.3-4

KENO Model UNITS 1-8, plus

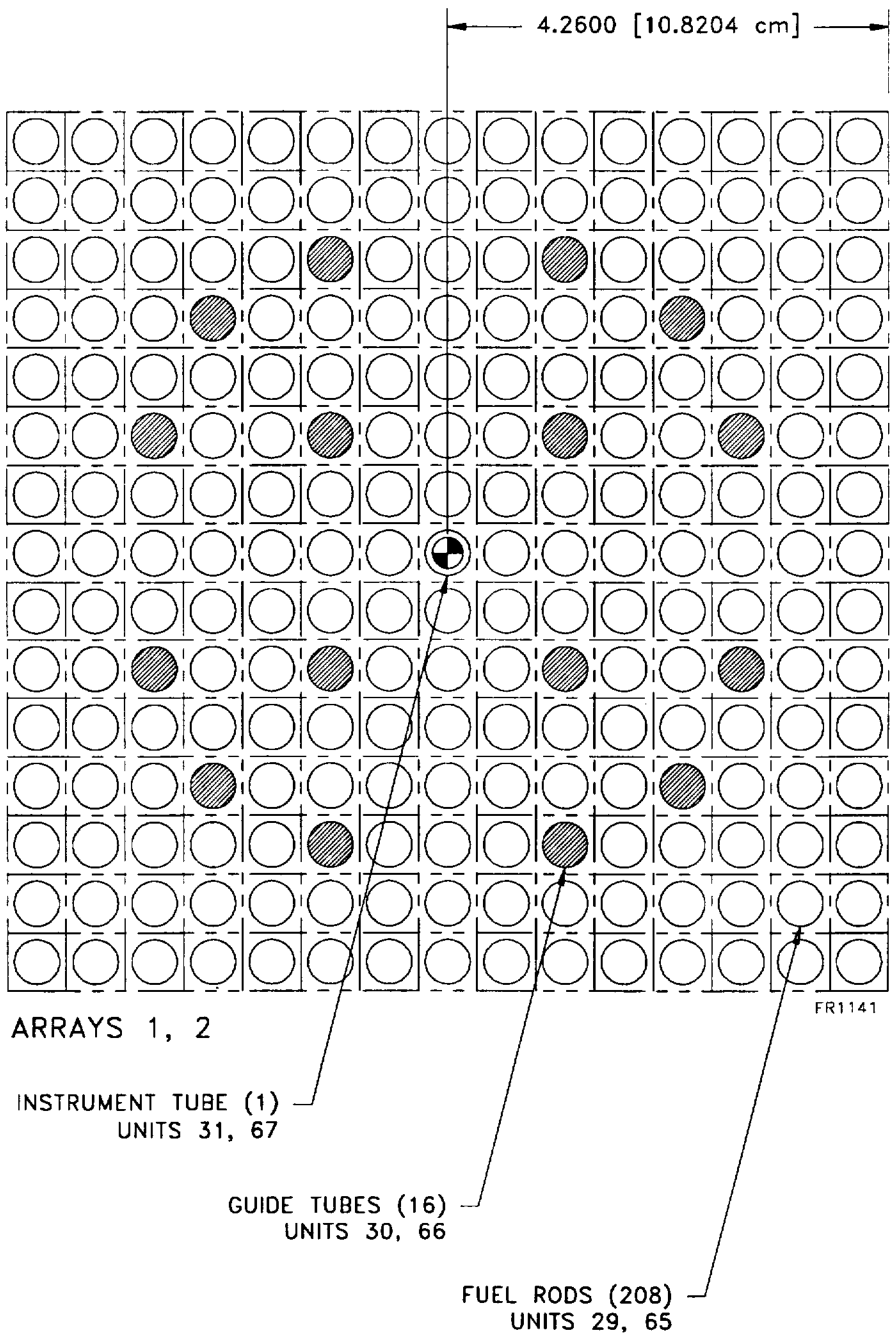

Figure 6.3-5

KENO Model of a Design Basis Fuel Assembly

6.3.3 NUHOMS®-MP187 Cask/FF-DSC Model

The NUHOMS®-MP187 Cask/FF-DSC KENO model is constructed in the same "slice of the cask" style as the MP187/FO-DSC model. The major differences are:

- 13 storage locations
- stainless steel fuel cans, no absorber panels/guide tubes
- different spacer disc pitch
- different support rod orientation (note that the support plates are modeled as an equivalent cylinder)
- Since SA240 Type XM-19 stainless steel has similar neutronic characteristics as carbon steel, it is an acceptable material for the spacer disc and support plate fabrication.

6.3.4 Package Regional Densities

Table 6.3-1 and Table 6.3-2 summarize the calculated atom densities used in the KENO models. Note that, when using the Hansen-Roach working library, resonance nuclides are specified by their σ_{peff}, thus the U235 and U238 atom density specifications in Table 6.3-1 are unique to each moderator state.

Table 6.3-1

KENO Model Atom Densities

Fuel Pellet			**Aluminum**		
Element	H-R ID No.	atom/b-cm	Element	H-R ID No.	atom/b-cm
Oxygen	8100	4.6540E-02	Aluminum	13100	6.0552E-02
U235	(run-unique)	8.0802E-04			
U238	(run-unique)	2.2462E-02			
Zircaloy-4			**Absorber Plate**		
Element	H-R ID No.	atom/b-cm	Element	H-R ID No.	atom/b-cm
Chromium	24100	7.5166E-05	Aluminum	13100	3.9268E-02
Iron	26100	1.4696E-04	Boron	5100	2.4879E-02
Nickel	28100	2.3299E-06	Carbon	6100	7.6705E-03
Zirconium	40100	4.2711E-02			
C-Steel			**Lead**		
Element	H-R ID No.	atom/b-cm	Element	H-R ID No.	atom/b-cm
Iron	26100	8.3801E-02	Lead	82100	3.2960E-02
Manganese	25100	8.6048E-04			
S_Steel			**NS-3**		
Element	H-R ID No.	atom/b-cm	Element	H-R ID No.	atom/b-cm
Chromium	24100	1.7274E-02	Aluminum	13100	7.0275E-03
Iron	26100	5.9042E-02	Calcium	20100	1.4835E-03
Manganese	25100	1.7210E-03	Carbon	6100	8.2505E-03
Nickel	28100	7.4481E-03	Hydrogen	1101	5.0996E-02
			Iron	26100	1.0628E-04
			Oxygen	8100	3.7793E-02
			Silicon	14100	1.2680E-03

Table 6.3-2

KENO Model Moderator Atom Densities

Density (g/cc)	Scaling Factor	Hydrogen (at/b-cm)	Oxygen (at/b-cm)
1.00000	1.00177	6.68544e-02	3.34272e-02
0.99823	1.00000	6.67361e-02	3.33680e-02
0.90000	0.90160	6.01690e-02	3.00845e-02
0.80000	0.80142	5.34835e-02	2.67418e-02
0.70000	0.70124	4.67981e-02	2.33990e-02
0.60000	0.60106	4.01126e-02	2.00563e-02
050000	0.50089	3.34272e-02	1.67136e-02
0.40000	0.40071	2.67418e-02	1.33709e-02
0.30000	0.30053	2.00563e-02	1.00282e-02
0.20000	0.20035	1.33709e-02	6.68544e-03
0.10000	0.10018	6.68544e-03	3.34272e-03
0.0500	0.05009	3.34272e-03	1.67136e-03
0.00000	0.00000	0.00000e-00	0.00000e-00

6.4 Criticality Calculation

6.4.1 Calculational Method

Criticality calculations for the NUHOMS®-MP187 Package are performed using the microcomputer application KENO5A [6.8] and the Hansen-Roach 16-group (HR-16) cross section working library. In order to use the HR-16 library, σ_{peff}, the effective resonance cross section, must be calculated for each resonance nuclide of interest (for this work, U235 and U238). σ_{peff} includes both resonance self shielding and heterogeneous effects. The proper working library nuclide, or more generally nuclides, must be selected from the HR-16 library based on σ_{peff}.

Corrections for resonance and heterogeneous effects are performed using the Transnuclear proprietary program PN-HET. PN-HET was developed during TN's validation of KENO5A as a means to streamline and unify the analytical approach used to calculate σ_{peff}. The calculational procedure is to:

A. Calculate σ_{peff} for U235 and U238 in the fuel rods.

B. Select H-R library nuclides with σ_{peff} above and below the calculated value.

C. Perform a weighted average to accurately represent the resonance nuclide using a mixture of the two selected nuclides.

The major assumptions made in the KENO modeling are:

A. Unirradiated fuel - no credit taken for fissile depletion or fission product poisoning.

B. No credit taken for fuel control components (applies to FC-DSC only).

C. Fuel is intact with no gross damage or missing rods (applies to FO/FC-DSCs only).

D. The fuel enrichment is modeled as uniform throughout the assembly. The maximum pellet enrichment is assumed to exist everywhere.

E. Fuel and cask are modeled as having finite length (water reflection is specified top and bottom) in allmodels.

F. Only 75% credit is taken for boron in neutron absorber panels.

G. All fuel rods are assumed to be filled with 100% moderator in the fuel cladding gap.

6.4.2 Fuel Loading Optimization

THIS SECTION CONTAINS
PROPRIETARY INFORMATION

Table 6.4-1

Summary of KENO Parametric Studies

Study	DSC Moderator Density	Ex-Cask Moderator Density	Neutron Shield	Radial Boundary Condition	Addresses
FONIF	Varies	1.0	Intact	Specular	§71.55(b)
FONXF	1.0	Varies	Intact	Specular	§71.59(a1)
FOHIF	Varies	1.0	None	Specular	§71.55(e)
FOHXF	1.0	Varies	None	Specular	§71.59(a2)
GSDEF*	1.0	0.70	None	Specular	§71.55(e)
FOCL	1.0	0.70	Varies	Specular	§71.55(b-3)
IFNCI	Varies	1.0	Intact	Water	§71.55(b)
IFNCX	1.0	Varies	Intact	Specular	§71.59(a2)
FFDSI	Varies	1.0	Intact	Water	§71.55(b)
FFDSX	1.0	Varies	Intact	Specular	§71.59(a2)

*This parametric study only applies to the FO Can.

The results of the studies are shown in graphic and tabular form at the end of this Section.

6.4.2.1 NUHOMS®–MP187 Cask/FO-DSC Summary

The highest calculated k_{eff} was for the Hypothetical Accident Condition, Cask Layer Removal Study (cask structural shell vanished) with 0.70 g/cc moderator interspersed between an infinite array of packages. The reactivity was 0.94015 ± 0.00148. With a 95% confidence (2σ), the maximum k_{eff} is 0.94311. The KENO5A/HR-16/PN-HET calculational bias is zero.

6.4.2.2 NUHOMS®–MP187 Cask/FF-DSC Summary

The highest calculated k_{eff} was for the Hypothetical Accident Condition (neutron shield vanished) with double-ended shear, one row of half length rods failed, 1.0 g/cc internal moderator, 0.80 g/cc external moderator in a single package with specular reflection at all boundaries. The hypothetical accident calculations were performed assuming the fuel will be in the most reactive credible post-drop condition as described above. The reactivity was

0.94598 ± 0.00185. With a 95% confidence (2σ), the maximum k_{eff} is 0.94968. The KENO5A/HR-16/PN-HET calculational bias is zero.

Table 6.4-2

MP187/FO-DSC KENO Results (Guide Sleeve Deformation)

Model	k_{eff}	+/-	1 s	$k_{eff} + 2\sigma$
gsdef00.ko	0.93271	+/-	0.00152	0.93575
gsdef025.ko	0.93097	+/-	0.00149	0.93395
gsdef05.ko	0.93197	+/-	0.00143	0.93483
gsdef08.ko	0.93093	+/-	0.00157	0.93407
gsdef10.ko	0.93337	+/-	0.00154	0.93645
gsdef11.ko	0.93221	+/-	0.00157	0.93535
gsdef12.ko	0.93610	+/-	0.00152	0.93914
gsdef14.ko	0.93672	+/-	0.00142	0.93956
gsdef16.ko	0.93723	+/-	0.00162	0.94047
gsdef18.ko	0.93966	+/-	0.00157	0.94280

A graphical representation of the results for Table 6.4-2 is shown in Figure 6.4-1.

Table 6.4-3

MP187/FO-DSC KENO Results (Cask Layer Removal)

Model	k_{eff}	+/-	1 s	$k_{eff} + 2\sigma$
FOCLA.KO	0.93818	+/-	0.00158	0.94134
FOCLB.KO	0.93758	+/-	0.00155	0.94068
FOCLC.KO	0.93966	+/-	0.00157	0.94280
FOCLD.KO	0.94015	+/-	0.00148	0.94311
FOCLE.KO	0.93513	+/-	0.00157	0.93827
FOCLF.KO	0.93859	+/-	0.00155	0.94169

Table 6.4-4

MP187/FO-DSC KENO Results

Model	keff	+/-	1 σ	Model	keff	+/-	1 σ
FONIF00.KO	0.33984	+/-	0.00095	FOHIF00.KO	0.34009	+/-	0.00100
FONIF05.KO	0.37054	+/-	0.00084	FOHIF05.KO	0.37023	+/-	0.00085
FONIF10.KO	0.53723	+/-	0.00110	FOHIF10.KO	0.53972	+/-	0.00112
FONIF20.KO	0.60799	+/-	0.00110	FOHIF20.KO	0.61329	+/-	0.00120
FONIF30.KO	0.66953	+/-	0.00126	FOHIF30.KO	0.67393	+/-	0.00123
FONIF40.KO	0.71959	+/-	0.00136	FOHIF40.KO	0.72584	+/-	0.00140
FONIF50.KO	0.76679	+/-	0.00141	FOHIF50.KO	0.76799	+/-	0.00134
FONIF60.KO	0.80562	+/-	0.00145	FOHIF60.KO	0.81102	+/-	0.00146
FONIF70.KO	0.84433	+/-	0.00149	FOHIF70.KO	0.84750	+/-	0.00156
FONIF80.KO	0.87400	+/-	0.00156	FOHIF80.KO	0.88223	+/-	0.00144
FONIF90.KO	0.90667	+/-	0.00167	FOHIF90.KO	0.91096	+/-	0.00158
FONIF100.KO	0.93159	+/-	0.00158	FOHIF100.KO	0.93389	+/-	0.00151

Model	keff	+/-	1 σ	Model	keff	+/-	1 σ
FONXF00.KO	0.93436	+/-	0.00152	FOHXF00.KO	0.93548	+/-	0.00156
FONXF05.KO	0.93290	+/-	0.00158	FOHXF05.KO	0.93524	+/-	0.00153
FONXF10.KO	0.93030	+/-	0.00151	FOHXF10.KO	0.93899	+/-	0.00153
FONXF20.KO	0.93116	+/-	0.00149	FOHXF20.KO	0.93712	+/-	0.00158
FONXF30.KO	0.93397	+/-	0.00147	FOHXF30.KO	0.93950	+/-	0.00156
FONXF40.KO	0.93330	+/-	0.00159	FOHXF40.KO	0.93607	+/-	0.00152
FONXF50.KO	0.93269	+/-	0.00148	FOHXF50.KO	0.93604	+/-	0.00152
FONXF60.KO	0.93100	+/-	0.00149	FOHXF60.KO	0.93885	+/-	0.00147
FONXF70.KO	0.93331	+/-	0.00153	FOHXF70.KO	0.93966	+/-	0.00157
FONXF80.KO	0.93052	+/-	0.00161	FOHXF80.KO	0.93600	+/-	0.00156
FONXF90.KO	0.93074	+/-	0.00153	FOHXF90.KO	0.93734	+/-	0.00158
FONXF100.KO	0.93159	+/-	0.00158	FOHXF100.KO	0.93389	+/-	0.00151

Table 6.4-5

MP187/FF-DSC KENO Results

Model	keff	+/-	1 σ	Model	keff	+/-	1 σ
IFNCI000.KO	0.26349	+/-	0.00070	FFDSI000.KO	0.25584	+/-	0.00081
IFNCI005.KO	0.37248	+/-	0.00098	FFDSI005.KO	0.36074	+/-	0.00098
IFNCI010.KO	0.60350	+/-	0.00143	FFDSI010.KO	0.59256	+/-	0.00143
IFNCI020.KO	0.67650	+/-	0.00158	FFDSI020.KO	0.67131	+/-	0.00159
IFNCI030.KO	0.72586	+/-	0.00173	FFDSI030.KO	0.72868	+/-	0.00172
IFNCI040.KO	0.76875	+/-	0.00186	FFDSI040.KO	0.77097	+/-	0.00183
IFNCI050.KO	0.80214	+/-	0.00186	FFDSI050.KO	0.80398	+/-	0.00176
IFNCI060.KO	0.83485	+/-	0.00184	FFDSI060.KO	0.83614	+/-	0.00186
IFNCI070.KO	0.86550	+/-	0.00195	FFDSI070.KO	0.87030	+/-	0.00184
IFNCI080.KO	0.88686	+/-	0.00184	FFDSI080.KO	0.89273	+/-	0.00185
IFNCI090.KO	0.90846	+/-	0.00184	FFDSI090.KO	0.91861	+/-	0.00184
IFNCI100.KO	0.93493	+/-	0.00205	FFDSI100.KO	0.94382	+/-	0.00192

Model	keff	+/-	1 σ	Model	keff	+/-	1 σ
IFNCX000.KO	0.93065	+/-	0.00195	FFDSX000.KO	0.94015	+/-	0.00182
IFNCX005.KO	0.93402	+/-	0.00186	FFDSX005.KO	0.94498	+/-	0.00183
IFNCX010.KO	0.93828	+/-	0.00198	FFDSX010.KO	0.94164	+/-	0.00188
IFNCX020.KO	0.93636	+/-	0.00184	FFDSX020.KO	0.94164	+/-	0.00194
IFNCX030.KO	0.94004	+/-	0.00186	FFDSX030.KO	0.93913	+/-	0.00196
IFNCX040.KO	0.93472	+/-	0.00186	FFDSX040.KO	0.94024	+/-	0.00190
IFNCX050.KO	0.93430	+/-	0.00194	FFDSX050.KO	0.94159	+/-	0.00198
IFNCX060.KO	0.93829	+/-	0.00189	FFDSX060.KO	0.94471	+/-	0.00193
IFNCX070.KO	0.93336	+/-	0.00189	FFDSX070.KO	0.94150	+/-	0.00189
IFNCX080.KO	0.93152	+/-	0.00186	FFDSX080.KO	0.94598	+/-	0.00185
IFNCX090.KO	0.92930	+/-	0.00187	FFDSX090.KO	0.94417	+/-	0.00189
IFNCX100.KO	0.93405	+/-	0.00192	FFDSX100.KO	0.94015	+/-	0.00189

Single-ended Shear

Model	keff	+/-	1 σ	Model	keff	+/-	1 σ
FFSS010.KO	0.92971	+/-	0.00209	FFSS020.KO	0.93198	+/-	0.00195
FFSS030.KO	0.93866	+/-	0.00190	FFSS040.KO	0.93735	+/-	0.00194
FFSS048.KO	0.93920	+/-	0.00183				

Table 6.4-6

MP187/FF-DSC KENO Results (Cask Layer Removal)

File	Cask Layer	K_{eff}	+/-	1σ	$K_{eff} + 2\sigma$
FFCL80A.KO	Nominal	0.94248	+/-	0.00194	0.94636
FFCL80B.KO	N Shield Panel	0.94008	+/-	0.00180	0.94368
FFCL80C.KO	N Shield	0.94598	+/-	0.00185	0.94968
FFCL80D.KO	Cask Structural Shell	0.94336	+/-	0.00184	0.94704
FFCL80E.KO	Gamma Shield	0.93934	+/-	0.00189	0.94312
FFCL80F.KO	Cask Inner Shell	0.94492	+/-	0.00191	0.94874

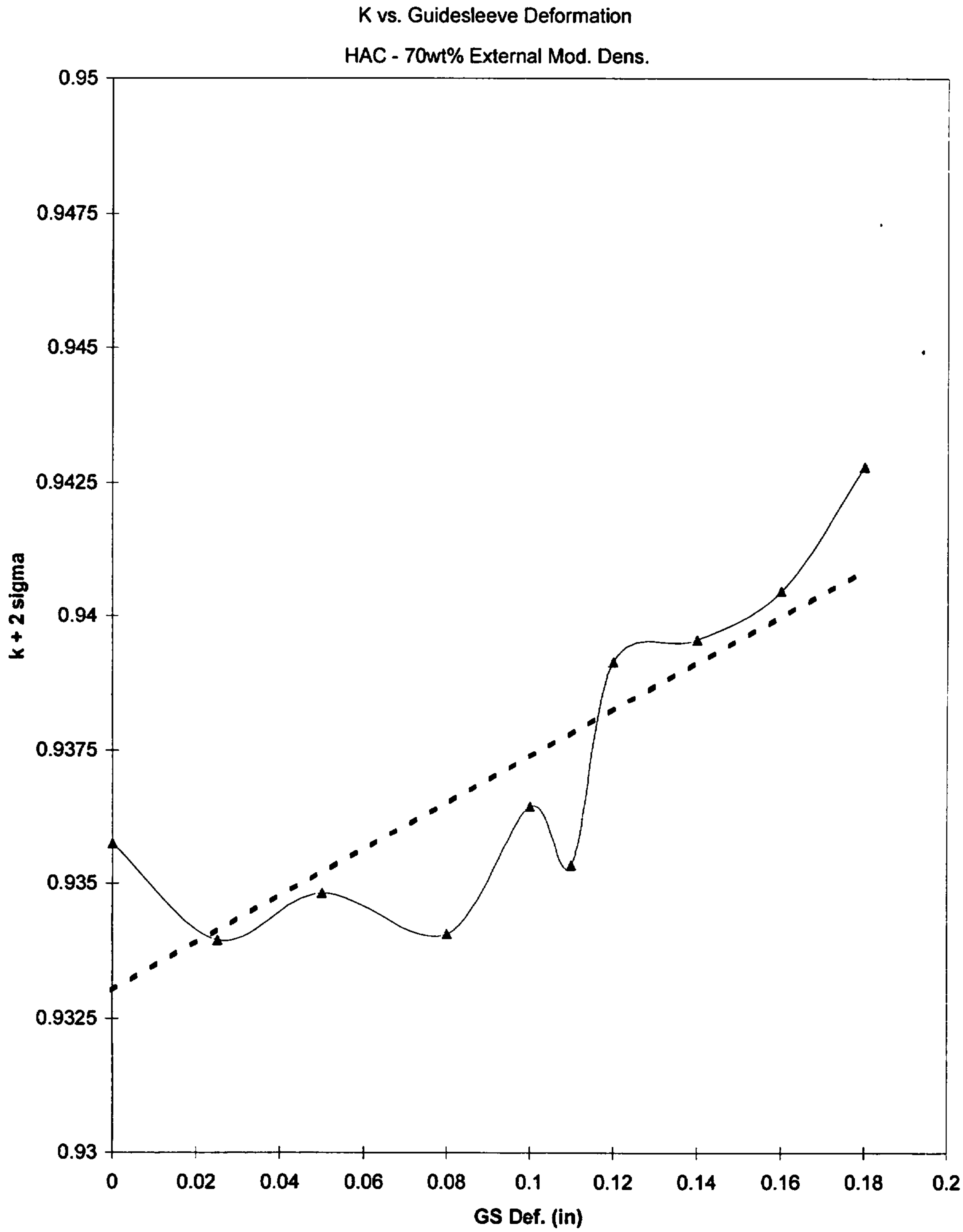

Figure 6.4-1

K vs. Guide Sleeve Deformation

THIS SECTION CONTAINS
PROPRIETARY INFORMATION

Figure 6.4-2

FF-DSC Broken Fuel Rod Models

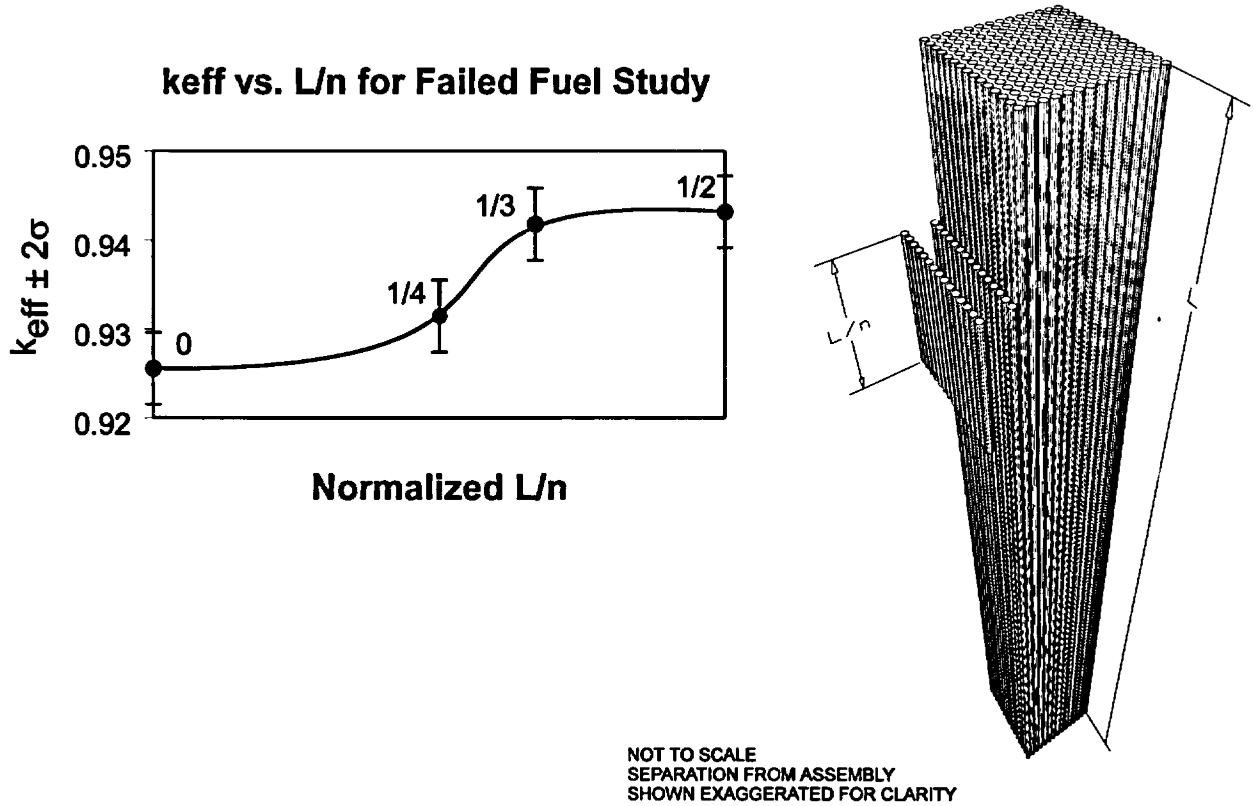

Figure 6.4-3

FF-DSC Double-Ended Rod Break Models

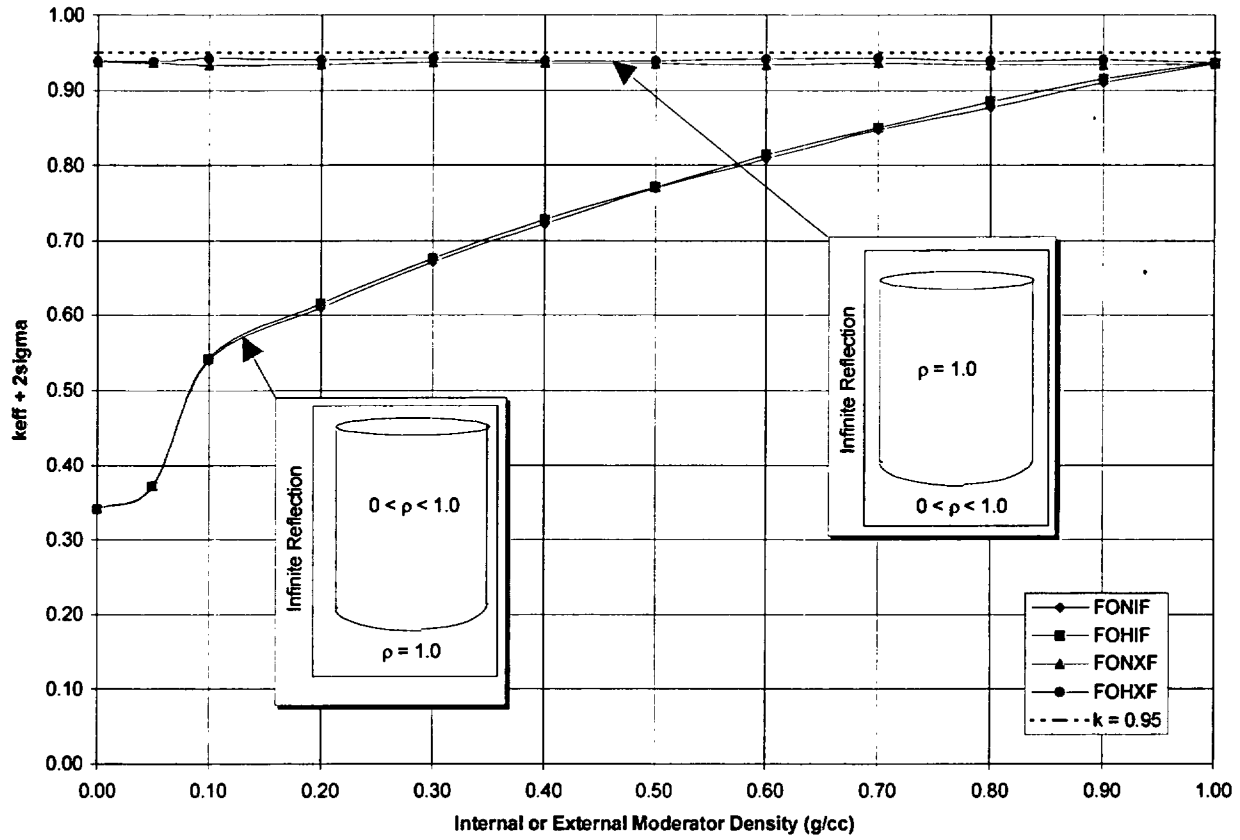

± 2σ error bars omitted for clarity

Figure 6.4-4

NUHOMS®-MP187 Cask/FO-DSC Criticality Results

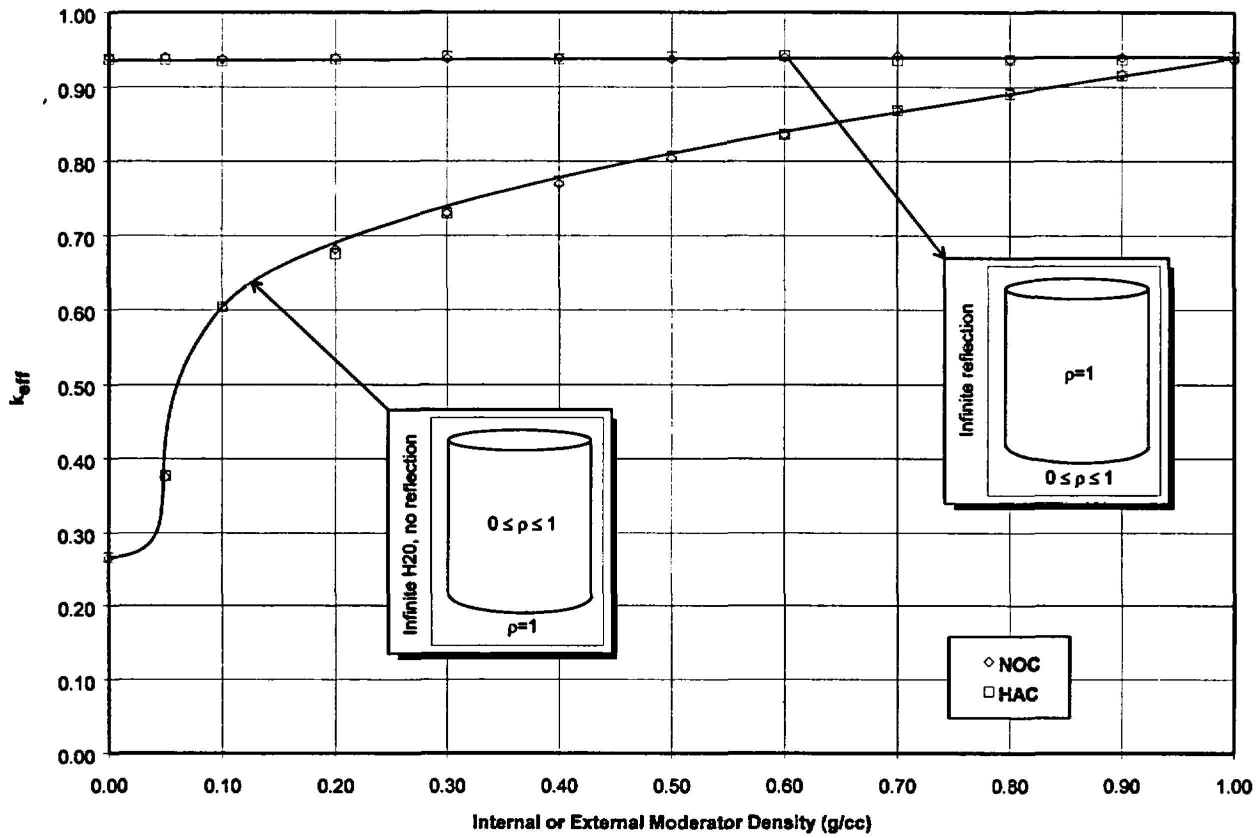

± 2σ error bars omitted for clarity

Figure 6.4-5

NUHOMS®-MP187 Cask/FF-DSC Criticality Results

6.5 Critical Benchmark Experiments

6.5.1 Benchmark Experiments and Applicability

A suite of 150 critical and subcritical LWR fuel benchmark cases was run by Transnuclear to validate KENO5A, the Hansen-Roach 16 group working cross section library, and PN-HET [6.9] (a TN proprietary code for performing nuclear resonance/heterogeneous effects calculations). The large number of cases was necessary to evaluate parameter dependencies, such as fuel enrichment, fuel rod pitch, absorber material, absorber thickness, absorber to cluster distance, reflector material, reflector to cluster distance, and critical cluster separation.

The benchmark problems are representative of critical or subcritical arrays of commercial light water reactor (LWR) fuels with the following characteristics:

A. water moderation

B. neutron absorbers:

- no special neutron absorbers,
- neutron absorption by fixed sheets,
- neutron absorption by aqueous solutions

C. unirradiated light water reactor type fuel (no fission products or "burnup credit") near room temperature (vs. reactor operating temperature)

D. close reflection:

- no specific reflector,
- steel,
- lead, and
- depleted uranium

A statistical analysis of the largest statistical population of benchmark cases was performed to determine if the KENO-Va/HR-16/PN-HET methodology produces any bias due to fuel enrichment, fuel rod pitch, absorber material, absorber thickness, absorber to cluster distance, reflector material, reflector to cluster distance, critical cluster separation, or other parameters. This population consisted of 134 benchmark experiments performed on critical arrays of fuel rods, References [6.11] through [6.14]. Of the 150 cases originally run by Transnuclear West, 14 B&W critical experiments (Reference 6.15) and two subcritical experiments (Reference 6.16) were not included with the 134 cases because they contained experimental or empirical uncertainties not related to the benchmark bias.

A subset of the 134 cases was chosen to be most representative of the NUHOMS®–MP187 Package design for the purpose of establishing a calculational bias. The criterion used to select the subset of cases was the neutron absorber material since that parameter most strongly influences the behavior of the system. From the set of 134 cases, those with cadmium, copper, copper/cadmium, unborated aluminum, Zircaloy, Boroflex, and no neutron absorbers were discarded. There were six benchmark cases with borated absorber panels (similar to the FO- and FC-DSC absorber panels) and 13 cases with stainless steel neutron absorbing panels (thick stainless steel guide tubes are used in the FF-DSC design, thin stainless sheets are used for guide tubes in the FO- and FC-DSCs).

6.5.2 Details of Benchmark Calculations

The KENO5A code and HR-16 library were used to model the critical configurations. The modeling technique incorporated a rod-by-rod representation of the fuel assemblies with explicit models of the material interspersed between assemblies. The cross section library identifiers for resonance materials were selected using PN-HET. All pertinent data for each critical configuration are documented in References [6.11] through [6.16] to permit use of these data for validating calculational methods in accordance with ANSI N16.9-1976 [6.5].

6.5.3 Results of Benchmark Calculations

Statistical analysis of the 134 critical benchmark cases showed that there are no systematic biases for fuel enrichment, fuel rod pitch, absorber material, absorber thickness, absorber to cluster distance, reflector material, reflector to cluster distance, and critical cluster separation. One dependency was noted on reflector to cluster distance for depleted uranium (DU) reflected benchmarks. The source of this bias could not be determined, but since the MP187 cask does not use a DU shielding, no corrections were made to the criticality results and the DU criticals were not used to calculate the final calculational bias for the KENO-Va/HR-16/PN-HET methodology. Figure 6.5-1 shows the results of the benchmark calculations.

Once the conclusion was drawn that the KENO-Va/HR-16/PN-HET methodology produces no systematic biases that would affect the MP187 calculations, a subset of cases most like the MP187 system were chosen as described above for the purpose of calculating the final calculational bias. The results of the nineteen most applicable benchmark critical cases are shown in bold face type in Table 6.5-1. The results are summarized below:

	Absorber Plates	
	Borated	Stainless
Cases	6	13
Maximum k_{eff}	1.01064	1.01405
Average k_{eff}	1.00819	1.00897
Minimum k_{eff}	1.00499	1.00254
Standard Deviation	0.00197	0.00372

The calculational bias is the maximum difference between any applicable calculated critical benchmark k_{eff} and unity, excluding any cases where the calculated k_{eff} was greater than unity. The calculated k_{eff}, without its associated uncertainty, is used for determining the bias. The group of applicable critical benchmark experiments is the nineteen cases described above.

Since all cases had a calculated k_{eff} greater than unity, the calculational bias is zero.

Table 6.5-1

Benchmark Calculation Results

Note: ***Bold face*** benchmarks are most applicable to MP187

THIS SECTION CONTAINS
PROPRIETARY INFORMATION

THIS SECTION CONTAINS
PROPRIETARY INFORMATION

Figure 6.5-1
Critical Benchmark Results

6.6 Appendix

6.6.1 References

6.6.2 KENO Input Files

6.6.1 References

6.1 Code of Federal Regulations, Title 10, Part 71, "Packaging and Transportation of Radioactive Material."

6.2 ANSI/ANS-8.1-1983, "Nuclear Criticality Safety in Operations with Fissionable Materials Outside Reactors."

6.3 ANSI/ANS-8.17-1984, "Criticality Safety Criteria for the Handling, Storage, and Transportation of LWR Fuel Outside Reactors."

6.4 USNRC Regulatory Guide 3.41, "Validation of Calculational Methods for Nuclear Criticality Safety," Revision 1, May, 1977.

6.5 ANSI N16.9-1975, "Validation of Calculational Methods for Nuclear Criticality Safety."

6.6 USNRC Regulatory Guide 1.13, "Spent Fuel Storage Facility Design Basis," Proposed Revision 2, December 1981 (for guidance only).

6.7 "Safety Analysis Report for the Standardized NUHOMS® Horizontal Modular Storage System for Irradiated Nuclear Fuel," NUH-003, Revision 4A, TNW, June 1996.

6.8 "KENO5A-PC, Monte Carlo Criticality Program with Supergrouping," CCC-548, Oak Ridge National Laboratory, June, 1990.

6.9 Thomas, B. D., "QA Category 2 Computer Code Verification Document - KENO5A," Pacific Nuclear Version 1.2.0," Revision 2, TNW Proprietary.

6.10 Burn, Reed R., "Boral Accelerated Radiation Aging Tests," Nuclear Reactor Laboratory, University of Michigan, Ann Arbor, Michigan, May 9, 1990.

6.11 Bierman, S.R., et al., "Criticality Experiments with Subcritical Clusters of 2.35 Wt% and 4.31 Wt% ^{235}U Enriched UO_2 Rods in Water With Steel Reflecting Walls," Battelle Pacific Northwest Laboratories, NUREG/CR-1784, April, 1981.

6.12 Bierman, S.R., et al., "Critical Separation Between Subcritical Clusters of 4.29 Wt% ^{235}U Enriched UO_2 Rods in Water With Fixed Neutron Poisons," Battelle Pacific Northwest Laboratories, NUREG/CR-0073, May 1978.

6.13 Bierman, S.R., et al., "Criticality Experiments with Subcritical Clusters of 2.35 Wt% and 4.31 Wt% ^{235}U Enriched UO_2 Rods in Water With Uranium or Lead Reflecting Walls," Battelle Pacific Northwest Laboratories, NUREG/CR-0796, August, 1981.

6.14 Bierman, S.R., et al., "Critical Separation Between Subcritical Clusters of 2.35 Wt% ^{235}U Enriched UO_2 Rods in Water with Fixed Neutron Poisons," Battelle Pacific Northwest Laboratories, PNL-2438, October, 1977.

6.15 Baldwin, M.N., et al., "Critical Experiments Supporting Close Proximity Water Storage of Power Reactor Fuel," BAW-1484-7, Babcock & Wilcox Company, Lynchburg, Virginia, July, 1979.

6.16 Bierman, S.R., "Reactivity Measurements on an Experimental Assembly of 4.31 Wt% ^{235}U Enriched UO_2 Fuel Rods Arranged in a Shipping Cask Geometry," Battelle Pacific Northwest Laboratories, PNL-6838, October, 1989.

6.6.2 KENO Input Files

THIS SECTION CONTAINS
PROPRIETARY INFORMATION

7. OPERATING PROCEDURES

7.1 Procedures for Loading the Package

The NUHOMS®-MP187 Cask can be used (1) to transport fuel offsite; (2) to transfer fuel to horizontal storage modules (HSMs) in an onsite storage facility; or (3) an onsite storage container. Each of these modes of use requires (1) preparation of the cask for use; (2) verification that the fuel assemblies to be loaded meet the criteria set forth in this document; and (3) installation of a DSC and fuel assemblies into the cask.

Onsite storage involves transfer of the DSC to the storage facility where it is either inserted into an HSM, or left inside the cask for storage. Offsite transport involves (1) preparation of the cask for transport; (2) assembly verification leakage-rate testing of the package containment boundary; (3) placement of the cask onto a transportation vehicle; and (4) installation of the impact limiters.

During shipment, the packaging contains up to 24 spent fuel assemblies in the FO-DSC or FC-DSC, or up to 13 spent fuel assemblies in the FF-DSC. Procedures are provided in this section for three different handling/storage schemes, as shown in Figure 7.1-1. These include transport of the cask/DSC directly from the plant fuel pool, transport after storage in a NUHOMS® Horizontal Storage Module (HSM), and transport after onsite storage in the NUHOMS®-MP187 cask. Additional procedures are provided for handling a DSC which has leaked during storage in an HSM. A glossary of terms used in this section is provided in Section 7.1.9.

7.1.1 Preparation of the NUHOMS®-MP187 Cask for Use

Procedures for preparing the cask for use after receipt at the site are provided in this section.

a. Remove the impact limiter attachment bolts from each impact limiter and remove the impact limiters from the cask.

b. Anytime prior to removing the lid, sample the cask cavity atmosphere through the vent port. Flush the cask interior gases to the site radwaste systems if necessary.

c. Remove the transportation skid closure assembly.

d. Take contamination smears on the outside surfaces of the cask. If necessary, decontaminate the cask until smearable contamination is at an acceptable level.

e. Inspect the cask hardware (including closure plates, rupture discs, and vent/drain/test ports) for damage which may have occurred during transportation. Repair or replace as required. Metallic O-ring seals shall be discarded after each use.

f. Place suitable slings around the cask top and bottom ends, lift cask and place on suitable cribbing.

g. Remove the cask trunnion plugs. Inspect the trunnion sockets as discussed in Section 8.2.3.4, and install the upper and lower trunnions. Torque the trunnion attachment screws for each of the four trunnions in accordance with the drawings in Appendix 1.3.2.

h. Using slings, lift the cask and place it onto the onsite transfer trailer.

i. Remove the slings from the cask.

j. Install the onsite support skid pillow block covers.

7.1.2 Wet Loading the NUHOMS®-MP187 Cask and DSC

The procedure for wet loading the cask and DSC is summarized in this section. This procedure is intended to describe the type and quality of work performed to load and seal a DSC. Actual DSC loading procedures may vary slightly from tasks described below. The cask/DSC wet loading procedure is shown in Figure 7.1-2. The NUHOMS®-MP187 Cask is designed to transport one FO-DSC or FC-DSC containing twenty-four PWR fuel assemblies or one FF-DSC containing 13 PWR fuel assemblies. Fuel assemblies with missing fuel pins shall not be shipped in the FO-DSC or FC-DSC unless dummy fuel pins that displace an equal amount of water have been installed in the fuel assembly. All fuel assembly locations are to be loaded with design basis fuel assemblies or dummy assemblies of the same weight. Verification that the burnup, enrichment, and cooling time of the assemblies are all within acceptable ranges will be performed by site personnel, prior to shipment, as discussed below.

a. Verify that the fuel assemblies to be placed in the DSC meet the maximum burnup, maximum initial enrichment, minimum cooling time, and maximum decay heat limits for Type I or Type II fuel assemblies as specified in Section 1.2.3 of this document.

   Note: All damaged fuel assemblies to be loaded into the FF-DSC must meet the criteria in Section 1.2.3 for damaged fuel, having no more than 15 known or suspected damaged fuel rods.

   The potential of fuel misloading is essentially eliminated through the implementation of multiple procedural and administrative barriers. The controls instituted to ensure that fuel assemblies are loaded into a known cell location within a DSC will typically take the following form:

   - A cask/DSC loading plan is developed to compare various parameters including decay heat values to guarantee that Type I fuel assemblies are identified to be placed only in the four innermost cells of the DSC. This loading plan is the same procedure that verifies the fuel assemblies to be placed in the DSC meet the maximum burnup, maximum initial enrichment, and minimum cooling time requirements.

- The loading plan is independently verified and approved.
- A fuel movement schedule is then written, verified and approved based upon the loading plan. All fuel movements from any rack location are performed under strict verbatim compliance of the fuel movement schedule.
- All fuel assemblies are videotaped and independently verified by ID number to match the movement schedule prior to the placement of the shield plug.
- A third verification is performed by the Special Nuclear Materials Manager in preparation for the DOE reporting requirements. This third verification independently verifies that fuel in the DSC is placed per the original cask loading plan.

b. Using a suitable prime mover, position the cask and onsite transfer trailer below the plant crane.

c. Remove the ram closure plate, inspect the sealing surfaces, and re-install the ram closure plate. If the cask is to be used for transportation offsite, new metallic seals shall be installed with the ram closure plate. If the cask is to be used for onsite transfer of the DSC, a single, elastomeric seal may be installed in the ram closure in lieu of the dual metallic seals specified on the drawings. The purpose of this seal is only to protect the cask cavity from contamination. This seal is not intended to act as a containment boundary. Inspect the rupture discs for damage during prior operations. Repair or replace as necessary.

d. Remove the onsite support skid pillow block covers.

e. Engage the cask upper trunnions with the lifting yoke using the plant crane, rotate the cask to a vertical orientation, lift the cask from the onsite support skid, and place the cask in the plant decon area.

Note: The empty cask may be uprighted and lifted using the lifting yoke either with the top closure installed or removed.

f. If the cask top closure plate has not already been removed, remove the bolts from the cask top closure plate and lift the top closure plate and seals (if present) from the cask.

g. Discard the used metallic seals.

h. Install the cask shear key plug assembly.

i. Place an empty DSC in the cask. Align DSC to ensure proper positioning of DSC grapple ring key within cask bottom forging keyway.

j. Fill the DSC cavity and the cask/DSC annulus with clean, demineralized water and install the cask annulus seal.

Note: The DSC cavity may optionally be filled with borated spent fuel pool water if required by plant specific procedures.

k. Lower the cask and DSC into the fuel pool and load 24 PWR fuel assemblies into the DSC (13 assemblies for the FF-DSC). In accordance with Chapter 1, no more than four Type I assemblies shall be installed in the center fuel spaces. Location of Type I assemblies shall be verified to be the center four fuel spaces.

Note: Failed fuel assemblies may be placed into their removable cans directly in the FF-DSC and then the can lids installed, or loaded in a separate area and the loaded failed fuel can placed into the DSC.

l. Place the DSC top shield plug onto the DSC.

m. Lift the cask/canister/fuel from the fuel pool and place it in the plant decon area.

n. Remove surface water from the top of the DSC and the cask/DSC annulus seal.

o. Decontaminate the cask surfaces such that smearable surface contamination on the cask is less than 2200 dpm/100 cm^2 from beta and gamma emitting sources and 220 dpm/100 cm^2 from alpha emitting sources.

p. Install the DSC inner top cover plate and place the inner seal weld.

q. Drain the DSC and draw and hold a vacuum of three torr or less for a minimum of 30 minutes in the DSC cavity.

r. Backfill the DSC cavity with helium to 0 psig to 2.5 psig.

s. Install and seal weld the DSC vent and siphon port cover plates.

t. Install and seal weld the DSC outer top cover plate.

u. Remove the cask drain port screw and drain the cask/DSC annulus.

v. Install the drain port screw and tighten in accordance with the drawings in Appendix 1.3.2. Install and tighten the drain port plug to the torque specified in the Appendix 1.3.2 drawings.

7.1.3 Transferring the DSC to an Onsite Storage Facility

DSCs may be stored onsite in a 10 CFR Part 72 licensed facility prior to transportation. This section provides an outline of the procedure for transferring the DSC from the Auxiliary/Fuel building to an onsite ISFSI for storage either in the NUHOMS®-MP187 Cask or in an HSM. Note that the NUHOMS®-MP187 Cask or an alternate NRC approved onsite transfer cask may be used for onsite movements of the DSC. This procedure is described herein to provide a general description of 10 CFR 72 operations to be performed with the MP187 cask. These operations are governed by a 10 CFR 72 license. For onsite transfer operations, the DSC provides the fuel containment boundary and the cask is used for physical protection and shielding. The cask cavity, therefore, need not be sealed during onsite movements of the DSC.

a. Install the cask top closure and install a minimum of 12 top closure bolts snug tight. The top closure seals are not required to be installed.

b. Using the cask lifting yoke engage the upper trunnions, lift the cask from the decon area, and place the cask in the onsite support skid.

c. Install the onsite support skid pillow block covers.

d. Using a suitable prime mover, tow the onsite transfer trailer to the onsite storage facility.

7.1.4 Placing the DSC in an HSM for Storage

The procedure for loading a DSC into an HSM is summarized in this section. As noted above, either the NUHOMS®-MP187 Cask or an alternate onsite transfer cask may be used during HSM loading. This procedure is described herein to provide a general description of 10 CFR 72 operations to be performed with the MP187 cask. These operations are governed by a 10 CFR 72 license. This procedure is typical of NUHOMS® ISFSIs and some of the steps listed below may not be required and/or may be performed in a different order.

a. Position the onsite transfer trailer in front of the module face.

b. Remove the cask ram closure plate.

c. Install the ram trunnion support assembly.

d. Remove the HSM door.

e. Use the trailer skid positioning system and optical surveying transits to align the cask with the HSM.

f. Remove the cask top closure.

g. Dock the cask with the HSM and install the cask/HSM restraints.

h. Install and align the hydraulic ram cylinder in the ram trunnion support assembly.

i. Extend the ram hydraulic cylinder until the grapple contacts the DSC bottom cover.

j. Engage the DSC grapple ring with the ram grapple.

k. Extend the ram hydraulic cylinder until the DSC is fully inserted in the HSM.

l. Disengage the grapple from the DSC.

m. Remove the hydraulic ram from the cask.

n. Remove the cask from the HSM.

o. Install the HSM door and DSC seismic restraint.

7.1.5 Loading the DSC into the Cask from an HSM

The procedure for loading a DSC into the cask from a NUHOMS® Horizontal Storage Module (HSM) is summarized in this section. DSCs stored in HSMs have previously been loaded and sealed as described in Section 7.1.2 above. The cask/HSM loading procedure is shown in Figure 7.1-3. Depending on the most recent use of the cask, several of the initial steps listed below may not be necessary.

a. Using a suitable prime mover, bring the onsite transfer trailer (and cask) to the ISFSI site and back the trailer in front of the module face.

b. Remove the ram closure plate and the top closure plate.

c. Install the ram trunnion support assembly.

d. Remove the HSM door and the DSC seismic restraint assembly from the HSM.

e. Use the trailer skid positioning system and optical surveying transits to align and dock the cask with the HSM.

f. Install the cask/HSM restraints.

g. Install and align the hydraulic ram cylinder in the ram trunnion support assembly.

h. Extend the ram hydraulic cylinder until the grapple contacts the DSC bottom cover.

i. Engage the DSC grapple ring with the ram grapple.

j. Retract the ram hydraulic cylinder until the DSC is fully seated in the cask.

k. Disengage the grapple from the DSC.

l. Remove the hydraulic ram and ram trunnion support assembly from the cask.

m. Install the ram closure plate. If the DSC transfer is to result in long term storage or transportation, install a new set of metallic O-ring seals and perform the procedure described in Section 7.1.7. If the DSC is being moved to another HSM or the plant fuel pool, then a single O-ring (metallic or elastomeric) may be installed.

n. Remove the cask/HSM restraints.

o. Using the skid positioning system, move the cask to the transfer position and secure the onsite support skid to the onsite transfer trailer.

p. Install the cask toop closure. If the transfer is to result in long term storage or transportaion, install metallic O-ring seals and perform the procedure described in Section 7.1.7. If the DSC is being transferred on site, then install the cask top closure per Step “a” of Section 7.1.3.

7.1.6 Placing the DSC in Metal Cask Storage at an Onsite Facility

The procedure for placing the NUHOMS®-MP187 cask containing intact or failed DSCs into onsite storage is summarized in this section. This procedure is described herein to provide a general description of 10 CFR 72 operations to be performed with the MP187 cask. These operations are governed by a 10 CFR 72 license. DSCs to be stored have previously been loaded, sealed, and transferred to the facility as described in Sections 7.1.2 and 7.1.1 above.

a. If the DSC is stored in an HSM, retrieve the DSC as described in Section 7.1.5.

b. Install a new set of top closure seals.

c. If necessary, apply vacuum grease to the seals and the adjoining sealing surfaces on the cask top closure.

d. Install the cask top closure. Lubricate, install and preload the top closure bolts per the drawing requirements.

e. Install a new set of ram closure seals.

f. If necessary, apply vacuum grease to the seals and the adjoining sealing surfaces on the cask ram closure.

g. Install the cask ram closure plate. Lubricate, install, and preload the ram closure bolts per the drawing requirements.

h. Using a suitable vacuum pump, evacuate the cask cavity and backfill with helium.

i. Perform an assembly verification leak test as specified in Appendix 7.4.2.

j. Set the cask on the storage pad and if required install the shear key plug assembly and the cask weather shield/tip over impact limiter device.

7.1.7 Preparing the Cask for Transportation

Once a loaded DSC has been placed inside the NUHOMS®-MP187 Cask, the following tasks are performed to prepare the cask for transportation. The cask is assumed to be seated horizontally in the onsite support skid. Note that steps 7.1.7(a) through 7.1.7(e) have already been performed for DSCs stored in the cask and need not be repeated.

a. Verify that all metallic O-ring seals are new. Discard any seals that have previously been installed in the cask.

b. If necessary, apply vacuum grease to the seals and the adjoining sealing surfaces on the cask top closure.

c. Install the cask top closure plate. Lubricate, install and preload the top closure bolts per the drawing requirements.

d. If necessary, apply vacuum grease to the seals and the adjoining sealing surfaces on the cask ram closure.

e. Install the cask ram closure plate. Lubricate, install and preload the ram closure bolts per the drawing requirements.

f. If necessary, remove the shear key plug assembly from the cask.

g. Verify that the drain port screw is installed and torqued in accordance with the drawings in Appendix 1.3.2.

h. Verify that the fuel assemblies meet the burnup, initial enrichment, cooling time, and decay heat criteria set forth in Section 1.2.3.

i. Not used.

j. Verify that the cask surface removable contamination levels meet the requirements of 49 CFR 173.443 [7.2] and 10 CFR 71.87 [7.3].

k. Perform the assembly verification leakage rate testing specified in Appendix 7.4.2. This test must be performed within 12 months prior to the shipment. This test includes drawing a vacuum in the cavity between the cask and DSC, which ensures that any water has been removed.

7.1.8 Placing the Cask onto the Railcar

The procedure for placement of the cask on the railcar is given in this section and shown in Figure 7.1-4.

a. Using a suitable prime mover, bring the cask and onsite transfer trailer to the transportation railcar.

b. Remove the onsite support skid pillow block covers.

c. Install suitable slings around the cask top and bottom ends.

d. Lift the cask from the onsite transfer trailer.

e. Remove the cask upper and lower trunnions and install the trunnion plugs.

f. Place the cask onto the railcar transportation skid.

g. Remove the lifting slings from the cask.

h. Install the skid closure assembly and insert the locking wedges.

i. Install the impact limiters on the cask and torque the mounting bolts in accordance with the drawings in Appendix 1.3.2.

j. Install the cask tamperproof seals.

k. Monitor the cask radiation levels per 49 CFR 173.441 [7.2] and 10 CFR 71.47 [7.3] requirements.

Note: The procedure outlined above may also be used to transfer the cask directly from the fuel pool to a rail car, without using the transfer trailer, should appropriate facilities be available for such a transfer. The procedures outlined in Section 7.1.7 would also be applicable to such a scenario.

7.1.9 Glossary

The following terms, used in the above procedures, are defined below. See Table 1.0-1 for terms relating to the package.

a.	Horizontal Storage Module (HSM):	Concrete shielded structure used for onsite storage of DSCs.
b.	Onsite Transfer Trailer:	A hydraulically supported trailer used for onsite movements of the cask.
c.	Onsite Support Skid:	Skid present on the onsite transfer trailer used to support the cask during onsite movements.
d.	Cask/DSC Annulus Seal:	Pneumatic seal placed between the cask and DSC during operations in the fuel pool.
e.	Cask Lifting Yoke:	Passive, open hook lifting yoke used for vertical lifts of the cask.
f.	Ram Trunnion Support Assembly:	Frame attached to the cask bottom which provides an anchor for the hydraulic ram during DSC insertion and retrieval.
g.	Skid Positioning System:	Hydraulically operated alignment system that provides the interface between the onsite transfer trailer and the onsite support skid.
h.	Hydraulic Ram:	Hydraulic cylinder used to insert/withdraw DSCs to/from HSMs.
i.	Cask/HSM Restraints:	Provides the load path between the cask and HSM during DSC transfer operations.
j.	Cask Weather Shield/ Tip Over Impact Limiter Device:	Provides environmental protection of the cask top cover during storage and protects cask contents in event of cask tipover.

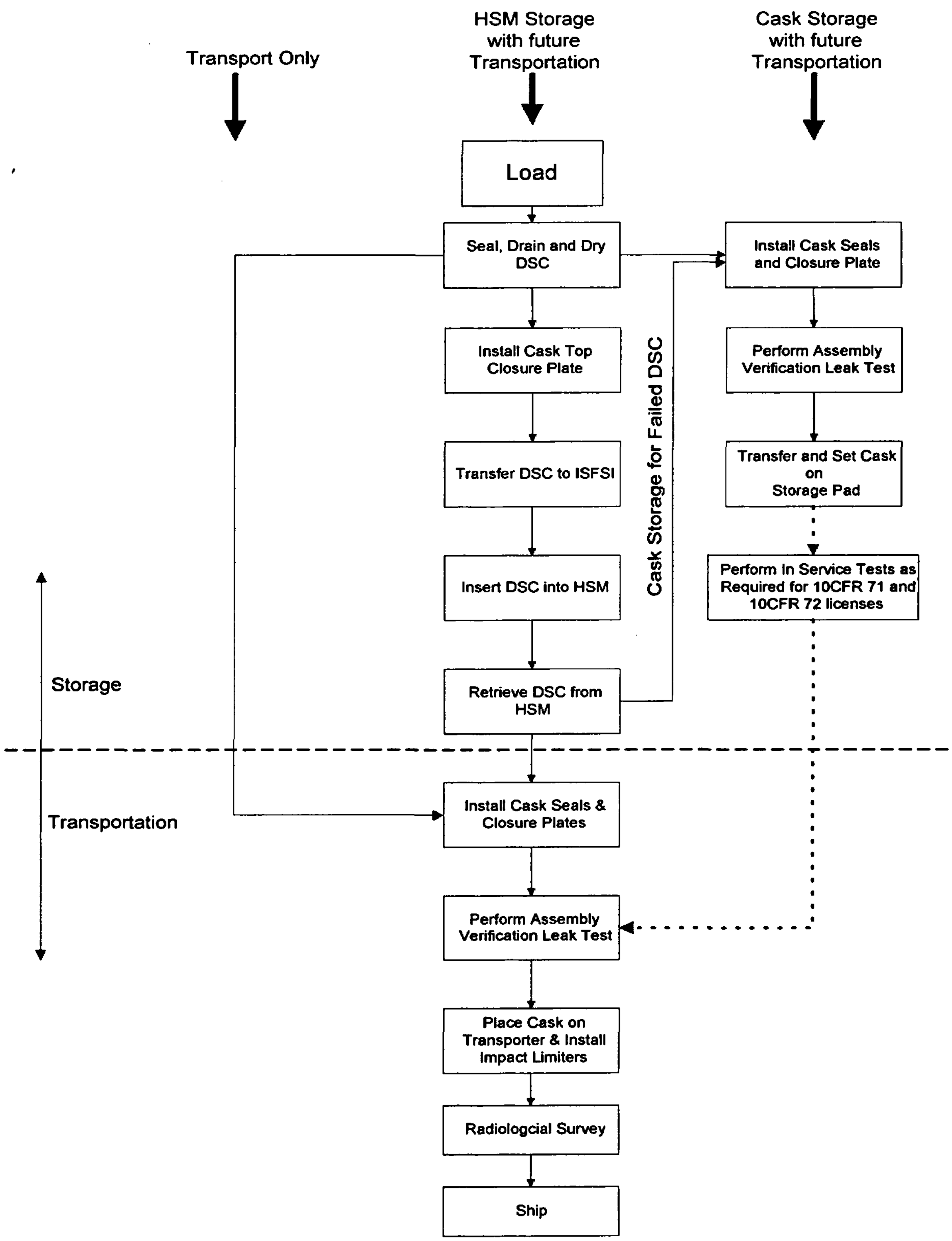

Figure 7.1-1

NUHOMS®-MP187 Cask Operating Procedures Flow Chart

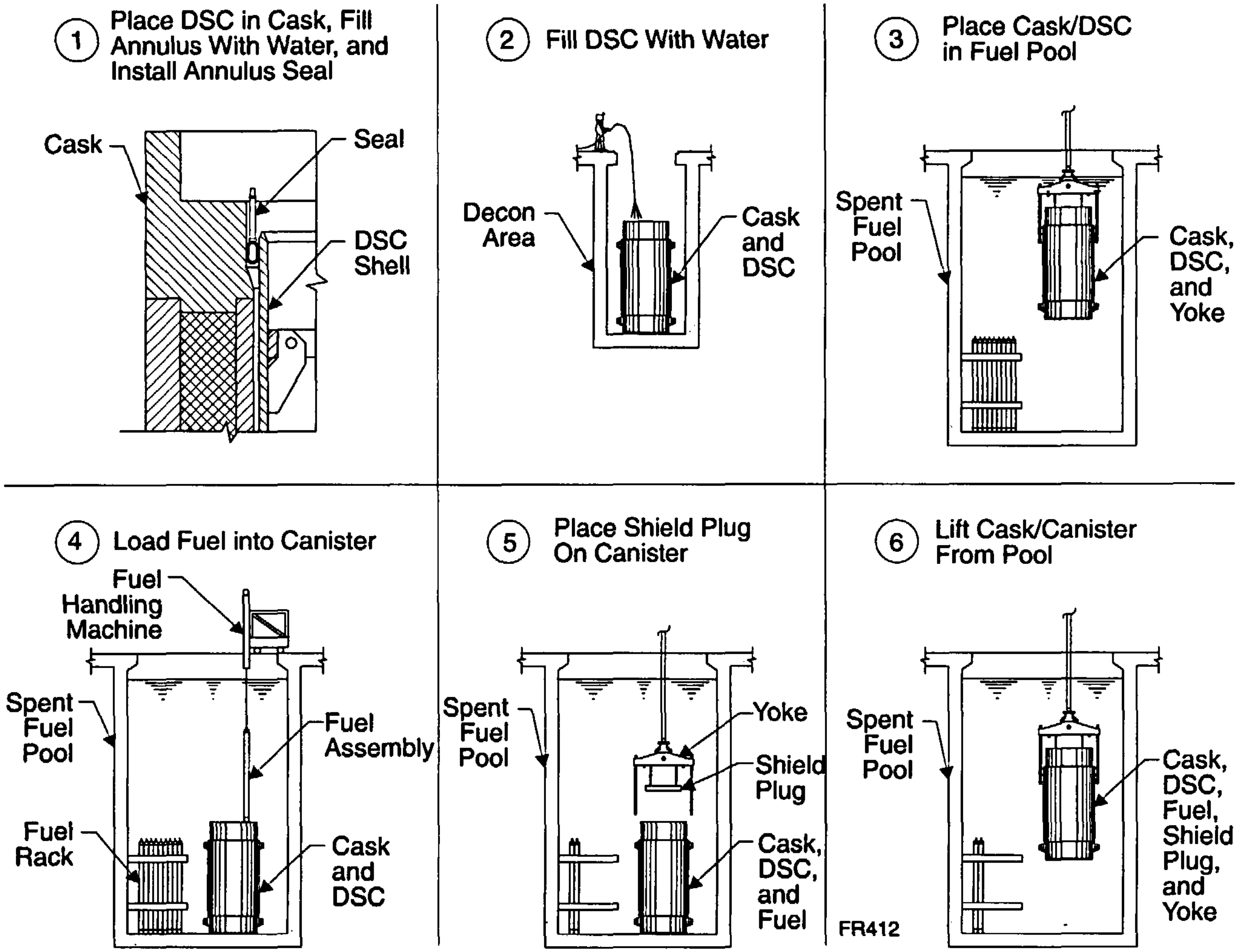

Figure 7.1-2
NUHOMS®-MP187 Wet Loading Procedure

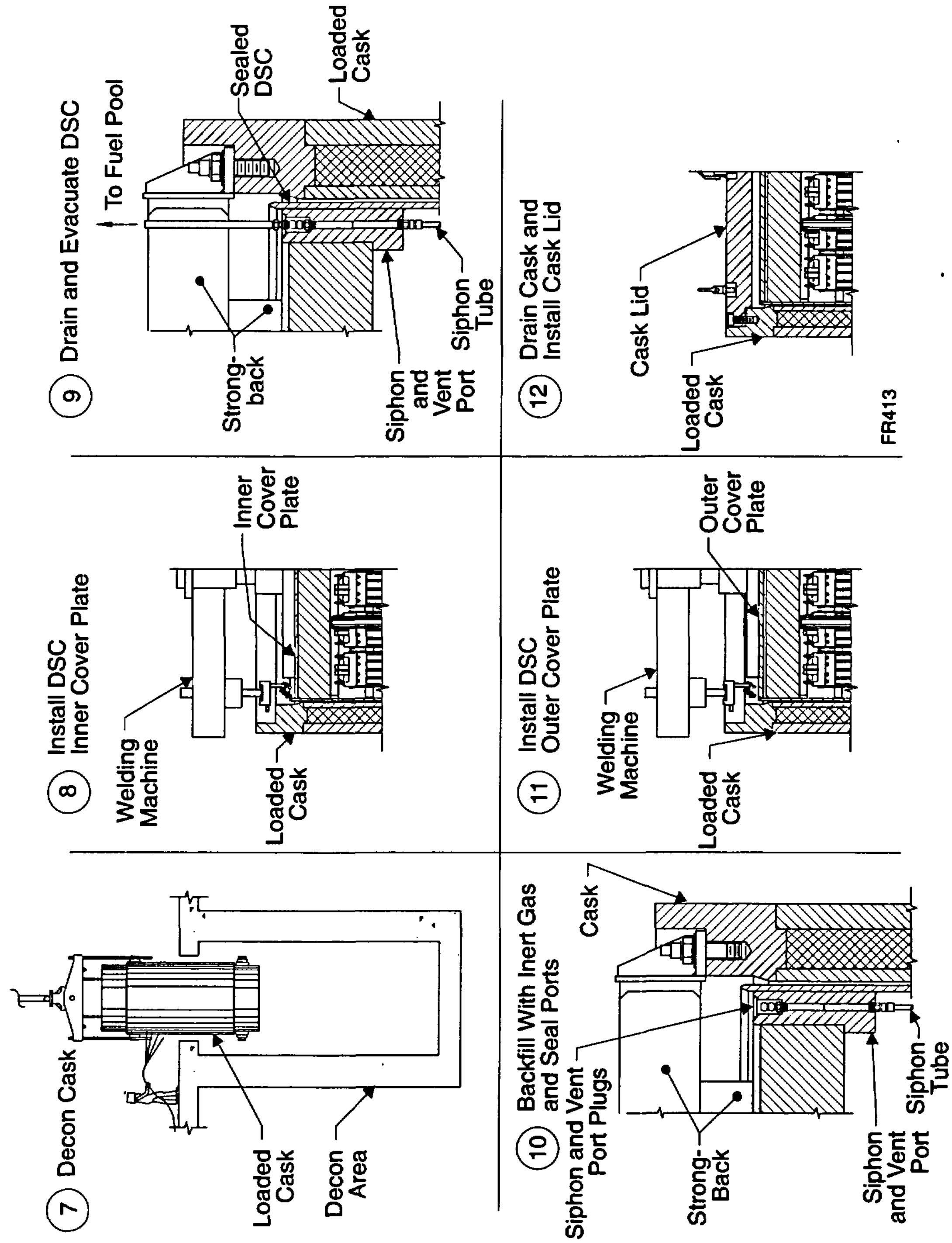

Figure 7.1-2

NUHOMS®-MP187 Wet Loading Procedure (concluded)

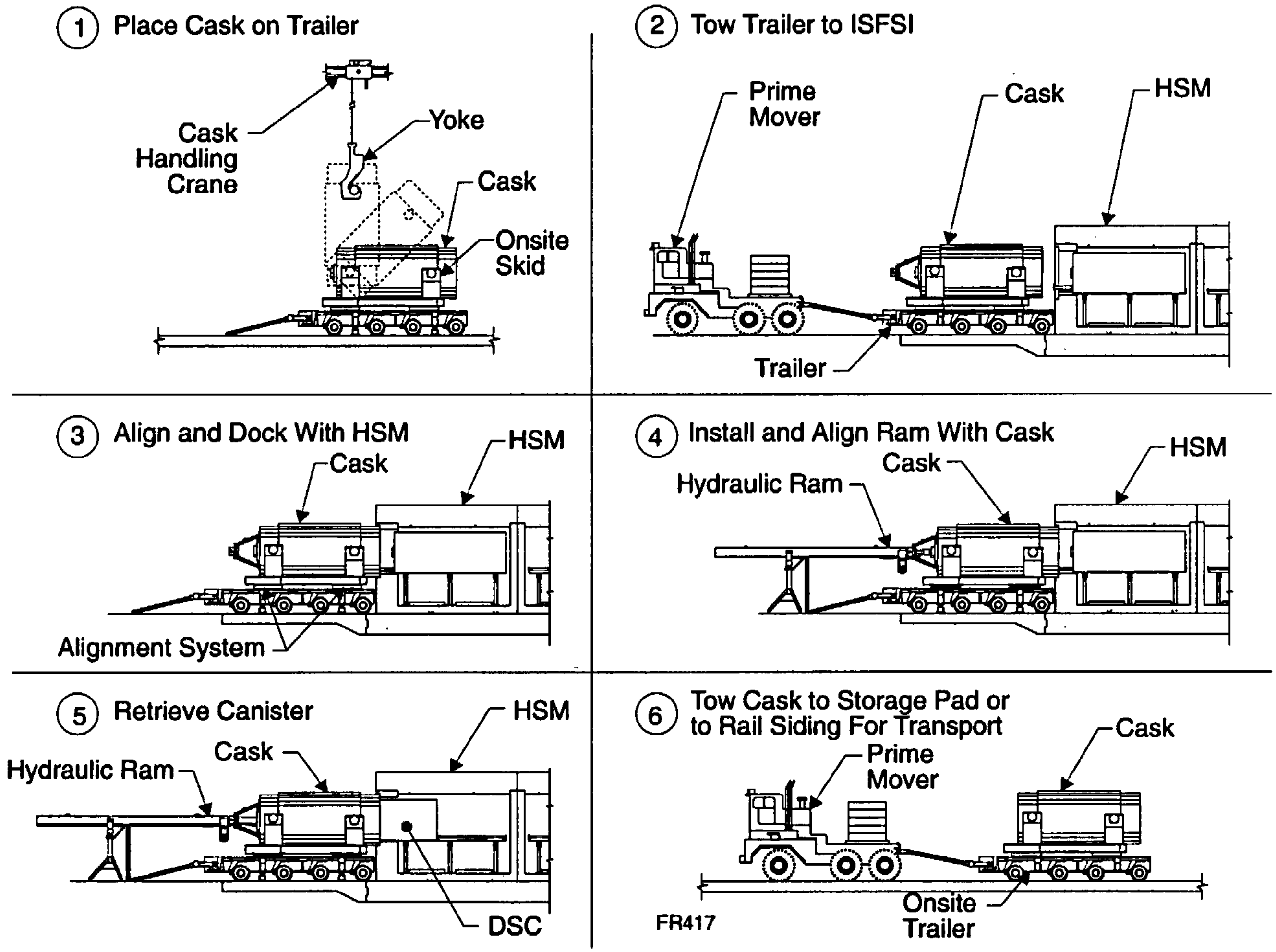

Figure 7.1-3
NUHOMS®-MP187 Dry Loading Procedure

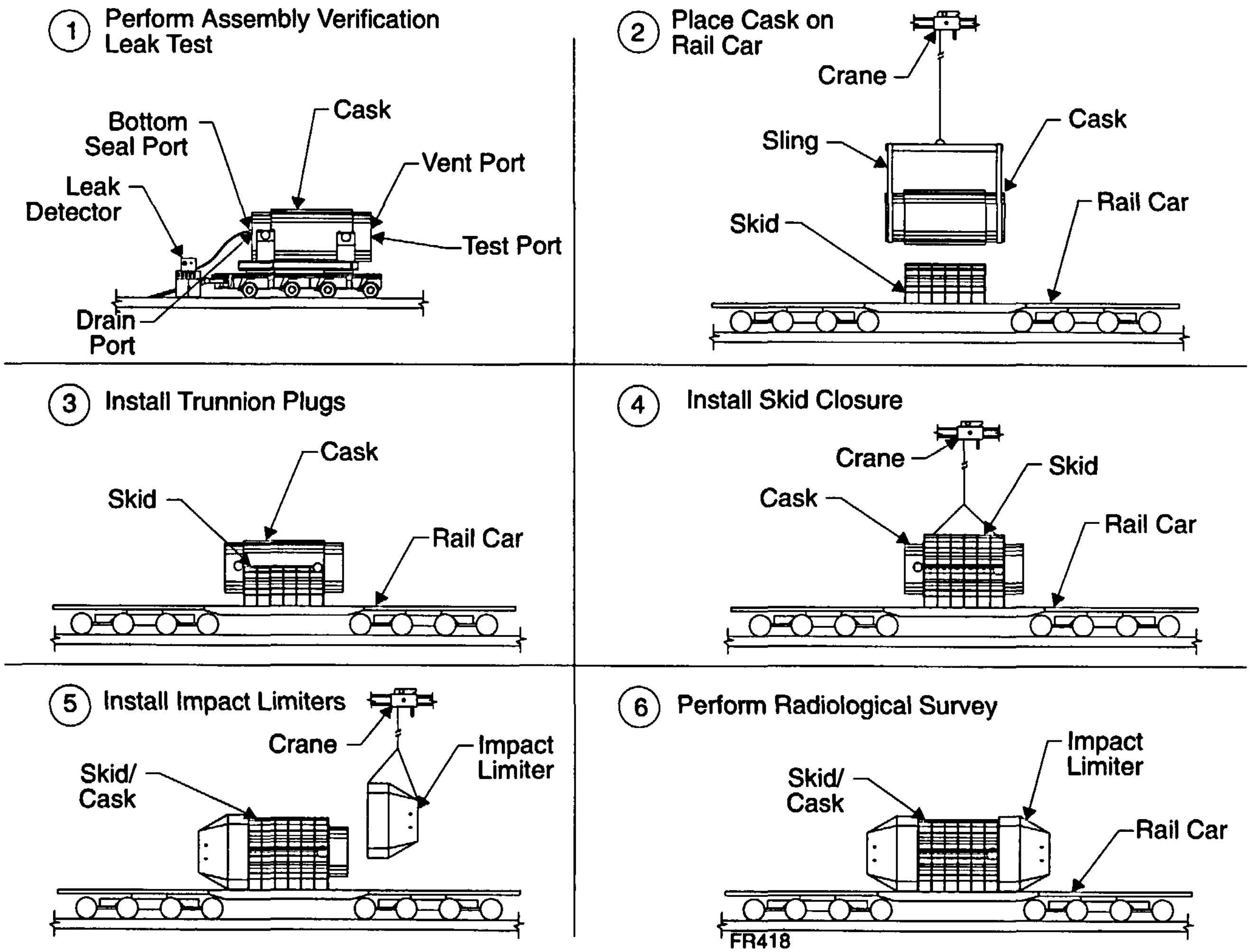

Figure 7.1-4
NUHOMS®-MP187 Preparation for Transportation

7.2 Procedures for Unloading the Cask

Unloading the NUHOMS®-MP187 Cask after transport involves removing the cask from the railcar and removing the canister from the cask. The cask is designed to allow the canister to be unloaded from the cask into a NUHOMS® staging module, or hot cell, and provisions exist to allow wet unloading into a fuel pool. The necessary procedures for these tasks are essentially the reverse of those described in Section 7.1.

7.2.1 Receipt of the Loaded NUHOMS®-MP187 Cask

Procedures for receiving the loaded cask after shipment are described in this section. Procedures for receiving an empty cask are provided in Section 7.1.1.

a. Verify that the tamperproof seals are intact.

b. Remove the tamperproof seals.

c. Remove the impact limiter attachment bolts from each impact limiter and remove the impact limiters from the cask.

d. Remove the transportation skid closure assembly.

e. Take contamination smears on the outside surfaces of the cask. If necessary, decontaminate the cask until smearable contamination is at an acceptable level.

f. Place suitable slings around the cask top and bottom ends.

g. Using a suitable crane, lift the cask from the railcar and remove the cask trunnion plugs. Inspect the trunnion sockets as discussed in Section 8.2.3.4 and install the upper and lower trunnions. Torque the trunnion attachment screws for each of the four trunnions in accordance with the drawings in Appendix 1.3.2. Place cask onto the onsite transfer trailer. Remove the slings from the cask.

h. Install the onsite support skid pillow block covers.

i. Transfer the cask to a staging module, fuel pool, or dry cell and unload using the procedures described in the following sections.

7.2.2 Unloading the NUHOMS®-MP187 Cask to a Staging Module

The procedure for unloading a DSC from the cask into an HSM is summarized in this section. This procedure is typical of NUHOMS® ISFSIs and some of the steps listed below may be performed in a different order.

a. Position the onsite transfer trailer in front of the module face.

b. Sample the cask cavity atmosphere through the vent port. Flush the cask interior gases to the site radwaste systems if necessary.

c. Remove the cask ram closure plate. Discard the metallic ram closure seals.

d. Install the ram trunnion support assembly.

e. Remove the HSM door.

f. Use the skid positioning system and optical surveying transits to align the cask with the HSM.

g. Remove the cask top closure. Discard the metallic top closure seals.

h. Dock the cask with the HSM and install the cask/HSM restraints.

i. Install and align the hydraulic ram cylinder in the ram trunnion support assembly.

j. Extend the ram hydraulic cylinder until the grapple contacts the DSC bottom cover.

k. Engage the DSC grapple ring with the ram grapple.

l. Extend the ram hydraulic cylinder until the DSC is fully inserted in the HSM.

m. Disengage the grapple from the DSC.

n. Remove the hydraulic ram from the cask.

o. Remove the cask from the HSM.

p. Install the HSM door and DSC seismic restraint.

q. Move the onsite transfer trailer and cask to a low-dose maintenance area.

r. Inspect the cask hardware (including covers and vent/drain/test ports) for damage that may have occurred during transportation. Repair or replace as necessary.

7.2.3 Unloading the NUHOMS®-MP187 Cask to a Fuel Pool

The procedure for unloading the cask and DSC into a fuel pool is summarized in this section. This procedure is intended to describe the type and quality of work performed to unload a DSC. Actual DSC unloading procedures may vary slightly from the tasks described below. Note that the NUHOMS®-MP187 cask or an alternate suitable cask may be used for onsite movements of the DSC.

a. Tow the onsite transfer trailer to the fuel receiving area.

b. Remove the onsite support skid pillow block covers.

c. Using the cask lifting yoke, engage the upper trunnions, rotate the cask to a vertical orientation, lift the cask from the onsite support skid, and place the cask in the decon pit.

d. Sample the cask cavity atmosphere through the vent port. Flush the cask interior gases to the site radwaste systems if necessary.

e. Remove the bolts from the cask top closure and lift the top closure plate from the cask.

f. Remove and discard the cask top closure seals.

g. Install the shear key plug assembly.

h. Locate the DSC siphon and vent ports using the indications on the DSC outer top cover plate.

i. Drill a hole in the DSC outer top cover plate and remove the siphon closure plug to expose the siphon port quick connect.

j. Drill a hole in the DSC outer top cover plate and remove the vent closure plug to expose the vent port quick connect.

k. Sample the DSC cavity atmosphere. If necessary, flush the DSC cavity gases to the site radwaste systems.

l. Fill the DSC with demineralized water through the siphon port with the vent port open and routed to the plant's off-gas system.

Note: The DSC cavity may optionally be filled with borated water.

m. Install a debris shield over the cask/DSC annulus.

n. Use plasma arc-gouging, a mechanical cutting system, or other suitable means remove the closure weld from the outer top cover plate.

o. Remove the DSC outer top cover plate.

p. Remove the closure weld from the DSC inner top cover plate.

q. Remove the DSC inner top cover plate.

r. Fill the cask/DSC annulus with demineralized water and install the cask/DSC annulus seal.

s. Remove excess material on the DSC inside shell surface which will interfere with top shield plug removal.

t. Clean the cask surface of dirt and debris that may have accumulated during transportation or weld removal.

u. Engage the cask lifting yoke to the upper trunnions and install the shield plug cables between the yoke and the DSC top shield plug.

v. Lower the cask into the fuel pool.

w. Disengage the lifting yoke from the cask trunnions and remove the top shield plug.

x. Remove the fuel assemblies (or fuel cans for the FF-DSC) from the DSC.

y. Engage the lifting yoke to the cask upper trunnions, remove the cask from the pool, and place it in the decon area.

z. Remove the water from the DSC cavityand DSC/Cask annulus.

aa. Remove the DSC from the cask and handle in accordance with low-level waste procedures.

bb. Decontaminate the cask inner and outer surfaces as necessary.

cc. Inspect the cask hardware (including covers and valves) for damage that may have occurred during transportation. Repair or replace as necessary.

7.2.4 Unloading the NUHOMS®-MP187 Cask to a Dry Cell

The procedure for handling a DSC in a dry cell is highly dependent on the design of the dry cell and on the intended future use of the DSC. The procedure described below is intended to show the type of operations that will be performed and is not intended to be limiting.

a. Tow the onsite transfer trailer to the hot cell area.

b. Remove the onsite support skid pillow block covers.

c. Using the cask lifting yoke, engage the upper trunnions, rotate the cask to a vertical orientation, lift the cask from the onsite support skid, and place the cask in the appropriate handling area.

d. Sample the cask cavity atmosphere through the vent port. Flush the cask interior gases to the site radwaste systems if necessary.

e. Remove the bolts from the cask top closure and lift the top closure plate from the cask.

f. Remove and discard the cask top closure seals.

g. Install the shear key plug assembly, if required.

h. Transfer the cask into the hot cell using suitable handling equipment.

i. Remove the DSC from the cask and handle according to appropriate procedures.

j. Remove the cask from the hot cell.

k. Decontaminate the cask inner and outer surfaces as necessary.

l. Inspect the cask hardware (including covers and vent/drain/test ports) for damage that may have occurred during transportation. Repair or replace as necessary.

7.3 Preparation of an Empty Cask for Transport

Previously used and empty NUHOMS®-MP187 casks shall be prepared for transport per the requirements of 49 CFR 173.427 [7.2].

7.4 Appendix

7.4.1 References

7.1 ANSI N14.5-1987, "American National Standard for Radioactive Materials - Leakage Tests on Packages for Shipment," American National Standards Institute, Inc., New York, 1987.

7.2 Title 49, Code of Federal Regulations, Part 173 (49 CFR 173), "Shippers - General Requirements for Shipments and Packaging."

7.3 Title 10, Code of Federal Regulations, Part 71 (10 CFR 71), "Packaging and Transportation of Radioactive Material."

7.4.2 Leakage Rate Testing of the Containment Boundary

The procedure for leak testing the cask containment boundary prior to shipment is given in this section. Assembly verification leak testing shall conform to the requirements of Section 6.5 and Section A3.5 of ANSI N14.5-1987, "American National Standard for Radioactive Materials - Leakage Tests on Packages for Shipment [7.1]". A flow chart of the assembly verification leak test is provided in Figure 7.4-1. The order in which the leak tests of the various seals are performed may vary. If more than one leak detector is available then more than one seal may be tested at a time.

a. Remove the cask vent port plug.

b. Install the cask port tool in the cask vent port. (The port tool is designed to replace the vent/drain and test prot plugs and provide a means for loosening the vent/drain and test port screw in a controlled volume. This volume can be isolated from the cask volume by an externally accessible valve to ensure personell protection during cask venting operations.)

c. Turn the cask port tool handle to open the cask vent port.

d. Attach a suitable vacuum pump to the cask port tool.

e. Reduce the cask cavity pressure to below 1.0 psia.

f. Attach a source of helium to the cask port tool.

g. Fill the cask cavity with helium to atmospheric pressure.

h. Close the vent port screw by turning the cask port tool handle. Tighten the vent port screw in accordance with the drawings in Appendix 1.3.2.

i. Remove the helium saturated cask port tool and install a clean (helium free) cask port tool.

j. Connect a mass spectrometer leak detector capable of detecting a leak of $5x10^{-8}$ standard cubic centimeters per second to the cask port tool.

k. Evacuate the vent port until the vacuum is sufficient to operate the leak detection equipment per the manufacturer's recommendations.

l. Perform the leak test. If the leakage rate is greater than $1x10^{-7}$ standard cubic centimeters per second repair or replace the vent port screw and/or seal as required and retest.

Note: Upon removing the vent port screw, it will be necessary to reduce the cask cavity pressure below 1.0 psia and refill with helium through the vent port.

m. Remove the leak detection equipment from the cask vent port.

n. Remove the cask port tool from the vent port and replace the vent port plug.

o. Remove the top test port plug.

p. Install the cask port tool in the top test port.

q. Turn the cask port tool handle to open the top test port.

r. Connect the vacuum pump to the cask port tool.

s. Connect the leak detector to the cask port tool.

t. Evacuate the top test port until the vacuum is sufficient to operate the leak detection equipment per the manufacturer's recommendations. Perform a pressure rise leak test to confirm leakage past the outer seal is less than $7x10^{-3}$ std-cc/sec of air.

u. Perform the helium leak test. If the leakage rate is greater than $1x10^{-7}$ standard cubic centimeters per second repair or replace the cask top closure or the cask top closure O-ring seals as required and retest.

Note: Upon removing and reinstalling the cask top closure, it will be necessary to reduce the cask cavity pressure below 1.0 psia and refill with helium through the vent port. The vent port assembly verification test must also be retested as described above.

v. Remove the leak detection equipment from the top test port.

w. Tighten the top test port screw in accordance with the drawings in Appendix 1.3.2. Remove the cask port tool from the top test port and replace the top test port plug.

x. Remove the cask drain port plug.

y. Install the cask port tool in the cask drain port.

z. Turn the cask port tool handle to verify that the cask drain port is closed.

aa. Connect the vacuum pump to the cask port tool.

bb. Connect the leak detector to the cask port tool.

cc. Evacuate the drain port until the vacuum is sufficient to operate the leak detection equipment per the manufacturer's recommendations.

dd. Perform the leak test. If the leakage rate is greater than $1x10^{-7}$ standard cubic centimeters per second repair or replace the drain port screw and/or seal as required and retest.

Note: Upon removing the drain port screw, it will be necessary to reduce the cask cavity pressure below 1.0 psia and refill with helium through the vent port. The vent port assembly verification test must also be retested as described above.

ee. Remove the leak detection equipment from the drain port.

ff. Tighten the drain port screw in accordance with the Drawings in Appendix 1.3.2. Remove the cask port tool from the cask drain port and replace the drain port plug.

gg. Remove the bottom test port plug.

hh. Install the cask port tool in the bottom test port.

ii. Turn the cask port tool handle to open the bottom test port.

jj. Connect the vacuum pump to the cask port tool.

kk. Connect the leak detector to the cask port tool.

ll. Evacuate the bottom test port until the vacuum is sufficient to operate the leak detection equipment per the manufacturer's recommendations. Perform a pressure rise leak test to confirm leakage past the outer seal is less than $7x10^{-3}$ std-cc/sec of air.

mm. Perform the helium leak test. If the leakage rate is greater than $1x10^{-7}$ standard cubic centimeters per second repair or replace the cask ram closure or the cask ram closure O-ring seals as required and retest.

Note: Upon removing the cask ram closure, it will be necessary to reduce the cask cavity pressure below 1.0 psia and refill with helium through the vent port. The vent port assembly verification test must also be retested as described above.

nn. Remove the leak detection equipment from the bottom test port.

oo. Tighten the bottom test port screw in accordance with the drawings in Appendix 1.3.2. Remove the cask port tool from the bottom test port and replace the bottom test port screw.

This concludes the assembly verification leak test procedure.

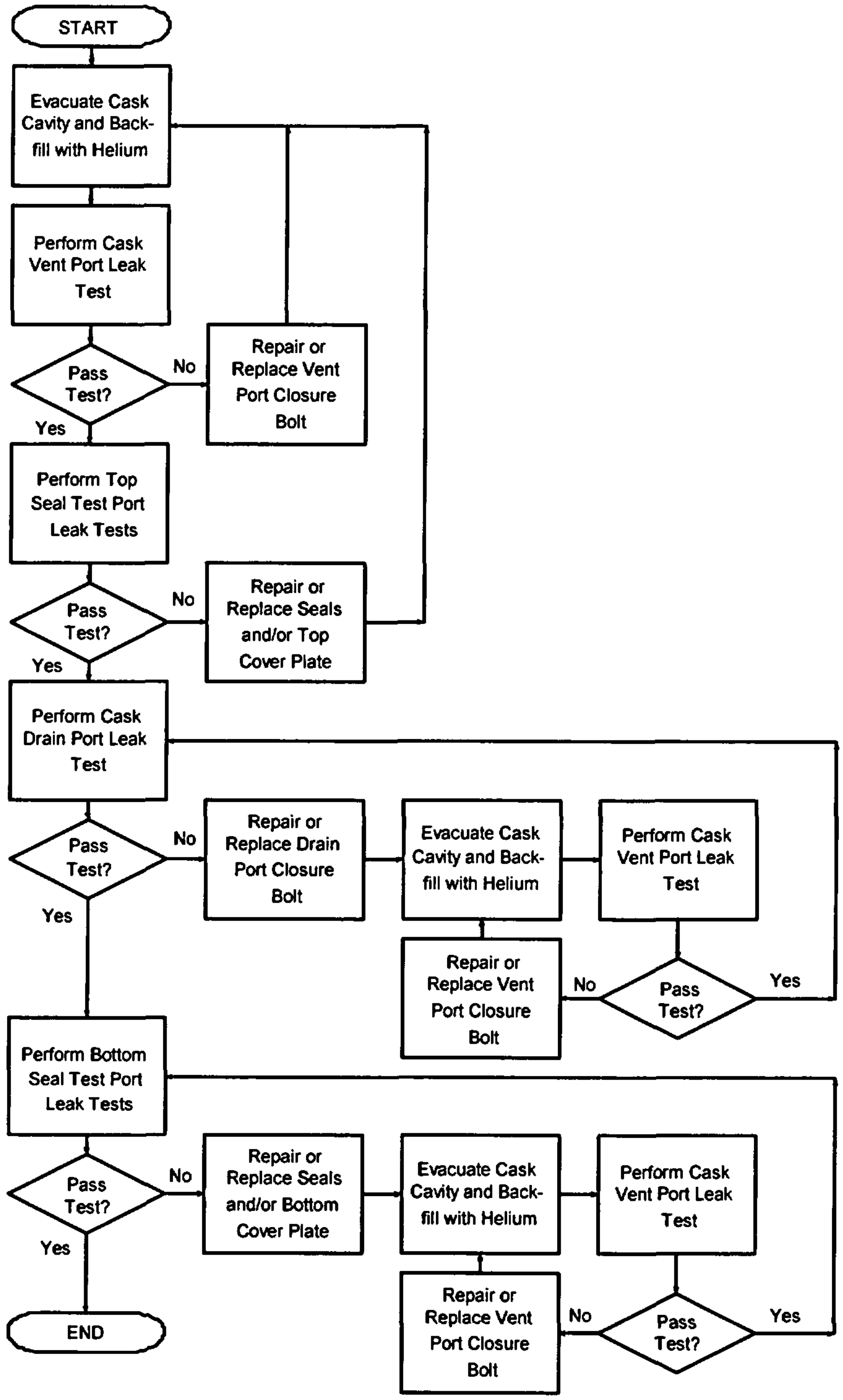

Figure 7.4-1

Assembly Verification Leak Test Flow Chart

8. ACCEPTANCE TESTS AND MAINTENANCE PROGRAM

8.1 Acceptance Tests

This section discusses the tests to be performed prior to first use of the package.

8.1.1 Visual Inspection

All NUHOMS®-MP187 Multi-Purpose Cask materials of construction and welds shall be examined in accordance with the specifications delineated on the Packaging General Arrangement Drawing in Appendix 1.3.2.

8.1.2 Structural and Pressure Tests

The maximum working load for each of the lifting trunnions (the two trunnions closest to the top of the cask) is one-half the weight of the NUHOMS®-MP187 cask, canister and fuel, without impact limiters and lids, and including the weight of the cask cavity full of water. Each of the lifting trunnions will be load tested to 150% of this maximum working load per ANSI N14.6 - 1986 [8.2], as specified in the design drawings provided in Appendix 1.3.2.

Per the drawings in Appendix 1.3.2, all welds and material in the lifting load path for the trunnions shall be visually inspected for plastic deformation or cracking, visually inspected and liquid penetrant inspected or magnetic particle inspected per ASME Boiler and Pressure Vessel Code [8.1], Section V, Article 6 and Section III, Division 1, Subsection NB, Article NB-5000 as called for in ANSI N14.6-1986 [8.2]. Any indication of cracking or distortion shall be recorded on a Nonconformance Report and dispositioned prior to final acceptance in accordance with the Transnuclear Quality Assurance Program.

The cask containment boundary shall be pressure tested to 150% of the maximum normal operating pressure per the requirements of Reference 8.3, Paragraph 71.85(b) to verify structural integrity. The cask containment maximum design pressure is 50 psig which is greater than the maximum normal operating pressure calculated in Section 3.1.3 of 45.1 psia. The containment vessel will be tested to 75 psig which is 150% of the design pressure. Accessible weld and material inspections will be performed after the pressure test to verify maintenance of structural integrity and absence of any permanent deformations.

8.1.3 Leak Tests

The fabrication verification leak test will be performed after initial fabrication to verify package configuration and performance to design criteria in accordance with Reference 8.3, Paragraph 71.85(a) and ANSI 14.5 [8.4].

The fabrication verification leak test can be separated into the following five tests: 1) cask leakage integrity, 2) cask vent port closure bolt seal integrity, 3) cask drain port closure bolt seal integrity, 4) cask top closure plate seal integrity, and 5) ram closure plate seal integrity. The testing will be accomplished in accordance with the ANSI N14.5 [8.4]. Typical methodology for complying with ANSI N14.5 are presented below. These sections also include the typical rework steps in the event of test failure. The tests need not be performed concurrently or in the specific order provided herein.

All references to the vent, test and drain port closure bolts reflect the assembly which is made up of a slotted cap screw and a metallic O-ring.

8.1.3.1 Prerequisites

a. Obtain a helium mass spectrometer leak detector capable of detecting a leak of $5x10^{-8}$ standard cubic centimeters per second, or better.

b. Calibrate the leak detector according to the manufacturer's recommendations such that the leak detector sensitivity is $5x10^{-8}$ standard cubic centimeters per second, or better.

8.1.3.2 Testing the Cask Leakage Integrity

Prior to lead pour and final machining of the inner shell, the cylindrical portion of the containment boundary including the bottom end closure will be leak tested in accordance with the requirements of ANSI N14.5, using temporary closures and seals for the ram and top closure plates. Final machining of the inner shell I.D. may be performed after completion of the lead pour when the lead and structural shell will provide support to the inner shell during final machining. For this test the interior of the cask cavity will be flooded with a helium atmosphere while vacuum is drawn on the lead cavity to determine the leak rate. If a leak is discovered the source will be determined, repaired and the shells retested to ensure that the measured leak rate is less than 1×10^{-7} standard cubic centimeters per second.

A leak test at this interim stage of fabrication will ensure leak tightness of the containment shell. The test will be performed in conjunction with the non-destructive examination of the inner shell welds in accordance with ASME BPVC, Section III, Subsection NB, a PT examination of every weld layer in the shell to top forging closure weld, and a PT examination of all final machined surfaces of the inner shell per the ASME Code. These examinations combined with the fabrication leak test, plus a second helium leak test performed on the completed cask, will ensure that the containment is leak tight.

On the completed cask, the cask body integrity is tested as follows:

a. Clean and inspect O-ring top and ram closure plate seals. Sparingly apply new vacuum grease to the seals and adjoining seal areas if needed. Install O-ring seals into the O-ring grooves.

b. Remove the protective cover from the vent port, followed by the vent port closure bolt.

c. Install a vent port tool into the vent port.

d. Sparingly apply new vacuum grease to the seal area on the cask body. Inspect the cask top closure bolts for signs of damage or wear. Replace defective bolts. Install the cask top closure plate, tightening the thirty-six (36) 2 inch bolts in accordance with the preload requirements of the Packaging General Arrangement Drawings, Appendix 1.3.2.

e. Clean and inspect both ram closure port cover O-ring seals. Sparingly apply new vacuum grease to the seals and adjoining seal areas if needed. Install the O-ring seals into the O-ring grooves.

f. If needed, sparingly apply new vacuum grease to the seal area on the ram closure plate. Inspect the ram closure plate bolts for signs of damage or wear. Install the ram closure plate, tighten twelve (12) 1 inch bolts in accordance with the torque requirements found on the Packaging General Arrangement Drawings in Appendix 1.3.2.

g. Utilizing appropriate fittings, attach a leak detector and a source of helium gas, in parallel, to the vent port tool. Install valves on each of the lines to allow independent isolation of the leak detector and the source of the helium gas to the vent port tool. Close the valve to the helium gas source and open the valve to the leak detector.

h. Evacuate the system through the vent port tool until the vacuum is adequate to operate the leak detector per the manufacturer's instructions.

i. Provide a helium atmosphere about the exterior of the cask body, taking care to purge all other gases from any pockets or cavities adjacent to the cask body.

j. Determine the leak rate of the system using the leak detector manufacturer's recommendations, and so note.

k. If the leak rate of the system is determined to be greater than 1×10^{-7} standard cubic centimeters per second, release the vacuum, disassemble the system and utilize appropriate methods to locate/isolate the leak path. Repair the leak path and repeat Steps c. through m. to verify cask leakage integrity.

l. Remove the leak detector from the vent port tool.

8.1.3.3 Testing the Cask Vent Port Closure Bolt Seal Integrity

a. Open the isolation valve to the source of helium gas thereby allowing free passage of the gas into the evacuated cask cavity.

NOTE: The next step must be performed quickly to reduce the loss of helium gas from the cask cavity.

b. When the internal pressure of the system reaches atmospheric, remove the helium-saturated vent port tool and install the vent port closure bolt, pressure tight.

c. Install a clean (helium-free) vent port tool.

d. Rotate the handle on the vent port tool closed to verify the vent port closure bolt is properly seated. Torque the vent Port closure bolt in accordance with the requirements on the drawings in Appendix 1.3.2.

e. Utilizing appropriate fittings, attach the leak detector to the vent port tool.

f. Evacuate the system through the vent port tool until the vacuum is sufficient to operate the leak detector as per the manufacturer's recommendations. Note any adjustments made to the connecting fittings required to achieve sufficient vacuum.

g. Determine the leak rate of the system using the leak detector manufacturer's recommendations, and so note.

h. If the leak rate of the system is determined to be greater than $1x10^{-7}$ standard cubic centimeters per second, release the vacuum, remove the vent port closure bolt, and inspect the vent port closure bolt seal for cuts, tears, or abrasion, and the seal area for cleanliness and surface condition. If necessary, replace the seal and/or repair the seal area. Repeat Steps a through h. If, after repeated testing, it has been determined that the vent port closure bolt cannot be made to pass the test, utilize appropriate methods to locate and isolate the leak path. Repair the leak path and repeat Steps a through h to verify vent port closure bolt seal integrity.

NOTE: Upon removing and replacing the vent port closure bolt, it will be necessary to plug the vent port to reduce the loss of helium from the cask cavity prior to retesting.

i. Remove the vent port tool/leak detector assembly from the vent port and replace the vent port plug.

8.1.3.4 Testing the Cask Drain Port Closure Bolt Seal Integrity

a. Verify that the drain port closure bolt has been installed properly with the seal. The closure bolt should be torqued in accordance to the requirements on the drawings in Appendix 1.3.2.

b. Verify that the cask has been evacuated and filled with helium.

c. Install a clean (helium-free) port tool at the drain port.

d. Rotate the handle on the port tool closed to verify the drain port closure bolt is properly seated and tighten in accordance with the requirements of the drawings in Appendix 1.3.2.

e. Utilizing appropriate fittings, attach the leak detector to the port tool.

f. Evacuate the system through the port tool until the vacuum is sufficient to operate the leak detector as per the manufacturer's recommendations. Note any adjustments made to the connecting fittings required to achieve sufficient vacuum.

g. Determine the leak rate of the system using the leak detector manufacturer's recommendations, and so note.

h. If the leak rate of the system is determined to be greater than 1×10^{-7} standard cubic centimeters per second, release the vacuum, remove the drain port closure bolt, and inspect the drain port closure bolt seal for cuts, tears, or abrasion, and the seal area for cleanliness and surface condition. If necessary, replace the seal and/or repair the seal area. Repeat Steps a through h. If, after repeated testing, it has been determined that the drain port closure cannot be made to pass the test, utilize appropriate methods to locate/isolate the leak path. Repair the leak path and repeat Steps a through h to verify drain port closure bolt seal integrity.

NOTE: Upon removing and replacing the drain port closure bolt, it will be necessary to plug the drain port to reduce the loss of helium from the cask cavity prior to retesting.

i. Remove the vent port tool/leak detector assembly from the drain port and replace the drain port plug.

8.1.3.5 Testing the Cask Top Closure Plate Seal Integrity

a. Rotate the handle on the cask top closure plate test port tool to open the test port closure bolt. Continue to rotate the knurled handle until it stops.

b. Utilizing appropriate fittings, attach the leak detector to the lid test port tool.

c. Evacuate the system through the test port tool until the vacuum is sufficient to operate the leak detector per the manufacturer's recommendations. Note any adjustments made to the connecting fittings required to achieve sufficient vacuum. Determine the leak rate of the outer seal by performing a pressure rise test.

d. Determine the helium leak rate of the system using the leak detector manufacturer's recommendations, and so note.

e. If the leak rate of the system is determined to be greater than 3×10^{-3} std-cc/sec of air for the pressure rise test or greater than 1×10^{-7} standard cubic centimeters per second of helium, release the vacuum, remove the top closure plate, and inspect the O-ring seals for cuts, tears, or abrasion, and the seal areas for cleanliness and surface condition. If necessary, replace the seal(s) and/or repair the seal area(s). Repeat Steps a through e. If, after repeated testing, it has been determined that the cask top closure seals cannot be made to pass the test, utilize appropriate methods to locate/isolate the leak path. Repair the leak path and repeat Steps a through e to verify top closure seal integrity.

NOTE:: Upon removing and replacing the top closure, it will be necessary to reduce the cavity pressure below 1.0 psia and refill the cask cavity with helium through the vent port.

8.1.3.6 Testing the Ram closure Seal Integrity

a. Remove the protective cover from the ram closure test port and, in its place, install a test port tool.

b. Rotate the handle on the test port tool to open the test port closure bolt. Continue to rotate the handle until it stops.

c. Utilizing appropriate fittings, attach the leak detector to the test port tool.

d. Evacuate the system through the test port tool until the vacuum is sufficient to operate the leak detector as per the manufacturer's recommendations. Note any adjustments made to the connecting fittings required to achieve sufficient vacuum. Determine the leak rate of the outer seal by performing a pressure rise test.

e. Determine the helium leak rate of the system using the leak detector manufacturer's recommendations, and so note.

f. If the leak rate of the system is determined to be greater than $3x10^{-3}$ std-cc/sec of air for the pressure rise test or greater than $1x10^{-7}$ standard cubic centimeters per second of helium, release the vacuum, remove the ram closure plate, and inspect the O-ring seals for cuts, tears, or abrasion, and the seal areas for cleanliness and surface condition. If necessary, replace the seal(s) and/or repair the seal area(s). Repeat Steps a through f. If, after repeated testing, it has been determined that the ram closure seals cannot be made to pass the test, utilize appropriate methods to locate/isolate the leak path. Repair the leak path and repeat Steps a through f to verify ram closure seal integrity.

NOTE: Upon removing and replacing the ram closure plate, it will be necessary to reduce the cavity pressure below 1.0 psia and refill the cask cavity with helium through the vent port.

This concludes the fabrication verification leak test of the cask.

8.1.4 Component Tests -Impact Limiter - Energy Absorption Material

8.1.4.1 Polyurethane Foam

Foam will be installed within the NUHOMS®-MP187 Multi-Purpose Cask impact limiters and tested to ensure conformance with the required foam material properties. To ensure that the samples tested are representative of the installed foam, the foam will be installed according to the following:

The foam shall be polyurethane closed-cell material with a density of approximately 15 pounds per cubic foot. The shells shall be cleaned of scale, oils, grease and debris prior to waxing to prevent foam adhesion.

With the aluminum honeycomb type materials in place or equivalent dunnage to simulate the honeycomb material, the liquid foam material shall be poured directly into the cavity. Each pour shall be carefully controlled so that the liquid components will react to form the rigid foam, and rise in such a way that the entire volume of the foamed assembly will be filled with expanded foam with a density of approximately fifteen pounds per cubic foot (15 pcf). The direction of foam rise shall be parallel to the vertical (axial) axis of the impact limiters. The temperature of the mixed foam components shall be maintained at a minimum of 60°F. The surrounding walls of the impact limiter shall be maintained at a minimum of 55°F prior to the foam installation.

The foam shall be poured in small batches to ensure uniformity of the final foam assembly. The level of each batch pour shall be recorded.

Bracing and shoring of the surrounding impact limiter walls shall be provided as necessary to prevent distortion due to internal foam pressures. The method used for bracing must be adequate to maintain the required dimensions specified on the Packaging General Arrangement Drawings in Appendix 1.3.2. If a simulated honeycomb block was used as shoring to pour the foam, it shall be removed after the foam pour and replaced with the actual honeycomb assembly.

Production records for each foam pouring operation shall be compiled during the operation. At a minimum, the record shall include pour dates, operator name, shell part number and serial number, Quality Assurance acceptance, and material traceability identified by batch.

Upon completion of production, a certification referencing the production record data and all testing data pertaining to each impact limiter shall be issued by the foam supplier. Test data relevant to the pouring operation shall be included with the certification. All QA data submittals shall be dated and signed by the foam supplier's designated QA representative.

Each production pour, including its properties, shall be completely recorded. Test samples representing the production pour shall be formed using test boxes or containers with material from the actual production pour stream. Test specimens shall be taken from each sample box prepared during production. Test samples shall be tested prior to installation of the next pour.

The test specimens shall be tested for compressive strength within the parameters presented in Appendix 2.10.8, in accordance with the requirements of Reference 8.5. Stress-strain plots, similar to those shown in Appendix 2.10.8 shall be prepared for the parallel-to-rise orientation. The test data will be recorded and reviewed to ensure compliance with the foam structural acceptance criteria outlined in Appendix 2.10.8. The average compressive stress of the sample properties from each pour shall be within $\pm$15% of the specified stress in the above referenced figures at foam strains of 10%, 40% and 70%. The average compressive stress of all pours into a single limiter shall be within $\pm$10%.

At the time of polyurethane foam installation, test samples will be retained from each foam pour, as discussed above. Using these samples, each foam pour will be tested for flame retardancy in accordance with the requirements of Section 853(c) and Part I(d), Appendix F, of 14 CFR 25, Reference 8.6. In addition, foam samples shall be tested to verify leachable chloride levels below detectable levels.

8.1.4.2 Aluminum Honeycomb Type Material

The aluminum honeycomb type material utilized in the fabrication of the impact limiters shall be manufactured as a homogenous block of sufficient size to provide the joint configuration shown in the drawings in Appendix 1.3.2. Each block of material shall be tested to demonstrate that the static strength, density and dynamic strength at -20°F and at +200°F meet the specification in Appendix 2.10.8. The number of samples tested dynamically from each block, may be reduced, or deleted, if a reliable correlation between density and static and dynamic strengths is clearly established.

8.1.5 Tests for Shielding Integrity

8.1.5.1 Gamma Shield

The MP-187 cask body poured lead shielding integrity will be confirmed via gamma scanning prior to installation of the neutron shield. There are at least two different methods available to scan the cask body. The principal difference in the methods is the location of the source and the method of scanning. In the first method the source is placed at the cask centerline, on the bottom of the cask cavity, and the detector is rotated around the exterior of the cask body parallel to the source. After each rotation the source and detector are raised a predetermined distance, typically six inches, and the full circumference scan repeated, until the full height of the body has been scanned. An alternative method places the source and detector on a frame separated by a distance greater than the cask wall thickness. The frame is lowered to the bottom of the cask and the body is rotated through the full circumference. The frame/source is raised and the process repeated until the cask body has been fully scanned. The integrity of the FF and FC-DSC poured lead shield plugs will be checked using a similar gamma scan procedure to that described above, or other methods such as X-ray or UT measurement of lead thickness.

The outer cask surface is gridded and a chart is made to reflect the gridded surface. The gamma scan will be performed using a detector with a detection area enveloping the grid minimum area (e.g., for a 6" x 6" grid, the detector will encompass a 6" x 6" square). This data serves as the raw gamma scan results in milliroentgens per hour (mR/hr). The dose rates are evaluated by comparing them to predetermined dose rate values for the nominal (as designed) lead thickness and the nominal less 5% lead thickness. The acceptance criteria are determined by utilizing test blocks made up from nominal thicknesses for the lead and steel sheets. The source is placed behind the test block assembly and dose readings recorded. This test sequence is repeated on the nominal less 5% test block assembly and the dose rate established. Additional dose readings are taken in incremental thicknesses between and beyond the two base readings. The resultant data is then plotted on a chart of dose values versus lead thickness. The dose rate at the nominal less 5% lead thickness is used as the maximum acceptable dose reading for the inspected cask.

The probe time and source/detector distances used in the inspection shall be the same as that used in establishing the minimum dose rates in the mockup. Dose rates for minimum cask shell thickness shall be at least three times the background dose rate.

8.1.5.2 Neutron Shield

The cask annulus neutron shield and miscellaneous components are filled with NS-3 cementitious material with 2w/o B4C. As successfully demonstrated during the fabrication of the NuPac 125B cask [8.7] confirmation of acceptable placing of the NS-3 will be established using a combination of mockup testing, in-process production controls, and measurement of cask surface dose rates.

To account for potential stratification, a full scale mockup of a cask segment will be constructed with transparent panels in the face to permit monitoring of the pour process. The NS-3 material will be mixed and placed in accordance with the manufacturer's instructions. A sample of the NS-3 material will be retained from each pour for chemical testing to verify the elemental composition. The cured NS-3 mockup will be sectioned and chemical tests performed to establish the hydrogen and boron densities of each segment. A linear fit of the resultant densities will be performed to determine the direction and magnitude of any mockup stratification of boron or hydrogen. NS-3 test acceptance criteria will demonstrate that the densities of the boron and hydrogen meet the manufacturer's minimum specified values and exceed those assumed in the shielding analysis.

Production controls verified by the mockup test, and similar to those adopted for the fabrication of the NuPac 125B cask, will be used to ensure that the production placement will be performed in the same manner as the mockup test. This will include the use of a metered pump to ensure that the predetermined volume of material is poured into the neutron shield. Samples of each pour will be taken for chemical verification of the density, boron, and hydrogen concentrations to demonstrate compliance with the mockup test results and analytical requirements.

In addition to the controls described above, a confirmatory neutron scan may be performed either on the empty cask, or upon completion of the initial fuel load, but prior to placing the cask on the transportation skid. The empty cask test would be accomplished by inserting a known neutron source into the cask cavity and scanning the exterior surface with a neutron flux detector. The outer cask surface is gridded and a chart is made to reflect the gridded surface. The neutron scan will be performed using a detector with a detection area enveloping the grid minimum area (e.g., for a 6" x 6" grid, the detector will encompass a 6" x 6" square). This data serves as the raw neutron scan results in milliroentgens per hour (mR/hr). The measured dose rates will be evaluated by comparing them to predetermined dose rates developed from a calibration block equal to the nominal design thickness less 5%. The acceptance criteria are determined by utilizing test blocks made up from nominal thicknesses for the lead, NS3, and steel sheets. The source is placed behind the test block assembly and dose readings recorded. This test sequence is repeated on the nominal less 5% test block assembly and the dose rate established. Additional dose readings are taken in incremental thicknesses between and beyond the two base readings. The resultant data is then plotted on a chart of dose values versus NS3 thickness. The dose rate at the nominal less 5% NS3 thickness is used as the maximum acceptable dose reading for the inspected cask.

If the measurements are taken after the initial fuel load then the acceptance criteria will be developed based on the design limits ratioed by the fuel neutron source term to the design fuel basis source term.

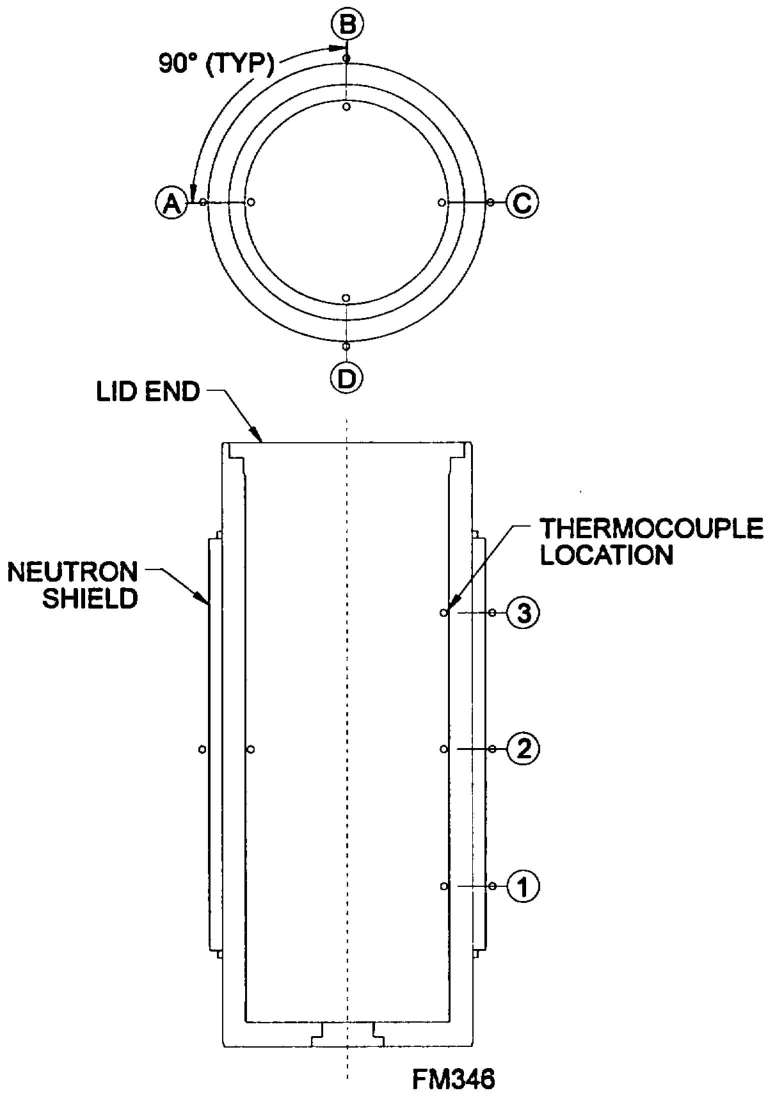

Figure 8.1-1

Thermocouple Locations for Thermal Acceptance Test

8.1.6 Thermal Acceptance Tests

8.1.6.1 Prior to First Use

Material properties established in Section 3.0 are conservative for the analyses performed. As such, acceptance tests for material thermal properties are not performed.

The complete cask shall be subjected to a thermal heat rejection test to demonstrate satisfactory operation of the as-built shells, top lid , and shielding materials but without the ram closure installed. This test is required for certification of the cask for transportation and will be performed following completion of fabrication and prior to first use as a transport cask. The cask shall be supported vertically with an internal heat source capable of producing a minimum of 4.5 kW suitably supported within the cask cavity. As shown in Figure 8.1-1, a minimum of six pairs of thermocouples will be attached on the containment shell and the neutron shield shell to record the thermal gradient between the cask cavity and the external surface. Power and instrumentation cables may exit the cask through the ram access port. A special temporary cover plate is not required. Power shall be applied to the heaters for sufficient time for the cask to reach thermal equilibrium with temperatures recorded at least every 30 minutes. The cask shall be held at equilibrium for a minimum of one hour then the power turned off and the cask allowed to cool without any mechanical cooling. The acceptance criteria shall be calculated for the change in temperature across the cask wall based on the specific internal heat and the exterior environmental conditions using the same analytical methods used to predict the cask performance for the normal and accident conditions.

8.1.6.2 Thermal Acceptance Test During Storage

When the MP187 cask is used in storage mode for time periods greater than 5 years, the thermal performance of the cask will be verified by performing a thermal acceptance test as follows. The test will be performed prior to shipment of the cask.

The cask is assumed to be in the vertical orientation on the storage pad at the ISFSI site. The total decay heat from the fuel assemblies in the cask will be calculated at the time of the thermal test. The steady state condition of the cask for the ambient conditions present will be verified prior to the start of the test. The temperature on the outside surface of the cask in the radial direction at four locations (90° from each other at the cask mid-plane) will be measured. Similarly, the temperature on the top surface of the cask top cover in the axial direction at four locations (90° from each other in line with the radial measurement locations) will be measured.

The acceptance criteria shall be calculated for the ratio of axial to radial temperature for the given heat load and ambient conditions using the same analytical methods used to predict the cask performance for the normal and accident conditions.

8.1.7 Lead Installation Tests

Testing during the lead installation process involves pre- and post-pour diameter and straightness measurements of the cask shells and close monitoring of the cask temperatures during the preheat, lead pour, and cool-down processes. A more detailed description of the lead installation and testing is presented in Section 8.3.2.

8.1.8 Neutron Absorber Plates

The neutron absorber plates are verified to have their minimum total B^{10} per unit area (areal density) of the sandwiched material as specified on the drawings in Appendix 1.3.2.

Samples from each sheet of the neutron absorber are retained for testing and record purposes. The minimum B^{10} content per unit area and the uniformity of dispersion within a panel are verified by wet chemical analysis and/or neutron attenuation testing. All material certifications, lot control records, and test records are maintained to assure material traceability.

Chemical (destructive) testing is the preferred method because the B^{10} areal density, which is the primary requirement for the material, can be directly measured. This is done by first taking two one inch square samples from each end of the rolled product. This one square inch sample size is small compared to the finished panel size, 1300 in^2, so that non-uniformities in B^{10} areal density would be readily apparent between the samples. The material on the ends of the rolled product is known to be thinner than the rest of the panel because of the rolling process. This characteristic of the finished product is confirmed by examination of thickness in four locations on 100% of the panels. The thinnest of these samples is used for destructive chemical determination of the amount of boron in the sample using written, approved procedures and standard laboratory processes and equipment. Using the measured thickness of the sample, the area of the sample, and the mass of boron in the sample, the areal boron density may be calculated. Once the areal boron density is known, the areal B^{10} density is calculated using the isotopic assay of the B_4C powder used to manufacture the product. The sample frequency is determined using standard statistical procedures to assure that minimum B^{10} areal densities are achieved with a 95/95 confidence level.

Neutron attenuation testing may be performed to augment or replace chemical (destructive) testing as required to demonstrate acceptable minimum areal B^{10} loading of the neutron absorber plates. Neutron transmission measurements may be performed on samples, or completed panels, using a neutron diffractometer. The neutron transmission measurements shall be performed using written, approved procedures in accordance with applicable portions of ASTM E94, "Recommended Practice for Radiographic Testing", ASTM E142, "Controlling Quality of Radiographic Testing", and ASTM E545, " Standard Method for Determining Image Quality in Thermal Radiographic Testing". Since this type of testing does not measure directly the B^{10} areal density of the panels, the results of neutron attenuation tests shall be demonstrated by calculation to show that the minimum specified B^{10} areal densities are achieved with a 95/95 confidence level.

8.2 Maintenance Program

This section describes the maintenance program used to ensure continued performance of the packaging.

8.2.1 Structural and Pressure Tests

Other than the tests required prior to first use, no structural or pressure tests are necessary to ensure continued performance of the packaging.

8.2.2 Leak Tests

The metallic containment seals are to be replaced after each use and shall be leak tested to show a leak rate less than 1×10^{-7} standard cubic centimeters per second of helium, (with a test sensitivity of at least 5×10^{-8} standard cubic centimeters per second). This test is to be performed for the inner seals, and a leak rate less than 7×10^{-3} std-cc/sec of air for the top closure and ram closure outer seals, (with a test sensitivity of at least 3.5×10^{-3} std-cc/sec), within the 12-month period prior to each shipment and after each seal replacement.

Appropriate sections of the maintenance verification leak test shall be performed during routine maintenance to verify cask configuration and performance to design criteria. Tests of the top closure, ram access and drain and vent port O-ring seals are to be performed upon replacement, but not necessarily at the same time (seals are to be replaced annually or when damaged). The maintenance verification leak test shall also be performed after the third use of the system per Section 6.5 of ANSI N14.5-1987 [8.4].

For the NUHOMS®-MP187 Multi-Purpose Cask the assembly verification leak test, the fabrication leak test for the seal integrity and the maintenance verification leak test all use the same methodology. Therefore, the maintenance verification leak test will be performed using the steps outlined for the assembly verification leak test in Appendix 7.4.2.

8.2.3 Subsystems Maintenance

This section describes the inspection and replacement schedule for packaging subsystems.

8.2.3.1 Fasteners

All threaded parts will be inspected after each use, and annually, for deformed or stripped threads. Damaged parts shall be evaluated for continued use and replaced as required. At a minimum, the replacement schedule for package fasteners is given below for the transportation mode. The replacement interval is initiated at the time of fastener torquing for package transportation. Pre-loading of bolts as part of a demonstration or training program would not initiate the five year interval. If the cask is used in a storage mode, the fasteners need not be inspected or replaced until after the first shipment if the replacement interval has been exceeded.

Component Fastener	Replacement Interval (years)
Vent/Test/Drain Ports	5
Impact Limiter Attachment	5
Cask Top Closure Plate	5
Ram closure Plate	5

8.2.3.2 Impact Limiters

A sound industrial maintenance program will be followed to assure the integrity of the impact limiters. The impact limiter attachment fastener and hole threads will be inspected after each use, and annually, when in use as a transportation cask for damaged or stripped threads. Damaged parts shall be evaluated for continued use and corrected as required. Additionally, plastic pipe plugs at the ends of the impact limiters shall be inspected for damage and replaced prior to further use if damage is present.

The impact limiters are sealed so that no water is expected to enter the internal cavity. The foam is a closed cell foam which in similar applications has not deteriorated or absorbed significant water in over 10 years of use. To ensure that no significant amount of water is absorbed in the impact limiter, the impact limiters shall be inspected within one year of use. The inspection shall consist of a visual inspection of the foam for water absorption or degradation by removing the plastic pipe plugs in the shell. Each impact limiter shall also be weighed at the time of inspection. The impact limiter shall be restricted from use if there is more than a 3% weight increase.

8.2.3.3 Seal Areas and Grooves

Sealing surfaces and O-ring grooves shall be inspected at the time of seal replacement, for potentially damaging burrs or scratches. Damaged parts shall be evaluated for continued use/repair and replaced as required (e.g., 400-600 grit emery cloth to polish the surface). More extensive damage may be repaired by the use of surface welding procedures and grinding to restore the original surface, or similar processes.

8.2.3.4 Trunnions Sockets

The trunnions sockets shall be inspected annually and before each use for excessive wear, galling, or distortion. Trunnions sockets exhibiting excessive wear, galling, or distortion shall be documented for proper QA disposition (e.g. use "as is" or repair).

8.2.4 Valves, Rupture Disks, and Gaskets

All containment O-ring seals and gaskets shall be replaced after each use per specifications as delineated on the Packaging General Arrangement Drawing in Appendix 1.3.2. Following seal replacement and prior to a loaded shipment, the seal(s) shall be leak tested to the requirements of Section 8.2.2.

There are no valves or rupture disks used on the NUHOMS®-MP187 cask that are in the containment boundary. The rupture disks in the lower neutron shield ring protect the neutron shield cavity from over-pressurization and require annual visual inspection to verify there is no evidence of damage when the cask is in use for transportation. The neutron shield rupture disks require no special maintenance.

8.2.5 Shielding

Other than the tests required prior to first use, no shielding tests are necessary to ensure continued performance of the package.

8.2.6 Thermal

The heat removal capacity of the cask shall be verified periodically by performing the applicable test described in section 8.1.6.1. The test shall be performed within five years of each use of the cask for transportation purposes. An increase of the temperature drop across the wall of more than 25°F from the previous test is unacceptable.

The test described in section 8.1.6.1 is to be performed if the cask is used in the storage mode for time periods greater than five years.

8.3 Appendix

8.3.1 References

8.1 American Society of Mechanical Engineers (ASME) Boiler and Pressure Vessel Code.

8.2 ANSI N14.6-1986, American National Standard for Radioactive Materials -Special Lifting Devices for Shipping Containers Weighing 10,000 Pounds (4,500 kg) or More.

8.3 Title 10, Code of Federal Regulations, Part 71 (10 CFR 71), Packaging and Transportation of Radioactive Materials.

8.4 ANSI N14.5-1987, American National Standard for Radioactive Materials - Leakage Tests on Packages for Shipment.

8.5 ASTM D1623-73, Method of Test for Tensile Properties of Rigid Cellular Plastics.

8.6 Title 14, Code of Federal Regulations, Part 25, (14 CFR 25), Airworthiness Standards: Transport Category Airplanes, July 21, 1986.

8.7 Pacific Nuclear, "Consolidated Safety Analysis Report for the NuPac 125-B Fuel Shipping Cask," NRC Docket No. 71-9200, April 1991.

8.3.2 Lead Installation Procedure

The following delineates a representative procedure for installation of poured lead into the NUHOMS®-MP187 Multi-Purpose Cask structural shell/inner shell cavity. The procedure presents pre-pour cask inner shell dimensional inspection requirements, lead pour, gamma scan or X-ray inspection of the lead shielding, and post-pour cask inner shell dimensional inspection requirements. Note: The neutron shield is attached after lead pour and cool down.

a. Record the cask, inner and outer shell diameter and straightness in accordance with the requirements of ASME Boiler and Pressure Vessel Code [8.1], Section III, Subsection NE, Article NE-4220. At a minimum, record the inside diameter at five locations approximately four equal spaces along the inside diameter length, and at 8 points 45° apart along the circumference at each of the five locations along the cask longitudinal axis as shown in Figure 8.3-1.

b. All cask inner and outer surfaces shall be supported or braced, as necessary, depending on the shell thickness and based upon shell buckling calculations for the anticipated loading during lead pour.

c. The lead shall be poured with the cask in the vertical position. The lead may be pumped from below the cask or poured from above the cask. The cask may be positioned with either the open end up or down.

   Stand pipes or equivalent shall be placed on the top of the cask to insure an excess head of liquid lead when the cask lead cavity is full (during cooling operation). This excess head shall be maintained during the cooling operation. Vent risers shall be provided to allow for escape of air and impurities.

d. The cask shall be instrumented with thermocouple wires at a minimum of twelve (12) locations on the inside and outside to monitor temperature differentials between the two shells as shown in Figure 8.3-1.

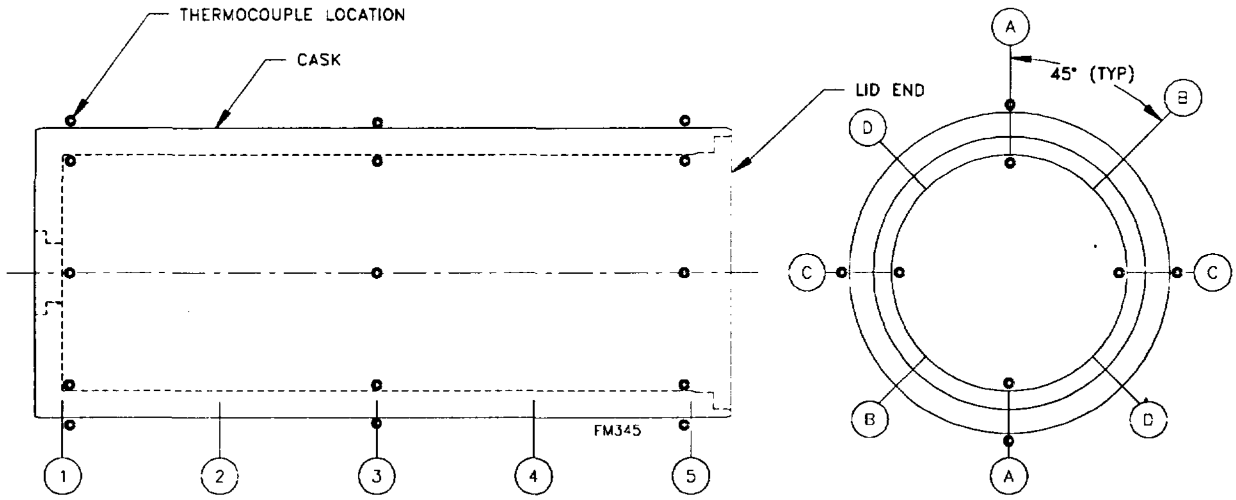

Figure 8.3-1

Thermocouple Locations for Lead Installation

e. All cask components (i.e., outer shell, inner shell, top end forging and bottom end closure) shall be uniformly preheated at a maximum heat up rate of 150 °F per hour to a temperature between 500°F and 725°F over the entire surface prior to lead pouring. No temperature deviation between any two points on the cask shell shall exceed 250°F. Maximum differential temperature between inner and outer shell shall not be greater than 100°F.

f. The temperature of the lead at the time of lead pour shall be above 625°F and less than 790°F.

g. The rate of lead flow shall be controlled to fill the cask lead cavity as rapidly and evenly as possible. The lead shall enter the cavity, and flow shall be controlled, in such a way as to minimize impingement on the cask shells.

h. Heat sources shall be controlled during the cool-down period so that the cask is cooled to insure that only one solidifying front exists in the lead. Cooling shall be initiated from the lowest portion of the cask as it is positioned for lead pour. Maximum cool-down rate shall not exceed 100°F per hour. No deviation between 2 points from top to bottom shall be more than 250°F.

i. Molten lead shall be added to the standpipes at a rate consistent with normal shrinkage.

j. After cool-down is complete, the thermocouples and any internal and/or external bracing shall be removed and the outer cask gamma scanned or X-ray examined in accordance with the tests delineated in Section 8.1.5.

k. Upon a successful gamma scan inspection, the cask shell diameter and straightness shall be measured. All measurements after lead pour must meet the requirements specified on the Packaging General Arrangement Drawing in Appendix 1.3.2.

l. Remove all fill, vent, and standpipes, or equivalent, clean the holes thoroughly of all lead, and install plugs of a material that is compatible with the base material.

8.3.3 NS-3 Specification

Specific Gravity	1.76
Hydrogen	5.14e+22 atom/cc
Thermal Aging:	
100 hrs. @ 150°F	Wt. loss=2.15%, H loss=4.68%
100 hrs. @ 200°F	Wt. loss=2.90%, H loss=6.33%
2 hrs. @ 340°F	Wt. loss=4.16%, H loss=8.90%
Radiation Exposure:	
Gamma	1.5e+10 Rads Gamma
Thermal Neutron (<.55eV)	1.5e+19 n/cm^2
Epithermal Neutron (.55eV-1keV)	9.3e+16 n/cm^2
Fast Neutron (> 1MeV)	1.6e+17 n/cm^2
Wt. Loss	7.17%
Hydrogen loss	13.4%
Thermal Conductivity	5.86 Btu-in/hr-ft^2-°F)
Coefficient of Thermal Expansion	7.81e-6 in/in/°F
Compressive Strength	4500 psi

Theoretical Elemental Composition:

Hydrogen 4.85 wt. %	Oxygen 57.05 wt. %	Iron 0.56 wt. %
Carbon 9.35 wt. %	Silicon 3.36 wt. %	Trace 1.33 wt. %
Calcium 5.61 wt. %	Aluminum 17.89 wt. %	

Maximum B_4C Loading 11.25 wt. %